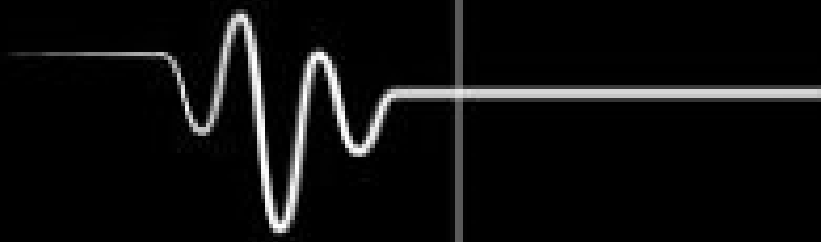


J. Arrillaga | N.R. Watson

power system harmonics

Second Edition

WILEY



VISIT…



1

Subject Definition and Objectives

1.1 Introduction

When an electrical signal is sent to an oscilloscope its waveform is observed in the time domain; that is, the screen shows the signal amplitude at each instant in time. If the same signal is applied to a hi-fi amplifier, the resulting sound is a mix of harmonic frequencies that constitute a complete musical chord. The electrical signal, therefore, can be described either by time-domain or frequency-domain information. This book describes the relationships between these two domains in the power system environment, the causes and effects of waveform distortion and the techniques currently available for their measurement, modelling and control.

Reducing voltage and current waveform distortion to acceptable levels has been a problem in power system design from the early days of alternating current. The recent growing concern results from the increasing use of power electronic devices and of waveform-sensitive load equipment.

The utilisation of electrical energy is relying more on the supply of power with controllable frequencies and voltages, while its generation and transmission take place at nominally constant levels. The discrepancy, therefore, requires some form of power conditioning or conversion, normally implemented by power electronic circuitry that distorts the voltage and current waveforms.

The behaviour of circuits undergoing frequent topological changes that distort the waveforms can not be described by the traditional single-frequency phasor theory. In these cases the steady state results from a periodic succession of transient states that require dynamic simulation. However, on the assumption of reasonable periods of steady-state behaviour, the voltage and current waveforms comply with the requirements permitting Fourier analysis [1], and can, therefore, be expressed in terms of harmonic components. A harmonic is defined as the content of the function whose frequency is an integer multiple of the system fundamental frequency.

1.2 The Mechanism of Harmonic Generation

Electricity generation is normally produced at constant frequencies of 50 Hz or 60 Hz and the generators' e.m.f. can be considered practically sinusoidal. However, when

Power System Harmonics, Second Edition J. Arrillaga, N.R. Watson
© 2003 John Wiley & Sons, Ltd ISBN: 0-470-85129-5

a source of sinusoidal voltage is applied to a nonlinear device or load, the resulting current is not perfectly sinusoidal. In the presence of system impedance this current causes a non-sinusoidal voltage drop and, therefore, produces voltage distortion at the load terminals, i.e. the latter contains harmonics.

To provide an intuitive view of this phenomenon let us consider the circuit of Figure 1.1, where generator G feeds a purely resistive load R_l through a line with impedance $(R_s + jX_s)$ and a static converter.

The generator supplies power (P_{g1}) to the point of common coupling (PCC) of the load with other consumers. Figure 1.1(a) shows that most of this power (P_{l1}) is transferred to the load, while a relatively small part of it (P_{c1}) is converted to power at different frequencies in the static converter. Besides, there is some additional power loss (P_{s1}) at the fundamental frequency in the resistance of the transmission and generation system (R_{s1}).

Figure 1.1(b) illustrates the harmonic power flow. As the internal voltage of the generator has been assumed perfectly sinusoidal, the generator only supplies power at the fundamental frequency and, therefore, the generator's e.m.f. is short-circuited in this diagram, i.e. the a.c. line and generator are represented by their harmonic impedances $(R_{sh} + jX_{sh})$ and $(R_{gh} + jX_{gh})$, respectively. In this diagram the static converter appears as a source of harmonic currents. A small proportion of fundamental power (P_{c1}) is transformed into harmonic power: some of this power $(P_{sh} + P_{gh})$ is consumed in the system (R_{sh}) and generator (R_{gh}) resistances and the rest (P_{lh}) in the load.

Thus the total power loss consists of the fundamental frequency component (P_{s1}) and the harmonic power caused by the presence of the converter $(P_{sh} + P_{gh} + P_{lh})$.

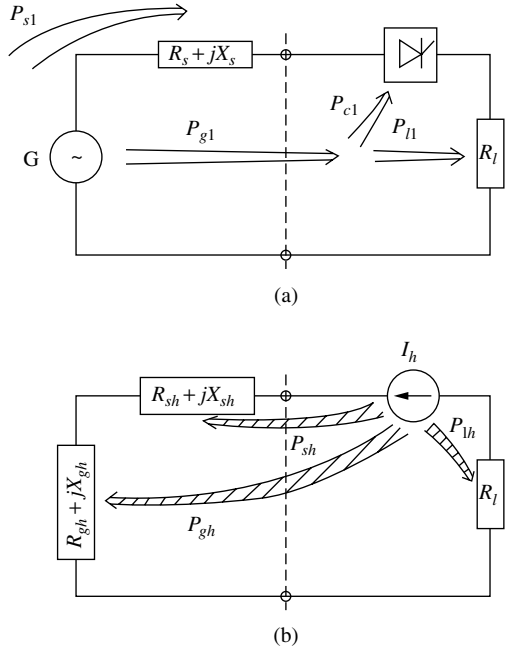


Figure 1.1 (a) Power flow at the fundamental frequency; (b) harmonic power flow

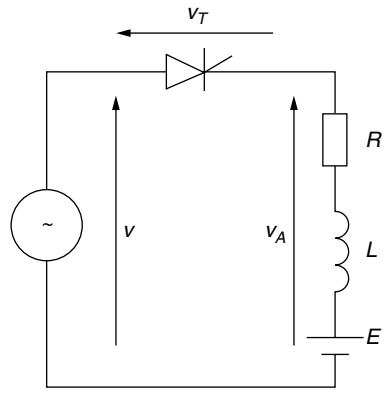


Figure 1.2 Basic circuit to explain the conversion mechanism

For a more rigorous interpretation of the conversion mechanism, let us consider the case of Figure 1.2, where v is a source of sinusoidal voltage and E the constant e.m.f. of a battery with negligible internal resistance.

The thyristor turns ON at $\omega t = \alpha$ and OFF at $\omega t = \beta$ and its voltage drop during conduction is neglected.

Figure 1.3(a), (b) and (c) display respectively the source voltage, the voltage across the thyristor and the load voltage, while Figure 1.3(d) displays the current waveform.

The load voltage V_{A} can be replaced by the three components shown in Figure 1.4, derived from the Fourier transformation, i.e.

$$V_A = V_{A1} + V_{Ah} + V_{A0} \tag{1.1}$$

where

$$V_{A1} = \sqrt{2} V_{A1} \sin(\omega t + \theta_1) \tag{1.2}$$

is the fundamental component,

$$V_{Ah} = \sum_{h=2}^{n} \sqrt{2} V_{Ah} \sin(h\omega t + \theta_h) \tag{1.3}$$

is the harmonic content, and

$$V_{A0} = \frac{1}{T} \int_0^{\mathrm{T}} V_A \, \mathrm{d}t = V_{\mathrm{dc}} \tag{1.4}$$

is the d.c. component.

Equally, the current can be replaced by the following three components:

$$i_1 = \sqrt{2} I_1 \sin(\omega t + \xi_1) \tag{1.5}$$

$$i_h = \sum_{h=2}^{n} \sqrt{2} I_h \sin(h\omega t + \xi_h) \tag{1.6}$$

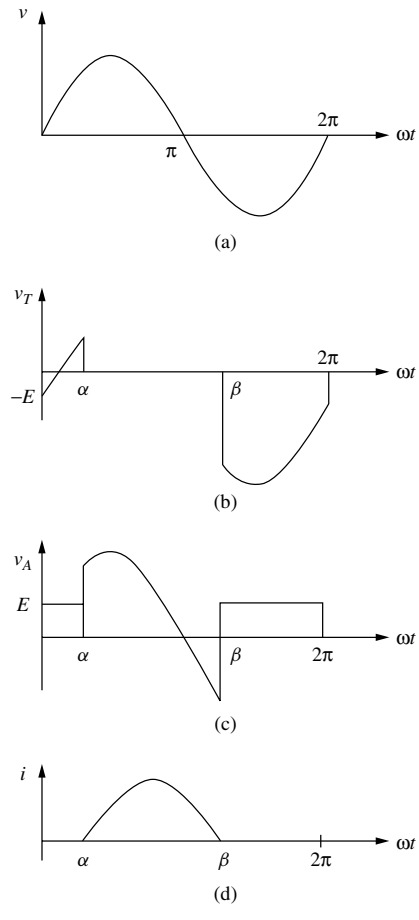


Figure 1.3 Waveforms of the circuit of Figure 1.2: (a) voltage source; (b) voltage across the thyristor; (c) load voltage; (d) current

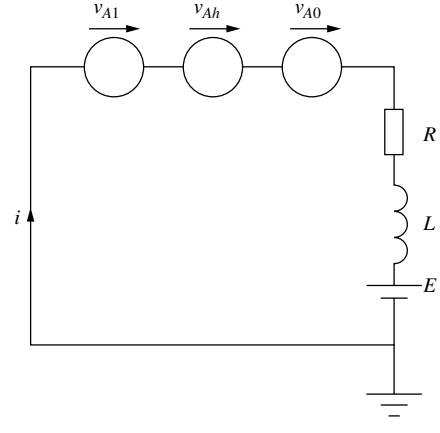


Figure 1.4 Load voltage components of the circuit of Figure 1.2

$$I_0 = \frac{V_{\mathrm{dc}} - E}{\mathrm{R}} \tag{1.7}$$

Next let us consider the energy aspects.

The active power generated by the source is

$$P_G = V_1 I_1 \cos\xi_1 \tag{1.8}$$

and the power supplied to the load

$$P_A = P_{A1} + P_{Ah} + P_{A0} \tag{1.9}$$

where

$$P_{A1} = V_{A1} I_1 \cos(\theta_1 - \xi_1) = I_1^2 R \tag{1.10}$$

is the power supplied to the fundamental component,

$$P_{Ah} = \sum_{h=2}^{n} V_{Ah} I_h \cos(\theta_h - \xi_h) = \sum_{h=2}^{n} I_h^2 R \tag{1.11}$$

is the power supplied to the harmonics, and

$$P_{A0} = V_{\mathrm{dc}} I_0 = E I_0 + I_0^2 R \tag{1.12}$$

is the d.c. power.

Therefore the thyristor behaves like an energy converter, i.e. the ideal voltage source combines with the fundamental component of the current waveform to generate the total power P_G.

As the thyristor losses have been ignored $P_G = P_A$ and the following relationship applies:

$$P_G = P_A = I^2 R + E I_0 \tag{1.13}$$

where

$$I = \sqrt{I_0^2 + I_1^2 + \sum_{h=2}^{n} I_h^2}$$

is the current root mean square (r.m.s.) value

1.3 Definitions and Standards

Power system harmonics are defined as sinusoidal voltage and currents at frequencies that are integer multiples of the main generated (or fundamental) frequency. They constitute the major distorting components of the mains voltage and load current waveforms. However, the increasing content of power system inter-harmonics, i.e.

distorting components at frequencies that are not integer multiples of the fundamental, has prompted a need to give them greater attention.

Most countries have in the past developed their own harmonic standards or recommendations, to suit local conditions. However, with the growth of global trade, the need for equipment manufactured in one country to comply with standards in another has prompted concerted effort in formulating international standards on harmonics and inter-harmonics.

The rationale is to maintain a globally acceptable electromagnetic environment that co-ordinates the setting of emission and immunity limits. This is achieved using reference levels of electromagnetic disturbance, referred to as compatibility levels. The latter are recognised as the levels of severity which can exist in the relevant environment; therefore all equipment intended to operate in that environment is required to have immunity at least at that level of disturbance and, thus, a margin appropriate to the equipment concerned is normally provided between the compatibility and immunity levels.

In determining the appropriate emission limits, the concept of planning level is also used. This is a locally specific level of disturbance adopted as a reference for the setting of emission limits from large installations in order to co-ordinate those limits with the limits adopted for equipment intended to be connected to the power system. Again, the planning level is generally lower than the compatibility level by a specific margin that takes into account the structure and electrical characteristics of the local supply network. This margin is necessary to make allowance for possible system resonance and for an upward drift in the levels on the network due to future loads that may be connected where there is no consent required. Such loads include computers and other home and office electronic equipment that contain switched-mode power supplies. In addition there is uncertainty about the impedance of the supply systems and the customers' equipment at harmonic frequencies.

The relationship between the various levels defined above is illustrated in Figure 1.5.

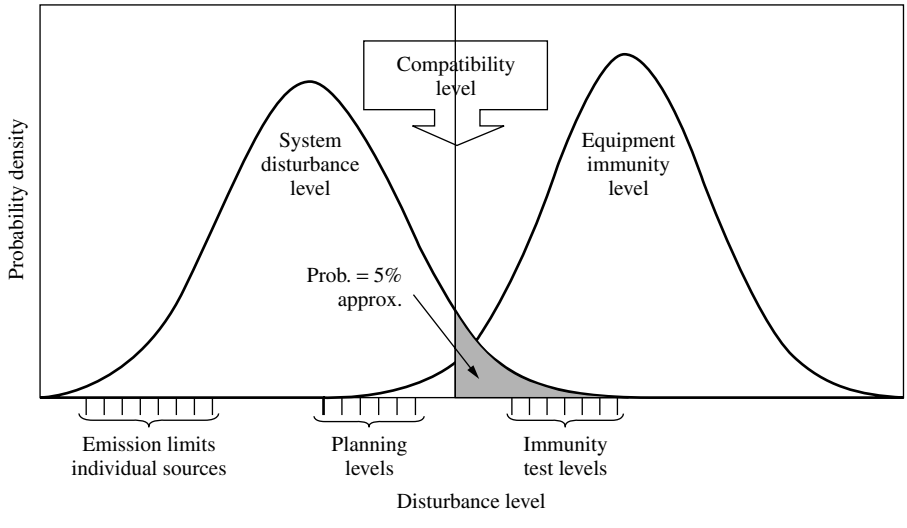


Figure 1.5 Relation between compatibility, immunity, planning and emission levels

1.3.1 Factors Influencing the Development of Standards

The development of harmonic standards is centred around the following issues:

- description and characterisation of the phenomenon;
- major sources of harmonic problems;
- impact on other equipment and on the power system;
- mathematical description of the phenomenon using indices or statistical analysis to provide a quantitative assessment of its significance;
- measurement techniques and guidelines;
- emission limits for different types and classes of equipment;
- immunity or tolerance level of different types of equipment;
- testing methods and procedures for compliance with the limits;
- mitigation guidelines.

The standards themselves may be either system standards, connection standards or, more usually, some combination of the two. In a system standard the emphasis is on the levels of harmonics that can be tolerated in the system, with little or no reference within the body of the standard to the source of harmonics. Details of the harmonic sources, and their likely influence on system harmonic content, are usually given as associated material in appendices.

The limits may be expressed as absolute levels of current or voltage, which may not be exceeded, or as incremental limits allowing small changes to the harmonic source with limited consideration of system effects. The former approach usually permits the connection of certain types and ratings of distorting loads (e.g. converters) to the system without reference to existing harmonic levels. With higher converter ratings the existing harmonic content needs to be established prior to connection, and the proposed additional harmonic source considered in relation to these levels, in order to determine if the limits are likely to be exceeded.

The application of absolute harmonic current limits for individual consumers would seem to provide equal rights for all consumers, large or small. However, this may be considered an unfair distribution by a large consumer connected to a PCC together with a number of small consumers, as it takes no account of their share of the total load. If, instead, the limit is expressed in a way which takes account of the consumer's share of the total load, then this may well be seen as overly restrictive, particularly if a large consumer has little or no disturbing load.

If the limits are expressed in terms of the levels of harmonic voltage at the PCC, then consumers connected to a strong PCC may well benefit relative to a consumer connected to a weak PCC. The adoption of harmonic voltage limits may also mean that, where existing levels are high, new consumers may be forced to install expensive additional circuitry before, connection is permitted. This latter situation constitutes the 'first come, first served' approach.

In considering the type and nature of the limits to be adopted, the different problems presented by the various types of load must be taken into account; the two extremes are groups of small distributed disturbing loads (normally domestic) and large industrial loads. An industrial consumer may also have a number of individual components of

plant, each capable of generating significant harmonic content. Such a consumer is faced with the double problem of ensuring that no harmonic-induced effects occur within its own system, and maintaining the levels at the PCC within the prescribed limits. Experience shows that in many instances where high harmonic levels exist at points within the consumer's own network, these levels do not necessarily penetrate to the external system.

The way in which the harmonics from a number of sources interact on the power system is governed by the random nature of such sources and the variation of their distribution throughout the system, both physically and with time. The random nature of the sources can be accounted for by introducing a diversity factor. This changes the actual ratings of the disturbing loads into an effective rating, which is then used in assessing its relationship with the standard.

1.3.2 Existing Harmonic Standards

The organisation widely recognised as the curator of electric power quality standards is the IEC (International Electrotechnical Commission or Commission Electrotechnique Internationale), based in Geneva. The IEC has defined a series of standards, called Electromagnetic Compatibility (EMC) Standards, to deal with power quality issues. The IEC 61000 series [2] includes harmonics and inter-harmonics as one of the conducted low-frequency electromagnetic phenomena. A widespread alternative to the IEC series is the IEEE 519–1992 document [3], which provides guidelines on harmonics.

There are also standards dealing with specific equipment under the influence of harmonic distortion, such as those of references [4–7], and their relevance will be discussed in Chapter 4.

While the international standards are used as a basis for global co-ordination, individual countries make their own adjustments to accommodate various national priorities. These are normally motivated by the special characteristics of their power system configuration and load management (e.g. the use of ripple control in some countries). Consider as an illustration the power systems of the UK and New Zealand. In the UK a highly interconnected power system with distributed generation serves a large number of load centres, always relatively close to the points of generation. This contrasts with the New Zealand situation, where remote generation centres provide supply to a few, widely separated, major load centres and a large number of scattered small loads. The resulting long transmission lines and comparatively low fault levels increase the vulnerability of the system to harmonic penetration. These factors, taken together with the extensive use made of ripple control, present very different problems than those encountered in the UK to their respective standards committees.

The European Union, through the Electromagnetic Compatibility Directive, has sought to ensure the removal of technical barriers to trade by requiring equipment to operate satisfactorily in its specified electromagnetic environment, and by protecting the public electricity distribution from disturbances emitted by equipment through limiting these emissions. Engineering recommendation ER G5/4 came into force in the UK in March 2001 to ensure that the objectives of the Directive are met for harmonic disturbances. In the revised recommendation planning levels for individual harmonics and for total harmonic distortion (THD) are given for all system voltages from 400 V to 400 kV.

It must also be recognised that no standard relating to system harmonic content can be regarded as permanent, but rather as the current interpretation of system requirements, taking into account the state of monitoring and modelling techniques. As understanding improves through the application of improved measurements and analytical techniques, so must the standards change.

The IEC 61000 Series This section provides a concise description of the documents of the IEC series, which provide internationally accepted information for the control of power system harmonic (and inter-harmonic) distortion. Specific details of their content will be used as needed in the following chapters.

IEC 61000 1-4 Provides the rationale for limiting power frequency conducted harmonic and inter-harmonic current emissions from equipment in the frequency range up to 9 kHz. Relevant background for this document can be found in Chapters 2 and 3.

IEC 61000 2-1 Outlines the major sources of harmonics in three categories of equipment: power system equipment, industrial loads and residential loads.

The increasing use of HVd.c. converters and FACTS devices has become the main source of harmonic distortion originating in the transmission system. Static power converters and electric arc furnaces are the main contributors in the industrial category, and appliances powered by rectifiers with smoothing capacitors (mostly PCs and TV receivers) the main distorting components in the residential category.

IEC 61000 2-2 Contains a section on the compatibility levels of the harmonic and inter-harmonic voltage distortion in public low-voltage power industry systems.

IEC 61000 2-4 Provides harmonic and inter-harmonic compatibility levels for industrial plant. It also describes the main effects of inter-harmonics, a subject discussed in Chapter 3.

IEC 61000 2-12 Similarly to 61000 2-4, this document deals with compatibility levels for low-frequency conducted disturbances, in this case relating to medium voltage power supply systems. It also covers the subject of injected signals such as those used in ripple control.

IEC 61000 3-2 and 3-4 Contain limits for harmonic current emissions by equipment with input currents of 16 A and below per phase. It also specifies the measurement circuit, supply source and testing conditions as well as the requirements for the instrumentation.

IEC 61000 3-6 First, indicates the capability levels for harmonic voltages in low- and medium-voltage networks as well as planning levels for MV, HV and EHV power systems. It then makes an assessment of emission limits for distorting loads in MV and HV power systems.

IEC 61000 3-12 Provides limits for the harmonic currents produced by equipment connected to low-voltage systems with input currents equal to and below 75 A per phase and subject to restricted connection.

IEC 61000 4-7 This is perhaps the most important document of the series, covering the subject of testing and measurement techniques. It is a general guide on harmonic and inter-harmonic measurements and instrumentation for power systems and equipment connected thereto. The application of this document is discussed in Chapter 5.

IEC 61000 4-13 This is also a document on testing and measurement techniques with reference to harmonics and inter-harmonics, including mains signalling at a.c. power ports as well as low-frequency immunity tests.

IEEE 519-1992 [3] Document IEEE 519-1992 identifies the major sources of harmonics in power systems. The harmonic sources described in this standard include power converters, arc furnaces, static VAR compensators, inverters of dispersed generation, electronic phase control of power, cycloconverters, switch mode power supplies and pulse-width modulated (PWM) drives. The document illustrates the typical distorted wave shapes, the harmonic order numbers and the level of each harmonic component in the distortion caused by these devices. It also describes how the system may respond to the presence of harmonics. The discussion on responses comprise parallel resonance, series resonance and the effect of system loading on the magnitude of these resonances. Based on typical characteristics of low-voltage distribution systems, industrial systems and transmission systems, this document discusses the general response of these systems to harmonic distortion.

The effects of harmonic distortion on the operation of various devices or loads are also included in the standard. These devices comprise motors and generators, transformers, power cables, capacitors, electronic equipment, metering equipment, switchgear, relays and static power converters. Interference to the telephone networks as a result of harmonic distortion in the power systems is discussed with reference to the C-message weighting system created jointly by Bell Telephone Systems and Edison Electric Institute (described in Chapter 4). The standard outlines several possible methods of reducing the amount of telephone interference caused by harmonic distortion in the power system.

This standard also describes the analysis methods and measurement requirements for assessing the levels of harmonic distortion in the power system. It summarises the methods for the calculation of harmonic currents, system frequency responses and modelling of various power system components for the analysis of harmonic propagation. The section on measurements highlights their importance and lists various harmonic monitors that are currently available. It describes the accuracy and selectivity (the ability to distinguish one harmonic component from others) requirements on these monitors; it also describes the averaging or snap-shot techniques that can be used to 'smooth-out' the rapidly fluctuating harmonic components and thus reduce the overall data bandwidth and storage requirements.

The standard describes methods for designing reactive compensation for systems with harmonic distortion. Various types of reactive compensation schemes are discussed, indicating that some of the equipment, such as TCR and TSC, are themselves

sources of harmonic distortion. It also outlines the various techniques for reducing the amount of harmonic current penetrating into the a.c. systems. Recommended practices are suggested to both individual consumers and utilities for controlling the harmonic distortion to tolerable levels. This standard concludes with recommendations for evaluating new harmonic sources by measurements and detailed modelling and simulation studies. It provides several examples to illustrate how these recommendations can be implemented effectively in practical systems.

Notching, the distortion caused on the line voltage waveform by the commutation process between valves in some power electronic devices, is described in detail. The document analyses the converter commutation phenomenon and describes the notch depth and duration with respect to the system impedance and load current. Limits are outlined in terms of the notch depth, THD of supply voltage and notch area for different supply systems.

1.3.3 General Harmonic Indices

The most common harmonic index, which relates to the voltage waveform, is the THD, which is defined as the root mean square (r.m.s.) of the harmonics expressed as a percentage of the fundamental component, i.e.

$$\mathrm{THD} = \frac{\sqrt{\sum_{n=2}^{N} V_n^2}}{V_1}$$

where V_n is the single frequency r.m.s. voltage at harmonic n, N is the maximum harmonic order to be considered and V_1 is the fundamental line to neutral r.m.s. voltage.

For most applications, it is sufficient to consider the harmonic range from the 2nd to the 25th, but most standards specify up to the 50th.

Current distortion levels can also be characterised by a THD value but it can be misleading when the fundamental load current is low. A high THD value for input current may not be of significant concern if the load is light, since the magnitude of the harmonic current is low, even though its relative distortion to the fundamental frequency is high. To avoid such ambiguity a total demand distortion (TDD) factor is used instead, defined as:

$$\mathrm{TDD} = \frac{\sqrt{\sum_{n=2}^{N} I_n^2}}{I_R}$$

This factor is similar to THD except that the distortion is expressed as a percentage of some rated or maximum load current magnitude, rather than as a percentage of the fundamental current. Since electrical power supply systems are designed to withstand the rated or maximum load current, the impact of current distortion on the system will be more realistic if the assessment is based on the designed values, rather than on a reference that fluctuates with the load levels.

Consider as an example the case of a three-phase purely resistive load of 50 kW rating supplied directly from a 50 Hz three-phase 415 V (phase-to-phase) bus. At the time of measuring, the load was consuming 41.5 kW and the voltage waveform contained 11 V of negative-sequence fifth harmonic and 8 V of positive-sequence seventh harmonic. Assuming that the load resistance varies with the square root of the harmonic order h, the following steps are used to calculate the THD and TDD indices at the point of connection:

Load resistance values:

$$R_1 = \frac{V_1^2}{P_1} = \frac{(415/\sqrt{3})^2}{(41\,500/3)} = 4.15\ \Omega$$

$$R_5 = R_1\sqrt{h} = 4.15\sqrt{5}$$

$$R_7 = R_1\sqrt{h} = 4.15\sqrt{7}$$

Load current components:

$$I_r = \frac{50}{415\sqrt{3}} = 69.56\ \text{A}$$

$$I_1 = \frac{(V_1/\sqrt{3})}{R_1} = \frac{(415/\sqrt{3})}{4.15} = 57.735\ \text{A}$$

$$I_5 = \frac{(V_5/\sqrt{3})}{R_5} = \frac{(11/\sqrt{3})}{(4.15\sqrt{5})} = 0.6844\ \text{A}$$

$$I_7 = \frac{(V_7/\sqrt{3})}{R_7} = \frac{(8/\sqrt{3})}{(4.15\sqrt{7})} = 0.4207\ \text{A}$$

$$\text{THD}v = \frac{\sqrt{(V_5^2 + V_7^2)}}{V_1} = \frac{\sqrt{(11^2 + 8^2)}}{415} = 0.03276$$

$$\text{THD}i = \frac{\sqrt{(I_5^2 + I_7^2)}}{I_1} = \frac{\sqrt{(0.68438)^2 + (0.42066)^2}}{57.735} = 0.01391$$

$$\text{TDD}i = \frac{\sqrt{(I_5^2 + I_7^2)}}{I_r} = \frac{\sqrt{(0.68438)^2 + (0.42066)^2}}{69.56} = 0.01155$$

An important question left out of present standards is how to apply the indices to three-phase systems. It is, of course, possible to calculate the indices in each phase individually and apply the limits to the highest. Alternatively, some type of averaging could be carried out. This matter is discussed further in Chapter 4 with reference to telephone interference.

1.4 Relevance of the Topic

Perhaps the most noticeable consequence of power system harmonics is the degradation of telephone communications caused by induced harmonic noise. There are,

however, more disastrous effects, such as the maloperation of important control and protection equipment and the overloading of power plant. Very often the presence of harmonics is only detected following an expensive casualty (like the destruction of power factor correction capacitors). Normally these components have to be replaced, and the equipment protected by filters, at the customer's expense.

In recent times there have been considerable developments in industrial processes that rely on controlled rectification for their operation, and therefore generate harmonic currents. The design of such equipment often assumes the existence of a symmetrical voltage source free of harmonic distortion, a situation that only occurs in the absence of other harmonic sources or when the supply system is very strong (i.e. of negligible impedance). Consequently, the smaller industrial users of electricity are being subjected to increasing operating difficulties as a result of the harmonic interaction of their own control equipment with the power supply.

With open electricity markets, the number of players will increase considerably. The competitive electricity trade should not degrade the level of security, for which the requirements of clients are likely to be more stringent. A general power quality standard, although difficult to define, must be guaranteed by the system operator. However, power quality can raise complicated problems that require detailed information and technical skills to find adequate solutions.

Although interruptions and voltage dips can, to a certain extent, be mastered by the system operator, harmonic voltage fluctuations cannot, since they are generally customers' emissions. It is not clear, then, who should take the risk of ensuring specified levels of harmonic distortion. The obvious thing to do is to put standards on emission limits, but the question is to decide who will control the users' voltage disturbance emissions and who will charge them for this. An innovative approach is for the distribution companies to be responsible for supplying electricity to any user with defined disturbances levels, with a system of penalisation or compensation if these levels are exceeded.

Utilities are likely to accept different levels of compromise between security and cost, and the consequence of this difference is that the party with stricter standards might be left to solve its neighbours' 'problems'. In practice, the party with relaxed standards will rely on others for the provision of support services. If it is not possible to harmonise the power quality standards between the interconnected utilities, proper commercial arrangements will be needed to reflect the consequences of these differences. While it may seem obvious that hardware and software systems should be installed to monitor performance and delivery of agreed service provision, in reality these are not always available.

Power quality awareness in general, and waveform distortion in particular, is likely to increase with deregulation as the competitive environment will try to drive to the limit the use of existing facilities and networks with as little expenditure as possible. The risk of harmonic resonances and their effect on shunt capacitor destruction is well documented. However, some of the negative consequences of this approach may not be immediately obvious, particularly the effect of harmonics on equipment overloading. For instance, the life of a transformer will be considerably reduced by the extra current loading imposed by harmonics. Thus there is a need to adapt existing recommendations, put in place appropriate commercial arrangements and, most of all, monitor their implementation more rigorously than in the past.

In pre-deregulation days, the allocation of responsibilities to maintain adequate standards, largely determined by the supply companies, given the inadequate simulation and monitoring tools available, could not be technically challenged effectively. Deregulation will encourage the use of advanced simulation and assessment tools for the customer to make informed decisions when dealing with the power supply companies.

The competitive electricity market has made utilities more conscious of the need to satisfy their customers' needs and not simply to supply them with electricity. For instance, Electricité de France conducts surveys to analyse customers' expectations.

The new environment provides a considerable challenge that will force the utilities to ensure that individual customer's needs are met. This implies developing complementary services taking into account the customer's specific requirements.

The lack of enforceable harmonic standards in the past did not encourage the use of expensive monitoring, testing and software tools. The development of such tools has accelerated with the acceptance of more stringent standards. Deregulation is leading to more transparent considerations of power quality issues and to a more contestable environment, where the independent parties can be adequately represented. In this environment, information about harmonics itself has become a valuable commodity, giving rise to profitable consulting services. This presents an important problem for the system operators, that of maintaining power quality when the parties are reluctant to provide all the necessary information.

In the competitive environment, waveform distortion can be jeopardised by excessive confidentiality. To allow the interconnected network to maintain adequate harmonic levels at low cost, this must be given priority over confidentiality. To ensure this policy, it is essential that the system operator obtains information and makes it generally available to all market participants. Determining limits on harmonic levels is a difficult exercise. Current knowledge is still insufficient to ascertain the extent to which any given power system can sustain a particular level of harmonics and remain viable in terms of the functions that the system has to perform. Two major impediments to such understanding are the ability to make accurate measurements (discussed in Chapter 5) and the state of computer simulation (discussed in Chapters 7 and 8).

It is relatively easy, though expensive, to keep the harmonic contribution of large nonlinear plant components such as HVd.c. converters under control, normally by the connection of passive filters. The situation is less straightforward in power distribution systems, where the exact location and/or operating characteristics of the dispersed loads are not well defined. Moreover, the harmonic distortion levels of distribution systems appear to be increasing at a consistent rate. A report [8] on extensive field tests carried out in several New England Power Service Co. distribution feeders indicated an increase in THD of the order of 0.1% per year, with the fifth harmonic causing the greatest concern. There is a need for more global planning for the limitation of harmonic distortion in distribution systems.

Concern for waveform distortion must be shared by all the parties involved in order to establish the right balance between exercising control by distortion and keeping distortion under control. Early co-ordination between the interested parties is essential to achieve acceptable economic solutions.

1.5 References

1. Fourier, J.B.J. (1822) *Théorie Analytique de la Chaleur*, Paris.
2. IEC 61000-2-1 (1990) Electromagnetic Compatibility (EMC)—Part 2: Environment—Section 1: Description of the Environment–Electromagnetic Environment for Low-Frequency Conducted Disturbances and Signalling in Public Power Supply Systems. IEC, Geneva.
3. IEEE 519-1992, IEEE Recommended Practices and Requirements for Harmonic Control in Electrical Power Systems (ANSI). IEEE, New York.
4. CCITT (1963) Directives Concerning the Protection of Telecommunication Lines against Harmful Effects from Electricity Lines, International Telecommunications Union, Geneva.
5. Engineering Reports of the Joint Subcommittee on Development and Research of the Edison Electric Institute and the Bell telephone System, New York, 5 volumes, July 1926 to January 1943.
6. IEEE/ANSI C57.110-1998, IEEE Recommended Practice for Establishing Transformer Capability when Supplying Nonsinusoidal Load Currents. IEEE, New York.
7. IEEE/ANSI Std 18–2002 (Reaff 1991), IEEE Standard for Shunt Power Capacitors. IEEE, New York.
8. Nejdawi, I.M., Emmanuel, A.E., Pileggi, D.J., Corridori, M.J. and Archambeault, R.D. (1999) Harmonic trends in NE USA: a preliminary view, *Trans. IEEE Power Delivery*, **14**(4), 1488–1494.

2

Harmonic Analysis

2.1 Introduction

The voltage and current waveforms at points of connection of nonlinear devices can either be obtained from appropriate transducers or calculated for a given operating condition, from knowledge of the devices' nonlinear characteristics. In 1822 J.B.J. Fourier [1] postulated that any continuous function repetitive in an interval T can be represented by the summation of a d.c. component, a fundamental sinusoidal component and a series of higher-order sinusoidal components (called *harmonics*) at frequencies which are integer multiples of the fundamental frequency.

Harmonic analysis is then the process of calculating the magnitudes and phases of the fundamental and higher-order harmonics of the periodic waveform. The resulting series, known as the Fourier series, establishes a relationship between a time-domain function and that function in the frequency domain.

The Fourier series of a general periodic waveform is derived in the first part of this chapter and its characteristics discussed with reference to simple waveforms.

More generally, the Fourier transform and its inverse are used to map any function in the interval from $-\infty$ to ∞, in either the time or frequency domain. The Fourier series therefore represents the special case of the Fourier transform applied to a periodic signal.

In practice, data is often available in the form of a sampled time function, represented by a time series of amplitudes, separated by fixed time intervals of limited duration. When dealing with such data, a modification of the Fourier transform, the discrete Fourier transform (DFT), is used. The implementation of the DFT by means of the so-called Fast Fourier transform (FFT) forms the basis of most modern spectral and harmonic analysis systems.

The voltage and current waveforms captured from the power system, however, may contain transient or time-varying components. Even stationary signals when viewed from limited data (due to finite sampling) will introduce errors in the frequency spectrum of the signal. A variety of techniques have been developed to derive the frequency spectrum under those conditions. The chapter ends with a brief review of these alternative techniques.

Power System Harmonics, Second Edition J. Arrillaga, N.R. Watson
© 2003 John Wiley & Sons, Ltd ISBN: 0-470-85129-5

2.2 Fourier Series and Coefficients [2,3]

The Fourier series of a periodic function $x(t)$ has the expression

$$x(t) = a_0 + \sum_{n=1}^{\infty} \left(a_n \cos\left(\frac{2\pi nt}{T}\right) + b_n \sin\left(\frac{2\pi nt}{T}\right)\right) \tag{2.1}$$

This constitutes a frequency-domain representation of the periodic function.

In this expression a_0 is the average value of the function $x(t)$, while a_n and b_n, the coefficients of the series, are the rectangular components of the nth harmonic. The corresponding nth harmonic vector is

$$A_n \angle \phi_n = a_n + jb_n \tag{2.2}$$

with magnitude

$$A_n = \sqrt{a_n^2 + b_n^2}$$

and phase angle

$$\phi_n = \tan^{-1}\left(\frac{b_n}{a_n}\right)$$

For a given function $x(t)$, the constant coefficient, a_0, can be derived by integrating both sides of equation (2.1) from $-T/2$ to $T/2$ (over a period T):

$$\int_{-T/2}^{T/2} x(t)\mathrm{d}t = \int_{-T/2}^{T/2} \left[a_0 + \sum_{n=1}^{\infty} a_n \cos\left(\frac{2\pi nt}{T}\right) + b_n \sin\left(\frac{2\pi nt}{T}\right)\right] \mathrm{d}t \tag{2.3}$$

The Fourier series of the right-hand side can be integrated term by term, giving

$$\int_{-T/2}^{T/2} x(t)\mathrm{d}t = a_0 \int_{-T/2}^{T/2} \mathrm{d}t + \sum_{n=1}^{\infty} \left[a_n \int_{-T/2}^{T/2} \cos\left(\frac{2\pi nt}{T}\right) \mathrm{d}t + b_n \int_{-T/2}^{T/2} \sin\left(\frac{2\pi nt}{T}\right) \mathrm{d}t \right] \tag{2.4}$$

The first term on the right-hand side equals Ta_0, while the other integrals are zero. Hence, the constant coefficient of the Fourier series is given by

$$a_0 = 1/T \int_{-T/2}^{T/2} x(t)\, \mathrm{d}t \tag{2.5}$$

which is the area under the curve of $x(t)$ from $-T/2$ to $T/2$, divided by the period of the waveform, T.

The a_n coefficients can be determined by multiplying equation (2.1) by $\cos(2\pi mt/T)$, where m is any fixed positive integer, and integrating between $-T/2$ and $T/2$, as previously:

$$\int_{-T/2}^{T/2} x(t)\cos\left(\frac{2\pi mt}{T}\right)\mathrm{d}t = \int_{-T/2}^{T/2}\left[a_0 + \sum_{n=1}^{\infty}\left[a_n\cos\left(\frac{2\pi nt}{T}\right) + b_n\sin\left(\frac{2\pi nt}{T}\right)\right]\right]\cos\left(\frac{2\pi mt}{T}\right)\mathrm{d}t$$

$$= a_0\int_{-T/2}^{T/2}\cos\left(\frac{2\pi mt}{T}\right)\mathrm{d}t + \sum_{n=1}^{\infty}\left[a_n\int_{-T/2}^{T/2}\cos\left(\frac{2\pi nt}{T}\right)\times\cos\left(\frac{2\pi mt}{T}\right)\mathrm{d}t + b_n\int_{-T/2}^{T/2}\sin\left(\frac{2\pi nt}{T}\right)\cos\left(\frac{2\pi mt}{T}\right)\mathrm{d}t\right] \tag{2.6}$$

The first term on the right-hand side is zero, as are all the terms in b_n since $\sin(2\pi nt/T)$ and $\cos(2\pi mt/T)$ are orthogonal functions for all n and m.

Similarly, the terms in a_n are zero, being orthogonal, unless $m = n$. In this case, equation (2.6) becomes

$$\int_{-T/2}^{T/2} x(t)\cos\left(\frac{2\pi mt}{T}\right)\mathrm{d}t = a_n\int_{-T/2}^{T/2}\cos\left(\frac{2\pi nt}{T}\right)\mathrm{d}t$$

$$= \frac{a_n}{2}\int_{-T/2}^{T/2}\cos\left(\frac{4\pi nt}{T}\right)\mathrm{d}t + \frac{a_n}{2}\int_{-T/2}^{T/2}\mathrm{d}t \tag{2.7}$$

The first term on the right-hand side is zero while the second term equals $a_nT/2$. Hence, the coefficients a_n can be obtained from

$$a_n = \frac{2}{T}\int_{-T/2}^{T/2} x(t)\cos\left(\frac{2\pi nt}{T}\right)\mathrm{d}t \quad \text{for } n = 1 \to \infty \tag{2.8}$$

To determine the coefficients b_n, equation (2.1) is multiplied by $\sin(2\pi mt/T)$ and, by a similar argument to the above,

$$b_n = \frac{2}{T}\int_{-T/2}^{T/2} x(t)\sin\left(\frac{2\pi nt}{T}\right)\mathrm{d}t \quad \text{for } n = 1 \to \infty \tag{2.9}$$

It should be noted that because of the periodicity of the integrands in equations (2.5), (2.8) and (2.9), the interval of integration can be taken more generally as t and $t + T$.

If the function $x(t)$ is piecewise continuous (i.e. has a finite number of vertical jumps) in the interval of integration, the integrals exist and Fourier coefficients can be calculated for this function.

Equations (2.5), (2.8) and (2.9) are often expressed in terms of the angular frequency as follows:

$$a_0 = \frac{1}{2\pi}\int_{-\pi}^{\pi} x(\omega t)\,\mathrm{d}(\omega t) \tag{2.10}$$

$$a_n = \frac{1}{\pi}\int_{-\pi}^{\pi} x(\omega t)\cos(n\omega t)\,\mathrm{d}(\omega t) \tag{2.11}$$

$$b_n = \frac{1}{\pi}\int_{-\pi}^{\pi} x(\omega t)\sin(n\omega t)\,\mathrm{d}(\omega t) \tag{2.12}$$

so that

$$x(t) = a_0 + \sum_{n=1}^{\infty} [a_n\cos(n\omega t) + b_n\sin(n\omega t)] \tag{2.13}$$

2.3 Simplifications Resulting From Waveform Symmetry [2,3]

Equations (2.5), (2.8) and (2.9), the general formulas for the Fourier coefficients, can be represented as the sum of two separate integrals:

$$a_n = \frac{2}{T}\int_0^{T/2} x(t)\cos\left(\frac{2\pi nt}{T}\right)\mathrm{d}t + \frac{2}{T}\int_{-T/2}^{0} x(t)\cos\left(\frac{2\pi nt}{T}\right)\mathrm{d}t \tag{2.14}$$

$$b_n = \frac{2}{T}\int_0^{T/2} x(t)\sin\left(\frac{2\pi nt}{T}\right)\mathrm{d}t + \frac{2}{T}\int_{-T/2}^{0} x(t)\sin\left(\frac{2\pi nt}{T}\right)\mathrm{d}t \tag{2.15}$$

Replacing t by $-t$ in the second integral of equation (2.14), and changing the limits produces

$$\begin{aligned} a_n &= \frac{2}{T}\int_0^{T/2} x(t)\cos\left(\frac{2\pi nt}{T}\right)\mathrm{d}t + \frac{2}{T}\int_{+T/2}^{0} x(-t)\cos\left(\frac{-2\pi nt}{T}\right)\mathrm{d}(-t) \\ &= \frac{2}{T}\int_0^{T/2} [x(t) + x(-t)]\cos\left(\frac{2\pi nt}{T}\right)\mathrm{d}t \end{aligned} \tag{2.16}$$

Similarly,

$$b_n = \frac{2}{T}\int_0^{T/2} [x(t) - x(-t)]\sin\left(\frac{2\pi nt}{T}\right)\mathrm{d}t \tag{2.17}$$

Odd Symmetry The waveform has odd symmetry if $x(t) = -x(-t)$. Then the a_n terms become zero for all n, while

$$b_n = \frac{4}{T}\int_0^{T/2} x(t)\sin\left(\frac{2\pi nt}{T}\right)\mathrm{d}t \tag{2.18}$$

The Fourier series for an odd function will, therefore, contain only sine terms.

Even Symmetry The waveform has even symmetry if $x(t) = x(-t)$. In this case $b_n = 0$ for all n and

$$a_n = \frac{4}{T}\int_0^{T/2} x(t)\cos\left(\frac{2\pi nt}{T}\right)\mathrm{d}t \tag{2.19}$$

The Fourier series for an even function will, therefore, contain only cosine terms.

Certain waveforms may be odd or even depending on the time reference position selected. For instance, the square wave of Figure 2.1, drawn as an odd function, can be transformed into an even function by shifting the origin (vertical axis) by $T/2$.

Halfwave Symmetry A function $x(t)$ has halfwave symmetry if

$$x(t) = -x(t + T/2) \tag{2.20}$$

i.e. the shape of the waveform over a period $t + T/2$ to $t + T$ is the negative of the shape of the waveform over the period t to $t + T/2$. Consequently, the square wave function of Figure 2.1 has halfwave symmetry.

Using equation (2.8) and replacing (t) by $(t + T/2)$ in the interval $(-T/2,0)$

$$a_n = \frac{2}{T}\int_0^{T/2} x(t)\cos\left(\frac{2\pi nt}{T}\right)\mathrm{d}t + \frac{2}{T}\int_{-T/2+T/2}^{0+T/2} x(t+T/2)\cos\left(\frac{2\pi n(t+T/2)}{T}\right)\mathrm{d}t$$

$$= \frac{2}{T}\int_0^{T/2} x(t)\left[\cos\left(\frac{2\pi nt}{T}\right) - \cos\left(\frac{2\pi nt}{T} + n\pi\right)\right]\mathrm{d}t \tag{2.21}$$

since by definition $x(t) = -x(t + T/2)$.

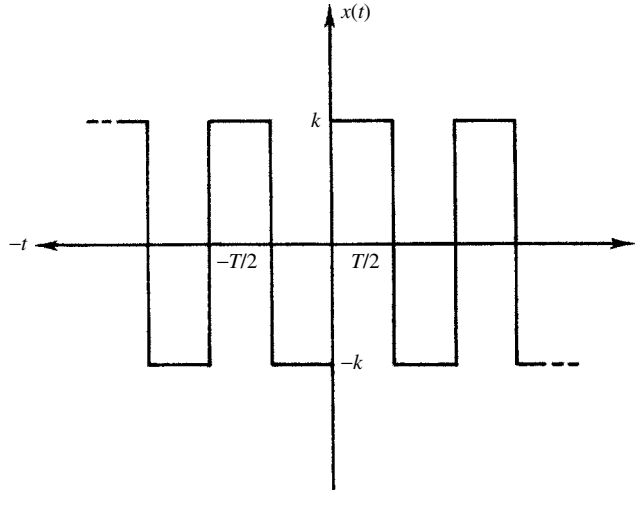


Figure 2.1 Square wave function

If n is an odd integer then

$$\cos\left(\frac{2\pi nt}{T}+n\pi\right)=-\cos\left(\frac{2\pi nt}{T}\right)$$

and

$$a_n=\frac{4}{T}\int_0^{T/2}x(t)\cos\left(\frac{2\pi nt}{T}\right)\mathrm{d}t \tag{2.22}$$

However, if n is an even integer then

$$\cos\left(\frac{2\pi nt}{T}+n\pi\right)=\cos\left(\frac{2\pi nt}{T}\right)$$

and

$$a_n=0.$$

Similarly,

$$\begin{aligned}\mathrm{b}_n&=\frac{4}{T}\int_0^{T/2}x(t)\sin\left(\frac{2\pi nt}{T}\right)\mathrm{d}t \quad \text{for } n \text{ odd}\\ &=0 \quad \text{for } n \text{ even}\end{aligned} \tag{2.23}$$

Thus, waveforms which have halfwave symmetry contain only odd order harmonics.

The square wave of Figure 2.1 is an odd function with halfwave symmetry. Consequently, only the b_n coefficients and odd harmonics will exist. The expression for the coefficients taking into account these conditions is

$$b_n=\frac{8}{T}\int_0^{T/4}x(t)\sin\left(\frac{2\pi nt}{T}\right)\mathrm{d}t \tag{2.24}$$

which can be represented by a line spectrum of amplitudes inversely proportional to the harmonic order, as shown in Figure 2.2.

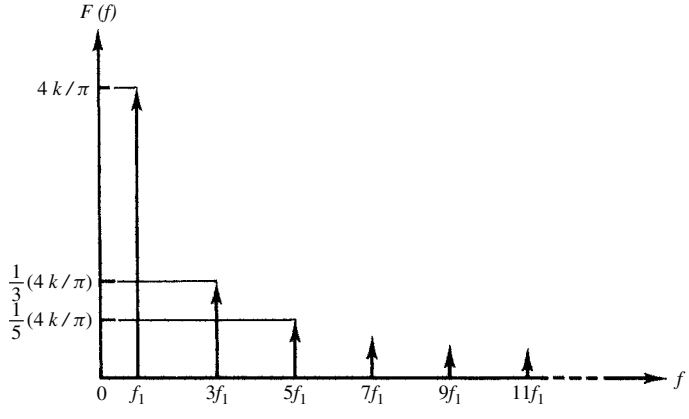


Figure 2.2 Line spectrum representation of a square wave

2.4 Complex Form of the Fourier Series

The representation of the frequency components as rotating vectors in the complex plane gives a geometrical interpretation of the relationship between waveforms in the time and frequency domains.

A uniformly rotating vector $A/2e^{j\phi}(X(f_n))$ has a constant magnitude $A/2$, and a phase angle ϕ, which is time varying according to

$$\phi = 2\pi fT + \theta \tag{2.25}$$

where θ is the initial phase angle when $t = 0$.

A second vector $A/2e^{-j\phi}$ $(X(-f_n))$ with magnitude $A/2$ and phase angle $-\phi$ will rotate in the opposite direction to $A/2e^{+j\phi}$ $(X(f_n))$. This negative rate of change of phase angle can be considered as a negative frequency.

The sum of the two vectors will always lie along the real axis, the magnitude oscillating between A and $-A$ according to

$$\frac{A}{2}e^{j\phi} + \frac{A}{2}e^{-j\phi} = A\cos\phi \tag{2.26}$$

Thus, each harmonic component of a real valued signal can be represented by two half-amplitude contra-rotating vectors as shown in Figure 2.3, such that

$$X(f_n) = X^*(-f_n) \tag{2.27}$$

where $X^*(-f_n)$ is the complex conjugate of $X(-f_n)$.

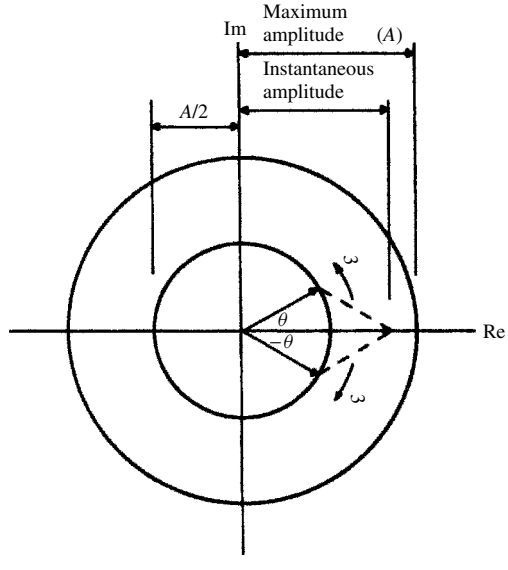


Figure 2.3 Contra-rotating vector pair producing a varying amplitude (pulsating) vector

The sine and cosine terms of equations (2.11) and (2.12) may, therefore, be solved into positive- and negative-frequency terms using the trigonometric identities

$$\cos(n\omega t) = \frac{e^{jn\omega t} + e^{-jn\omega t}}{2} \tag{2.28}$$

$$\sin(n\omega t) = \frac{e^{jn\omega t} - e^{-jn\omega t}}{2j} \tag{2.28a}$$

Substituting into equation (2.13) and simplifying yields

$$x(t) = \sum c_n e^{jn\omega t} \tag{2.29}$$

where

$$c_n = \tfrac{1}{2}(a_n - jb_n), \qquad n > 0$$
$$c_{-n} = c_n$$
$$c_0 = a_0$$

The c_n terms can also be obtained by complex integration:

$$c_n = \frac{1}{\pi}\int_{-\pi}^{\pi} x(\omega t) e^{-jn\omega t}\, d(\omega t) \tag{2.30}$$

$$c_0 = \frac{1}{2\pi}\int_{-\pi}^{\pi} x(\omega t)\, d(\omega t) \tag{2.31}$$

If the time domain signal $x(t)$ contains a component rotating at a single frequency nf, then multiplication by the unit vector $e^{-j2\pi nft}$, which rotates at a frequency $-nf$, annuls the rotation of the component, such that the integration over a complete period has a finite value. All components at other frequencies will continue to rotate after multiplication by $e^{-j2\pi nft}$, and will thus integrate to zero.

The Fourier series is most generally used to approximate a periodic function by truncation of the series. In this case, the truncated Fourier series is the best trigonometric series expression of the function, in the sense that it minimises the square error between the function and the truncated series. The number of terms required depends upon the magnitude of repeated derivatives of the function to be approximated. Repeatedly differentiating equation (2.30) by parts, it can readily be shown that

$$c_n = \frac{1}{2\pi}\frac{1}{n^{m+1}}\int_{-\pi}^{\pi} f^{(m+1)}(\omega t)\, d(\omega t) \tag{2.32}$$

Consequently, the Fourier series for repeatedly differentiated functions will converge faster than that for functions with low-order discontinuous derivatives.

The complex Fourier series expansion is compatible with the FFT, the method of choice for converting time-domain data samples into a Nyquist rate-limited frequency

spectrum. The trigonometric Fourier expression can also be written as a series of phase-shifted sine terms by substituting

$$a_n \cos n\omega t + b_n \sin n\omega t = d_n \sin(n\omega t + \psi_n) \tag{2.33}$$

into equation (2.13), where

$$\begin{aligned} d_n &= \sqrt{a^2{}_n + b^2{}_n} \\ \psi_n &= \tan^{-1} \frac{b_n}{a_n} \end{aligned} \tag{2.34}$$

Finally, the phase-shifted sine terms can be represented as peak value phasors by setting

$$\Psi_n = d_n \mathrm{e}^{j\psi_n} \tag{2.35}$$

so that

$$\begin{aligned} d_n \sin(n\omega t + \psi_n) &= I\{\Psi_n \mathrm{e}^{jn\omega t}\} \\ &= |\Psi_n| \sin(n\omega t + \angle \Psi_n) \end{aligned} \tag{2.36}$$

The harmonic phasor Fourier series is, therefore,

$$f(t) = \sum_{n=0}^{\infty} I\{\Psi_n \mathrm{e}^{jn\omega t}\} \tag{2.37}$$

which does not contain negative-frequency components. Note that the d.c. term becomes

$$\begin{aligned} \Psi_0 &= \frac{a_0}{2} \mathrm{e}^{j\pi/2} \\ &= j\frac{a_0}{2} \end{aligned} \tag{2.38}$$

In practice, the upper limit of the summation is set to n_h, the highest harmonic order of interest.

2.5 Convolution of Harmonic Phasors

Viewing a continuous function through a sampling period of interval T seconds is equivalent to multiplying the signal in the time domain by a rectangular pulse of length T (Figure 2.4). This corresponds to the convolution in the frequency domain of their respective frequency spectra.

In general, the point-by-point multiplication of two time-domain waveforms is expressed in the harmonic domain by a discrete convolution of their Fourier series. When two harmonic phasors of different frequencies are convolved, the results are harmonic phasors at sum and difference harmonics. This is best explained by multiplying the corresponding sinusoids using the trigonometric identity for the product of sine waves,

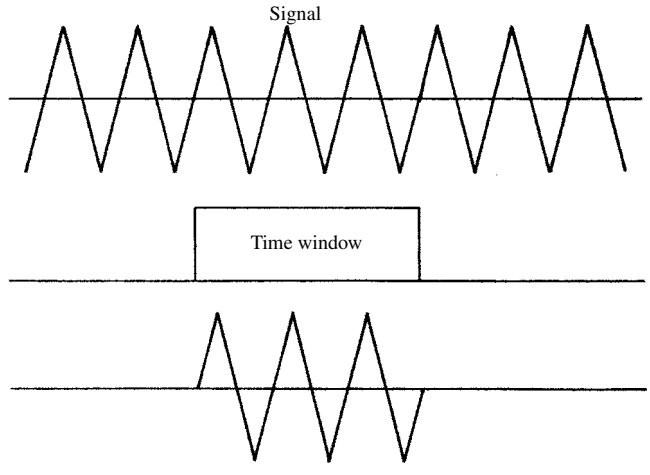


Figure 2.4 Influence of viewing a continuous function through a rectangular time window

and then converting back to phasor form. Given two phasors, A_k and B_m, of harmonic orders k and m, the trigonometric identity for their time-domain multiplication is:

$$|A_k|\sin(k\omega t + \angle A_k)|B_m|\sin(m\omega t + \angle B_m) = \tfrac{1}{2}|A_k|\ |B_m| \left[\sin\left((k-m)\omega t + \angle A_k - \angle B_m + \frac{\pi}{2}\right) - \sin\left((k+m)\omega t + \angle A_k + \angle B_m + \frac{\pi}{2}\right)\right] \tag{2.39}$$

Converting to phasor form:

$$\begin{aligned} A_k \otimes B_m &= \tfrac{1}{2}|A_k||B_m|\left[e^{j(\angle A_k - \angle B_m + \pi/2)}|_{(k-m)} - e^{j(\angle A_k - \angle B_m + \pi/2)}|_{(k+m)}\right] \\ &= \tfrac{1}{2}\left[(|A_k|e^{j\angle A_k}|B_m|e^{-j\angle B_m}e^{j\pi/2})|_{(k-m)} - (|A_k|e^{j\angle A_k}|B_m|e^{j\angle B_m}e^{j+\pi/2})_{k+m}\right] \\ &= \tfrac{1}{2}j[(A_k B^*{}_m)_{k-m} - (A_k B_m)_{k+m}] \end{aligned} \tag{2.40}$$

If k is less than m, a negative harmonic can be avoided by conjugating the difference term. This leads to the overall equation:

$$A_k \otimes B_m = \begin{cases} \frac{1}{2}j(A_k B^*{}_m)_{(k-m)} - \frac{1}{2}j(A_k B_m)_{(k+m)} & \text{if } k \geq m \\ \frac{1}{2}j(A_k B^*{}_m)^*_{(m-k)} - \frac{1}{2}j(A_k B_m)_{(k+m)} & \text{otherwise} \end{cases} \tag{2.41}$$

The multiplication of two non-sinusoidal periodic waveforms leads to a discrete convolution of their harmonic phasor Fourier series:

$$\begin{aligned} f_a(t)\,f_b(t) &= \sum_{k=0}^{n_h} |A_k|\sin(k\omega t + \angle A_k) \sum_{m=0}^{n_h} |B_k|\sin(m\omega t + \angle B_m) \\ &= \sum_{k=0}^{n_h}\sum_{m=0}^{n_h} |A_k|\sin(k\omega t + \angle A_k)|B_k|\sin(m\omega t + \angle B_m) \end{aligned} \tag{2.42}$$

Rewriting this in terms of phasors yields

$$\mathbf{F}_{\mathrm{A}} \otimes \mathbf{F}_{\mathrm{B}} = \sum_{k=0}^{n_h} \sum_{m=0}^{n_h} A_k \otimes B_m \tag{2.43}$$

Equation (2.43) generates harmonic phasors of order up to $2n_h$, due to the sum terms. Substituting the equation for the convolution of two phasors, equation (2.41), into (2.43) and solving for the lth order component yields

$$(A \otimes B)_l = \tfrac{1}{2} j \left[\sum_{k=1}^{n_h} A_k B^*{}_{k-l} + \sum_{k=1}^{n_h} (A_k B^*{}_{k+l})^* - \sum_{k=0}^{n_h} A_k B^*{}_{l-k} \right], l > 0 \tag{2.44}$$

$$(A \otimes B)_l = \tfrac{1}{2} j \left[-A_0 B_0 + \sum_{k=0}^{n_h} A_k B^*{}_k \right], l = 0 \tag{2.45}$$

The convolution equations are non-analytic in the complex plane but are differentiable by decomposing into two real valued components (typically rectangular).

If negative frequencies are retained, the convolution is just the multiplication of two series:

$$\begin{aligned} f_{a(t)} f_{b(t)} &= \sum_{n=-n_h}^{n_h} c_{an} \mathrm{e}^{jn\omega t} \sum_{l=-n_h}^{n_h} c_{bl} \mathrm{e}^{jl\omega t} \\ &= \sum_{n=-n_h}^{n_h} \sum_{l=-n_h}^{n_h} c_{an} c_{bl} \mathrm{e}^{j(l+n)\omega t} \end{aligned} \tag{2.46}$$

In practice, the discrete convolution can be evaluated faster using FFT methods.

2.6 The Fourier Transform [3,4]

Fourier analysis, when applied to a continuous, periodic signal in the time domain, yields a series of discrete frequency components in the frequency domain.

By allowing the integration period to extend to infinity, the spacing between the harmonic frequencies, ω, tends to zero and the Fourier coefficients, c_n, of equation (2.30) become a continuous function, such that

$$X(f) = \int_{-\infty}^{\infty} x(t) \mathrm{e}^{-\mathrm{j}2\pi f T} \, \mathrm{d}t \tag{2.47}$$

The expression for the time domain function $x(t)$, which is also continuous and of infinite duration, in terms of $X(f)$ is then

$$x(t) = \int_{-\infty}^{\infty} X(f) \mathrm{e}^{\mathrm{j}2\pi f T} \, \mathrm{d}f \tag{2.48}$$

$X(f)$ is known as the spectral density function of $x(t)$.

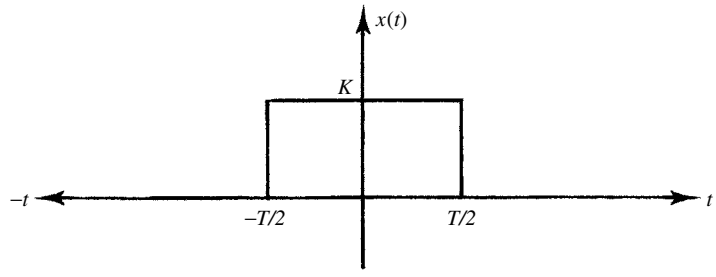


Figure 2.5 Rectangular function

Equations (2.47) and (2.48) form the Fourier transform pair. Equation (2.47) is referred to as the 'forward transform' and equation (2.48) as the 'reverse' or 'inverse transform'.

In general, $X(f)$ is complex and can be written as

$$X(f) = \text{Re } X(f) + j \text{ Im } X(f) \tag{2.49}$$

The real part of $X(f)$ is obtained from

$$\text{Re } X(f) = \frac{1}{2}[X(f) + X(-f)] = \int_{-\infty}^{\infty} x(t) \cos 2\pi f t \, \mathrm{d}t \tag{2.50}$$

Similarly, for the imaginary part of $X(f)$

$$\text{Im } X(f) = \frac{1}{2} j[X(f) - X(-f)] = -\int_{-\infty}^{\infty} x(t) \sin 2\pi f T \, \mathrm{d}t \tag{2.51}$$

The amplitude spectrum of the frequency signal is obtained from

$$|X(f)| = [(\text{Re } X(f))^2 + (\text{Im } X(f))^2]^{\frac{1}{2}} \tag{2.52}$$

The phase spectrum is

$$\phi(f) = \tan^{-1}\left[\frac{\text{Im } X(f)}{\text{Re } X(f)}\right] \tag{2.53}$$

Using equations (2.49) to (2.53), the inverse Fourier transform can be expressed in terms of the magnitude and phase spectra components:

$$x(t) = \int_{-\infty}^{\infty} |X(f)| \cos[2\pi f T - \phi(f)] \, \mathrm{d}f \tag{2.54}$$

As an example, let us consider a rectangular function such as Figure 2.5, defined by

$$x(t) = K \text{ for } |t| \leq T/2$$
$$= 0 \text{ for } |t| > T/2$$

i.e. the function is continuous over all t but is zero outside the limits $(-T/2, T/2)$.

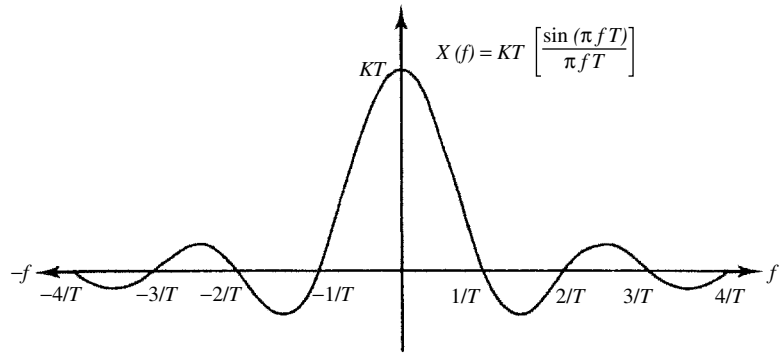


Figure 2.6 The sinc function, $\sin(\pi fT)/(\pi fT)$

Its Fourier transform is

$$\begin{aligned} X(f) &= \int_{-\infty}^{\infty} x(t)\mathrm{e}^{-j2\pi fT}\,\mathrm{d}t \\ &= \int_{-T/2}^{T/2} K\mathrm{e}^{-j2\pi fT}\,\mathrm{d}t \\ &= \frac{-K}{\pi f}\cdot\frac{1}{2j}[\mathrm{e}^{-j\pi fT} - \mathrm{e}^{j\pi fT}] \end{aligned} \tag{2.55}$$

and using the identity

$$\sin\phi = \frac{1}{2j}(\mathrm{e}^{j\phi} - \mathrm{e}^{-j\phi})$$

yields the following expression for the Fourier transform:

$$\begin{aligned} X(f) &= \frac{K}{\pi f}\sin(\pi fT) \\ &= KT\left[\frac{\sin(\pi fT)}{\pi fT}\right] \end{aligned} \tag{2.56}$$

The term in brackets, known as the sinc function, is shown in Figure 2.6.

While the function is continuous, it has zero value at the points $f = n/T$ for $n = \pm1, \pm2, \ldots$ and the side lobes decrease in magnitude as $1/T$. This should be compared to the Fourier series of a periodic square wave, which has discrete frequencies at odd harmonics. The interval $1/T$ is the effective bandwidth of the signal.

2.7 Sampled Time Functions [4,5]

With an increase in the digital processing of data, functions are often recorded by samples in the time domain. Thus, the signal can be represented as in Figure 2.7,

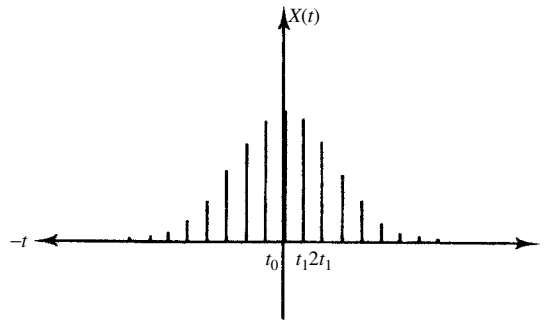


Figure 2.7 Sampled time-domain function

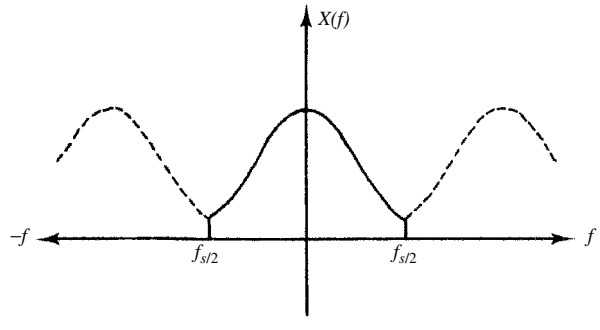


Figure 2.8 Frequency spectrum for discrete time-domain function

where $f_s = 1/t_1$ is the frequency of the sampling. In this case, the Fourier transform of the signal is expressed as the summation of the discrete signal where each sample is multiplied by $e^{-j2\pi fnt_1}$:

$$X(f) = \sum_{n=-\infty}^{\infty} x(nt_1)e^{-j2\pi fnt_1} \tag{2.57}$$

The frequency domain spectrum, shown in Figure 2.8, is periodic and continuous. The inverse Fourier transform is thus

$$x(t) = 1/f_s \int_{-f_s/2}^{f_s/2} X(f)e^{j2\pi fnt_1} df \tag{2.58}$$

2.8 Discrete Fourier Transform (DFT) [4,5]

In the case where the frequency domain spectrum is a sampled function, as well as the time domain function, we obtain a Fourier transform pair made up of discrete components:

$$X(f_k) = 1/N \sum_{n=0}^{N-1} x(t_n)e^{-j2\pi kn/N} \tag{2.59}$$

and

$$x(t_n) = \sum_{k=0}^{N-1} X(f_k) e^{j2\pi kn/N} \tag{2.60}$$

Both the time domain function and the frequency domain spectrum are assumed periodic as in Figure 2.9, with a total of N samples per period. It is in this discrete form that the Fourier transform is most suited to numerical evaluation by digital computation.

Consider equation (2.59) rewritten as

$$X(f_k) = 1/N \sum_{n=0}^{N-1} x(t_n) W^{kn} \tag{2.61}$$

where $W = e^{-j2\pi/N}$.

Over all the frequency components, equation (2.61) becomes a matrix equation.

$$\begin{bmatrix} X(f_0) \\ X(f_1) \\ \vdots \\ X(f_k) \\ \vdots \\ X(f_{N-1}) \end{bmatrix} = 1/N \begin{bmatrix} 1 & 1 & \cdots & 1 & \cdots & 1 \\ 1 & W & \cdots & W^k & \cdots & W^{N-1} \\ \vdots & \vdots & & \vdots & & \vdots \\ 1 & W^k & \cdots & W^{k^2} & \cdots & W^{k(N-1)} \\ \vdots & \vdots & & \vdots & & \vdots \\ 1 & W^{N-1} & \cdots & W^{(N-1)k} & \cdots & W^{(N-1)^2} \end{bmatrix} \cdot \begin{bmatrix} x(t_0) \\ x(t_1) \\ \vdots \\ x(t_k) \\ \vdots \\ x(t_{N-1}) \end{bmatrix} \tag{2.62}$$

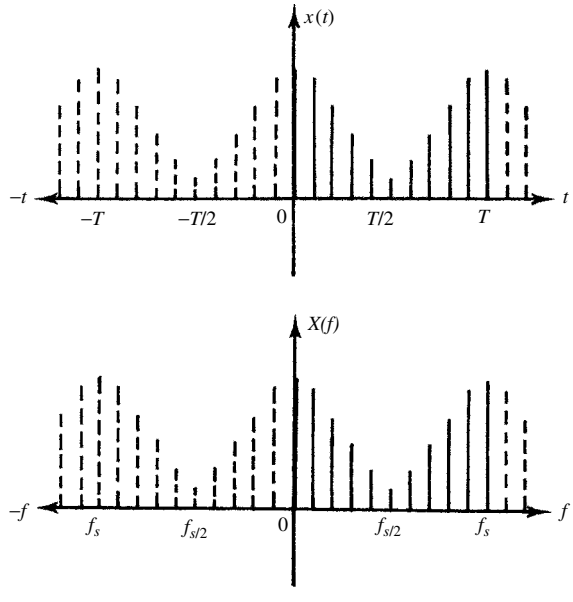


Figure 2.9 Discrete time- and frequency-domain function

or in a condensed form

$$[X(f_k)] = 1/N[W^{kn}][x(t_n)] \tag{2.63}$$

In these equations, $[X(f_k)]$ is a vector representing the N components of the function in the frequency domain, while $[x(t_n)]$ is a vector representing the N samples of the function in the time domain.

Calculation of the N frequency components from the N time samples, therefore, requires a total of N^2 complex multiplications to implement in the above form.

Each element in the matrix $[W^{kn}]$ represents a unit vector with a clockwise rotation of $2n\pi/N$ ($n = 0, 1, 2, \ldots, (N-1)$) introduced between successive components. Depending on the value of N, a number of these elements are the same.

For example, if $N = 8$ then

$$\begin{aligned} W &= \mathrm{e}^{-j2\pi/8} \\ &= \cos\frac{\pi}{4} - j\sin\frac{\pi}{4} \end{aligned}$$

As a consequence

$$\begin{aligned} W^0 &= -W^4 = 1 \\ W^1 &= -W^5 = (1/\sqrt{2} - j1/\sqrt{2}) \\ W^2 &= -W^6 = -j \\ W^3 &= -W^7 = -(1/\sqrt{2} + j1/\sqrt{2}) \end{aligned}$$

These can also be thought of as unit vectors rotated through $\pm 0^\circ$, $\pm 45^\circ$, $\pm 90^\circ$ and $\pm 135^\circ$, respectively.

Further, W^8 is a complete rotation and hence equal to 1. The value of the elements of W^{kn} for $kn > 8$ can thus be obtained by subtracting full rotations, to leave only a fraction of a rotation, the values for which are shown above. For example, if $k = 5$ and $n = 6$, then $kn = 30$ and $W^{30} = W^{3\times 8+6} = W^6 = j$.

Thus, there are only four unique absolute values of W^{kn} and the matrix $[W^{kn}]$, for the case $N = 8$, becomes

1	1	1	1	1	1	1	1
1	W	$-j$	W^3	-1	$-W$	j	$-W^3$
1	$-j$	-1	j	1	$-j$	-1	j
1	W^3	j	W	-1	$-W^3$	$-j$	$-W$
1	-1	1	-1	1	-1	1	-1
1	$-W$	$-j$	$-W^3$	-1	W	j	W^3
1	j	-1	$-j$	1	j	-1	$-j$
1	$-W^3$	j	$-W$	-1	W^3	$-j$	W

It can be observed that the d.c. component of the frequency spectrum, $X(f_0)$, obtained by the algebraic addition of all the time domain samples, divided by the number of samples, is the average value of all the samples.

Subsequent rows show that each time sample is weighted by a rotation dependent on the row number. Thus, for $X(f_1)$ each successive time sample is rotated by $1/N$ of a revolution; for $X(f_2)$ each sample is rotated by $2/N$ revolutions, and so on.

2.9 The Nyquist Frequency and Aliasing [4]

With regard to equation (2.62) for the DFT and the matrix $[W^{kn}]$, it can be observed that for the rows $N/2$ to N, the rotations applied to each time sample are the negative of those in rows $N/2$ to 1. Frequency components above $k = N/2$ can be considered as negative frequencies, since the unit vector is being rotated through increments greater than π between successive components. In the example of $N = 8$, the elements of row 3 are successively rotated through $-\pi/2$. The elements of row 7 are similarly rotated through $-3\pi/2$, or in negative frequency form through $\pi/2$. More generally, a rotation through

$$2\pi(N/2 + p)/N \text{ radians}$$
$$\text{for } p = 1,\ 2,\ 3\ldots,\ (N/2 - 1) \quad [\text{with } N \text{ even}]$$

corresponds to a negative rotation of

$$-2\pi(N/2 - p)/N \text{ radians}$$

Hence, $-X(k)$ corresponds to $X(N - k)$ for $k = 1$ to $N/2$ as shown by Figure 2.10.

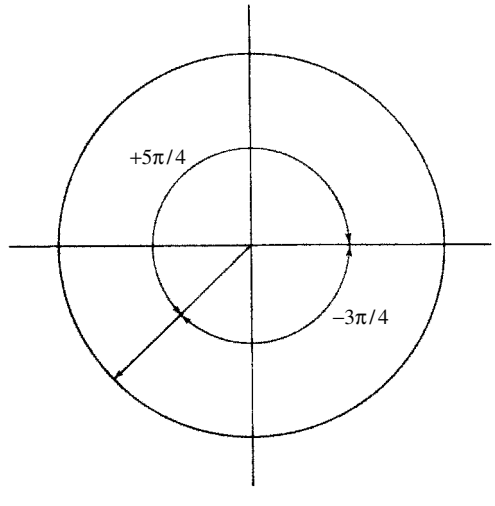


Figure 2.10 Correspondence of positive and negative angles

This is an interpretation of the sampling theorem, which states that the sampling frequency must be at least twice the highest frequency contained in the original signal for a correct transfer of information to the sampled system.

The frequency component at half the sampling frequency is referred to as the Nyquist frequency.

The representation of frequencies above the Nyquist frequency as negative frequencies means that if the sampling rate is less than twice the highest frequency present in the sampled waveform, then these higher frequency components can mimic components below the Nyquist frequency, introducing error into the analysis.

It is possible for high-frequency components to complete many revolutions between samplings; however, since they are only sampled at discrete points in time, this information is lost.

This misinterpretation of frequencies above the Nyquist frequency, as lower frequencies, is called *aliasing* and is illustrated in Figure 2.11.

To prevent aliasing it is necessary to pass the time domain signal through a band-limited low-pass filter, the ideal characteristic of which is shown in Figure 2.12, with a cut-off frequency, f_c, equal to the Nyquist frequency.

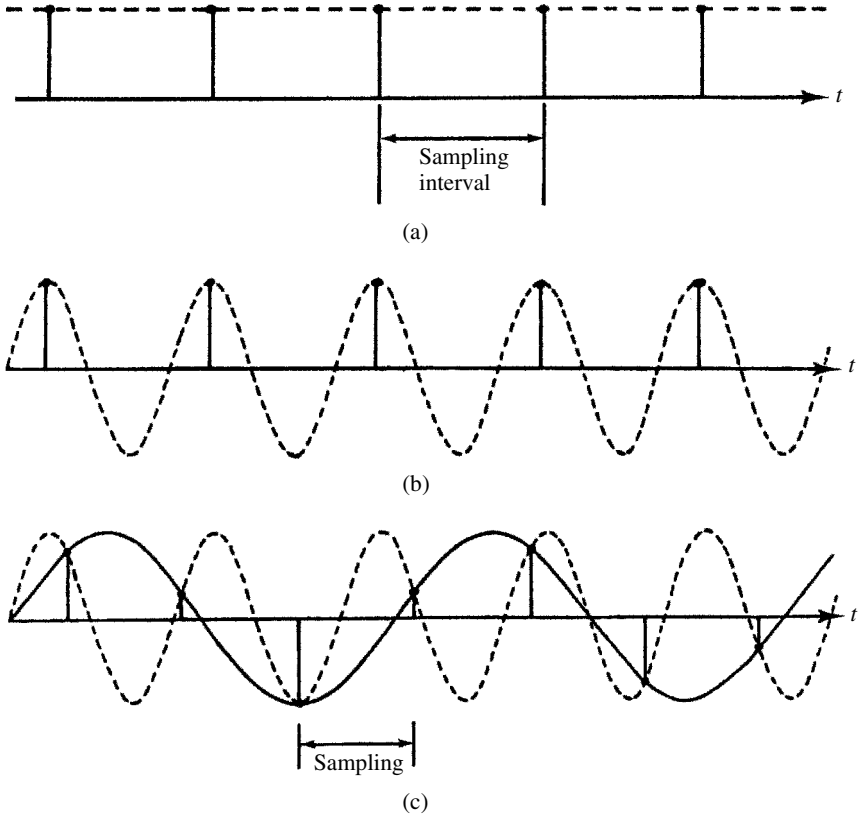


Figure 2.11 The effect of aliasing: (a) $x(t) = k$; (b) $x(t) = k \cos 2\pi nft$. For (a) and (b) both signals are interpreted as being d.c. In (c) the sampling can represent two different signals with frequencies above and below the Nyquist or sampling rate

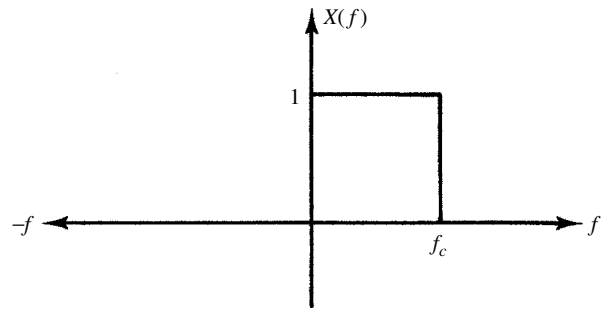


Figure 2.12 Frequency domain characteristics of an ideal low-pass filter with cut-off frequency f_c

Thus, if sampling is undertaken on the filtered signal and the DFT applied, the frequency spectrum has no aliasing effect and is an accurate representation of the frequencies in the original signal that are below the Nyquist frequency. However, information on those frequencies above the Nyquist frequency is lost due to the filtering process.

2.10 Fast Fourier Transform (FFT) [4–7]

For large values of N, the computational time and cost of executing the N^2 complex multiplications of the DFT can become prohibitive.

Instead, a calculation procedure known as the FFT, which takes advantage of the similarity of many of the elements in the matrix $[W^{kn}]$, produces the same frequency components using only $N/2 \log_2 N$ multiplications to execute the solution of equation (2.63). Thus, for the case $N = 1024 = 2^{10}$, there is a saving in computation time by a factor of over 200. This is achieved by factorising the $[W^{kn}]$ matrix of equation (2.63) into $\log_2 N$ individual or factor matrices such that there are only two non-zero elements in each row of these matrices, one of which is always unity. Thus, when multiplying by any factor matrix only N operations are required.

The reduction in the number of multiplications required, to $(N/2)\log_2 N$, is obtained by recognising that

$$W^{N/2} = -W^0$$
$$W^{(N+2)/2} = -W^1 \text{ etc.}$$

To obtain the factor matrices, it is first necessary to re-order the rows of the full matrix. If rows are denoted by a binary representation, then the re-ordering is by bit reversal.

For the example where $N = 8$, row 5, represented as 100 in binary (row 1 is 000), now becomes row 2, or 001 in binary. Thus, rows 2 and 5 are interchanged. Similarly, rows 4 and 7, represented as 011 and 110, respectively, are also interchanged. Rows 1, 3, 6 and 8 have binary representations which are symmetrical with respect to bit reversal and hence remain unchanged.

The corresponding matrix is now

1	1	1	1	1	1	1	1
1	-1	1	-1	1	-1	1	-1
1	$-j$	-1	j	1	$-j$	-1	j
1	j	-1	$-j$	1	j	-1	$-j$
1	W	$-j$	W^3	-1	$-W$	j	$-W^3$
1	$-W$	$-j$	$-W^3$	-1	W	j	W^3
1	W^3	j	W	-1	$-W^3$	$-j$	$-W$
1	$-W^3$	j	$-W$	-1	W^3	$-j$	W

This new matrix can be separated into $\log_2 8$ (=3) factor matrices:

1	1						
1	-1						
		1	$-j$				
		1	j				
				1	W		
				1	$-W$		
						1	W^3
						1	$-W^3$

1		1					
	1		1				
1		-1					
	1		-1				
				1		$-j$	
					1		$-j$
				1		j	
					1		j

1				1			
	1				1		
		1				1	
			1				1
1				−1			
	1				−1		
		1				−1	
			1				−1

As previously stated, each factor matrix has only two non-zero elements per row, the first of which is unity.

The re-ordering of the $[W^{kn}]$ matrix results in a frequency spectrum which is also re-ordered. To obtain the natural order of frequencies, it is necessary to reverse the previous bit reversal.

In practice, a mathematical algorithm implicitly giving factor matrix operations is used for the solution of an FFT [8].

Using $N = 2^m$, it is possible to represent n and k by m bit binary numbers such that:

$$n = n_{m-1}2^{m-1} + n_{m-2}2^{m-2} + \cdots + 4n_2 + 2n_1 + n_0 \tag{2.64}$$

$$k = k_{m-1}2^{m-1} + k_{m-2}2^{m-2} + \cdots + 4k_2 + 2k_1 + k_0 \tag{2.65}$$

where

$$n_i = 0, 1 \text{ and } k_i = 0, 1$$

For $N = 8$:

$$n = 4n_2 + 2n_1 + n_0$$

and

$$k = 4k_2 + 2k_1 + k_0$$

where n_2, n_1, n_0 and k_2, k_1, k_0 are binary bits (n_2, k_2 most significant and n_0, k_0 least significant).

Equation (2.61) can now be rewritten as:

$$X(k_2, k_1, k_0) = \sum_{n_2=0}^{1} \sum_{n_1=0}^{1} \sum_{n_0=0}^{1} \frac{1}{N} x(n_2, n_1, n_0) W \tag{2.66}$$

Defining n and k in this way enables the computation of equation (2.61) to be performed in three independent stages computing in turn:

$$A_1(k_0, n_1, n_0) = \sum_{n_2=0}^{1} \frac{1}{N} x(n_2, n_1, n_0) W^{4k_0 n_2} \tag{2.67}$$

$$A_2(k_0, k_1, n_0) = \sum_{n_1=0}^{1} A_1(k_0, n_1, n_0) W^{2(k_0+2k_1)n_1} \tag{2.68}$$

$$A_3(k_0, k_1, k_2) = \sum_{n_0=0}^{1} A_2(k_0, k_1, n_0) W^{(k_0+2k_1+4k_2)n_0} \tag{2.69}$$

From equation (2.69) it is seen that the A_3 coefficients contain the required $X(k)$ coefficients but in reverse binary order:

Order of A_3 in binary form is $k_0k_1k_2$

Order of $X(k)$ in binary form is $k_2k_1k_0$

Hence

		Binary		Reversed		
$A_3(3)$	=	$A_3(011)$	=	$X(110)$	=	$X(6)$
$A_3(4)$	=	$A_3(100)$	=	$X(001)$	=	$X(1)$
$A_3(5)$	=	$A_3(101)$	=	$X(101)$	=	$X(5)$

2.11 Window Functions [9]

In any practical measurement of a time domain signal, it is normal to limit the time duration over which the signal is observed. This process is known as *windowing* and is particularly useful for the measurement of non-stationary signals, which may be divided into short segments of a quasi-stationary nature with an implied infinite periodicity. Furthermore, in the digital analysis of waveforms, only a finite number of samples of the signal is recorded on which a spectral analysis is made. Thus even stationary signals are viewed from limited time data and this can introduce errors in the frequency spectrum of the signal.

The effect of windowing can best be seen by defining a time domain function which lies within finite time limits. Outside of these, the function is zero. The simplest window function is the rectangular window of Figure 2.13(a). The frequency spectrum of this function, obtained in Section 2.6, is also included.

The application of a window function has the effect of multiplying each point of a time domain signal by the corresponding time point of the window function. Thus, within a rectangular window, the signal is just itself, but outside of this the signal is completely attenuated although a periodicity of the signal within the window is implied outside the defined window. This time domain multiplication has its equivalent in the frequency domain as the convolution of the spectra of the window function and the

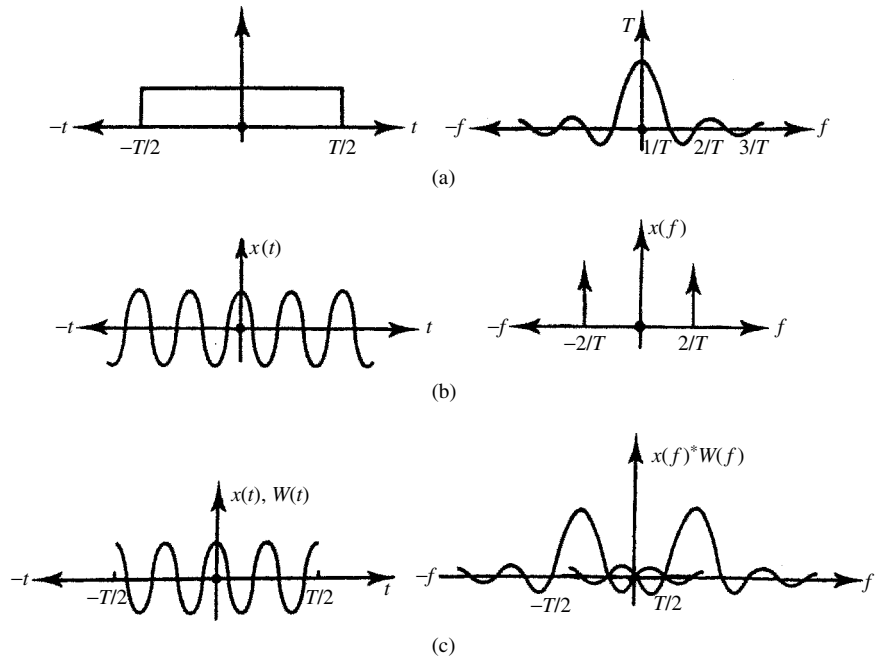


Figure 2.13 Infinite periodic function processed with a rectangular window function: (a) rectangular window function and frequency spectrum; (b) periodic function $x(t) = A \cos(4\pi t/T)$ and frequency spectrum; (c) infinite periodic function viewed through a rectangular time window

signal. This is illustrated for an infinite periodic function and a rectangular window function in Figure 2.13(b) and (c). It can be observed that there is significant power in the frequencies of the side lobes about the fundamental frequency, which is not present in the infinite fundamental frequency waveform.

"In this sample case where the signal $x(t)$ is of fundamental frequency f_1 only, with a sampled frequency spectrum, the spectral components of the function $x(t)$. $W(t)$ are integer multiples of f_1 and lie at the zero crossings of $X(f)$. Hence the only spectral component which contributes is that being evaluated, i.e. the component at f_1."

However, it is highly likely that waveforms will be made up of many frequency components, not necessarily integer multiples of the fundamental window frequency f_1. Consequently, discontinuities will exist between the function at the start and finish of the window, which will introduce uncertainty in the identification of the periodic components present, since Fourier analysis assumes periodicity of functions and continuity at the boundaries. The resulting error is known as spectral leakage and is the non-periodic noise contributing to each of the periodic spectral components present.

As an illustration of spectral leakage with respect to a single-frequency periodic waveform Fig. 14(a) shows the case where the time window is an exact multiple of the waveform period, 14(b) the phase discontinuity for a worst case sample and 14(c) when viewed as a discrete frequency spectrum. Besides the main frequency component there are high side lobes and d.c.

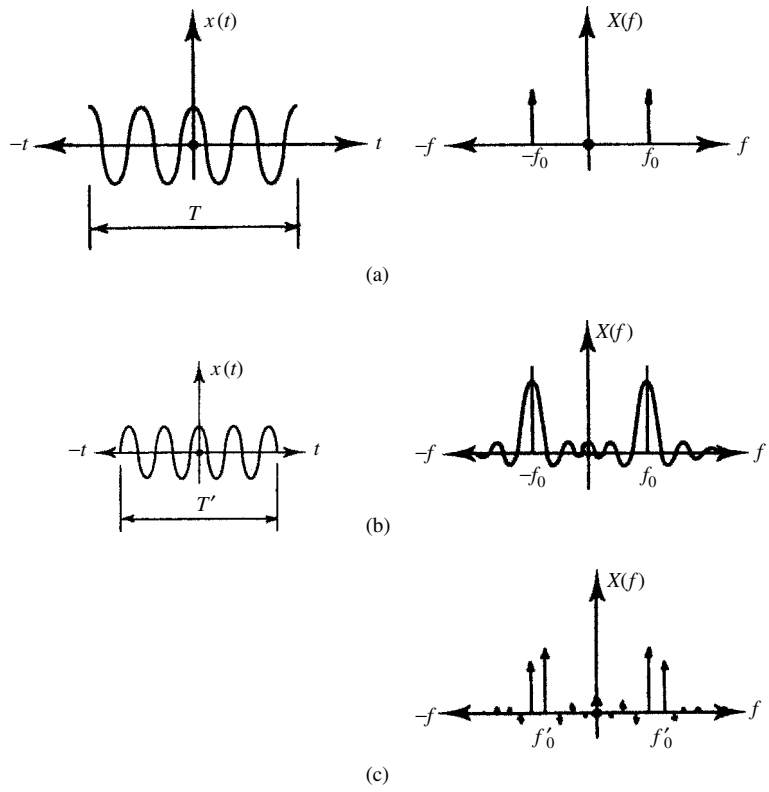


Figure 2.14 Infinite periodic signal viewed during different duration time windows with periodicity implied: (a) the time window is an exact multiple of the period of the waveform; (b) the time window is a $(2n + 1)/2$ multiple of the period of the waveform; (c) case (b) viewed as a discrete frequency spectrum

2.11.1 The Picket Fence

The combination of the DFT and window function produces a response equivalent to filtering the time domain signal through a series of filters with centre frequencies at integer multiples of $1/T$, where T is the sampling period. The filter characteristic and the associated leakage are determined by the particular window function chosen. The resulting spectrum can therefore be considered as the true spectrum viewed through a picket fence with only frequencies at points corresponding to the gaps in the fence being visible.

When the signal being analysed is not one of these discrete, orthogonal frequencies, then, because of the non-ideal nature of the DFT filter, it will be seen by more than one such filter, but at a reduced level in each. The effect can be reduced by adding a number of zeros, usually equivalent to the original record length, to the data to be analysed. This is called zero padding. This effective increase in the sampling period T introduces extra DFT filters at points between the original filters. The bandwidth of the individual filters still depends upon the original sample period and is therefore unchanged.

2.11.2 Spectral Leakage Reduction

The effect of spectral leakage can be reduced by changing the form of the window function. In particular, if the magnitude of the window function is reduced towards zero at the boundaries, any discontinuity in the original waveform is weighted to a very small value and thus the signal is effectively continuous at the boundaries. This implies a more periodic waveform, which has a more discrete frequency spectrum.

A number of window functions are shown in Figure 2.15, along with their Fourier transforms, which give a measure of the attenuation of the side lobes that give rise to spectral leakage.

2.11.3 Choice of Window Function

The objective in choosing a window to minimise spectral leakage is to obtain a main-lobe width which is as narrow as possible, so that it only includes the spectral component of interest, with minimal side-lobe levels to reduce the contribution from interfering spectral components. These two specifications are interrelated for realisable windows and a compromise is made between main-lobe width compression and side-lobe level reduction.

The rectangular window function, defined by

$$W(t) = \begin{cases} 1 & \text{for } -T/2 < t < T/2 \\ 0 & \text{otherwise} \end{cases} \tag{2.70}$$

has a noise or effective bandwidth of $1/T$, where T is the window length; the side-lobe levels are large (-13 dB from the main lobe for the first side lobe), and their rate of decay with frequency is slow (being 20 dB per decade). This means that when evaluating the fundamental component of a signal, interfering spectral components near to it will be weighted heavily, contributing greater interference to the fundamental component than for the other windows illustrated in Figure 2.15.

However, as mentioned previously, there is one situation where the rectangular window ideally results in zero spectral leakage and high spectral resolution. This situation occurs when the duration of the rectangular window is equal to an integer multiple of the period of a periodic signal. When the rectangular window spans exactly one period, the zeros in the spectrum of the window coincide with all the harmonics excepting one. This results in no spectral leakage under ideal conditions. Consequently, spectrum analysers often incorporate the rectangular window function facility for the analysis of periodic waveforms, to which the duration of the window can be matched. This is achieved through the use of a phase-locked loop. This frequency matching gives the greatest resolution of the periodic frequency.

The triangular window, defined by

$$W(t) = \begin{cases} 1 + 2t/T & \text{for } -T/2 < t < 0 \\ 1 - 2t/T & \text{for } 0 < t < -T/2 \\ 0 & \text{otherwise} \end{cases} \tag{2.71}$$

is a simple modification of the rectangular window, where the amplitude of the multiplying window is reduced linearly to zero from the window centre. The reduction of

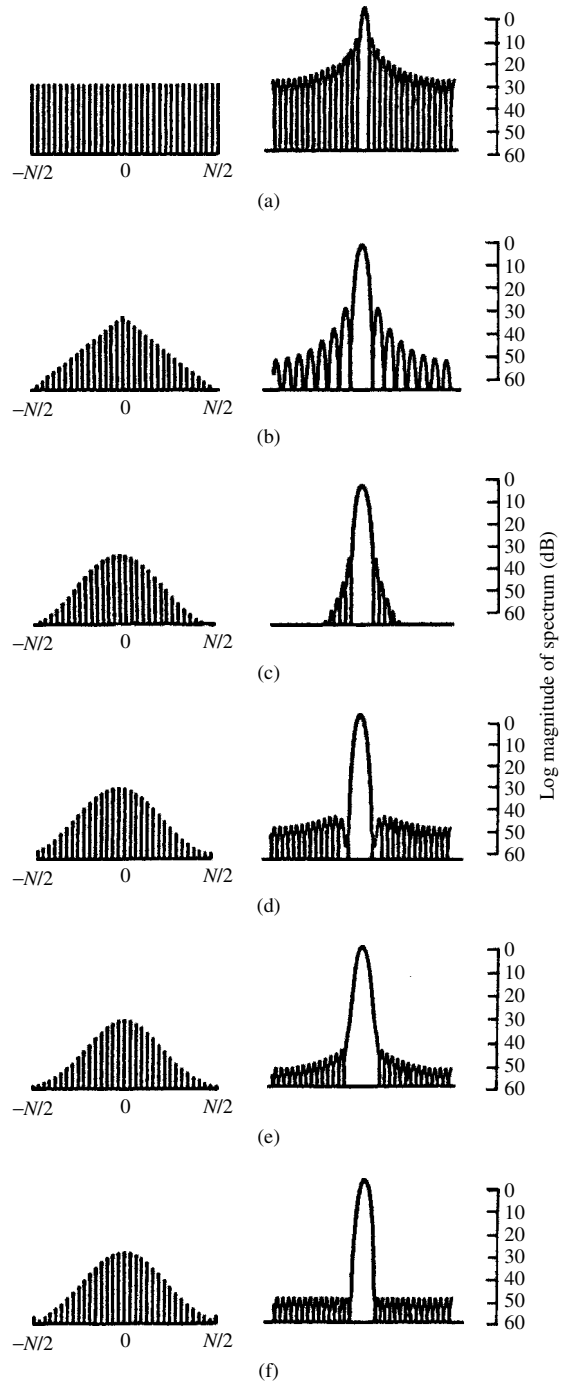


Figure 2.15 Fourier transform pairs of common window functions (a) rectangular; (b) triangular; (c) cosine squared (Hanning); (d) Hamming; (e) Gaussian; (f) Dolph-Chebyshev

the side-lobe is readily seen in Figure 2.15(b), but this is at the expense of main-lobe width and a consequent reduction in frequency resolution.

An international standard window function often incorporated into spectrum analysers is the cosine-squared or Hanning window, defined by

$$W(t) = \frac{1}{2}\left(1 - \cos\frac{2\pi t}{T}\right) \quad \text{for } -\frac{T}{2} < t < \frac{T}{2} \tag{2.72}$$

and in which it is the power term that is cosine squared. This function is easily generated from sinusoidal signals and in FFT analysers a table of cosine values can be utilised for generating the window. The main lobe noise bandwidth is greater than that for the rectangular window, being $1.5T$; however, the highest side lobe is at -32 dB and the side-lobe fall-off rate is 60 dB per decade, thus reducing the effect of spectral leakage. This is illustrated in Figure 2.16, where the Hanning window is compared to the rectangular window for side-lobe level reduction.

By mounting the Hanning window on a small rectangular pedestal (but limiting the maximum of the function to unity), the Hamming window is obtained. This is described in its amplitude form as

$$W(t) = 0.54 - 0.46\cos\frac{2\pi t}{T} \quad \text{for } -\frac{T}{2} < t < \frac{T}{2} \tag{2.73}$$

The second side lobe of the rectangular function coincides with the first side lobe of the Hanning function, and since these are in opposite phase, they can be scaled to cancel

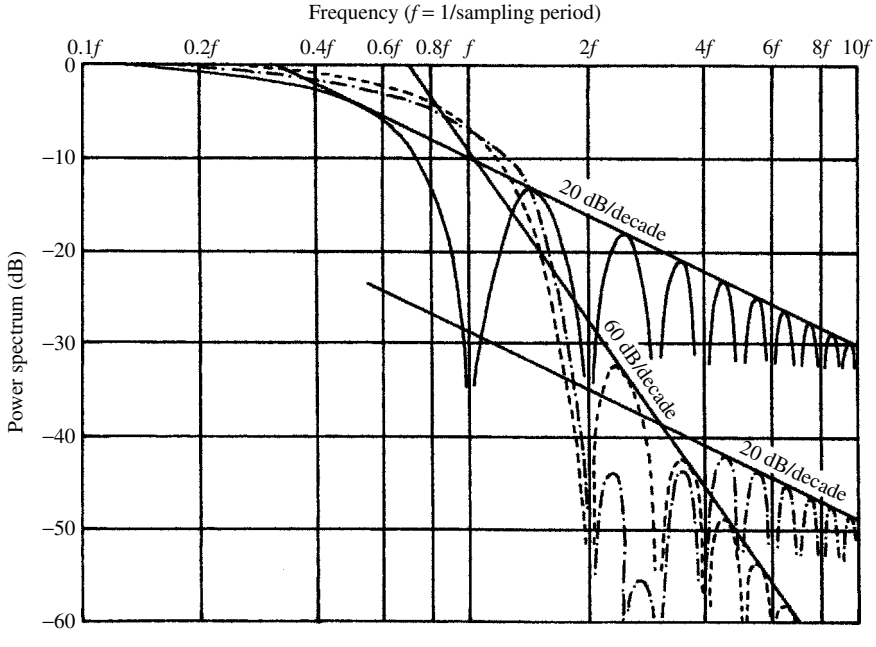


Figure 2.16 Power spectrum *versus* log(frequency) for selected window functions. (———), Rectangular window; (- - - -), Hanning window; (-·-·-·-), Hamming window

each other. As a consequence, the highest side-lobe level is −42 dB (Figure 2.16). The remaining side lobes are dominated by the rectangular function and have a fall-off rate of 20 dB per decade. A slight improvement in main-lobe noise bandwidth (to $1.4/T$) is observed also.

The ideal window, which has a single main lobe and no side lobes, is in the form of a Gaussian function:

$$W(t) = \exp(-t^2/2\sigma^2) \tag{2.74}$$

The Gaussian function has the property of transforming, by the Fourier transform, to another Gaussian function. On a decibel scale, its shape is that of an inverted parabola, with a characteristic which becomes successively steeper. Theoretically, the Gaussian function is defined between infinite time limits. For practical use, the function is truncated at three times the half-amplitude width, which is 7.06 times the standard deviation. As a consequence, side lobes are established in the power spectrum but these are of the order of −44 dB down. The main-lobe noise bandwidth is wider than the previous windows, being $1.9/T$.

The final window, presented in Figure 2.15(f), is the Dolph-Chebyshev function, the discrete form of which is defined as

$$W(t) = \frac{(-1)^r \cos[N \cos^{-1}[\beta \cos(\pi r/N)]]}{\cosh[n \cosh^{-1}(\beta)]} \quad \text{for } 0 < r < N-1 \tag{2.75}$$

where r is an integer, N is the number of discrete samples of the window function,

$$\beta = \cosh\left[\frac{1}{N}\cosh^{-1}(10^{\alpha})\right]$$

and the inverse hyperbolic cosine is defined by

$$\cosh^{-1} x = \begin{cases} \pi/2 - \tan^{-1}[x/\sqrt{(1-x^2)}] & \text{for } |x| < 1.0 \\ 1n[x + \sqrt{(x^2-1)}] & \text{for } |x| > 1.0 \end{cases}$$

This function provides the narrowest possible main-lobe width for a given specified side-lobe level, which is constant on a decibel scale. The side-lobe levels are controlled by the parameter in equation (2.75). With $\alpha = 4.0$ the side lobes are at −80 dB (0.01%) with respect to the main lobe.

2.11.4 Main-Lobe Width Reduction

In obtaining low side-lobe levels to reduce spectral leakage, in all the window functions previously mentioned, there has been a sacrifice of main-lobe bandwidth. It is possible that in harmonic analysis, when evaluating, for example, the fundamental of a waveform, the resolution is such that the d.c. component and the second and third harmonics are included within the main lobe. This causes considerable interference in the individual harmonic evaluations and restricts the identification of spectral leakage effects to higher order frequencies and noise, outside the main lobe.

However, with the ability to change the side-lobe level with the Dolph-Chebyshev window, an algorithm presents itself to effectively reduce the main-lobe bandwidth.

Consider the complex fundamental Fourier component of the waveform, multiplied by the Dolph-Chebyshev window function, i.e. $W(r) \cdot x(r)_{r=1}^{N}$, obtained by the application of the DFT (using the FFT technique):

$$X_1 = W_0C_1 + W_1C_2 + W_2C_3 + W_{-2}C_{-1} + W_{-3}C_{-2} + W_{-4}C_{-3} + W_{-1}C_0 + \sum_{n=3}^{N/2} W_nC_{n+1} + \sum_{n=4}^{N/2-1} W_{-n+1}C_{-n} \tag{2.76}$$

where W are the discrete window coefficients in the frequency domain and $C_n = C_{-n}$ are the complex periodic Fourier coefficients of harmonic order n.

By pre-processing the waveform, the d.c. component can be removed, thereby eliminating C_0 in equation (2.76). In addition, since the last two terms of this equation include all the higher-order harmonics and noise, but are weighted with window coefficients of the order of 0.01%, they can also be neglected. Equation (2.76) can therefore be reduced to:

$$X_1 = C_1(W_0 + \mathrm{W}_{-2}) + \mathrm{C}_2(W_1 + W_{-3}) + \mathrm{C}_3(\mathrm{W}_2 + \mathrm{W}_{-4}) \tag{2.77}$$

Application of the DFT to the windowed discrete time-domain waveform yields a value for X_1. The window coefficients in the frequency domain are known by the defining equation (2.73) and hence only the three harmonic terms C_1, C_2, C_3 are known.

The use of three windows, each with a different α parameter, and the application of the DFT three times to the same waveform, produces three simultaneous equations of the same form as equation (2.77). The solution of these leads directly to the values of C_1, C_2 and C_3, i.e. the fundamental component and second and third harmonics of the original waveform.

As an illustration of the effectiveness of this algorithm, consider the function defined by

$$x(t) = C_1 \cos(2\pi f_1 t + \phi_1) + \sum_{n=2}^{7} C_n \cos(n2\pi f_1 + \phi_n) \tag{2.78}$$

where $C_1 = 1.0$ and $C_n = 0.2$ for $n = 2$ to 7, for which 32 samples were available.

With window filtering the error introduced by the higher harmonics in the identification of C_1 was limited to 0.16%. However, when a non-periodic component of frequency $5.65 f_1$ and magnitude 0.2 was introduced into $x(t)$, the error in identifying C_1 without window filtering was 2%. With the Dolph-Chebyshev window and using α values of 3.2, 3.5 and 3.8, the error was reduced to 0.36%.

2.11.5 Application to Inter-Harmonic Analysis [10]

If frequencies not harmonically related to the sampling period are present or the waveform is not periodic over the sampling interval, errors are encountered due to spectral leakage.

Section 2.11 has shown that the method normally used to minimise spectral leakage and obtain accurate magnitude and frequency information involves the use of windows. Windowing functions weight the waveform to be processed by the FFT in such a way as to taper the ends of the sample to near zero.

Figure 2.17 illustrates a waveform containing the six steady-state frequency components shown in Table 2.1. The resulting waveform is not periodic and appears even asymmetric depending on the observation interval.

Applying the Hanning window to the waveform of Figure 2.17 produces the waveform shown in Figure 2.18 and spectrum shown in Figure 2.19.

Even with the use of windowing functions, closely spaced inter-harmonic frequencies are hard to determine due to the resolution of the FFT as determined by the original

Table 2.1 Frequency components of example system

Frequency	Magnitude
50	1.0
104	0.3
117	0.4
134	0.2
147	0.2
250	0.5

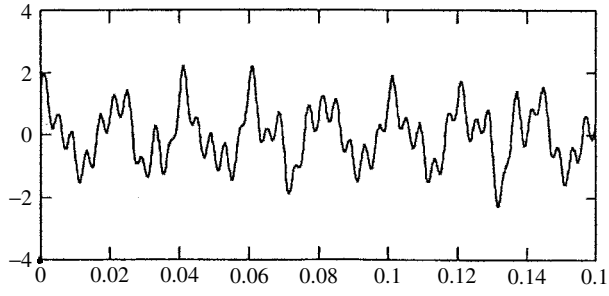


Figure 2.17 Waveform with harmonic and inter-harmonic components

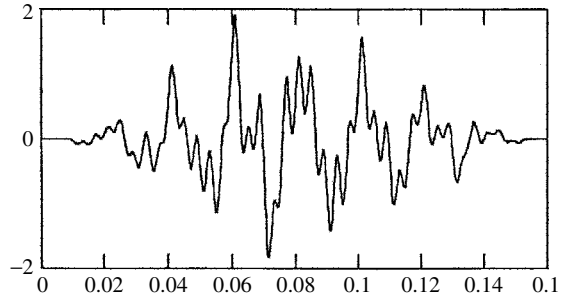


Figure 2.18 Result of Hanning window

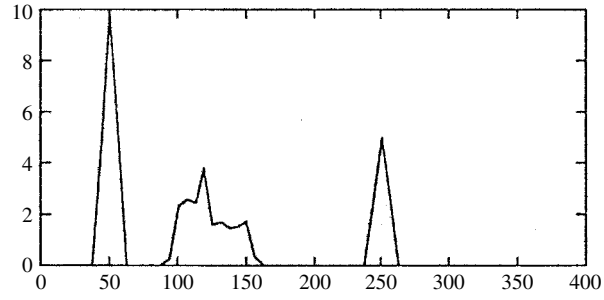


Figure 2.19 FFT spectrum of Figure 2.17

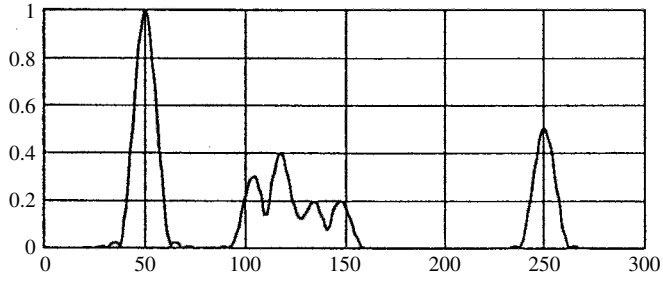


Figure 2.20 Result of FFT analysis of Figure 2.19 with four-fold zero padding

sampling period, which is 8 cycles of 50 Hz in this case. The use of the zero padding technique can result in a much more accurate determination of the actual inter-harmonic frequency component magnitudes and frequencies. Figure 2.20 shows the results of applying a four-fold zero padding before performing the FFT.

Note that the resolution has been improved enough to accurately determine the magnitude and frequency of each component even though the sampled waveform was not periodic and some of the inter-harmonic components are very close to each other.

2.12 Efficiency of FFT Algorithms

2.12.1 The Radix-2 FFT

The complex radix-2 [11] is the standard FFT version and is usually available in DSP libraries. A number of alternative algorithms, such as the higher radix, mixed radix and split radix, have been developed but the radix-2 is still widely used. It relies on a decomposition of the set of N inputs into successively smaller sets on which the DFT is computed until sets of length 2 remain. Figure 2.21 represents this approach, which requires that the number of input points N is a power of two ($N = 2^v$). The decomposition in this way can then be performed v times.

Each of the 2-point DFTs consists of a *butterfly* computation as depicted in Figure 2.22. It involves the two complex numbers a and b, where b is multiplied by the complex phase factor and then the product is added and subtracted from a.

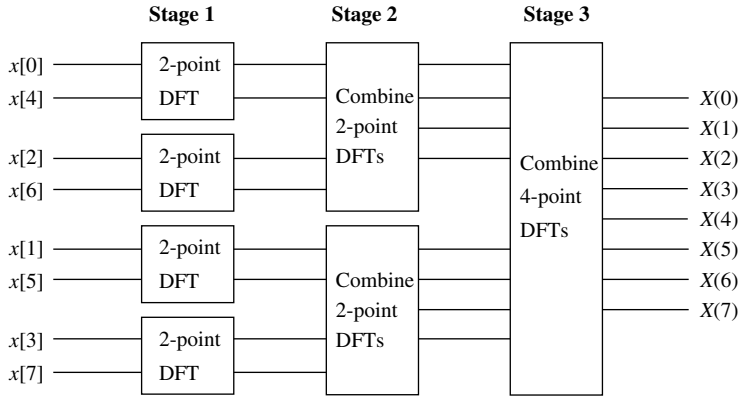


Figure 2.21 Decomposition of an 8-point DFT into 2-point DFTs by the radix-2 FFT algorithm

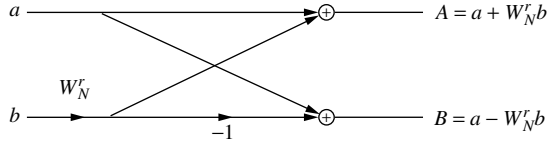


Figure 2.22 Butterfly computation with twiddle factor W_N^r

One butterfly hence requires one complex multiplication and two complex additions. Each of the stages consists of $N/2$ butterflies. Thus to compute the radix-2 FFT, $vN/2$ butterflies are required. The total number of real operations is $5vN$, consisting of $2vN$ multiplications and $3vN$ additions.

2.12.2 Mixed-Radix FFT

The sampling rate of measurement equipment (and step-length for time-domain simulation) is not often chosen to result in 2^n sample points for one period of the fundamental frequencies of 50 Hz or 60 Hz. With the increase in computer power, the mixed-radix FFT is useful and practical for power system studies, giving flexibility in transform data size and sampling rate, and eliminating the leakage problem that often occurs with radix-2 FFT.

FFT algorithms are not limited to the radix-2 family of algorithm's only. Reference [12] describes an improvement of these algorithms where radix-2 and radix-4 routines are mixed to produce a more efficient FFT. Single-radix FFTs such as the radix-3 and the radix-5 require 3, 9, 27, 81, 243, ... data points and 5, 25, 125, 625, ... data points, respectively. Algorithms based on routines higher than radix-10 require too many points for efficient computation.

More flexibility in the selection of data size is therefore provided by the mixed-radix FFT. For example, a 2000-point DFT can be achieved using a mixed-radix FFT

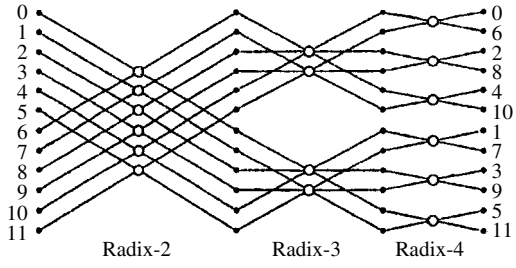


Figure 2.23 12-point $2 \times 3 \times 2$ FFT flow chart

to perform the DFT in $2 \times 2 \times 2 \times 2 \times 5 \times 5 \times 5$ or $2 \times 10 \times 10 \times 10$. Single-radix FFTs for radices 2, 3, 4, 5, 6, ... can be stacked in any order to accommodate the desired number of data points. Figure 2.23 gives a simple flow chart showing a 12-point ($2 \times 3 \times 2$) FFT.

2.12.3 Real-Valued FFTs

FFT algorithms are designed to perform complex multiplications and additions but the input sequence may be real. This can be exploited to compute the DFT of two real-valued sequences of length N by one N-point FFT. This is based on the linearity of the DFT and on the fact that the spectrum of a real-valued sequence has complex conjugate symmetry, i.e.

$$X(k) = X^*(N-k), \qquad k = 1 \ldots \frac{N}{2} - 1 \tag{2.79}$$

while $X(k)$ and $X(N/2)$ are real. A complex-valued sequence $x[n]$ defined by two real-valued sequences $x_1[n]$ and $x_2[n]$ such that

$$x[n] = x_1[n] + jx_2[n] \tag{2.80}$$

has a DFT that, due to the linearity of the transform, may be expressed as

$$X(k) = X_1(k) + jX_2(k) \tag{2.81}$$

The DFTs of the original sequences are then given by

$$\begin{aligned} X_1(k) &= \tfrac{1}{2}[X(k) + X^*(N-k)] \\ X_2(k) &= \tfrac{1}{(2j)}[X(k) + X^*(N-k)] \end{aligned} \tag{2.82}$$

The extra amount of computation needed to recover the DFTs according to equation (2.82) is small. Since $X_1(k)$ and $X_2(k)$ represent the DFTs of real sequences, they must have complex conjugate symmetry (equation (2.79)) and only the values for $k = 0 \ldots N/2$ need to be computed. For $k = 0$ or $k = N/2$ the result will be real. Thus for two length N real-valued sequences, the total number of computations amounts to

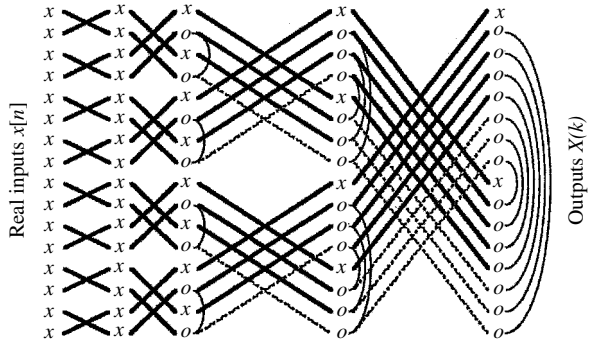


Figure 2.24 Radix-2 FFT of length 16 with real inputs. Real values are indicated by x, complex ones by o. The complex values connected by arcs are conjugates of each other. The solid lines represent the butterflies that need to be computed. Reproduced from [13]

one N-point FFT plus $2N - 4$ extra additions, which essentially means that the number of operations compared to the standard FFT is halved by this technique.

An even more efficient technique [13] is based on the fact that complex conjugate symmetry not only exists at the output of the FFT algorithm (coefficients $X(k)$) but also at every stage. This is shown in Figure 2.24 for a 16-point FFT with real-valued inputs. Thus the complex conjugate values need not be calculated (saving five butterflies in Figure 2.24).

Although the concept can be applied to any kind of FFT algorithm, the *split-radix* FFT algorithm is recommended because it requires fewer operations than a radix-2 FFT, a radix-4 FFT or any higher radix FFT. It is called 'split-radix' because an N-point DFT is broken up into a length $N/2$ DFT over the inputs with even indices and two length $N/4$ DFTs over the inputs with odd indices. This scheme is then iterated through all stages of the transform. A corresponding real-valued inverse split-radix FFT exists (in this case the outputs being real-valued).

The computational complexity of the real-valued split-radix FFT is reduced to:

$$\begin{aligned} \#_{\text{mul}} &= \tfrac{2}{3} v N - \tfrac{19}{9} N + 3 + \frac{(-1)^v}{9} \\ \#_{\text{add}} &= \tfrac{4}{3} v N - \tfrac{17}{9} N + 3 - \frac{(-1)^v}{9} \\ \hline \#_{\text{total}} &= 2 v N - 4 N + 6 \end{aligned} \tag{2.83}$$

where $2^v = N$.

2.12.4 Partial FFTs

FFT algorithms generally compute N frequency samples for a length N input sequence. If only a narrow band of the spectrum is of interest, i.e. fewer than the N outputs are needed, there are methods to reduce the complexity of the FFT accordingly.

One way is to compute the desired DFT points directly using digital filters, which resonate at the corresponding frequencies [14]. Another well-known technique is FFT *pruning* [15] where the branches in the tree-like FFT flow graph (see Figure 2.24) that lead to unwanted outputs are removed. Instead of a full set of N points, a smaller subset of L points, which must occur in a sequence, can be calculated.

A more flexible and efficient method is *transform decomposition* (TD) [16], where S output points, which need not be in a sequence, are computed by decomposing the N-point DFT into Q P-point DFTs ($N = PQ$). Subsequently, each of the P-point DFTs is computed and recombination (multiplication by the phase factors and summation) leads to the desired S output points. This process is shown in the block diagram of Figure 2.25 for an 8-point DFT. Any FFT algorithm may be used and therefore the real-valued split-radix algorithm described in the previous section is the best choice.

The overhead for the transform decomposition amounts to:

$$\begin{aligned} \#_{\text{mul}} &= 4QS \\ \#_{\text{add}} &= 4QS - 2S \\ \#_{\text{total}} &= 8QS - 2S \end{aligned} \tag{2.84}$$

To obtain the total number of operations for the TD, the computations for the Q length P split-radix have to be added. These follow from equation (2.83), RFFTs where the operation counts of an N-point split-radix RFFT are given, and the total becomes:

$$\#_{\text{total}} = 2N[\log_2 P - 2 + (3 + 4S)/P] - 2S \tag{2.85}$$

Table 2.2 lists the number of operations required by each of the FFT algorithms discussed in this section to compute the DFT for a number of inputs and outputs. The savings achieved by the TD are more than 75%.

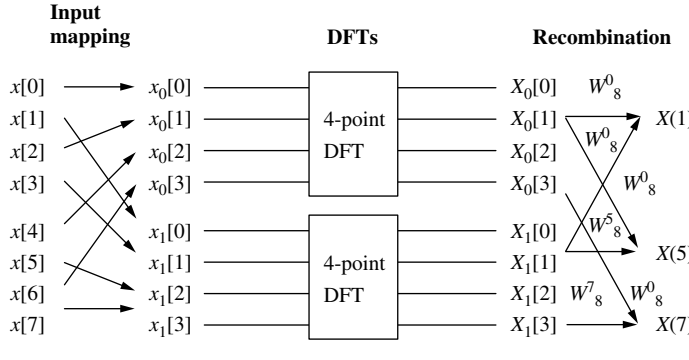


Figure 2.25 Transform decomposition of an 8-point DFT ($Q = 2$, $P = 4$). Only $S = 3$ output points are computed

Table 2.2 Number of operations (real multiplications and additions) required for the DFT computation by the discussed FFT algorithms. The last column indicates the savings of the transform decomposition over a standard FFT

Number of DFTs		Number of operations			Reduction (%)
Inputs N	Outputs S (0–5 Hz)	Standard FFT	Split-radix RFFT	TD + split-radix RFFT	
512	9	23 040	7 174	4 302	81.3
1024	17	51 200	16 390	10 430	79.6
2048	33	112 640	36 870	24 734	78.0
4096	65	245 760	81 926	57 438	76.6
8192	129	532 480	180 230	131 038	75.4

2.13 Alternative Transforms

Traditionally, the Fourier transform has almost exclusively been used in power as well as most other engineering fields, therefore this book concentrates on assessment techniques based on Fourier analysis.

Three principal alternatives have been discussed at great length in recent literature with reference to potential power system applications. These are the Walsh, Hartley and Wavelets transforms.

As in the Fourier case, the Walsh transform [17] constitutes a set of orthogonal functions. It is extremely simple conceptually, as it involves only square wave components, but for accurate results it needs a large number of terms for the processing of power system waveforms. Moreover, it does not benefit from the differential-to-phasor transformation, and handling differentiation and integration, common operations in power systems.

The Hartley transform [17], also using the orthogonal principle, is expressed as

$$F(v) = \frac{1}{\sqrt{2\pi}} \int_{-\infty}^{\infty} f(t)\ \mathrm{cas}(vt)\, \mathrm{d}t \tag{2.86}$$

where

$$\mathrm{cas}(vt) = \cos(vt) + \sin(vt)$$

and v is identical to the ω of Fourier, i.e. radians/second.

Moreover, its inverse, i.e.

$$f(t) = \frac{1}{\sqrt{2\pi}} \int_{-\infty}^{\infty} F(v)\ \mathrm{cas}(vt)\ \mathrm{d}t \tag{2.87}$$

has exactly the same form, and this leads to simpler software. An important difference between the Fourier and Hartley transforms is that the latter is all real and thus requires only one half of the memory for storage (i.e. one real quantity as compared with one complex quantity of Fourier's). Also, the convolution operation requires only one real multiplication as compared with four multiplications in the Fourier domain.

However, the Fourier transform is widely spread throughout the power system field and permits a very convenient assessment of magnitude and phase information. The latter is not always required, however, and in such cases the efficiency of the Hartley transform may be sufficiently attractive for it to be used as an alternative to the traditional philosophy.

Owing to the interest generated in the potential applications of wavelets, this transform is given special consideration in the next section.

2.13.1 The Wavelet Transform

The WT, originally derived to process seismic signals, provides a fast and effective way of analysing non-stationary voltage and current waveforms. As in the Fourier case, the Wavelet transform decomposes a signal into its frequency components. Unlike the Fourier transform, the wavelet can tailor the frequency resolution, a useful property in the characterisation of the source of a transient.

The ability of wavelets to focus on short time intervals for high-frequency components and long intervals for low-frequency components improves the analysis of signals with localised impulses and oscillations, particularly in the presence of a fundamental and low-order harmonics.

A wavelet is the product of an oscillatory function and a decay function. A *mother* wavelet is expressed as [18]

$$g(t) = \mathrm{e}^{-\alpha t^2}\mathrm{e}^{j\omega t} \tag{2.88}$$

An example of a mother wavelet is shown in Figure 2.26.

A variety of wavelets originating from a mother wavelet can be used to approximate any given function. These wavelets are derived by scaling and shifting (in time) mother wavelets as shown in Figure 2.27, and can be expressed as

$$g'(a, b, t) = \frac{1}{\sqrt{a}} g\left(\frac{t-b}{a}\right) \tag{2.89}$$

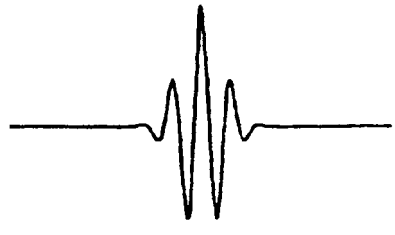


Figure 2.26 A sample mother wavelet



Figure 2.27 A sample daughter wavelet

The WT of a continuous signal $x(t)$ is defined as

$$\text{WT}\ (a, b) = \frac{1}{\sqrt{a}} \int_{-\infty}^{\infty} f(t) g\left(\frac{t-b}{a}\right) \mathrm{d}t \tag{2.90}$$

The time extent of the wavelet $g(t - b/a)$ is expanded or contracted in time depending on whether $a > 1$ or $a < 1$. A value of $a > 1$ ($a < 1$) expands (contracts) $g(t)$ in time and decreases (increases) the frequency of the oscillations in $g(t - b/a)$. Hence, as a is ranged over some interval, usually beginning with unity and increasing, the input is analysed by an increasingly dilated function that is becoming less and less focused in time.

The WT has a digitally implementable counterpart, the discrete wavelet transform (DWT).

In DWT, the scale and translation variables are discretised but not the independent variable of the original signal. It is to be noted that the two variables a and b are continuous in the continuous transform. However, in the reconstruction process, the independent variable will be broken down into small segments for ease of computer implementations. A DWT gives a number of wavelet coefficients depending upon the integer number of the discretisation step in scale and translation, denoted by m and n, respectively. So any wavelet coefficient can be described by two integers, m and n. If a_0 and b_0 are the segmentation step sizes for the scale and translation, respectively, the scale and translation in terms of these parameters will be $a = a_0^m$ and $b = nb_0a_0^m$.

In terms of the new parameters a_0, b_0, m and n, equation (2.89) becomes

$$g'(m, n, t) = \frac{1}{\sqrt{{a_0}^m}} g\left(\frac{t - nb_0{a_0}^m}{{a_0}^m}\right) \tag{2.91}$$

or

$$g'(m, n, t) = \frac{1}{\sqrt{{a_0}^m}} g(ta_0 - nb_0) \tag{2.92}$$

and the discrete wavelet coefficients are given by

$$\text{DWT}(m, n) = \int_{-\infty}^{\infty} \frac{1}{\sqrt{{a_0}^m}} f(t) g({a_0}^{-m} t - nb_0)\, \mathrm{d}t \tag{2.93}$$

Although the transformation is over continuous time, the wavelets representation is discrete and the discrete wavelet coefficients represent the correlation between the original signal and wavelets for different combinations of m and n.

The inverse DWT is given by

$$f(t) = K \sum_{m=0}^{\infty} \sum_{n=0}^{\infty} W_g f(m, n) \frac{1}{\sqrt{{a_0}^m}} g({a_0}^{-m} t - nb_0) \tag{2.94}$$

where $K = (A + B)/2$, and A and B are the frame bounds (maximum values of a and b).

Wavelet analysis is normally implemented using multi-resolution signal decomposition (MSD). High- and low-pass equivalent filters, h and g respectively, are

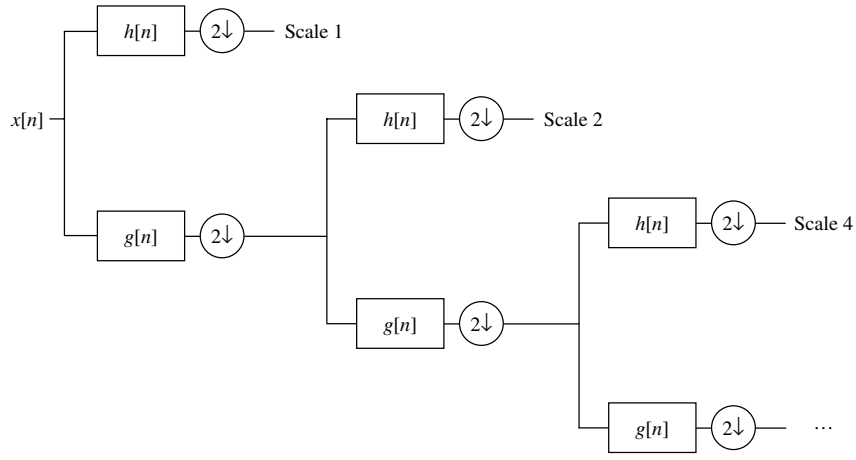


Figure 2.28 Multi-resolution signal decomposition implementation of wavelet analysis

formed from the analysing wavelet. The digital signal to be analysed is then decomposed (filtered) into smoothed and detailed versions at successive scales, as shown in Figure 2.28, where (2↓) represents a down-sampling by half.

Scale 1 in Figure 2.28 contains information from the Nyquist frequency (half the sampling frequency) to one quarter the sampling frequency; scale 2 contains information from one quarter to one eighth of the sampling frequency, and so on.

Choice of Analysing Wavelets The decomposition can be halted at any scale, with the final smoothed output containing the information of all of the remaining scales, i.e. scales 8, 16, 32, ... if it is halted at scale 4, one of the desirable properties of MSD.

The choice of mother wavelet is different for each problem at hand and can have a significant effect on the results obtained. Orthogonal wavelets ensure that the signal can be reconstructed from its transform coefficients [19]. Wavelets with symmetric filter coefficients generate linear phase shift, and some wavelets have better time localisation than others.

The wavelet family derived by Daubechies [20] covers the field of orthonormal wavelets. This family is very large and includes members ranging from highly localised to highly smooth. For short and fast transient disturbances, Daub4 and Daub6 wavelets are the best choice, while for slow transient disturbances, Daub8 and Daub10 are particularly good.

However, the selection of an appropriate mother wavelet without knowledge of the types of transient disturbances (which is always the case) is a formidable task. A more user-friendly solution [21] utilises one type of mother wavelet in the whole course of detection and localisation for all types of disturbances.

In doing so, higher-scale signal decomposition is needed. At the lowest scale, i.e. scale 1, the mother wavelet is most localised in time and oscillates most rapidly within a very short period of time. As the wavelet goes to higher scales, the analysing wavelets become less localised in time and oscillate less due to the dilation nature of the wavelet transform analysis. As a result of higher-scale signal decomposition, fast and short

transient disturbances will be detected at lower scales, whereas slow and long transient disturbances will be detected at higher scales.

Example of Application [21] Figure 2.29(a) shows a sequence of voltage disturbances. To remove the *noise* present in the waveform, squared wavelet transform coefficients (SWTC) are used at scales $m = 1$, 2, 3 and 4 (shown in Figure 2.29(b), (c), (d) and (e), respectively); these are analysed using the Daub4 wavelet.

Figure 2.29(a) contains a very rapid oscillation disturbance (high frequency) before time 30 ms, followed by a slow oscillation disturbance (low frequency) after time 30 ms. The SWTCs at scales 1, 2 and 3 catch these rapid oscillations, while scale 4 catches the slow oscillating disturbance which occurred after time 30 ms. Note that the high SWTCs persist at the same temporal location over scales 1, 2 and 4.

It must be pointed out that the same technique can be used to detect other forms of waveform distortion (like notches and harmonics) and other types of disturbance such as momentary interruptions, sags and surges.

However, rigorous uniqueness search criteria must be developed for each disturbance for the wavelet transform to be accepted as a reliable tool for the automatic classification of power quality disturbances.

2.13.2 Automation of Disturbance Recognition

Some proposals are being made to automate the process of disturbance recognition [22,23] to improve the speed, reliability and ease of data collection and storage.

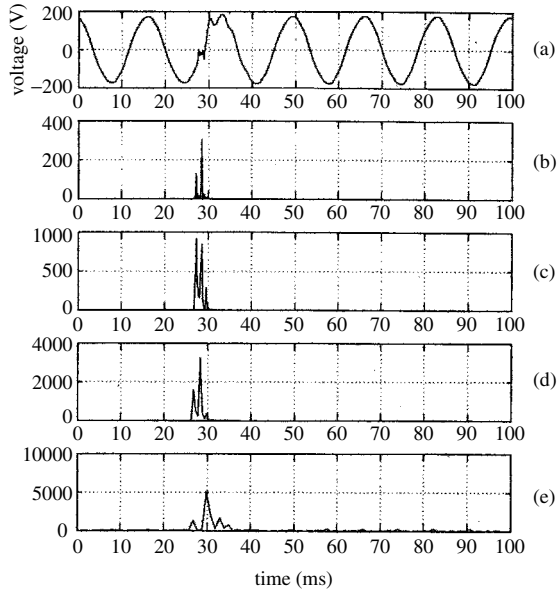


Figure 2.29 Wavefault disturbance detection using Daub4: (a) the voltage disturbance signal; (b), (c), (d) and (e) the squared WTCs at scales 1, 2, 3 and 4, respectively. Copyright 1996 IEEE

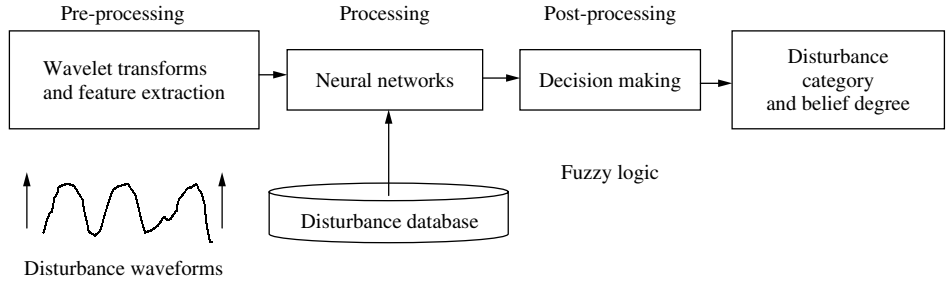


Figure 2.30 Block diagram of the automatic disturbance recognition system

Such a scheme involves the three separate stages illustrated in Figure 2.30. These are a pre-processing stage to extract the disturbance information from the generated power signal, a main processing stage to carry out pattern recognition on the disturbance data, and a post-processing stage to group the output data and form decisions on the possible nature and cause of the disturbance.

The WT described in Section 2.13.1 is an obvious candidate to extract the disturbance information owing to its greater precision and speed over Fourier methods. A collection of standard libraries of wavelets can be developed to fit specific types of disturbance or transient.

Artificial neural networks can be used in the main processing stage to perform pattern recognition. The neural network can be trained to classify the preliminary information extracted in the pre-processing stage.

The most commonly used type of neural network for pattern recognition is the multi-layered perceptron. These are constructed as shown in Figure 2.31 and are usually trained using the recursive error back-propagation algorithm or a modification thereof [24].

The output of the network is

$$y_k(p) = \varphi_k\left(\sum_j w_{kj}(p) \cdot y_j(p)\right) \tag{2.95}$$

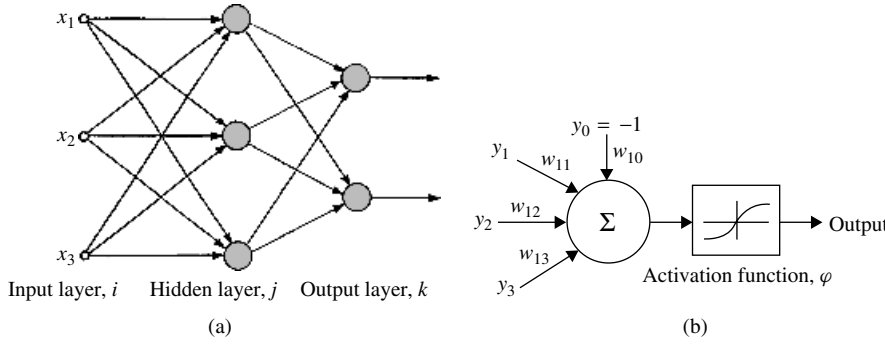


Figure 2.31 (a) Multi-layered perceptron; (b) Configuration of an individual neuron

Finally, fuzzy logic [25,26] is well suited in the post-processing stage to make decisions on the disturbance category. It is simple and fast to compute.

Fuzzy rules must be derived in order to take the information provided by the neural networks and produce a 'belief' in each disturbance category. These rules take the form of IF ... THEN relations based on human knowledge of the problem.

The output of the disturbance recognition system is produced as one or a list of disturbance categories with an associated degree of belief. A list of disturbance categories with belief degree is necessary, as pattern recognition systems are inexact by nature. The system should, however, produce high belief degrees only for disturbance categories that are likely causes.

2.14 Discussion

The Fourier transform is still the most widely utilised signal processing tool in power system harmonic analysis. For efficient computation its use has been enhanced by the development of a variety of algorithms under the general heading of the Fast Fourier transform. The development of effective windows, essential to the analysis of non-stationary signals, as well as inter-harmonic information, is another important addition to Fourier assessment.

The main alternatives to the Fourier transform under consideration in power system analysis are the Walsh, Hartley and wavelets transforms. Although harmonic analysis implies steady-state conditions, the information recorded from actual measurements is not necessarily of that type and thus the wavelet approach, although initially designed for the processing of transients, can also be used to extract harmonic content from practical power system recordings.

Finally, with the greater availability of computing power it is possible to make more extensive use of computer-demanding heuristic techniques, such as neural networks and fuzzy logic, in the processing of power system signals, although at the point of writing these are mainly confined to the technical literature.

2.15 References

1. Fourier, J.B.J. (1822) *Theorie analytique de la chaleur*, Paris.
2. Kreyszig, E. (1967) *Advanced Engineering Mathematics*, 2nd edn. John Wiley & Sons.
3. Kuo, F.F. (1966) *Network Analysis and Synthesis*. John Wiley & Sons.
4. Brigham, E.O. (1974) *The Fast Fourier Transform*. Prentice-Hall.
5. Cooley, J.W. and Tukey, J.W. (1965) An algorithm for machine calculation of complex Fourier series, *Math. Comp.*, **19**, 297–301.
6. Cochran, W.T., Cooley, J.W., Favin, D.L., Helms, H.D., Kaenal, R.A., Lang, W.W., Maling Jr, G.C., Nelson, D.E., Rader, C.M. and Welch, P.D. (1967) What is the fast Fourier transform?, *IEEE Trans Audio and Electroacoustics*, special issue on fast Fourier transform and its application to digital filtering and spectral analysis, **AU-15**(2), pp. 45–55.
7. Bergland, G.D. (1969) A guided tour of the fast Fourier transform. *IEE Spectrum*, July, 41–42.
8. Bergland, G.D. (1968) A fast Fourier transform algorithm for real-values series, *Numerical Analysis*, **11**(10), 703–10.

9. Harris, F.J. (1978) On the use of windows for harmonic analysis with the discrete Fourier transform, *Proc. IEEE*, **66**, 51–84.
10. IEEE Task Force on Interharmonics and CIGRE WG 36.05/CIRED 2-CCO2.
11. Lu, I.D. and Lee, P. (1994) Use of mixed radix FFT in electric power system studies, *IEEE Trans. Power Delivery*, **9**(3), 1276–80.
12. Sorensen, H.V., Heiderman, M.T. and Burrus, C.S. (1986) On computing the split-radix FFT, *IEEE Trans. Acoustics, Speech Signal Process.*, **ASSP-34** 152–6.
13. Sorensen, H.V., Jones, D.L., Heiderman, M.T. and Burrus, C.S. (1987) Real-valued FFT algorithms, *IEEE Trans Acoustics, Speech Signal Process.*, **35**(6), 849–64.
14. Soertzel, G. (1958) An algorithm for the evaluation of finite trigonometric series, *Am. Math. Monthly*, **65**(1), 34–5.
15. Markel, J.D. (1971) FFT pruning, *IEEE Trans. Audio Electroacoustics*, **19**(4), 305–11.
16. Sorensen, H.V. and Burrus, C.S. (1993) Efficient computation of the DFT with only a subset of input or output points, *IEEE Trans. Signal Process.*, **41**(3), 1184–1200.
17. Heydt, G.T. (1991) *Electric Power Quality*, Stars in a Circle Publications, West LaFayette.
18. Ribeiro, P.F., Haque, T., Pillay P. and Bhattacharjee, A. (1994) Application of wavelets to determine motor drive performance during power systems switching transients, *Power Quality Assessment*, Amsterdam.
19. Chui, C.K. (1992) *An Introduction To Wavelets*, Academic Press, pp. 6–18.
20. Daubechies, I. (1988) Orthonormal bases of compactly supported wavelets, *Comm. Pure Appl. Math.*, **41**, 909–96.
21. Santoso, S., Powers, E.J., Grady W.M. and Hofmann, P. (1996) Power quality assessment via wavelet transform analysis, *IEEE Trans. Power Delivery*, **11**(2), 924–30.
22. Ringrose, M. and Negnevitsky, M. (1998) *Automated disturbance recognition in power systems*, Australasian Universities Power Engineering Conference (AUPEC'98), Hobart, pp. 593–7.
23. Ribeiro, P.F. and Celio, R. (1994) Advanced techniques for voltage quality analysis: unnecessary sophistication or indispensable tools, paper A-206. *Power Quality Assessment*, Amsterdam.
24. Haykin, S. (1994) Neural Networks: A Comprehensive Foundation. Macmillan, pp. 138–229.
25. Zadeh, L. (1965) Fuzzy sets, *Inform. Control*, **8**(3), 338–54.
26. Tanaka, K. (1997) *An Introduction to Fuzzy Logic for Practical Applications*. Springer.

3

Harmonic Sources

3.1 Introduction

Prior to the appearance of power semiconductors, the main sources of waveform distortion were electric arc furnaces, the accumulated effect of fluorescent lamps, and to a lesser extent electrical machines and transformers.

The increasing use of power electronic devices for the control of power apparatus and systems has been the reason for the greater concern about waveform distortion in recent times. A power electronic converter can be viewed as a matrix of static switches that provides a flexible interconnection between input and output nodes of an electrical power system. Through these switches power can be transferred between input and output systems operating at the same or different frequencies (one or both of which can be d.c.).

The most common power electronic aid is the single-phase rectifier, used to power most modern office and domestic appliances. Although the individual ratings are always small, their combined effect can be an important source of waveform distortion.

Because of their considerable power ratings, three-phase static power converters are the main contributors to the harmonic problem. The terms *rectification* and *inversion* are used for power transfers from a.c. to d.c. or d.c. to a.c., respectively and the term *conversion* is used when the power electronic device has bi-directional power transfer capability.

According to the relative position of the firing instant of the switches from one cycle to the next on the steady state, four basically different power electronic control principles are in common use:

(1) Constant phase-angle control produces consecutive valve firings equally spaced with reference to their respective commutating voltages.

(2) Equidistant firing control produces consecutive firings at equal intervals of the supply frequency.

(3) Modulated phase-angle control produces time-varying phase-modulated firings.

(4) Integral cycle control selects an integer number of complete cycles or half cycles of the supply frequency.

Power System Harmonics, Second Edition J. Arrillaga, N.R. Watson
© 2003 John Wiley & Sons, Ltd ISBN: 0-470-85129-5

The Fourier analysis as described in Chapter 2 is directly applicable to the phase-angle controlled and equidistant-firing controlled waveforms, whereas modulated firing and integral cycle controls require special analysis.

Inverter fed a.c. drives are normally supplied from the a.c. power system through a line-commutated three-phase rectifier and thus their harmonic contribution to the power network is covered under the various static converter categories. However, the inverter side of the drive uses either pulse width modulation (PWM) and/or multi-level configurations to reduce the harmonic content and, thus requires special consideration.

3.2 Transformer Magnetisation Nonlinearities

3.2.1 Normal Excitation Characteristics

At no-load the primary of a transformer is practically balanced by the back e.m.f. because the effect of winding resistance and leakage reactance is negligible at low currents. At any instant, therefore, the impressed voltage v_1 for a sinusoidal supply is

$$v_1 = -e_1 = -E_m \sin \omega t = N_1 \frac{\mathrm{d}\phi}{\mathrm{d}t} \tag{3.1}$$

From equation (3.1) the following expression is obtained for the main flux:

$$\phi = -\int \frac{e_1}{N_1}\,\mathrm{d}t = \frac{E_m}{N_1 \omega} \cos \omega t = \phi_m \cos \omega t \tag{3.2}$$

i.e. a sinusoidal primary voltage produces a sinusoidal flux at no-load. The primary current, however, will not be purely sinusoidal, because the flux is not linearly proportional to the magnetising current, as explained in the next section.

3.2.2 Determination of the Current Waveshape

In an ideal core without hysteresis loss the flux ϕ and the magnetising current needed to produce it are related to each other by the magnetising curve of the steel used in the laminations, as shown in Figure 3.1(a). In Figure 3.1(b), where ϕ represents the sinusoidal flux needed to balance the primary voltage, the magnetising current is plotted against time for each value of ϕ and the resulting waveform is far from sinusoidal. However, when operating at or close to the nominal voltage, the transformer magnetising current is only 1–2% of the rated current and presents no special problem.

When the hysteresis effect is included, as in the case of Figure 3.2, the non-sinusoidal magnetising current wave is no longer symmetrical about its maximum value. In this case the current corresponding to any point on the flux density wave of Figure 3.2(b) is determined from Figure 3.2(a), the ascending portion of the hysteresis being used for the ascending portion of the flux density wave.

The distortion illustrated in Figures 3.1 and 3.2 is mainly caused by zero-sequence triplen harmonics and particularly the third. Thus, in order to maintain a reasonably

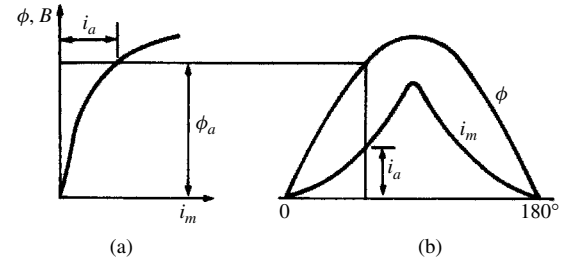


Figure 3.1 Transformer magnetisation (without hysteresis): (a) magnetisation curve; (b) flux and magnetisation current waveforms

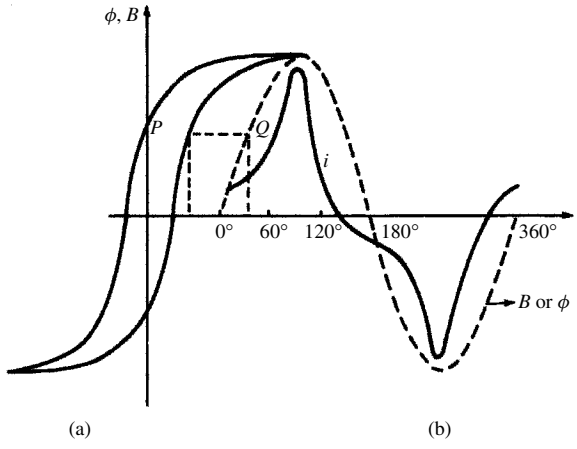


Figure 3.2 Transformer magnetisation (including hysteresis): (a) magnetisation curve; (b) flux and magnetisation current waveforms

sinusoidal voltage supply, it is necessary to provide a path for the zero-sequence current harmonics and this is normally achieved by the use of delta-connected windings.

With three-limb transformers the triplen harmonic m.m.f.s are all in phase and they act in each limb in the same direction. Hence the path of triplen harmonic flux must return through the air (or rather through the oil and transformer tank) and the higher reluctance of such a path reduces the triplen harmonic flux to a very small value (about 10% of that appearing in independent core phases). Thus, flux density and e.m.f. waveforms remain sinusoidal under all conditions in this case. However, the elimination of triplen harmonics in the delta-connected windings is only fully effective when the voltages are perfectly balanced. The magnetising current harmonics often rise to their maximum levels in the early hours of the morning, i.e. when the system is lightly loaded and the voltage high.

3.2.3 Symmetrical Overexcitation

For economic reasons transformers are normally designed to make good use of the magnetic properties of the core material. This means that a typical transformer using a

good quality grain-oriented steel might be expected to run with a peak magnetic flux density in the steady state of the order of 1.6–1.7 T. If a transformer running with this peak operating magnetic flux density is subjected to a 30% rise in voltage, the core material may be subjected to a magnetic flux density of, say, 1.9–2.0 T, which will produce considerable saturation.

The problem of overvoltage saturation is particularly onerous in the case of transformers connected to large rectifier plant following load rejection. It has been shown [1] that the voltage at the converter terminals can reach a level of 1.43 per unit, thus driving the converter transformer deep into saturation.

The symmetrical magnetising current associated with a single transformer core saturation contains all the odd harmonics. If the fundamental component is ignored, and if it is assumed that all triplen harmonics are absorbed in delta windings, then the harmonics being generated are of orders 5, 7, 11, 13, 17, 19 . . ., i.e. those of orders $6k \pm 1$, where k is an integer. In conventional six-pulse rectifier schemes it is usual to filter these harmonics from the a.c. busbars as they are exactly of the same order as the theoretical harmonics produced by a six-pulse converter. If, however, a twelve-pulse converter configuration is used, the theoretical harmonics are of orders $12k \pm 1$, where k is an integer. In this case the fifth- and seventh-order harmonics produced by a saturated converter transformer are not filtered and have to be absorbed by the a.c. system.

The composition of the magnetising current versus the exciting voltage is typically as shown in Figure 3.3.

3.2.4 Inrush Current Harmonics

If a transformer is switched off it can be left with a residual flux density in the core of magnitude $+B_r$ or $-B_r$ (or under some circumstances zero). When the transformer is re-energised the flux density illustrated in Figure 3.4 can reach peak levels of $2B_{\max}$ or

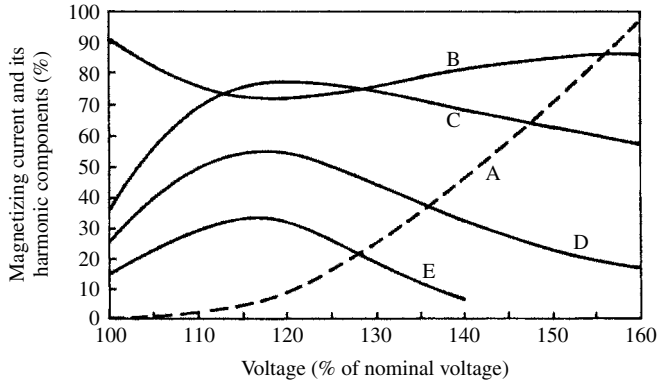


Figure 3.3 Harmonic components of transformer exciting current: A, magnetising current (% of rated current); B, fundamental component (% of total magnetising current); C, third harmonic (% of fundamental current); D, fifth harmonic (% of fundamental current); E, seventh harmonic (% of fundamental current)

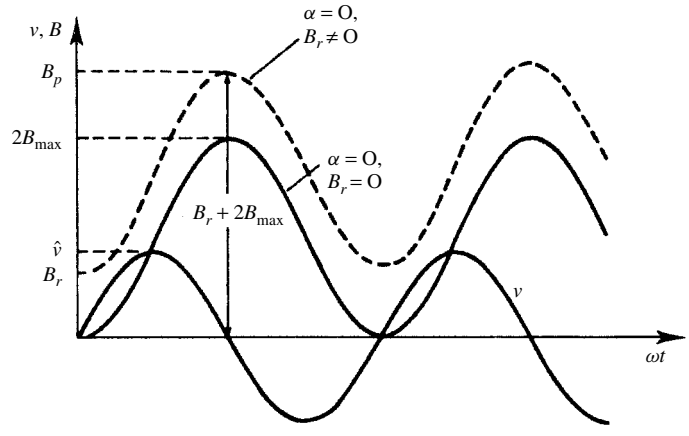


Figure 3.4 Transformer energisation flux density with and without remanence

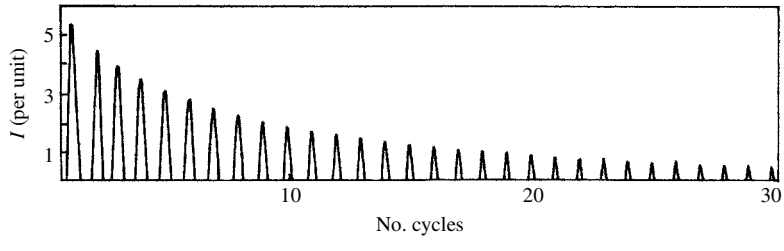


Figure 3.5 Inrush current of a 5 MVA transformer: $B_r = 1.3$ T, $\alpha = 0$

$B_r + 2B_{\max}$ (almost three times the working flux). For a normally designed transformer this can create peak flux densities of about 3.4 or 4.7 T, respectively [2]. When this is compared to the saturation flux density levels of around 2.05 T to be expected from symmetrical overexcitation, it can be seen that the transformer core will be driven to extreme saturation levels and will thus produce excessive ampere-turns in the core. This effect gives rise to magnetising currents of up to 5–10 per unit of the rating (as compared to the normal values of a few percentage points). Such an inrush current is shown in Figure 3.5.

The decrement of the inrush current with time is mainly a function of the primary winding resistance. For the larger transformers this inrush can go on for many seconds because of their relatively low resistance.

By way of illustration, the Fourier series of the waveshape of Figure 3.5 yields the harmonic profile shown in Figure 3.6.

The harmonic content, shown as a percentage of the rated transformer current, varies with time, and each harmonic has peaks and nulls.

3.2.5 D.C. Magnetisation

It has been shown in previous sections that a transformer excited by sinusoidal voltage produces a symmetrical excitation current that contains only odd harmonics. If a linear

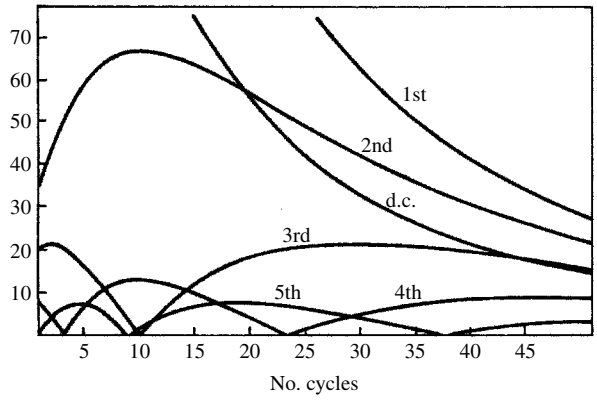


Figure 3.6 The variation of harmonic content (as a percentage of the rated current) with time

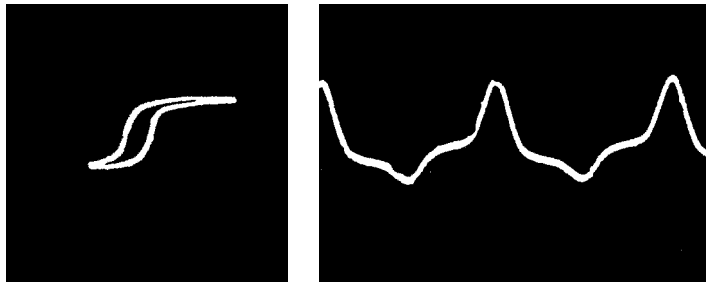


Figure 3.7 (a) Excitation characteristic; (b) exciting current waveform

or a nonlinear load is connected to this transformer, the excitation current will again contain only odd harmonics, provided that the load does not produce a direct component of current.

Under magnetic imbalance, the shape of the magnetising characteristic and the excitation current are different from those under no-load conditions. If the flux is unbalanced, as shown in Figure 3.7(a), the core contains an average value of flux ϕ_{dc} and the a.c. flux component is offset by a value equal to ϕ_{dc}. The existence of an average flux implies that a direct component of excitation current is present in Figure 3.7(b).

Under such unbalanced conditions, the transformer excitation current contains both odd and even harmonic components. The asymmetry can be caused by any load connected to the secondary of the transformer, leading to a direct component of current, in addition to the sinusoidal terms. The direct current may be a feature of the design, as in a transformer feeding a half-wave rectifier, or may result from the unbalanced operation of some particular piece of equipment, such as a three-phase converter with unbalanced firing.

A similar effect can occur as a result of geomagnetically induced currents (GIC). These are very low frequency currents (typically 0.001–0.1 Hz) and can reach levels as high as 200 A. They enter the transformer windings by way of earthed star connections and produce asymmetrical flux, causing half-cycle saturation.

It has been shown [3] that the magnitude of the harmonic components of the excitation current in the presence of direct current on the secondary side of the transformer increases almost linearly with the direct current content. The linearity is better for the lower-order harmonics.

Moreover, the harmonics generated by the transformer under d.c. magnetisation are largely independent of the a.c. excitation. Therefore there appears to be no advantage in designing a transformer to run 'underfluxed' in the presence of direct current. This independence is most noticeable at low levels of the direct current and for the lower harmonic orders.

3.3 Rotating Machine Harmonics

3.3.1 M.m.f. Distribution of A.C. Windings

Figure 3.8 shows the m.m.f. and flux distribution in one phase of a full-pitched poly-phase winding with one slot per pole per phase on the assumption of a constant air gap and in the absence of iron saturation.

Under such idealised conditions the air-gap m.m.f. is uniform and has a maximum value $(iN)/2$, where i is a maximum instantaneous current per conductor and N is the number of conductors per slot.

The frequency-domain representation of the rectangular m.m.f. space distribution of Figure 3.8 is

$$F(x) = \frac{2\sqrt{2}IN}{\pi}\left\{\sin\frac{2\pi x}{\lambda} + \frac{1}{3}\sin\left(3\frac{2\pi x}{\lambda}\right) + \frac{1}{5}\sin\left(5\frac{2\pi x}{\lambda}\right) + \cdots\right\} \tag{3.3}$$

Thus, the rectangular m.m.f. distribution is reduced to a fundamental and harmonic components. The amplitude of the nth harmonic is $1/n$ times the fundamental pole pitch.

In general, for an alternating current of angular frequency $\omega = 2\pi f$, equation (3.3) becomes

$$F(x) = \frac{2\sqrt{2}IN}{\pi}\sin(\omega t)\sum_{n=1}^{\infty}\frac{1}{n}\sin\left(n\frac{2\pi x}{\lambda}\right), \quad \text{for } n \text{ odd} \tag{3.4}$$

where λ is the wavelength and I the r.m.s. value of the current.

However, in practice the windings are distributed along the surface with g slots per pole per phase and the m.m.f.s of the g coils are displaced from each other in space.

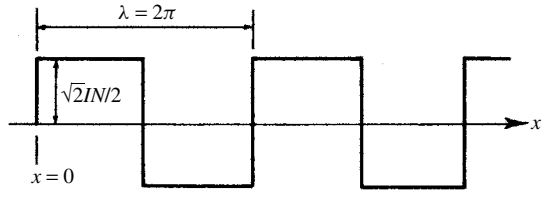


Figure 3.8 M.m.f. and flux distribution of full-pitch winding with one slot per pole

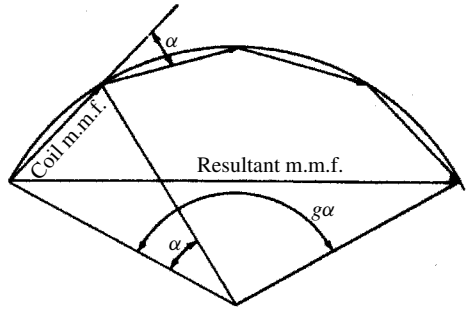


Figure 3.9 Determination of distribution factor

Moreover, the displacement angle is different for the various harmonics since their pole pitches are different.

For an m-phase machine, the number of slots per pole is $Q = mg$ and the electrical angle between slots $\alpha = \pi/Q$.

The distribution factor is

$$K_d = \frac{\text{Resultant m.m.f.}}{\text{Sum of m.m.f.s of individual coils}}.$$

From the geometry of Figure 3.9,

$$k_d = \frac{\sin(g\alpha/2)}{g\sin(\alpha/2)} \tag{3.5}$$

for the fundamental frequency, and

$$k_{dn} = \frac{\sin(ng\alpha/2)}{g\sin(n\alpha/2)} \tag{3.6}$$

for the nth harmonic.

Hence the m.m.f. of one phase of a poly-phase winding is

$$F(x) = \frac{2\sqrt{2}IN}{\pi} g\sin(\omega t)\sum_{n=1}^{\infty}\frac{k_{dn}}{n}\sin\left(n\frac{2\pi x}{\lambda}\right), \text{ for } n \text{ odd} \tag{3.7}$$

3.3.2 Three-Phase Winding

The phase windings of a three-phase machine are displaced by $2\pi/3$ in space and the currents by $2\pi/3$ in time. The corresponding m.m.f.s are

$$F_1(x) = \frac{2\sqrt{2}IN}{\pi} g\sin\omega t\left\{\sum_{n=1}^{\infty}\frac{k_{dn}}{n}\sin\left(n\frac{2\pi x}{\lambda}\right)\right\} \tag{3.8}$$

$$F_2(x) = \frac{2\sqrt{2}IN}{\pi} g \sin\left(\omega t - \frac{2\pi}{3}\right) \left\{\sum_{n=1}^{\infty} \frac{k_{dn}}{n} \sin\left[n\left(\frac{2\pi x}{\lambda} - \frac{2\pi}{3}\right)\right]\right\} \quad (3.9)$$

$$F_3(x) = \frac{2\sqrt{2}IN}{\pi} g \sin\left(\omega t - \frac{4\pi}{3}\right) \left\{\sum_{n=1}^{\infty} \frac{k_{dn}}{n} \sin\left[n\left(\frac{2\pi x}{\lambda} - \frac{4\pi}{3}\right)\right]\right\} \quad (3.10)$$

The total m.m.f. is $F(x) = F_1(x) + F_2(x) + F_3(x)$, and its nth harmonic term is

$$\begin{aligned}
&\frac{2\sqrt{2}IN}{\pi} g \frac{k_{dn}}{n} \left\{\sin\left(n\frac{2\pi x}{\lambda}\right) \sin\omega t + \sin\left[n\left(\frac{2\pi x}{\lambda} - \frac{2\pi}{3}\right)\right] \sin\left(\omega t - \frac{2\pi}{3}\right)\right. \\
&\quad \left. + \sin\left[n\left(\frac{2\pi x}{\lambda} - \frac{4\pi}{3}\right)\right] \sin\left(\omega t - \frac{4\pi}{3}\right)\right\} \\
&= \frac{2\sqrt{2}IN}{\pi} g \frac{k_{dn}}{2n} \left\{\cos\left[\frac{2\pi nx}{\lambda} - \omega t\right] - \cos\left[\frac{2\pi nx}{\lambda} + \omega t\right]\right. \\
&\quad + \cos\left[\frac{2\pi nx}{\lambda} - \omega t - (n-1)\frac{2\pi}{3}\right] - \cos\left[\frac{2\pi nx}{\lambda} + \omega t - (n+1)\frac{2\pi}{3}\right] \\
&\quad \left. + \cos\left[\frac{2\pi nx}{\lambda} - \omega t - (n-1)\frac{4\pi}{3}\right] - \cos\left[\frac{2\pi nx}{\lambda} + \omega t - (n+1)\frac{4\pi}{3}\right]\right\} \quad (3.11)
\end{aligned}$$

Putting in turn $n = 1, 3, 5$, etc.

$$\begin{aligned}
F(x) = \frac{3\sqrt{2}IN}{\pi} g &\left\{(k_{d1}) \cos\left(\frac{2\pi x}{\lambda} - \omega t\right) + \left(\frac{k_{d5}}{5}\right) \cos\left(5 \times \frac{2\pi x}{\lambda} + \omega t\right)\right. \\
&\left. + \left(\frac{k_{d7}}{7}\right) \cos\left(7 \times \frac{2\pi x}{\lambda} - \omega t\right) + \cdots\right\} \quad (3.12)
\end{aligned}$$

It can be seen that the fundamental is a travelling wave moving in the positive direction, triplen harmonics (3, 9, 15, etc.) are absent, the fifth harmonic is a wave travelling in the negative direction, the seventh travels in the positive direction, etc.

3.3.3 Slot Harmonics

If the machine has mg slots per pole (as shown in Figure 3.10), the variation of permeance in the air gap can be approximated by

$$A_1 + A_2 \sin\left(2mg\frac{2\pi x}{\lambda}\right) \quad (3.13)$$

Since the fundamental m.m.f. varies as $B\sin(2\pi x/\lambda)$, the resultant flux density variation is

$$\left\{B \sin\frac{2\pi x}{\lambda}\right\} \left\{A_1 + A_2 \sin\left(2mg\frac{2\pi x}{\lambda}\right)\right\} \quad (3.14)$$

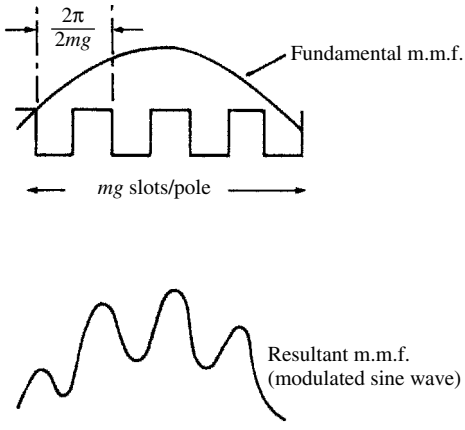


Figure 3.10 Slot harmonics

which has a fundamental frequency component, i.e.

$$A_1 B \sin\left(\frac{2\pi x}{\lambda}\right) \tag{3.15}$$

and frequency components expressed as

$$A_2 B \sin\frac{2\pi x}{\lambda} \sin\left(2mg\frac{2\pi x}{\lambda}\right) = \frac{A_2 B}{2}\left\{\cos\left(\frac{2\pi x}{\lambda}(2mg-1)\right) - \cos\left(\frac{2\pi x}{\lambda}(2mg+1)\right)\right\} \tag{3.16}$$

Therefore slotting gives rise to harmonics of orders $2mg \pm 1$.

3.3.4 Voltage Harmonics Produced by Synchronous Machines

If the magnetic flux of the field system is distributed perfectly sinusoidally around the air gap, then the e.m.f. generated in each full-pitched armature coil is $2\pi f\phi \sin \omega t$ volts per turn. Here ϕ is the total flux per pole and the frequency f is related to speed N (in revolutions per second) and pole pairs p by $f = Np$. However the flux is never exactly distributed in this way, particularly in salient pole machines. A non-sinusoidal field distribution can be expressed as a harmonic series:

$$F(x) = F_1 \sin\left(\frac{2\pi x}{\lambda}\right) + F_3 \sin\left(\frac{3 \times 2\pi x}{\lambda}\right) + F_5 \sin\left(\frac{5 \times 2\pi x}{\lambda}\right) + \cdots \tag{3.17}$$

The machine can be considered to have $2p$ fundamental poles together with $6p, 10p, \ldots, 2np$ harmonic poles, all individually sinusoidal and all generating e.m.f.s in an associate winding. The winding e.m.f. can be expressed as a harmonic series:

$$E(t) = E_1 \sin \omega t + E_3 \sin 3\omega t + E_5 \sin 5\omega t + \cdots \tag{3.18}$$

The magnitudes of the harmonic e.m.f.s are determined by the harmonic fluxes, the effective electrical phase spread of the winding, the coil span, and the method of interphase connection.

For an integral slot winding with g slots per pole per phase and an electrical angle α between slots, the distribution factor for the nth harmonic is

$$k_{dn} = \frac{\sin(ng\alpha/2)}{g\sin(n\alpha/2)} \tag{3.19}$$

If the coils are chorded to cover $(\pi \pm \theta)$ electrical radians, the flux linked is reduced by $\cos(\theta/2)$ and the e.m.f. is reduced in proportion. The effective chording angle for harmonics of order n is $n\theta$. Hence the general coil-span factor is

$$k_{sn} = \cos(n\theta/2) \tag{3.20}$$

By suitable choice of k_d and k_s many troublesome e.m.f. harmonics can be minimised or even eliminated. The triplen harmonics in a three-phase machine are generally eliminated by phase connection, and it is usual to select the coil span to reduce fifth and seventh harmonics.

Standby generators with neutral require special consideration in this respect, as illustrated by the following example.

A standby generator had to be designed to supply a 250 kVA load consisting mainly of fluorescent lighting appliances. A neutral current of 40 A was considered sufficient for the generator design. However, in practice the machine generated 250 A of third-harmonic zero sequence and had to be rewound with a two-thirds pitch (i.e. $k_{s3} = \cos(3 \times 60/2) = 0$).

Slotting (the slots being on the stator) produces variation of permeance, which may be represented as $A_2 \sin[2mg(2\pi x/\lambda)]$. The fundamental rotor m.m.f. can be represented as a travelling wave $F_1 \cos[(2\pi x/\lambda - \omega t)]$. The slot ripple component of flux density is of the form

$$F_1 A_2 \sin\left(2mg\frac{2\pi x}{\lambda}\right)\cos\left(\frac{2\pi x}{\lambda} - \omega t\right) \tag{3.21}$$

This can be resolved into two counter-rotating components, i.e.

$$\frac{F_1 A_2}{2}\left\{\sin\left[(2mg+1)\frac{2\pi x}{\lambda} - \omega t\right] + \sin\left[(2mg-1)\frac{2\pi x}{\lambda} + \omega t\right]\right\} \tag{3.22}$$

which are slow-moving multi-pole harmonics. Their wavelengths are $\lambda/(2mg \pm 1)$ and the corresponding velocities are $f\lambda/(2mg \pm 1)$. As the number of waves passing any point on the stator per second is (speed $\div$ wavelength), obviously each component induces an e.m.f. of fundamental frequency in the armature.

Relative to the rotor, however, these two waves have different velocities. The rotor velocity being $f\lambda$, the waves travel at velocities $f\lambda - [f\lambda/(2mg+1)]$ and $f\lambda + [f\lambda/(2mg-1)]$ with respect to the rotor. In any closed rotor circuit each of these will generate currents of frequency $2mgf$ (by considering the ratio of speed to wavelength) and these superimpose a time-varying m.m.f. at frequency $2mgf$ on the rotor

fundamental m.m.f. This can be resolved into two counter-rotating components relative to the rotor, each travelling at high velocity $2mgf\lambda$, and therefore at $2mgf\lambda \pm f\lambda$ relative to the stator. The resultant stator e.m.f.s have frequencies $(2mg \pm 1)f$.

Slot harmonics can be minimised by skewing the stator core, displacing the centre line of damper bars in successive pole faces, offsetting the pole shoes in successive pairs of poles, shaping the pole shoes, and by the use of composite steel–bronze wedges for the slots of turboalternators.

It can be shown that the distribution factor for slot harmonics is the same as for the fundamental e.m.f.; it is not reduced by spreading the winding. Fractional instead of integral slotting should be used.

3.3.5 Rotor Saliency Effects

In the extreme case of perfect saliency, the flux concentrates exclusively in the direct axis of the rotor. If the stator current is of positive sequence, the field produced by this current in the rotor is stationary, and only causes armature reaction at the fundamental frequency. On the other hand, the flux produced by a negative sequence stator current can be divided into two components rotating in opposite senses, which therefore induce two e.m.f.s in the stator, one of them of negative sequence at the fundamental frequency and the other of positive sequence at third harmonic. The latter, using the same reasoning, will produce fifth-harmonic voltage and this in turn will create some seventh harmonic, etc. This mechanism is illustrated in Figure 3.11 for the case of a machine connected to an asymmetrical transmission line.

The above reasoning can be extended to the presence of harmonic currents in the stator. If the stator contains a current of harmonic order h and positive sequence, the rotor flux will include two opposite rotating fields of order $(h-1)$ that will induce a positive sequence voltage of order h and a negative sequence voltage of order $(h-2)$. Similarly the negative sequence current of order h will produce two opposite rotating fields of order $(h+1)$ that will cause a negative sequence voltage of order h and another positive sequence of order $(h+2)$. This effect is illustrated in Figure 3.12 with reference to the presence of seventh harmonic, of either positive or negative sequence.

In practice, as the machine poles are not completely salient and the transmission line is approximately symmetrical, the effect discussed above is not significant. Consequently, when carrying out harmonic penetration studies, the salient pole effect is normally neglected and the synchronous machine represented as a linear impedance.

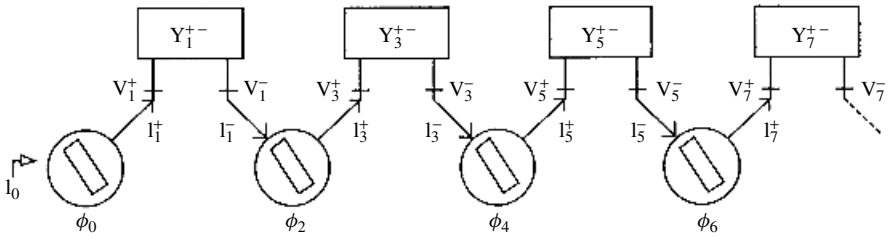


Figure 3.11 Mechanism of harmonic generation in a machine with salient poles

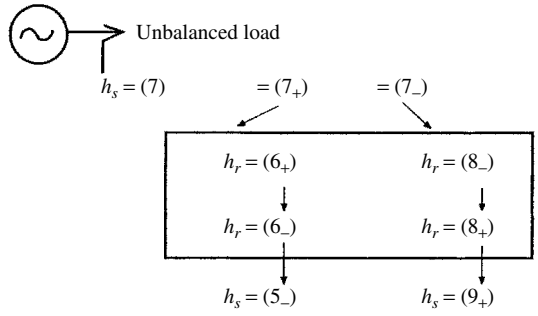


Figure 3.12 Response of a salient-pole synchronous generator to the presence of a harmonic current

However, in special cases when either the load is asymmetrical or the generator feeds static converter equipment the machine can be an important source of harmonic generation.

3.3.6 Voltage Harmonics Produced by Induction Motors

The speed of the synchronous rotating field of the stator of an induction motor is the fundamental frequency times the wavelength, i.e. $f_1\lambda$. For a slip s, the rotor speed is thus $f_1\lambda(1-s)$ and the frequency of the rotor currents sf_1.

Time harmonics are produced by induction motors as a result of the harmonic content of the m.m.f. distribution and are speed dependent.

A harmonic of order n in the rotor m.m.f. (i) has a wavelength λ/n; (ii) travels at a speed $\pm(sf)\lambda/n$ with respect to the rotor; and (iii) travels at a speed $f\lambda(1-s) \pm (sf)\lambda/n$ with respect to the stator.

This harmonic induces an e.m.f. in the stator at a frequency equal to the ratio speed ÷ wavelength, i.e.

$$f^1 = \frac{f\lambda(1-s) \pm (sf)(\lambda/n)}{\lambda/n} = f\{n - s(n \pm 1)\} \tag{3.23}$$

the positive sign being taken when the harmonic rotor m.m.f. travels in the opposite direction to the fundamental.

Harmonics can also occur as a result of electrical asymmetry. Consider an electrically unbalanced rotor winding, the stator winding being balanced such that the supply voltage produces a pure rotating field travelling at speed $f\lambda$. Slip frequency e.m.f. is induced in the rotor but, since the rotor winding is unbalanced, both positive and negative phase sequence currents will flow, giving fields in the forward and reverse directions. These travel at speed $\pm sf\lambda$ with respect to the rotor, and therefore at $f\lambda(1-s) \pm sf\lambda$ with respect to the stator. The frequencies of stator e.m.f.s induced by these fields are f and $(1-2s)f$, the latter being considered here as a harmonic frequency. Interaction of harmonic and mains frequency currents results in beats at this low frequency $2sf$ being registered on connected meters.

Table 3.1 Typical harmonic currents produced by a wound-rotor induction motor

Frequency (Hz)	Current as a percentage of fundamental	Cause
20	3.0	Pole unbalance
40	2.4	Rotor phase unbalance
50	100.0	Fundamental mutual
80	2.3	Pole unbalance
220	2.9	5th and 7th harmonic
320	3.0	mutuals
490	0.3	11th and 13th harmonic
590	0.4	mutuals

Source: [4]

An idea of the relative magnitudes of the harmonic current produced by a wound-rotor induction motor and their cause is given in Table 3.1 for a six-pole motor running at a speed of 0.9 per unit.

3.4 Distortion Caused by Arcing Devices

The voltage-current characteristics of electric arcs are highly nonlinear. Following arc ignition the voltage decreases due to the short-circuit current, the value of which is only limited by the power system impedance.

The main harmonic sources in this category are the electric arc furnace, discharge-type lighting with magnetic ballasts, and to a lesser extent arc welders.

3.4.1 Electric Arc Furnaces

The voltage-current characteristic of an arc furnace has a quasi-trapezoidal shape and its magnitude is a function of the length of the arc. The current levels, limited mainly by the furnace cables (and leads) and transformer, can reach values of over 60 kA. Those impedances have a buffering effect on the supply voltage and thus the arcing load appears as a relatively stable current harmonic source.

However, the stochastic voltage changes due to the sudden alterations of the arc length produce a spread of frequencies, predominantly in the range 0.1–30 Hz [5] about each of the harmonics present. This effect is more evident during the melting phase, caused by continuous motion of the melting scrap and the interaction of electromagnetic forces between the arcs.

During the refining part of the process the arc is better behaved, but there is still some modulation of the arc length by waves on the surface of the molten metal.

Typical time-averaged frequency spectra of the melting and refining periods are shown in Figure 3.13.

However, the levels of harmonic currents vary markedly with time, and are better displayed in the form of probabilistic plots, such as that shown in Figure 3.14.

Three sets of averaged harmonic current levels obtained by different investigators are listed in Table 3.2 as percentages of the fundamental.

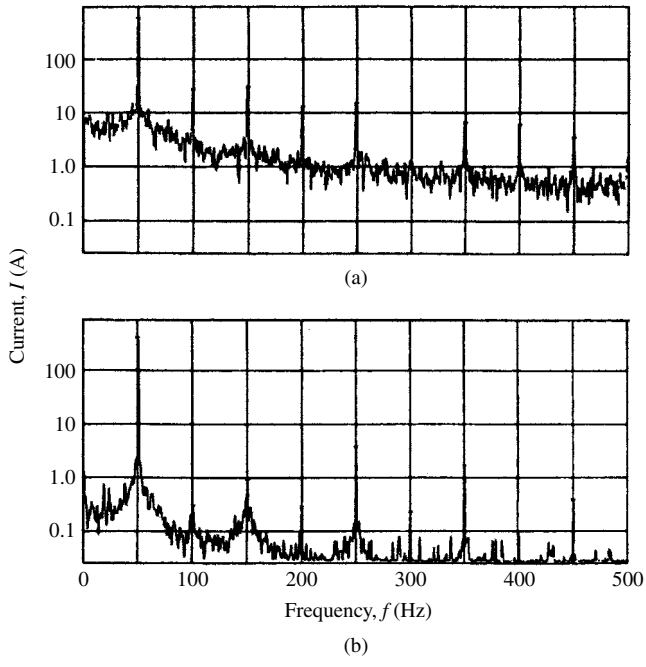


Figure 3.13 Frequency spectra for (a) melting and (b) refining periods

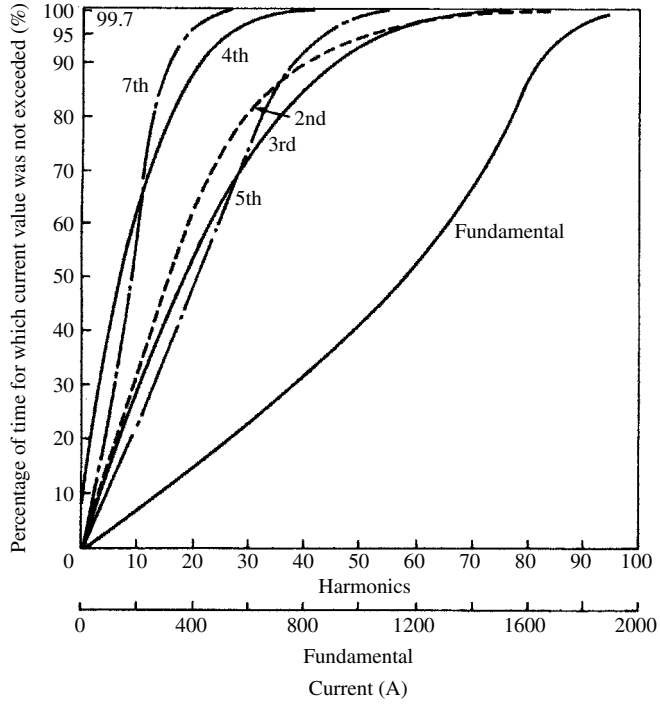


Figure 3.14 Probabilistic harmonic magnitude plots

Table 3.2 Average harmonic levels from arc furnaces expressed as percentages of the fundamental

Order	Level		
	[7]	[5]	[6]
2	3.2	4.1	4.5
3	4.0	4.5	4.7
4	1.1	1.8	2.8
5	3.2	2.1	4.5
6	0.6	Not given	1.7
7	1.3	1.0	1.6
8	0.4	1.0	1.1
9	0.5	0.6	1.0
10	>0.5	>0.5	>1.0

Note: [6] also found levels of 1% at the 22nd harmonic

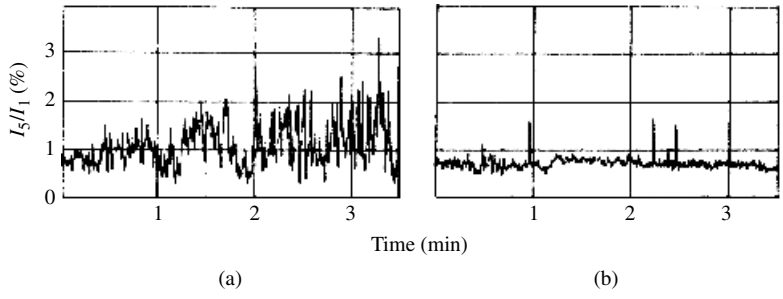


Figure 3.15 Fifth harmonic as a percentage of the fundamental with time [5]: (a) melting; (b) refining

Finally, the time variation of the harmonic currents is exemplified by the records shown in Figure 3.15 for the fifth harmonic, an important point being that the harmonic current varies not only with time but also in respect to the fundamental component.

3.4.2 Discharge-Type Lighting

Luminous discharge lighting is highly nonlinear and gives rise to considerable odd-ordered harmonic currents. This effect is clearly illustrated in Figure 3.16, which shows the current waveform and harmonic spectrum of a high-efficiency lamp.

This effect is particularly important in the case of fluorescent lamps, given the large concentration of this type of lighting. Additional magnetic ballasts are needed to limit the current to within the capability of the fluorescent tube and stabilise the arc.

In a three-phase, four-wire load the triplen harmonics are basically additive in the neutral, the third being the most dominant.

With reference to the basic fluorescent circuit of Figure 3.17, a set of voltage and current oscillograms is displayed in Figure 3.18. These waveforms are shown with

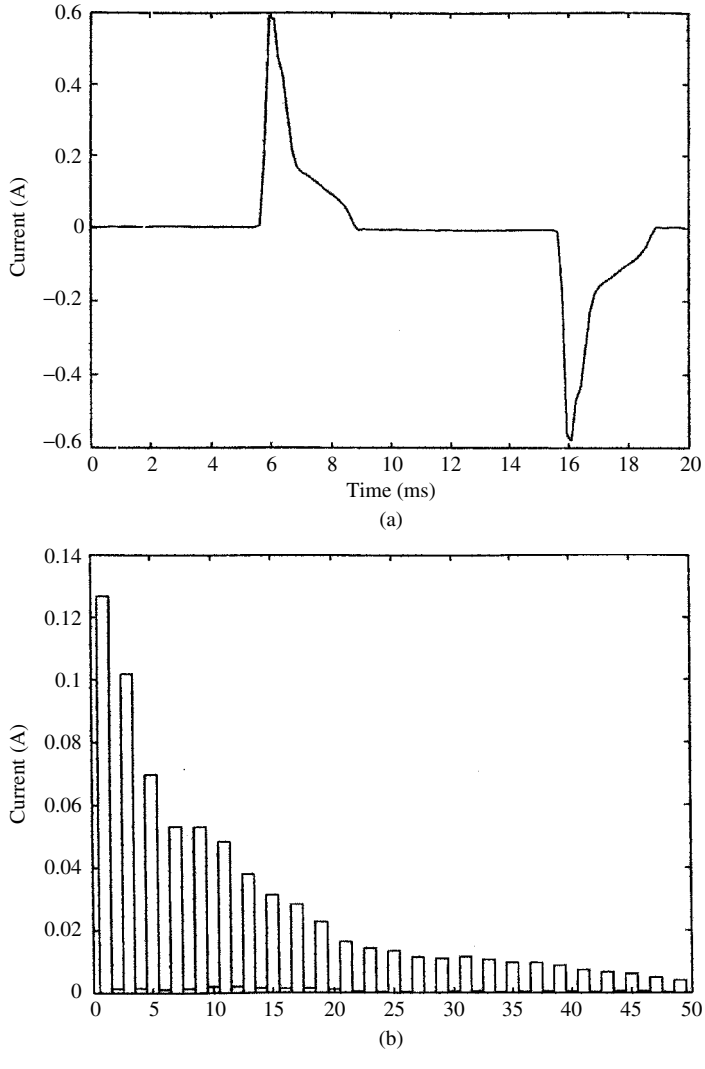


Figure 3.16 Current wave (a) and spectrum (b) of a high-efficiency discharge lamp

reference to the sinusoidal phase voltage supply. The voltage across the tube itself (Figure 3.18(a)) clearly illustrates the nonlinearity. The waveform in Figure 3.18(b) shows the phase current, and the waveform in Figure 3.18(c) the neutral current for a case of three banks of three lamps connected in star. The latter consists almost exclusively of third harmonic.

Lighting circuits often involve long distances and have very little load diversity. With individual power factor correction capacitors, the complex LC circuit can approach a condition of resonance at third harmonic. This effect has been illustrated by laboratory results in a balanced three-phase fluorescent lamp installation [8]. The results of greatest interest refer to the effects of increasing the neutral reactance and isolating the capacitor star point (see Figure 3.17). In the graph of Figure 3.19 the abscissa used is

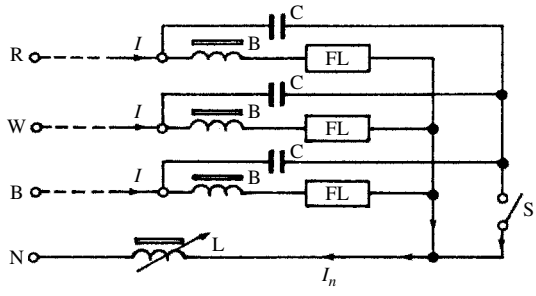


Figure 3.17 Three-phase fluorescent lighting test circuit. FL, fluorescent lamp; B, ballast; C, power factor correction capacitor; L, variable inductor; S, switch to isolate capacitor star point

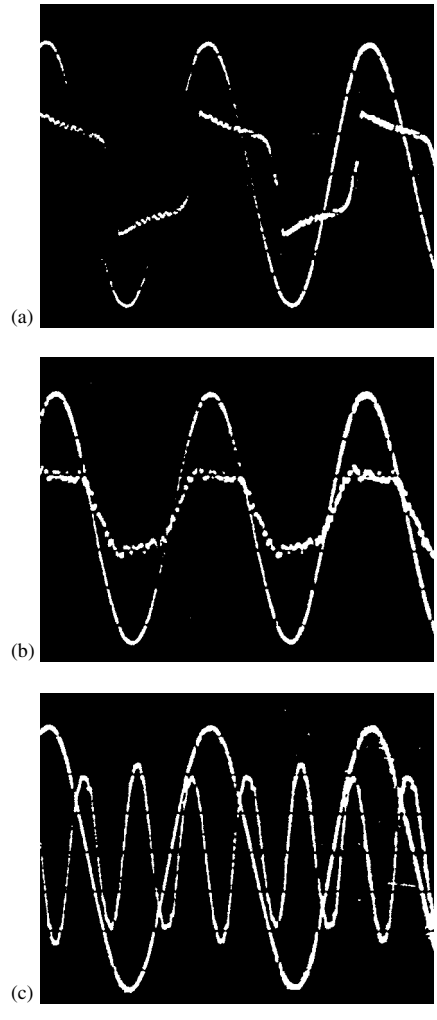


Figure 3.18 (a) Tube voltage; (b) phase current with capacitor, one lamp, 240 mA/division; (c) neutral current, three banks of three lamps in star, 240 mA/division

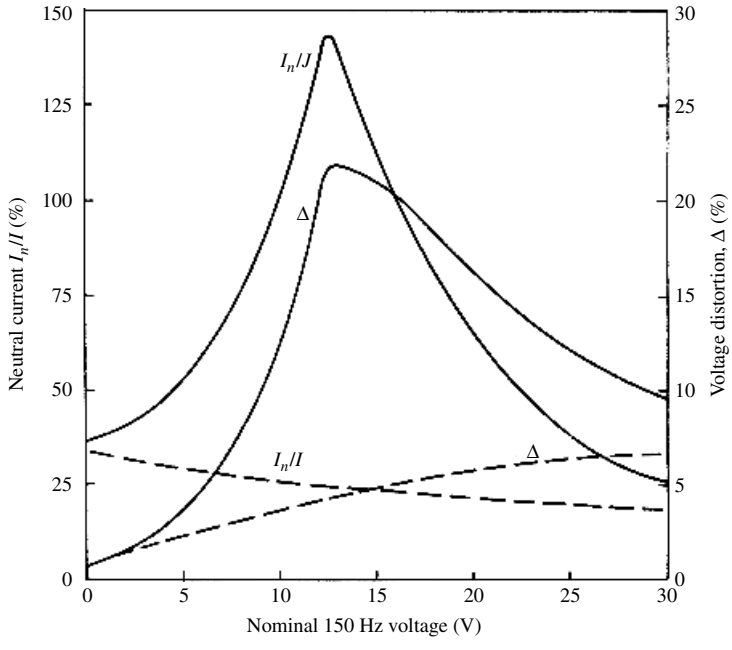


Figure 3.19 Characteristics of the fluorescent lighting test circuit. The nominal 150 Hz voltage is the calculated product of the 150 Hz lamp current per phase and the circuit zero-sequence impedance (150 Hz). (———), Switch S closed (star point connected to neutral); (- - - -), switch S open (star point floating)

the nominal third harmonic voltage, i.e. the product of the lamp third harmonic current per phase and the corresponding circuit third harmonic zero-sequence impedance. It can be seen that with the capacitor star point connected to the neutral, the third harmonic neutral current can by far exceed the nominal value calculated by the conventional method based on three times the nominal lamp current. With the star point disconnected the neutral current is less than the nominal value.

The results demonstrated in the laboratory test were in fact a confirmation of actual field test results taken on a 900 kVA fluorescent installation. In this case the full load condition operated well above the resonant point; at about half load some neutral current values exceeded the corresponding phase current values, and the voltage distortion at some distribution boards exceeded 20%.

Whenever possible, the design procedure recommended to avoid resonance is to try to avoid individual lamp compensation, providing, instead, capacitor banks adjacent to distribution boards connected either in star with floating neutral or in delta.

3.5 Single-Phase Rectification

3.5.1 D.C. Power Supplies

Many commercial and domestic appliances require direct current for their operation. The single-phase diode bridge rectifier (Figure 3.20) has become a popular power

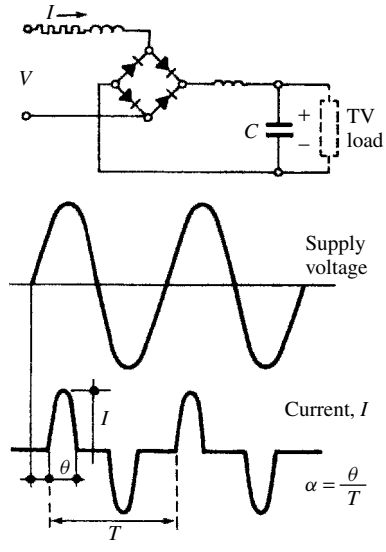


Figure 3.20 Single-phase diode rectifier bridge and d.c. capacitor power source

source for these appliances because of its reduced cost and relatively low sensitivity to supply voltage variations under normal operating conditions.

The circuit of Figure 3.20 produces a very narrow current pulse at every half-cycle of the supply frequency, because the d.c. capacitor is recharged only when the supply voltage exceeds the d.c. level (i.e. close to the peak of the voltage sine wave).

The Fourier series of the current pulse of Figure 3.20 has the expression:

$$I_n = \frac{8\alpha I}{\pi} \sum_{n=1,3,5}^{\infty} \frac{\cos n\alpha\pi}{1 - n^2\alpha^2\pi^2} \cos n\omega t \tag{3.24}$$

where I is the impulse peak value and $\alpha = \theta/T$ its duration as a proportion of the fundamental wave.

Earlier technology used a transformation stage to control the required low voltage levels and the transformer leakage inductance had a smoothing effect that resulted in low harmonic current levels.

Instead, modern appliances use the switch-mode power supply concept, whereby the input rectifier is directly connected to the a.c. source, as in Figure 3.20; however, in this case the rectified voltage is converted back to a.c. at a very high frequency and then rectified again. This process provides a very compact design and efficient operation, tolerating large variations in input voltage. Personal computers and most office and domestic appliances, as well as the electronic ballast of modern fluorescent lighting systems, are now of this type. However, the lack of a.c. side inductance smoothing lets the narrow current pulses pass directly into the a.c. system, thus increasing considerably the current harmonic content. Particularly troublesome is the third harmonic, which adds arithmetically in the neutral of the three-phase network.

The current harmonics calculated from equation (3.24) assume that the supply voltage is itself undistorted. In practice, however, the accumulation of current pulses, placed

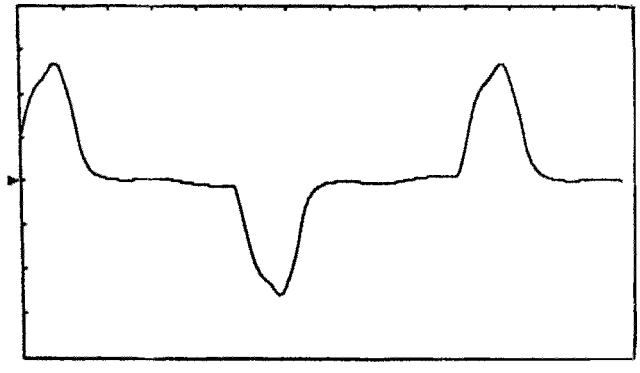
at the centre of the voltage waveform, flattens the voltage sine wave at the peak; the flat top has the effect of widening the current pulses used to charge the capacitors, thus reducing the harmonic current injections.

Typical examples of single-phase distorting appliances are TV receivers, personal computers and microwave ovens.

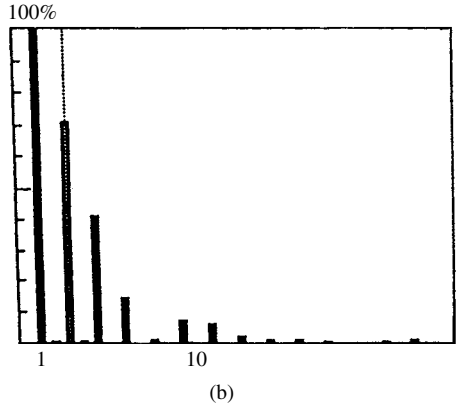
TV Receivers Figure 3.21 shows the current waveform and its harmonic spectrum (as a percentage of the fundamental component) of a 23″ TV set obtained from a harmonic analyser. The main harmonics are in order of magnitude the third, fifth, seventh and ninth.

PC and Printer Figure 3.22 shows the harmonic spectrum generated by a combination of a personal computer and a printer. Again, the main component is the third (72%), followed by the fifth (60%), seventh (40%) and ninth (22.6%).

To illustrate the cumulative effect of this type of load, imagine the case of a high office block, which may have up to 1000 personal computers. If a 1000 kVA, 11 kV/440 V transformer supplies the building at say 0.95 power factor, the rated fundamental current will be 1248 A. From the spectrum of Figure 3.22, and assuming a



(a)



(b)

Figure 3.21 (a) Current waveform and (b) harmonic spectrum generated by a 23″ TV set

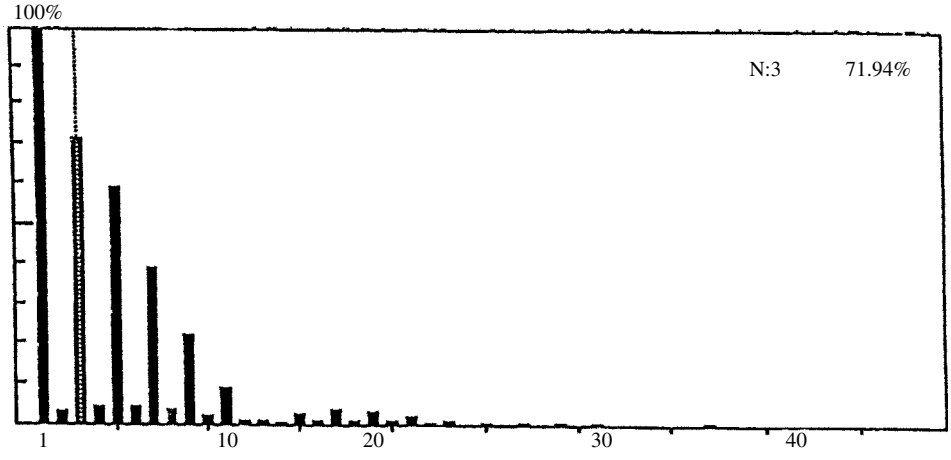


Figure 3.22 Harmonic currents generated by a PC/printer combination

1 A fundamental current per PC, the main harmonic current components per phase will be approximately:

$$I_3 = (1000/3)(0.72) = 240 \text{ A}$$
$$I_5 = (1000/3)(0.6) = 200 \text{ A}$$
$$I_7 = (1000/3)(0.4) = 133 \text{ A}$$
$$I_9 = (1000/3)(0.226) = 75 \text{ A}$$

The corresponding total demand distortion is:

$$\text{TDD}(\%) = 100\frac{\sqrt{(240^2 + 200^2 + 133^2 + 75^2)}}{1248} = 28\%$$

Moreover, the transformer neutral current will contain 720 A (3×240) of third harmonic and 225 A (3×75) of ninth harmonic, i.e. practically the same rating as the phase conductors!

Microwave Oven Figure 3.23 shows a recording of the current waveform and corresponding spectrum generated by a domestic microwave appliance, which again consists mainly of third, fifth and seventh harmonics.

3.5.2 Line-Commutated Railway Rectifiers

The application of single-phase rectification in hundreds of kilowatts is widespread in the railway electrification industry. A typical configuration of the locomotive power supply, shown in Figure 3.24, uses individual bridge control of two groups of two bridge converters connected in series to a parallel connection of two d.c. locomotive

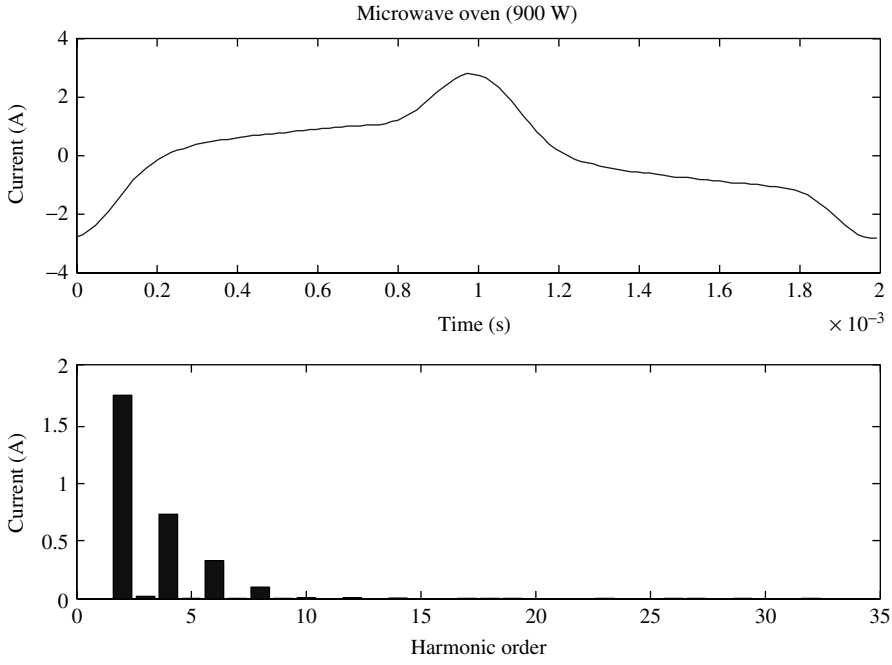


Figure 3.23 Current harmonics generated by a microwave oven

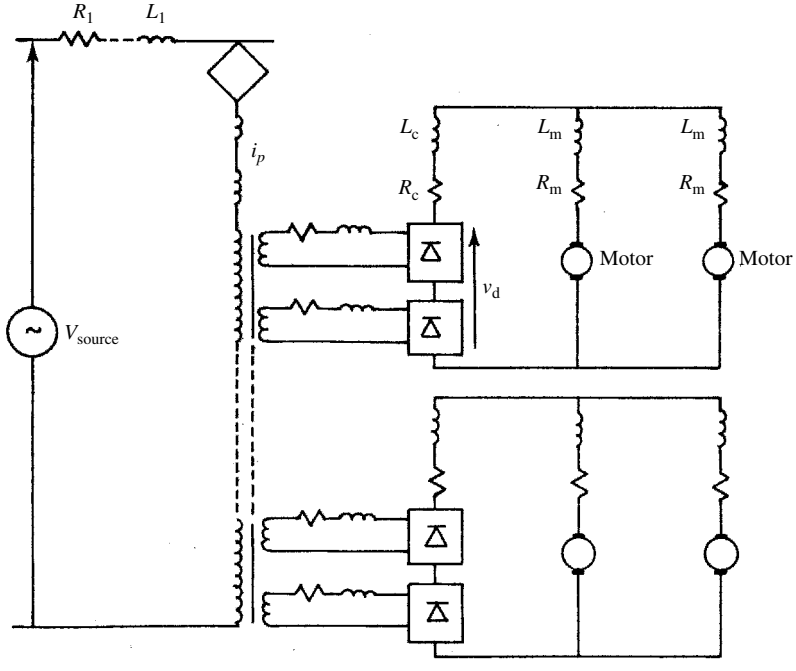


Figure 3.24 Typical locomotive power circuit

motors. At the start, the back e.m.f. of the d.c. motors is zero, the supply d.c. voltage is low and the delay angle large. Therefore during the initial accelerating period, with maximum d.c. motor current, the bridge rectifier produces the worst harmonic currents and operates with the lowest power factor. To alleviate the situation at low speeds, one of the bridges is often bypassed and phase control exercised on the other. When the speed builds up, and the second bridge operates on minimum delay, phase control is exercised on the first bridge. The relevant waveforms are illustrated in Figure 3.25.

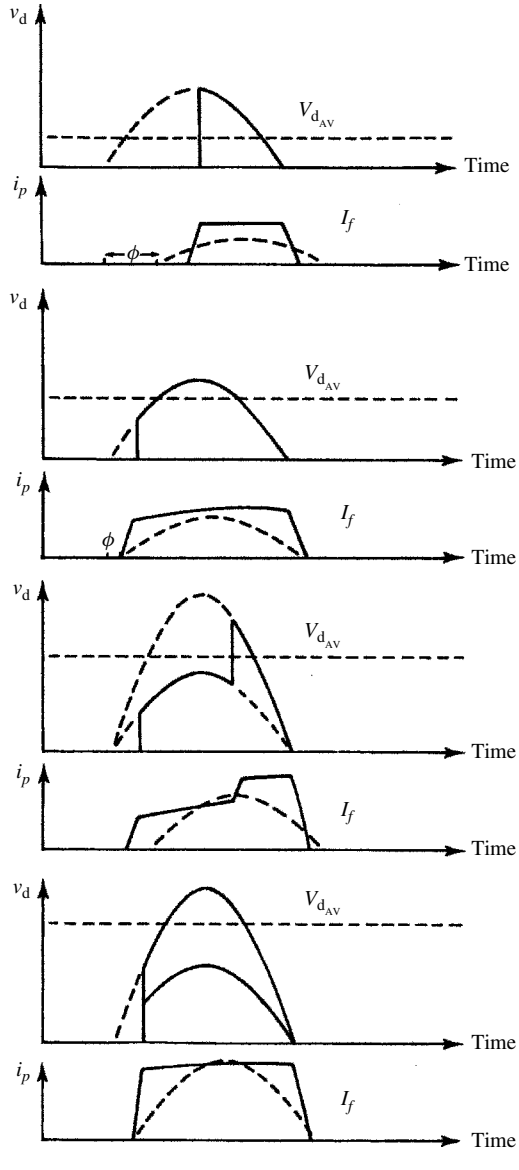


Figure 3.25 Voltage and current waveforms of a double bridge individually controlled converter

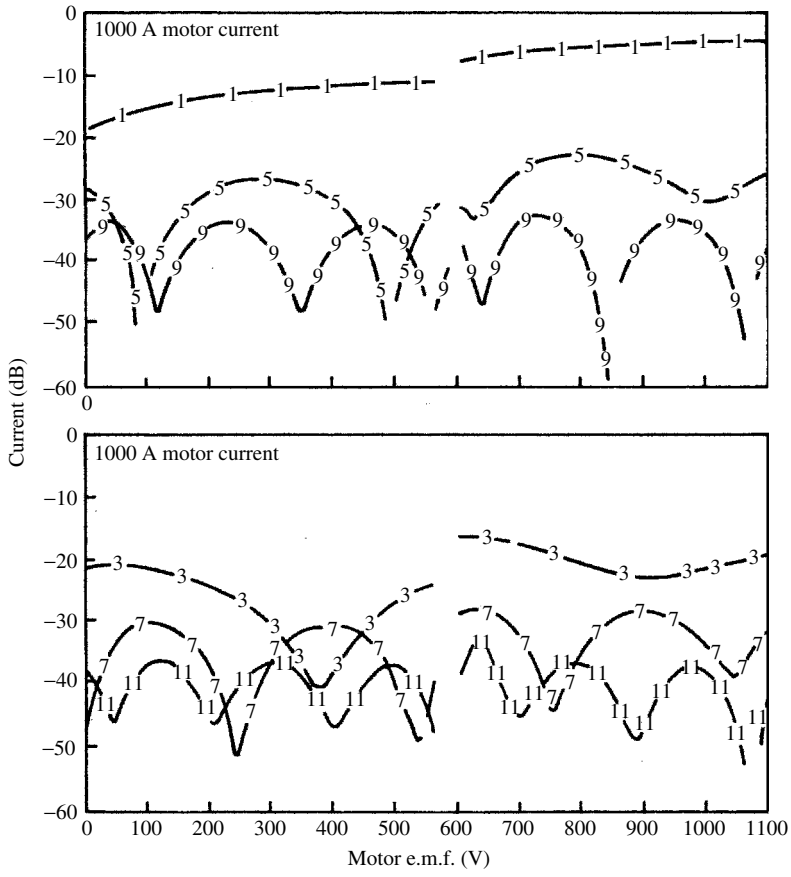


Figure 3.26 Variation in harmonic currents with locomotive operation

An indication [9] of the wide variation in harmonic current magnitudes corresponding to the waveform of Figure 3.25 is given in Figure 3.26.

3.6 Three-Phase Current-Source Conversion

A current-source converter is characterised by a very inductive d.c. side configuration relative to the a.c. system side. This is achieved by means of a series smoothing reactor on the d.c. side. As the a.c. system is predominantly inductive, some shunt capacitance (normally in the form of tuned filters) must be connected to the a.c. side of the converter. Under these conditions, the d.c. current is reasonably constant and the converter acts as a source of harmonic voltage on the d.c. side and of harmonic current on the a.c. side. The switches must block voltages of both polarities, but are only required to conduct current in one direction. Thus, large converters have traditionally been of the current-source type because of the availability of efficient highly rated thyristors.

Under perfectly symmetrical a.c. system conditions the resulting currents are exactly the same in all phases.

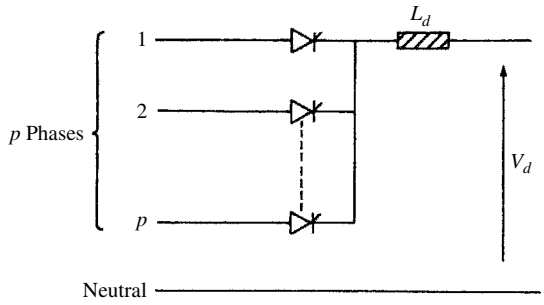


Figure 3.27 p-Phase one-way converter

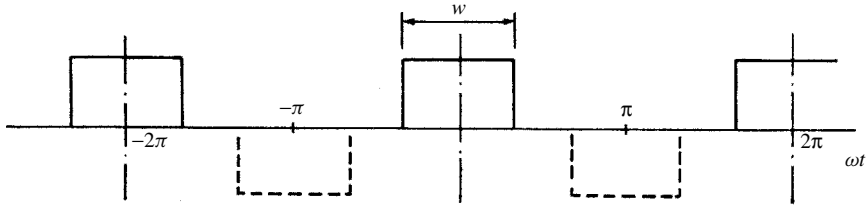


Figure 3.28 Trains of positive and negative pulses

The ideal p-phase one-way converter, illustrated in Figure 3.27, has zero a.c. system impedance and infinite smoothing inductance. Under these conditions the phase currents consists of periodic positive rectangular pulses of width $w = 2\pi/p$, repeating at the supply frequency.

If in the analysis of the waveform of Figure 3.28, the origin is taken at the centre of the pulse, $F(\omega t)$ is shown to be an 'even' function (i.e. $f(x) = f(-x)$) and the Fourier series has only cosine terms. The relevant Fourier coefficients, with reference to a 1 per unit-d.c. current, are

$$A_0 = \frac{1}{2\pi}\int_{-w/2}^{w/2} \mathrm{d}(\omega t) = \frac{w}{2\pi} = \frac{1}{p} \tag{3.25}$$

$$A_n = \frac{1}{\pi}\int_{-w/2}^{w/2} \cos(n\omega t)\,\mathrm{d}(\omega t) = \frac{2}{n\pi}\sin\left(\frac{n\pi}{p}\right) \tag{3.26}$$

The corresponding Fourier series for the positive current pulses is

$$F_p = \frac{2}{\pi}\left(\frac{w}{4} + \sin\left(\frac{w}{2}\right)\cos(\omega t) + \frac{1}{2}\sin\left(\frac{2w}{2}\right)\cos(2\omega t) + \frac{1}{3}\sin\left(\frac{3w}{2}\right)\cos(3\omega t) + \frac{1}{4}\sin\left(\frac{4w}{2}\right)\cos(4\omega t) + \cdots\right) \tag{3.27}$$

An ideal p-phase, two-way converter producing positive and negative current pulses is shown in Figure 3.29.

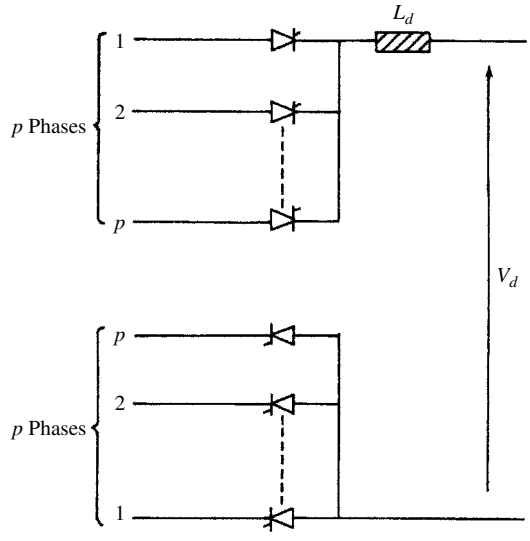


Figure 3.29 p-Phase two-way converter

Applying equations (3.25) and (3.26) to the negative group gives the following Fourier series

$$F_n = \frac{2}{\pi}\left(-\frac{w}{4} + \sin\left(\frac{w}{2}\right)\cos(\omega t) - \frac{1}{2}\sin\left(\frac{2w}{2}\right)\cos(2\omega t) + \frac{1}{3}\sin\left(\frac{3w}{2}\right)\cos(3\omega t) - \frac{1}{4}\sin\left(\frac{4w}{2}\right)\cos(4\omega t) + \cdots\right) \tag{3.28}$$

The phase current of the two-way configuration consists of alternate positive and negative pulses such that $F(\omega t + \pi) = -F(\omega t)$. Its Fourier series is obtained by combining equations (3.27) and (3.28)

$$F = F_p + F_n = \frac{4}{\pi}\left(\sin\left(\frac{w}{2}\right)\cos(\omega t) + \frac{1}{3}\sin\left(\frac{3w}{2}\right)\cos(3\omega t) + \frac{1}{5}\sin\left(\frac{5w}{2}\right)\cos(5\omega t) + \cdots\right) \tag{3.29}$$

in which the d.c. component and even-ordered harmonics have been eliminated.

For the square wave of Figure 3.30(a) $w = \pi$ which on substituting into equation (3.29) gives as the equation for the waveform in the frequency domain

$$F(t) = \frac{4}{\pi}\left(\cos(\omega t) - \frac{1}{3}\cos(3\omega t) + \frac{1}{5}\cos(5\omega t) - \frac{1}{7}\cos(7\omega t) + \cdots\right) \tag{3.30}$$

in which harmonics of order $n = 1, 5, 9$, etc. are of positive sequence and those of order $n = 3, 7, 11$, etc. are of negative sequence.

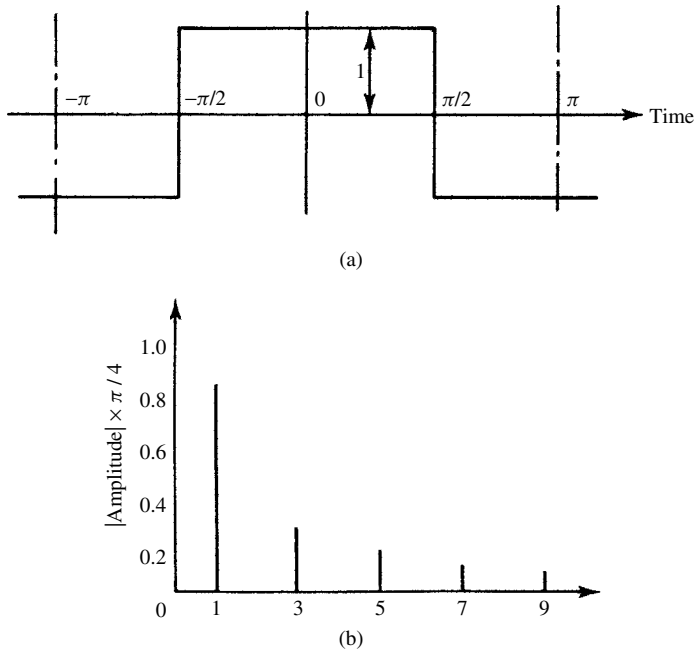


Figure 3.30 (a) Time-domain representation and (b) frequency-domain representation of a square wave

The frequency-domain representation of the square wave harmonic amplitudes is shown in Figure 3.30(b).

The time-domain waveforms can also be synthesised from the combination of the time-domain representation of the individual harmonics. Figure 3.31 shows this synthesis process for the square wave considered above. For clarity only the fundamental, third and fifth harmonics have been shown and the complex waveform produced is therefore not complete.

3.6.1 Basic (Six-Pulse) Configuration

Six-pulse rectification (and inversion) is obtained from three-phase two-way configurations. Substituting $w = 2\pi/3$ in equation (3.29) and inserting the actual d.c. current I_d, the frequency domain representation of the a.c. current in phase a is

$$i_a = \frac{2\sqrt{3}}{\pi} I_d \left(\cos(\omega t) - \frac{1}{5}\cos(5\omega t) + \frac{1}{7}\cos(7\omega t) - \frac{1}{11}\cos(11\omega t) + \frac{1}{13}\cos(13\omega t) - \frac{1}{17}\cos(17\omega t) + \frac{1}{19}\cos(19\omega t) \cdots \right) \tag{3.31}$$

The three-phase currents are shown in Figure 3.32(b), (c) and (d), respectively. Some useful observations can now be made from equation (3.31):

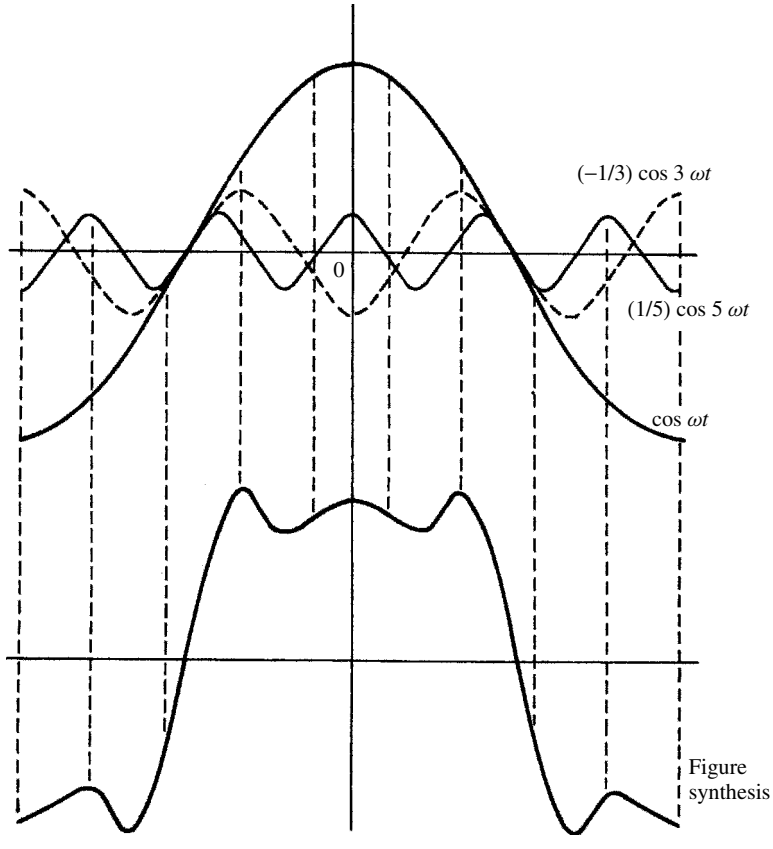


Figure 3.31 Waveform synthesis of a square wave

(1) The absence of triple harmonics.

(2) The presence of harmonics of orders $6k \pm 1$ for integer values of k.

(3) Those harmonics of orders $6k + 1$ are of positive sequence and those harmonics of orders $6k - 1$ are of negative sequence. This statement may not be obvious. Let us clarify it with reference to the fundamental, third (although not present in the symmetrical case) and fifth harmonic current components.
The three-phase currents of the fundamental frequency are

$$R(1_{\angle 0})$$
$$Y(1_{\angle -120})$$
$$B(1_{\angle 120})$$

i.e. of positive-sequence rotation.
The three-phase currents of the third harmonic component (had it existed) would be

$$R(1/3)_{\angle 0}$$

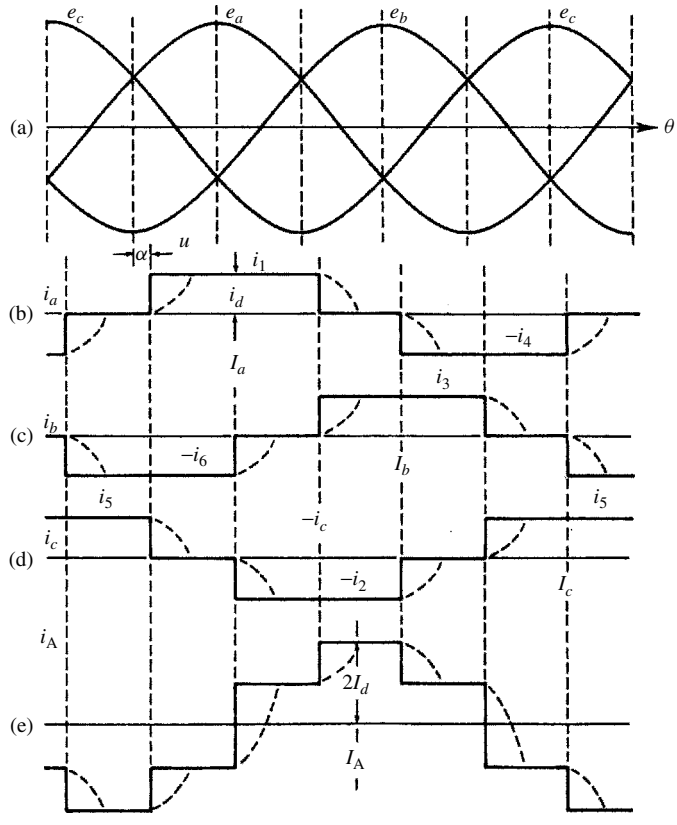


Figure 3.32 Six-pulse bridge waveforms: (a) phase to neutral voltages; (b)–(d) phase currents on the converter side; (e) phase current on the system side with delta–star transformer

$$Y(1/3)_{\angle(-120\times3)} = (1/3)_{\angle 0}$$
$$B(1/3)_{\angle(+120\times3)} = (1/3)_{\angle 0}$$

i.e. of zero-sequence rotation (however, it will be shown later that when the supply voltage is unbalanced, some positive-sequence third harmonic current will be produced).

The three-phase currents of the fifth harmonic component are

$$R(1/5)_{\angle 0}$$
$$Y(1/5)_{\angle(-120\times5)} = (1/5)_{\angle 120}$$
$$B(1/5)_{\angle(+120\times5)} = (1/5)_{\angle -120}$$

i.e. of negative-sequence rotation.

(4) The r.m.s. magnitude of the fundamental frequency is

$$I_1 = (1/\sqrt{2})(2\sqrt{3}/\pi)I_d = (\sqrt{6}/\pi)I_d \tag{3.32}$$

(5) The r.m.s. magnitude of the nth harmonic is

$$I_n = I_1/n \tag{3.33}$$

3.6.2 Effect of Transformer Connection

If either the primary or secondary three-phase windings of the converter transformer are connected in delta, the a.c. side current waveforms consist of the instantaneous differences between two rectangular secondary currents 120° apart as shown in Figure 3.32(e).

The Fourier series of the waveform shown in Figure 3.32(e) can be easily obtained from the general equation (3.29) by superimposing the results of two component pulses of widths π and $\pi/3$, respectively.

Moreover, to maintain the same primary and secondary voltages as for the star–star connection, a factor of $\sqrt{3}$ is introduced in the transformer ratio, and the current waveform is as shown in Figure 3.33.

The resulting Fourier series for the current in phase a on the primary side is

$$i_a = \frac{2\sqrt{3}}{\pi} I_d \left(\cos(\omega t) + \frac{1}{5}\cos(5\omega t) - \frac{1}{7}\cos(7\omega t) - \frac{1}{11}\cos(11\omega t) + \frac{1}{13}\cos(13\omega t) + \frac{1}{17}\cos(17\omega t) - \frac{1}{19}\cos(19\omega t) \cdots \right) \tag{3.34}$$

This series only differs from that of a star–star connected transformer by the sign of harmonic orders $6k \pm 1$ for odd values of k, i.e. the 5th, 7th, 17th, 19th, etc.

3.6.3 Twelve-Pulse Related Harmonics

Twelve-pulse configurations consist of two six-pulse groups fed from two sets of three-phase transformers in parallel, with their fundamental voltage equal and phase-shifted by 30°; a common 12-pulse configuration is shown in Figure 3.34.

Moreover, to maintain 12-pulse operation the two six-pulse groups must operate with the same control angle and therefore the fundamental frequency currents on the a.c. side of the two transformers are in phase with one another.

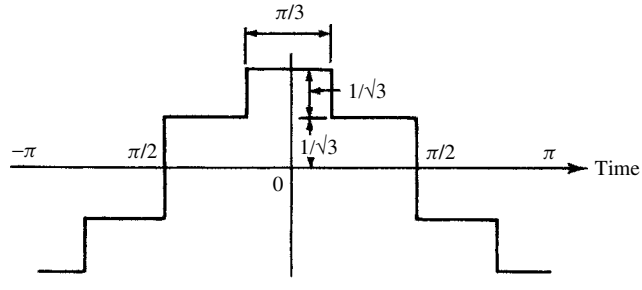


Figure 3.33 Time-domain representation of a six-pulse waveform with delta–star transformer

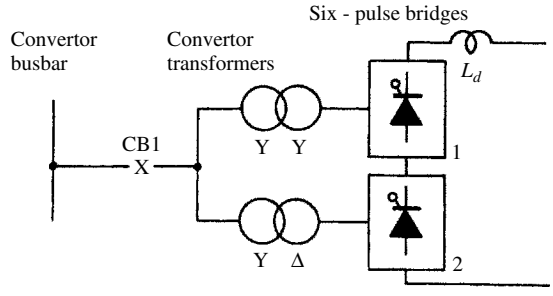


Figure 3.34 Twelve-pulse converter configuration

The resultant a.c. current is given by the sum of the two Fourier series of the star–star (equation (3.31)) and delta–star (equation (3.34)) transformers, i.e.

$$(i_a)_{12} = 2\left(\frac{2\sqrt{3}}{\pi}\right) I_d \left(\cos(\omega t) - \frac{1}{11}\cos(11\omega t) + \frac{1}{13}\cos(13\omega t) - \frac{1}{23}\cos(23\omega t) + \frac{1}{25}\cos(25\omega t)\cdots\right) \tag{3.35}$$

This series only contains harmonics of order $12k \pm 1$. The harmonic currents of orders $6k \pm 1$ (with k odd), i.e. $k = 5, 7, 17, 19$, etc., circulate between the two converter transformers but do not penetrate the a.c. network. The time-domain representation of the 12-pulse waveform is shown in Figure 3.35(a) and the corresponding frequency domain representation in Figure 3.35(b).

3.6.4 Higher-Pulse Configurations

In the last section, the use of two transformers with a 30° phase-shift has been shown to produce 12-pulse operation. The addition of further appropriately shifted transformers in parallel provides the basis for increasing pulse configurations.

For instance, 24-pulse operation is achieved by means of four transformers with 15° phase-shifts and 48-pulse operation requires eight transformers with 7.5° phase-shifts. Although theoretically possible, pulse numbers above 48 are rarely justified due to the practical levels of distortion found in the supply voltage waveforms, which can have as much influence on the voltage crossings as the theoretical phase-shifts.

Similarly to the case of the 12-pulse connection, the alternative phase-shifts involved in higher pulse configurations require the use of appropriate factors in the parallel transformer ratios to achieve common fundamental frequency voltages on their primary and secondary sides.

The theoretical harmonic currents are related to the pulse number (p) by the general expression $pk \pm 1$ and their magnitudes decrease in inverse proportion to the harmonic order. Generally harmonics above the 49th can be neglected as their amplitude is too small.

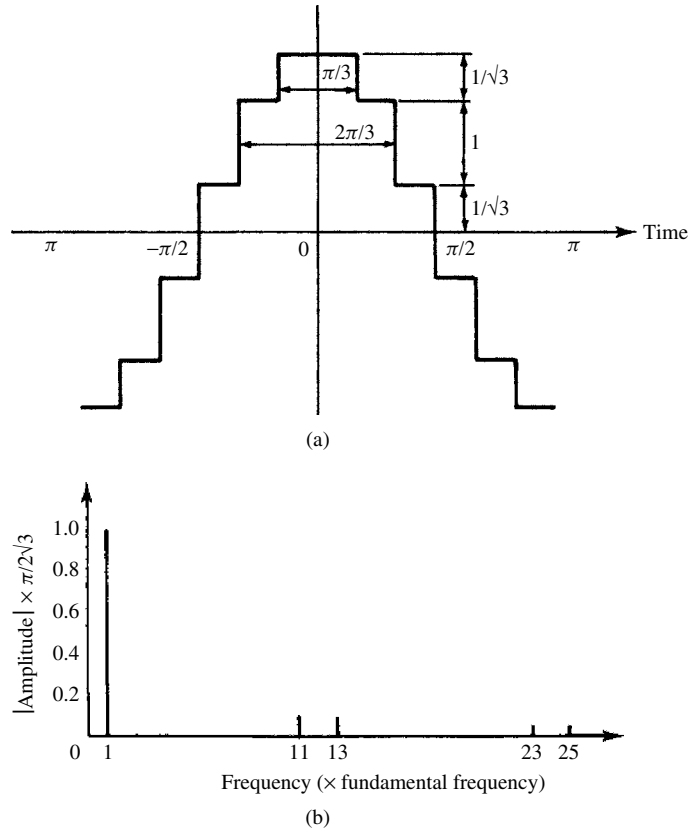


Figure 3.35 (a) Time-domain representation of the 12-pulse phase current; (b) frequency-domain representation of 12-pulse operation

3.6.5 Effect of Transformer and System Impedance

In practice the existence of reactance in the commutation circuit causes conduction overlap of the incoming and outgoing phases.

As we have seen in previous sections, high-pulse configurations are combinations of three-pulse groups, i.e. the commutation overlaps are those of the three-pulse groups as shown by the broken lines in Figure 3.32.

The current waveform has now lost the even symmetry with respect to the centre of the idealised rectangular pulse. Using as a reference the corresponding commutating voltage (i.e. the zero-voltage crossing) and assuming a purely inductive commutation circuit, the following expression defines the commutating current [10]

$$i_c = \frac{E}{\sqrt{2}X_c}(\cos(\alpha) - \cos(\omega t)) \tag{3.36}$$

where X_c is the reactance (per phase) of the commutation circuit, which is largely determined by the transformer leakage reactance.

At the end of the commutation $i_c = I_d$ and $\omega t = \mu$, and equation (3.36) becomes

$$I_d = \frac{E}{\sqrt{2}X_c}[\cos(\alpha) - \cos(\alpha + \mu)] \tag{3.37}$$

Dividing (3.36) by (3.37),

$$i_c = I_d \left(\frac{\cos(\alpha) - \cos(\omega t)}{\cos(\alpha) - \cos(\alpha + \mu)} \right) \tag{3.38}$$

and this expression applies for $\alpha < \omega t < \alpha + \mu$.

The rest of the positive current pulse is defined by

$$i = I_d \quad \text{for } \alpha + \mu < \omega t < \alpha + 2\pi/3 \tag{3.39}$$

and

$$i = I_d - I_d \left[\frac{\cos(\alpha + 2\pi/3) - \cos(\omega t)}{\cos(\alpha + 2\pi/3) - \cos(\alpha + 2\pi/3 + \mu)} \right]$$
$$\text{for } \alpha + \frac{2\pi}{3} < \omega t < \alpha + \frac{2\pi}{3} + \mu \tag{3.40}$$

The negative current pulse still possesses half-wave symmetry and therefore only odd-ordered harmonics are present. These can now be expressed in terms of the delay (firing), and overlap angles and their magnitudes, related to the fundamental components, are illustrated in Figures 3.36–3.39, for the 5th, 7th, 11th and 13th harmonics, respectively [10].

In summary, the existence of system impedance is seen to reduce the harmonic content of the current waveform, the effect being much more pronounced in the case of uncontrolled rectification. With large firing angles the current pulses are practically unaffected by a.c. system reactance.

To illustrate the use of these graphs let us consider the case of a six-pulse rectifier connected via a 50 MVA Y–Y transformer of unity turns ratio to the 110 kV system. If the rated d.c. current is 300 A, the transformer leakage reactance 10.73%, and assuming that the maximum steady-state delay is $\alpha = 30^\circ$, determine the levels of the first four characteristic harmonic currents.

From Equation (3.37) the value of the commutation angle is:

$$\mu = \arccos \left[\cos\alpha - \frac{\sqrt{2}X_c I_d}{E} \right] - \alpha$$

where

$$X_c = x_t X_B = x_t \frac{(\text{kV})^2}{\text{MVA}} = (10.73)(110 \times 10^3)^2/(50) = 25.9\ \Omega.$$

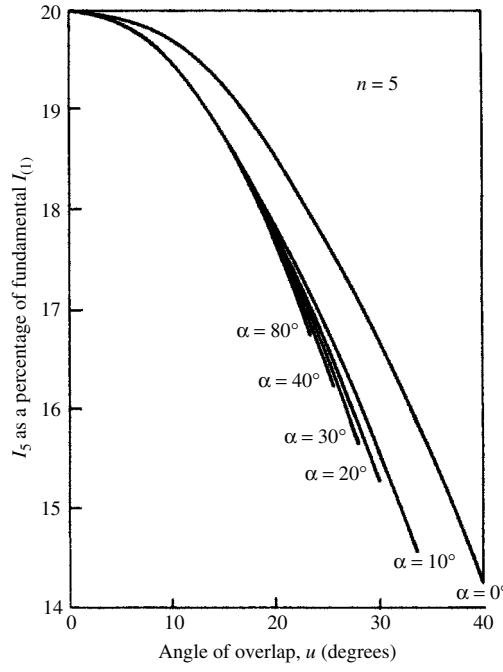


Figure 3.36 Variation of fifth harmonic current in relation to angles of delay and commutation overlap

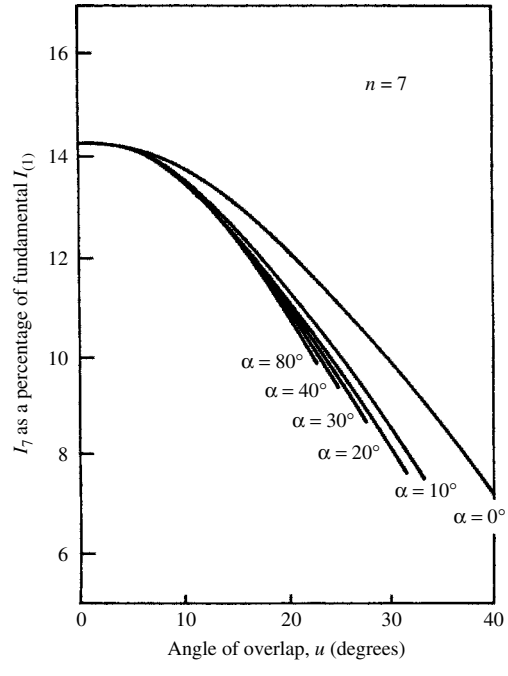


Figure 3.37 Variation of seventh harmonic current in relation to angles of delay and commutation overlap

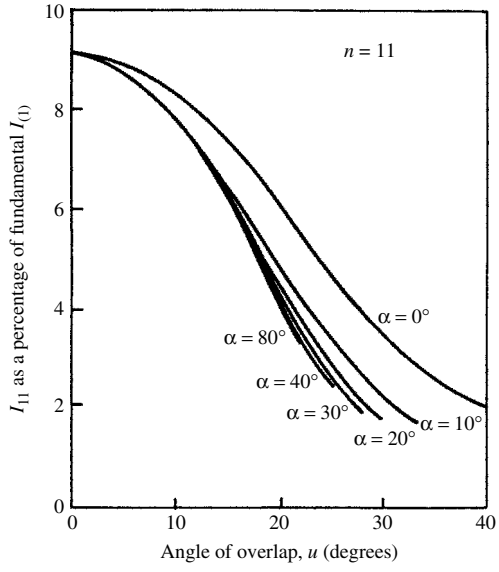


Figure 3.38 Variation of 11th harmonic current in relation to angles of delay and overlap

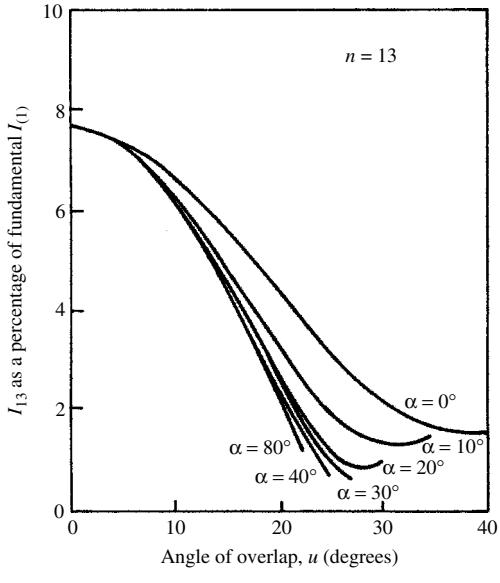


Figure 3.39 Variation of 13th harmonic current in relation to angles of delay and overlap

Therefore,

$$\mu = \arccos\left[\cos 30^\circ - \frac{\sqrt{2}(25.9)(300)}{110 \times 10^3}\right] - 30^\circ = 10^\circ$$

From Figures 3.36–3.39 the following harmonic currents as percentages of the fundamental component are obtained for $\alpha = 30^\circ$ and $\mu = 10^\circ$:

19.398%(5th), 13.4335%(7th), 7.772%(11th) and 6.1585%(13th)

and using equation (3.32)

$$I_1 = (\sqrt{6}/\pi)I_d = (\sqrt{6}/\pi)300 = 233.91 \text{ A}$$

Finally, the harmonic currents are:

$$I_5 = 45.37 \text{ A} \quad I_7 = 31.27 \text{ A} \quad I_{11} = 19.08 \text{ A} \quad I_{13} = 14.03 \text{ A}$$

3.6.6 Direct Voltage Harmonics

For the three-phase bridge configuration the orders of the harmonic voltages are $n = 6k$. The corresponding d.c. voltage waveforms are illustrated in Figure 3.40.

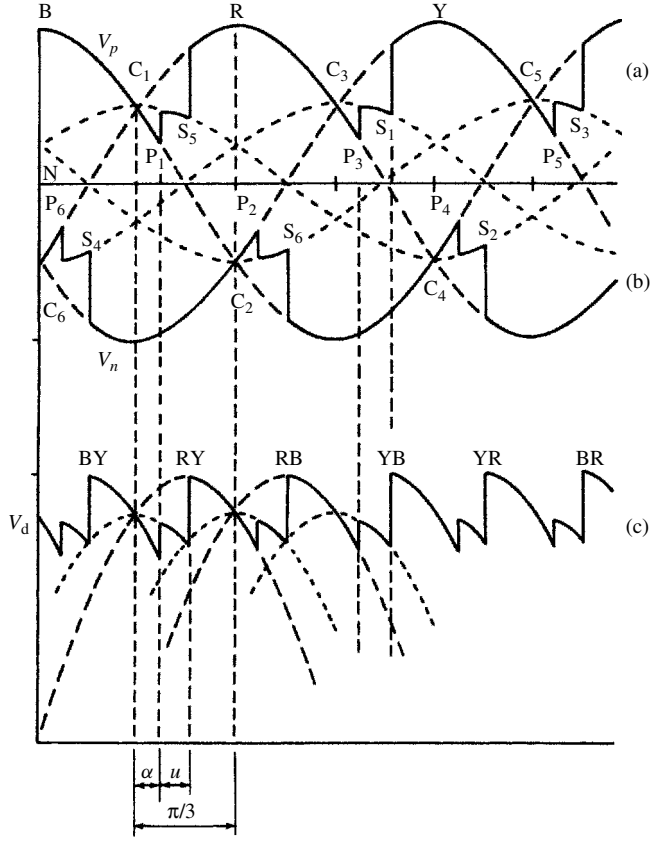


Figure 3.40 Six-pulse converter d.c. voltage waveforms: (a) at the positive terminal; (b) at the negative terminal; (c) across the output terminals

The repetition interval of the waveform shown in Figure 3.40(c) is $\pi/3$ and it contains the following three different functions with reference to voltage crossing C_1:

$$v_d = \sqrt{2}V_c \cos\left(\omega t + \frac{\pi}{6}\right) \quad \text{for } 0 < \omega t < \alpha \tag{3.41}$$

$$v_d = \sqrt{2}V_c \cos\left(\omega t + \frac{\pi}{6}\right) + \frac{1}{2}\sqrt{2}V_c \sin(\omega t) = \frac{\sqrt{6}}{2}V_c \cos(\omega t)$$
$$\text{for } \alpha < \omega t < \alpha + \mu \tag{3.42}$$

$$v_d = \sqrt{2}V_c \cos\left(\omega t - \frac{\pi}{6}\right) \quad \text{for } \alpha + \mu < \omega t < \frac{\pi}{3} \tag{3.43}$$

where V_c is the (commutating) phase to phase r.m.s. voltage.

From equations (3.41), (3.42) and (3.43) the following expression is obtained for the r.m.s. magnitudes of the harmonic voltages of the d.c. voltage waveform:

$$V_n = \frac{V_{c0}}{\sqrt{2}(n^2-1)}\left[(n-1)^2\cos^2\left((n+1)\frac{\mu}{2}\right) + (n+1)^2\cos^2\left((n-1)\frac{\mu}{2}\right)\right.$$
$$\left. - 2(n-1)(n+1)\cos\left((n+1)\frac{\mu}{2}\right)\cos\left((n-1)\frac{\mu}{2}\right)\cos(2\alpha+\mu)\right]^{\frac{1}{2}} \tag{3.44}$$

Figures 3.41 and 3.42 illustrate the variation of the 6th and 12th harmonics as a percentage of V_{c0}, the maximum average rectified voltage, which for the six-pulse bridge converter is $3\sqrt{2}V_c/\pi$. These curves and equations show some interesting facts. Firstly, for $\alpha = 0$ and $\mu = 0$, equation (3.44) reduces to

$$V_{n0} = \sqrt{2}V_{c0}/(n^2-1) \tag{3.45}$$

or

$$\frac{V_{n0}}{V_{c0}} = \sqrt{2}/(n^2-1) \approx \sqrt{2}/n^2 \tag{3.46}$$

giving 4.04%, 0.99% and 0.44% for the 6th, 12th and 18th harmonics, respectively.

Generally, as α increases, harmonics increase as well, and for $\alpha = \pi/2$ and $\mu = 0$

$$\frac{V_{n0}}{V_{c0}} = \sqrt{2}n/(n^2-1) \approx \sqrt{2}/n \tag{3.47}$$

which produces n times the harmonics content corresponding to $\alpha = 0$. This means that the higher harmonics increase faster with α. Equation (3.47) is of some importance as it represents the maximum proportion of harmonics in the system, particularly when it is considered that at $\alpha = 90^\circ$ μ is likely to be very small.

If the converter involves two bridges, one with a star–star or delta–delta transformer and the other with a delta–star or star–delta transformer, their respective voltages will be 30° out of phase and so the harmonics will accordingly be out of phase. Since 30° of mains frequency correspond to a half-cycle of the 6th harmonic, this harmonic will be in phase opposition in the two bridges. Similarly for the 12th

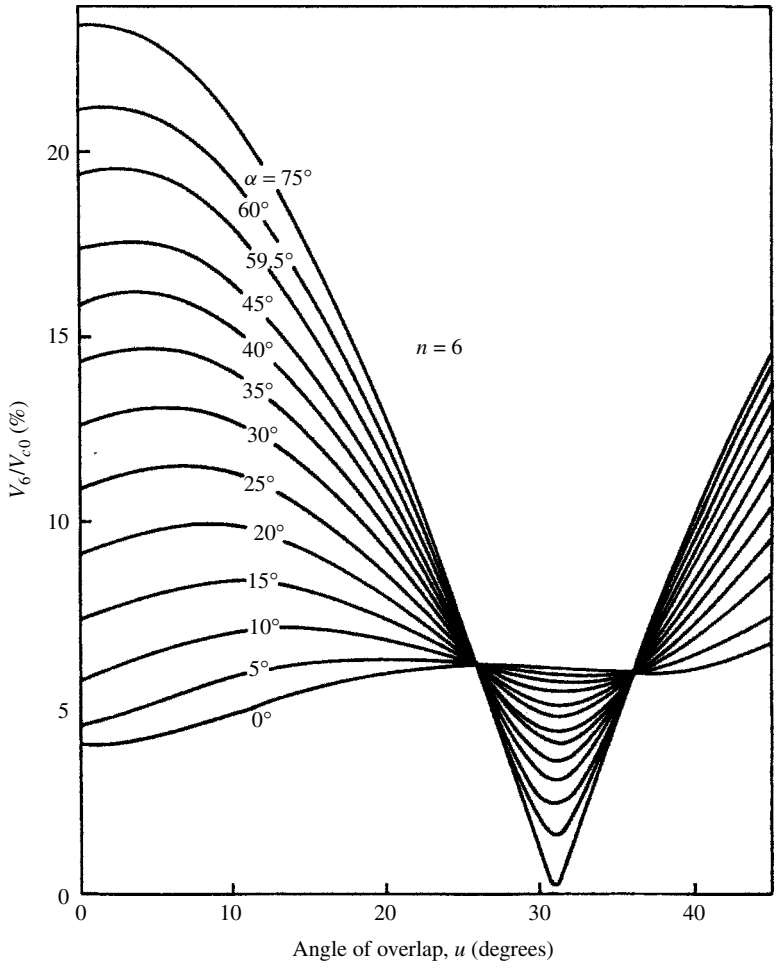


Figure 3.41 Variation of the sixth harmonic voltage in relation to angles of delay and overlap

harmonic, 30° corresponds to one cycle, giving harmonics in phase; for the 18th harmonic, 30° corresponds to one and a half cycles, giving harmonics in opposition and so on.

3.6.7 Imperfect D.C. Voltage Smoothing

Considering the limited inductance of the motor armature winding and the larger variation of firing angle, the constant d.c. current assumption of the large size converters cannot be justified in the case of a d.c. drive.

The d.c. load must now be represented as an equivalent circuit which in its simplest form includes resistance, inductance and back e.m.f. (as shown in Figure 3.43).

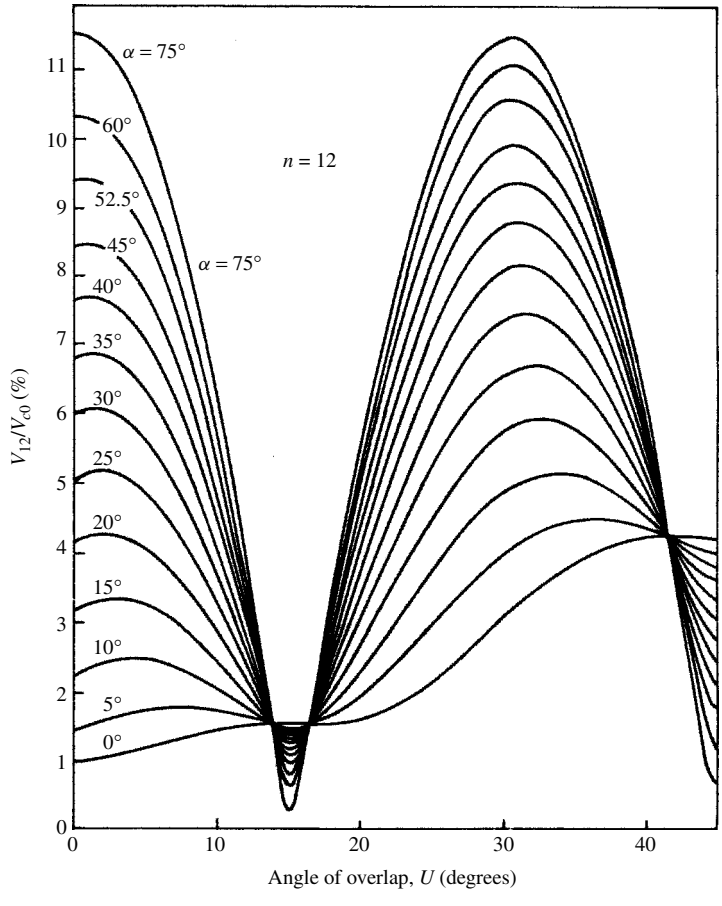


Figure 3.42 Variation of the 12th harmonic voltage in relation to angles of delay and overlap

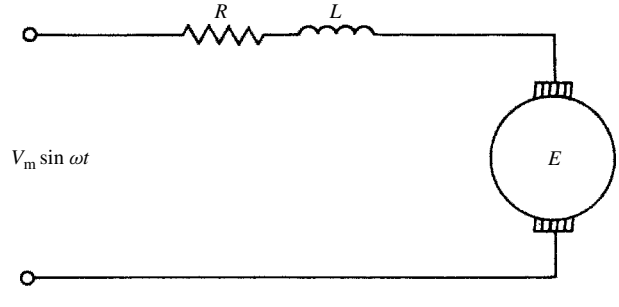


Figure 3.43 D.c. motor equivalent circuit

With sinusoidal supply voltage $V_m \sin \omega t$, the following equation applies:

$$V_m \sin(\omega t) = Ri + L\left(\frac{\mathrm{d}i}{\mathrm{d}t}\right) + E \tag{3.48}$$

and the load current has the form

$$i = Ke^{-Rt/L} + \frac{V_m}{\sqrt{R^2 + (\omega L)^2}} \sin(\omega t - \phi) - \frac{E}{R} \tag{3.49}$$

where

$$\phi = \tan^{-1}(\omega L/R)$$

and the constant K is derived from the particular initial conditions.

Under nominal loading the firing delay is kept low, but during motor start or light load conditions the delay increases substantially and the current may even be discontinuous. This extreme operating condition is illustrated in Figure 3.44 for a six-pulse rectifier. Each phase consists of two positive and two negative current pulses, which are derived from the general expression (3.49) by using the appropriate voltage phase relationships with a common reference.

The current in phase R with reference to the instant when V_{RY} is maximum in Figure 3.44 has the following components:

(1) Over the range $\theta_1 < \omega t < \theta_2$

$$i = \frac{V_m}{R}\left(\cos(\phi)\cos(\omega t - \phi) - \frac{E}{V_m} + \left[\frac{E}{V_m} - \cos(\phi)\cos(\theta_1 - \phi)\right] e^{(-R/\omega L)(\omega t - \theta_1)}\right) \tag{3.50}$$

(2) When $\theta_3 < \omega t < \theta_4$ where $\theta_3 = (\theta_1 + \pi/3)$,

$$i = \frac{V_m}{R}\left(\cos(\phi)\cos\left(\omega t - \frac{\pi}{3} - \phi\right) - \frac{E}{V_m} + \left[\frac{E}{V_m} - \cos(\phi)\cos(\theta_1 - \phi)\right] e^{(-R/\omega L)(\omega t - \pi/3 - \theta_1)}\right) \tag{3.51}$$

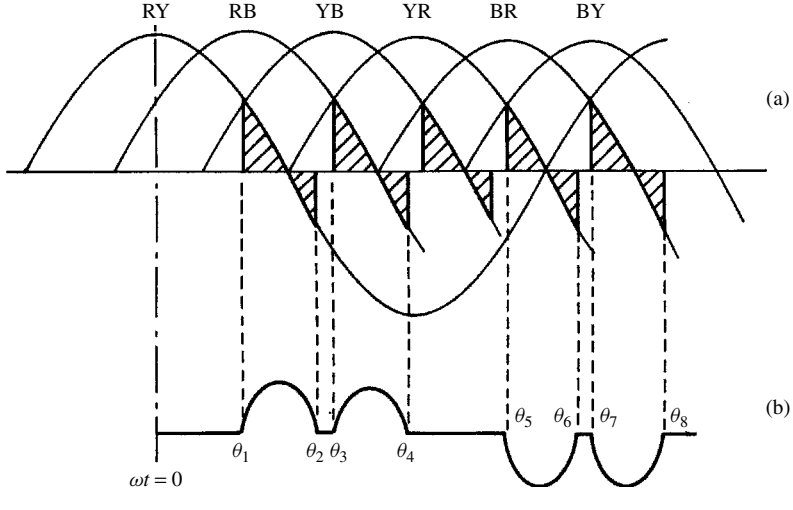


Figure 3.44 Discontinuous waveforms: (a) d.c. voltage; (b) a.c. current in phase R

(3) When $\theta_5 < \omega t < \theta_6$ where $\theta_5 = (\theta_1 + \pi)$,

$$i = -\frac{V_m}{R}\left(\cos(\phi)\cos(\omega t - \pi - \phi) - \frac{E}{V_m} + \left[\frac{E}{V_m} - \cos(\phi)\cos(\theta_1 - \phi)\right] e^{(-R/\omega L)(\omega t - \pi - \theta_1)}\right) \tag{3.52}$$

(4) When $\theta_7 < \omega t < \theta_8$ where $\theta_7 = (\theta_1 + 2\pi/3)$,

$$i = -\frac{V_m}{R}\left(\cos(\phi)\cos\left(\omega t - \frac{2\pi}{3} - \phi\right) - \frac{E}{V_m} + \left[\frac{E}{V_m} - \cos(\phi)\cos(\theta_1 - \phi)\right] e^{(-R/\omega L)(\omega t - 2\pi/3 - \theta_1)}\right) \tag{3.53}$$

Application of Fourier analysis to these current pulses indicates that the fifth harmonic can reach peak levels of up to three times those of the rectangular wave shape with the same fundamental component.

When d.c. motors are designed specifically for use with thyristor converters their armature inductance is often increased to avoid current discontinuities and the above analysis can then be simplified considerably. An approximate method described by Dobinson [11] derives the harmonic components of the a.c. current in terms of the ripple ratio, i.e.

$$r = \frac{I_r}{I_d} \tag{3.54}$$

where I_r is the alternating ripple of the direct current and I_d is the mean direct current, flowing in the motor armature circuit (Figure 3.45) at the relevant speed and load. The method ignores the effect of the commutation reactance, which at large delay angles is negligible.

With reference to Figure 3.45, a further approximation is made by assuming that the ripple is part of a sine wave displaced by a value θ relative to the zero direct-current level.

The information included in Figures 3.45(b) and (c) results in the following functions:

$$f(\theta) = 0 \qquad \text{for } 0 < \theta < \pi/6 \tag{3.55}$$

$$f(\theta) = I_d\left[7.46r\sin\left(\theta + \frac{\pi}{6}\right) - 7.13r + 1\right] \qquad \text{for } \pi/6 < \theta < \pi/2 \tag{3.56}$$

$$f(\theta) = I_d\left[7.46r\sin\left(\theta - \frac{\pi}{6}\right) - 7.13r + 1\right] \qquad \text{for } \pi/2 < \theta < 5\pi/6 \tag{3.57}$$

$$f(\theta) = 0 \qquad \text{for } 5\pi/6 < \theta < \pi \tag{3.58}$$

Application of Fourier analysis yields the following expression for the fundamental:

$$I_1 = I_d(1.102 + 0.014r) \tag{3.59}$$

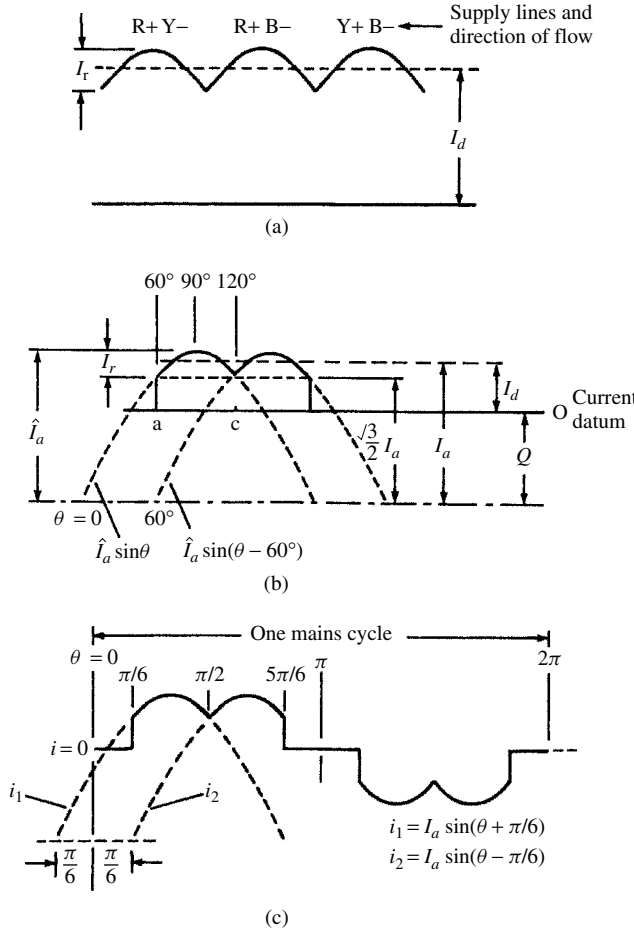


Figure 3.45 Converter output and input current waveforms: (a) armature current; (b) thyristor current; a.c. current

Also, the magnitudes of the characteristic harmonics (expressed as a percentage of the fundamental) are

$$I_n = 100\left(\frac{1}{n} + \frac{6.46r}{n-1} - \frac{7.13r}{n}\right)(-1)^k \quad \text{for } n = kp - 1 \tag{3.60}$$

and

$$I_n = 100\left(\frac{1}{n} + \frac{6.46r}{n+1} - \frac{7.13r}{n}\right)(-1)^k \quad \text{for } n = kp + 1 \tag{3.61}$$

These are plotted in Figure 3.46 as a function of r covering the whole range from zero ripple (i.e. infinite inductance) to the limit case of continuous current (at $r = 1.5$).

Figure 3.46 shows that although the fifth harmonic increases substantially with output current ripple, all the other harmonics reduce.

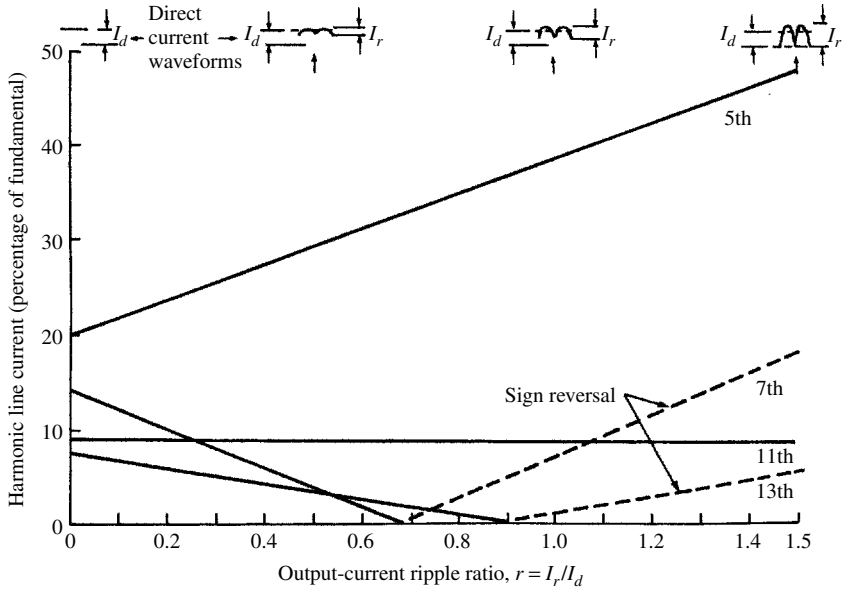


Figure 3.46 Harmonic content of the supply current for six-pulse converter with finite inductive load

3.6.8 Half-Controlled Rectification

Because of the cheapness of its design, the half-controlled version of the variable speed d.c. drive has been popular in some countries. When operating at full load (i.e. with zero firing delay) these controllers produce virtually the same harmonic currents as the fully controlled converter and operate very efficiently.

However, under operating conditions requiring firing delays, the half-wave symmetry of the current waveform is lost, as shown in Figure 3.47.

At low loads these controllers not only have a very poor power factor but introduce severe waveform distortion, particularly at even harmonics. More often than not the controllers and motors initially installed are larger than required to cope with future expansion, and operation is then at a fraction of the full load. Under these conditions the second harmonic component often reaches levels close to the fundamental current.

3.6.9 Uncharacteristic Harmonic and Inter-Harmonic Generation

The harmonic effects caused by imperfect system conditions encountered in practice cannot be derived from the idealised models described in Section 3.6.

In general each of the main three parts of the system is always in error to a lesser or greater extent:

(1) The a.c. system voltages are never perfectly balanced and undistorted, and the system impedances, in particular the converter transformer, are not exactly equal in the three phases.

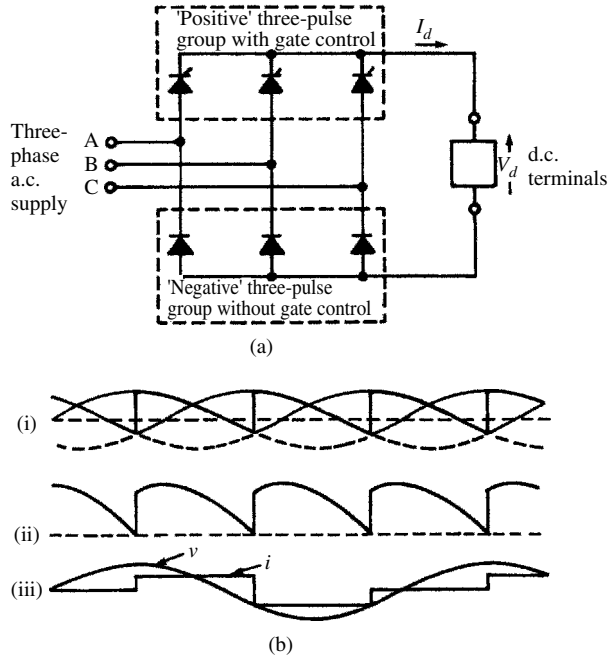


Figure 3.47 (a) Three-phase 'half-controlled' converter and (b) theoretical waveforms for $\alpha = 60$. Trace (i) shows the voltage of a 'positive' group at the d.c. terminal with respect to the supply neutral (———) and the voltage of a 'negative' group at the d.c. terminal with respect to the supply neutral (- - - -). Trace (ii) shows the d.c. terminal voltage of the bridge. Trace (iii) shows the supply voltage and current of phase A

(2) The d.c. current may be modulated from another converter station in the case of a rectifier-inverter link.

(3) The firing angle control systems often given rise to substantial errors in their implementation.

As a result the large static converters often produce harmonic orders and magnitudes not predicted by the Fourier series of the idealised waveforms.

The uncertain nature of these 'uncharacteristic' harmonics makes it difficult to prevent them at the design stage. Filters are not normally provided for uncharacteristic harmonics and as a result their presence often causes more problems than the characteristic harmonics.

By way of example, Table 3.3 shows the results of harmonic measurements during back-to-back testing of the New Zealand d.c. converter station at Benmore. All the harmonic voltages are unbalanced, particularly the third and ninth. The table also illustrates the presence of all current harmonic orders, odd and even, with the uncharacteristic orders causing higher voltage distortion than the characteristic ones. A realistic quantitative analysis of the uncharacteristic harmonic components can only be achieved by a complete three-phase computer model of the system behaviour with detailed representation of the converter controls. A mostly qualitative assessment of the main problem

Table 3.3 Harmonic measurements during back-to-back testing of the New Zealand high voltage d.c. converters

Harmonic	400 A d.c. (one-third full load) current; phase-to-neutral voltages at Benmore on 220 kV		
	Red phase (%)	Yellow phase (%)	Blue phase (%)
1	100	100	100
2	0.5	0.7	1.0
3	2.9	0.3	1.0
4	0.6	0.3	0.4
5	0.25	0.15	0.25
6	0.25	0.30	0.35
7	0.15	0.15	0.1
8	0	0.05	0.1
9	0.05	0.05	0.15
10	0.05	0.05	0.05
11	0.1	0.15	0.1
12	0.15	0.05	0.15
13	0.05	0.05	0.05
14	0.05	0.05	0.05
15	0.15	0	0.2
16	0	0.1	0.15
17	0.3	0.3	0.3
18	0	0.05	0.1
19	0.3	0.3	0.7
20	–	–	–
21	–	–	–
22	0.2	0.2	0.5
23	0.4	0.2	0.3
24	0.2	0.2	0.15

areas and the sensitivity of the system to small deviations from the ideal conditions are considered in this section.

Imperfect a.c. Source Deviations from the perfectly balanced sinusoidal supply can be caused by (i) presence of negative sequence fundamental frequency in the commutating voltage; (ii) harmonic voltage distortion of positive or negative sequence; and (iii) asymmetries in the commutation reactances. In general an imperfect a.c. source produces asymmetrical firing references and d.c. current modulation. The first problem can be eliminated by using equidistant firing control but the second problem still remains. This effect, illustrated in Figure 3.48 for the case of an unrealistically high level of fundamental voltages asymmetry, produces considerable second harmonic content on the d.c. side and third harmonic on the a.c. side [12].

Under normal operating conditions the expected levels of asymmetry and distortion are small and their effects can be approximated with reasonable accuracy.

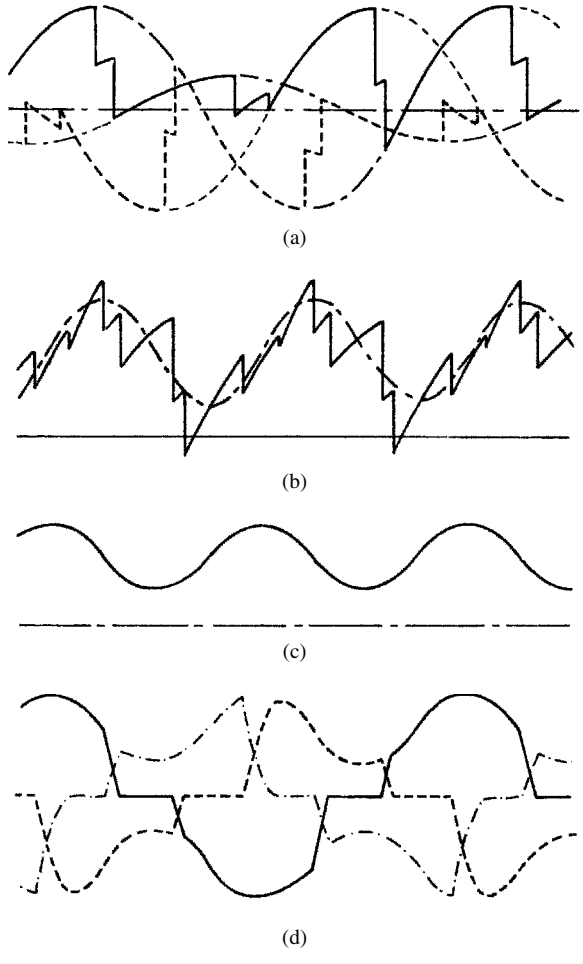


Figure 3.48 Sustained unbalanced voltages on a single converter bridge: (a) three-phase voltages; (b) direct voltage; (c) direct current; (d) three-phase currents

With reference to unbalance conditions, a CIGRE working group [13] examined the effect of different factors of asymmetry (one at the time) on an otherwise standard 12-pulse converter. The a.c. system was assumed of negligible impedance (i.e. the terminal voltage perfectly sinusoidal) and the d.c. current ripple was ignored. In practice, of course, the result of unbalance is a combination of each effect, which may either increase or decrease the harmonic content of the individual cases.

Five cases were considered, as follows:

(1) The voltage in one phase is reduced by 1% with respect to the other two.

(2) The transformer leakage reactances are 20% (for five of the phases) and 21% (for the sixth phase).

(3) Different transformer reactances, i.e. 20% (for the star–star) and 21% (for the star–delta).

Table 3.4 Harmonic currents (in as a percentage of the fundamental) generated by different types of unbalance

	Unbalance type				
Harmonic order	(1)	(2)	(3)	(4)	(5)
1	100.00	100.00	100.00	100.00	100.00
2					0.0279
3	0.069	0.130			0.0268
4					0.0253
5		0.208	0.414	0.0666	0.0234
6					0.0213
7		0.0184	0.366	0.0516	0.0189
8					0.0163
9	0.043	0.0904			0.0136
10					0.0109

(4) Different transformer turns ratios, i.e. 100% (for the star–star) and 100.5% (for the star–delta).

(5) The firing angles are 15° (for five valves) and 15.2° (for the remaining valve).

The effect of each of these cases on the first ten harmonic currents generated by the converter are shown in Table 3.4. These results show that the effects of phase reactance unbalance and firing angle unbalance are different for the two types of converter transformer. These are more severe for the star–star transformer (i.e. in the absence of a delta winding).

With reference to supply distortion, if a small positive- or negative-sequence signal V_n (per unit of the normal fundamental voltage) is added to the otherwise ideal three-phase supply of a 12-pulse converter configuration, the order and maximum level (V_k) of uncharacteristic harmonic voltage at the rectified output come under one of the following categories [14]:

Case 1: If $n + k = 12p_1 + 1$ and $n - k = 12p_2 + 1$, where p_1 and p_2 are any integers, then

$$V_k = \begin{cases} V_n \left(\dfrac{n\sqrt{2}}{n^2 - k^2} \right) & \text{if } n^2 > k^2 \quad (3.62) \\ V_n \left(\dfrac{k\sqrt{2}}{k^2 - n^2} \right) & \text{if } k^2 > n^2 \quad (3.63) \end{cases}$$

Case 2: If $n + k = 12p_1 + 1$ but $n - k \neq 12p_2 + 1$, then

$$V_k = V_n \frac{1}{\sqrt{2}(n + k)} \quad (3.64)$$

Table 3.5 Resulting harmonic voltages for interfering harmonics of orders −5 to +5

Interfering a.c. voltage harmonic order, n	Harmonic voltage on d.c. side	
	Order, k	Amplitude, V_k/V_n
−1	2	0.707
+2	1	0.707
−2	3	0.707
+3	2	0.707
−3	4	0.707
−4	5	0.707
−5	6	0.707

Case 3: If $n - k = 12p_1 + 1$ but $n + k \neq 12p_2 + 1$, then

$$V_k = V_n \frac{1}{\sqrt{2}(n-k)} \tag{3.65}$$

Case 4: If $n + k \neq 12p_1 + 1$ and $n - k \neq 12p_2 + 1$, then

$$V_k = 0 \tag{3.66}$$

A summary of all resulting harmonic voltages up to order 6 is given in Table 3.5 for interfering harmonics of orders −5 to +5. (There are also higher-order harmonics in each case, not shown, of much lower amplitude.)

The tabulated V_k is expressed per unit of the maximum average d.c. voltage and V_n per unit of the normal a.c. voltage.

The values given above are in practice applicable also to converters of higher pulse number. Thus, while characteristic harmonics can be reduced by using high pulse number, the uncharacteristic harmonics due to a.c. unbalance cannot.

It should be noted that the above is an approximation due to neglect of commutation reactance but is generally sufficiently valid at low harmonic orders (below the fifth).

The cause of the imperfection may also be some asymmetry in the commutation reactances, i.e.

$$X_a = X_0(1 + g_a)$$
$$X_b = X_0(1 + g_b)$$
$$X_c = X_0(1 + g_c)$$

where X_0 is the mean reactance and each value of g can vary between $\pm g_0$.

In this case the maximum level of uncharacteristic a.c. harmonic currents I_n of order n (in phase a) for the case of a six-pulse bridge occurs when

$$g_a = 0, \quad g_b = \pm g_0, \quad g_c = \mp g_0 \quad \text{for } n = 3, 9, 15, \text{ etc.}$$

or

$$g_a = \pm g_0, \quad g_b = \mp g_0, \quad g_c = 0 \quad \text{for } n = 5, 7, 11, 13, \text{ etc.}$$

The maximum value of I_n neglecting changes of d.c. current and a.c. voltage is obtained from the expression

$$I_n = \frac{I_1 g_0}{n(n^2-1) i_d X_0 \sqrt{3}} \times \{n^4[\cos(\alpha+\mu) - \cos\alpha]^2 + 2n^3 \sin(\alpha)\sin(n\mu[\cos(\alpha+\mu) - \cos\alpha]) + n^2[\sin^2(\alpha) + \sin^2(\alpha+\mu) + 2\cos n\mu(\cos^2\alpha - \cos\mu) + 2\cos(\alpha)(\cos(\alpha+\mu) - \cos\alpha)] + 2n\cos(\alpha)\sin(n\mu)(\sin\alpha + \sin(\alpha+\mu)) + 2\cos^2\alpha(1-\cos n\mu)\}^{1/2} \quad (3.67)$$

for $n = 3, 9, 15$, etc., where I_1 is the fundamental r.m.s. current, i_d is the d.c. current per unit, X_0 is the mean commutation reactance per unit, α is the firing angle and μ is the overlap (or commutation) angle. For $n = 5, 7, 11, 13$, etc., the above expression should be divided by 2.

Table 3.6 gives values for a typical case of $X_0 = 0.2$ per unit, $\alpha = 15°$, $g_0 = 0.075$.

Unequal commutation reactances also cause uncharacteristic voltages on the d.c. side. The highest magnitude of these occurs when $g_a = 0$, $g_b = +g_0$ and $g_c = -g_0$. Only even harmonics occur, given by

$$V_n(\text{max.}) = \frac{i_d X_0 g_0 V_{dio}}{2\sqrt{6}} \quad (3.68)$$

where V_{dio} is the theoretical no-load d.c. voltage.

As an example for $i_d = 1$, $X_0 = 20\%$ and $g_0 = 0.075$, V_n(max.) is 0.31% of V_{dio} for $n = 2, 4, 8, 10, 14, 16$, etc., independent of harmonic order or of firing angle.

D.c. Current Modulation [14] If we now assume a perfect three-phase supply and equidistant firing, the addition of a small current harmonic component I_k of order k on the d.c. side will generate a component I_n of different order but of the same sequence on the a.c. side, the maximum level of which is given in Table 3.7.

The amplitude I_n is in multiples of $I_1 I_k / I_d$, where I_1 is the r.m.s. fundamental current at the a.c. busbar, I_k is the r.m.s. interfering current on the d.c. side at order k and I_d is the d.c. current.

Table 3.6 Values for a typical case

n	I_n (% of I_1)
3	0.70
5	0.33
7	0.29
9	0.50
11	0.22
13	0.19
15	0.31

Table 3.7 Maximum level of I_n

Harmonic order, k, of modulating current on d.c. side	Harmonic current on a.c. side	
	Order n	Amplitude, I_n
1	0	0.707
	+2	0.707
2	−1	0.707
	+3	0.707
3	−2	0.707
4	−3	0.707
	+5	0.707

Table 3.7 is independent of the prime cause of the d.c. current modulation. It is again approximate, valid only at low frequencies, because the commutation reactance has been neglected.

Control System Imperfections No general rules can be given in this case. By way of example, Ainsworth [14] describes the effect of modulating the harmonic content of the voltage applied to the oscillator of the d.c. current control system using the phase-locked oscillator principle [15]. Assuming constant d.c. current and a.c. voltages, a V_c modulating harmonic signal of order n (in per unit, referred to the normal steady-state control voltage), causes d.c. voltage components of orders $n_1 = \pm n \pm 12p$ in a 12-pulse convertor, where p is any integer.

The magnitude (in per unit of the maximum average rectified voltage) of the d.c. voltage modulation is

$$V = \frac{V_c \sin(\alpha_0) \cos(n_1 \mu_0/2)}{n_1} \tag{3.69}$$

where α_0 and μ_0 are the mean firing and overlap angles, respectively.

The total a.c. current magnitude referred to one phase of one valve winding at harmonic order n_2 due to a similar excitation is

$$I_A(n_2) = \frac{I_d V_c \cdot 2\sqrt{3} \sin(n_2 \mu_0/2)}{n_2(\cos(\alpha_0) - \cos(\alpha_0 + \mu_0))} \tag{3.70}$$

for $n_2 = \pm n \pm$ (1, 11, 13, ...) only.

Firing Asymmetry A.c. system imperfections or firing errors result in pulse-width deviations from the characteristic quasi-rectangular current waveform. Kimbark [16] describes the effect of late and early firings with reference to a six-pulse bridge converter.

If the positive current pulses start early by an angle ε and the negative ones start late by the same angle, the non-conductive intervals are increased by 2ε. The even symmetry, which eliminates the even-ordered harmonics, is now lost and the even

harmonics for small overlap angles are given by the expression

$$\frac{I_n}{I_1} = \frac{2\sin(n\varepsilon)}{2n\cos(\varepsilon)} \approx \varepsilon \tag{3.71}$$

For example, for $\varepsilon = 1^\circ$ the second and fourth harmonics are each approximately 1.74% of the fundamental current.

If the firings of the two valves connected to the same phase are late by ε then the positive and negative current pulses of that phase are ε degrees shorter than the normal. Moreover, the current pulses of one of the remaining phases (the leading phase) are increased by ε while those of the lagging phase remain unaltered. This produces triplen harmonic currents. On the assumption of zero overlap angle the ratio of the triplen harmonics ($h = 3q$) to the fundamental current are expressed by

$$\frac{I_n}{I_1} = \frac{\sin(q\pi \pm 1.5q\varepsilon)}{3q\sin(\pi/3 \pm \varepsilon/2)} \tag{3.72}$$

For small values of ε the approximate levels of third harmonic are given by

$$\frac{I_3}{I_1} \approx \frac{1.5q\varepsilon}{3q\sqrt{3}/2} = 0.577\varepsilon \tag{3.73}$$

For example, for $\varepsilon = 1^\circ$, $I_3 = 1\%$ of the fundamental.

3.6.10 Frequency Cross-Modulation in Line-Commutated Converter Systems

The Modulation Process The harmonic transfers through the a.c.–d.c. converter are best explained using modulation theory [17,18]. The voltage and current relationships across the converter can be expressed as follows:

$$v_d = \sum Y_{\psi \mathrm{dc}} v_\psi \tag{3.74}$$

$$i_d = Y_{\psi \mathrm{ac}} \cdot i_{\mathrm{dc}} \tag{3.75}$$

where $Y_{\psi \mathrm{dc}}$ and $Y_{\psi \mathrm{ac}}$ are transfer functions for the voltages and current, respectively, and $\psi = 0^\circ$, 120°, 240° for the three phases.

This process is illustrated in Figure 3.49, which shows the modulated output current on the a.c. side of the converter in response to a d.c. current that contains a ripple frequency [19]. In the absence of commutation overlap, the transfer functions are rectangular, as shown in Figure 3.49.

The simplified modulation process, explained above, can be extended to the more realistic case where the commutation process is included. This extension, explained further in Chapter 8, is necessary to derive accurate quantitative information from the generalised table to be described in the following section.

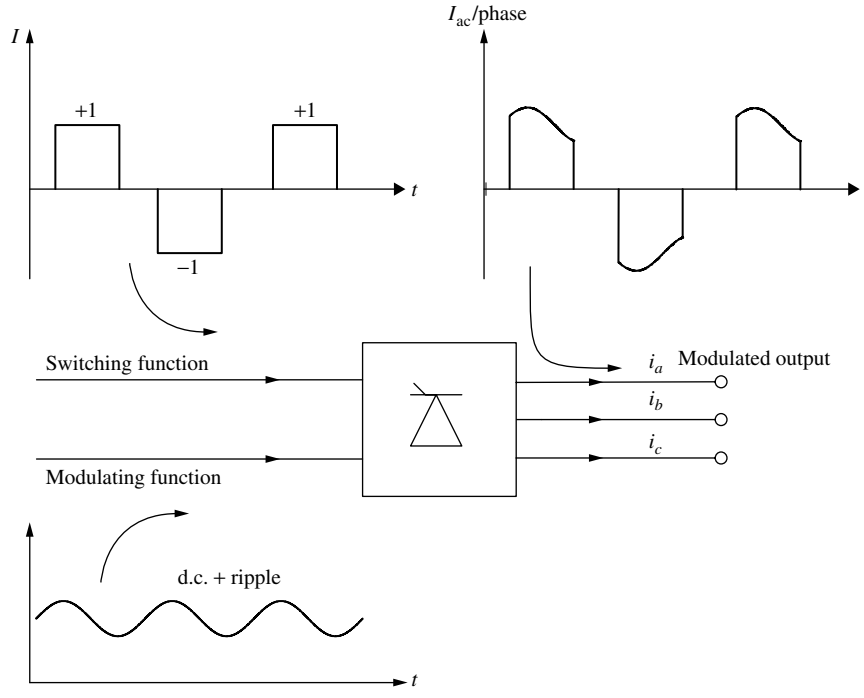


Figure 3.49 A.c. current modulation under ideal converter switching

Cross-Modulation Across an a.c.–d.c.–a.c. Link The frequency transfer relationships in the cross-modulation process of a line-commutated 12-pulse a.c.–d.c.–a.c. link have been collected together in Figure 3.50 [20]. The link can be an HVd.c. interconnection between two a.c. systems of frequencies f_1 and f_2 or the supply system for a synchronous variable speed drive.

The 'exciting' harmonic sources are multiples, integers or non-integer, of the frequency in system 1.

k_1 is a current harmonic source, whereas $k_1 - 1$ and $k_1 + 1$ are voltage harmonic sources.

The resulting harmonic orders in system 2 are related to the frequency of system 2.

The DC column refers to the d.c. side of the link; the $AC_1{}^+$ and $AC_1{}^-$ columns represent the positive and negative sequences of system 1, and $AC_2{}^+$ and $AC_2{}^-$ represent the positive and negative sequences of system 2, respectively.

When the d.c. link interconnects separate power systems, either of the same nominal (but in practice slightly different) frequency or different nominal frequencies, there will be a wide range of harmonic and non-harmonic frequency transfers. These can be divided into two groups:

(1) Frequencies at terminal 1 caused by the characteristic d.c. voltage harmonics $(12nf_2)$ and their consequential currents from terminal 2. These are represented in the expression

$$f_{ac1} = (12m \pm 1) f_1 \pm 12nf_2 \tag{3.76}$$

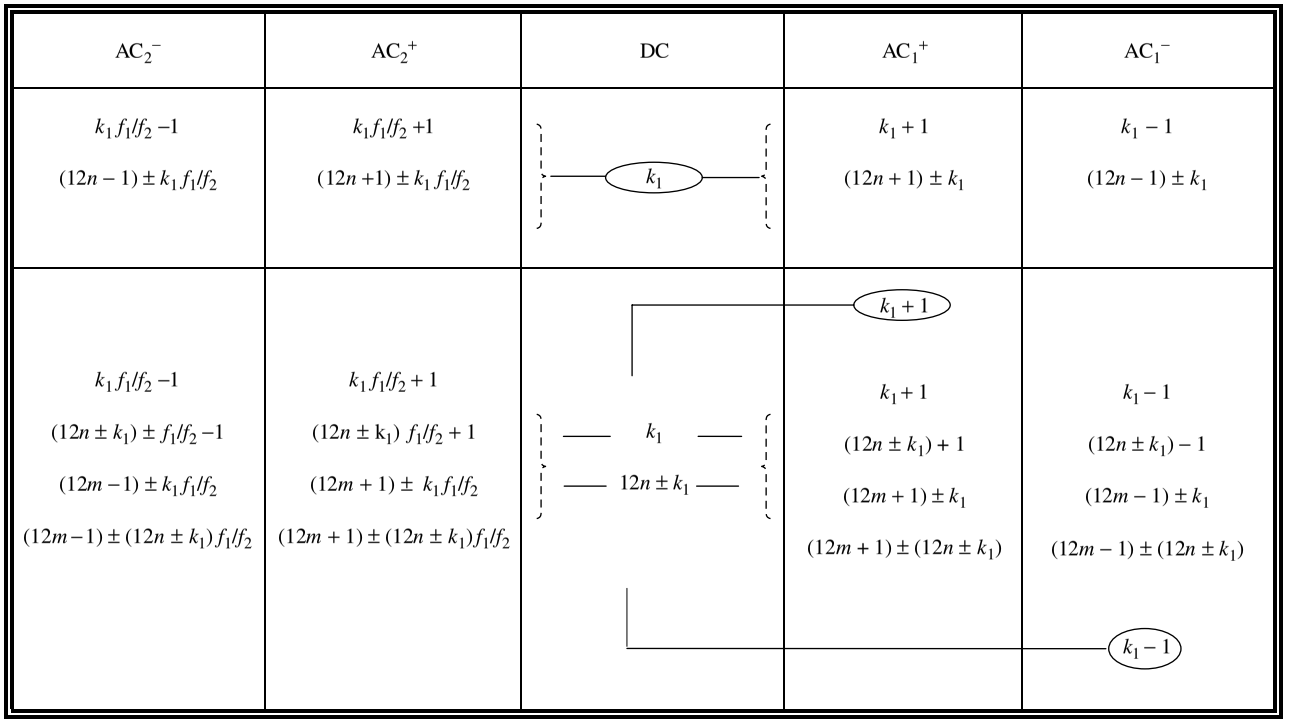


Figure 3.50 Harmonic transfers across a 12-pulse a.c.–d.c.–a.c. link. The encircled elements indicate harmonic sources and $m, n \in (1, 2, 3 \ldots)$

where $m, n \varepsilon (0, 1, 2, 3\ldots)$ which can have any frequency, including frequencies below the fundamental.

The back-to-back frequency conversion schemes represent the worst condition for non-integer harmonic frequencies. In this case, with small smoothing reactors the d.c. side coupling is likely to be strong which means that the flow of harmonically unrelated currents on the d.c. side can be large. In six-pulse operation such schemes can produce considerable subharmonic content even under perfect a.c. system conditions. However, 12-pulse converters do not produce subharmonic content under symmetrical and undistorted a.c. system conditions. These will produce inter-harmonic currents as defined by equation (3.76).

When the link interconnects two isolated a.c. systems of the same nominal frequency but they differ by a small increment Δf_0, then the characteristic harmonics are different by $12n\Delta f_0$. A d.c. side voltage at frequency $12n(f_0 + \Delta f_0)$ is generated by one converter, and this will be modulated down again at the other converter by a characteristic frequency in the thyristor switching pattern in accordance with equation (3.76) i.e.

$$(12m \pm 1) f_0 \pm 12n(f_0 + \Delta f_0)$$

which on the a.c. side, among other frequencies, includes (for $m = n$):

$$f_0 \pm 12n\Delta f_0$$

The latter will beat with the fundamental component at a frequency $12n\Delta f_0$, which at some values of n will allow flicker-inducing currents to flow.

(2) Frequencies caused in system 1 by unbalance or distortion in the supply voltage of system 2. Negative sequence voltages at frequencies $(k-1)f_2$ produce the following non-characteristic frequencies on the d.c. side:

$$f_{dc} = (12n \pm k) f_2 \quad (n = 0, 1, 2\ldots) \tag{3.77}$$

Cross-modulation of these current components produces the following frequencies in system 1

$$f_{ac1} = (12m \pm 1) f_1 \pm (12n \pm k) f_2. \tag{3.78}$$

Let us first consider a frequency conversion scheme with a sinusoidal but negative sequence unbalanced voltage in system 2, i.e. $(k-1) = 1$ (and therefore $k = 2$). Substituting $m = n = 0$ and $k = 2$ in equation (3.76) yields currents (and therefore voltage) at frequencies

$$f_{ac1} = \pm f_1 \pm 2 f_2 \tag{3.79}$$

One of these frequencies $(f_1 - 2f_2)$ will beat with the fundamental frequency voltage of system 1 at a frequency

$$f_1 + (f_1 - 2f_2) = 2(f_1 - f_2) \tag{3.80}$$

which for a 50–60 Hz conversion scheme becomes 20 Hz. This is a flicker-producing frequency. This same frequency will be referred to generator rotor shaft torque at 20 Hz, which may excite mechanical resonances.

Again, this type of cross-modulation effect is most likely to happen in back-to-back schemes due to the stronger coupling between the two converters, although it is also possible with any HVd.c. scheme in the presence of a suitable resonance.

Now consider two a.c. systems of the same nominal (but slightly different) frequency.

Substituting $m = n = 0$ and $k = 2$, for fundamental frequency f_0 into equation (3.78), a current and resultant voltage (through the a.c. system impedance) of frequency

$$f_{ac1} = \pm f_0 \pm 2(f_0 + \Delta f_0) \tag{3.81}$$

which leads to $f_0 \pm 2\Delta f_0$ is induced on the a.c. side. This will either beat with the fundamental frequency f_0 or produce generator/motor shaft torques at $2\Delta f_0$. This frequency is generally too low to produce flicker but may induce mechanical oscillations.

Substituting $m = n = 1$ and $k = 2$ in equation (3.78) gives, among others, a current (and thus voltage) at the frequency

$$(12 + 1) f_0 - (12 + 2)(f_0 - \Delta f)$$

and for $f_0 = 50$ Hz and $\Delta f = 1$ Hz, the resulting a.c. current (and thus voltage) in system 1 is:

$$13 \times 50 - 14 \times 49 = 36 \text{ Hz}$$

This distorting voltage will, therefore, beat with the fundamental, producing 14 Hz flicker. However, the subharmonic levels expected from this second-order effect will normally be too small to be of consequence.

3.7 Three-Phase Voltage-Source Conversion

A voltage-source converter (VSC) is characterised by a predominantly capacitive d.c. side and an inductive a.c. system. Under these conditions the d.c. voltage is well defined, while the a.c. side currents are controlled by the converter modulation process.

The simplest VSC configuration is the six-pulse diode bridge with a large capacitor across the output terminals. In this circuit the capacitor is charged every half-cycle of the supply frequency by two short current pulses, typically as shown in Figure 3.51. The corresponding harmonic content can reach levels of up to 90% (5th), 80% (7th), 75% (11th) and 70% (13th). However, unlike the single-phase power supply rectifier, the absence of neutral connection in the three-phase case eliminates the triplen harmonics. The addition of an a.c. line choke provides a substantial reduction in the harmonic current levels and is often used with adjustable speed drives (ASD) of the pulse width modulation (PWM) type.



Figure 3.51 Harmonic current waveform of a VSC converter

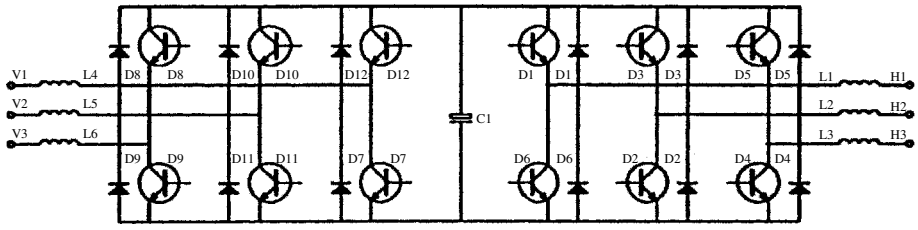


Figure 3.52 A voltage-sourced rectifier inverter cascade

When the converter is required to alter the d.c. side capacitor voltage, the diodes must be replaced by controlled rectifiers. Moreover, when bi-directional power flow is designed for, the switches must block a unidirectional voltage but be capable of conducting current in either direction.

This type of converter suits the a.c. motor drive because both the a.c. system and motor load are predominantly inductive. A typical voltage-sourced rectifier/inverter cascade is shown in Figure 3.52. Advances in the ratings of GTO and IGBT devices is extending the application of the voltage-sourced conversion concept to very large motor drives and even to light HVd.c. applications [21].

3.7.1 Multi-Level VSC Configurations

Manufacturers are introducing high voltage drives rated above 200 kW using IGBT technology. However the switching transients caused by the higher voltages impose additional stresses on the motor windings. The multi-level solution has been developed to generate high voltage waveforms using relatively low voltage switching devices.

A multi-level voltage-source converter can switch its output between multiple voltage levels within each cycle, thus creating a better voltage waveform for a particular switching frequency, when compared to a conventional two-level inverter. Theoretical phase output voltages for three- and five-level configurations are illustrated in Figure 3.53.

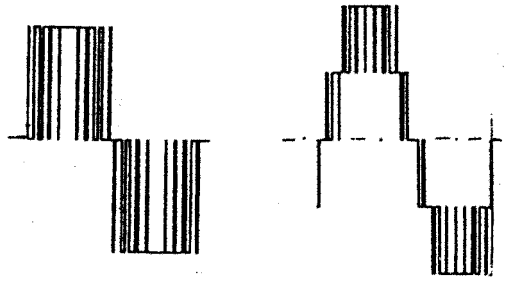


Figure 3.53 Phase output voltage waveforms for three- and five-level inverters. Source: C. Newton, M. Sumner, 'multi-level convertors: a real solution to medium/high-voltage drives?', *Power Engineering Journal*, February 1998, pp. 21–26

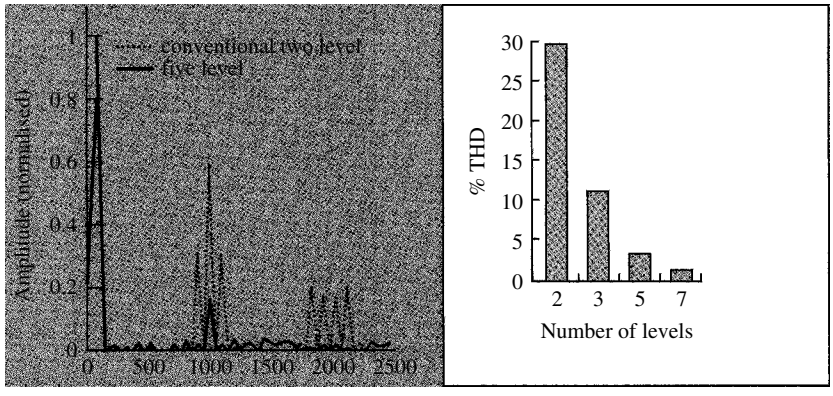


Figure 3.54 Comparison of phase voltage spectra and THD for multi-level inverters. Source: C. Newton, M. Sumner, 'multi-level convertors: a real solution to medium/high-voltage drives?', *Power Engineering Journal*, February 1998, pp. 21–26

The reduced harmonic content achieved by the multi-level solution is further illustrated in Figure 3.54, where the phase output voltage spectrum of a five-level inverter is compared with that of the standard two-level case. The figure also shows the voltage THD calculated for two-, three-, five- and seven-level output waveforms.

The following d.c.–a.c. multi-level configurations have been identified:

(1) Multiple bridge configuration, using transformer or inductor summing arrangements [22]. In this configuration the harmonic cancellation is achieved through the phase displacement of the voltage waveforms of phase-shifted transformer secondary windings.

(2) Multiple bridge using direct series connection [23]. This is a variation of the previous case, its main difference being the elimination of the phase-shifting transformers, i.e. it is directly connected to the a.c. side. Each phase consists of series connected single-phase full bridges, each bridge requiring an isolated d.c. bus.

(3) The multi-level diode clamped converter [24]. This alternative achieves the multi-level waveforms by the series or parallel connection of switches within the converter bridge itself.

(4) The multi-level flying capacitor converter [25]. In previous configurations each phase leg consisted of a switch pair in parallel with a bus capacitor, and must be always connected to either the positive or negative node of the capacitor. In this alternative the switch pair/capacitor cell is isolated and inserted within a similar cell. Thus this inner pair of switches/capacitors now 'fly' as the outer pair of devices switch.

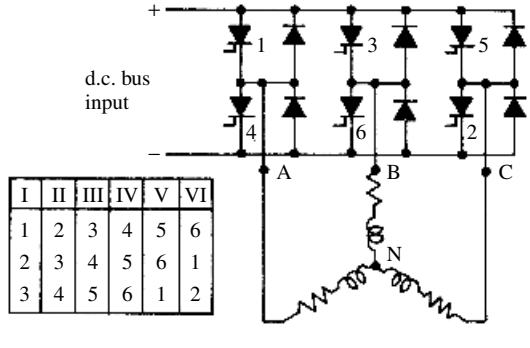
(5) The chain circuit converter [26]. This configuration consists of individually controlled units, which can then be assembled to form the three-phase converter. It provides modularity and ease of expansion.

(6) A d.c. voltage reinjection scheme [27]. Unlike the previous multi-level configurations, where all the switches form part of the main conversion process, the pulse increase is now achieved by separate switching circuitry at reduced current levels.

3.8 Inverter-Fed A.C. Drives

Although the thyristor-controlled d.c. drive still holds a large share of the market in the large power rating group, the emphasis has shifted towards the use of inverters and induction motors. This trend has been helped by substantial increases in the ratings of the more controllable GTO thyristors and IGBT switching devices.

The basic three-phase inverter bridge commonly used for a.c. motor control is made up of six controlled semiconductors, each having a feedback diode connected in inverse parallel, as shown in Figure 3.55. The inverter can be of the voltage source (VSI) or current source (CSI) types. The VSI requires a constant d.c. voltage input, which is normally achieved with a large capacitor or LC filter, whereas the CSI needs a constant current input, obtained by means of a series inductor in the d.c. link. CSI drives have better speed characteristics but require a motor with leading power factor (either synchronous or induction-type with capacitors); however, the use of turn-off switching devices removes this restriction.



I	II	III	IV	V	VI
1	2	3	4	5	6
2	3	4	5	6	1
3	4	5	6	1	2

Figure 3.55 Basic three-phase inverter and balanced motor load showing an elementary switch-closing sequence

The inverter bridge is normally supplied from a line-commutated controlled converter and thus, the harmonic content injected into the a.c. power system is as described in Section 3.6 (for the CSI drive) or Section 3.7 (for the VSI drive).

Motor Phase Voltage In the circuit of Figure 3.55 the inverter phase output voltage is always at one of two distinct voltage levels. The floating neutral voltage with respect to ground, expressed in terms of the inverter phase output voltage waveforms v_A, v_B, v_C is

$$v_N = \frac{1}{3}(v_A + v_B + v_C) \tag{3.82}$$

so that a typical motor phase voltage is

$$v_{AN} = v_A - v_N = \frac{1}{3}(2v_A - v_B - v_C) \tag{3.83}$$

For a balanced linear, bilateral motor load impedance, the motor phase voltage of a harmonic of order n can be expressed as

$$\begin{aligned} v_{AN(n)} &= \frac{1}{3}[2v_{A(n)} - v_{B(n)} - v_{C(n)}] \\ &= \frac{1}{3}[2v_{mn}\sin(n\omega_1 t) - v_{mn}\sin(n(\omega_1 t + 2\pi/3)) - v_{mn}\sin(n(\omega_1 t - 2\pi/3))] \\ &= \frac{2}{3}v_{mn}\sin(n\omega_1 t)[1 - \cos(2n\pi/3)] \\ &= \frac{2}{3}v_{A(n)}[1 - \cos(2n\pi/3)] \end{aligned} \tag{3.84}$$

and similarly for phases B and C:

$$v_{BN(n)} = \frac{2}{3}v_{B(n)}[1 - \cos(2n\pi/3)] \tag{3.85}$$

$$v_{CN(n)} = \frac{2}{3}v_{C(n)}[1 - \cos(2n\pi/3)] \tag{3.86}$$

Moreover, for all the positive and negative sequence harmonics

$$\cos(2n\pi/3) = -\frac{1}{2}$$

so that

$$v_{AN(n)} = v_{A(n)},\ v_{BN(n)} = v_{B(n)},\ v_{CN(n)} = v_{C(n)} \tag{3.87}$$

and in the balanced three-phase system, for the zero sequence harmonics,

$$\cos(2n\pi/3) = 1$$

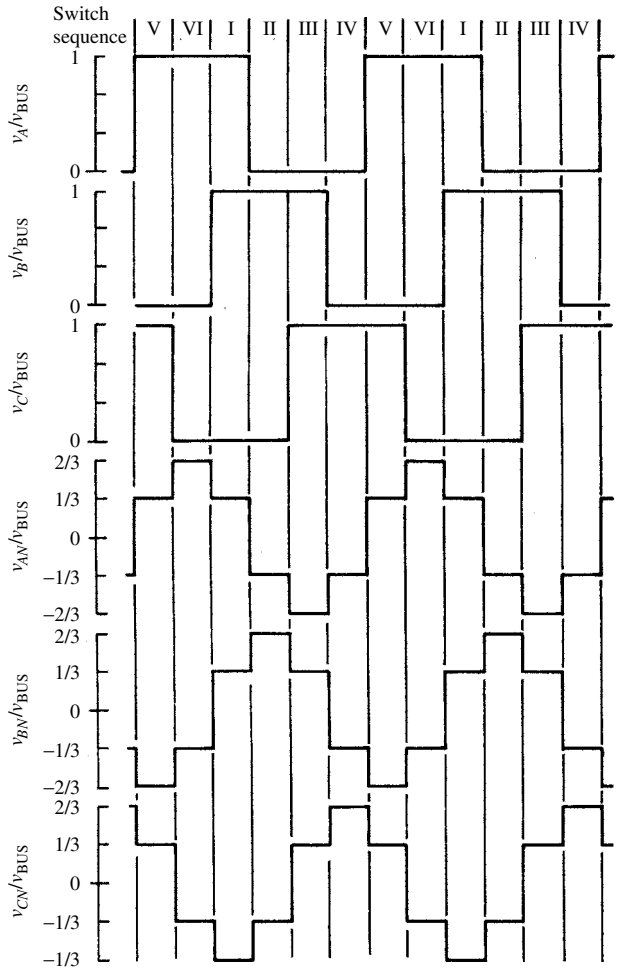


Figure 3.56 Basic six-step waveforms

so that

$$v_{AN(n)} = v_{BN(n)} = v_{CN(n)} = 0 \tag{3.88}$$

Thus, for the basic six-pulse voltage sourced inverter, the motor phase input voltage is identical to that of the corresponding inverter phase output voltage, with the exception that all inverter phase triplen harmonics have been eliminated. The effect of triplen harmonic elimination is shown in Figure 3.56 for the inverter output voltage waveforms resulting from the basic switch-closing sequence indicated in Figure 3.55. Since each motor phase input waveform results from square inverter phase voltage waveforms, the motor phase voltage in the frequency domain is

$$v_p = \frac{2}{\pi} v_{\text{BUS}} \sum_{k=0}^{\infty} \left(\frac{1}{(6k+1)} \sin((6k+1)\omega_1 t) + \frac{1}{(6k+5)} \sin((6k+5)\omega_1 t) \right) \tag{3.89}$$

Magnetising Current and Flux The motor phase magnetising inductance, L_m, acts as an integrating filter for the input voltage waveform, i.e.

$$i_p = \frac{1}{L_m}\int_{t_0}^{t} v_p \, \mathrm{d}t \tag{3.90}$$

Therefore for the nth harmonic phase voltage

$$v_{p(n)} = \frac{2}{n\pi} v_{\mathrm{BUS}} \sin(n\omega_1 t) \tag{3.91}$$

$$i_{p(n)} = \frac{2v_{\mathrm{BUS}}}{n\pi L_m}\int_{t_0}^{t} \sin(n\omega_1 t)\, \mathrm{d}t = \frac{2v_{\mathrm{BUS}}}{n^2\pi\omega_1 L_m}\cos(n\omega_1 t) \tag{3.92}$$

and the magnetising current resulting from equation (3.89) is

$$i_p = \frac{2v_{\mathrm{BUS}}}{\pi\omega_1 L_m}\sum_{k=0}^{\infty}\left[\frac{1}{(6k+1)^2}\cos((6k+1)\omega_1 t) + \frac{1}{(6k+5)^2}\cos((6k+5)\omega_1 t)\right] \tag{3.93}$$

For a motor phase magnetising inductance of an equivalent N turns, the resultant motor phase air gap flux phasor is

$$\phi_p = \frac{2v_{\mathrm{BUS}}}{\pi\omega_1 N}\sum_{k=0}^{\infty}\left[\frac{1}{(6k+1)^2}\cos((6k+1)\omega_1 t) + \frac{1}{(6k+5)^2}\cos((6k+5)\omega_1 t)\right] \tag{3.94}$$

The relative amplitudes of these motor phase harmonic quantities are summarised in Table 3.8.

Voltage Control and its Effect on Harmonics The peak amplitude of the fundamental frequency voltage in equation (3.89) is

$$v_{p(1)} = (2v_{\mathrm{BUS}})/\pi$$

and from equation (3.94) the peak amplitude of the fundamental air gap flux phasor is

$$\phi_{p(1)} = \frac{1}{\omega_1 N}\frac{2v_{\mathrm{BUS}}}{\pi} = \frac{v_{p(1)}}{\omega_1 N} \tag{3.95}$$

Table 3.8 Relative amplitudes of motor phase harmonics

Quantity	Harmonic number, n								
	1	5	7	11	13	17	19	23	25
v_p	1.000	0.200	0.143	0.091	0.077	0.059	0.053	0.043	0.040
i_p	1.000	0.040	0.020	0.008	0.006	0.004	0.003	0.002	0.002
ϕ_p	1.000	0.040	0.020	0.008	0.006	0.003	0.003	0.002	0.002

To maintain $\phi_{p(1)}$ constant when the fundamental frequency ω_1 varies, it is evident from equation (3.95) that $v_{p(1)}$ must be made a linear function of ω_1.

Some high-power inverter-fed a.c. motor speed controllers employ a separate d.c. chopper power supply in the d.c. bus to vary the voltage linearly with frequency. In this case the inverter output voltage waveforms are always square waves, as shown in Figure 3.56, and the air gap harmonic flux vectors have the relative amplitudes indicated in Table 3.8.

An alternative to independent d.c. voltage control is the use of pulse width modulation, discussed in the next section.

Pulse Width Modulation A popular drive configuration consists of a VSI operating on the PWM concept in order to economise on power semiconductor switching stages. The operating principle consists of chopping the basic inverter square wave output voltage of Figure 3.56 in order to control the fundamental frequency voltages.

In its simplest form a saw-tooth wave [28] is used to modulate the chops, as shown in Figure 3.57. The saw-tooth has a frequency which is a multiple of three times the sine wave frequency, allowing symmetrical three-phase voltages to be generated from a three-phase sine wave set and one saw-tooth waveform. This method controls line-to-line voltage from zero to full voltage by increasing the magnitude of the saw-tooth or a sine-wave signal, with little regard to the harmonics generated.

The most significant areas of voltage in the spectrum, apart from the fundamental, occur at the carrier frequency (saw-tooth frequency) and its two sidebands, and to a significant extent at each multiple of these frequencies in the spectrum. When the carrier frequency is six times the fundamental, the triplen harmonics cancel in the system; however, the phase waveforms of Figure 3.57 do not have half-wave symmetry, hence even harmonics are present.

If the carrier frequency is a large multiple of the fundamental, the first large harmonics encountered are high in the harmonic spectrum.

Single-phase bridge inverters can use either bipolar or unipolar PWM switching schemes. With bipolar switching two legs of the bridge are synchronised so that either $+V_d$ or $-V_d$ appears across the load. The harmonics in the inverter output voltage

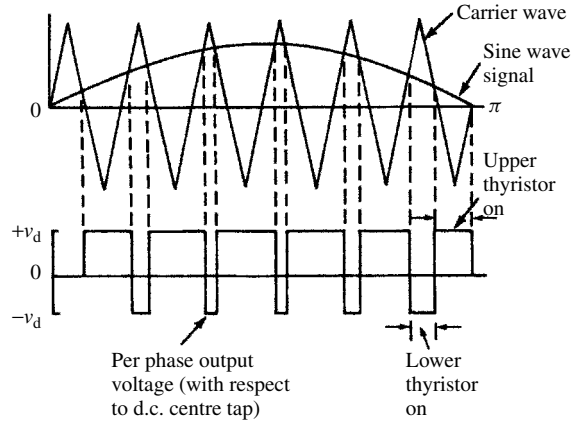


Figure 3.57 Principle of PWM

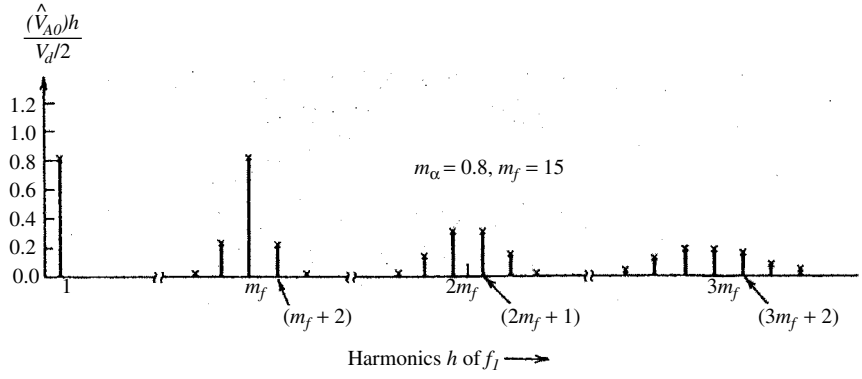


Figure 3.58 Harmonic spectrum with bipolar switching

are sidebands centred around the switching frequency and its multiples, as shown in Figure 3.58, the harmonic orders being given by:

$$\bullet \; h = km_f \pm n$$

where m_f is the frequency modulation ratio, and k and n are integers.

For odd values of k, harmonics only exist for even values of n and vice versa.

With unipolar switching, each leg of the inverter is controlled independently so that there are periods when both sides of the load are connected to the same d.c. rail, resulting in zero output voltage. This has the effect of doubling the switching frequency as now the harmonics present are given by:

$$\bullet \; h = k2m_f \pm n.$$

The spectrum for the unipolar switching scheme is shown in Figure 3.59.

PWM with Selected Harmonic Elimination More efficient PWM techniques have been developed to control the fundamental and harmonic voltages simultaneously [29–32]. For this purpose the chops can be created at predetermined angles of the

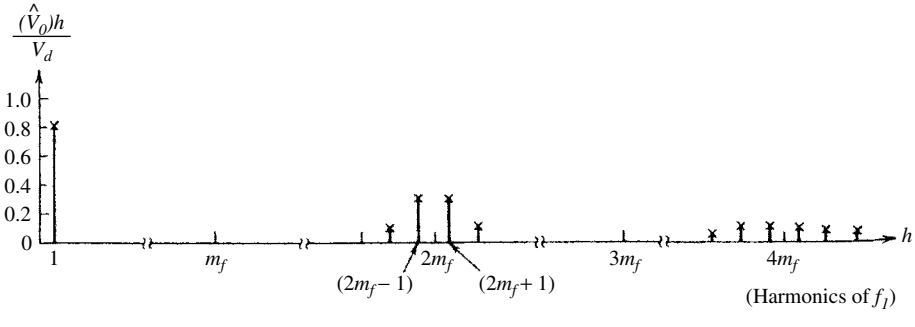


Figure 3.59 Harmonic spectrum with unipolar switching

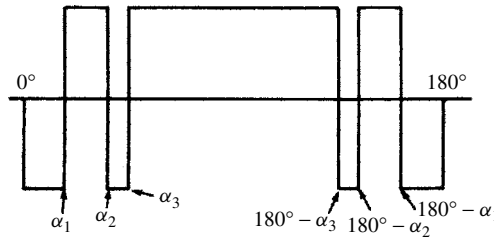


Figure 3.60 PWM wave on the basis of selected harmonic elimination by a look-up table

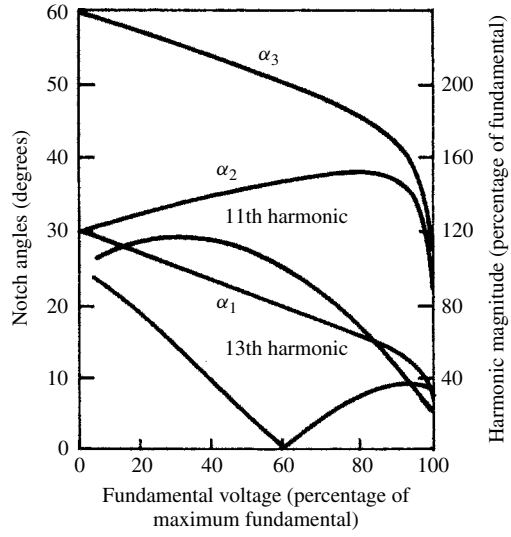


Figure 3.61 Notch angle curves with voltage control and selected elimination (for 5th and 7th harmonics)

square wave as shown in Figure 3.60. By way of example, Figure 3.61 illustrates the case where the fifth and seventh harmonics are eliminated with the help of a look-up table storing the angles required.

In the method of reference [32] the period is divided into six regions. If the second and fifth regions of each phase waveform are filled with a train of pulses, or chops, only these pulses appear in the line-to-line voltage.

Harmonic voltages occur at multiples of the carrier frequency (i.e. the chop number per half-wave of the phase voltage (m) times six) with sidebands, given by $L(6m \pm 1)$, where $L = 1, 3, 5, 7$.

Here also the carrier is a triplen harmonic and is cancelled out in a three-phase system. Moreover, the phase waveforms have such symmetry that there are no even harmonics. The higher m is, the higher up the spectrum the harmonic voltages occur.

The number of inverter switchings per second, $F(2m + 1)$, limits the number of chops allowable as fundamental frequency increases, e.g. for eight chops there are 17 on/off switchings per period.

In order to keep harmonic orders high in the spectrum, the number of chops is changed as fundamental frequency increases.

Further reduction of lower-order harmonics can be achieved by the use of complex PWM control waveform strategies, at the cost of increasing the inverter switching rate. For a given maximum inverter phase switching rate, the problem is to choose that PWM control strategy which will achieve the desired linear variation of fundamental voltage amplitude with frequency and reduce the effect of harmonic torques, or minimise the harmonic power losses within the motor.

Generally, at any fundamental switching frequency, each chop per half cycle of the inverter phase voltage waveform can eliminate one harmonic of the waveform or reduce a group of harmonic amplitudes [29]. Thus for m chops per half cycle one chop must be utilised to control the fundamental harmonic amplitude, so $m - 1$ degrees of freedom remain. The $m - 1$ degrees of freedom may be utilised to eliminate completely $m - 1$ specified low-order harmonics or to minimise motor power losses caused by a specified range of harmonics within the motor.

At any fundamental frequency, elimination of the lower-order harmonics from the phase waveforms will cause the portion of the r.m.s. which was provided by the eliminated harmonics to be spread over the remaining harmonic magnitudes. This occurs because the total harmonic r.m.s. voltage cannot change. The effect of this shifting motor performance needs to be determined, but the integrating filter characteristic of the motor should be more effective in reducing the current harmonics at higher orders.

Multi-Stepped Converters Rather than increasing the frequency of the PWM pattern to reduce the harmonic content of the output voltage, a multi-bridge configuration with parallel connected units can be subjected to a phase-shifted carrier, as shown in Figure 3.62. Considering n units, each carrier is shifted by T/n, where T is the period of the fundamental reference wave. Thus the voltage harmonic components of the individual units are shifted with respect to each other and can be designed to be cancelled when the outputs of the various bridges are added. In the case illustrated in Figure 3.62(b) the carrier to fundamental frequency ratio is 9 and thus the individual bridges have harmonic orders around the 9th and multiples of it. However, the use of four units produces the spectrum shown in Figure 3.62(e), where the lowest dominant harmonic orders are in the region of the 36th.

3.9 Thyristor-Controlled Reactors

3.9.1 The Static VAR Compensator (SVC)

Static VAR compensators using thyristor-controlled reactors, such as shown in Figure 3.63, are in common use in high-voltage transmission systems and some industrial plant like electric arc furnaces. Their main purpose is to provide fast voltage controllability and various other related effects such as flicker reduction, power factor improvement, phase balancing and power system stability.

Figure 3.64 shows a typical three-phase SVC circuit connected in delta. The currents in the three coils are delayed by almost 90° with respect to their corresponding voltages because the resistive effect is not significant.

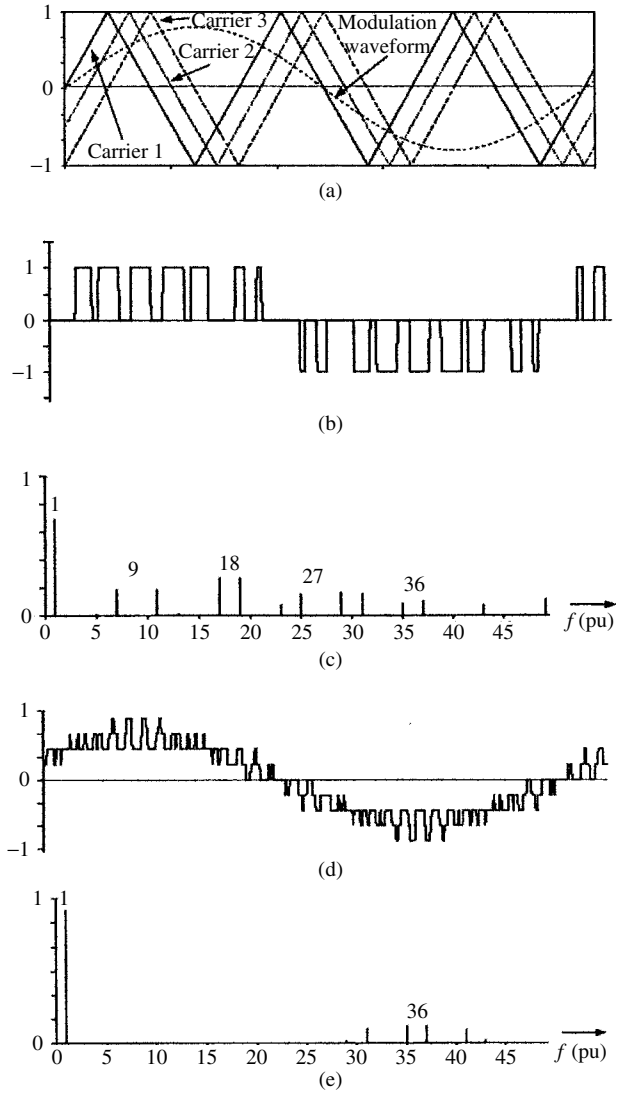


Figure 3.62 Multi-module harmonic reduction by carrier phase shifting. (a) Phase shifting carrier principle; (b) output voltage of the individual units; (c) harmonic spectrum of the individual units; (d) total output voltage; (e) harmonic spectrum for four units IEE © copyright

As illustrated in Figure 3.65(a), under uninterrupted current conditions the current is sinusoidal; however, the firing delays reduce the magnitude of the currents and distort their waveforms.

The instantaneous current has the expression:

$$i = \sqrt{2}\frac{V}{X_L}(\cos(\alpha) + \cos(\omega t)) \quad \text{for } \alpha < \omega t < \alpha + \sigma$$

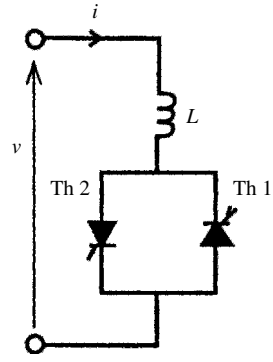


Figure 3.63 A thyristor-controlled reactor

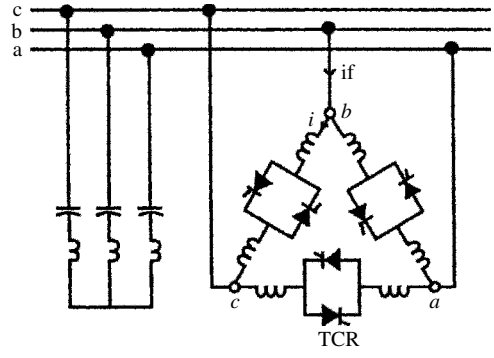


Figure 3.64 Three-phase configuration of a TCR in parallel with a shunt capacitor bank

and

$$i = 0 \quad \text{for } \alpha + \sigma < \omega t < \alpha + \pi \tag{3.96}$$

where V is the r.m.s. value of the supply voltage, $X_L = \omega L$ is the coil reactance at the fundamental frequency and α is the firing delay with respect to the corresponding voltage.

The harmonic currents produced by the partial conduction are of odd orders, provided that the firing delays are the same in the two back-to-back thyristor valves.

The r.m.s. value of the harmonic currents is given by the expression [33]:

$$I_n = \frac{4V}{\pi X_L}\left[\frac{\sin((n+1)\alpha)}{2(n+1)} + \frac{\sin((n-1)\alpha)}{2(n-1)} - \cos(\alpha)\frac{\sin(n\alpha)}{n}\right] \text{ for } n = 3, 5, 7, \ldots \tag{3.97}$$

Table 3.9 includes the maximum values of the first 37 harmonics as a percentage of the fully conducting fundamental component, but the maximum values do not occur for the same firing delays. Under perfectly symmetrical voltage conditions the values in brackets (of triplen harmonics) are present in the individual phases but are kept out of the line by the delta connection. However, in applications like the electric arc

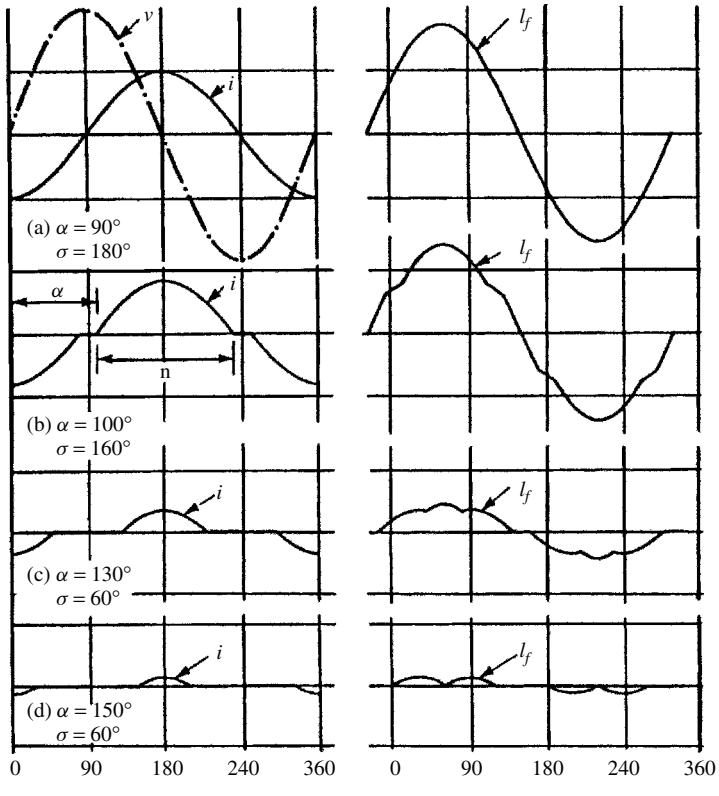


Figure 3.65 Current waveforms in the TCR of Figures 3.63 and 3.64

furnace, where the voltages are unbalanced due to the unstable arc periods, the third harmonic currents also appear in the line currents.

3.9.2 Thyristor-Controlled Series Compensation (TCSC)

The TCSC consists of a capacitor bank and a thyristor-controlled inductor connected in parallel as shown in Figure 3.66.

When the thyristor valve is triggered before the capacitor voltage crosses the zero line the device is in the capacitive boost mode and a capacitor discharge current pulse will circulate through the inductor, as shown in Figure 3.67.

When the thyristor is triggered after the capacitor voltage crosses the zero line the device is in the inductive boost mode, giving rise to the waveforms shown in Figure 3.68. As the capacitor provides a low impedance path for the harmonic frequencies, very little current will pass to the transmission line, the main interest being the harmonic voltages created at the terminals of the TCSC; these can be calculated by representing the thyristor branch as a current source. Normally the TCSC operates in the capacitive boost mode, under which condition only the lowest-order harmonics will have any practical significance.

Table 3.9 Maximum amplitude of the current harmonics produced by the TCR

Harmonic order	%
1	100
3	(13.78)
5	5.05
7	2.59
9	(1.57)
11	1.05
13	0.75
15	(0.57)
17	0.44
19	0.35
21	(0.29)
23	0.24
25	0.20
27	(0.17)
29	0.15
31	0.13

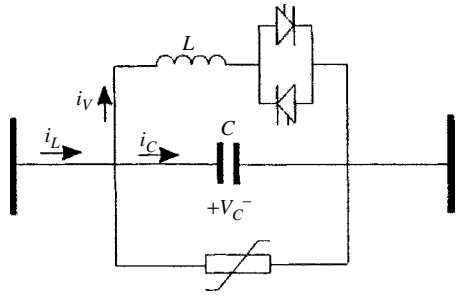


Figure 3.66 TCSC circuit

3.10 Modulated Phase Control

The main application of modulated phase control is the cycloconverter, which provides static power conversion from one frequency to another. The basic three-phase cycloconverter, shown in Figure 3.69 feeding an induction motor, consists of a dual configuration (A and B) of three pairs of six-pulse bridges connected in anti-parallel; $i+$ and $i-$ are the output currents, $u+$ and $u-$ the output voltages, i_R i_Y i_B the stator currents and u_R u_Y u_B the stator voltages. The mains and motor frequencies are f_1 and f_2, respectively.

The cycloconverter configuration is controlled through time-varying phase-modulated firing pulses so that it produces an alternating, instead of a direct, output voltage per phase as illustrated in Figure 3.70(a). The output current phase relationship and waveform (Figure 3.70(b)) depend on the load. The rectifier and inverter operating regions for each converter are shown in Figure 3.70(c) and (d).

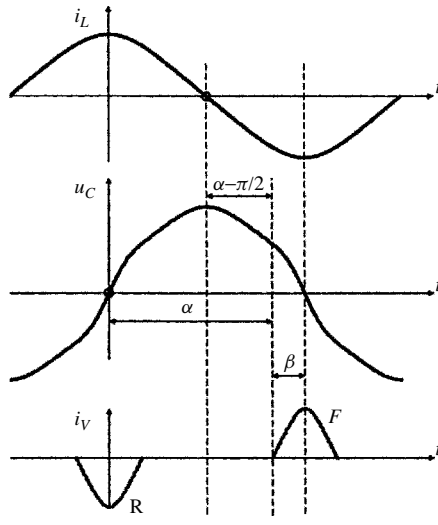


Figure 3.67 Voltage and current waveforms in the capacitive boost mode IEE © copyright

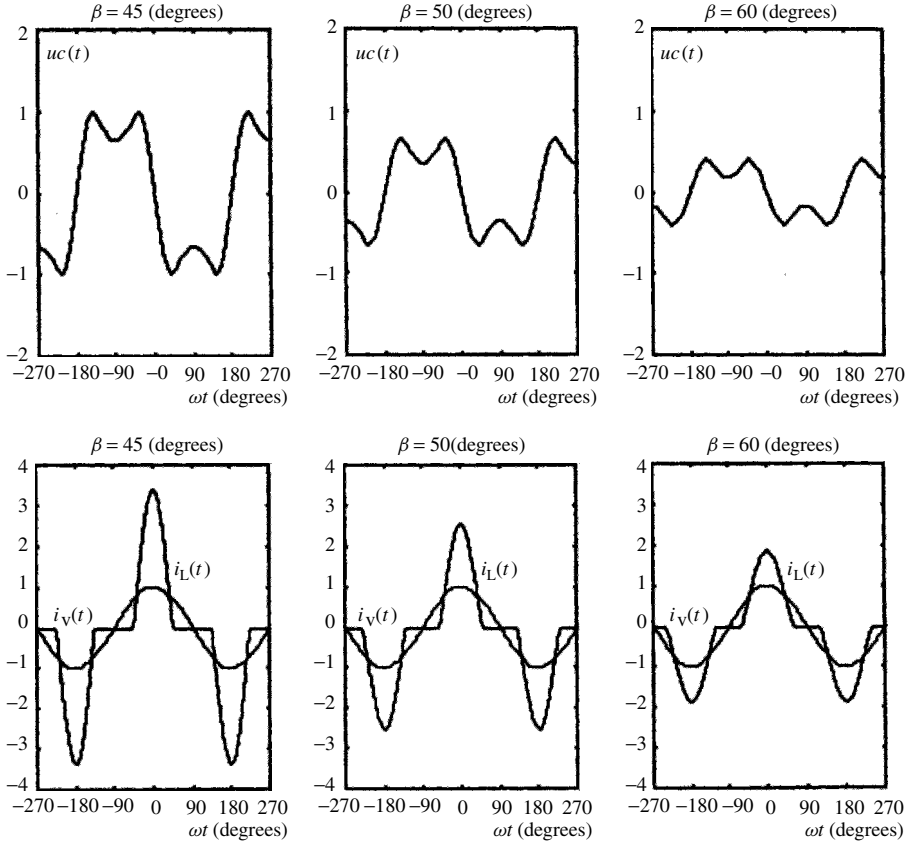


Figure 3.68 TCSC waveforms in the inductive boost mode IEE © copyright

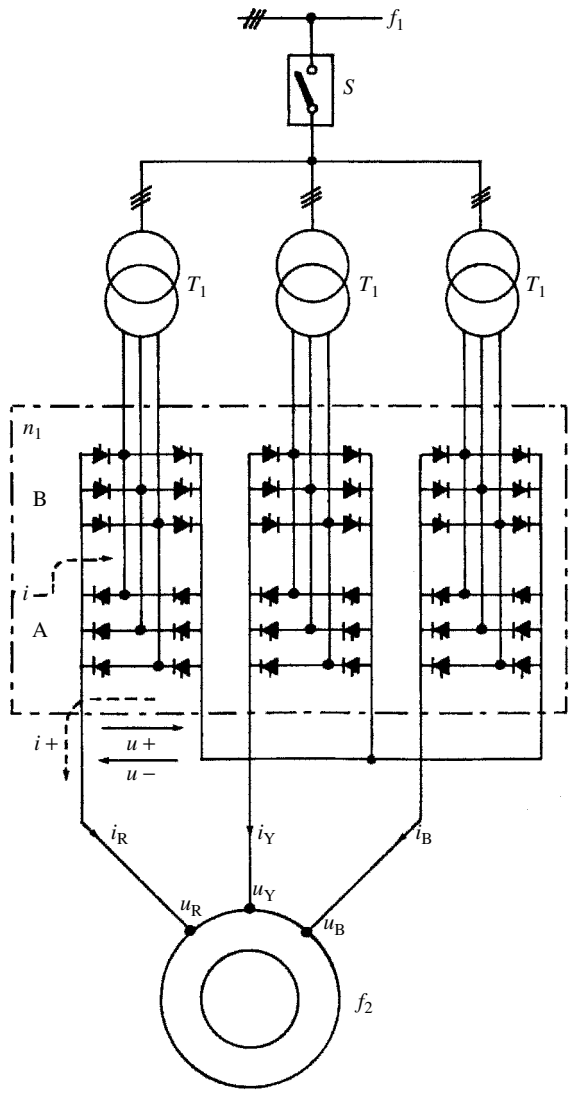


Figure 3.69 Basic circuit diagram of a six-pulse cycloconverter-fed a.c. motor

Similar to the phase-controlled converter, the input current will in general contain in-phase, quadrature and harmonic components. Practical cycloconverters operate with negligible internal circulating current between the two converters and thus only the circulating current-free mode of operation is of importance with regard to harmonic assessment.

The output voltage waveform is formed by selected intervals of the three-phase input voltage supply and the input current in each phase by selected intervals of the output currents.

All practical converter configurations used for large power ratings are combinations of the basic three-pulse group. Moreover, the harmonic content of these multipulse

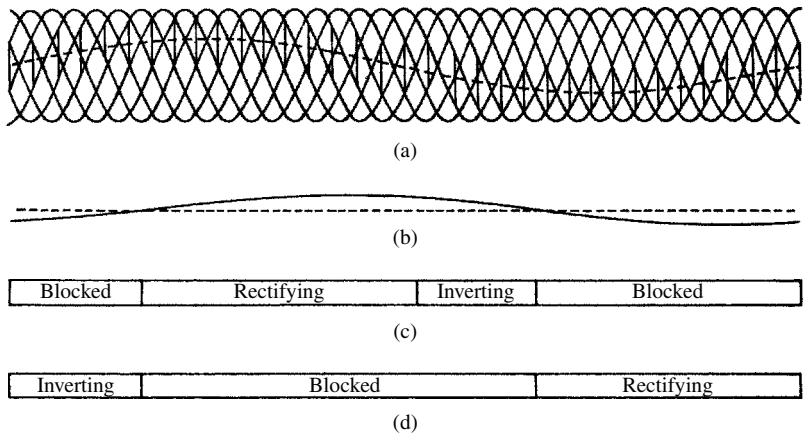


Figure 3.70 Theoretical waveforms for a six-pulse cycloconverter on half-maximum output voltage ($r = 0.5$) with a displacement angle of 60° and one-sixth output frequency: (a) output voltage; (b) output current; (c) A bridge operating mode; (d) B bridge operating mode

circuits can easily be derived from the basic harmonic series of the three-pulse phase-controlled converter. The three-pulse waveform with arbitrary firing angle control should therefore provide the most general case for harmonic analysis.

The conventional Fourier analysis (described in Chapter 2) is not practical for the derivation of cycloconverter harmonic components since the frequency spectra of the output voltage and input current waveforms are related to both the main input and output frequencies; they produce 'beat frequencies' which are both the sums and differences of multiples of both these frequencies. Classical Fourier analysis resolves a periodic waveform into a fundamental component, the frequency of which is equal to the fundamental repetition frequency of the wave, and a series of harmonic components, which are multiples of the fundamental frequency. The cycloconverter waveforms, on the other hand, contain frequencies which are not integer multiples of the main output frequency. In fact, there may not even be a clearly defined fundamental output frequency. Only when the output frequency is an exact submultiple of the product of the input frequency and the converter pulse number, is each output cycle identical with the next, i.e.

$$f_0 = \frac{3f_i}{k} \tag{3.98}$$

where k is an integer.

A more general method is described in the next section, which provides the output voltage and input current harmonic component in terms of each of the independent variables.

3.10.1 The Switching Function Approach [34]

The general method is illustrated in Figure 3.71, where the effect of each thyristor switching is derived independently and the overall output waveform is then expressed

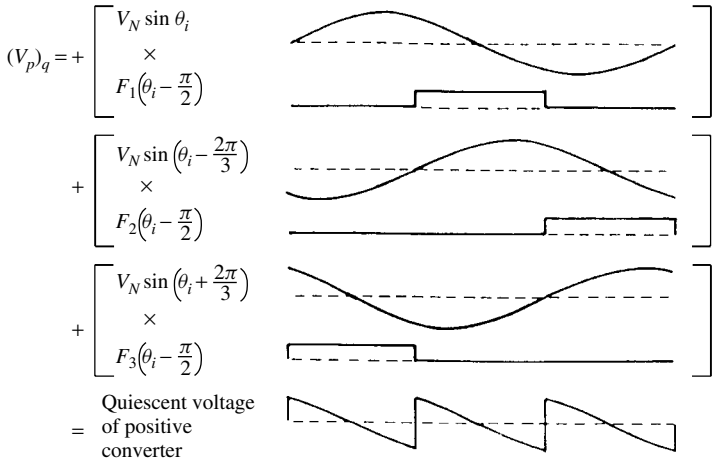


Figure 3.71 Derivation of voltage waveforms of the positive converter for quiescent ($\alpha = 90^\circ$) operation. From [34]

as the addition of all the wave segments generated by the individual thyristors. The effect of each thyristor is expressed as the product of the appropriate input voltage (or output current) waveform and a 'switching function', of unity and zero amplitudes when the thyristor is ON and OFF, respectively.

By expressing the switching function as a phase-modulated harmonic series, a general harmonic series can be derived for the output voltage (or input current) waveform in terms of the independent variables.

The quiescent firing (90°) is used as a reference for the modulated firings. The quiescent firing produces zero voltage in both the positive and negative converters.

By way of illustration the quiescent voltage waveform of the positive converter, shown in Figure 3.71, is given by

$$(v_p)_q = V_N \sin\theta_i \cdot F_1\left(\theta_i - \frac{\pi}{2}\right) + V_N \sin\left(\theta_i - \frac{2\pi}{3}\right) \cdot F_2\left(\theta_i - \frac{\pi}{2}\right) + V_N \sin\left(\theta_i + \frac{2\pi}{3}\right) \cdot F_3\left(\theta_i - \frac{\pi}{2}\right). \tag{3.99}$$

The modulated firing control provides a 'to and fro' phase modulation $f(\theta_0)$ of the individual firings with respect to the quiescent firing.

In general the value of $f(\theta_0)$ will oscillate symmetrically to and from about zero, at a repetition frequency equal to the selected output frequency. The limits of control on either side of the quiescent point are then $\pm\pi/2$. Thus the general expressions for the switching function of the positive and negative converters are

$$F\left(\theta_i - \frac{\pi}{2} + f(\theta_0)\right) \quad \text{and} \quad F\left(\theta_i + \frac{\pi}{2} - f(\theta_0)\right)$$

since the phase modulation of the firing angles of the positive and negative converters is equal but of opposite sign.

Moreover, it has been shown [34] that the optimum output waveform, i.e. the minimum r.m.s. distortion, is achieved when the firing angle modulating function is derived by the 'cosine wave crossing' control. Under this type of control the phase of firing of each thyristor is shifted with respect to the quiescent position by

$$f(\theta_0) = \sin^{-1}(r)\sin(\theta_0), \tag{3.100}$$

where r is the ratio of amplitude of wanted sinusoidal component of output voltage to the maximum possible wanted component of output voltage, obtained with 'full' firing angle modulation, with no commutation overlap.

3.10.2 Derivation of Input Current Harmonics

For the derivation of the input current waveform it is more convenient to use two switching functions, i.e. the thyristor and the converter (i.e. the conducting half of the dual converter) switching functions.

It is also necessary to make the following approximations: (i) the output current is purely sinusoidal; and (ii) the source impedance (including transformer leakage) is neglected. A single-phase output is illustrated in Figure 3.72, and the current in each phase of the supply is given by

$$\begin{aligned} i_A = {} & I_0 \sin(\theta_0 + \phi_0) \cdot F_1\left(\theta_i - \frac{\pi}{2} + f(\theta_0)\right) \cdot F_p(\theta_0) \\ & + I_0 \sin(\theta_0 + \phi_0) \cdot F_1\left(\theta_i + \frac{\pi}{2} - f(\theta_0)\right) \cdot F_N(\theta_0) \end{aligned} \tag{3.101}$$

From conventional Fourier analysis F_1, F_p and F_N can be expressed in terms of the following series:

$$\begin{aligned} F_1\left(\theta_i \mp \frac{\pi}{2} \pm f(\theta_0)\right) = \frac{1}{3} + \frac{\sqrt{3}}{\pi}\Bigg[& \sin\left(\theta_i \pm \frac{\pi}{2} \mp f(\theta_0)\right) \\ & - \frac{1}{2}\cos 2\left(\theta_i \pm \frac{\pi}{2} \mp f(\theta_0)\right) \\ & - \frac{1}{4}\cos 4\left(\theta_i \pm \frac{\pi}{2} \mp f(\theta_0)\right)\Bigg] \end{aligned} \tag{3.102}$$

$$F_p(\theta_0) = \frac{1}{2} + \frac{2}{\pi}\left[\sin(\theta_0 + \phi_0) + \frac{1}{3}\sin 3(\theta_0 + \phi_0) + \frac{1}{5}\sin 5(\theta_0 + \phi_0) + \cdots\right] \tag{3.103}$$

$$F_N(\theta_0) = \frac{1}{2} - \frac{2}{\pi}\left[\sin(\theta_0 + \phi_0) + \frac{1}{3}\sin 3(\theta_0 + \phi_0) + \frac{1}{5}\sin 5(\theta_0 + \phi_0) + \cdots\right] \tag{3.104}$$

Substituting in i_A and reducing,

$$\begin{aligned} i_A = I_0 \sin(\theta_0 + \phi_0)\Bigg\{ & \frac{1}{3} + \frac{\sqrt{3}}{\pi}\Bigg[\sin\theta_i \sin f(\theta_0) + \frac{1}{2}\cos 2\theta_i \cos 2f(\theta_0) \\ & - \frac{1}{4}\cos 4\theta_i \cos 4f(\theta_0) - \frac{1}{5}\sin 5\theta_i \sin 5f(\theta_0) + \cdots\Bigg] \end{aligned}$$

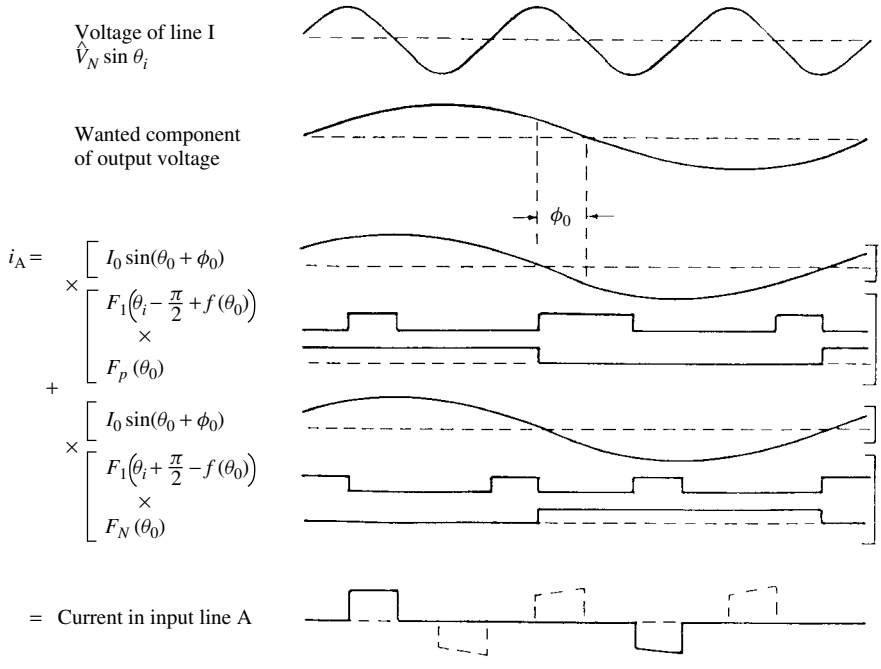


Figure 3.72 Derivation of the input line current of a cycloconverter. The current is shown in the bottom part of the figure as a continuous line for a single-phase load and as a broken line for a three-phase load. From [34]

$$+\frac{4\sqrt{3}}{\pi^2}\left[-\cos\theta_i\cos f(\theta_0) - \frac{1}{2}\sin 2\theta_i \sin 2f(\theta_0) + \frac{1}{4}\sin 4\theta_i \sin 4f(\theta_0)\right.$$
$$\left.+\frac{1}{5}\cos 5\theta_i \cos 5f(\theta_0)\ldots\right]\left[\sin(\theta_0+\phi_0) + \frac{1}{3}\sin 3(\theta_0+\phi_0)\right.$$
$$\left.+\frac{1}{5}\sin 5(\theta_0+\phi_0) + \cdots\right]\Bigg\} \tag{3.105}$$

In the above expression $f(\theta_0) = \sin^{-1}(r)\sin(\theta_0)$ (see equation (3.100)) as explained above when the modulating function uses the cosine wave crossing control method.

In general, however, the output will also be three-phase and, assuming perfectly balanced input and output waveforms, each phase of the input will include the contribution of the three output currents, i.e., $i_A = i_{A1} + i_{A2} + i_{A3}$, and the corresponding waveform is illustrated by the broken line in Figure 3.72.

The above procedure can be extended to cases of three-phase output, under different transformer connections and different converter configurations. This, however, is a very long and tedious task, thoroughly documented in Pelly's book [34] and will not be detailed here. The chart of Figure 3.73 contains the main results of the harmonic analysis for the case of a balanced three-phase output; it gives the relationships which exist between the predominant harmonic frequencies present in the three-pulse input current waveform versus the output to input frequency ratio. It also indicates the groups of harmonics eliminated by the use of higher pulse numbers.

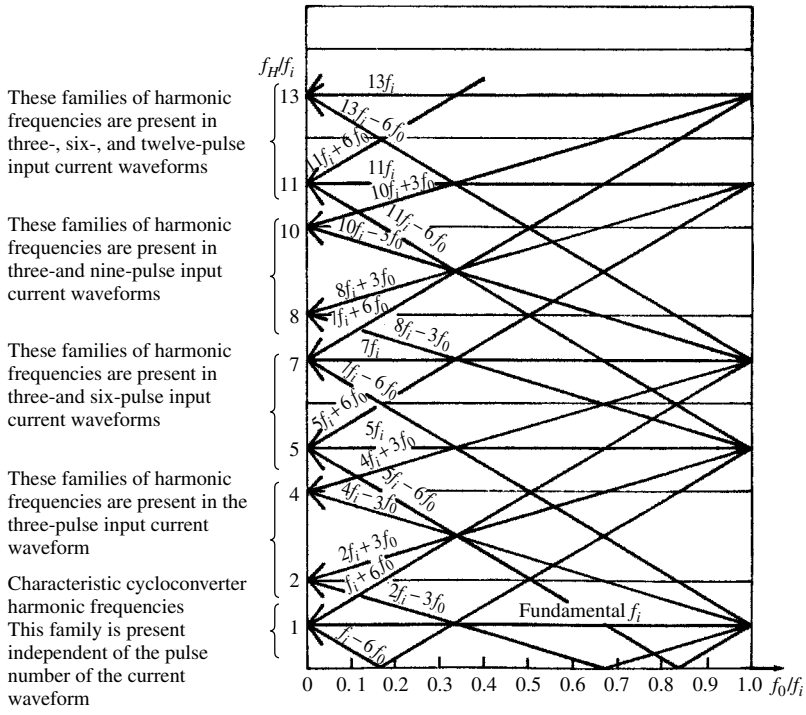


Figure 3.73 Relationships between the predominant harmonic frequencies of a cycloconverter and the output to input frequency ratio. From [34]

3.11 A.C. Regulators

3.11.1 Single-Phase Full-Wave Controller

The main application of this type of controller is in single-phase resistive loads, particularly as dimmers for incandescent lighting. They consist of a back-to-back thyristor pair in series with the load as shown in Figure 3.74. The output voltage waveform, controlled by firing delay with reference to the voltage zero crossings, is as shown in Figure 3.75 and its harmonic content, plotted as a function of the firing angle, is illustrated in Figure 3.76.

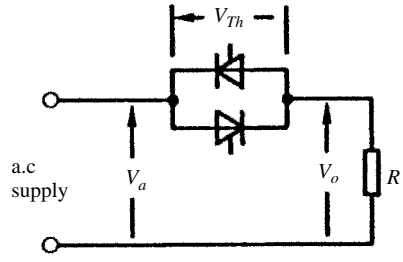


Figure 3.74 Single-phase full-wave regulator

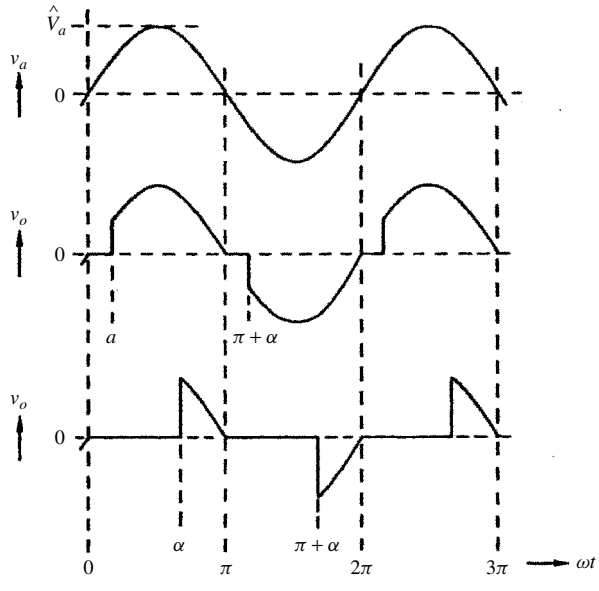


Figure 3.75 Waveforms of the single-phase regulator of Figure 3.74

3.11.2 Integral Cycle Control

Instead of point on wave switching selection, this type of control is based on the switching of entire voltage half-cycles using a pair of back-to-back thyristors, as shown in Figure 3.77. It is often called 'burst-firing' and has found application in long time constant loads (e.g. temperature control in electric ovens).

The fundamental supply frequency cannot be used as a basis for the Fourier analysis in this case, because the period of repetition, and thus the lowest frequency produced, is now a variable subharmonic frequency.

If the number of ON cycles is N and the number of cycles over which the pattern is repeated is M the period of repetition is M/f, where f is the supply frequency.

The lowest frequency, which now becomes the fundamental frequency, is f/M Hz. With reference to this lowest frequency, the current being analysed can be expressed as

$$i = I_{\max} \sin(M\omega t) \tag{3.106}$$

Using the time reference indicated in Figure 3.77(b), the A_0 and A_n Fourier coefficients are zero, i.e. there are only sine terms, their general expression being

$$\begin{aligned} B_n &= \frac{2}{\pi} \int_0^{2\pi f/M} [-I_{\max} \sin(M\omega t) \sin(n\omega t)] \, \mathrm{d}(\omega t) \\ &= -I_{\max} \cdot \frac{2M}{\pi} \cdot \frac{\sin((N/M)n\pi)}{M^2 - n^2} \end{aligned} \tag{3.107}$$

Consider as an example the case where $M = 5$ and $N = 1$.

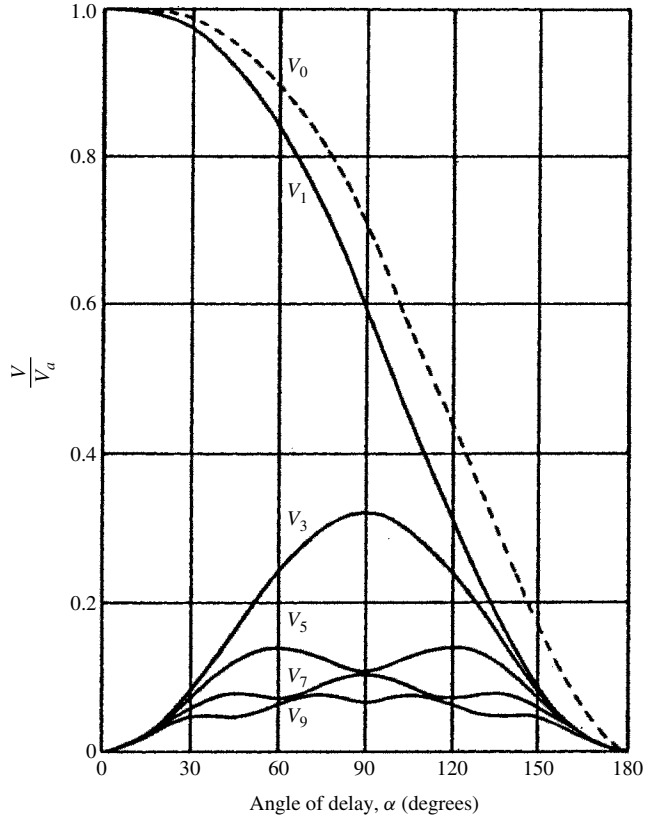


Figure 3.76 Harmonic content of the a.c. regulator of Figure 3.74

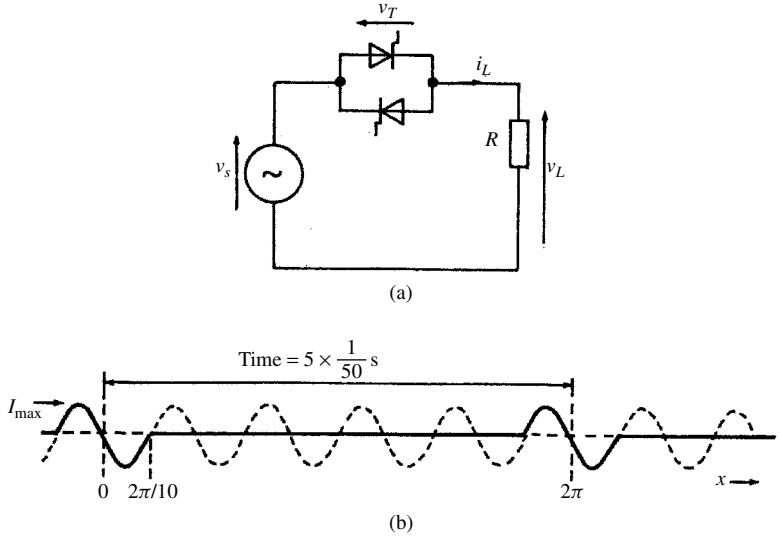


Figure 3.77 Integral cycle control: (a) basic circuit; (b) voltage waveform

The lowest repetition frequency for a 50 Hz supply is therefore

$$f_1 = \frac{f}{M} = \frac{50}{5} = 10, \tag{3.108}$$

i.e. $n = 1$ corresponds with 10 Hz.

The per unit levels of the various frequencies present, obtained from equation (3.107), are

$$\begin{aligned} f_1(10\text{ Hz}) &= 0.078 & f_8(80\text{ Hz}) &= 0.078 \\ f_2(20\text{ Hz}) &= 0.14 & f_9(90\text{ Hz}) &= 0.033 \\ f_3(30\text{ Hz}) &= 0.189 & f_{10}(100\text{ Hz}) &= 0 \\ f_4(40\text{ Hz}) &= 0.208 & f_{11}(110\text{ Hz}) &= 0.019 \\ f_5(50\text{ Hz}) &= 0.2 & f_{12}(120\text{ Hz}) &= 0.025 \\ f_6(60\text{ Hz}) &= 0.17 & f_{13}(130\text{ Hz}) &= 0.021 \\ f_7(70\text{ Hz}) &= 0.126 & f_{14}(140\text{ Hz}) &= 0.01 \end{aligned}$$

When n is multiple of M the coefficients are zero, i.e. for 100 Hz, 150 Hz, etc.

This clearly shows that integral cycle control produces no harmonic frequencies. It does, however, produce inter-harmonic and subharmonic frequencies.

3.12 Discussion

Within the normal operating range the harmonic content of the transformer magnetising current is not significant. It is only during energisation and when operating above their normal voltage that transformers can considerably increase their harmonic contribution.

Similarly, the harmonic content of the internal e.m.f. of well-designed synchronous machines is also small. Rotor saliency in the presence of transmission system unbalance and/or load-injected harmonic currents is likely to be the main source of generator e.m.f. distortion. Induction motors produce time harmonics as a result of the harmonic content of the m.m.f. distribution, and these are speed dependent. However, the impact on the power system is small, partly due to operational diversity and partly to the smaller rating of these machines, when compared with the synchronous generators.

Power electronic devices constitute the main sources of harmonic current distortion. The characteristics of the main power electronic devices have been described in this chapter with reference to their harmonic contribution under the assumption of specified terminal conditions. For most applications this is an acceptable approximation. However the input terminal conditions (normally the voltage waveform) can change as a result of the interaction that exists between the nonlinear power electronic component and the rest of the system. A more rigorous analysis of the harmonic sources taking this effect into account is described in Chapter 8.

3.13 References

1. Bowles, J.P. (1980) Alternative techniques and optimisation of voltage and reactive power control at h.v.d.c. convertor stations. Paper presented at the IEEE Conference on Overvoltages and Compensation on Integrated A.C.–D.C. Systems, Winnipeg.
2. Yacamini, R. (1981) *Harmonics caused by transformer saturation. Presented at the International Conference on Harmonics in Power Systems*, UMIST, Manchester.
3. Yacamini, R. and de Oliveira, J.C. (1978) Harmonics produced by direct current in converter transformers, *Proc. IEE*, **125**, 873–8.
4. Wallace A.K., Ward, E.S. and Wright, A. (1974) Sources of harmonic current in slip-ring induction motors, *Proc. IEE*, **121**, 1495–1500.
5. Jahn, H.H. and Kauferle, J. (1974) Measuring and evaluating current fluctuations of arc furnaces, *IEE Conf. Publ.*, **110**, 105–9.
6. Coates, R. and Brewer, G.L. (1974) The measurement and analysis of waveform distortion caused by a large multi-furnace arc furnace installation, *IEE Conf. Publ.*, **110**, 135–43.
7. Lemoine, M. (1978) Resonances en presence des harmoniques crees par les convertisseurs de puissance et les fours a arcs associes a des dispositifs de compensation, *Revue Gen. Electricite*, **87**, 945–62.
8. Muntz, V.A. and Jones, R.M. (undated) *Control of third harmonic current in three-phase neutrals, e.g. large fluorescent lighting installations*, Monograph MT, No. 3, State Electricity Commission of Victoria, Australia.
9. Harker, B.J. (1983) Estimation of the harmonic currents entering the power system as a result of a.c. electrified railway traction. Paper presented at the Annual General Meeting, IPENZ, New Zealand.
10. Adamson, C. and Hingorani, N.G. (1960) *High Voltage Direct Current Power Transmission*, Garraway, London, Ch. 3.
11. Dobinson, L.G. (1975) Closer accord on harmonics. *Electronics and Power*, May, 567–72.
12. Giesner, D.B. and Arrillaga, J. (1972) Behaviour of h.v.d.c. links under unbalanced a.c. fault conditions. *Proc. IEE*, **119**, 209–15.
13. CIGRE WG 14-03 (1989) AC harmonic filters and reactive compensation with particular reference to non-characteristic harmonics, *Complement to Electra*, **63** (1979).
14. Ainsworth, J.D. (1981) Harmonic instabilities. Paper presented at the Conference on Harmonics in Power Systems, UMIST, Manchester.
15. Ainsworth, J.D. (1968) The phase-locked oscillator—a new control system for controlled static convertors, *Trans. IEEE*, **PAS-87**(3), 859–65.
16. Kimbark, E.W. (1971) *Direct Current Transmission,* vol. I, John Wiley & Sons, New York.
17. Swartz, M., Bennett, W.R. and Stein, S. (1966) *Communication Systems and Techniques*. McGraw-Hill, New York.
18. Persson, E.V. (1970) Calculation of transfer functions in grid controlled converter system. *IEE Proc.*, **117**(5), 989–97.
19. Hu, L. and Yacamini, R. (1992) Harmonic transfer through converters and HVdc links. *IEEE Trans. Power Electronics*, **7**(4), 514–25.
20. CIGRE SC-14, WG 14.25 (1997) Harmonic cross-modulation in HVdc transmission, HVdc colloquium, Johannesburgh.
21. Asplund, G., Eriksson, K. and Svensson, K. (1997) DC transmission based on voltage source converters, CIGRE sc-14 colloquium, Johannesburgh, paper 5.7.
22. Mori, S., Matsuno, K., Hasegawa, T., Ohnishi, S., Takeda, M., Seto, M., Murakarni, S. and Ishiguro, F. (1993) Development of a large static VAR generator using self-commutated inverters for improving power system stability, *IEEE Trans. Power*, **8**(1), 371–7.
23. Song Y.H. and Johns A.T. (1999) *Flexible a.c. Transmission Systems* IEE Power and Engineering series 30, IEEE, Ch. 2.

24. Ooi, B.T., Joos, G. and Huang, X. (1997) Operating principles of shunt STATCOM based on three-level diode-clamped converters and twelve-phase magnetics, *IEEE Trans. Power Delivery*, **V14**(4).
25. Meynard, T. and Foch, H. (1993) Imbricated cells multi-level voltage source inverters for high voltage applications, *Eur. Power Electronics J.*, **V3**(2).
26. Lai, J.S. and Peng, F.Z. (1996) Multi-level converters—a new breed of power converters, *IEEE Trans. Industry Applications*, **32**(3), 509–17.
27. Liu, Y.H., Arrillaga, J. and Watson, N.R. (2002) Multi-level voltage-sourced conversion by voltage reinjection at six times the fundamental frequency, *IEE Proc. Electric Power Applications*, **V149**(3), 201–7.
28. Schonung, A. and Stemmler, H. (1973) Reglage d'un motor triphase reversible a l'aide d'un convertisseur statique de frequence commande suivant le procede de la sous-oscillation, *Rev. Brown Boveri*, **51**, 557–76.
29. Patel, H.S. and Hoft, R.G. (1973) Generalised technique of harmonic elimination in voltage control in thyristor inverters. Part 1. Harmonic elimination, *Trans. IEEE*, **IA-9**(3), 310–17.
30. Patel, H.S. and Hoft, R.G. (1974) Generalised technique of harmonic elimination and voltage control in thyristor inverters. Part 2. Voltage control techniques, *Trans IEEE*, **IA-10**(5), 666–73.
31. Buja, E.S. and Indri, G.B. (1977) Optimal pulse width modulation for feeding a.c. motors, *Trans. IEEE*, **IA-13**(1), 38–44.
32. Byers, D.J. and Harman, R.T.C. (1976) Control of a.c. motors in a new concept of electric town car, paper presented to the Institute of Engineers, Australia.
33. Miller, T.J.E. (1982) Reactive Power Control in Electric Systems, Wiley Interscience, New York.
34. Pelly, B.R. (1971) *Thyristor Phase-controlled Converters and Cycloconverters*, Wiley Interscience, New York.

4

Effects of Harmonic Distortion

4.1 Introduction

Once the harmonic sources are clearly defined, they must be interpreted in terms of their effects on the rest of the system and on personnel and equipment external to the power system.

Each element of the power system must be examined for its sensitivity to harmonics as a basis for recommendations on the allowable levels. The main effects of voltage and current harmonics within the power system are:

- The possibility of amplification of harmonic levels resulting from series and parallel resonances.
- A reduction in the efficiency of the generation, transmission and utilisation of electric energy.
- Ageing of the insulation of electrical plant components with consequent shortening of their useful life.
- Malfunctioning of system or plant components.

Among the possible external effects of harmonics are a degradation in communication systems performance, excessive audible noise and harmonic-induced voltage and currents.

4.2 Resonances

The presence of capacitors, such as those used for power factor correction, can result in local system resonances, which lead in turn to excessive currents and possibly subsequent damage to the capacitors [1].

4.2.1 Parallel Resonance

Parallel resonance results in a high impedance at the resonant frequency being presented to the harmonic source. Since the majority of harmonic sources can be considered as

Power System Harmonics, Second Edition J. Arrillaga, N.R. Watson
© 2003 John Wiley & Sons, Ltd ISBN: 0-470-85129-5

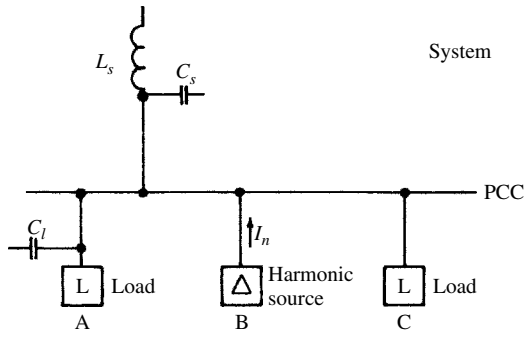


Figure 4.1 Parallel resonance at a point of common coupling (PCC)

current sources, this results in increased harmonic voltages and high harmonic currents in each leg of the parallel impedance.

Parallel resonances can occur in a variety of ways, the simplest perhaps being that where a capacitor is connected to the same busbar as the harmonic source. A parallel resonance can then occur between the system impedance and the capacitor.

Assuming the system impedance to be entirely inductive, the resonant frequency is

$$f_p = f\sqrt{\left(\frac{S_s}{S_c}\right)} \tag{4.1}$$

where f is the fundamental frequency (Hz), f_p is the parallel resonant frequency (Hz), S_s is the short-circuit rating (VAr) and S_c is the capacitor rating (VAr).

Further opportunities for parallel resonance can occur with a more detailed representation of the system. For instance in Figure 4.1 the harmonic current from consumer B encounters a high harmonic impedance at the busbar. This may be due to a resonance between the system inductance (L_s) and the system (C_s) and/or load capacitance (C_l).

To determine which resonance condition exists it is necessary to measure the harmonic currents in each consumer load and in the supply, together with the harmonic voltage at the busbar. In general, if the current flowing into the power system from the busbar is small, while the harmonic voltage is high, resonance within the power system is indicated. If instead a large harmonic current flows in consumer A's load and leads the harmonic voltage at the busbar, resonance between the system inductance and the load capacitor is indicated.

4.2.2 Series Resonance

Consider the system of Figure 4.2. At high frequencies the load can be ignored as the capacitive impedance reduces. Under these conditions a series resonant condition will exist when

$$f_s = f\sqrt{\left(\frac{S_t}{S_c Z_t} - \frac{S_l^2}{S_c^2}\right)}, \tag{4.2}$$

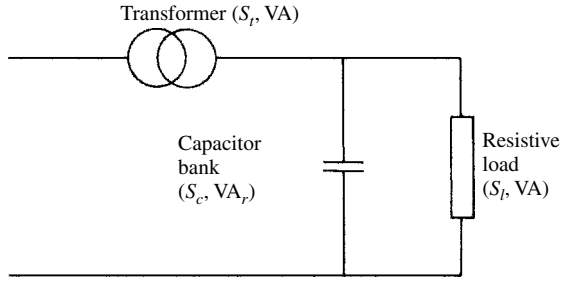


Figure 4.2 Series resonance circuit

where f_s is the series resonant frequency (Hz), S_t is the transformer rating, Z_t is the transformer per unit impedance, S_c is the capacitor rating and S_l is the load rating (resistive).

The concern with series resonance is that high capacitor currents can flow for relatively small harmonic voltages. The actual current that will flow will depend upon the quality factor Q of the circuit. This is typically of the order of 5 at 500 Hz.

4.2.3 Effects of Resonance on System Behaviour

Power Factor Correction Capacitors Harmonic resonances affect the design of power factor correction capacitors. The overload current capability of these capacitors is discussed in Section 4.4.3.

This problem can be illustrated with reference to a study carried out for an iron-sand mining plant consisting of six-pulse rectifiers and fed from a long-distance 11 kV line. The original rating of the scheme (8 MW at 0.85 power factor) was to be increased to 10 MW by the shunt connection of power factor correction capacitors at the plant terminals.

The minimum fault level at the point of connection was 35.4 MVA, which (on a 10 MW power base) is equivalent to a per unit maximum system impedance of

$$x_s = (V^2)/(\text{MVAF/MVAB}) = (1)/(35.4/10) = 0.28 \text{ p.u.}$$

The conversion from 8 to 10 MW required 3 MVAR (or 0.3 p.u. on the 10 MVA base), the corresponding capacitance being

$$x_c = V^2/\text{MVAR} = 1/(0.3) = 3.3 \text{ p.u.}$$

and this capacitance was divided into three independently switched banks.

The converter harmonic currents were now injected into the a.c. system impedance in parallel with the PF correction capacitors, the corresponding parallel resonant frequency resulting from the equation:

$$n\, x_s = (1/n)x_c \qquad \text{where } n = \omega_n/\omega$$

Therefore $n^2 = x_c/x_s = 3.3/0.28 = 11.8$, and $n = 3.4$ (when all the capacitance is connected), $n = 4.2$ (with one of the three banks disconnected) and $n = 5.9$ (with two banks disconnected).

However, measurements carried out at the plant indicated that the levels of third ($n = 3$) and fourth ($n = 4$) harmonic current content were insignificant, and the decision was made to eliminate the possibility of fifth harmonic resonance by placing 4% inductance in series with the capacitors.

Another area where resonance effects may lead to component failure is associated with the application of power line signalling (ripple control) for load management. In such systems tuned stoppers (filters) are often used to prevent the signalling frequency from being absorbed by low-impedance elements such as power factor correction capacitors. A typical installation is shown in Figure 4.3.

Where local resonances exist, excessive harmonic currents can flow, resulting in damage to the tuning capacitors. Figure 4.4 shows the harmonic currents recorded at one such installation where failure of this type occurred.

In another installation tuned stoppers (at 530 Hz) were fitted to 15 × 65 kVAr steps of power factor correction capacitance, each stopper rated at 100 A. Most of the stopper tuning capacitors failed within two days. The problem was eventually traced to a local

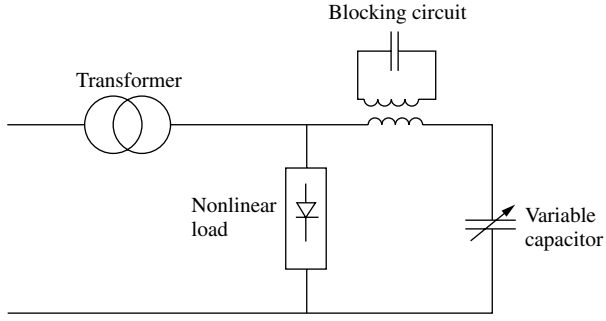


Figure 4.3 Tuned stopper circuit for ripple control signal

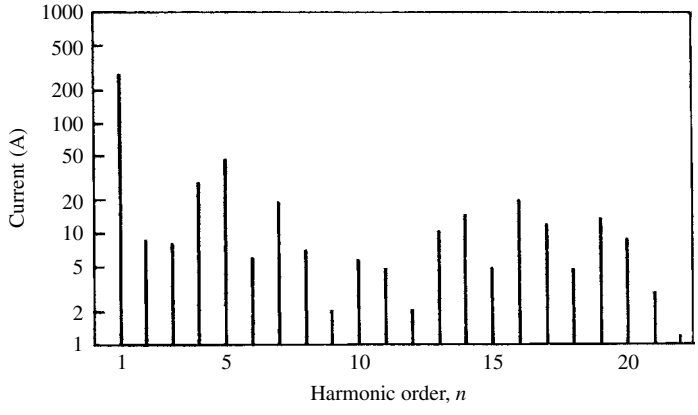


Figure 4.4 Harmonic currents measured through a blocking circuit

power system harmonic at 350 Hz, near to which frequency the tuned stoppers were found to series resonate with the power factor correction capacitors.

Magnification of Low-Order Harmonics The following simplified reasoning explains the harmonic magnification phenomena. Let us consider the case of a static converter (represented as a harmonic current injector) fed from an a.c. system of internal impedance Z_r at the h harmonic.

The a.c. system admittance at the fundamental and low-order harmonics is predominantly inductive, i.e.

$$Y_r = G_r - jB_r$$

In the absence of filters or compensation, the harmonic current (I_h) generates at the point of connection a harmonic voltage of amplitude

$$V_h = Z_r I_h = I_h / Y_r$$

When a capacitor bank or filters of admittance Y_f are present, the harmonic voltage at the point of connection becomes:

$$V_h' = I_h / (Y_r + Y_f)$$

and, since the admittance of a filter bank is predominantly capacitive ($Y_f = jB_f$),

$$V_h' = I_h / (G_r - jB_r + jB_f)$$

When $B_r = B_f$ the harmonic voltage is only limited by the system resistance, which is generally very small. Thus, when $Y_r + Y_f < Y_r$ the harmonic distortion is magnified, the magnification factor being:

$$V_h' / V_h = Y_r / (Y_r + Y_f)$$

Consequently, a low-order non-characteristic harmonic current, which has no practical adverse effect in the absence of the capacitor or filter banks, can be amplified to give a voltage greater that the filtered harmonics.

4.2.4 Complementary and Composite Resonances

The traditional definition of resonance as described above is used with reference to isolated parts of an overall system (e.g. the a.c. or d.c. sides of a static converter). This sort of resonance is well defined, being the frequency at which the capacitive and inductive reactances of the circuit impedance are equal. At the resonant frequency, a parallel resonance has a high impedance and a series resonance a low impedance.

This approach has led to the concept of *complementary resonance*, i.e. a high-impedance parallel resonance at a harmonic on the a.c. side closely coupled to a low-impedance series resonance at an associate frequency on the d.c. side. The first-order associate a.c. and d.c. side frequencies, derived from the general table of

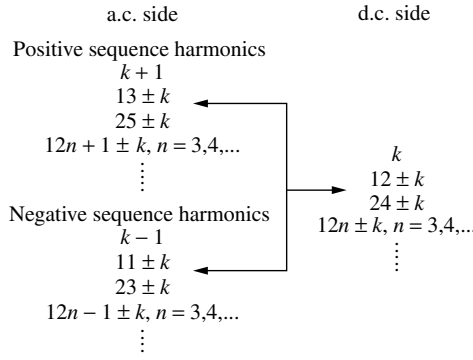


Figure 4.5 Associate three-port harmonic orders

Figure 3.50, are shown in the three-port model of Figure 4.5. A reported experience of this condition, and used in the commonly used CIGRE benchmark HVd.c. test system [2], involves a second-harmonic parallel resonance on the a.c. side and a fundamental frequency series resonance on the d.c. side.

Moreover, when the a.c. and d.c. systems are interconnected by a static converter, the system impedances interact via the converter characteristics to create entirely different resonant frequencies. The term 'composite resonance' has been proposed [3] to describe this sort of resonance, emphasising its dependence on all the components of the system

A composite resonance may be excited by a relatively small distortion source in the system, or by an imbalance in the converter components or control. The resulting amplification of the small source by the resonant characteristics of the system can compromise the normal operation of the converter and even lead to instability. A true instability results when, at the composite resonant frequency, the resistance of the overall circuit is negative. This can occur at non-integer frequencies and is driven by conversion from the fundamental frequency and d.c. components to the composite resonance frequency via the converter control. A detailed representation of the control, firing angle and end-of-commutation angle modulation is needed to model this operating condition; this can be done using the advanced models described in Chapter 8.

A frequently reported case of this type in HVd.c. converters is the so-called core saturation instability [4]. This type of instability can be explained with reference to the block diagram of Figure 4.6. If a small level of positive-sequence second-harmonic voltage distortion exists on the a.c. side of the converter, a fundamental frequency distortion will appear on the d.c. side. Through the d.c. side impedance, a fundamental frequency current will flow, resulting in a positive-sequence second-harmonic current and a negative-sequence d.c. flowing on the a.c. side. The negative-sequence d.c. will begin to saturate the converter transformer, resulting in a multitude of harmonic currents being generated, including a positive-sequence second-harmonic current. Associated with this current will be an additional contribution to the positive-sequence second-harmonic voltage distortion and in this way the feedback loop is completed. The stability of the system is determined by this feedback loop.

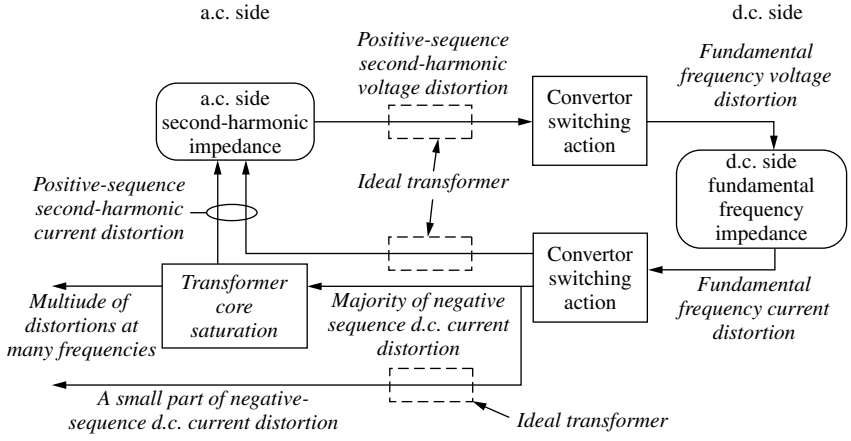


Figure 4.6 Mechanism of core saturation instability

Due to the dynamics of the instability, the d.c distortion is never exactly at the fundamental frequency, therefore the so-called negative sequence d.c. is not a true d.c. but is varying slowly, hence the use of the otherwise inappropriate term 'negative-sequence d.c.' The same mechanism could be triggered by the presence of some d.c. side fundamental frequency current induced by the proximity of an a.c. transmission system.

4.2.5 Poor Damping

Considerable power at the consumer's end of the system is controlled by power electronics to be constant power loads.

A constant power load, such as a motor variable speed drive or a switched mode power supply, presents a small-signal impedance or resistance to the power system that is negative; that is, any rise in voltage causes the current to fall. This removes the damping, or broadband energy absorption capability, from the power system. It can be expected that the continuous addition of such loads to the power system will cause instabilities or poor performance in the future

4.3 Effects of Harmonics on Rotating Machines

4.3.1 Harmonic Losses

Non-sinusoidal voltages applied to electrical machines may cause overheating. Motors are not normally derated so long as the harmonic distortion remains within the 5% normally recommended by the regulations. Above that limit they will often experience excessive heating problems. On the positive side, motors contribute to the damping of the system harmonic content by virtue of the relatively high X/R ratio of their blocked rotor circuit.

Harmonic voltages or currents give rise to additional losses in the stator windings, rotor circuits, and stator and rotor laminations. The losses in the stator and rotor conductors are greater than those associated with the d.c. resistances because of eddy currents and skin effect.

Leakage fields set up by harmonic currents in the stator and rotor end-windings produce extra losses. In the case of induction motors with skew rotors the flux changes in both stator and rotor and high frequency can produce substantial iron loss. The magnitude of this loss depends upon the amount of skew, and the iron-loss characteristics of the laminations.

As an illustration of the effect of supply waveform distortion on the power loss, reference [5] reports on the case of a 16 kW motor, operating at full output and rated fundamental voltage (at 60 Hz). With a sinusoidal voltage supply the total loss is 1303 W, whereas with a quasi-square voltage supply the total loss is 1600 W.

The following typical distribution of losses caused by supply harmonics has been reported [6] for the case of an inverter-fed machine: stator winding, 14.2%; rotor bars, 41.2%; end region, 18.8%; skew flux, 25.8%.

It would be inappropriate to apply the above loss breakdown to individual harmonics or to extend them to other machines, but it is clear that the major loss component is in the rotor. With the exception of the skew losses, the loss subdivision of a synchronous machine should follow a similar pattern.

When considering the harmonic heating losses in the rotor of synchronous machines it must be remembered that pairs of stator harmonics produce the same rotor frequency. For example the fifth and seventh harmonics both give induced rotor currents at frequency $6f_1$. Each of these currents takes the form of an approximately sinusoidal spatial distribution of damper bar currents travelling around the rotor at velocity $6\omega_1$, but in opposite directions. Thus for a linear system, the average rotor surface loss density around the periphery will be proportional to $(I_5^2 + I_7^2)$; however, because of their opposing rotations, at some point around the periphery the local surface loss density will be proportional to $(I_5 + I_7)^2$. If the fifth and seventh harmonic currents are of similar magnitude then the maximum local loss density would be about twice the average loss density caused by these two currents.

Extra power loss is probably the most serious effect of harmonics upon a.c. machines. An approximate assessment of the additional thermal stress of the coils can be achieved with the help of a weighted distortion factor adapted to inductance, i.e.

$$\mathrm{THD}_L = \frac{\sqrt{\sum_{n=2}^{N} \left(\frac{V_n^2}{n^\alpha} \right)}}{V_1} \tag{4.3}$$

where $\alpha = 1$ to 2, V_n is the single frequency r.m.s. voltage at harmonic n, N is the maximum order of harmonic to be considered and V_1 is the fundamental line to neutral r.m.s. voltage.

The capability of a machine to cope with extra harmonic currents will depend on the total additional loss and its effect on the overall machine temperature rise and local overheating (probably in the rotor). Cage-rotor induction motors tolerate higher rotor losses and temperatures provided that these do not result in unacceptable stator

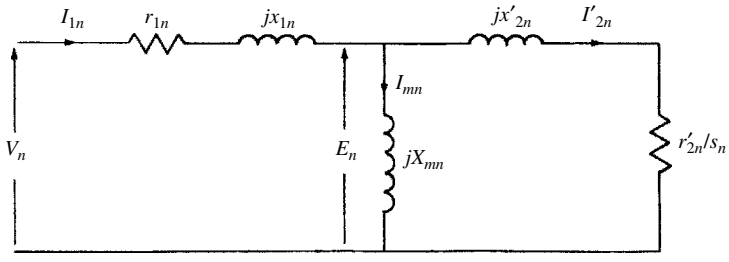


Figure 4.7 Equivalent circuit of induction machine per phase for harmonic n

temperatures, whereas machines with insulated rotor windings may be more limited. Some guidance as to the probably acceptable levels may be obtained from the fact that the level of continuous negative-sequence current is limited to about 10% for generators, and negative-sequence voltage to about 2% for induction motors. It is therefore reasonable to expect that if the harmonic content exceeds these negative-sequence limits, then problems will occur.

4.3.2 Harmonic Torques

The familiar equivalent circuit of an induction machine can be drawn for each harmonic as in Figure 4.7, where all the parameters correspond to actual frequencies of winding currents.

Harmonic currents present in the stator of an a.c. machine produce induction motoring action (i.e. positive harmonic slips S_n). This motoring action gives rise to shaft torques in the same direction as the harmonic field velocities so that all positive-sequence harmonics will develop shaft torques aiding shaft rotation whereas negative-sequence harmonics will have the opposite effect.

For a harmonic current I_n, the torque per phase is given by $I_n^2(r'_{2n}/s_n)$ watts at harmonic velocity. Referred to fundamental velocity this becomes

$$T_n = (I_n^2/n)(r'_{2n}/s_n) \text{ synchronous watts} \tag{4.4}$$

with the sign of n giving the torque direction.

Since s_n is approximately 1.0, equation (4.4) can be written as

$$T_n = (I_n^2/n)r'_{2n} \text{ per unit} \tag{4.5}$$

if I_n and r'_{2n} are per unit.

Using the relationship $V_n = I_n Z_n$ and $Zn \sim nZ_1$, the torque can be expressed in terms of the harmonic voltages, i.e.

$$T_n = (V_n^2/n^3)(r'_{2n}/X_1^2) \tag{4.6}$$

Because the slip to harmonic frequencies is almost unity, the torques produced by practical per unit values of harmonic currents is very small, and moreover the small

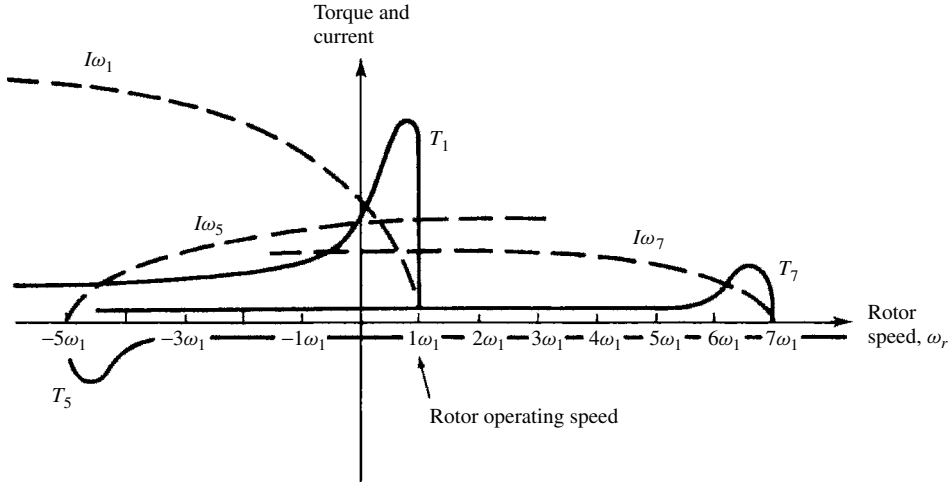


Figure 4.8 Rotor harmonic torques and currents

torques occur in pairs, which tend to cancel. This effect is illustrated in Figure 4.8. Therefore the effects of harmonics upon the mean torque may, in most cases, be neglected.

Although harmonics have little effect upon mean torque, they can produce significant torque pulsations.

Williamson [7] has developed the following approximate expression for the magnitudes of torque pulsations based on nominal voltage:

$$T_{3k} = [I_{n+}^2 + I_{n-}^2 - 2I_{n+}I_{n-}\cos(\phi_{n+} - \phi_{n-})]^{1/2} \text{ per unit}$$

where I_{n+} and I_{n-} are per unit values, $n+$ represents the $1 + 3k$ harmonic orders and $n-$ represents the $1 - 3k$ harmonic orders. This expression permits the preliminary assessment of possible shaft torsional vibration problems.

As an example, let us take the case of a supply voltage with total harmonic distortion of about 4%, resulting in machine currents of 0.03 and 0.02 per unit for the fifth and seventh harmonics, respectively. If both harmonics have the same phase angle, then for a 50 Hz machine on full voltage the torque will have a varying component at 300 Hz with an amplitude of 0.01 per unit. If the harmonics have the most adverse phase relationship, the amplitude will be 0.05 per unit.

4.3.3 Other Effects

The perturbation of the speed/torque characteristic by the presence of harmonics can cause clogging, a term used to describe the failure of an induction motor to run up to normal speed due to a stable operating point occurring at a lower frequency.

The stray capacitances in ASD-fed electric motors in the presence of harmonics cause capacitive currents to flow through the motor bearings and are often a source of their failure [8].

4.4 Effect of Harmonics on Static Power Plant

4.4.1 Transmission System

The flow of harmonic currents in the transmission network produces two main effects. One is the additional power loss caused by the increased r.m.s. value of the current waveform, i.e.

$$\sum_{n=2}^{\infty} I_n^2 R_n$$

where I_n is the nth harmonic current and R_n the system resistance at that harmonic frequency. Skin and proximity effects are functions of frequency and raise the value of the a.c. resistance of the cable, thus increasing the conductor I^2R losses.

The second effect of the harmonic current flow is the creation of harmonic voltage drops across the various circuit impedances. This means in effect that a 'weak' system (of large impedance and thus low fault level) will result in greater voltage disturbances than a 'stiff' system (of low impedance and high fault level).

In the case of transmission by cable, harmonic voltages increase the dielectric stress in proportion to their crest voltages. This effect shortens the useful life of the cable. It also increases the number of faults and therefore the cost of repairs.

The effects of harmonics on Corona starting and extinction levels are a function of peak-to-peak voltage. The peak voltage depends on the phase relationship between the harmonics and the fundamental. It is thus possible for the peak voltage to be above the rating while the r.m.s. voltage is well within this limit.

The IEEE 519 standard provides typical capacity derating curves for cables feeding six-pulse convertors.

4.4.2 Transformers

The primary effect of power system harmonics on transformers is the additional heat generated by the losses caused by the harmonic content of the load current. Other problems include possible resonances between the transformer inductance and system capacitance, mechanical insulation stress (winding and lamination) due to temperature cycling and possible small core vibrations.

The presence of harmonic voltages increases the hysteresis and eddy current losses in the laminations and stresses the insulation. The increase in core losses due to harmonics depends on the effect that the harmonics have on the supply voltage and on the design of the transformer core.

The flow of harmonic currents increases the copper losses; this effect is more important in the case of converter transformers because they do not benefit from the presence of filters, which are normally connected on the a.c. system side. Apart from the extra rating required, converter transformers often develop unexpected hot spots in the tank.

Delta-connected windings can be overloaded by the circulation of triplen frequency zero-sequence currents, unless these extra currents are taken into account in the design. Under this condition a three-legged transformer design can be effectively overloaded

by zero-sequence-caused harmonic fluxes. These fluxes cause additional heating in the tanks, core clamps, etc.

If the load current contains a d.c. component, the resulting saturation of the transformer magnetic circuit (described in Section 3.2) greatly increases the harmonic content of the excitation current.

Guidelines for transformer derating to take into account the harmonic content are given in the ANSI/IEEE standard C57.110 based on a derating factor [9] expressed as

$$K = \sqrt{\frac{\sum_h (I_h^2 h^2)}{\sum_h I_h^2}} \tag{4.7}$$

In terms of the above K factor, the following expression is used to determine the derated (or maximum allowed) current:

$$I_{\max} = \sqrt{\frac{1 + P_{EC.R}}{1 + KP_{EC.R}}}(I_R) \tag{4.8}$$

where I_R is the fundamental r.m.s. current under rated load conditions and $P_{EC.R}$ is the ratio of eddy-current loss to rated I^2R loss (I being the total r.m.s. current).

Examples of K-Factor Application

(i) Assume that the converter transformer used in Section 3.6.5 has a P_{EC} (eddy current loss) of 12 kW and an I^2R loss on rating of 100 kW.

In that example the calculated values of the fundamental and harmonic currents were

233.91 A(fundamental), 45.37 A(5th), 31.27 A(7th), 19.08 A(11th) and 14.03 A(13th)

Therefore $P_{EC.R} = 12/100 = 0.12$ and I_R (rated fundamental current) $= 233.91$ A.

From Equation (4.7)

$$K = \sqrt{\frac{\left(\frac{233.91}{233.91}\right)^2 1^2 + \left(\frac{45.84}{233.91}\right)^2 5^2 + \left(\frac{31.27}{233.91}\right)^2 7^2 + \left(\frac{19.08}{233.91}\right)^2 11^2 + \left(\frac{14.03}{233.91}\right)^2 13^2}{\left(\frac{233.91}{233.91}\right)^2 + \left(\frac{45.84}{233.91}\right)^2 + \left(\frac{31.27}{233.91}\right)^2 + \left(\frac{19.08}{233.91}\right)^2 + \left(\frac{14.03}{233.91}\right)^2}}$$

$$= 1.996$$

and from Equation (4.8) the maximum allowed current is

$$I_{\max} = \sqrt{\frac{1 + 0.12}{1 + (1.985)(0.12)}} \times (233.91) = 222 \text{ A}$$

Therefore the transformer will be overloaded if used with the nominal (i.e. 233.91 A) a.c. current rating.

Table 4.1 Harmonic currents of two heat pumps operating at nominal speed

h	Pump A		Pump B	
	Amplitude (A)	Phase (degrees)	Amplitude (A)	Phase (degrees)
1	11.87	17	14.4	2
3	7.487	0228	12.18	−10
5	3.003	−125	9.84	−17
7	1.329	−89	6.88	−24
9	0.582	67	3.99	−34
11	0.499	−55	1.63	−50
13	0.309	−227	0.39	−141
15	0.273	−68	0.88	151
17	0.154	−164	0.94	132

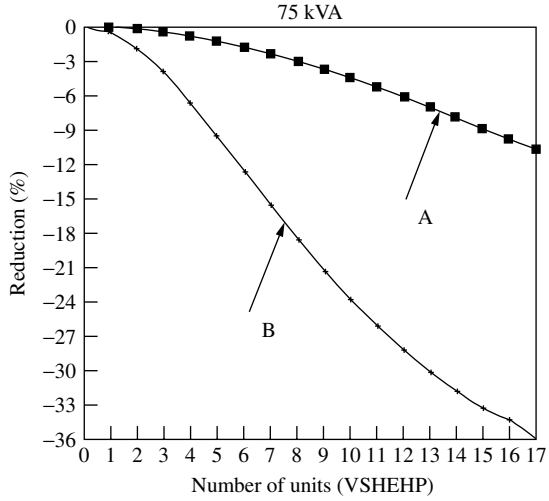


Figure 4.9 Reduction of the nominal capacity of a 75 kVA distribution transformer feeding two types of heat pump

(ii) A 75 kVA single-phase transformer feeds different proportions of heat pumps (VSHEHP) [10], involving rectification with high harmonic content (shown in Table 4.1). The derated levels, using the ANSI-C57.110 recommendation, are plotted in Figure 4.9 for different numbers of pump units.

4.4.3 Capacitor Banks

The presence of voltage distortion increases the dielectric loss in capacitors, the total loss being expressed by

$$\sum_{n=1}^{\infty} C(\tan\delta)\omega_n V_n^2 \tag{4.9}$$

where $\tan\delta = \mathrm{R}/(1/\omega C)$ is the loss factor, $\omega_n = 2\pi f_n$ and V_n is the r.m.s. voltage of the nth harmonic.

The additional thermal stress of capacitors directly connected to the system (i.e. without series inductance) is assessed approximately with the help of a special capacitor weighted THD factor defined as

$$\mathrm{THD}_C = \frac{\sqrt{\sum_{n=1}^{N}(n \cdot V_n^2)}}{V_1} \tag{4.10}$$

Series and parallel resonances (discussed in Section 4.2) between the capacitors and the rest of the system can cause overvoltages and high currents, thus increasing dramatically the losses and overheating of capacitors, and often leading to their destruction. Therefore all possible resonances must be taken into account in the design of power factor correction capacitors and in other applications, such as those used with single-phase induction motors and in converter transients damping. These capacitors are rated according to overcurrent limiting standards, such as ANSI/IEEE 18–1980, typical values being 15% in the UK, 30% in Europe and 80% in the USA.

Moreover, the total reactive power, including fundamental and harmonics, i.e.

$$Q = \sum_{n=1}^{N} Q_n$$

should not exceed the rated reactive power (taking into account the effect of permissible overvoltage and component manufacturing tolerances).

Power factor correction capacitors are often tuned to about the third or fifth harmonic frequency by adding a small series inductance (about 9% and 4%, respectively). This makes the capacitor look inductive to frequencies above the third (or fifth) harmonic and thus avoids parallel resonances.

4.5 Power Assessment with Distorted Waveforms

4.5.1 Single-Phase System

Early attempts to include waveform distortion in the power definitions were made by Budeanu [11] and Fryze [12].

Budeanu divided the apparent power into three orthogonal components, i.e.

$$S^2 = P^2 + Q_B^2 + D^2 \tag{4.11}$$

and defined the terms reactive power

$$Q_B = \sum_{l=1}^{n} V_l I_l \sin(\varphi_l) \tag{4.12}$$

accepted by the IEC and IEEE, and complementary power (which Budeanu called fictitious)

$$P_c = \sqrt{S^2 - P^2} \tag{4.13}$$

Fryze separated the current into two orthogonal components, i_a (active) and i_b (reactive)

$$i = i_a + i_b \tag{4.14}$$

and proposed for the reactive power the following definition:

$$Q_F = V I_b = \sqrt{S^2 - P^2} \tag{4.15}$$

To add some physical meaning to the matter, Shepherd and Zakikhani [13] proposed the following decomposition for the apparent power:

$$S^2 = S_R^2 + S_X^2 + S_D^2 \tag{4.16}$$

being

$$S_R^2 = \sum_1^n V_n^2 \sum_1^n I_n^2 \cos^2(\varphi_n) \tag{4.17}$$

$$S_X^2 = \sum_1^n V_n^2 \sum_1^n I_n^2 \sin^2(\varphi_n) \tag{4.18}$$

$$S_D^2 = \sum_1^n V_n^2 \sum_1^p I_p^2 + \sum_1^m V_m^2 \left(\sum_1^n I_n^2 + \sum_1^p I_p^2 \right) \tag{4.19}$$

In these expressions, S_R is said to be active apparent power, S_X reactive apparent power and S_D distortion apparent power.

The main advantage of this decomposition is that the minimisation of S_X immediately leads to the optimisation of the power factor via the addition of a passive linear element, a property not available when applying Budeanu's definition; however, there is no justification for a power decomposition with an active component that differs from the mean value of the instantaneous power over a period (i.e. the active power).

An alternative model also involving three components was proposed by Sharon [14]

$$S^2 = P^2 + S_Q^2 + S_C^2 \tag{4.20}$$

where

$$P \sim \text{ active power}$$

$$S_Q = V \sqrt{\sum_1^n I_n^2 \sin^2(\varphi_n)} \sim \text{ a reactive power in quadrature} \tag{4.21}$$

and

$$S_C \sim \text{ a complementary reactive power}$$

Similarly to the model of Shepherd and Zakikhani, the minimisation of S_Q in this model results in maximum power factor via the connection of linear passive elements. Moreover, Sharon replaces the questionable term S_R by the more acceptable active power P.

Taking into account that, in general, the main contribution to reactive power comes from the fundamental component of the voltage, Emanuel [15] proposed the following definitions:

$$Q_1 = V_1 I_1 \sin(\varphi_1) \tag{4.22}$$

and a complementary power

$$P_C^2 = S^2 - P^2 - Q_1^2 \tag{4.23}$$

Based on Fryze's theory, Kusters and Moore [16] proposed a power definition in the time domain with the current divided into three components:

i_p	an active component with a waveform identical to that consumed in an ideal resistance
i_{ql}/i_{qc}	a reactive component, corresponding to either a coil or a capacitor
i_{qlr}/i_{qcr}	a residual reactive component, the remaining current after removing the active and reactive, i.e.

$$i_{qr} = i - i_p - i_q \tag{4.24}$$

Furthermore, Kusters and Moore suggested the following decomposition for the apparent power:

$$S = P^2 + Q_l^2 + Q_{lr}^2 = P^2 + Q_c^2 + Q_{cr}^2 \tag{4.25}$$

where $P = VI_p$ is the active power, $Q_l = VI_{ql}$ the inductive reactive power, $Q_c = VI_{qc}$ the capacitive reactive power, and Q_{lr}/Q_{cl} the remaining reactive powers obtained from equation (4.24).

Also based on Fryze's definition, Emanuel [17] proposed two alternative decompositions distinguishing between the power components of the fundamental frequency (P_1, Q_1) and harmonics (P_H, Q_H), i.e.

$$S^2 = (P_1 + P_H)^2 + Q_F^2 \tag{4.26}$$

being

$$Q_F^2 = Q_B^2 + D^2 \tag{4.27}$$

and

$$S^2 = (P_1 + P_H)^2 + Q_1^2 + Q_H^2 \tag{4.28}$$

where

$$Q_H^2 = Q_F^2 - Q_1^2 \tag{4.29}$$

Further articles elaborating on the decomposition of power under non-sinusoidal conditions have been published by Czarnecki [18] and Slonin and Van Wyk [19].

In a recent contribution, Emanuel [20] makes the following statements:

- All forms of non-active powers stem from energy manifestations that have a common mark: energy oscillations between different sources, sources and loads or loads and loads. The net energy transfer linked with all the non-active powers is nil.
- Due to the unique significance of the fundamental powers, S_1, P_1 and Q_1, that comes from the fact that electric energy is a product expected to be generated and delivered and bought in the form of a 60 or 50 Hz electromagnetic field, it is useful to separate the apparent power S into fundamental S_1 and the non-fundamental S_N apparent powers:

$$S^2 = S_1^2 + S_N^2. \tag{4.30}$$

- As well as all the non-active powers, the term S_N contains also a minute amount of harmonic active power, P_H. The harmonic active power rarely exceeds $0.005P_1$. Thus, in a first approximation, an industrial nonlinear load can be evaluated from the measurements of P_1, Q_1 and S_N.
- The further subdivision of S_N into other components provides information on the required dynamic compensator or static filter capacity and level of current and voltage distortion.

Illustrative Example [21] To illustrate the practical consequences of using each of the above definitions, a comparative test study is shown with four single-phase networks with identical r.m.s. values of voltage (113.65 V) and current (16.25 A). In case A, the applied voltage is sinusoidal and the load nonlinear; case B contains voltage and current of the same, non-sinusoidal, waveform and in phase with each other; in case C the two identical waveforms are out of phase, and finally in D the voltage and current have harmonics of different orders.

The numerical information corresponding to these four cases is listed in Table 4.2 and the time-domain variation of the voltages and currents is shown in Figure 4.10.

Table 4.3 lists, for each case, the values of the powers previously defined, i.e. active P, reactive Q_B, apparent reactive S_X, reactive in quadrature Q_S, reactive of fundamental component Q_1, Fryze's reactive Q_F, distortion D, apparent S and also the power factor PF.

Table 4.2 Voltage and current phasors $V = 113.65$ V, $I = 16.25$ A

Case		$V_1\angle\alpha_1$	$V_3\angle\alpha_3$	$V_5\angle\alpha_5$	$V_7\angle\alpha_7$
A	v_A	$113.65\angle 0^\circ$			
	i_A	$15\angle -30^\circ$	$5.8\angle 0^\circ$	$2\angle 0^\circ$	$1\angle 0^\circ$
B	v_B	$105\angle 0^\circ$	$35\angle 0^\circ$	$21\angle 0^\circ$	$15\angle 0^\circ$
	i_B	$15\angle 0^\circ$	$5\angle 0^\circ$	$3\angle 0^\circ$	$(15/7)\angle 0^\circ$
C	v_C	$105\angle 0^\circ$	$35\angle 0^\circ$	$21\angle 0^\circ$	$15\angle 0^\circ$
	i_C	$15\angle -30^\circ$	$5\angle -90^\circ$	$3\angle -150^\circ$	$(15/7)\angle 150^\circ$
D	v_D	$105\angle 0^\circ$	$40.82\angle 180^\circ$		$15\angle 0^\circ$
	i_D	$15\angle -30^\circ$		$5.44\angle -60^\circ$	$3\angle -30^\circ$

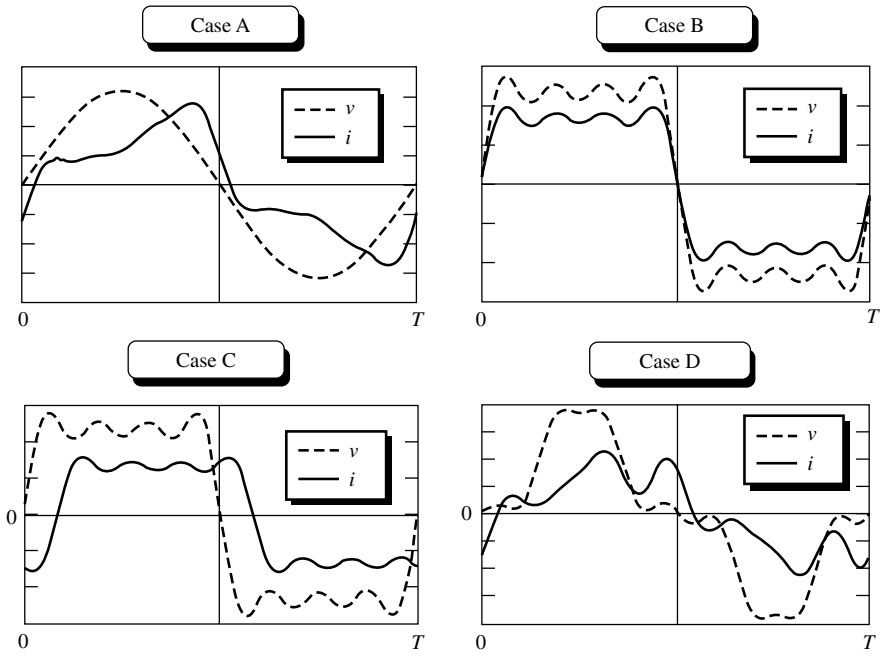


Figure 4.10 Voltage and current waveforms

Table 4.3 Alternative powers for four circuits with the same r.m.s. voltage and current but with different waveforms

Magnitude		Case A	Case B	Case C	Case D
Active	$P(W)$	1476	1845	1282	1403
Budeanu	$Q_B(Var)$	852	0	978	810
Shepherd	$S_X(VA)$	852	0	1046	811
Sharon	$Q_S(Var)$	852	0	1046	870
Emanuel	$Q_I(Var)$	852	0	788	788
Fryze	$Q_F(Var)$	1107	0	1327	1198
Budeanu	$D(VA)$	707	0	897	883
Apparent	$S(VA)/PF$	1845/0.80	1845/1	1845/0.695	1845/0.76

The rest of this section describes the results of three different comparisons made between cases A, C and D.

The first method, type 1 in Table 4.4, relates to the conventional capacitive compensation, and the table indicates the value of the capacitor that optimises the power factor $PF_{\max 1}$ and the required apparent power $S_{\min 1}$.

The second method, type 2, consists of a sinusoidal current injection of fundamental frequency that cancels the reactive current i_{r1} in the load; the corresponding apparent power and power factor are $S_{\min 2}$ and $PF_{\max 2}$, respectively.

Finally, in type 3 compensation, the current injection not only cancels the reactive component i_{r1}, but also the harmonic currents; $S_{\min 3}$ and $PF_{\max 3}$, are the apparent power and power factor, respectively.

Table 4.4 $S_{\min}$ and $PF_{\max}$ values for different compensation techniques

	Compensation	Case A	Case B	Case C
Type 1	$S_{\min 1}(VA)/C(\mu F)/PF_{\max 1}$	1636/210/0.902	1693/98/0.757	1759/81/0.798
Type 2	$S_{\min 2}(VA)/PF_{\max 2}$	1636/0.92	1636/0.785	1636/0.858
Type 3	$S_{\min 3}(VA)/PF_{\max 3}$	1476/1	1476/0.869	1476/0.950

The more relevant comments resulting from the comparison are:

(1) When the voltage is sinusoidal and the current non-sinusoidal (case A), the load is nonlinear; in this case, all the reactive powers obtained are identical, except Fryze's, which includes the distortion component. With reference to the optimisation process, $PF_{\max 1} = PF_{\max 2}$, as could be expected considering the sinusoidal nature of the voltage.

(2) If the voltage and current are in phase and of the same waveform (case B) the instantaneous power never reaches negative values; therefore $P = S$, the reactive and distortion powers are zero and the power factor unity, the load equivalent impedance being a linear resistance.

(3) When the voltage and current have the same waveform but are out of phase with each other (case C) the reactive powers calculated according to the various definitions proposed are different. In this case, the passive circuit does not distort the current waveform but alters its phase such that the power factor increases from an initial value of 0.695 to an optimal value $PF_{\max 3}$ of 0.869.

(4) Case D, due to the load nonlinearity, contains different harmonics; the third harmonic is only present in the voltage and the fifth in the current waveforms, respectively. This is the most general case; all the reactive powers calculated are different and the maximum power factor ($PF_{\max 3}$) is 0.95.

(5) The reactive powers calculated according to the various definitions are all different; the smallest is Emanuel's, since he only considers the fundamental component, and the largest Fryze's, which also includes distortion. In general,

$$Q_1 \leq Q_B \leq S_X \leq Q_S \leq Q_F \tag{4.31}$$

4.5.2 Three-Phase System

Apparent power in unbalanced three-phase systems is currently calculated using several definitions that lead to different power factor levels. Consequently the power bills will also differ, due to the reactive power tariffs and, in some countries, to the direct registration of the maximum apparent power demand.

Four different expressions have been proposed for the apparent reactive power, two of them based on Budeanu's and the other two on Fryze's definitions [22]:

(i)
$$S_v = \sqrt{\left(\left(\sum_k P_k\right)^2 + \left(\sum_k Q_{bk}\right)^2 + \left(\sum_k D_k\right)^2\right)} \tag{4.32}$$

or vector apparent power;

(ii) $$S_a = \sum_k \sqrt{(P_k^2 + Q_{bk}^2 + D_k^2)} \tag{4.33}$$

or arithmetic apparent power.

In the above expressions P_k represents the active power, Q_{bk} Budeanu's reactive power and D_k the distortion power in phase k; these terms are generally accepted by the main international organisations, such as the IEEE and IEC.

(iii) $$S_e = \sum_k \sqrt{(P_k^2 + Q_{fk}^2)} = \sum_k V_k I_k \tag{4.34}$$

an apparent r.m.s. power, that considers independently the power consumed in each phase.

(iv) $$S_s = \sqrt{(P^2 + Q_f^2)} = \sqrt{\sum_k V_k^2} \sqrt{\sum_k I_k^2} \tag{4.35}$$

a system apparent power, that considers the three-phase network as a unit.

The last two expressions use the reactive powers as defined by Fryze, Q_f and Q_{fk}, which include not only the reactive but also the distortive effects.

In the vector apparent power the phase reactive powers compensate each other, but not in the other expressions; the system apparent power calculates the voltage and current of each phase individually and therefore yields the highest apparent power. In general, the following applies:

$$S_v \leq S_a \leq S_e \leq S_s \tag{4.36}$$

The power factor of a load or system is generally accepted as a measure of the power transfer efficiency and is defined as the ratio between the electric power transformed into some other form of energy and the apparent power, i.e.

$$PF = P/S \tag{4.37}$$

Correspondingly, the relative magnitudes of the power factors calculated from the different definitions are

$$PF_v \geq PF_a \geq PF_e \geq PF_s \tag{4.38}$$

where PF_v, PF_a, PF_e and PF_s are the power factors corresponding to the vector, arithmetic, r.m.s. and system apparent powers, respectively.

For the power factor to reflect the system efficiency in three-phase networks with neutral wire, the neutral (zero sequence) currents must be included in the calculation of the equivalent current, i.e. in equation (4.35):

$$I_k^2 = I_a^2 + I_b^2 + I_c^2 + I_n^2 \tag{4.39}$$

and

$$V_k^2 = V_a^2 + V_b^2 + V_c^2 \tag{4.40}$$

where a, b, c indicate the individual phase values and n the neutral.

Illustrative Example [23,24] The simple test system shown in Figure 4.11 is used to illustrate the different performance of the proposed three-phase power definitions. Asymmetrical three-phase networks, even with sinusoidal voltage excitation and linear resistive loading, interchange reactive energy between the generator phases, despite the absence of energy storing elements. To show this effect, the circuit of Figure 4.11 is further simplified by making the line resistances equal to zero and assuming that the load is purely resistive, i.e. $Z_a = R_a$, $Z_b = R_b$, $Z_c = R_c$. Moreover, the three-phase source is assumed to be balanced and sinusoidal.

The following different operating conditions are compared in Table 4.5.

Case i	$R_a = 0\ \Omega$	$R_b = 5\ \Omega$	$R_c = 25\ \Omega$	without neutral wire
Case ii	$R_a = 5\ \Omega$	$R_b = 5\ \Omega$	$R_c = 25\ \Omega$	without neutral wire
Case iii	$R_a = 5\ \Omega$	$R_b = 5\ \Omega$	$R_c = 25\ \Omega$	with neutral wire
Case iv	$R_a = 5\ \Omega$	$R_b = 5\ \Omega$	$R_c = 5\ \Omega$	without neutral wire

As shown in Table 4.5, in case i, phases a and c generate reactive power while phase b absorbs reactive power, even though the overall reactive power requirement is zero. The effect is attenuated when a load is connected to phase a (case ii), but

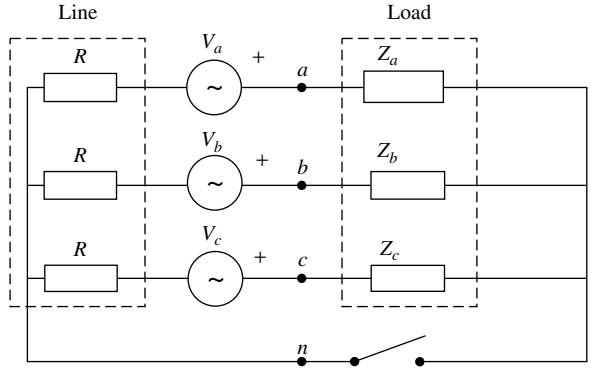


Figure 4.11 Three-phase test system

Table 4.5 Apparent powers and power factors for test cases i to iv

Case	SV_a	SV_b	SV_c	SV	$S_a = S_e$	S_s	PF_v	$PF_a = PF$	PF_s
i	$32.4 - j12.46$	$27 + j15.58$	$5.4 - j3.11$	64.8	72.12	81.52	1	0.898	0.794
ii	$14.7 - j5.7$	$14.7 + j5.7$	4.9	34.36	36.47	39.58	1	0.942	0.868
iii	18	18	3.6	39.6	39.6	44.53	1	1	0.889
iv	18	18	18	54	54	54	1	1	1

*All the powers are expressed in kVA.

there is still reactive power in two phases. When the circuit topology is changed by connecting a neutral wire (case iii) the generating source stops generating reactive power; the reactive power generation is also absent when phase c is made equal to phases a and b (case iv), i.e. when the network is perfectly balanced, and this is the case of maximum efficiency.

Table 4.5 shows for each case the apparent powers resulting from the different definitions as well as the corresponding power factors. The table also shows the complex apparent powers generated by the sources V_a, V_b, V_c. It can be seen that the most pessimistic power factor is PF_s, which only gives the value of one when the resistive load is perfectly balanced; on the other hand PF_v remains unity in all cases since the total load demand for reactive power, being resistive, is zero.

Next, a set of test cases v to x involve the circuit of Figure 4.11 with a perfectly balanced source feeding either linear or nonlinear loads.

The calculations performed in each case involve the four power factors defined above, the resistive losses in the line, and the line loss ratios of each of the cases to that of case v (the balanced case), which is used as a reference; the latter will show that only one of the definitions coincides with that ratio.

As the powers consumed by the load are different in all cases, for the purpose of comparison, the power of case v is also used as a reference, i.e. 54 kW in the test system.

Case v: V_{ns} (non-sinusoidal voltages), balanced load, 3 or 4 wires

$$R_a = R_b = R_c = 5\ \Omega,\ R = 0.2\ \Omega/\text{phase}$$
$$v_a = 298.51\sqrt{2}\sin(\omega t) + 29.85\sqrt{2}\sin(5\ \omega t);\quad V_a = 300\ \text{V}$$
$$i_a = 59.70\sqrt{2}\sin(\omega t) + 5.97\sqrt{2}\sin(5\ \omega t);\quad I_a = 60\ \text{A}$$
$$P = 3 \times 298.51 \times 59.70 + 3 \times 29.85 \times 5.97 = 54\,000\ \text{W}$$

The power loss in the line is $P_v = 3 \times (60)^2 \times 0.2 = 2160$ W. It should be noted that this value is the same as case iv (the balanced sinusoidal circuit) for the same line resistance.

Case vi(a): V_{ns}, unbalanced load, 4 wires

$$R_a = R_b = 5\ \Omega,\ R_c = 25\ \Omega$$
$$v_a = 298.51\sqrt{2}\sin(\omega t) + 29.85\sqrt{2}\sin(5\ \omega t)$$
$$i_a = 59.70\sqrt{2}\sin(\omega t) + 5.97\sqrt{2}\sin(5\ \omega t);\quad I_a = 60\ \text{A}$$
$$i_b = 59.70\sqrt{2}\sin(\omega t - 120) + 5.97\sqrt{2}\sin(5\ \omega t + 120);\quad I_b = 60\ \text{A}$$
$$i_c = 11.94\sqrt{2}\sin(\omega t + 120) + 1.19\sqrt{2}\sin(5\ \omega t - 120);\quad I_c = 12\ \text{A}$$

The topology of this case does not permit distorted or reactive power. To calculate the line loss in relation to the power base, the calculated currents are multiplied by factor K, which is the ratio of the power in case v to that of vi(a); therefore

$$K = 54\,000/39\,600 = 1.36$$
$$P_{\text{vi}} = [(60 \times 1.3636)^2 + (60 \times 1.3636)^2 + (12 \times 1.3636)^2] \times 0.2 = 2731.23\ \text{W}$$

The ratio $P_{\text{v}}/P_{\text{vi}} = 0.79$ is the square of PF_s. It is observed that although the consumed power has no reactive or distorted component, due to load unbalance, line losses

are larger and the power factors PF_{v}, PF_a and PF_e do not reflect that loss of network efficiency; on the other hand PF_s represents faithfully this increment. It should be noted that the value P_{iii} (of case iii) would be identical to P_{vi} if the line resistance (i.e. 0.2 Ω/phase) had been represented.

Case vi(b): V_{ns}, unbalanced load, 3 wires

$$R_a = R_b = 5\ \Omega,\ R_c = 25\ \Omega,\ R = 0.2\ \Omega/\text{phase}$$
$$v_a = 298.51\sqrt{2}\sin(\omega t) + 29.85\sqrt{2}\sin(5\ \omega t)$$
$$i_a = 52.34\sqrt{2}\sin(\omega t + 21.05) + 5.234\sqrt{2}\sin(5\ \omega t - 21.05); \quad I_a = 52.60\ \text{A}$$
$$i_b = 52.34\sqrt{2}\sin(\omega t - 141.05) + 5.234\sqrt{2}\sin(5\ \omega t + 141.05); \quad I_b = 52.60\ \text{A}$$
$$i_c = 16.34\sqrt{2}\sin(\omega t + 120) + 1.628\sqrt{2}\sin(5\ \omega t - 120); \quad I_c = 16.36\ \text{A}$$

The different behaviour in this case with respect to reactive and distorted power is due to the new topology, which excludes the neutral wire.

The line losses, normalised to 54 kW, are $P_{\mathrm{vi}}(\mathrm{b}) = 2865.3$ and the ratio $P_{\mathrm{v}}/P_{\mathrm{vi}} = 0.75$ is again the square of PF_s.

Case vii: V_{s} (sinusoidal), nonlinear load, I_{ns} (non sinusoidal) and balanced

$$R = 0.2\ \Omega/\text{phase}$$
$$v_a = 300\sqrt{2}\sin(\omega t).$$
$$i_a = 60\sqrt{2}\sin(\omega t) + 6\sqrt{2}\sin(5\ \omega t); \quad I_a = I_b = I_c = 60.3\ \text{A}$$

In this case the load nonlinearity produces a harmonic component not present in the voltage source. The power consumed is 54 kW and the values of the various power factors are identical and close to unity, in spite of the fifth harmonic current, because the fundamental component of the current is balanced and its power factor is unity.

Case viii: V_{s}, nonlinear load, I_{ns} unbalanced

$$R = 0.2\ \Omega/\text{phase}$$
$$v_a = 300\sqrt{2}\sin(\omega t).$$

This case has the same currents as in vi(b), yielding lower power factors, due to the fact that the load active power decreases in the absence of fifth harmonic voltage.

Case ix: V_{ns}, nonlinear load, I_{ns} balanced

$$R = 0.2\ \Omega/\text{phase}$$
$$v_a = 298.51\sqrt{2}\sin(\omega t) + 29.85\sqrt{2}\sin(5\ \omega t)$$
$$i_a = 59.70\sqrt{2}\sin(\omega t) + 5.97\sqrt{2}\sin(5\ \omega t) + 10\sqrt{2}\sin(7\ \omega t); \quad I_a = 60.83\ \text{A}$$

In this case the currents are as in v, but the load nonlinearity injects seventh harmonic, which results in a reduction of power factors with respect to the base case.

Case x: V_{ns}, nonlinear load, I_{ns} unbalanced

$$R = 0.2\ \Omega/\text{phase}$$
$$v_a = 298.51\sqrt{2}\sin(\omega t) + 29.85\sqrt{2}\sin(5\ \omega t)$$
$$i_a = 59.70\sqrt{2}\sin(\omega t); \quad I_a = 59.70\ \text{A}$$
$$i_b = 59.70\sqrt{2}\sin(\omega t - 120) + 5.97\sqrt{2}\sin(5\ \omega t + 120); \quad I_b = 60\ \text{A}$$
$$i_c = 59.70\sqrt{2}\sin(\omega t + 120) + 11.94\sqrt{2}\sin(5\ \omega t - 120); \quad I_b = 60.88\ \text{A}$$

Table 4.6 Circuit characteristics for test cases v to x

Case	Volt components	Impedance	Neutral	Current components
v	ωi, ω5	$R_a = R_b = R_c = 5\ \Omega$	No	ω1, ω5, balanced
vi(a)	ωi, ω5	$R_a = R_b = 5;\ R_c = 25\ \Omega$	Yes	ω1, ω5, unbalanced
vi(b)	ω1, ω5	$R_a = R_b = 5;\ R_c = 25\ \Omega$	No	ω1, ω5, unbalanced
vii	ω1	Nonlinear	Yes	ω1, ω5, balanced
viii	ω1	Nonlinear	Yes	ω1, ω5, unbalanced
ix	ω1, ω5	Nonlinear	Yes	ω1, ω5, balanced
x	ω1, ω5	Nonlinear	Yes	ω1, balanced; ω5, unbalanced

Table 4.7 Apparent powers and power factors of test cases v to x

Case	S_v	$S_a = S_e$	S_s	PF_v	$PF_a = PF_e$	PF_s	P_j	P_v/P_j	PF_s^2
v	54 000	54 000	54 000	1	1	1	2160	1	1
vi(a)	39 600	39 600	44 529.5	1	1	0.889	2731.2	0.790	0.790
vi(b)	34 436.8	36 470.1	39 578.3	0.997	0.942	0.868	2865.3	0.753	0.753
vii	54 269.3	54 269.3	54 269.3	0.995	0.995	0.995	2181.6	0.990	0.990
viii	34 385.1	36 470.1	39 578.3	0.994	0.937	0.863	2893.9	0.746	0.746
ix	54 744.8	54 744.8	54 744.8	0.986	0.986	0.986	2220	0.972	0.972
x	54 117.5	54 176.0	54 177.9	0.997	0.996	0.996	2174.2	0.993	0.993

The fundamental component is as in case v; the nonlinear load contains unbalanced fifth harmonic, chosen to ensure that the consumed active power is the same as that of the base circuit; this case also shows a decrease of the power factors with respect to the base case.

The main characteristics of the seven cases considered in this section are shown in Table 4.6. Table 4.7 illustrates, for each case, the magnitudes of the apparent powers; P_j is the power loss in the line, normalised to the base power of case v, P_v/P_j is the ratio of the line power loss for the balanced line and that corresponding to each case. Finally, the table lists the magnitude of PF_s (the square of the system power factor), which coincides always with P_v/P_j.

4.5.3 Power Factor Under Harmonic Distortion [25]

In general, the instantaneous values of the voltage and current components can be expressed as

$$v = \sum_{1}^{n} \sqrt{2} V_n \sin(n\omega t + \alpha_n) + \sum^{m} \sqrt{2} V_m \sin(m\omega t + \alpha_m) \tag{4.41}$$

$$i = \sum_{1}^{n} \sqrt{2} I_n \sin(n\omega t + \alpha_n + \phi_n) + \sum^{p} \sqrt{2} I_p \sin(p\omega t + \alpha_p) \tag{4.42}$$

and the power factor is given by

$$\text{p.f.} = \frac{1/T \int_0^T vi \, \mathrm{d}t}{V_{\text{rms}} I_{\text{rms}}} = \frac{\sum_1^n V_n I_n \cos(\phi_n)}{\left\{ \left(\sum_1^n V_n^2 + \sum^m V_m^2 \right) \left(\sum_1^n I_n^2 + \sum^p I_p^2 \right) \right\}^{1/2}} \tag{4.43}$$

This factor represents a figure of merit of the character of the power consumption. A low value indicates poor utilisation of the source-power capacity needed by the load.

If the voltage waveform is sinusoidal, equation (4.43) reduces to

$$\text{p.f.} = \frac{V_1 I_1 \cos(\phi_1)}{V_1 I_{\text{rms}}} = \frac{I_1}{I_{\text{rms}}} \cdot \cos(\phi_1) = \mu \cos(\phi_1) \tag{4.44}$$

where $\cos(\phi_1)$ is the displacement power factor (DPF) between the fundamental components of voltage and current, and μ is a current distortion factor. It is worth mentioning that only DPF information is available from conventional instrumentation.

Thus unity power factor can only be achieved when $\mu = 1$ since $\cos(\phi_1)$ in equation (4.44) can not be greater than one.

Power factor compensation is not straightforward with distorted waveforms. As lossless devices are normally used for the compensation, the minimisation of the apparent power should lead directly to the optimum power factor. If, for example, a capacitance C is added in parallel to the load characterised by equations (4.41) and (4.42), the general expression for the apparent power in terms of C is

$$S = \left(\sum_1^n V_n^2 + \sum^m V_m^2 \right)^{1/2} \cdot \left\{ \sum_1^n (I_n^2 + V_n^2 n^2 \omega^2 C^2 + 2 V_n I_n n \omega C \sin(\phi_n)) + \sum^m V_m^2 m^2 \omega^2 C^2 + \sum^p I_p^2 \right\}^{1/2} \tag{4.45}$$

The differentiation of this equation with respect to C and its subsequent equating to zero leads to an optimum value of the linear capacitance, i.e.

$$C_{\text{opt}} = -\frac{1/\omega \sum_1^n V_n n I_n \sin(\phi_n)}{\sum_1^n V_n^2 n^2 + \sum^m V_m^2 m^2} \tag{4.46}$$

The object of capacitor compensation is to improve the displacement factor if the voltage is sinusoidal. Improvement in the values of distortion factor are achieved by filters, higher pulse numbers, or current waveform modification. These techniques are discussed in Chapter 6.

4.5.4 Effect of Harmonics on Measuring Instruments

Measuring instruments initially calibrated on purely sinusoidal alternating current and subsequently used on a distorted electricity supply can be prone to error. The magnitude and direction of the harmonic power flow are important for revenue considerations as the sign of the meter error is decided by the direction of flow.

Studies have shown that errors due to harmonic content vary greatly as to the type of meter, and that both positive and negative metering errors are possible.

The classic energy measuring instrument is the Ferraris motor type kilowatt-hour meter. Its inherent design is electromagnetic, producing driving and braking fluxes which impinge on its rotor, developing a torque. Secondary flux-producing elements are provided for compensation purposes to improve the instrument accuracy and to compensate for friction in the register. These flux-producing elements, providing primary and secondary torques, are essentially nonlinear in regard to amplitude and frequency. The nonlinear elements include the voltage and current elements and overload magnetic shunts, and the frequency-sensitive elements include the disc, the quadrature and anti-friction loops.

The response of this meter to frequencies outside the design parameter is inefficient, and large inaccuracies result. An expression for total power as seen by a meter is

$$\underset{(P_{\mathrm{T}})}{\text{Total power}} = \underset{(P_{\mathrm{dc}})}{V_{\mathrm{dc}} I_{\mathrm{dc}}} + \underset{(P_{\mathrm{F}})}{V_F I_F \cos\phi_F} + \underset{(P_{\mathrm{H}})}{V_H I_H \cos\phi_H} \tag{4.47}$$

The meter will not measure P_{dc} but will be sensitive to its presence; it will measure P_{F} accurately and P_{H} inaccurately, the error being determined by the frequency. The total harmonic power P_{H} is obtained by adding all components derived from the products of voltages and currents of the same frequencies, both above and below the fundamental frequency.

Any d.c. power supplied to or generated by the customer will cause an error proportional to the power ratio $P_{\mathrm{dc}}/P_{\mathrm{T}}$, with the error sign related to the direction of power flow. Similarly, any deficiency in measuring harmonic power P_{H} will cause an error represented by $\pm KP_{\mathrm{H}}/P_{\mathrm{T}}$, where the factor K is dependent on the frequency-response characteristics of the meter, and the error sign again will be related to power flow direction.

D.c. power and harmonic voltages or currents alone should not produce torques, but will degrade the capability of a meter to measure fundamental frequency power. Direct currents distort the working fluxes and alter the incremental permeability of the magnetic elements. Fluxes produced by harmonic currents combine with spurious fluxes of the same frequency that may be present due to the imperfection of the meter element and produce secondary torques.

The kilowatt-hour meter, based on the Ferraris (eddy current) motor principle, has been found generally to read high to the extent of up to several percentage points with a consumer generating harmonics through thyristor-controlled variable speed equipment (particularly if even harmonics and d.c. are involved) and notably if there is also a low power factor.

Converter loads using the 'burst firing' principle can cause kilowatt-hour meters to read high by several percentage points (cases in excess of 6% have been quoted), largely attributable to the lack of current damping during the no-load interval.

It appears that consumers that generate harmonics are automatically penalised by a higher apparent electricity consumption, which may well offset the supply authority's additional losses [26]. It is therefore in the consumer's own interest to reduce harmonic generation to the greatest possible extent.

There is no evidence that the reading of kVA-demand meters is affected by network harmonics. However, kW-demand meters operating on the time interval Ferraris motor principle will read possibly a few percentage points high, as shown earlier for energy meters.

Harmonics present a problem to measurement of VAR values, since this is a quantity defined with respect to sinusoidal waveforms.

The present trend is to use solid state instruments which can measure true power irrespective of the waveforms. Modern r.m.s. responding voltmeters and ammeters are relatively immune to the influences of waveform distortion. In such meters, the input voltage or current is processed using an electronic multiplier type, such as variable transconductance, log/antilog, time division, and thermal and digital sampling. All these can be configured to respond to the r.m.s. value independently of the harmonic amplitude or phase, as long as the harmonics are within the operating bandwidth of the instrument and the crest factor (the ratio of peak to r.m.s.) of the waveform is not excessively large. However, absolute average and peak responding meters which are calibrated in r.m.s. are not suitable in the presence of harmonic distortion.

A seldom mentioned effect, but nevertheless an important one, is that measurement and calibration laboratories, working to small tolerances of accuracy, may lose confidence in their results.

4.6 Harmonic Interference with Ripple Control Systems

Ripple signals are often used for the remote control of street lighting circuits and for load reduction (such as domestic hot water heaters) during peak times of the day.

Electricity suppliers have in the past experienced some practical difficulties with their ripple control equipment as a result of harmonic interference.

Since ripple relays are essentially voltage-operated (high-impedance) devices, harmonic interference can cause signal blocking or relay maloperation if present in sufficient amplitude. The exact amplitude at which the voltage harmonic will affect the relay is a function of the relay detection circuit (sensitivity and selectivity) and the proximity of the ripple injection frequency of the interfering harmonic.

Signal blocking occurs when sufficient interfering voltage renders the relay unable to detect the presence of the signal. Capacitors can produce the same effect due to their capability to absorb the ripple signal. Relay maloperation occurs when the presence of the harmonic voltage (usually in the absence of the signal) causes the relay to change state. The latter problem has effectively been solved by the use of suitably encoded switching signals in present generations of ripple relays.

Earlier ripple relays were electromechanical devices employing mechanical filter assemblies. Although their response was slow, they did achieve very good selectivity. However, these relays commonly suffered from maloperation because they had inadequate signal encoding to cater for any harmonic interference which got pass the filters.

However, modern ripple relays are basically electronic equivalents of their electromechanical forerunners. They usually employ piezoelectric or active filter circuits and a high degree of signal encoding to minimise maloperation. They have filter response curves defined by international standards [27] and they require the use of precision electronic components (high stability and reliability) to ensure a satisfactory performance over the life of the relay. Even better immunity can be achieved with the use of digital filtering techniques, which are ideally suited for the detection of signals of a specified frequency in the presence of harmonic voltages.

4.7 Harmonic Interference with Power System Protection

Harmonics can distort or degrade the operating characteristics of protective relays depending on the design features and principles of operation. Digital relays and algorithms that rely on sample data or zero crossings are particularly prone to error when harmonic distortion is present.

In most cases, the changes in operating characteristics are small and do not present a problem. Early tests [28] indicate that for most types of relays operation is not affected significantly for harmonic voltage levels of less than 20%. Most studies carried out so far conclude that it is difficult to predict relay performance without testing; the studies published have evaluated electromechanical and electronic relays but there is no information on digital relays [29]. However with the increased content of large power conversion equipment, this can be a potential problem.

Current harmonic distortion can also affect the interruption capability of circuit breakers and fuses. Possible reasons are higher $\mathrm{d}i/\mathrm{d}t$ at zero crossings, the current sensing ability of thermal magnetic breakers and a reduction in the trip point due to extra heating of the solenoid. The fuses, being thermally activated, are inherently r.m.s. overcurrent devices; the fuse ribbons are also susceptible to the extra skin effect of the harmonic frequencies.

4.7.1 Harmonic Problems During Fault Conditions

Protective functions are usually developed in terms of fundamental voltages and/or currents, and any harmonics present in the fault waveforms are either filtered out or ignored altogether. The latter is particularly the case for electromagnetic relay applications, such as overcurrent protection. Electromechanical relays have significant inertia associated with them such that often they are inherently less sensitive to higher harmonics.

More important is the effect of harmonic frequencies on impedance measurement. Distance relay settings are based on fundamental impedances of transmission lines, and the presence of harmonic current (particularly third harmonic) in a fault situation could cause considerable measurement errors relative to the fundamental-based settings.

High harmonic content is common where fault current flows through high resistivity ground (i.e. the ground impedance is dominant) so the possibility of maloperation is great unless only the fundamental waveforms are captured.

In solid fault situations, the fundamental components of current and voltage are much more dominant (notwithstanding the d.c. asymmetry associated with fault waveforms).

However, because of current transformer saturation, secondary induced distortion of current waveforms, particularly with large d.c. offsets in the primary waveforms, will occur. The presence of secondary harmonics in such instances can be a real problem, i.e. whenever current transformer saturation occurs it is very difficult to recover the fundamental current waveform.

Whenever high secondary e.m.f. exists during steady-state conditions, the nonlinear current transformer exciting impedance only causes odd harmonic distortion. During saturation under transient conditions, however, any harmonics can be produced, with dominance of second and third harmonic components [30].

Fortunately, these are often design problems. Correct choice of equipment in relation to the system requirements can eliminate many of the difficulties associated with the current and voltage transformers.

Filtering of the current and voltage waveforms, particularly in digital protection systems, is of special importance to distance protection schemes. Although the implementation is not always simple, the recovery of fundamental frequency data has been greatly improved by the use of digital techniques [31].

4.7.2 Harmonic Problems Outside Fault Conditions

The effective insensitivity of protective apparatus to normal system load conditions implies that, generally, the harmonic content of the waveforms is not a problem outside fault conditions.

The most notable exemption is probably the problem encountered in energisation of power transformers. In practice, constructive use of the high harmonic content of magnetising inrush currents prevents (most of the time!) tripping of the high voltage circuit breaker by the transformer protection due to the excessively high peaks experienced during energisation.

The actual peak magnitude of the inrush current depends on the air-core inductance of the transformer and the winding resistance plus the point on the voltage wave at which switching occurs [32]. Residual flux in the core prior to switching also increases the problem or alleviates it slightly, depending on the polarity of flux with regard to the initial instantaneous voltage.

Since the secondary current is zero during energisation, the heavy inrush current would inevitably cause the differential protection to operate unless it is rendered inoperative.

The simple approach is to use a time-delay differential scheme, but this could result in serious damage to the transformer should a fault be present at energisation.

In practice, information on the uncharacteristic second harmonic component present during inrush is used to restrain the protection, but protection is still active should an internal fault develop during energisation.

4.8 Effect of Harmonics on Consumer Equipment

This is a broad subject discussed in many journal articles; a selected bibliography on the topic can be found in a paper by the IEEE Task Force on the Effects of Harmonics on Equipment [33]. A concise summary of the main effects is made below:

(1) *Television receivers* Harmonics which affect the peak voltage can cause changes in TV picture size and brightness. Inter-harmonics cause amplitude modulation of the fundamental frequency; even a 0.5% inter-harmonic level can produce periodic enlargement and reduction of the image of the cathode ray tube.

(2) *Fluorescent and mercury arc lighting* These appliances sometimes have capacitors which, with the inductance of the ballast and circuit, produce a resonant frequency. If this corresponds to a generated harmonic, excessive heating and failure may result. However, the resonant frequency of most lamps is in the range 75–80 Hz and should not interact with the power supply. Audible noise is another possible effect of harmonic voltage distortion.

(3) *Computers* [34] There are designer-imposed limits as to acceptable harmonic distortion in computer and data processing system supply circuits. Harmonic rate (geometric) measured in vacuum must be less than −3% (Honeywell, DEC) or 5% (IBM). CDC specifies that the ratio of peak to effective value of the supply voltage must equal 1.41 ± 0.1.

(4) *Power electronic equipment* Notches in the voltage waveform resulting from current commutations may affect the synchronisation of other converter equipment or any other apparatus controlled by voltage zeros. Harmonics could theoretically affect thyristor-controlled variable-speed drives of the same consumer in several ways: (i) voltage notching (causing brief voltage dips in the supply) can cause maloperation via a thyristor through misfiring; (ii) harmonic voltages can cause the firing of the gating circuits at other than the required instant; (iii) resonance effects between different equipment can result in over-voltages and hunting.

The problems described above could also be experienced by other consumers if connected to the same (415 V or 11 kV) busbar. Consumers without problems with the simultaneous operation of their own thyristor-controlled equipment are unlikely to interfere with other consumers. Consumers on different busbars could interfere with each other but 'electrical' remoteness (separation by impedances in the form of lines and transformers) will tend to reduce the problem.

4.9 Interference with Communications

Noise on communication circuits degrades the transmission quality and can interfere with signalling. At low levels noise causes annoyance and at high levels loss of information, which in extreme cases can render a communication circuit unusable.

The continuously changing power transmission environment demands regular reconsideration of the interference problem when telephone lines are placed in the vicinity of the power system.

The signal to noise ratio commonly used in communication circuits as a measure of the transmission quality must be used with caution when considering power system interference because of the different power levels of the signals involved, i.e. in megawatts (power circuit) and milliwatts (communication circuit). Thus even a small unbalanced audio-frequency component within the power network may easily produce unacceptable noise level when coupled into a metallic communication circuit.

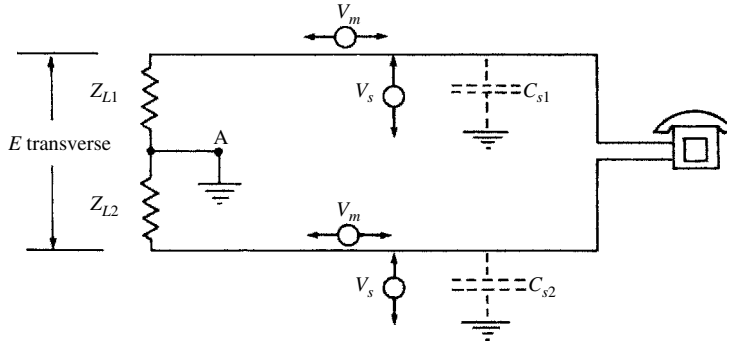


Figure 4.12 Simple model of a telephone circuit

Moreover, the purpose of the power system is to transmit energy at high efficiency but with relatively low waveform purity; on the other hand, in a communication circuit the waveform must not be significantly distorted, as the intelligence being conveyed may be destroyed, while the power efficiency is of secondary importance.

This section describes the factors influencing communication interference and the means by which noise may be reduced to within acceptable levels

4.9.1 Simple Model of a Telephone Circuit

A physical telephone circuit consists of a twisted pair of wires with associated terminal equipment, and a simplified model of such a circuit is illustrated in Figure 4.12.

For safety and practical reasons telephone circuits are referenced to earth and thus the equivalent circuit of the telephone system of Figure 4.12 includes the terminal impedances Z_{L1} and Z_{L2} to earth. An electromagnetic induced voltage is modelled as voltage source V_m, and an electrostatic induced voltage as V_s. The terminal impedances, Z_{L1} and Z_{L2}, are generally of high value and the telephone line self-impedance, being much smaller, may be neglected.

In the absence of an earth conductor the earth return circuit is completed by the stray capacitances C_{S1} and C_{S2}.

4.9.2 Factors Influencing Interference

Three factors combine to produce a noise problem on a communication line:

(1) *Power system influence* This depends on the source of audio-frequency components within the power system and the relative magnitude of unbalanced harmonic currents and voltages present in the power circuit in the vicinity of the communication circuit.

(2) *Coupling to communication circuits* This factor involves the coupling of interfering currents and voltages into a communication system.

(3) *Effect on communication circuits (susceptiveness)* The effect of the noise interference on a communication circuit is dependent on the characteristics of the circuit and associated apparatus.

All three factors must be present for the problem to develop. Complete elimination of the interference problem is usually impractical, and the degree of the problem will be a function primarily of the basic factors that have the highest influence.

Some harmonic currents in the power line are confined to the phase conductors, thus flowing in one phase and returning by the other two (the 'balanced' circuit); these are the positive- and negative-sequence harmonic currents. Other harmonic components flow in phase with each other in the phase conductors and return through the neutral or earth; these are the zero-sequence or residual currents.

4.9.3 Coupling to Communication Circuits

Coupling refers to the mutual impedance existing between the power and telephone lines. It depends on the separation between them, the length of exposure, earth resistivity and frequency.

Noise voltages may be impressed on telephone circuits in several ways, i.e. by loop induction, by longitudinal electromagnetic induction, by longitudinal electrostatic induction and by conduction.

Loop Induction Loop induction occurs when a voltage is induced directly into the metallic loop formed by the two wires of a telephone circuit. This type of induction manifests itself directly as a transverse voltage across the terminations of the telephone circuit. It is cancelled out by regular transpositions of aerial wires or by the use of twisted pairs of cables. As these are standard practices in communication circuits, loop induction is not generally a problem.

In the case of crossings, telephone lines often come so near the power line that the loop effect may be important [35].

Longitudinal Electromagnetic Induction Longitudinal electromagnetic induction occurs when an e.m.f. is induced along the conductors of a telephone circuit. The residual current in a power line sets up a magnetic field, which causes flux lines to intersect with any neighbouring telephone line and induces an e.m.f. longitudinally on it. This type of coupling, illustrated in Figure 4.13, constitutes the most common form of noise induction into communication lines.

For the close spacing of joint overhead transmission power and telephone lines, the magnetic coupling from balanced currents is important. For roadside spacings or greater, the earth return or residual current is the predominant source of interference.

The residual current I_R in Figure 4.13 returns via earth to V_p, hence the current loop so formed has a large cross-sectional area for overhead transmission lines. Likewise, aerial open wire telephone circuits may have large cross-sectional areas.

This leads to a longitudinal electromagnetic induction on telephone circuits given by

$$V_m = MI_R \tag{4.48}$$

where M is the mutual impedance between the power and telephone systems.

The most widely accepted model for determining the mutual impedance between power and telephone systems was developed by Carson [36].

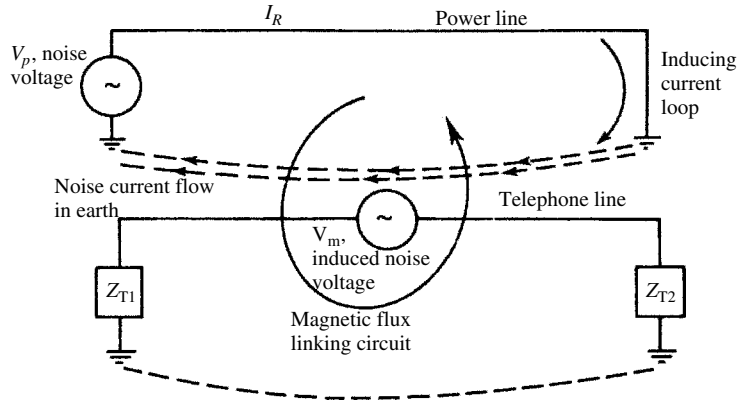


Figure 4.13 Electromagnetic induction

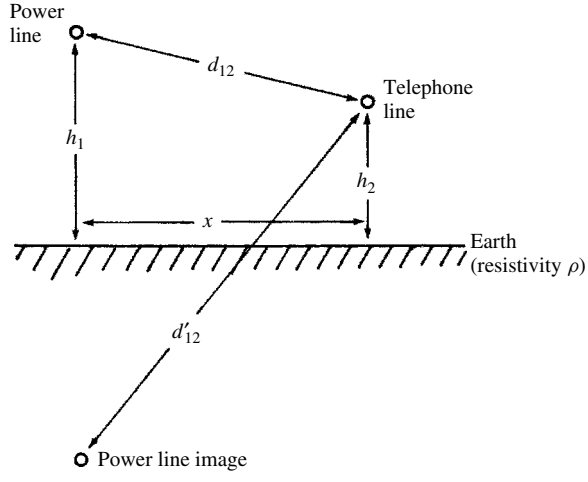


Figure 4.14 Power and telephone line configuration

In general, electromagnetic propagation at power frequencies is not very sensitive to earth structure and resistivity and so Carson's model (which assumes a uniform flat earth) is valid for most cases.

Carson's equation for the mutual impedance of a power line at height h_1 and a telephone line at height h_2, as in Figure 4.14, is given by

$$M = \frac{j\omega\mu_0}{2\pi}\left[\ln\frac{d'_{12}}{d_{12}} - 2j\int_0^\infty \left[\sqrt{(u^2+j)} - u\right] e^{-u\alpha(h_1+h_2)}\cos(u\alpha x)\,\mathrm{d}u\right] \qquad (4.49)$$

where M is the mutual impedance per unit length, x is the horizontal separation of power and telephone lines, h_1 is the height of the power line above ground (which is negative if below ground), h_2 is the height of the telephone line above ground (which is again negative if below ground), $d_{12} = \sqrt{[(h_1 - h_2)^2 + x^2]}$ is the radial distance

between lines, $d'_{12} = \sqrt{[(h_1 + h_2)^2 + x^2]}$ is the radial distance between one line and the underground image of the other, $\omega = 2\pi f$ is the angular frequency of the inducing current, μ_0 is the rationalised permeability of free space, $\alpha = \sqrt{2}/\delta$, $\delta = \sqrt{(2\rho/\mu_0\omega)}$, is the skin depth of uniform earth with resistivity ρ, and ρ is the resistivity of the earth in ohm-metres.

The first term of Carson's equation is the mutual impedance between two conductors as if they were above a perfectly conducting earth, while the second term 'corrects' for finite earth resistivity. Unfortunately, the second term usually dominates for typical parameters.

Carson's solution relies on measurements of the earth resistivity, which can be difficult to obtain, and simplified forms of Carson's equation are often used to obtain good approximations for the mutual impedance.

The factors influencing the mutual impedance between power and telecommunication lines can be summarised as follows: it increases with increasing values of the residual current loop area; it increases for increasing common distance run; it increases with frequency; it increases with earth resistivity; it decreases for increasing separation between circuits.

Longitudinal Electrostatic Induction Longitudinal electrostatic induction occurs when an e.m.f. is induced between the conductors and earth.

The simplest way of visualising electrostatic induction is by considering the capacitances in an exposure between a single power wire and a single telephone wire, as illustrated in Figure 4.15. The voltage of the power wire to ground (residual voltage), V_r, divides over the capacitance between the power and telephone wire, C_{PT} and the telephone wire and ground, C_{TC} in the ratio of their impedances, i.e.

$$V_s = \frac{Z_{\mathrm{T}}}{1/(j\omega C_{\mathrm{PT}}) + Z_{\mathrm{T}}} \cdot V_r \tag{4.50}$$

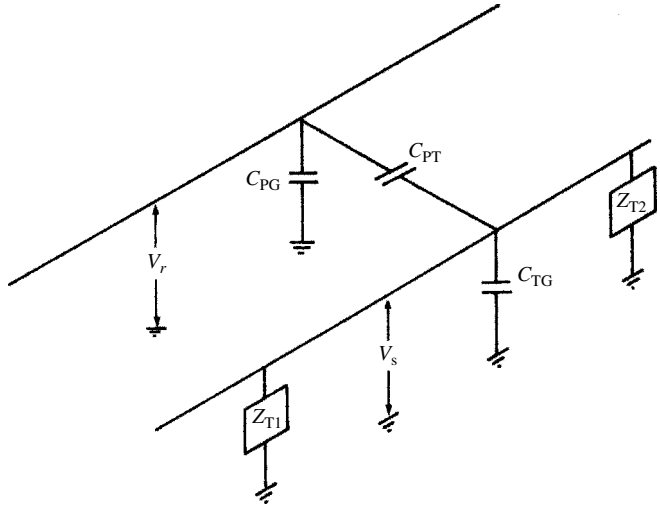


Figure 4.15 Electrostatic induction

where

$$Z_T = \frac{1}{j\omega C_{TG} + (1/Z_{T1}) + (1/Z_{T2})}$$

Because of the loading effect of Z_{T1} and Z_{T2} and the relative separations, V_s is very small as compared with V_m and can easily be neutralised by cable screening.

Electrostatic induction is serious only when the residual voltage, V_r is large (e.g. single-wire power lines) or when C_{PT} is large (for example, in joint construction and crossings, where the two lines are very close together). Generally the telephone line is terminated in impedances which are small compared to the capacitive impedances and thus reduce the induced voltage, V_s. This form of induction is often a problem on long telephone lines in the neighbourhood of very high voltage transmission lines.

For instance, for the case of roadside separation between the power and communication lines, with an earth resistivity of 100 metre-ohms, the 60 Hz mutual impedance is about one half ohm per mile. The longitudinal electric field in a telephone circuit on the same right of way as the power line is about 10 V per mile. Therefore five miles of exposure would induce 50 V on the telephone circuit.

Conductive Coupling There is always some residual current flowing in the neutral of the power system due to out-of-balance components. With a multiple earthed neutral (MEN) system, some of this residual current will return to the transformer by the neutral wire, and some via earth. The earth currents will cause a local rise of earth potential at the earth electrode.

If one end of a telephone line is earth referenced in the area of influence of this earth potential rise, then a longitudinal voltage may be impressed on the line.

In the circuit of Figure 4.12, if a local earth potential rise occurred at A this would cause unequal currents to flow through Z_{L1} and Z_{L2}, giving rise to a transverse noise voltage in the telephone circuit.

This source of interference is an increasing problem due to the following factors:

(1) MEN earth systems are carrying higher levels of noisy current.

(2) The earth resistances of telephone exchange earth systems are increasing as a result of the use of less lead armoured cable; it is very costly to achieve low earth resistance.

(3) Despite (2), the telephone exchange earth is often a relatively low impedance earth return circuit for a MEN earth system feeding the exchange, and hence a considerable noise voltage can be impressed onto the earth system from a MEN system.

4.9.4 Effect on Communication Circuits (Susceptiveness)

Telephone Circuit Susceptiveness A voice band telephone channel is normally designed to pass frequencies between 300 and 3000 Hz. Although harmonics in this range of frequencies are very small compared with the fundamental, they still have an effect on the telephone reception.

The effect that a 'noisy' power line will have on a communication line may be ascertained by considering the susceptiveness of the circuit to the effects of inductive interference. Three characteristics are of importance in this respect: (i) the relative interfering effects of different frequencies; (ii) the balance of the communication circuit; and (iii) shielding effects of metallic cable sheaths and other buried metallic plant.

Harmonic Weights Standard weighting curves are used to take into account the response of the telephone equipment and the sensitivity of the human ear to the harmonic frequencies. Two weighting factors are in common use:

(1) the psophometric weighting by the CCITT [37], extensively used in Europe;
(2) the C-message weighting by Bell Telephone Systems (BTS) and Edison Electric Institute (EEI) [38], used in the USA and Canada.

Figure 4.16 shows that the difference between these two weighting curves (when normalised) is very slight and that the human ear in combination with a telephone set has a sensitivity to audio-frequencies that peaks at about 1 kHz.

However, harmonics between 1000 and 3000 Hz are hardly diminished in the weighting curves and yet modern electronic telephone sets appear to be more sensitive to these higher frequencies; so perhaps the weightings should be revised accordingly.

Using these weighting factors, the total weighted transverse (or metallic) noise is obtained from the expression:

$$V_m = \sqrt{\sum_{n=1}^{N} (V_{cn} K_n B_n C_n)^2} \tag{4.51}$$

where V_m is the metallic mode weighted voltage, V_{cn} is the longitudinal induced voltage, N is the maximum order of harmonic to be considered, C_n is the psophometric or the C-message weighting factor of harmonic n, K_n is the telephone circuit shielding factor at harmonic n and B_n is the telephone circuit balance at harmonic n. The

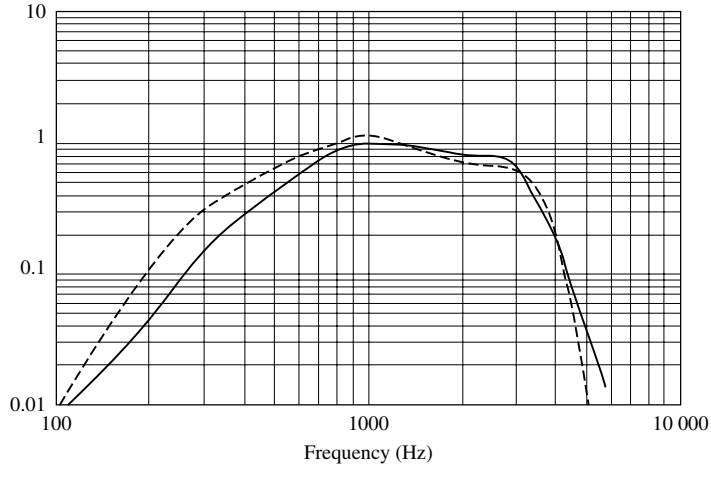


Figure 4.16 C-message (———) and psophometric weighting (– --- –) factors

last two coefficients require detailed information on the telephone systems cables and design as well as knowledge of the local earth resistivities.

Psophometric Weighting

Telephone Form Factor In the psophometric system the level of interference is described in terms of a telephone form factor (TFF), which is a dimensionless value that ignores the geometrical configuration of the coupling and is expressed as

$$\mathrm{TFF} = \sqrt{\sum_{n=1}^{N} \left(\frac{U_n}{U} . F_n \right)^2} \tag{4.52}$$

where U_n is the component at harmonic n of the disturbing voltage, N is the maximum harmonic order to be considered,

$$U = \sqrt{\sum_{n=1}^{N} U_n^2}$$

is the line to neutral total r.m.s. voltage, $F_n = p_n\, n f_0/800$, p_n is the psophometric weighting factor and f_0 is the fundamental frequency (50 Hz). The required limit of TFF is typically 1%.

The CCITT directives recommend that the total psophometric weighted noise on a telephone circuit has an e.m.f. (i.e. open circuit voltage) of less than 1 mV. When measuring the noise voltage the telephone circuit is terminated with its characteristic impedance (which is a resistance of the order of 600 Ω) and the noise voltage is measured across such resistance. Therefore, the psophometrically weighted noise across the terminating resistor must be less than 0.5 mV.

As a general rule, if the TFF is greater than 0.5 mV it is likely to cause interference to telephone services. It must be stressed that the TFF is only a guideline measurement; it is not satisfactory as the sole measure of interference to a communication line as it takes no account of coupling and exposure factors.

Equivalent Disturbing Current The CCITT also defines an equivalent disturbing current (I_P), expressed as

$$I_P = (1/p_{800}) \sqrt{\sum_f (h_f p_f I_f)^2} \tag{4.53}$$

where I_f is the component of frequency f of the current causing the disturbance, p_f is the psophometric weighting factor at frequency f, and h_f is a factor which is a function of frequency and takes into account the type of coupling between the lines concerned (by convention $h_{800} = 1$).

C-Message Weighting

Telephone Influence Factor The C-message weighting system uses the telephone influence factor (TIF) instead of the TFF of the psophometric system. Again, TIF

is a dimensionless value used to describe the interference of a power transmission line on a telephone line, and is expressed as

$$\text{TIF} = \frac{\sqrt{\sum_{n=1}^{N} (U_n W_n)^2}}{U} \tag{4.54}$$

where U_n is the single frequency r.m.s. voltage at harmonic n, N is the maximum harmonic order to be considered, U is the total line to neutral voltage (r.m.s.), C_n is the C-message weighting factor, f_0 is the fundamental frequency (60 Hz), and W_n is the single frequency TIF weighting at harmonic n (the relationship between the C-message and TIF weighting factors is $W_n = C_n\ 5n\ f_0$ and the corresponding coefficients for the first 25 harmonics are shown in Table 4.8).

The TIF weights account for the fact that mutual coupling between circuits increases linearly with frequency, while the C-message weights do not take this into consideration. Because of this coupling relationship the TIF weights peak at about 2.6 kHz (as compared with the 1 kHz peak of the C-message weighting curve). The TIF index

Table 4.8 C-message and TIF weighting coefficients

Frequency (Hz)	Harmonic	C-message weight, C	TIF W
60 (50)	1	0.0017	0.5 (0.71)
120 (100)	2	0.0167	10.0 (8.91)
180 (150)	3	0.0333	30.0 (35.5)
240 (200)	4	0.0875	105 (89.1)
300 (250)	5	0.1500	225 (178)
360 (300)	6	0.222	400 (295)
420 (350)	7	0.310	650 (376)
480 (400)	8	0.396	950 (484)
540 (450)	9	0.489	1320 (582)
600 (500)	10	0.597	1790 (661)
660 (550)	11	0.685	2260 (733)
720 (600)	12	0.767	2760 (794)
780 (650)	13	0.862	3360 (851)
840 (700)	14	0.912	3830 (902)
900 (750)	15	0.967	4350 (955)
960 (800)	16	0.977	4690 (1000)
1020 (850)	17	1.000	5100 (1035)
1080 (900)	18	1.000	5400 (1072)
1140 (950)	19	0.988	5630 (1109)
1200 (1000)	20	0.977	5860 (1122)
1260 (1050)	21	0.960	6050 (1109)
1320 (1100)	22	0.944	6230 (1072)
1380 (1150)	23	0.923	6370 (1035)
1440 (1200)	24	0.924	6650 (1000)
1500 (1250)	25	0.891	6680 (977)

Note: Number in brackets refer to the CCITT values and 50 Hz fundamental

models the effectiveness of induction between adjacent circuits, and is thus particularly useful to assess the interference of power distribution circuits on analogue-type telephone systems (many recent telephone circuits, however, are of digital-type design).

Instead of voltage, the TIF is more usefully expressed in terms of line current because the electromagnetic induction relates to line current amplitude. Also, the line currents are best represented by their sequence of rotation, i.e. positive, negative and zero sequences, respectively. The relationship between the phase and sequence currents is:

$$\begin{bmatrix} I^+ \\ I^- \\ I^0 \end{bmatrix} = 1/\sqrt{3} \begin{bmatrix} 1 & a & a^2 \\ 1 & a^2 & a \\ 1 & 1 & 1 \end{bmatrix} \begin{bmatrix} I_R \\ I_Y \\ I_B \end{bmatrix} \tag{4.55}$$

where $a = 1\angle 120^\circ$.

As the power circuit is three-phase and the audio circuit single phase, the latter can not distinguish between positive- and negative-sequence signals, but the effect of zero sequence is very different.

Telephone circuits are more affected by zero-sequence harmonics because these are in phase in the three phases and add arithmetically. Generally, standards are less tolerant of zero-sequence harmonics to take this fact into account. When only the zero-sequence signals are included in equation (4.54), the term *residual* is used in the TIF (which in the case of a balanced three-phase system include only triplen frequency components). The term balanced is used when the signals included in equation (4.54) are only of positive and negative sequence. The latter contribution to the induced noise is important in the immediate proximity of the transmission line, while the residual signals are the dominant ones at greater distances from the line. When the balanced signals are expected to contribute significantly to the induced noise, they must be included in the calculation of the TIF, i.e.

$$\mathrm{TIF} = \sqrt{\mathrm{TIF}_r^2 + \mathrm{TIF}_b^2} \tag{4.56}$$

where the suffixes r and b indicate residual and balanced, respectively.

Equivalent Disturbing Current

$$I_{\mathrm{eq}} = \sqrt{\sum_{n=1}^{N} (H_n C_n I_n)^2} \tag{4.57}$$

where I_n is the effective disturbing current at harmonic n (generally corresponding to residual mode currents), N is the maximum harmonic order to be considered, C_n is the C-message weighting factor, and H_n is the weighting factor normalised to reference frequency (1000 Hz) that accounts for the frequency dependence of mutual coupling, shielding and communication circuit balance at harmonic n.

Again, when the balanced mode harmonic currents are taken into account the effective disturbing current is then specified as

$$I_n = \sqrt{(I_{rn})^2 + (K_b I_{bn})^2} \tag{4.58}$$

where I_{rn} is the total residual mode current at harmonic n, I_{bn} is the balanced mode current at harmonic n, and K_b is the ratio of balanced mode coupling to the residual mode coupling at reference frequency.

IT and kVT Products The THD, TFF and TIF indices do not provide information about the amplitude of the voltage (or current) to which they relate. The IT and VT (or kVT) products incorporate that information. In these products the voltages or currents of the power transmission line are represented by a single voltage or current obtained by weighting each harmonic voltage or current with the corresponding factor of the system (BTS-EEI or CCITT) used.

The VT product incorporates the line-to-line voltage amplitude, i.e.

$$\mathrm{VT} = \sqrt{\sum_{n=1}^{N} (W_n V_n)^2} \tag{4.59}$$

where V_n is the single frequency r.m.s. line-to-line voltage at harmonic n, N is the maximum harmonic order to be considered and $W_n = C_n\ 5\ nf_0$ is the single frequency TIF weighting at harmonic n.

The IT product is derived similarly using currents instead of voltages. However, there is some confusion about whether to use the current in one phase or some kind of sum of the three phase currents; if the latter is used it would have to be a phasor sum, which is usually close to zero. Our interpretation is that when the analogue telephone circuit is far from the three-phase power line, the value to be used is the phasor combination of the three line currents. On the other hand, if the telephone circuit is in the vicinity of the power line then the calculation based on one phase current or a non-phasor combination of the three phases will be a better indicator of telephone interference. In [39] the line current is multiplied by a factor of $\sqrt{3}$ to account for the three-phase arrangement. Ideally, when assessing the interfering ability of a power line the effect of the balanced sequence components needs to be represented, including the geometry of the line, the separation of the telephone cable and the soil conditions; these effects are significant in typical road width type separations.

Taking into account the above ambiguities and the fact that analogue communication circuits are gradually being replaced by digital ones, the TIF and IT indices are not used extensively by telecommunication companies, as they do not reflect the vulnerabilities of services operating over telephone cables. The weightings currently used are based on the response of the human ear in conjunction with the telephone receiver. However, modern telecommunication devices tend to use all of the available spectrum that the cable can propagate. Even devices such as modems, which are restricted to the traditional telephony band from 300 Hz to 3400 Hz, utilise the high-frequency part of this band (1000 to 3400 Hz) much more extensively than the human voice does, and are consequently much more sensitive to interference at these frequencies. Thus it is possible to have acceptable TIF or psophometric noise on a telephone cable but still have severe service degradation.

More modern telecommunication services such as ADSL utilise the spectrum from about 25 kHz up to 1 MHz and beyond. As they are not using the low frequencies they are proving to be tolerant of typical power line noise, but they are likely to be sensitive to electrical fast transients.

Illustrative Example A 4.16 kV 60 Hz distribution system bus is selected to supply a three-phase 4.5 MVA purely resistive load. The corresponding fundamental frequency current in the line is

$$I_1 = (P_1/3)/(V_1/\sqrt{3}) = (4500/3)/(4.16/\sqrt{3}) = 624.5376 \text{ A}$$

and the load resistance is

$$R = (V_1/\sqrt{3})/I_1 = (4160/\sqrt{3})/(624.537) = 3.8457\ \Omega$$

Two different voltage waveforms, both with the same THD, are used to illustrate the relative effect of different frequencies on the IT and TIF indices. The voltage waveforms include either

(1) 75 V of zero sequence third harmonic and 177 V of negative sequence fifth, or

(2) 177 V of zero sequence third harmonic and 75 V of negative sequence fifth.

In both cases the total harmonic distortion (THD) is the same, i.e.

$$\text{THD} = 100\left(\sqrt{V_3^2 + V_5^2}/V_1\right) = 100\left(\sqrt{75^2 + 177^2}/4160\right) = 4.62\%$$

which is below the 5% limit recommended by IEEE standard 519 for the 4.16 kV distribution system.

The ANSI 368 standard indicates that telephone interference from a 4.16 kV distribution system is unlikely to occur when the IT index is below 10 000. Let us check the two cases against this limit using the TIF weightings (taken from Table 4.8) for the fundamental (0.5), the third (30) and fifth (225) harmonic frequencies:

Case (i):

$$I_3 = \frac{(V_3/\sqrt{3})}{R} = \frac{(75/\sqrt{3})}{3.8457} = 11.26 \text{ A}$$

$$I_5 = \frac{(V_5/\sqrt{3})}{R} = \frac{(177/\sqrt{3})}{3.8457} = 26.57 \text{ A}$$

Therefore the following IT indices result (using the questionable $\sqrt{3}$ factor as suggested in [39]):

$$\text{IT}_1 = (624.537)(0.5)\sqrt{3} = 540.865$$

$$\text{IT}_3 = (11.26)(30)\sqrt{3} = 585.071$$

$$\text{IT}_5 = (26.57)(225)\sqrt{3} = 10\,355.752$$

and the total IT including the balanced and residual components becomes:

$$\text{IT (total)} = \sqrt{(540.865)^2 + (585.087)^2 + (10\,354.63)^2} = 10\,386.358$$

which is above the ANSI standard limit.

The TIF index for this case is

$$\text{TIF} = \frac{\sqrt{(0.5x4160)^2 + (225x75)^2 + (30x177)^2}}{\sqrt{(4160)^2 + (75)^2 + (177)^2}} = 9.59$$

Case (ii):

$$I_3 = \frac{(177/\sqrt{3})}{3.8457} = 26.57 \text{ A}$$

$$I_5 = \frac{(75/\sqrt{3})}{3.8457} = 11.26 \text{ A}$$

and the corresponding ITs

$$IT_3 = (26.57)(30)\sqrt{3} = 1380.77$$

$$IT_5 = (11.26)(225)\sqrt{3} = 4388.103$$

$$\text{IT(total)} = \sqrt{(540.865)^2 + (1380.62)^2 + (4388.15)^2} = 4631.83$$

which is well below the 10 000 limit.

The total TIF index for this case is

$$\text{TIF} = \frac{\sqrt{(0.5x4160)^2 + (30x177)^2 + (225x75)^2}}{\sqrt{(4160)^2 + (177)^2 + (75)^2}} = 4.28$$

Typical requirements of TIF are between 15 and 50.

4.9.5 Telephone Circuit Balance to Earth

If the telephone line or terminal equivalent is not perfectly balanced with respect to earth, longitudinally induced voltage on that line can be transformed into transversed voltage, and it is as a transversed voltage across the ear piece that we can hear noise on the telephone.

Consider the simple telephone circuit of Figure 4.12. If the impedances to earth of the two wires that form a telephone circuit are different, and assuming that the two wires are subjected to the same longitudinal induction, different currents will flow in each wire. Because the self-impedances of the wires will be very similar, the different current flows will give rise to a transverse voltage between the pair.

Factors which may affect the telephone circuit balance to earth are (i) any leakage paths to earth, e.g. across-the-pole insulators or through-cable insulation; and (ii) any unbalanced terminal equipment, either subscriber's equipment (e.g. extension bells) or exchange equipment. Some of these factors may be corrected simply and quickly to reduce an induced noise problem, while others rely on the proper design and manufacture of the equipment or plant.

Balance is simply defined as

$$20\log_{10}\left(\frac{\text{Longitudinal voltage}}{\text{Transverse voltage}}\right)$$

and for the majority of relay sets it is of the order of 45–50 dB.

The most critical component balance-wise is generally any terminal relay set in a communication connection. As there are large numbers of such relay sets, it is not practical to set balance objectives at a very high level as this would significantly increase the cost of the communication network.

4.9.6 Shielding

A metallic or conducting earthed screen such as a cable sheath which encloses the telephone circuit over the length of an exposure is totally effective in eliminating electrostatic induction. Buried cables with a metallic screen or sheath are also immune to electrostatic induction due to the conducting effect of the earth.

Metallic screens or sheaths are only partly effective in reducing the effects of electromagnetic induction.

The mechanism of electromagnetic shielding is as follows. The power line current causes longitudinal voltages to be induced in the wires of the cable and also in the shield. The resulting current flow in the shield is in the opposite direction to the inducing current in the power line. This induced current in the shield generates in turn a voltage in the wires of the cable opposing the voltage induced by the power line current, thus tending to neutralise the latter.

If the shield current is large and/or well coupled to the inner conductors, reasonable shielding factors can be obtained.

The shielding factor of a cable is the fraction by which the shield reduces the voltage induced into the core; the shielding factor (K) of an installed shielded cable system is given by

$$K = \frac{\text{d.c. shield resistance} + \text{earth resistance}}{\text{a.c. shield resistance} + \text{earth resistance}} \tag{4.60}$$

This simple formula shows that the shielding factor may be reduced by decreasing the resistance and/or increasing the inductance of the sheath and/or decreasing the earth resistance.

A good shielding factor for a cable can be achieved if the following set of conditions hold:

(1) At points where the shield is earthed, the earth resistance must be low (typically 1–2 Ω).
(2) There is a low resistance shield, i.e. plenty of metal in the cable shield to keep the resistance low.
(3) Steel tapes are usually required.

All these factors mean that shielded cables used for noise shielding are relatively expensive; typically they can be expected to cost some 30–50% more than standard unshielded types.

4.9.7 Mitigation Techniques

The steps to be taken when a noise problem is known to exist are:

(1) Check the transverse noise voltage in the telephone circuit. If the e.m.f. is less than 1 mV no further steps need be taken; if it is greater than 1 mV, then proceed as below.
(2) Determine whether the mode of induction is of electrostatic or electromagnetic type.
(3) Test telephone line and termination balance to earth.
(4) Where considered useful, derive by test the telephone form factor in various parts of the power system to try to isolate the source of noise.

With the information gained from these tests, the following mitigation methods are considered:

(1) A reduction of the influence of the power system, which can be achieved by (i) physical relocation of either system (usually an expensive exercise); (ii) replacing the copper wire with light conducting fibres (fibre optics); or (iii) reduction of the harmonic content in the power system (the appropriate techniques are discussed in Chapter 6).
(2) Reducing coupling is not usually a practical proposition, except in cases of earth potential rise, where a noisy incoming multiple earthed neutral can be excluded if required.
(3) Reducing the susceptiveness of the communication circuits can be achieved by the use of noise chokes, noise-neutralising transformers, shielded cable and derived circuits.

Noise Chokes Reducing factors upwards of 25 dB are achievable in certain circumstances. Generally, noise chokes are only useful for improving the balance of substandard terminal relay sets. They work by increasing the a.c. longitudinal line impedance, thereby reducing the noise current and with it the transverse noise voltage level.

Noise-Neutralising Transformers These work by inducing an equal but opposite (in-phase) noise voltage in affected cable pairs, thus reducing the induced longitudinal noise. Reduction factors of 15–20 dB can be achieved.

Shielded Cable Reduction factors upward of 60 dB can easily be achieved, but it is costly. Generally the use of shielded cable is only applicable for new work.

Derived Circuits By providing the circuits via pulse code modulation (PCM) or frequency division multiplexing (FDM), the system can be made relatively immune to noise induction. In each case the degree of improvement depends on the circumstances.

It must be emphasised that the actual reduction factors depend on the particular circumstances and the factors mentioned above are not achievable in all cases.

4.10 Audible Noise from Electric Motors

The major causes of sound from electric motors are

- torque pulsations in induction and permanent magnet machines;
- torque and normal force pulsations in the doubly salient structure of the switched reluctance machines.

Motors powered by pulse width modulation exhibit their predominant sound levels at the modulating frequency. The level of sound is not a function of the load but is inversely proportional to the motor speed.

The highest levels are produced by switched reluctance motors and are related to the load torque.

4.11 Discussion

In the absence of an extremely intelligent harmonic traffic controller, the presence of waveform distortion is normally detected by its effects on power system components or on personnel or plant outside the power system. Some effects, such as telephone interference, are immediately obvious to the senses and can thus be mitigated at an early stage of the problem without excessive disturbance. Other effects, such as a resonant condition, can occur at unexpected locations lacking monitoring facilities and will often cause expensive damage to plant components such as capacitor banks and inadequate filter equipment. The financial consequences of harmonic overloading and equipment failure, not discussed in this chapter, should be an essential part in the design of modern power systems.

References

1. Ross, N.W. (1982) Harmonic and ripple control carrier series resonances with P.F. correction capacitors, *Trans. Electr. Supply Authority (N.Z.)*, **52**, 48–6.
2. Szechtman, M., Weiss, T. and Thio, C.V. (1991) First benchmark model for HVdc control studies, *Electra*, **135**, 55–75.
3. Wood, A.R. (1993) An analysis of non-ideal HVdc converter behaviour in the frequency domain, and a new control proposal, PhD thesis, University of Canterbury, New Zealand.
4. Chen, S., Wood, A.R. and Arrillaga, J. (1996) HVDC converter transformer core saturation instability: a frequency domain analysis, *IEE Proc. Generation Transmission and Distribution*, **143**(1), 75–81.
5. Kinghsirn, E.A. and Jordan, H.E. (1968) Polyphase induction motor performance and losses on non-sinusoidal voltage sources, *IEEE Trans*., **PAS-87**, 624–31.
6. Chalmers, B.J. and Srakar, B.R. (1968) Induction motor losses due to non-sinusoidal waveforms, *Proc. IEE*, **115**, 1777–82.
7. Williamson, A.C. (1981) The effects of system harmonics upon machines, International Conference on Harmonics in Power Systems, UMIST, Manchester.
8. Link, P.J. (1999) Minimizing electric bearing currents, *IEEE Industry Applications Magazine*, July/August.

9. Frank, J.M. (1994) Origin, development and design of K-factor transformers, Conference Record, IEEE Industry Applications Society Annual Meeting, Denver, pp. 2273–4.
10. Balda, J.C., Olejniczak, K.J., Wang, C., Barbré, B. and Samotyj, M. (1992) Comments on the derating of distribution transformers serving nonlinear loads, *Proceedings of the Second International Conference on Power Quality: End-Use Applications and Perspectives*, Atlanta, GA, September 28–30, pp. D-23:1–D-23:7.
11. Antoniu, S. (1984) Le régime énergétique déformant. Une question de priorité, *RGE*, **6/84**, 357–62.
12. Fryze, S. (1932) Wirk-, Blind- und Scheinleistung in Elektrischen Stromkreisen mit nichtsinusförmigen Verlauf von Strom und Spannung, *Elektrotecnische Zeitschrift*, June, 596–9.
13. Shepherd, W. and Zakikhani, P. (1972) Suggested definition of reactive power for nonsinusoidal systems, *Proc. IEE*, **119**, 1361–2.
14. Sharon, D. (1973) Reactive power definition and power factor improvement in nonlinear systems, *Proc. IEE*, **120**, 704–6.
15. Emanuel, A.E. (1977) Energetical factors in power systems with nonlinear loads, *Archiv für Elektrotechnik*, **59**, 183–9.
16. Kusters, N.L. and Moore, W.J.M. (1980) On definition of reactive power under nonsinusoidal conditions, *IEEE Trans. Power App. Systems*, **PAS-99**, 1845–50.
17. Emanuel, A.E. (1990) Power in nonsinusoidal situations. A review of definitions and physical meaning, *IEEE Trans. Power Delivery*, **PWRD-5**, 1377–83.
18. Czarnecki, L.S. (1987) What is wrong with the Budeanu concept of reactive and distortion power and why it should be abandoned, *IEEE Trans. Instr. Meas.*, **IM-36**(3), 834–7.
19. Slonin, M.A. and Van Wyk, J.D. (1988) Power components in a system with sinusoidal and nonsinusoidal voltages and/or currents, *Proc. IEE*, **135**, 76–84.
20. Emanuel, A.E. (1998) Apparent power: components and physical interpretation, *International Conference on Harmonics and Quality of Power (ICHQP'98)*, Athens, pp. 1–13.
21. Eguiluz, L.I. and Arrillaga, J. (1995) Comparison of power definitions in the presence of waveform distortion, *Int. J. Electrical Engineering Education*, **32**, 141–53.
22. Filipski, P.S. (1991) Polyphase apparent power and power factor under distorted waveform conditions, *IEEE Trans. Power Delivery*, **6**(3).
23. Eguiluz, L.I., Benito, P. and Arrillaga, J. (1996) Power factor and efficiency in three-phase distorted circuits, *Proc. IPENZ*, Dunedin, New Zealand, February, 131–40.
24. Eguiluz, L.I., Mañana, M., Benito, P. and Lavandero, J.C. (1995) El *PFs* un factor de potencia que relaciona las perdidas en la linea en circuitos trifasicos distorsionados, *4as J Luso-Espariholas de Engenharia Elecrotecnica*, **3**, 1212–20.
25. Shepherd, W. and Zand, P. (1979) *Energy Flow and Power Factor in Non-Sinusoidal Circuits*, Cambridge University Press, New York.
26. Baggott, A.G. (1974) The effect of waveform distortion on the measurement of energy tariff meters, IEE Conference Publication, 110.
27. CENELEC TC102 (1978) Harmonisation document for ripple controlled receivers.
28. Jost, F.A., Menzies, D.F. and Sachdev, M.S. (1974) Effect of system harmonics on power system relays, presented at a Power System Committee meeting, Canadian Electrical Association.
29. IEEE PES Power System Relaying Committee (1984) Sine-wave distortions in power systems and the impact on protective relaying, 84 TH 0115-6 PWR.
30. *GEC Protection Applications Guide*, GEC, London, ch. 5, pp. 76–8.
31. McClaren, P.G. and Redfern, M.A. (1975) Fourier series techniques applied to distance protection, *Proc. IEE*, **122**, 1301–5.
32. Van Warrington, A.R. (1971) *Protective Relays: Their Theory and Practice*, vol. 1, Chapman & Hall, London.
33. IEEE Task Force on the Effects of Harmonics on Equipment (1993) *IEEE Trans. Power Delivery*, **8**(2), 672–80.

34. Goldberg, G. (1975) Behaviour of apparatus under the influence of voltage and current harmonics, *Bull. Soc. R. Belg. Electr.*, **91**, 225–35.
35. Kuussaari, M. and Pessonen, A.J. (1976) Measured power line harmonic currents and induced telephone noise interference with special reference to statistical approach, Paper 36–05, CIGRE, Paris.
36. Carson, J.R. (1926) Wave propagation in overhead wires with ground return, *Bell Sys. Tech. J.*, **5**, 539–54.
37. CCITT (1963) Directives Concerning the Protection of Telecommunication Lines against Harmful Effects from Electricity Lines, International Telecommunications Union, Geneva.
38. Engineering Reports of the Joint Subcommittee on Development and Research of the Edisson Electric Institute and the Bell Telephone System, New York, 5 volumes, July 1926 to January 1943.
39. Heydt, G.T. (1991) *Electric Power Quality*, Stars in a Circle Publications, West LaFayette.

5

Harmonic Monitoring

5.1 Introduction

Harmonic monitoring involves the capturing and processing of voltage and current signals at various points of the power system. The signals to be captured are normally of high voltage and current levels, and thus require large transformation ratios before they can be processed by the instruments.

As an introduction to the subject, a summary of the harmonic measurement requirements specified by the IEC are considered first. This is followed by an assessment of the characteristics of conventional and special types of current and voltage transformers for use in harmonic measurements.

The transducers are normally placed in outdoor switchyards and the transformed low-level signals have to travel through a hostile electromagnetic environment before they reach the control rooms; thus the transmission of data in that environment also needs to be considered.

Once the captured signals reach the control room, the whole science of signal processing becomes available for the derivation of the harmonic spectrum. Chapter 2 has already described the main waveform processing techniques available with reference to the power system signals. The implementation of these techniques in modern digital instrumentation is also described in this chapter.

5.2 Measurement Requirements

5.2.1 The IEC 61000 4-7 Document [1]

Standard IEC 61000 4-7 describes the techniques for measuring harmonic distortion in the power system. For the purpose of formulating the requirements for measurement instruments the standard divides the harmonics broadly into three categories:

(1) quasi-stationary (slowly varying);

(2) fluctuating;

(3) rapidly changing (very short bursts of harmonics).

Power System Harmonics, Second Edition J. Arrillaga, N.R. Watson
© 2003 John Wiley & Sons, Ltd ISBN: 0-470-85129-5

The differing characteristics of the three categories of harmonics place different requirements on the design of the measuring instrument. For measuring quasi-stationary harmonics, there can be gaps between the rectangular observation window of 0.1–0.5 s wide. On the other hand, to access fluctuating harmonics, the rectangular window width has to be decreased to 0.32 s or a Hanning's window of 0.4–0.5 s width has to be used. Moreover, there should not be any gap between successive rectangular windows and there should be a half-by-half overlapping of the successive Hanning's window (described in Section 2.11.3). Lastly, rapidly changing harmonics have to be measured with a 0.08–0.16 s wide rectangular window without any gap between successive windows.

Instruments designed for measuring quasi-stationary harmonics are only appropriate to survey the long-term (such as thermal) effects of harmonics, or for the measurement of constant harmonic currents, such as those produced by television receivers. The measurement of fluctuating harmonic currents, such as those produced by motor reversal or speed change in household appliances with phase control and regulation, has to be made continuously without any gaps between successive observation intervals. Continuous real-time measurement capability is absolutely necessary for assessing the instantaneous effects of the rapidly changing harmonics, or short bursts of harmonics, on sensitive equipment such as electronic controls or ripple control receivers.

Measurements of up to the 50th harmonic order are commonly recommended but there are discussions on increasing it up to the 100th in certain cases. With such large amounts of data to be recorded, statistical evaluation over different observation intervals can be used to compress the data. Five time intervals are recommended in this standard:

(1) Very short interval (T_{vs}): 3 s

(2) Short interval (T_{sh}): 10 min

(3) Long interval (T_L): 1 h

(4) One-day interval (T_D): 24 h

(5) One-week interval (T_W): 7 d

If instantaneous effects are considered important, the maximum value of each harmonic should be recorded and the cumulative probability (at least 95% and 99%) of these maxima should be calculated. On the other hand, if long-term thermal effects are considered, the maximum of the r.m.s. value at each harmonic and its cumulative probabilities (at 1%, 10%, 50%, 90%, 95% and 99%) are to be calculated and recorded, i.e.

$$C_{n,rms} = \sqrt{\frac{\left(\sum_{k=1}^{M} C_{n,k}^2\right)}{M}} \tag{5.1}$$

where all the M single calculated values C_n shall be determined over the time interval T_{vs} for selectable individual harmonics (preferably up to $n = 50$).

5.2.2 Inter-Harmonics

IEC 61000 4-7 also contains a small subsection on inter-harmonics as a broad extension of harmonic phenomena. However, it leaves several important issues unresolved, and recommends that issues such as the range of frequencies to be considered and the centre frequency should be selected in accordance with the studied phenomenon, e.g. their influence on ripple control receivers or on flicker.

A study report prepared by a joint IEEE/CIGRE/CIRED working group on inter-harmonics [2] identifies the main problem associated with measurement of inter-harmonics as being that a waveform consisting of two or more non-harmonically related frequencies may not be periodic. Hence, most power system monitoring equipment, which is based on the FFT, will encounter errors due to the end-effect. This effect can be minimised by the signal processing techniques commonly used in the communication and broadcast industries, whereby the sampling of the signal need not be synchronised to the power frequency. The use of proper windowing functions and application of zero padding before performing the FFT can improve the frequency resolution of the measured inter-harmonic magnitudes significantly. For instance, the Hanning window with four-fold of zero padding technique [2] should also be suitable for measuring inter-harmonics in power systems.

The type of inter-harmonic measurement to be used also depends on the purpose of the assessment. Purposes include the diagnosis of a specific problem, general survey of an electromagnetic environment, compatibility testing and compliance monitoring. The IEC proposes to fix the sampling interval of the waveform to 10 and 12 cycles for 50 Hz and 60 Hz systems, resulting in a fixed set of spectra with 5 Hz resolution, for harmonic and inter-harmonic evaluation. The sampling will be phase-locked to the mains frequency, thereby minimising the contamination of the harmonic components by the inter-harmonic components. However, recent indications are that the IEC will opt to simplify the assessment process by summing the components between harmonics into one single inter-harmonic group, and reserving the original method of showing all inter-harmonic components at 5 Hz steps for specific cases. The frequency bins directly adjacent to the harmonic bins are omitted.

$$X_{IH}^2 = \sum_{i=2}^{8} X_{10n+i}^2 \quad \text{(50 Hz system)} \tag{5.2}$$

$$X_{IH}^2 = \sum_{i=2}^{10} X_{12n+i}^2 \quad \text{(60 Hz system)} \tag{5.3}$$

where n is the inter-harmonic group of interest and i is the inter-harmonic bin being summed.

Similarly, distortion indices equivalent to those for harmonics can be defined for inter-harmonics. The corresponding total inter-harmonic distortion (TIHD) factor is

$$\text{TIHD} = \frac{\sqrt{\sum_{i=1}^{n} V_i^2}}{V_1} \tag{5.4}$$

where i is the total number of inter-harmonics considered and n is the total number of frequency bins present including subharmonics (i.e. inter-harmonic frequencies that are less than the fundamental frequency). If the subharmonics are important, they can be analysed separately as another index called appropriately the total subharmonic distortion (TSHD).

$$\text{TSHD} = \frac{\sqrt{\sum_{s=1}^{S} V_s^2}}{V_1} \tag{5.5}$$

where S is the total number of frequency bins present below the fundamental frequency. Other distortion factors and statistical evaluation of harmonics can also be applied for the assessment of inter-harmonics in power systems.

5.2.3 Harmonic Phase-Angle Displacement

The measurement of phase angles between harmonic voltages and currents, together with their amplitudes, is required for the following purposes:

(1) to evaluate harmonic flows throughout the system;
(2) to identify harmonic sources and harmonic sinks;
(3) to assess summation factors of harmonic currents from different disturbing loads if they are connected to the same node;
(4) to establish system-equivalent circuits for calculating the impact of new disturbing loads, or the effectiveness of the countermeasures such as filters.

The direction of the active power flow at the harmonic order of interest can help to identify the source of the disturbance. To find the direction of the active power flow, the phase angle between the harmonic voltage at the point of common coupling and the plant feeder current has to be measured. If the active power flows into the public system, the plant is a harmonic source; otherwise it is a sink of harmonic currents from the system. The phase-lag of harmonic voltage and current in relation to the fundamental (absolute phase angle) need not be known in this case. Such absolute phase angle is only needed for evaluating the coupling between frequencies of nonlinear loads. However, the measurement of absolute phase angles provides the following additional advantages:

(1) Measurements at different nodes of similar or different systems can be compared.
(2) It becomes possible to deduce whether the connection or rearrangement of different systems, or locally spread disturbing loads, will increase or decrease the harmonic level in the system. Harmonic distortions with similar phase angles will superimpose, raising the harmonic level, while those with opposite phase angles will compensate each other, thereby lowering the harmonic level.
(3) Phase angles of disturbing loads, especially from rectifier circuits without firing control, can be detected in order to evaluate their overall disturbing effect or to find countermeasures.

Extra care is needed in operating the measuring instrument and in interpreting the results, when precise synchronisation across multiple channels is required to measure absolute phase angles.

5.2.4 Harmonic Symmetrical Components

If the loads and transmission and distribution systems are balanced, the three voltages and currents have identical wave shape and are separated by exactly $\pm\frac{1}{3}$ of the fundamental period. In such case, only characteristic harmonics exist: these are of zero sequence for orders $n = 3m(m = 1, 2, 3\ldots)$, of positive sequence for the $n = 3m - 2$ orders, and of negative sequence for the $n = 3m - 1$ orders. However, asymmetries always exists, causing non-characteristic harmonics in the system. These asymmetries can be evaluated by monitoring the symmetrical components of the harmonics.

Positive-sequence (or negative-sequence) impedances differ from zero-sequence impedances for nearly all loads and network equipment including transmission lines, cables and transformers. Therefore, a separate treatment of the system is necessary for assessing the harmonic voltages caused by the injected currents. Secondly, the effect of each sequence component differs for most loads and network equipment. Zero-sequence voltages do not affect delta-connected loads such as motors and capacitor banks. Only the non-characteristic components (positive sequence or negative sequence) of the third harmonic voltages cause additional losses in delta-connected motors. Moreover, commonly used transformers with delta–star or star–zigzag winding connections do not transfer zero-sequence currents and voltages.

5.3 Transducers

The function of a current or voltage transformer is to provide a replica of the power system current or voltage, at a level compatible with the operation of the instrumentation, in circumstances where direct connection is not possible.

While the behaviour of the conventional current and voltage transformers at fundamental frequency is well understood and defined, the behaviour at higher frequencies has not been as fully examined. With the need to measure power system harmonic content, their performance in transforming current and voltage signals containing harmonic components is essential to the measurement process.

Although the frequency response of a transducer may be poor, it can still be used for harmonic measurements if such a response is known and compensated for at the front end of the measuring instrument.

In line with the accuracy requirements suggested for instrumentation, the IEC 61000-4-7 standard indicates that the errors of voltage and current transformers shall not exceed 5% (related to the measured value) in magnitude and 5° in phase angle.

5.3.1 Current Transformers

The most common type of current transformer is the toroidally-wound transformer with a ferromagnetic core. This has, by virtue of its construction, low values of primary and

secondary leakage inductance and primary winding resistance. Under normal operating conditions, the transformer primary current will be substantially less than that required for saturation of the core, and operation will be on the nominally linear portion of the magnetisation characteristic.

The frequency response of current transformers is effectively determined by the capacitance present in the transformer and its relationship with the transformer inductance. This capacitance may be present as inter-turn, inter-winding or stray capacitance. Test have shown that while this capacitance can have a significant effect on the high-frequency response, the effect on frequencies to the 50th harmonic is negligible [3,4].

In addition to harmonic frequencies, it is also possible that the primary current will contain a d.c. component. If present, this d.c. component will not be transformed but will cause the core flux of the transformer to become offset. A similar condition could arise from remnant flux present in the transformer core as a result of switching.

For this reason, where the presence of a d.c. component is suspected, or remanence a possibility, a current transformer with an air gap in the core can be used. This air gap reduces the effect of the d.c. component by increasing core reluctance and enables linearity to be maintained. Because the current transformer burden tends to increase with frequency, the associated power factor reduces with increasing frequency and the transformer will produce a higher harmonic output voltage than it would for a purely resistive load. The resulting increased magnetising current will cause further error.

For measurements of harmonic currents in the frequency range up to 10 kHz, the normal current transformers that are used for switchgear metering and relaying have accuracies of better than 3%. If the current transformer burden is inductive, there will be a small phase shift in the current. Clamp-on current transformers are also available to give an output signal that can be fed directly into an instrument.

The following practical recommendations are worth observing whenever possible:

(1) If the current transformer is a multi-secondary type, the highest ratio should be used. Higher ratios require lower magnetising current and tend to be more accurate.

(2) The current transformer burden should be of very low impedance, to reduce the required current transformer voltage and, consequently, the magnetising current.

(3) The burden power factor should be maximised to prevent its impedance from rising with frequency and causing increased magnetising current errors.

(4) Whenever possible, it is suggested that the secondary of the measuring current transformer is short-circuited and the secondary current monitored with a precision clamp-on current transformer.

Unconventional Types of Current Transformer [5] Various alternatives to the conventional current transformer have been investigated, some of which are already finding a place in power system monitoring. Among them are:

- *Search coils*. The magnetic field in the proximity of a conductor or coil carries information on the components of the current which generates the field. The amplitude of the induced harmonic voltage in a search coil is proportional to the

effective coil area, number of turns, the amplitude of the harmonic magnetic field perpendicular to the coil surface and the frequency of the harmonics.

In such measurements, the measured magnetic field can arise from the contributions of more than one source. The magnetic field is inversely proportional to the distance from the source. Where it is possible to place the search coil at a small distance d from the conductor, while other conductors are located at distances larger than $20d$, the measurements of values in the chosen conductor are not substantially changed by fields of the other conductors.

- *Rogowski coils*. These devices are coils wound on flexible plastic mandrels, and they can be used as clamp-on devices. They have no metallic core, so problems of core saturation are avoided in the presence of very large currents, such as the 60–100 kA in the feed to an arc furnace or in the presence of direct current.
- *Passive systems*. In a passive system, a transmitted signal is modulated by a transducer mounted at the conductor. No power source is required at the conductor. Optical systems use the Faraday magneto-optic effect, by which the plane of polarisation of a beam of linear polarised light is rotated by a magnetic field along its axis.

  Designs for Faraday effect current transformers use either the open-path or the closed-path optical system [6].

  Microwave systems make use of gyromagnetic materials to modulate a microwave carrier by a magnetic field. The form of modulation is controlled by the arrangement of the gyromagnetic material and the form of polarisation of the microwave signal.
- *Active systems*. An active system uses a conductor-mounted transducer to provide a modulating signal for a carrier generated at the conductor. Transmission of the carrier to the receiving station is then achieved via a radio or fibre-optic link. The power for the transmitter is usually line derived using a magnetic current transformer together with some battery back-up.
- *Hall effect transducers*. The Hall effect is used in a variety of probes and transducers covering a range of current levels. For current transformer applications, a major problem is that of maintaining calibration over long periods.

5.3.2 Voltage Transformers

Only on low-voltage systems can the analyser be connected directly to the terminals where the voltage components must be determined. On medium- and high-voltage systems, means of voltage transformation are required.

Magnetic voltage transformers, of extensive use for medium voltage levels, are designed to operate at fundamental frequency. Harmonic frequency resonance between winding inductances and capacitances can cause large ratio and phase errors. For voltages to about 11 kV, and harmonics of frequencies under 5 kHz, the accuracy of most potential transformers is within 3%, which is satisfactory, the response being dependent upon the burden used with the transformer [7].

At higher voltage levels, the transformer tends to exhibit resonances at lower frequencies, as the internal capacitance and inductance values vary with insulation requirements

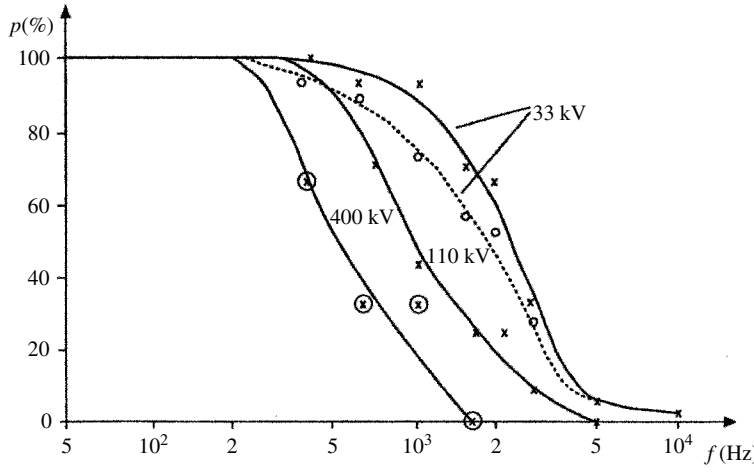


Figure 5.1 Percentage of voltage transformers, the transfer ratio of which has a maximum deviation (from the nominal value) of less than 5% or 5° up to the frequency f. (———) minimum error (5%); (- - - -) maximum error (5%)

and construction. The precise response for a particular unit will be a function of its construction [8].

Figure 5.1 contains test results carried out in over 40 voltage transformers at levels between 6 kV and 400 kV. The figure indicates the percentage of transformers that maintained the required precision (i.e. 5% and 5°) throughout the frequency range. The main conclusions are:

- At medium voltage, all the transformers perform adequately up to 1 kHz, while only 60% of them manage to cover the whole harmonic spectrum. The figures reduce further, to 700 Hz and 50% respectively, when the phase precision level requirement is included.
- At high voltage, the transformers' response deteriorates quickly for frequencies above 500 Hz unless special designs are introduced.
- The conventional voltage transformers of magnetic type do not provide accurate information for harmonic orders above the 5th.

Capacitive Voltage Transformer The capacitive voltage transformer (CVT) combines a capacitive potential divider with a magnetic voltage transformer, as shown in Figure 5.2. This combination enables the insulation requirements of the magnetic unit to be reduced, with an associated saving in cost.

The additional capacitance provided by the capacitive divider will influence the frequency response of the CVT, producing resonant frequencies as low as 200 Hz, which makes them unsuitable for harmonic measurements.

The form of frequency response obtained is also dependent upon the magnitude of the fundamental component and its relationship to any transition point in the magnetisation characteristic of the transformer steel.

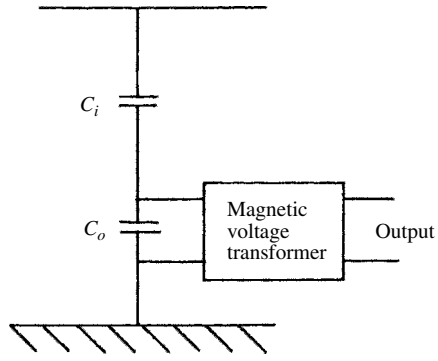


Figure 5.2 Capacitive voltage transformer (CVT)

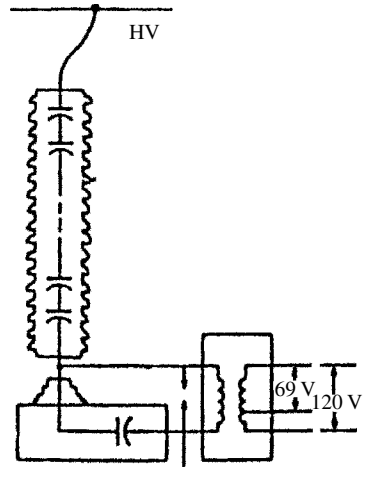


Figure 5.3 Capacitive voltage divider using a bushing tap

Capacitive Dividers For harmonics measurements, either a purpose-built divider could be assembled or, alternatively, use could be made of the divider unit of a capacitive voltage transformer, with the magnetic unit disconnected, or the loss tangent tap on an insulating bushing (Figure 5.3).

When subject to an impulse, such as might arise from local switching, the capacitive divider is subject to *ringing* due to the interaction between the divider capacitors and their internal inductances. This can lead to high common mode voltages, particularly in areas of high earth impedances. To minimise ringing, the capacitors forming the divider circuit should have a low inductance and the low-voltage capacitor should be screened.

In recent years, a number of amplifier-based capacitive divider systems have been developed [9,10]. Although intended primarily for use with high-speed protection schemes, they also have obvious application in harmonic measurements.

The basic arrangement for a single-phase unit is shown in Figure 5.4. High-input impedance instrumentation amplifiers must be included in such measurements. For best

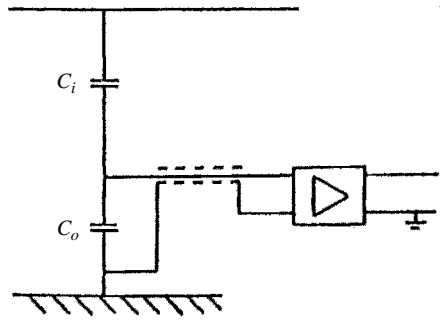


Figure 5.4 Capacitive voltage divider incorporating an amplifying circuit

results, the input amplifier should either be battery operated or use a suitably shielded and isolated supply. The leads from the low-voltage capacitors to the input amplifier should be as short as possible. In general, short leads from the amplifier to the analyser will greatly reduce the angle error when measuring phase angles. These devices have a limit on the burden that they can supply without saturation, hence the requirement for a high-impedance amplifier.

Unconventional Voltage Transformers [5] Electro-optical and electrogyration effects can be used to measure voltage in a manner akin to the Faraday effect used for current measurement.

The electro-optical effect causes linearly polarised light passing through the material to become elliptically polarised. As the two mutually perpendicular components propagate in the crystal at different velocities, they have a difference in phase as they emerge from the material. This phase difference will be proportional to the path length in the material and to either the field (the Pockels effect) or the square of the field (the Kerr effect). By measuring this phase difference, the electric field strength, and hence the voltage, can be obtained.

If a linearly polarised beam is propagated through an electrogyrational material in an electric field, the effect is to rotate the plane of polarisation in a manner analogous to that occurring in magneto-optic materials. The electrogyration effect can, therefore, be used to measure voltage in a manner similar to the Faraday effect current transformers.

5.4 Harmonic Instrumentation

The derivation of voltage and current harmonics is carried out in instrumentation systems that receive the line signals in the time domain and convert them into the frequency domain. The main purposes of a harmonic monitoring system are:

- capturing existing levels of harmonic distortion to check them against recommended or admissible limits;
- testing equipment that generates or causes harmonics in order to ensure its compliance to certain standards or guidelines;

- diagnosing or troubleshooting a situation in which some equipment performance is unacceptable to the utility or to the user;
- observing existing background levels and tracking the trends with time for any hourly, daily, weekly, monthly or seasonal patterns;
- verifying simulation studies or techniques and fine-tuning the modelling of the devices and the system under analysis;
- determining the driving point impedance at a given location. This impedance is useful for gauging the system capability to withstand power quality disturbances.

Monitoring background levels will require the system to be operated continuously over a long period of time and the measured data will have to be stored. The stored data may comprise the average, maximum and minimum values over predetermined intervals so as to provide an overall picture of the phenomenon. On the other hand, the testing of equipment simply requires the use of snapshots under certain operating modes. The captured data most likely will consist of several cycles of the time-domain waveforms, which can be further processed to extract the necessary information.

Some commercial instruments have been specifically designed for power systems use (e.g. harmonic analysers) while others are of more general use (signal analysers). The main difference between these two categories is the need to follow the variations in fundamental frequency in the case of harmonic analysis.

Portable instruments are of small size and lightweight, easy to set up and use in the field. The transducers (clip-on type) and interconnecting cable normally are part of the unit. They normally use microprocessor based circuitry to calculate the individual harmonics up to the 50th, as well as their r.m.s., THD and TIF indices. Some of these devices can also calculate harmonic powers and can upload stored waveforms and calculated data to a PC. Generally, the logging feature allows periodic downloading of the instrument readings to a PC through an RS323 interface.

To reduce cost, portable instruments are normally restricted to one or two channels. Battery operating is essential for usage flexibility without dependence on external wires and power supplies, particularly as the instrument has to be close to the measurement point due to the length of the clip-on cable. Generally, these instruments are not automated and therefore they need a person controlling their operation, although some now have a logging feature. The operator must control the transducer locations, what quantity is displayed, and the storing of data to memory or downloading to PC. The capabilities of these instruments are restricted to the features originally designed into the unit and cannot be changed. Therefore, upgrades are achieved by buying a newer model.

For permanent or semi-permanent monitoring, the instruments require many channels as they are intended to operate without human intervention and, generally, the channels are not designed to be moved from one location to another. Transducers do not come as part of these instruments, as it is assumed that the CTs or VTs already existing in the system will be used. Due to the high cost of such hardware, the functionality is designed into the software to permit upgrades. As some of the measuring points are likely to be in outdoor switchyards, the cables and transducers must be designed to withstand all weather conditions and operate satisfactorily in a hostile electromagnetic environment.

These instruments operate unattended over long periods and software is thus required to automate the data collection, processing and storage. Such instrumentation is normally required at a multitude of sites, therefore synchronisation and the ability to control them all from a central location are important features.

The processing of the waveforms can be carried out in analogue or digital form, although the latter has practically displaced the analogue-type analysers. Analogue instrumentation is based on the use of an adjustable filter which can be tuned to specific frequencies (heterodyne system) or a bank of filters, each of which detects a particular harmonic. The characteristics and implementation of the digital instrumentation are discussed in the following section.

5.4.1 Digital Instrumentation

As shown in Figure 5.5, A/D converters change the analogue signals into digital form as required by digital instruments; these signals are then processed by digital filters or the FFT.

Some digital analysers still use the digital filtering, method, which, in principle, is similar to analogue filtering. Before starting a series of measurements, the range of frequencies to be observed must be defined and this information selects the required digital filters. At the same time, the bandwidth is varied to optimise the capture of all the selected harmonics in the presence of a large fundamental frequency signal. All the recent instruments, however, use the FFT (described in Chapter 2), a very fast method of analysis that permits capturing several signals simultaneously via multi-channel instruments.

Generally, digital instruments use microprocessors for the processing of the signals and co-ordination of their functions. Some instruments include a PC with a data acquisition card that collects the voltage and current signals from the transducers; the PC contains a microprocessor that calculates the harmonic levels, a hard disk for data storage and a screen for the visual display of the results.

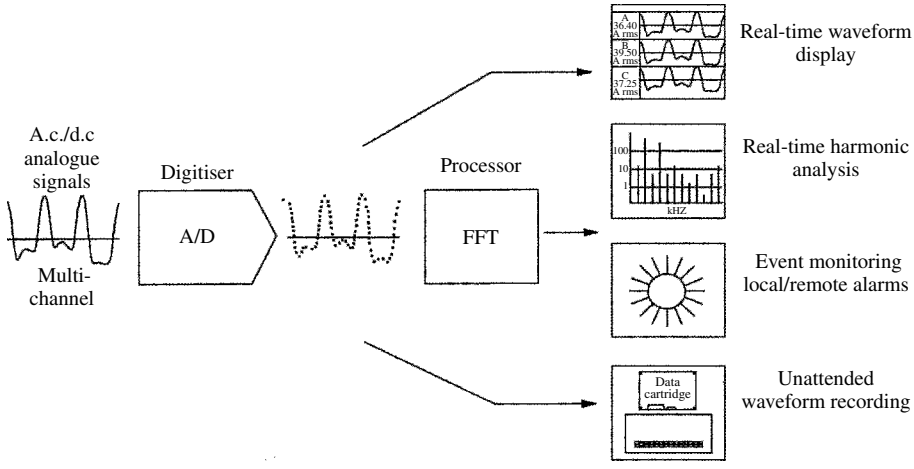


Figure 5.5 Components of a multiwave monitoring system (from Electric Research and Management Inc.)

The main components of an FFT-based instrument are illustrated in Figure 5.6. First, the signal is subjected to low-pass filtering to eliminate all the frequencies above the spectrum of interest; this is normally limited to orders below the 50th. Once filtered, the analogue signal is sampled, converted to digital and stored. The FFT is then applied to the 2^i samples included in a period T_w multiple of the fundamental wave period, i.e. $T_w = NT_1$, the sampling frequency being $f_s = 2^i/(NT_1)$.

To reduce spectral leakage, the samples contained in T_w are sometimes multiplied by a window function as described in Chapter 2.

The FFT process derives the Fourier coefficients a_k and b_k of frequencies $f_x = k(1/T_w)$ for $k = 0, 1, 2, \ldots 2^{i-1}$ and with adequate synchronisation the nth harmonic of the fundamental frequency is given by $n = k/N$.

Finally, an arithmetic processor calculates the harmonic amplitudes

$$C_n = \sqrt{a_n^2 + b_n^2} \tag{5.6}$$

and phases

$$\varphi_n = \arctan\left(\frac{b_n}{a_n}\right) \tag{5.7}$$

An FFT computation can be undertaken for each fundamental cycle, producing a set of harmonics every cycle, or several cycles of samples can be joined together before using a longer FFT to achieve better frequency resolution.

The frequency resolution of the FFT is given by the reciprocal of the record length

$$\Delta f = \frac{1}{T_0}$$

Hence to resolve harmonic values, separated by 50 Hz or 60 Hz, the record length must be one period of the fundamental frequency (20 ms or 16.7 ms). An FFT output bin is not, however, an impulse function centred on a particular harmonic. Instead, it has a non-zero response to frequencies between harmonics. This means that signals

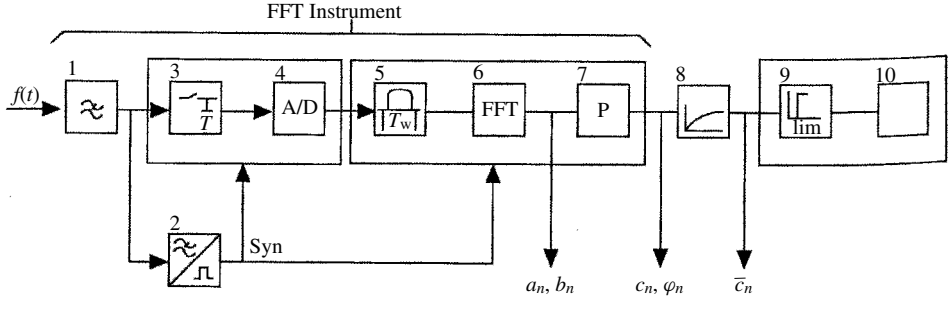


Figure 5.6 An FFT-based instrument 1, anti-aliasing low pass filter; 2, synchronisation; 3, sample and hold; 4, analogue/digital converter; 5, shape of window unit; 6, FFT processor; 7, arithmetic processor; 8, unit for evaluation of transitory harmonics; 9, programmable classifier; 10, counter and storage unit

present in the signal to be transformed, which are not harmonics, will contribute to particular harmonic outputs from the FFT, making them erroneous. The severity of this problem can be reduced by taking the FFT over longer time spans, thereby resolving inter-harmonic frequencies which would otherwise contribute to harmonic outputs. This does, however, require more data processing. In harmonic analysis this is seen as a disadvantage because only harmonics are required—as opposed to a spectrum analyser, which is required to have a very good resolution.

It is possible to achieve the same effect of taking the FFT over several periods by averaging several periods to one and computing the FFT of that, provided that sampling is synchronous with the fundamental. This preserves the bandwidth of the FFT with only a small processing overhead. It must be noted that if subharmonics are required, averaging is not suitable. Instead, the FFT must be taken over multiple cycles to produce the sub-multiples of the 50 Hz or 60 Hz fundamentals.

A modern monitoring system is divided into the three subsystems shown in Figure 5.7.

(1) *Input signal conditioning and acquisition subsystem.* The function of this unit is the conversion of analogue signals into digital formats. This digitisation simplifies the design of analogue circuitry and provides greater flexibility for altering the algorithms to be used for processing the data samples. The main factors to be considered in the design of this unit are:
   - the sampling rates, which for harmonic analysis are in the kHz range;
   - an anti-aliasing filtering, to be determined by the bandwidth of the signal to be measured;
   - provision of immunity to EMI susceptibility to the extremely noisy power system electromagnetic environment;
   - synchronisation and timing (when multiple channels are used);
   - automatic ranging, as the current can vary significantly between light and heavy loading conditions (this ensures that the full dynamic range is used).

(2) *Digital processing and storage subsystem.* Digital samples are transferred to this subsystem for processing and recording. This subsystem can simply be a data logger or a powerful parallel processing computer system. Generally, it is the design of this subsystem that determines if continuous real-time data acquisition is possible or only snapshots can be captured and stored for offline processing. The special requirements to achieve continuous real-time data acquisition are discussed in Section 5.4.2.

(3) *User interface subsystem.* The purpose of this unit is to provide users with access to the measured data, either through on-screen displays or in hard-copy forms. It also provides the users with the ability to control and configure the monitoring system. The basic requirement on this subsystem is to hide the complicated

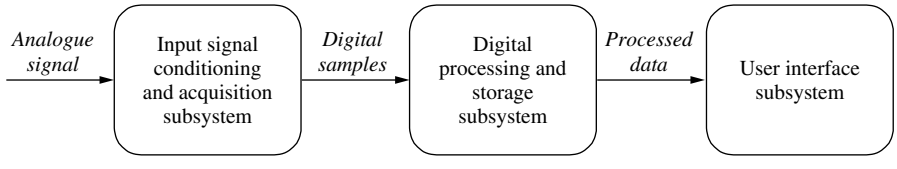


Figure 5.7 Major subsystems making up a monitoring system

details of the monitoring system from the users. A graphical user interface forms the essential 'face', representing the monitoring system, to the user.

5.4.2 Structure of a Modern Monitoring System

Ideally, the harmonic assessment should be carried out continuously over a wide bandwidth and with good resolution, usually at multiple nodes of the power network. Furthermore, in order to capture the very low magnitude higher-order harmonics in the presence of the large fundamental component, an adequate analogue to digital conversion resolution is required.

Most existing instruments are not equipped with the capability of synchronising the acquisition of data samples across multiple channels and between multiple instruments and/or nodes on a power network. Consequently, the steady-state assumption is again taken as implicit when snapshots, gathered at different parts of a power system network, are used alongside each other in order to make simultaneous power quality assessment of the system.

The need to know the precise state of the system at all times is particularly important when endeavouring to locate the distorting sources. This requires good magnitude and phase measurements, often at more than one location on the network and preferably synchronised.

Most existing data acquisition systems use the centralised processing architecture shown in Figure 5.8, which places a constraint on the data processing capability of the system. From the harmonic monitoring perspective, this limited real-time processing capacity results in offline post-processing of the acquired data to derive the necessary information. The lack of online analysis processing capability results in large volumes of raw data having to be acquired and stored. Consequently, the limited system throughput, bandwidth and storage volumes only allow the system to record snapshots.

The centralised configuration relies on the outputs of the CTs and VTs being directly routed to the metering room. Although this configuration is normally sufficient for relay operation or metering purposes, the limited bandwidth and EMI susceptibility of the long analogue communication links create serious concerns over the integrity of the measurements.

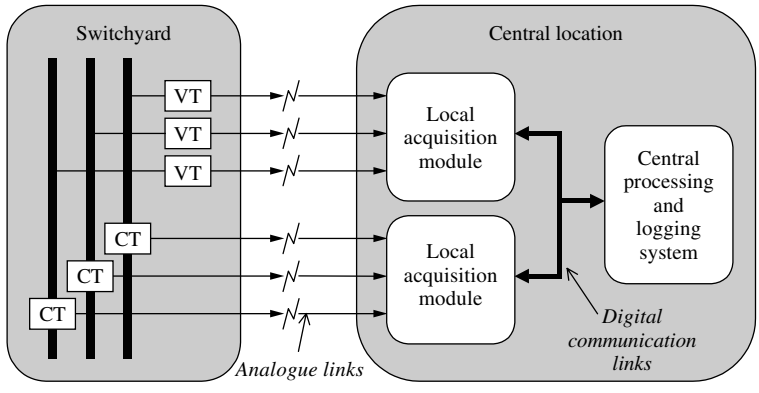


Figure 5.8 Conventional centralised processing architecture

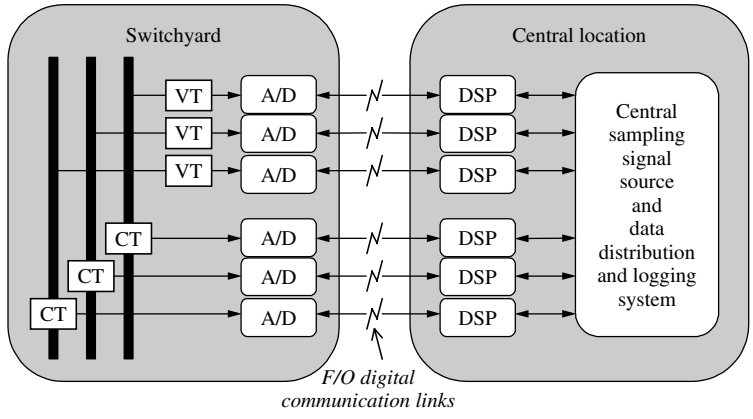


Figure 5.9 A possible distributed processing architecture

Therefore, some form of distributed processing architecture is preferred, such as shown in Figure 5.9. In this configuration the A/D conversion is shifted from the central location to the switchyard close to the transducers. This enables the use of digital communication links between the switchyard and the central system, thus improving the bandwidth, dynamic range and noise immunity of the acquired signals. The use of a fibre optic link reduces the system's susceptibility to electromagnetic noise, which can be significant in a switchyard environment. The second key element is the provision of a digital signal processor (DSP) to undertake the data processing for each individual channel. By dedicating a single DSP (or CPU) to every data channel, computationally intensive manipulations can be implemented online [11].

A centralised source of sampling signals provides the opportunity to synchronise the sampling across all data channels. The DSP usually communicates with the central data collection system through multi-processing bus architectures. This enables the DSP modules to be designed as plug-in cards, facilitating flexible expansion.

Sampling synchronisation between units at different sites can be achieved using GPS-generated timing signals.

5.5 Data Transmission

A high proportion of power system harmonic measurements will be made using instrumentation sited remotely from the transformers providing the replicas of system current and voltage. Some means of communication is, therefore, needed between the transformers and the instruments.

This communication link may pass wholly or partially through a high-voltage switchyard, in which case particular attention must be given to the effects of electrostatic and electromagnetic interference as well as the necessary screening.

The provision of increased noise immunity may require the use of other forms of data transmission such as current loop systems, modulated data or digitally encoded data.

Shielded conductors (coaxial or triaxial cables) are essential for accurate results, but proper grounding and shielding procedures should be followed to reduce the pick-up of parasitic voltages. Moreover, coaxial cable is only suitable for relatively short leads.

Where high common-mode voltages can occur, the communications link may be required to provide insulation up to several kilovolts to protect both users and equipment. This may require the use of isolation amplifiers or, where higher levels of isolation are required, fibre-optic links.

Information may be transmitted either as an analogue signal for direct connection of the instrument, or in a modulated or encoded form using both analogue and digital data systems. If direct analogue transmission is used, then a system of sufficiently high signal to noise ratio is obviously required. For certain harmonic measurements, a dynamic range of the order of 70 dB may well be needed and, hence, the achievable signal to noise ratio must be in excess of this figure.

5.6 Presentation of Harmonic Information

Figure 5.10 illustrates the capturing and transmission of information from the high-voltage network and its presentation in visual form by means of oscilloscopes and harmonic analysers. The former permit observing the time variation of the voltage and current waveforms, while the latter show their respective spectra.

The analogue-type analysers require minutes of processing time to gather the harmonic information and produce either graphs (as shown in Figure 5.11) or tables (e.g. the information corresponding to the graph of Figure 5.11 is shown in Table 5.1). The discrete measurement at widely separate times can lead to substantial interpretation errors. For instance, with reference to Figure 5.12, where the harmonic level varies with time, if the harmonic measurement is registered every 12 minutes as shown, the results will be very misleading.

When using digital systems the problem changes from one of insufficient data to one of extracting relevant information from the vast amount of recorder data. The captured information is often recorded for later offline processing.

As well as time-varying information (shown in Figure 5.12), it is possible to derive cumulative probability graphs (Figure 5.13) or histograms (Figure 5.14).

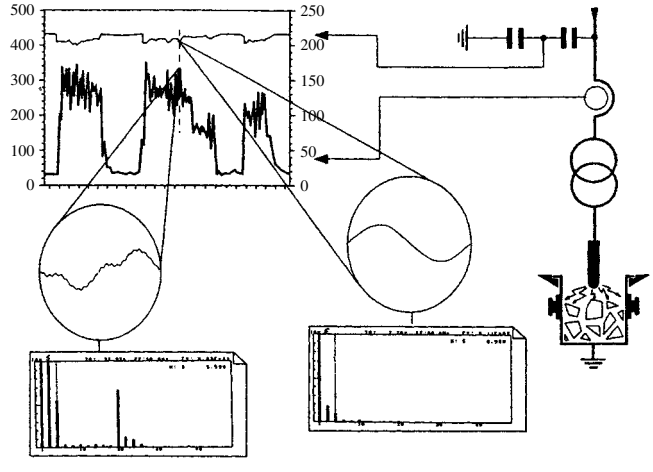


Figure 5.10 Captured and transmitted information from the grid

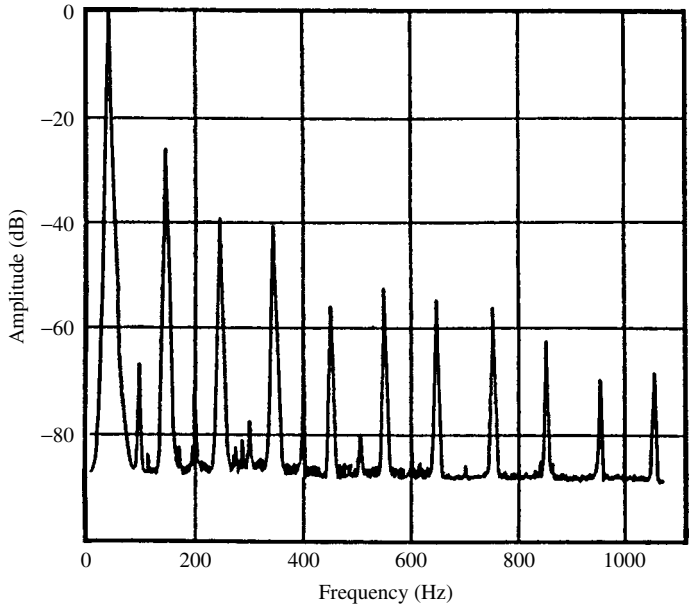


Figure 5.11 Typical harmonic plot from an analogue analyser

Table 5.1 Tabulated information corresponding to the plot in Figure 5.11

Frequency (Hz)	Amplitude (V)
50	240
100	0.1
150	12
200	0.1
250	2.7
300	0.0
350	2.1
400	0.0
450	0.3
500	0.0
550	0.6
600	0.0
650	0.4
700	0.0
750	0.3
800	0.0
850	0.2
900	0.0
950	0.1
1000	0.0

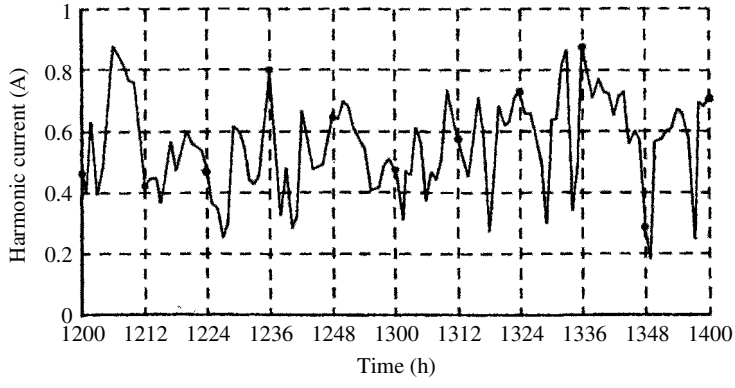


Figure 5.12 Recording of a current harmonic sampled at 12-minute intervals

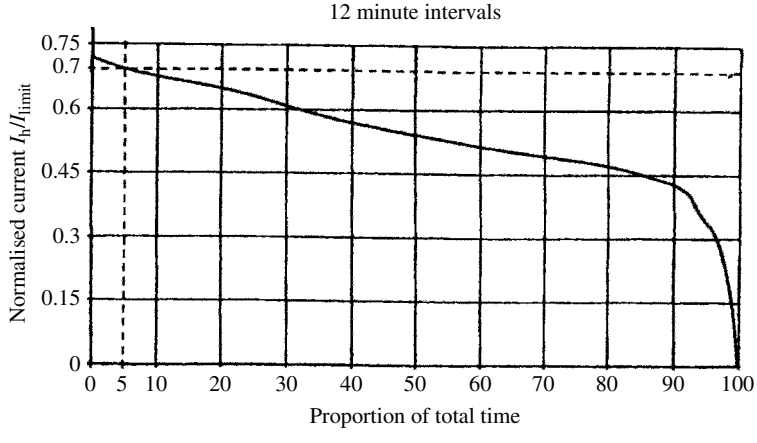


Figure 5.13 Cumulative probability graph

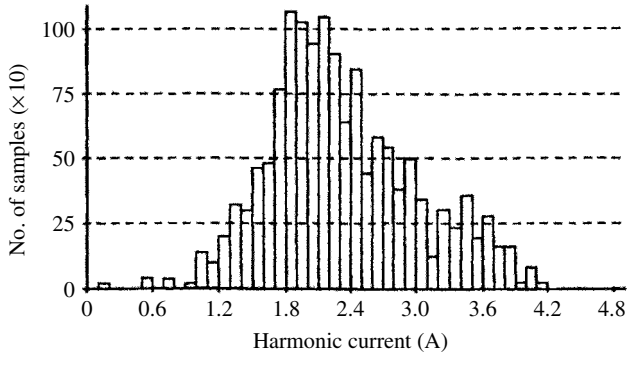


Figure 5.14 Histogram of harmonic amplitudes

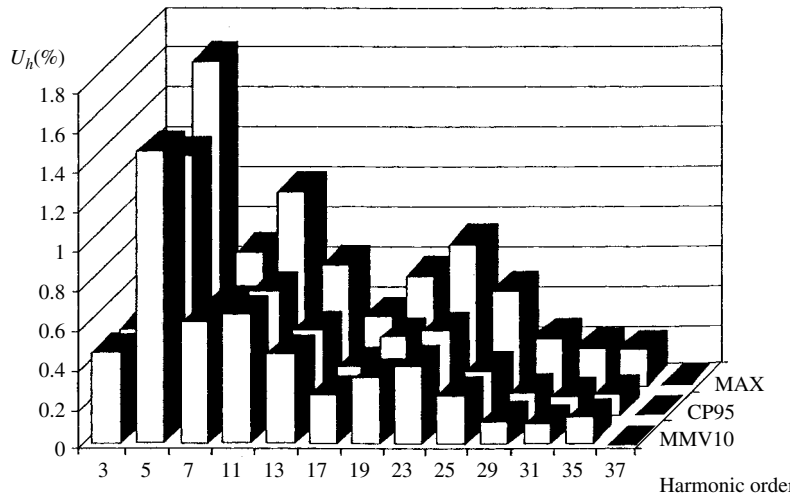


Figure 5.15 Levels of harmonic distortion not exceeded by 80% of the observation points

Another example of data presentation, shown in Figure 5.15, relates to the recommendation from a joint CIGRE/CIRED based on the IEC directives [1]. In this case the measurement at each observation point extends to several days (including the weekend), and for each harmonic and day the maximum value (MAX) the value not to be exceeded with a 95% probability (CP95) and the mean maximum value at 10-minute intervals (MMV10) are retained.

5.7 Examples of Application

This section reports on field measurements carried out in the New Zealand power system to illustrate the use and capability of modern digital instrumentation. The instrument used was CHART (Continuous Harmonic Analysis in Real Time) [11].

5.7.1 Synchronised Tests

Figure 5.16 shows the 220 kV network of New Zealand's South Island system. Between the Islington and North Makawera substations, there are a number of hydro stations and a HVd.c. scheme. The distribution network at Islington had reported a substantial amount of 5th harmonic distortion caused by the presence of a large number of industrial sites connected to this bus. The 5th harmonic current is largely absorbed by the compensation capacitors at the Islington substation. However, the capacitors are usually removed from service during light load conditions, causing the 5th harmonic current to flow into the 220 kV transmission system. On the other hand, at North Makawera, the opposite effect had been observed, with the 5th harmonic current flowing from the 220 kV transmission network into the distribution system. The main consumer of electrical power fed by the North Makawera substation is an aluminium smelter at the Tiwai bus. A recently installed 5th harmonic filter at Tiwai was

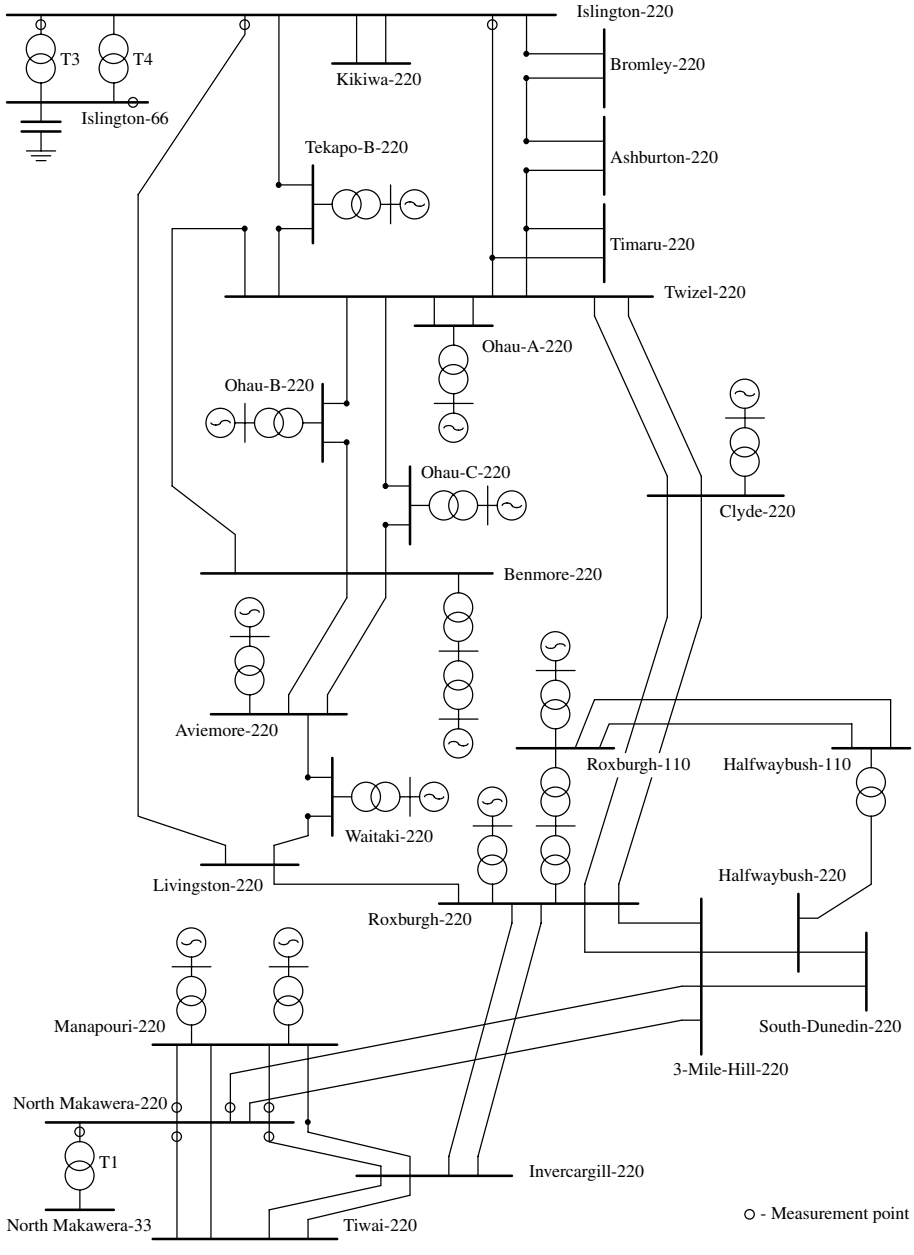


Figure 5.16 CHART measurement points in the synchronised test

frequently overloaded and the source of the 5th harmonic current distortion was traced to the 220 kV transmission system.

The first objective of the test was to decide whether there was any connection between the 5th harmonic problems at the Islington and North Makawera substations. If the two problems were related, the response of the 5th harmonic distortion at North

Makawera to the switching of capacitors at Islington was to be identified. This required that the measurements undertaken at both sites should be synchronised as accurately as possible. The 5th harmonic problems at both substations were known to vary with the daily operation of the South Island system. Therefore, the monitoring systems had to gather harmonic information over a fairly long period, covering a variety of operating conditions. CHART units were installed at the North Makawera and Islington substations (shown in Figure 5.17), to monitor the currents flowing between the 220 kV transmission system and the substations.

At Islington, the two transmission lines considered to have the lowest impedance between the substation and the generating stations around Benmore were the Islington–Livingston and Islington–Timaru–Twizel lines. The three phases on these two

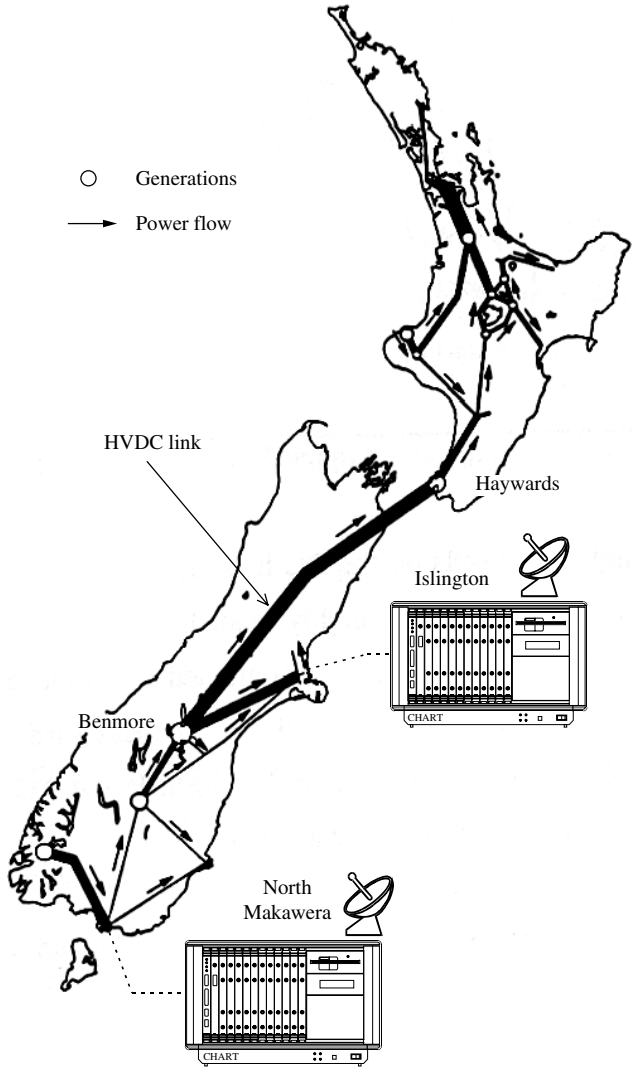


Figure 5.17 Location of CHART units in the synchronised test

circuits were therefore measured. Besides measurements on the 220 kV system, the voltage distortion on the 66 kV bus was also monitored. The CHART unit was also set up to record the current of one of the transformers (T3) interconnecting the 66 kV distribution network and the 220 kV transmission network.

At North Makawera, the main flow of power is between the generation at Manapouri and an aluminium smelter at Tiwai. The CHART unit was set up to monitor the current between these two places and the North Makawera substation. The connections from North Makawera to the rest of the 220 kV network were also monitored by measuring the current between North Makawera and 3-Mile Hill, and between North Makawera and Invercargill. Moreover, the current of transformer T1 feeding the 33 kV distribution network at North Makawera was monitored to determine if there is any 5th harmonic source within the local load. The voltage distortion on the 33 kV distribution busbar was also recorded. However, due to the limited number of channels available on this particular CHART unit (12 channels), it was necessary to forgo some of the phases at several measurement points.

The main requirement of this test was to record the harmonic distortion at both substation simultaneously. The data samples were time-stamped to enable them to be matched in time. It was decided to average the harmonics over one second and to compute the mean, maximum and minimum harmonics over a minute throughout the entire measurement.

The measured fundamental frequencies at Islington and North Makawera are shown in Figure 5.18. The fundamental frequencies are identical at both sites with similar deviations throughout the measurements. This ensured that the sampling processes were synchronised between the two CHART units.

A selection of acquired data is shown in Figure 5.19. A number of steps are observed on the 66 kV bus voltage which may be caused by the switching of the compensation capacitors. However, only three of these show concurrent changes in the 5th harmonic current flowing out of the Islington substation. The three cases are highlighted in the figure together with the possible capacitor switching instants. The currents in the

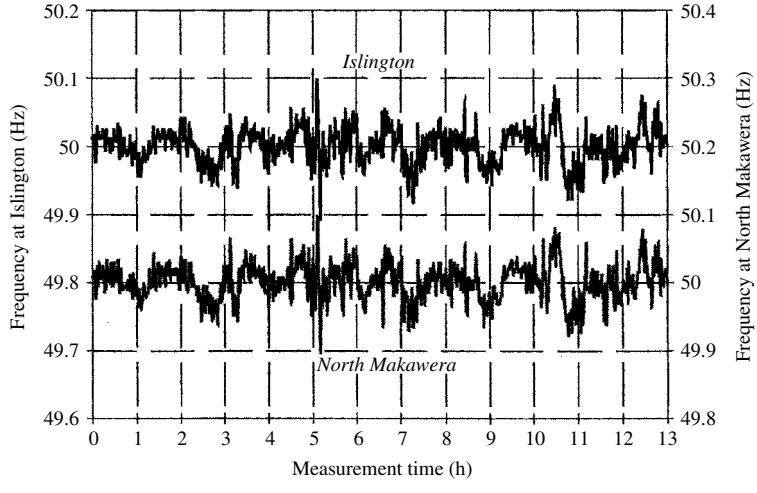


Figure 5.18 Fundamental frequency measured at Islington and North Makawera

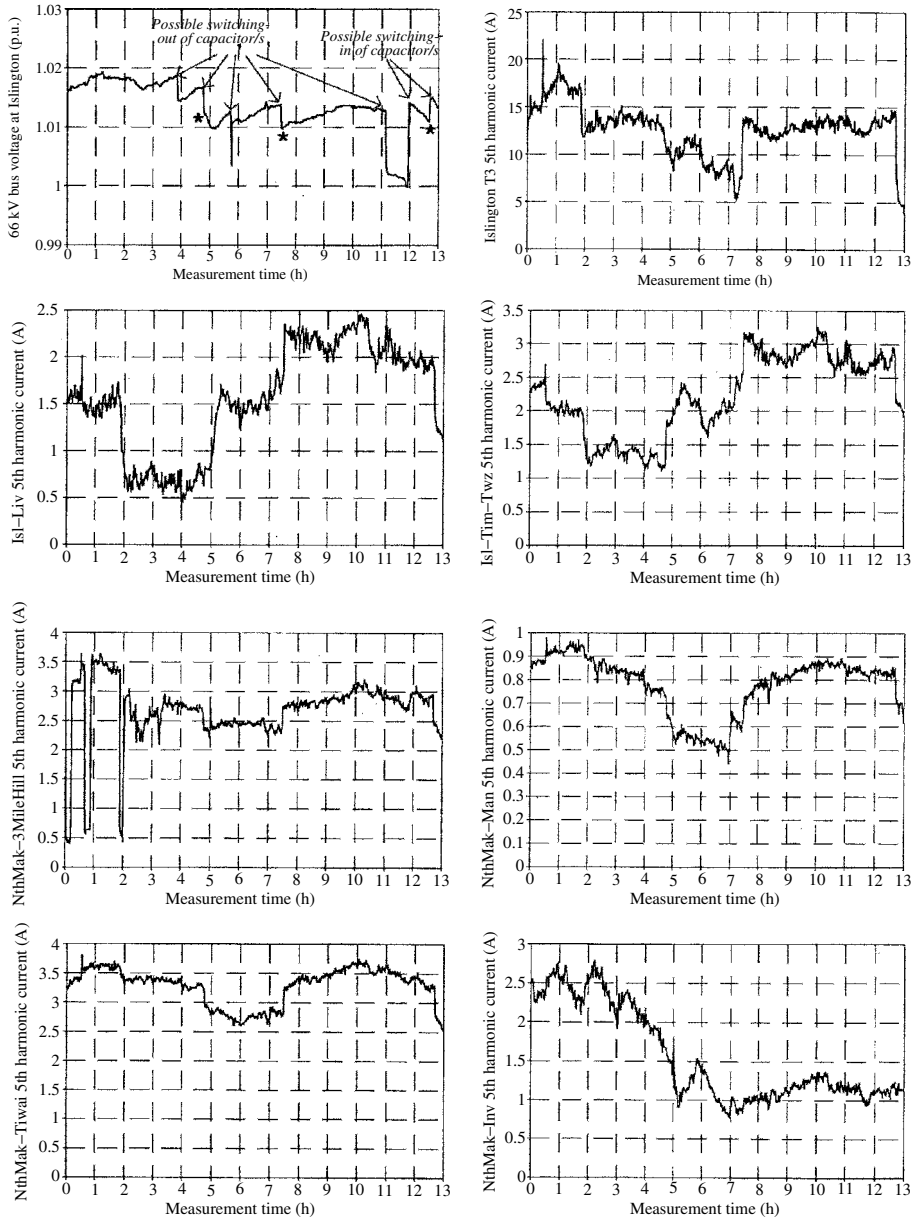

66 kV bus voltage at Islington (p.u.)
Possible switching-out of capacitor/s
Possible switching-in of capacitor/s
Measurement time (h)
Islington T3 5th harmonic current (A)
Isl–Liv 5th harmonic current (A)
Isl–Tim–Twz 5th harmonic current (A)
NthMak–3MileHill 5th harmonic current (A)
NthMak–Man 5th harmonic current (A)
NthMak–Tiwai 5th harmonic current (A)
NthMak–Inv 5th harmonic current (A)

Figure 5.19 Selection of data acquired in the South Island synchronised test

two transmission lines, Islington–Livingston and Islington–Timaru–Twizel, show an increase in the 5th harmonic current when the capacitors are switched out. A decrease in the 5th harmonic current is also observed when the capacitor is switched back into service towards the end of the test.

The variations in the 5th harmonic current at North Makawera do not always correspond with the changes at Islington. Among the three aforementioned instants

when there are changes to the 5th harmonic current flowing out of Islington, only the last two show corresponding changes in the distortion at North Makawera. At the second highlighted switching just after the 7th hour, when one of the capacitors is removed from service, the sudden increase in the 5th harmonic currents in the two outgoing lines from Islington coincides with similar increases in the lines between 3-Mile Hill, North Makawera and Tiwai. Similar coincidence is observed when one of the capacitors is put back into service near the end of the test. The decrease in the 5th harmonic current flowing out from the Islington 220 kV system coincides with the decreases in the 5th harmonic distortion around North Makawera.

These observations indicate that under certain operating conditions, the switching of capacitors at Islington substation can affect the 5th harmonic distortions at North Makawera. However, more detailed analyses of the system, in particular during the period when the measurement was carried out, will be required to finalise the above findings.

5.7.2 Group-Connected HVD.C. Converter Test

During a maintenance period at the Benmore HVd.c. converter station, the opportunity arose to test the possibility of operating the converter plant in the group-connection mode, i.e. islanded from the South Island a.c. network; as the filters are connected on the a.c. side of the converter transformers, the generators were subjected to greater harmonic distortion than under the normal configuration. Moreover, the fundamental frequency of the islanded network could deviate from the nominal 50 Hz depending on the d.c. load and the amount of generation.

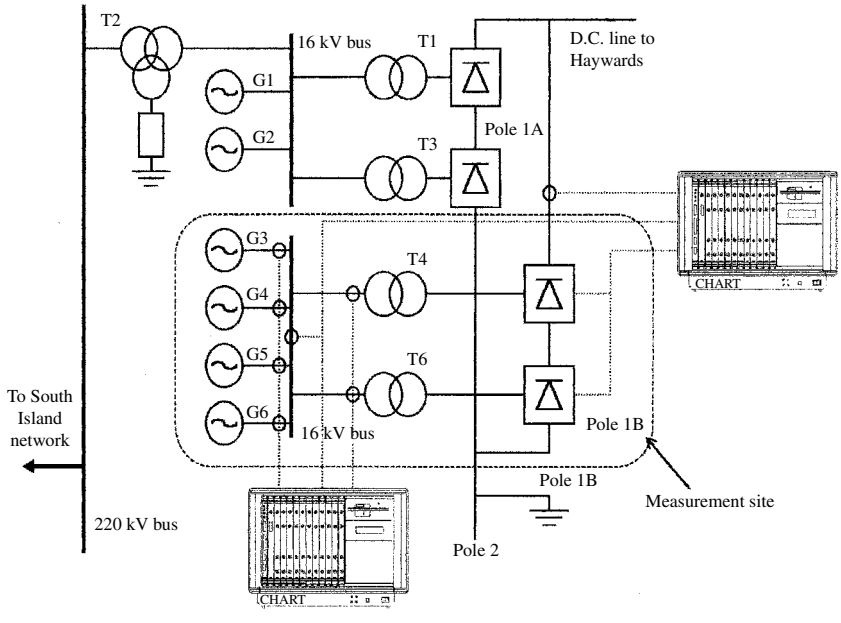


Figure 5.20 CHART measurement points in the Benmore test

Besides capturing the waveforms needed for validation of computer models, this test provided the opportunity to illustrate some of the capabilities of the digital instrumentation. These include the ability to perform alternative data processing tasks, the transparent handling of the different data formats of results from the tests, the ability to track the varying fundamental frequency in the islanded a.c. system and its use to ensure coherent sampling.

Figure 5.20 shows the islanded system at the Benmore converter station. Two CHART units were used to provide a total of 24 data channels. The measurements include the voltage at the 16 kV bus, generator currents, converter transformer currents, Pole 1B

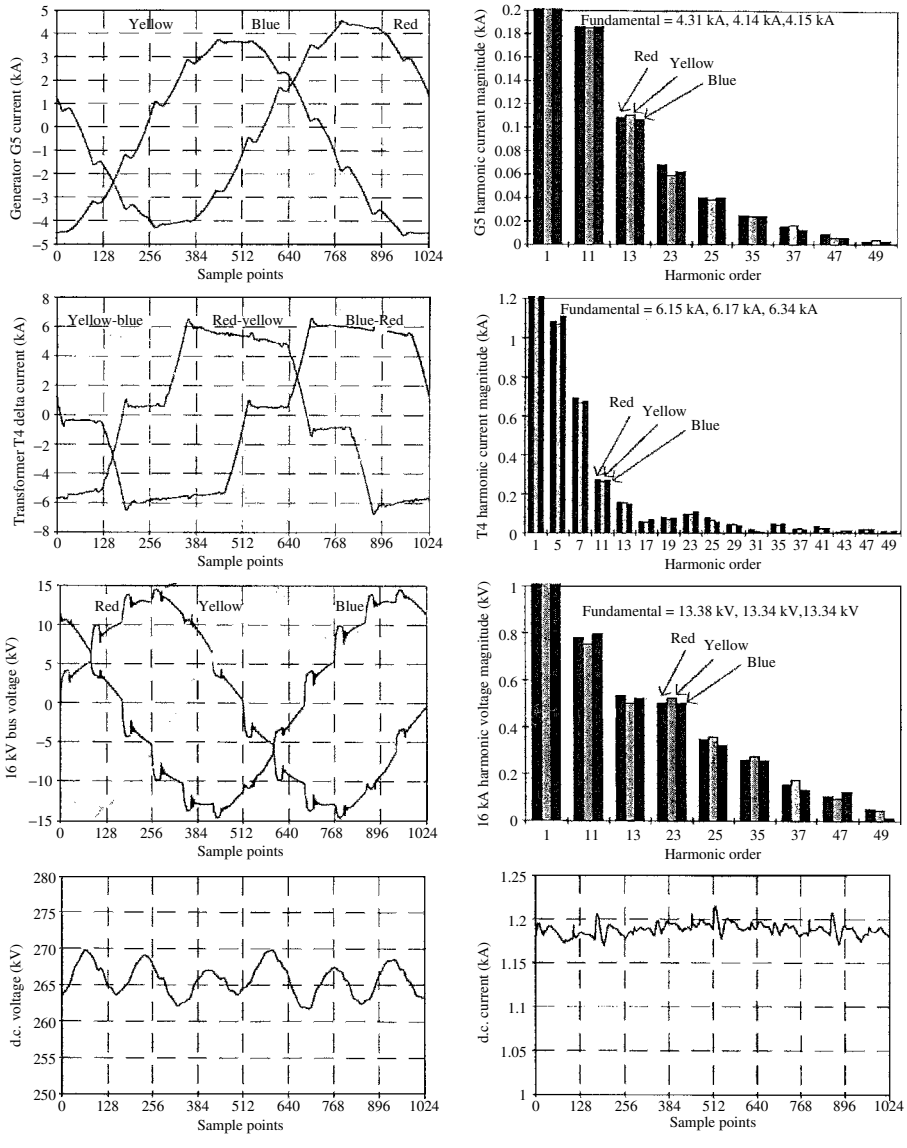


Figure 5.21 Selection of data acquired in the Benmore islanded converter test

d.c. line voltage and current, and the firing angle of the Pole 1B converter. The main task of the test system was to capture the time domain waveforms under different d.c. current and a.c. generation configurations. It was decided to capture two different forms of time-domain data, a small number of samples per fundamental cycle over a longer period for steady-state analysis and a handful of cycles of data with a higher sampling rate. A selection of data acquired during the islanded converter test at Benmore is shown in Figure 5.21.

5.8 Discussion

The main components of power system waveform monitoring, i.e. transducers and instrumentation, have been critically reviewed for their ability to transfer harmonic information. Adequate technology is now available for the transfer of voltage and current information and for their processing. The main limitation for reliable monitoring is its dependence on expensive high-voltage transducers; these are relatively few in number and primarily designed to obtain fundamental frequency related information. The inadequacy relates particularly to the use of capacitor voltage transformers.

A number of alternatives to improve the transducers' response at harmonic frequencies have been described in the literature and some of them are now produced by the industry. However, despite their limitations for harmonic monitoring, conventional CTs and CVTs are still the preferred options for general power system use. A possible solution is the re-calibration of the transducers' performance at the specified harmonic frequencies.

As the most popular technique, the chapter has discussed the FFT implementation of digital processing. Hardware and software system requirements have been described, both for single point and system-wide assessment, the latter requiring perfect sampling synchronisation at geographically separated buses. Examples of local and system-wide field test monitoring, using advanced digital instrumentation, have been included to illustrate their capability in the real environment.

5.9 References

1. IEC 61000-4-7 (1991), Electromagnetic Compatibility (EMC), Part 4: Limits, Section 7: General guide on harmonics and inter-harmonics measurements and instrumentation, for power supply systems and equipment connected thereto.
2. IEEE Inter-harmonic Task Force, CIGRE 36.05/CIRED 2 CC02 Voltage Quality Working Group, Inter-harmonics in Power Systems, January 1997.
3. Douglass, D.A. (1981) Current transformer accuracy with asymmetric and high frequency fault currents, *IEEE Trans.*, **PAS-100**, 1006–12.
4. Malewski, R. and Douville, J. (1976) Measuring properties of voltage and current transformers for the higher harmonics frequencies, Paper presented at the Canadian Communication and Power Conference, Montreal.
5. Mouton, L., Stalewski, A. and Bullo, P. (1978) Non-conventional current and voltage transformers, *Electra*, **59**, 91–122.
6. Rogers, A.J. (1979) Optical measurement of current and voltage on power system, *IEE Conf. Publ.* **174**, 22–6.

7. Douglass, D.A. (1981) Potential transformer accuracy at 60 Hz voltages above and below rating and at frequencies about 60 Hz, *IEEE Trans.*, **PAS-100**, 1370–75.
8. CIGRE Working Group 36-05 (Disturbing loads) (1981) Harmonics characteristics parameters, methods of study, estimating of existing values in the network, *Electra*, **77**, 35–54.
9. Lisser, J. (1976) High accuracy with amplifier type voltage transformer, *Electrical Review*, **198**(21), 31–33.
10. Gray, F.M., Hughes, M.A. and Stalewski, A. (1975) Monitoring of transmission line voltage for protective relaying purposes using capacitive dividers, *IEE Conf. Publ.*, **125**, 214–21.
11. Miller, A.J.V., Lake, C.B. and Dewe, M.B. (1990) Multichannel real-time harmonic analysis using the Intel Multibus II bus architecture, *Proc of the 7th International Intel Real-Time Users Group Conference*, St Louis, Missouri, October, pp. 11–24.

6

Harmonic Elimination

6.1 Introduction

When planning the installation of large nonlinear plant components the decision has to be made between designing the nonlinear devices for low levels of waveform distortion or installing harmonic compensation equipment at the terminals. The first solution is often possible by phase-shifting of the transformers and/or the control of converter bridges or by the use of switching devices with turn-off capability. These alternatives have been discussed under harmonic sources (Chapter 3). External harmonic compensation, on the other hand, is achieved by means of filters. In each case the decision will depend on factors like the power and voltage rating of the equipment to be installed and the effect of the local (internal) waveform distortion on the rest of the plant.

When the sole purpose is to prevent a particular frequency from entering selected plant components or parts of the power system (e.g. in the case of ripple control signals) it is possible to use a series filter consisting of a parallel inductor and capacitor which presents a large impedance to the relevant frequency. Such a solution, however, can not be extended to prevent the harmonics from arising at the source, because the production of harmonics by nonlinear plant components (like transformers and static converters) is essential to their normal operation.

In the case of static converters, the harmonic currents are normally prevented from entering the rest of the system by providing a shunt path of low impedance to the harmonic frequencies.

Although this chapter is mainly concerned with passive filters, a section is devoted to active filtering due to the increasing interest in this alternative.

6.2 Passive Filter Definitions

A shunt filter is said to be tuned to the frequency that makes its inductive and capacitive reactances equal.

The quality of a filter (Q) determines the sharpness of tuning and in this respect filters may be either of a high or a low Q type. The former is sharply tuned to one of the lower harmonic frequencies (e.g. the fifth) and a typical value is between 30

Power System Harmonics, Second Edition J. Arrillaga, N.R. Watson
© 2003 John Wiley & Sons, Ltd ISBN: 0-470-85129-5

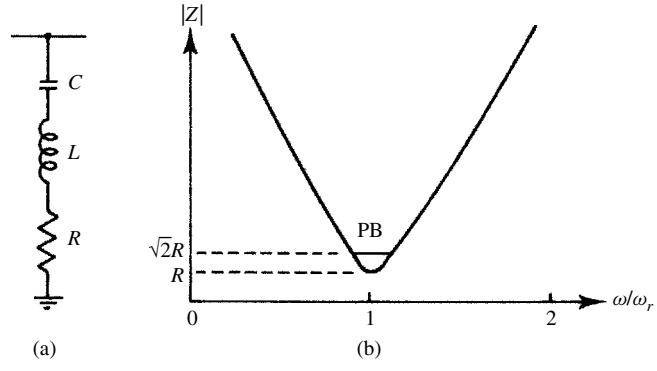


Figure 6.1 (a) Single-tuned shunt filter circuit; (b) single-tuned shunt filter impedance versus frequency

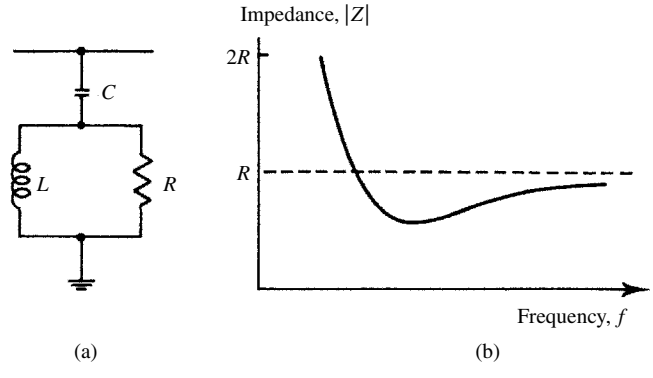


Figure 6.2 (a) Second-order damped shunt filter; (b) second-order damped shunt filter impedance versus frequency

and 60. The low Q filter, typically in the region of 0.5–5, has a low impedance over a wide range of frequency. When used to eliminate the higher-order harmonics (e.g. 17th up wards) it is also referred to as a high-pass filter. Typical examples of high and low Q filter circuits and their impedance variation with frequency are illustrated in Figures 6.1 and 6.2.

In the case of a tuned filter Q is defined as the ratio of the inductance (or the capacitance) to resistance at the resonant frequency, i.e.

$$Q = X_0/R \tag{6.1}$$

As shown in Figure 6.1(b), the filter pass band (PB) is defined as being bounded by the frequencies at which the filter reactance equals its resistance, i.e. the impedance angle is 45° and the impedance module $\sqrt{2}R$. The quality factor and pass band are related by the expression

$$Q = \omega_n/\text{PB} \tag{6.2}$$

where ω_n is the tuned angular frequency in radians per second. The sharpness of tuning in high-pass damped filters is the reciprocal of that of tuned filters, i.e. $Q = R/X$.

The extent of filter detuning from the nominal tuned frequency is represented by a factor δ. This factor includes various effects: (i) variations in the fundamental (supply) frequency; (ii) variations in the filter capacitance and inductance caused by ageing and temperature; and (iii) initial off-tuning caused by manufacturing tolerances and finite size of tuning steps.

The overall detuning, in per unit of the nominal tuned frequency, is

$$\delta = (\omega - \omega_n)/\omega_n \tag{6.3}$$

Moreover, a change of L or C of say 2% causes the same detuning as a change of system frequency of 1%. Therefore δ is often expressed as

$$\delta = \frac{\Delta f}{f_n} + \frac{1}{2}\left(\frac{\Delta L}{L_n} + \frac{\Delta C}{C_n}\right) \tag{6.4}$$

6.3 Filter Design Criteria

6.3.1 Conventional Criteria

The size of a filter is defined as the reactive power that the filter supplies at fundamental frequency. It is substantially equal to the fundamental reactive power supplied by the capacitors. The total size of all the branches of a filter is determined by the reactive power requirements of the harmonic source and by how much this requirement can be supplied by the a.c. network.

The ideal criterion of filter design is the elimination of all detrimental effects caused by waveform distortion, including telephone interference, which is the most difficult effect to eliminate completely. However, the ideal criterion is unrealistic for technical and economic reasons. From the technical point of view, it is very difficult to estimate in advance the distribution of harmonics throughout the a.c. network. On the economic side, the reduction of telephone interference can normally be achieved more economically by taking some of the preventive measures in the telephone system and others in the power system.

A more practical approach is to try to reduce the problem to an acceptable level at the point of common coupling with other consumers, the problem being expressed in terms of harmonic current, harmonic voltage, or both. A criterion based on harmonic voltage is more convenient for filter design, because it is easier to guarantee staying within a reasonable voltage limit than to limit the current level as the a.c. network impedance changes.

The voltage THD index is more representative than the arithmetic sum, because it corresponds to the power of the harmonics and is therefore more closely related to the severity of the disturbance. The recommended criteria for HVd.c. converter filters [1] is the maximum level of any single harmonic and the THD. In general it will be sufficient to include all harmonics up to the 25th order. The maximum values of individual harmonics generally occur for different conditions. It is therefore necessary

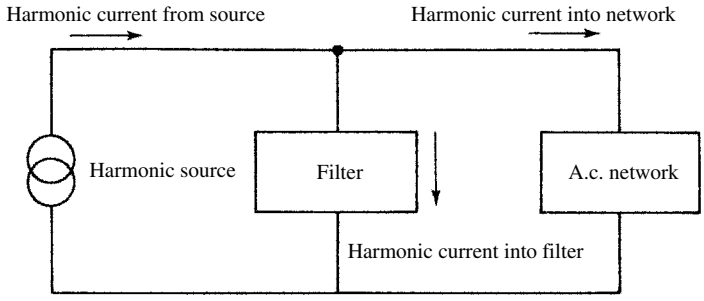


Figure 6.3 Circuit for the computation of voltage harmonic distortion

to clarify whether the THD should use those values of individual harmonics which are simultaneously present, or the non-coincident maximum values of each harmonic. Regarding telephone interference, although used in a number of projects, the IT index into a node of a meshed transmission system has little meaning. However, in cases when earth resistivity is high there is justification to limit the magnitudes of harmonic currents flowing in particular transmission lines which run close to telephone lines; this is normally achieved with the use of the 'equivalent disturbing current' concept.

To comply with the required harmonic limitations, the design of filters involves the following steps:

(1) The harmonic current spectrum produced by the nonlinear load is injected into a circuit consisting of filters in parallel with the a.c. system (Figure 6.3) and the harmonic voltages are calculated.

(2) The results of (1) are used to determine the specific parameters, i.e. the THD, TIF and IT factors.

(3) The stresses in the filter components, i.e. capacitors, inductors and resistors, are then calculated and with them their ratings and losses.

Three components require detailed consideration in filter design: the current source and the filter and system admittances.

The current source content should be varied through the range of load and (in the case of static converters) firing angle conditions. This subject has been discussed in Chapter 3. As far as system and filter admittances are concerned, it is essential to calculate the minimum total equivalent admittance at each harmonic frequency, which will result in maximum voltage distortion.

The obvious filter design is a single broad band-pass configuration capable of attenuating the whole spectrum of injected harmonics (e.g. from the fifth up in the case of a six-pulse converter). However, the capacitance required to meet such a target is too large, and it is usually more economical to attenuate the lower harmonics by means of single arm tuned filters.

6.3.2 Advanced Filter Design Criteria

The conventional criteria described above provide adequate filter designs for most applications. However, in cases where the nonlinear plant has a very large power

rating, such as an HVd.c. converter, these criteria can lead to inadequate solutions and even harmonic instabilities. The reason is that the conventional approach ignores the interaction that exists between the nonlinear device and the rest of the power system. Such interaction affects the harmonic current injections as well as the overall system harmonic impedances (which should include the effective contribution of the nonlinear device), and thus requires an iterative solution, rather than the direct solution of the conventional approach.

The derivation of advanced models of nonlinear plant, taking into account their harmonic interaction with the rest of the system, is described in Chapter 8.

6.4 Network Impedance for Performance Calculations

The network harmonic impedances change with system configuration and load conditions. Although these can be determined from measurements, it is difficult to monitor all possible network conditions; in particular, future changes can not be captured by measurements.

The use of computer programs provides greater flexibility. If the derived impedances are too pessimistic (i.e. unreasonably large and/or the damping too low), which is normally the case due to lack of accuracy in the parameters used for the calculation, the filter will be more expensive than necessary. Thus the correct modelling of the variation of component/branch resistance with frequency, particularly for transformers and loads, is important to determine accurately the damping of the network.

6.4.1 Size of System Representation

As the system harmonic impedances vary with the network configuration and load patterns, large amounts of data are generated. Considering the large number of studies involved in filter design, it is prohibitive to represent the whole system with the same degree of detail for every possible operating condition. The detail of component representation depends on their relative position to the harmonic source, as well as their size in comparison with that of the harmonic source. Any local plant components such as synchronous compensators, static capacitors and inductors, etc., will need to be explicitly represented.

As the high voltage transmission system has relatively low losses, it is also necessary to consider the effect of plant components with large (electrical) separation from the harmonic source. It would thus be appropriate to model accurately at least all of the primary transmission network. Moreover, due to the standing wave effect on lines and cables, a very small load connected via a line or cable can have a dramatic influence on the system response at harmonic frequencies.

It is recommended to consider the loads on the secondary transmission network in order to decide whether these should be modelled explicitly or as an equivalent circuit. If these loads are placed directly on the secondary side of the transformer, their damping can be overestimated when using simple equivalents.

Increasing network complexity results in a greater number of resonance frequencies. By way of illustration [2], Figure 6.4 shows the harmonic impedance at a converter

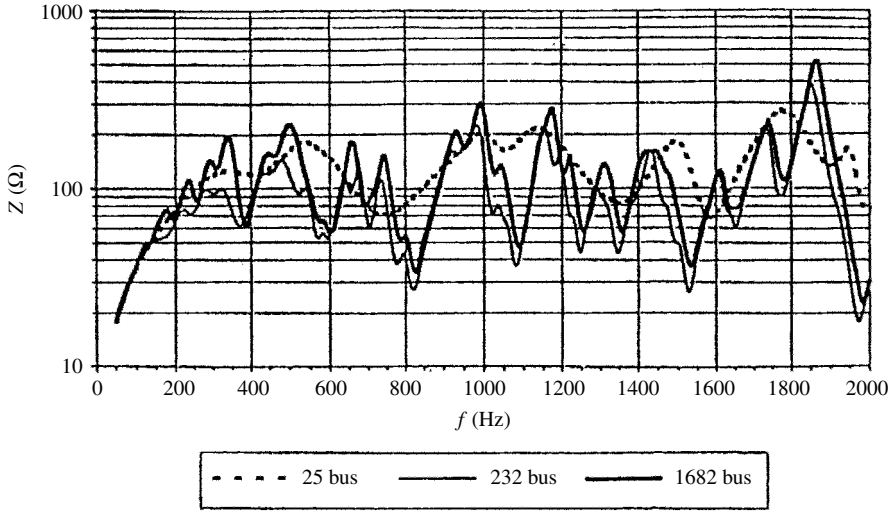


Figure 6.4 Effect of size of system representation [2]

bus of a primary (400 kV) system with either 25, 232 or 1682 buses included; the 25-bus case includes the nearest 400 kV lines terminated by equivalent circuits plus the transformers and large generators in this area. The continuous thick line shows the same information when the network consists of 1682 buses, which include the complete 400 kV, 220 kV and 110 kV networks plus the generators down to the 1 MVA size; however, it must be emphasised that the number of buses is not the only relevant criterion for increased accuracy. The considerable differences observed are due to the 'hand-made' formation of the small network while the large network is produced automatically from the network database. Because modern computers can handle the larger network in reasonable times, the larger representation must be recommended as it gives accurate results at any point in the network and only one model for the whole network has to be maintained.

Radial parts of the system or neighbouring interconnected systems that remain invariant when performing multiple case studies can be replaced by frequency-dependent circuits, or by their harmonic admittances at the point of connection.

6.4.2 Effect of A.C. Network Resistance at Low Frequencies [1]

When considering classical resonant filters, taking into account the damping of the a.c. network generally allows the use of smaller sized filters when a target of maximum harmonic voltage has been specified. This size reduction is a function of the maximum phase angle ($\phi_{h\,\max}$) of the network impedance at harmonic frequency h and is expressed by

$$1/(1 + \cos \phi_{h\,\max})$$

The filtering performance of damped filters (Section 6.6) for high frequencies does not depend much on the converter power rating or on the network impedance, the latter being generally higher than that of the filters.

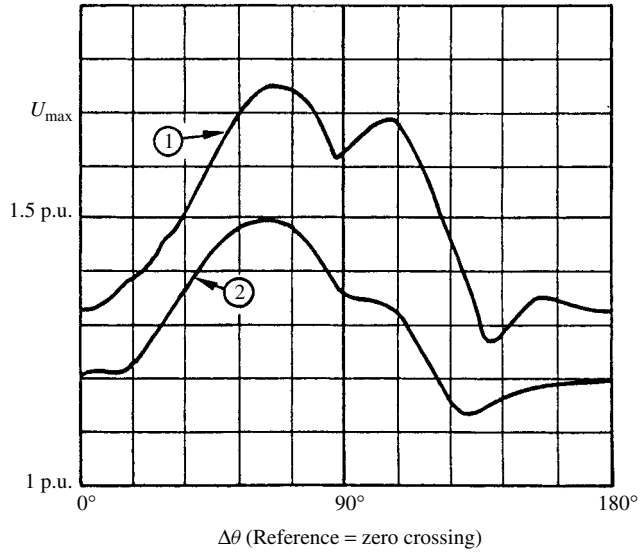


Figure 6.5 Influence of system damping on the maximum overvoltage during the energisation of a 150 MVAr filter bank. (1), Purely inductive system; (2), the real system (400 kV/4 GVA/50 Hz)

On the other hand, when designing a damped filter for stronger damping of a low-order harmonic voltage, it is essential to know accurately the network impedance at low frequencies. It is necessary to ensure that connecting the filter in parallel with the network impedance has a positive effect on the harmonic voltage and avoids excessive amplification of harmonic voltages of other orders, especially those which are close. These requirements must be fulfilled while keeping an acceptable level of losses.

The simulation of the transient overvoltages resulting from the energisation of the converter transformers and of compensation equipment also depend on the damping of the a.c. network at low frequencies. Figure 6.5 illustrates the calculated overvoltages due to switching of a second-order high-pass filter bank for different switching instants; these results show the influence of the damping representation of the network. Such analysis requires the determination of the network impedance locus for its various configurations and, especially, for the resonant frequencies between the a.c. network and the filters.

6.4.3 Impedance Envelope Diagrams

The results of the computer studies can be presented in the form of tables or, more effectively, as envelope diagrams, such as sector, polygon or circle diagrams. In the latter case an X/R area in the complex impedance diagram is defined for a certain frequency range. The locus of the a.c. system impedance for varying system conditions and at different harmonic frequencies is defined to be within the envelope of these areas. Envelope diagrams permit a systematic search for the worst-case impedance.

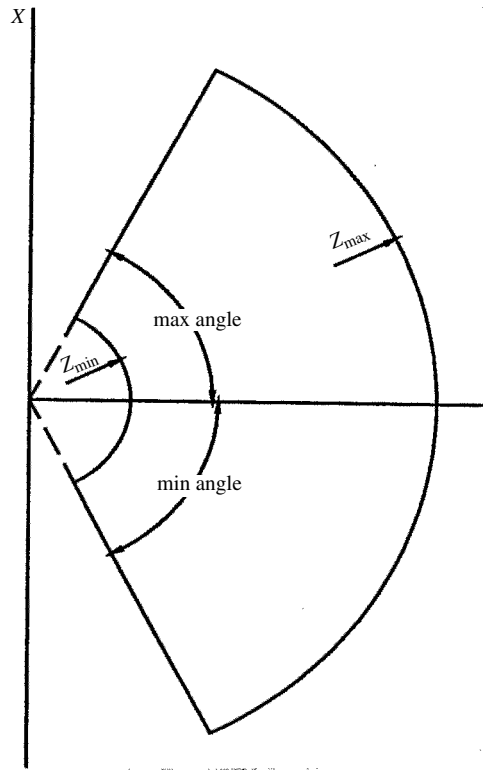


Figure 6.6 A.c. system impedance general sector diagram. CIGRE © copyright

Sector Diagrams The sector diagram restricts the area encompassing the loci of a particular harmonic impedance to a circular sector limited by maximum and minimum radii and angles, as shown in Figure 6.6. As the lower limit of the impedance, either the minimum impedance or the minimum resistance is given.

This diagram is very simple to define when little information about the network is available. The disadvantages of this representation are:

- Where the maximum R in a harmonic range is set by a system parallel resonance, this will define the maximum Z, and will produce corresponding reactance limits which often exceed their actual value.
- The maximum and minimum angles will normally be lower than those in the diagram for the higher reactance values.
- The relationship between the minimum limits of Z and R is unlikely to correspond to reality and yet it is an important factor in filter design.

Circle Diagram As Figure 6.7 illustrates, in this representation the locus of the system impedances is a circle with a radius selected to encompass the maximum impedance to be considered. In addition to the radius, the maximum and minimum angle and minimum resistance should be specified.

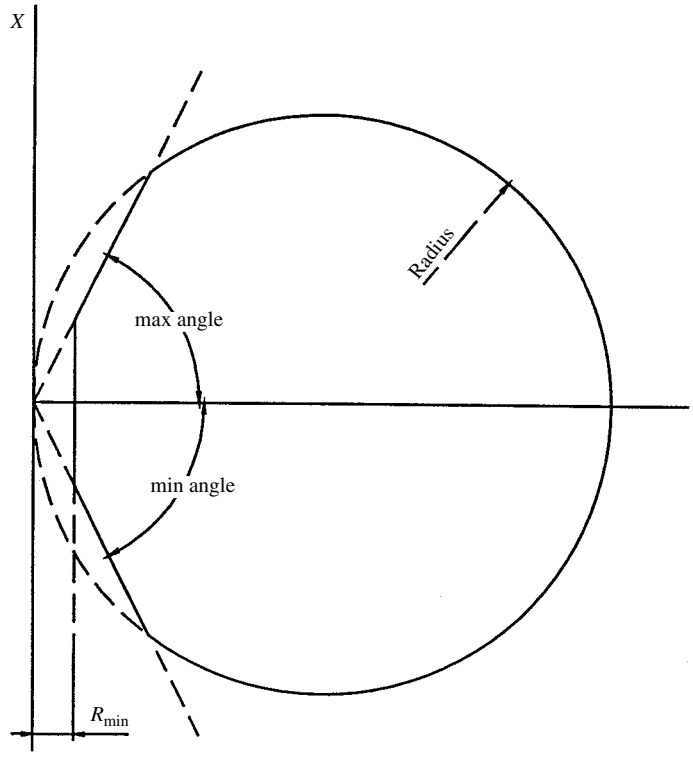


Figure 6.7 A.c. system impedance general circle diagram, with minimum resistance. CIGRE © copyright

This diagram provides a better fitting envelope for the real values than the sector diagram and a more realistic approximation for the characteristic harmonics. However, the radius is determined by the largest value of the impedance range, generally fixed by a parallel resonance which may apply over a more limited frequency range than that of the complete diagram (or there may be a set of resonances at different frequencies for different system conditions). Hence this approach could result in the inclusion of an even larger non-applicable area than the sector diagram, particularly in the capacitive reactance sector for the lower harmonic range.

Discrete Polygons For a more accurate representation of the network impedance, it is necessary to use different diagrams for different frequency ranges, as the system impedance is frequency dependent. In this way relatively limited impedance sectors can be defined for each harmonic, thus permitting a more exact matching of the a.c. filter design to the actual network conditions. This solution avoids filter over-designs of the low-order and 11th and 13th characteristic harmonics.

Care should be taken in specifying impedances for the low-order harmonics, particularly the second, third and fifth. If the values specified are too large the calculations may lead to filters tuned at these frequencies. Thus, it may be advisable to specify separate diagrams for these frequencies.

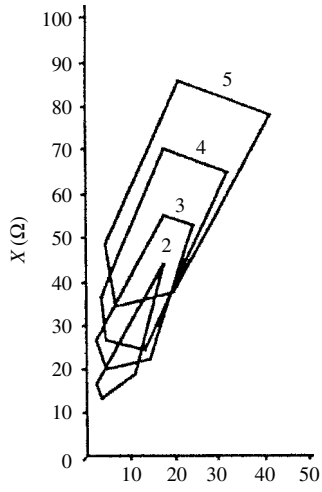


Figure 6.8 Discrete polygons for the 2nd to 5th harmonic impedances

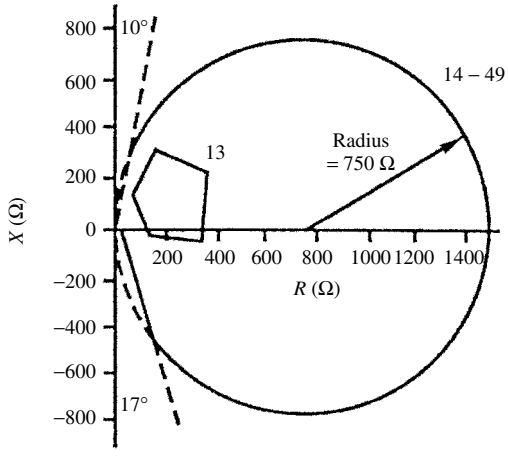


Figure 6.9 Harmonic impedance loci for the 13th and envelope of harmonic impedance loci for orders 14 to 49. Reproduced by permission of CIGRE

Figure 6.8 shows these polygons for the harmonic orders 2 to 5. In practice the polygons encompassing the impedances at high frequencies become rather large and it is more practical to use a circle diagram for these frequencies without introducing too much pessimism in the filter designs. A combination of polygons (up to the 13th harmonic) and circle diagram for the orders higher than the 13th is illustrated in Figure 6.9.

6.5 Tuned Filters

A single tuned filter is a series *RLC* circuit (as shown in Figure 6.1) tuned to the frequency of one harmonic (generally a lower characteristic harmonic). Its impedance

is given by

$$Z_1 = R + j\left(\omega L - \frac{1}{\omega C}\right) \tag{6.5}$$

which at the resonant frequency (f_n) reduces to R. There are two basic design parameters to be considered prior to the selection of R, L and C. These are the quality factor (Q), and the relative frequency deviation (δ), already defined.

In order to express the filter impedance in terms of Q and δ, the following relationships apply:

$$\omega = \omega_n(1 + \delta) \tag{6.6}$$

where

$$\omega_n = \frac{1}{\sqrt{LC}} \tag{6.7}$$

The reactance of inductor or capacitor in ohms at the tuned frequency is

$$X_0 = \omega_n L = \frac{1}{\omega_n C} = \sqrt{\frac{L}{C}} \tag{6.8}$$

$$Q = \frac{X_0}{R} \tag{6.9}$$

$$C = \frac{1}{\omega_n X_0} = \frac{1}{\omega_n R Q} \tag{6.10}$$

$$L = \frac{X_0}{\omega_n} = \frac{RQ}{\omega_n} \tag{6.11}$$

Substituting equations (6.6), (6.10) and (6.11) in equation (6.5) yields

$$Z_f = R\left(1 + jQ\delta\left(\frac{2+\delta}{1+\delta}\right)\right) \tag{6.12}$$

or, considering that δ is relatively small as compared with unity,

$$Z_f \approx R(1 + j2\delta Q) = X_0(Q^{-1} + j2\delta) \tag{6.13}$$

and

$$|Z_f| \approx R(1 + 4\delta^2 Q^2)^{1/2} \tag{6.14}$$

It is generally more convenient to deal with admittances rather than impedances in filter design, i.e.

$$Y_f \approx \frac{1}{R(1 + j2\delta Q)} = G_f + jB_f \tag{6.15}$$

where

$$G_f = \frac{Q}{X_0(1 + 4\delta^2 Q^2)} \tag{6.16}$$

$$B_f = -\frac{2\delta Q^2}{X(1 + 4\delta^2 Q^2)} \tag{6.17}$$

The harmonic voltage at the filter busbar is

$$V_n = \frac{I_n}{Y_{nf} + Y_{sn}} = \frac{I_n}{Y_n} \tag{6.18}$$

and therefore to minimise the voltage distortion it is necessary to increase the overall admittance of the filter in parallel with the a.c. system.

For a prediction of the largest V_n, the variables that are not accurately known have to be chosen pessimistically; these are the frequency deviation δ and the network admittance Y_{sn}. Since the harmonic voltage increases with δ, the largest expected deviation δ_m must be used in the analysis. Again, the worst realistic system condition (the lowest admittance) must be represented.

With certain limits the designer can decide on the values of Q and filter size (VA rating at the fundamental frequency).

In terms of Q and δ, equation (6.18) can be written as follows:

$$|V_n| = I_n \left\{ \left[G_{sn} + \frac{1}{R(1 + 4Q^2\delta^2)} \right]^2 + \left[B_{sn} - \frac{2Q\delta}{R(1 + 4Q^2\delta^2)} \right]^2 \right\}^{-1/2} \tag{6.19}$$

The case of a purely inductive a.c. network admittance, often used in filter design, is unduly pessimistic.

The impedance loci indicate that generally the harmonic impedances can be circumscribed in a region of R, jX determined by two straight lines and a circle passing through the origin (see Figure 6.7). The maximum phase angle of the network impedance can thus be limited to below 90° and generally decreases with increasing frequency (except in cable networks for high harmonic orders). The highest harmonic voltage is then obtained by using ϕ_{sn} with a sign opposite to that of δ.

Then equation (6.19) becomes

$$|V_n| = I_n\{(|Y_{sn}| \cos \phi_{sn} + G_f)^2 + (-|Y_{sn}| \sin \phi_{sn} + B_f)^2\}^{-1/2} \tag{6.20}$$

taking ϕ_{sn} positive and δ negative.

If $|Y_{sn}|$ is left unrestricted, the admittance giving maximum $|V_n|$ is

$$|Y_{sn}| = \frac{\cos \phi_{sn}(2Q\delta \tan \phi_{sn} - 1)}{R(1 + 4Q^2\delta^2)} \tag{6.21}$$

giving

$$|V_n| = I_n \omega_n L \left[\frac{1 + 4Q^2\delta^2}{Q(\sin \phi_{sn} + 2Q\delta \cos \phi_{sn})} \right] \tag{6.22}$$

There is an optimum Q which results in the lowest harmonic voltage, i.e.

$$Q = \frac{1 + \cos \phi_{sn}}{2\delta \sin \phi_{sn}} \tag{6.23}$$

for which

$$|V_n| = I_n \delta \omega_n L \left[\frac{4}{(1 + \cos \phi_{sn})} \right] = \frac{2 I_n R}{\sin \phi_{sn}} \tag{6.24}$$

Nevertheless, it should be noted that filters are not usually designed to give minimum harmonic voltage under these conditions. Normally a higher Q is selected in order to reduce losses.

A condition that also has to be considered in the design of filters, and which can restrict the operation of the converters, is an outage of one or more filter branches. The remaining filter branches may then be over-stressed as they have to take the total harmonic current generated by the converter.

6.5.1 Graphic Approach

A graphic explanation is given by Kimbark [3] which helps to understand the selection of optimum Q, i.e. the value that maximises Y_n.

For a given maximum value of the frequency deviation factor δ_m, and using a fixed reactance X_0 and variable resistance R, the locus of the filter admittance, i.e.

$$Y_f = \frac{1}{R(1 + j2\delta Q)}$$

is a semicircle of diameter $1/(2\delta_m X_0)$ tangent to the G-axis at the origin, as shown by the dashed line in Figure 6.10. The same figure displays (shaded area) the system

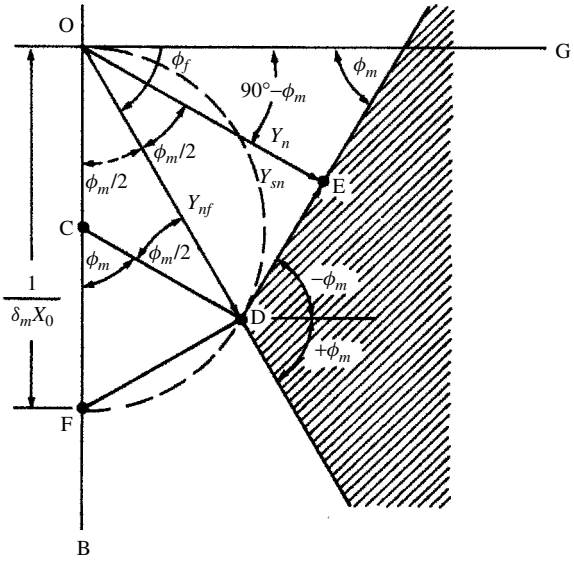


Figure 6.10 Construction for finding optimum Q and worst network admittance Y_{sn}, drawn for $\phi_m = 60°$. From [3]. Copyright 1971, John Wiley and Sons, Inc

admittance domain (Y_{sn}), obtained by inverting the impedance locus, and the minimum admittance for each frequency lies on the boundary of the shaded area.

For a given Y_{nf}, the shortest vector Y_n is perpendicular to and ends on the boundary. The vector diagram of Figure 6.10 drawn for a positive δ_m and negative $\phi = \phi_m$ produces the highest harmonic voltage. Moreover, the optimum value of Y_{nf} is that which terminates on the semicircle at a point where the boundary at angle $+\phi_m$ is the tangent to the semicircle. This optimum case is illustrated in Figure 6.10, where at point D, Y_{nf} maximises V_n and Y_{sn} minimises it.

For such conditions the filter admittance can be shown to be

$$|Y_{nf}| = \frac{\cos(\phi_m/2)}{2\delta_m X_0} \tag{6.25}$$

and

$$|Y_n| = |Y_{nf}|\cos(\phi_m/2) = \frac{1+\cos\phi_m}{4\delta_m X_0} \tag{6.26}$$

The quality factor of the chosen Y_{nf} is

$$Q = \frac{X_0}{R} = \frac{X_0}{X_f/(\tan\phi_f)} \tag{6.27}$$

but (from equation (6.13)

$$X_f = 2\delta_m X_0 \tag{6.28}$$

and (from Figure 6.10)

$$\tan\phi_f = \cot(\phi_m/2) \tag{6.29}$$

Therefore

$$Q = \frac{\cot(\phi_m/2)}{2\delta_m} = \frac{\cos\phi_m + 1}{2\delta_m \sin\phi_m} \tag{6.30}$$

After the individually tuned filter Qs values have been determined, the entire filter configuration must be used to determine the network admittance Y_n that yields the minimum total admittance Y at each harmonic frequency.

In practice, the minimal possible system admittances are also limited by a minimum conductance, thus resulting in the admittance domain shown shaded in Figure 6.11.

At any harmonic frequency the equivalent admittance of the filter configuration consists of a vector that ends at point O and starts in one of three regions of the admittance plane as shown in Figure 6.11.

At frequencies for which tuned filters are provided, the origin of the filter admittance is likely to lie in region 3, i.e. the total filter admittance is relatively large. At other frequencies, however, the filter admittance origin may lie in region 1 or 2.

The most pessimistic values of the network admittance are those which result in the lowest total admittance. These are clearly defined in the graph: (i) in region 1 the resultant admittance vector Y_n ends on the vertical (i.e. minimum conductance) part of the boundary; (ii) in region 2, Y_n ends on the corner of the boundary; and (iii) in region 3, Y_n is perpendicular to the nearer angular limit.

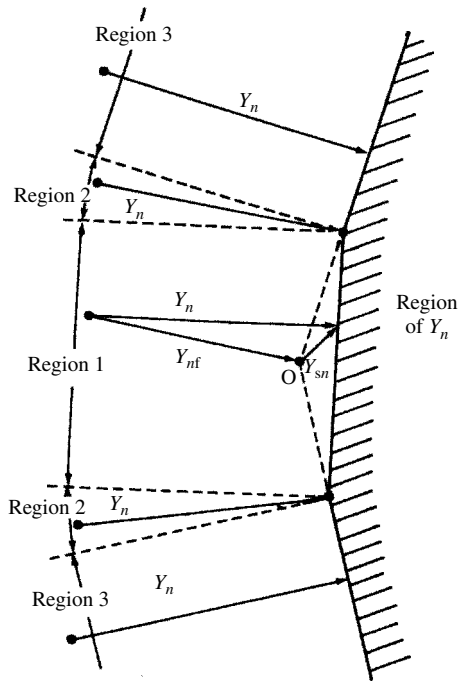


Figure 6.11 Determination of network admittance Y_{sn}, for minimum resultant admittance Y_n corresponding to filter admittances Y_f lying in different regions. From [3]. Copyright 1971, John Wiley & Sons, Inc

6.5.2 Double-Tuned Filters [4]

The equivalent impedances of two single-tuned filters (Figure 6.12(a)) near their resonance frequencies are practically the same as those of a double-tuned filter configuration, illustrated in Figure 6.12(b), subject to the following relationships between their components

$$C_1 = C_a + C_b \tag{6.31}$$

$$C_2 = \frac{C_a C_b (C_a + C_b)(L_a + L_b)^2}{(L_a C_a - L_b C_b)^2} \tag{6.32}$$

$$L_1 = \frac{L_a L_b}{L_a + L_b} \tag{6.33}$$

$$L_2 = \frac{(L_a C_a - L_b C_b)^2}{(C_a + C_b)^2 (L_a + L_b)} \tag{6.34}$$

$$R_2 = R_a \left[\frac{a^2 (1 - x^2)}{(1 + ax^2)^2 (1 + x^2)} \right] + R_b \left[\frac{1 - x^2}{(1 + ax^2)^2 (1 + x^2)} \right] + R_1 \left[\frac{(1 - x^2)(1 - ax^2)}{(1 + x^2)(1 + ax^2)} \right] \tag{6.35}$$

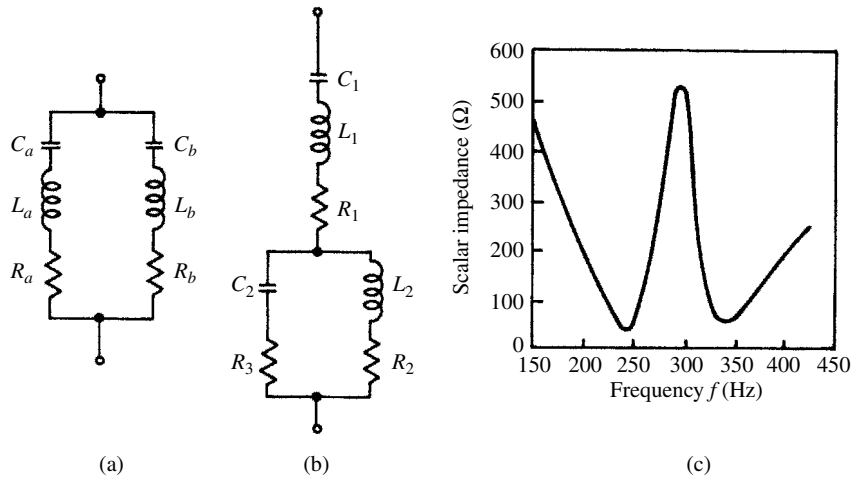


Figure 6.12 Transformation from (a) two single-tuned filters to (b) double-tuned filters. (c) The impedance versus frequency of filter double-tuned for 5th and 7th

where

$$a = \frac{C_a}{C_b} \text{ and } x = \sqrt{\frac{L_b C_b}{L_a C_a}}$$

The above practical approximation is carried out by omitting resistor R_1, which is therefore determined by the minimum resistances of the inductor L_1. This has the advantage of reducing the power loss at fundamental frequency as compared with the single-tuned filter configurations. The main advantage of the double-tuned filter is in high-voltage applications, because of the reduction in the number of inductors to be subjected to full line impulse voltages. Typical equivalent impedances of a double-tuned filter are illustrated in Figure 6.12.

A common design of double-tuned filter configurations is that of the Vindhyachal HVd.c. converter plant [1], shown in Figure 6.13. The scheme consists of three sets of double-tuned filters for 11/13, 3/27 and 5/24 harmonic orders. A filter for the third harmonic is needed to eliminate resonances with the a.c. network and the fifth harmonic filter is required to limit the individual harmonic distortion.

Triple- and quadruple-tuned filters can also be designed but these are rarely justified because of the difficulty of adjustment.

6.5.3 Automatically Tuned Filters

In tuned filter design it is advantageous to reduce the maximum frequency deviation. This can be achieved by making the filters tunable by either automatically switching the capacitance or by varying the inductance. A range of $\pm 5\%$ is usually considered adequate. A control system, which measures the harmonic frequency reactive power in the filter (both its sign and magnitude) and uses the information to alter the value of

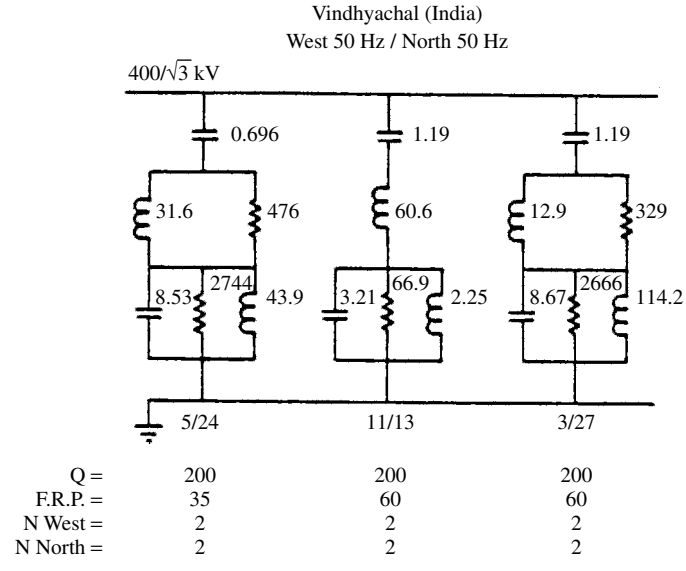


Figure 6.13 Filter configuration of the Vindhyachal HVd.c. scheme. CIGRE © copyright

the L or the C, has been used in HVd.c. converter filters. Automatically tuned filters offer the following advantages over fixed filters:

(1) The capacitor rating is lower.

(2) The capacitor used can combine a high temperature coefficient of capacitance and a high reactive power rating per unit of volume and per unit of cost.

(3) Because of the higher Q, the power loss is smaller.

Advantages (1) and (2) reduce the cost of the capacitor, which is the most expensive component of the filter. Advantage (3) reduces the cost of the resistor and the cost of the system losses.

6.6 Damped Filters

The damped filter offers several advantages:

(1) Its performance and loading are less sensitive to temperature variation, frequency deviation, component manufacturing tolerances, loss of capacitor elements, etc.

(2) It provides a low impedance for a wide spectrum of harmonics without the need for subdivision of parallel branches, which increases switching and maintenance problems.

(3) The use of tuned filters often results in parallel resonance between the filter and system admittances at a harmonic order below the lower tuned filter frequency, or in between tuned filter frequencies. In such cases the use of one or more damped filters is a more acceptable alternative.

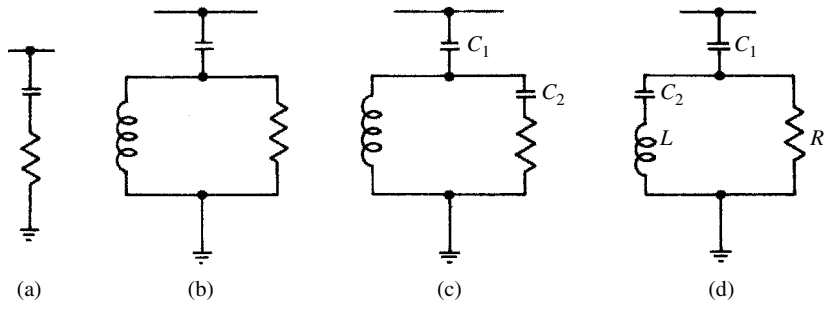


Figure 6.14 High-pass damped filters: (a) first order; (b) second order; (c) third order; (d) C-type

The main disadvantages of the damped filter are as follows:

(4) To achieve a similar level of filtering performance the damped filter needs to be designed for higher fundamental VA ratings, though in most cases a good performance can be met within the limits required for power factor correction.

(5) The losses in the resistor and reactor are generally higher.

6.6.1 Types of Damped Filters

Four types of damped filters are shown in Figure 6.14, first-order, second-order, third-order and C-type.

(1) The first-order filter is not normally used, as it requires a large capacitor and has excessive loss at the fundamental frequency.

(2) The second-order type provides the best filtering performance, but has higher fundamental frequency losses as compared with the third-order filters.

(3) The main advantage of the third-order type over the second-order type is a substantial loss reduction at the fundamental frequency, owing to the increased impedance at that frequency caused by the presence of the capacitor C_2. Moreover, the rating of C_2 is very small compared with C_1.

(4) The filtering performance of the C-type [5] filter lies in between those of the second- and third-order types. Its main advantage is a considerable reduction in fundamental frequency loss, since C_2 and L are series tuned at that frequency. However, this filter is more susceptible to fundamental frequency deviations and component value drifts.

6.6.2 Design of Damped Filters

When designing a damped filter the Q is chosen to give the best characteristic over the required frequency band and there is no optimal Q as with tuned filters.

The behaviour of damped filters has been described by Ainsworth [4] with the help of two parameters

$$f_0 = \frac{1}{2\pi CR} \tag{6.36}$$

$$m = \frac{L}{R^2 C} \tag{6.37}$$

Typical values of m are between 0.5 and 2. For a given capacitance these parameters (and hence L and R) are decided to achieve an appropriately high admittance over the required frequency range.

The conductance and susceptance terms of a second-order damped filter admittance are

$$G_f = \frac{m^2 x^4}{R_1[(1 - mx^2)^2 + m^2 x^2]} \tag{6.38}$$

$$B_f = \frac{x}{R_1}\left[\frac{1 - mx^2 + m^2 x^2}{(1 - mx^2)^2 + m^2 x^2}\right] \tag{6.39}$$

where $x = f/f_0$.

The minimum total admittance (i.e. the filter Y_F plus the a.c. system Y_{sn}) can be shown to be

$$Y = B_f \cos\phi_m + G_f \sin\phi_m \tag{6.40}$$

with both terms in equation (6.40) being positive and x being less than the value that gives

$$|\cot\phi_f| = |G_f/B_f| = |\tan\phi_m| \tag{6.41}$$

For greater values of x the minimum total admittance is that of the filter (i.e. with $Y_{sn} = 0$).

Figure 6.15 illustrates typical minimal admittances for a second-order damped filter in parallel with a lossless system (i.e. $\phi_m = \pm 90^\circ$). For comparison the conductance component G_f of a third-order damped filter, for the case of equal capacitors, is shown in Figure 6.16. These figures show that the third-order filter peaks are much sharper than those of the second order.

6.7 Conventional Filter Configurations

6.7.1 Six-Pulse Design

Static converters of large ratings are normally designed for at least 12-pulse operation. In many schemes, however, to cope with maintenance and other partial temporary outages, six-pulse operation is permitted. Under such conditions they produce considerable 5th and 7th harmonics as well as the characteristic 12-pulse-related orders. These are conventionally filtered by using a hybrid combination of tuned branches for the low

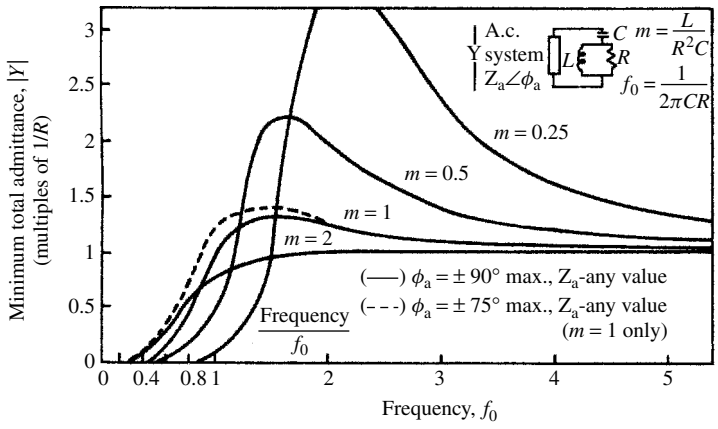


Figure 6.15 Admittance of second-order low-pass filter

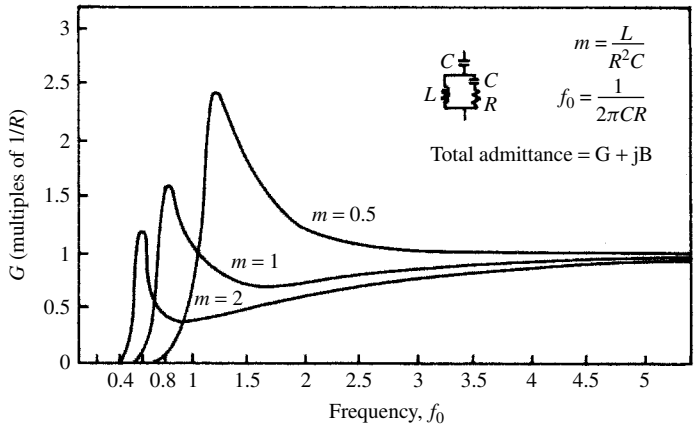


Figure 6.16 Conductance component for third-order low-pass filter

orders, i.e. 5th, 7th, 11th and 13th, and a high-pass damped filter for the 17th and higher orders.

The conventional design is best illustrated with some examples.

(i) Strong a.c. System Connection [4] A six-pulse converter bridge is rated at 100 kV, 100 MW d.c., operating at $\alpha = 15°$. The bridge is connected to a 275 kV, 50 Hz a.c. system via a 275/83 kV converter transformer with 15% leakage reactance. The secondary fundamental current is 780 A and that of the primary 236 A. The filters, to be connected to the primary side, consist of resonant arms for the 5th, 7th, 11th and 13th harmonics, and a second-order high-pass arm.

For a total filter size of 50 MVAr, and assuming that the capacitance is to be equally divided among the filter branches, each branch requires 0.421 μF. If the capacitor temperature coefficient is 0.05% per degree Celsius, the inductor temperature coefficient 0.01% per degree Celsius, ambient temperature ±20°C and frequency tolerance ±1%,

then from equation (6.4),

$$\delta = (1/100)[1 + 0.5(0.05 \times 20 + 0.01 \times 20)] = 0.016$$

Let the a.c. system impedance be of any magnitude but its phase angle restricted to $\phi_a < 75^\circ$ at any frequency. The optimum Q (giving the lowest harmonic voltage) is then obtained from equation (6.30), i.e.

$$Q = \frac{1 + \cos 75^\circ}{2(0.016) \sin 75^\circ} = 40.7.$$

With Q and C known, the values of L and R of the resonant arms can then be determined.

The damped arm components are found from equations (6.36) and (6.37) by choosing $m = 1$ and $f_0 = 17 \times 50 = 850$ Hz. Since C has been fixed above (i.e. 0.421 μF), the resulting values of inductor and resistor are 0.083 H and 444.9 Ω, respectively.

The complete circuit design is then as shown in Figure 6.17.

(ii) Weak a.c. System Connection Let us now consider the possible connection of the converter of the test system described above to a 110 kV instead of 275 kV network and assess whether the filters are effective at third harmonic. Let us further assume that the system third harmonic impedance may lie between 70 and 100 Ω, while the phase angle remains at 75°.

The total filter capacitance is now

$$C = \frac{\text{MVAr}}{(2\pi 50)(110)^2} = 13.15 \ \mu\text{F}$$

and that of the individual filter branches $C/5 = 2.631$ μF

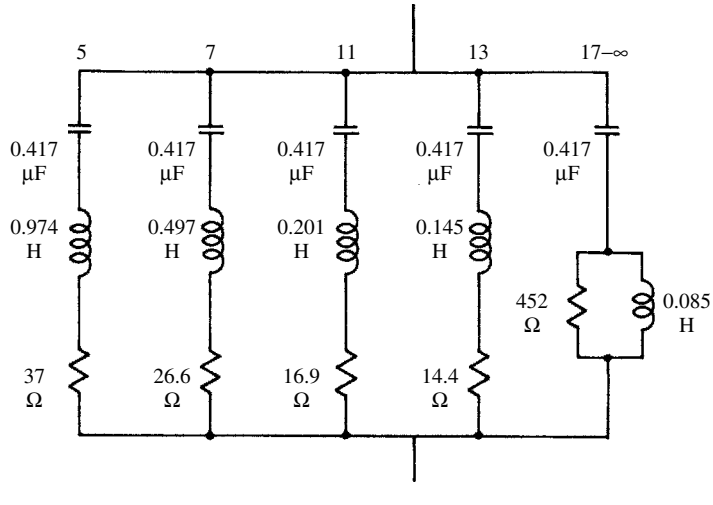


Figure 6.17 Example of a.c. filter design

Following the same reasoning as in case (i), equations (6.36) and (6.37) give the new values of the damped filter branch parameters, i.e.

$$R = 71.2\ \Omega \text{ and } L = 0.0133\ \text{H}$$

Similarly, equations (6.10) and (6.11) provide the following values for the remaining branches:

5th-tuned branch :	$R = 5.94\ \Omega$	$L = 0.1541$ H
7th-tuned branch :	$R = 4.24\ \Omega$	$L = 0.0786$ H
11th-tuned branch :	$R = 2.70\ \Omega$	$L = 0.0318$ H
13th-tuned branch :	$R = 2.29\ \Omega$	$L = 0.0228$ H

The filter branch impedances at the third harmonic are obtained by substituting $\omega_3 = 150$ Hz in the tuned and damped branch impedance equations. These are then inverted and added together to produce the total filter admittance, i.e.

$$Y_3^F = 0.00016 - j(0.01469)$$

The system harmonic impedance that yields the largest parallel impedance with the filter at 150 Hz has been found to be $Z_3 = 71\angle 75^\circ$, i.e.

$$Z_3^F = 71\ (\cos(75^\circ) - j\sin(75^\circ)) = 18.38 - j68.58$$

and

$$Y_3^F = 0.00365 - j0.01360$$

Thus, the parallel system and filter admittance is

$$Y_3^T = Y_3^F + Y_3^S = 0.00381 + j(0.00108)$$

The third harmonic voltage distortion is

$$V_3 = (I_3)/(Y_3^T)$$

where I_3 is the maximum expected level of injected third harmonic current. This is a difficult parameter to calculate, as it results from a number of different sources, among them the presence of some background third harmonic in the supply voltage, the presence of negative sequence, some unbalance in the commutation reactance and firing angle unbalance. Unbalance in the commutation reactances is the most likely cause of third harmonic generation, which can be typically up to 0.7% of the fundamental current (as shown in Table 3.7).

The fundamental frequency current for the 275 kV connection is 236 A and assuming that the new current is inversely proportional to the voltage, the 110 kV current will be

$$I_1 = 236 \times (275)/(110) = 588.5\ \text{A}$$

Therefore

$$I_3 = (0.7 \times I_1)/100 = 4.12 \text{ A}$$

and

$$V_3 = 4.12/(\sqrt{0.00381^2 + 0.00108^2}) = 1040.61 \text{ V or } 1.64\%$$

Although this value is within the 2% limit of the IEC standard (61000-3-6), it is very close to it, considering that only one of the possible third harmonic sources has been included in the calculation. A reduction of the filter capacity is introduced in the following case to further illustrate the problem.

(iii) Reduced Filter Capacitance Case (ii) is now repeated with a total filter capacity of 40 instead of 50 MVAr, with the capacitance still equally divided between the various filter branches.

At 110 kV the total capacitance required to supply 40 MVAr is 10.523 μF, or 2.105 μF per filter branch. Following the same process as for case (ii), the following values of R and L are obtained:

5th-tuned branch	$R = 7.428\ \Omega$	$L = 0.1926$ H
7th-tuned branch	$R = 5.306\ \Omega$	$L = 0.0983$ H
11th-tuned branch	$R = 3.376\ \Omega$	$L = 0.0398$ H
13th-tuned branch	$R = 2.857\ \Omega$	$L = 0.0285$ H

The new damped filter branch parameters are:

$$R = 88.97\ \Omega \text{ and } L = 0.0167 \text{ H}$$

The corresponding total filter admittance at 150 Hz is:

$$Y_3^F = 0.000131 + j(0.011748)$$

The third harmonic impedance for the system under consideration will typically lie within a sector limited by 70 Ω and 100 Ω radii and 75° and 80° phase angle. Within this range the impedance which in parallel with the filters produces the largest impedance value has been found to be $Z_3^S = 87\angle 80^\circ = 15.1074 + j85.6783$.

The corresponding system admittance is thus

$$Y_3^S = 0.0020 - j(0.01132)$$

The combined system/filter admittance becomes:

$$Y_3^T = Y_3^F + Y_3^S = 0.00213 + j(0.00043)$$

The uncorrected (i.e. before the filters) power factor of the converter load is approximately

$$\cos\phi = (1/2)(\cos\alpha + \cos(\alpha + \mu))$$

where $\cos(\alpha + \mu)$ is derived from the commutation equation (3.37) using the information of the test system (case (i) above), i.e. $V_1 = 83$ kV, $I_{dc} = 1000$ A, $\alpha = 15$ and $X = 15\%$; the resulting value of $\cos\phi$ is 0.878.

When corrected by the addition of the filters (40 MVAr), the power factor becomes 0.990 and the primary side fundamental current is:

$$I_1 = 1000\frac{\sqrt{6}}{\pi}\left(\frac{83}{110}\right) = 588.5 \text{ A}$$

Again, using the firing unbalance criterion of Table 3.7, the third harmonic current injection will be

$$I_3 = 588.5(0.7)/(100) = 4.12 \text{ A}$$

and

$$V_3 = \frac{4.12}{\sqrt{0.00213^2 + 0.00043^2}} = 1896.0022 \text{ V}$$

or

$$\frac{1896.0022}{(110/\sqrt{3}) \times 10^3} \times 100 = 2.99\%$$

which is well above the limit recommended by the IEC.

6.7.2 Twelve-Pulse Configuration

Whenever a reasonable twelve-pulse operation can be guaranteed under all operating conditions the fifth and seventh harmonic filters can be eliminated. An example of the configuration used in a high-voltage d.c. converter and its corresponding impedance locus are shown in Figure 6.18. The locus exhibits resonant points at the 11th, 13th and 27th harmonics, and reasonably low impedances to the fifth and seventh, which will cope with the levels expected under slight unbalanced power distribution between the individual bridges.

6.8 Band-Pass Filtering for Twelve-Pulse Converters

The conventional filter design for static converters, based on the use of separate tuned filters of the resonant type for the 11th and 13th harmonics and a high-pass filter for the higher orders, will usually provide a more effective reduction than required. This is because the minimum size of the filters is usually determined by the available economic size of the capacitor units and the minimum amount of reactive power generation required by the converters.

Therefore the filter design can be simplified, either by replacing the 11th and 13th tuned filters by a single filter of the damped type, or replacing all filters by a single damped filter. In the first case, the damped filter replacing the two tuned filters should be tuned to about the 12th harmonic and a fairly high Q can be selected (20–50),

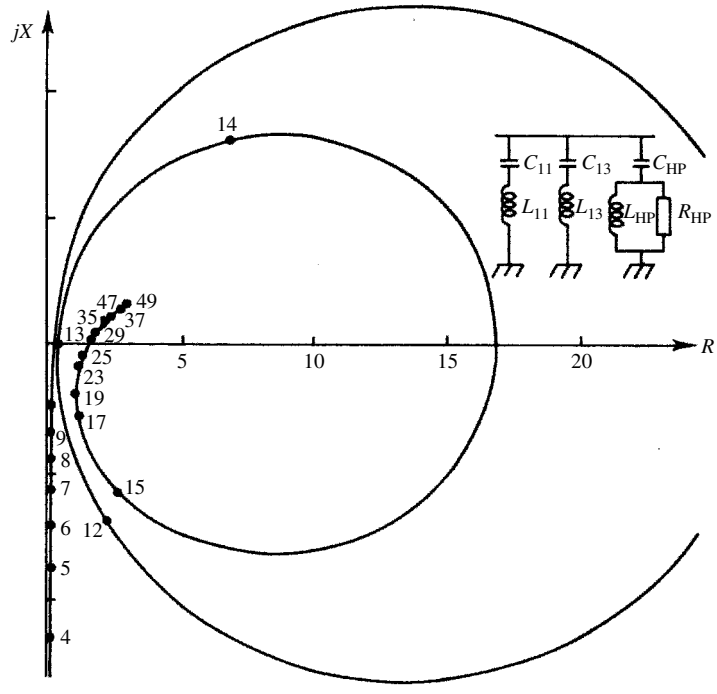


Figure 6.18 Filter configuration for 12-pulse operation and typical impedance locus

while the damped filter for the higher harmonics has a much smaller Q (2–4). In the second case, the single damped filter is also tuned to about the 12th harmonic but at a fairly low Q (2–6) to get a sufficiently low impedance at high harmonics.

Moreover, the hybrid design discussed in the last section (Figure 6.18) exhibits increasing impedance at the lower harmonic frequencies.

With the large ratings of some HVd.c. projects there is an increased probability of low-order non-characteristic harmonic resonance between the system impedance and the filter capacitance. This condition is more likely when the network includes cables or long a.c. overhead lines which provide substantial capacitive generation. The damping of a network tends to increase with increasing frequency; for low-order harmonics the limiting impedance angle can be high and severe resonances can occur. Moreover, in order to control the voltage profile of the a.c. network the tendency is to compensate totally, by local means, the reactive power absorbed by the converters. The high capacity of the filters or shunt capacitor banks decreases the resonant frequency with the network. A parallel resonance can amplify considerably several harmonics at different times, i.e. the critical frequency varies as a function of the a.c. system and of the configuration and number of capacitors in operation; in general, therefore, remedies can not be adopted only for one specific harmonic, but must avoid unacceptable amplification for a number of frequencies.

A very common condition resulting from system unbalance is the production of a significant third harmonic current by the converter (as explained in Section 3.6.9); this third harmonic is of positive sequence and will not be blocked by the transformer connection.

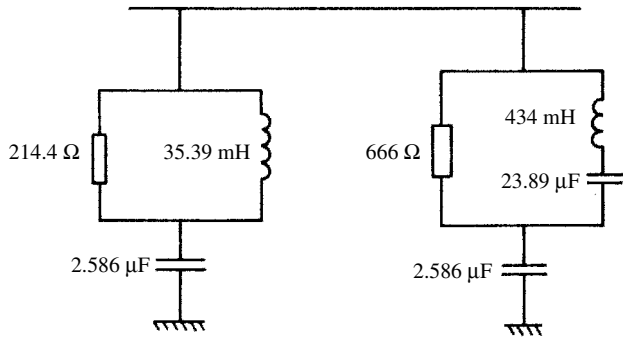


Figure 6.19 Combined second-order and C-type damped filters

An alternative filter design consisting of a C-type and a second-order damped filter (shown in Figure 6.19) can be used to eliminate the low-order resonance [5].

It is unduly pessimistic to consider the possibility of a number of harmonics in near resonance simultaneously. In the filter design of the 2000 MW cross-channel HVd.c. link the following combination of system impedances has been used:

(1) The harmonic order that produces the highest voltage distortion is assumed to be at or near resonance with the system.

(2) Other harmonics in the range 2–25 are selected from tables containing information about the system impedances under all likely system and planned outage conditions.

(3) The remaining harmonics in the range 25–49 are assumed to lie within a wide radius of 750 Ω, centred at $R = 750$ Ω, limited by impedance angles of 73° (capacitive) and 85° (inductive).

The filter configuration for this scheme (at the Sellindge end) is shown in Figure 6.20.

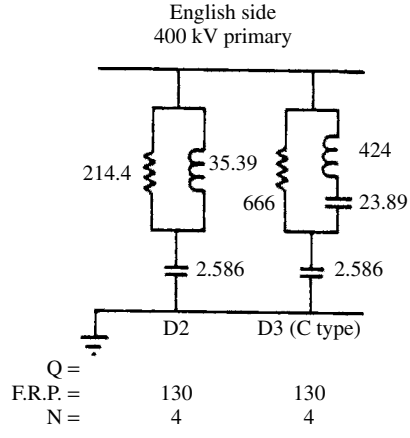


Figure 6.20 Filter configuration of the cross-channel scheme. CIGRE © copyright

Table 6.1 Derivation of the maximum r.m.s. distortion for the filter configuration of four second-order plus four C-type filters at 2000 MW d.c. load

Harmonic order	2	3	5	7	11
Pre-existing distortion on the a.c. system (%)	0.39	0.34	0.22	0.12	0.01
Distortion due to converter harmonic current (%)	0.13	0.42	0.56	0.29	0.43
Distortion from converter third harmonic current due to negative sequence on the a.c. system (%)	–	0.19	–	–	–
Distortion due to VAR compensator harmonic current (%)	–	0.03	0.03	0.02	0.01
Distortion due to compensator third harmonic current due to a.c. system unbalance (%)	–	0.17	–	–	–
Total contribution due to each harmonic (%)	0.41	1.16	0.60	0.31	0.43

Four of the 130 MVAr filter banks are second-order high-pass filters to absorb the characteristic harmonic currents. Large magnification factors for several system conditions are possible, particularly at the third harmonic, and therefore the remaining four filter banks are arranged as third-order C-type damped filters and have their minimum impedance at around 150 Hz.

The predicted performance characteristics are illustrated in Table 6.1. Since in this case the highest distortion is caused by the third harmonic, this harmonic is taken as the arithmetic sum of the contents produced by the various sources listed.

6.9 Distribution System Filter Planning [6]

The increasing levels of voltage distortion in some distribution systems can best be contained by the application of harmonic filters at strategic locations. In this respect, radial distribution systems have special characteristics that make filter planning and design different to those of industrial system plant. Among these are the differing X/R ratios and larger electrical distances, a wider variation in load with limited information on load characteristics, the use of capacitors for voltage control and power factor correction and the dispersed nature of the harmonic injections.

Dispersed distribution loads generate smaller currents at the higher harmonics and the phase angles of these currents are widely distributed [7, 8], resulting in a high degree of cancellation. At the lower frequencies, particularly the third, fifth and seventh harmonics, there is less cancellation and the resulting harmonic currents are higher.

Radial distribution systems with primary capacitor banks generally have resonances in the vicinity of the fifth and seventh harmonic frequencies involving the entire group of distributed capacitors. These resonances are much broader than the higher frequency resonances, which involve only one or two capacitor banks.

The trend in distribution planning is to consider simultaneously the optimised use of capacitances for the fundamental and harmonic frequencies. Although this can be

achieved very effectively by genetic algorithms, this solution is extremely demanding in computational requirements. Thus, generally, the locations and sizes of the reactive compensation in distribution systems are made on fundamental frequency considerations. Then the choice of capacitor banks to be tuned for filtering purposes is carried out based on harmonic flow considerations. Such tuning is first made to reduce the fifth harmonic content.

The effect of fifth harmonic tuning on the seventh harmonic voltage varies depending on the system configuration. In general, replacing a capacitor bank with a fifth harmonic filter tends to shift the resonance points above the fifth harmonic to a higher frequency, and the resulting voltages at the seventh harmonic will depend on the location and strength of these resonances.

On systems where a fifth harmonic filter also reduces the seventh harmonic voltage near the filter location, a choice exists as to the frequency of additional filters. Any further filtering investigation should include a comparison of both fifth and seventh harmonic filters, as the best choice is not necessarily at one or the other frequency.

On systems where a fifth harmonic filter increases the seventh harmonic voltages the frequencies must be treated separately. While additional filters at one frequency may raise voltage at the other, this is generally a second-order effect and the filter placement can be done independently.

6.10 Filter Component Properties

From knowledge of the fundamental and harmonic voltages at the relevant busbars the current and voltage ratings of the capacitors, inductors and resistors can be calculated, and with them the active and reactive powers and losses.

To prevent damage of these components their ratings must be based on the most severe conditions expected. These should include the highest fundamental voltage, the highest effective frequency deviation, and the harmonic currents from other sources and from possible resonances between the filter and a.c. system.

6.10.1 Capacitors

Capacitors are composed of standard units connected in series and/or parallel in order to achieve the desired overall voltage and kVA rating. The main factors involved in their design are [9]: temperature coefficient of capacitance, reactive power per unit volume, power loss, reliability and cost.

A very low temperature coefficient of capacitance is desirable for tuned filters in order to avoid detuning caused by change of capacitance with ambient temperature or with capacitor self-heating; this property, however, is unimportant for damped filters or power capacitors.

Capacitors obtain their high reactive power per unit volume by having low losses and by operating at very high voltage stresses. For this reason, prolonged operation at moderate over-voltage must be avoided to prevent thermal destruction of the dielectric; at higher over-voltages even brief periods of operation can produce destructive ionisation of the dielectrics.

The required reactive power rating of the capacitor is the sum of the reactive powers at each of the frequencies to which it is subjected.

6.10.2 Inductors

Inductors used in filter circuits need to be designed bearing in mind the high frequencies involved, i.e. skin effect and hysteresis losses must be included in the power loss calculation. Also, the effect of the flux level in the iron, i.e. the detuning caused by magnetic nonlinearity, must therefore be taken into account. This normally leads to the use of low flux densities when using iron cores. Alternatively, filter inductors are better designed with non-magnetic cores.

The Q at the predominant harmonic frequency may be selected for lowest cost and is usually between 50 and 150. However, lower Q values are normally required and these are derived by using a series resistor.

Inductor ratings depend mainly on the maximum r.m.s. current and on the insulation level required to withstand switching surges. Normally the R and L form the ground side of a tuned filter.

6.11 Filter Costs

An effective filter adequately suppresses harmonics at the least cost and supplies some reactive power, but perhaps not all that is required. The cost of losses incurred in the filters may be charged to reactive power supply and some to filtering, although there is no logical basis for the division.

The following assumptions are usually made in the cost analysis of filter components:

(1) In a typical installation, a capacitor bank consists of a 'matrix' of capacitor units, each having a nominal rating at the prescribed operating voltage and protected by an external fuse.

The cost of a capacitor bank is thus approximately constant up to the rating of the minimum matrix containing full units. For higher ratings, one or more units are added to each series group as required and a reasonably accurate cost per MVAr or SIZE can be arrived at. The situation is complicated further by the availability of standard units with different nominal ratings, e.g. 50, 100, 150 kVAr etc., and the incremental cost varies for different bands of capacitor bank SIZES. Although such factors would have to be included in the development of an accurate cost equation, here we are assuming that the capacitors' cost is proportional to their ratings.

(2) Although the cost of filter inductors depends greatly on the method of construction (e.g. oil insulated/cooled units, natural air-cooled reactors of open construction, etc.), their cost does not vary greatly for units of different rating. The cost approximation used in the analysis, therefore, is of the form

$$\text{Inductor cost} = U_K + U_L \times (\text{total MVAr rating})$$

where U_K is a constant cost component and U_L is the inductor incremental cost per MVAr rating.

(3) The power rating of the resistor necessary for Q-adjustment in each filter branch will affect the cost to some extent. However, the nominal resistance of the unit is difficult to predict in a general analysis, because it depends on the natural Q factor of the inductor. For this reason, and also because the cost of an air-cooled resistor is small compared with that of the other components, a constant cost per resistor is allocated in the analysis. If an air-cooled unit is used, the cost would be more significant but it would, in fact become virtually independent of power rating.

(4) Finally, it is assumed that the resistance of the inductor, for the purposes of power loss estimation, is constant at all frequencies.

6.11.1 Single-Tuned Filter

In a high-Q circuit it may be assumed that

$$V_c = V_L + V_s \tag{6.42}$$

where V_c, V_L and V_s represent the capacitor, inductor and supply voltages, respectively.

The filter SIZE is expressed as

$$S = \frac{V_s^2}{X_c - X_L} \tag{6.43}$$

where X_c and X_L are the fundamental frequency reactances of the capacitor and inductor.

But for a filter tuned to harmonic n,

$$X_0 = nX_L = X_c/n$$

i.e.

$$X_L = X_c/n^2 \text{ and } V_L = V_c/n^2$$

Therefore

$$S = V_s^2/[X_c(1 - 1/n^2)] = (V_s^2/X_c)[n^2/(n^2 - 1)] \text{ MVAr} \tag{6.44}$$

Also

$$V_c - V_L = V_c(1 - 1/n^2) = V_s$$

i.e.

$$V_c = [n^2/(n^2 - 1)]V_s \text{ kV} \tag{6.45}$$

The loadings for each filter component are determined for cost evaluation as follows:

Capacitor

Fundamental loading:

$$V_c^2/X_c = (V_s^2/X_c)[n^2/(n^2-1)]^2$$
$$= S[n^2/(n^2-1)] \text{ MVAr} \tag{6.46}$$

Harmonic loading:

$$I_n^2(X_c/n) = [(I_n^2.V_s^2)/(S.n)][n^2/(n^2-1)] \quad \text{MVAr} \tag{6.47}$$

Power loss:

$$K_{CL} \cdot (\text{total loading}) = K_{CL}[S + (I_n^2 \cdot V_s^2)/(S \cdot n)][n^2/(n^2-1)] \quad \text{kW} \tag{6.48}$$

where K_{CL} is the loss factor of the capacitors (in kW/MVAr).

Inductor

Fundamental loading:

$$V_L^2/X_L = (V_c/n^2)^2 \cdot (n^2/X_c) = V_c^2/n^2X_c$$
$$= (S/n^2)[n^2/(n^2-1)] \quad \text{MVAr} \tag{6.49}$$

Harmonic loading is the same as for the capacitor since the reactances are equal at harmonic frequency.

For cost purposes, it is convenient to consider the losses in the total effective resistance R, where

$$R = X_0/Q = X_c/nQ$$

The fundamental current is

$$I_1 = S/V_s \text{ kA}$$

and the total power loss

$$(I_1^2 + I_n^2)R = (S^2/V_s^2)X_c/nQ + I_n^2X_c/nQ$$
$$= [S^2/nQ](1/S)[n^2/(n^2-1)] + [I_n^2V_s^2/nSQ][n^2/(n^2-1)]$$
$$= [S/nQ + I_n^2V_s^2/nSQ][n^2/(n^2-1)] \times 10^3 \text{ kW} \tag{6.50}$$

For comparison purposes, the cost of energy losses is expressed in terms of equivalent capital cost by use of a present value factor:

$$P_v = [(1+i)^N - 1]/[i(1+i)^N] \tag{6.51}$$

where i is the interest rate and N is the budgeted filter life.

Thus the present value cost of energy losses is

$$\begin{aligned} &P_v U_u F_u \times 365 \times 24 \times (\text{total power loss}) \\ &\quad = 8760 P_v U_u F_u \times (\text{total power loss}) \end{aligned} \tag{6.52}$$

where U_u is the cost of energy loss per kilowatt-hour and F_u is the filter utilisation factor. The complete expression for the total cost is

$$\begin{aligned} \text{TCOST} = U_T + [n^2/(n^2-1)] \Bigg\{ U_c \left(S + \frac{V_s^2 I_n^2}{nS} \right) + U_L \left(\frac{S}{n^2} + \frac{V_s^2 I_n^2}{nS} \right) \\ + 8760 P_v U_u F_u \left[K_{CL} \left(S + \frac{V_s^2 I_n^2}{nS} \right) + 10^3 \left(\frac{S}{nQ} + \frac{I_n^2 V_s^2}{nSQ} \right) \right] \Bigg\} \end{aligned}$$

i.e.

$$\text{TCOST} = U_T + AS + \frac{B}{S} \tag{6.53}$$

where U_T is the total constant cost of the filter branch, U_c is the capacitor incremental cost per MVAr, U_L is the inductor incremental cost per MVAr,

$$A = [n^2/(n^2-1)] \left[U_c + \frac{U_L}{n^2} + 8760 P_v U_u F_u \left(K_{CL} + \frac{10^3}{nQ} \right) \right] \tag{6.54}$$

and

$$B = [n^2/(n^2-1)][V_s^2 I_n^2/n] \left[U_c + U_L + 8760 P_v U_u F_u \left(K_{CL} + \frac{10^3}{Q} \right) \right] \tag{6.55}$$

As SIZE S is varied, the minimum total cost occurs when

$$\mathrm{d}(\text{TCOST})/\mathrm{d}S = 0$$

i.e. when

$$S_{\text{MIN}} = \sqrt{\frac{B}{A}} \quad \text{MVAr} \tag{6.56}$$

6.11.2 Band-Pass Filter

The component loadings at fundamental and all harmonic frequencies may be determined as for the single-tuned filter, i.e.

$$S = (V_s^2/X_c)[n_0^2/(n_0^2-1)] \quad \text{MVAr} \tag{6.57}$$

where n_0 is the ratio of the tuned frequency to the supply frequency.

Capacitor rating

The fundamental loading is

$$S[n_0^2/(n_0^2-1)] \quad \text{MVAr} \tag{6.58}$$

The loading at harmonic n is

$$I_n^2(X_c/n) \tag{6.59}$$

and using equation (6.57) this becomes

$$\frac{1}{S}(I_n^2/n)V_s^2 n_0^2/(n_0^2-1) \tag{6.60}$$

Thus the total harmonic loading is

$$\left[\frac{1}{S}(V_s^2 n_0^2)/(n_0^2-1)\right]\sum_{n=n_{\min}}^{n_{\max}}(I_n^2/n) \quad \text{MVAr} \tag{6.61}$$

Inductor rating

Referring to Figure 6.2(a), for a Q value of 1.5, say,

$$R = 1.5X_0 = 1.5n_0X_L$$

Thus if the filter is tuned to a frequency close to the 17th harmonic

$$R \approx 25X_L$$

Since $I_c = I_L + jI_R$ it follows that, at fundamental frequency,

$$I_c \approx I_L$$

and the fundamental loading is

$$\begin{aligned} I_L^2X_L &= I_c^2X_c/n_0^2 \\ &= (S/V_s)^2[V_s^2/n_0^2S][n_0^2/(n_0^2-1)] \\ &= (S/n_0^2)[n_0^2/(2-1)] \quad \text{MVAr} \end{aligned} \tag{6.62}$$

At harmonic n,

$$(I_L)_n = I_nR/(R+jX_L) = I_nQ/[Q+(jn/n_0)] \tag{6.63}$$

and

$$|(I_L)_n| = I_nQ/[Q^2+(n/n_0)^2]^{1/2} \tag{6.64}$$

The inductive reactance at harmonic n is

$$\begin{aligned}(X_L)_n &= X_0(n/n_0) = (n/n_0)(X_c/n_0)\\ &= (n/n_0^2)(V_s^2/S)[n_0^2/(n_0^2-1)]\end{aligned}$$

Thus the loading at harmonic n is

$$(I_L)_n^2(X_L)_n = \frac{1}{S}Q^2V_s^2[n_0^2/(n_0^2-1)][nI_n^2/(Q^2n_0^2+n^2)] \quad \text{MVAr} \tag{6.65}$$

and the total harmonic loading is

$$\frac{1}{S}Q^2V_s^2[n_0^2/(n_0^2-1)]\sum_{n=n_{\min}}^{n_{\max}}\left[\frac{nI_n^2}{Q^2n_0^2+n^2}\right] \quad \text{MVAr} \tag{6.66}$$

Power losses

(1) The power loss in the capacitor is

$$K_{CL} \times (\text{total rating in kilowatts}) \tag{6.67}$$

(2) The inductor series resistance at fundamental frequency is

$$R_L = X_0/Q_L = (n_0/Q_L)X_L \tag{6.68}$$

where Q_L is the quality factor of the inductor, and the corresponding power loss is

$$\begin{aligned}I_L^2R_L &= (n_0/Q_L)\ (\text{MVAr loading})\\ &= [S/(n_0Q_L)][n_0^2/(n_0^2-1)] \quad \text{MW}\end{aligned} \tag{6.69}$$

Similarly, the harmonic power loss is

$$\sum (I_L)_n^2(R_L)_n = \frac{1}{S}(Q^2V_s^2n_0/Q_L)[n_0^2/(n_0^2-1)]\sum_{n=n_{\min}}^{n_{\max}}\frac{I_n^2}{Q^2n_0^2+n^2} \text{ MW} \tag{6.70}$$

(3) The power loss in the shunt resistor R may also be expressed as a fraction of the inductor loading. At the fundamental frequency,

$$R = QX_0 = Qn_0X_L,\ |I_R| = \frac{|I_L|X_L}{R} = \frac{I_LX_L}{Qn_0X_L} = \frac{I_L}{Qn_0} \tag{6.71}$$

and the power loss is

$$\begin{aligned}I_R^2R &= (1/Qn_0)I_L^2X_L\\ &= (1/Qn_0)\ (\text{MVAr loading})\\ &= [S/(Qn_0^3)][n_0^2/(n_0^2-1)] \times 10^3 \text{ kW}\end{aligned} \tag{6.72}$$

At harmonic n,

$$|(I_R)_n| = |(I_L)_n|(X_L/R) \tag{6.73}$$

and the power loss is

$$\sum (I_R)_n^2(R)_n = \frac{1}{S}(QV_s^2/n_0)[n_0^2/(n_0^2-1)] \sum_{n=n_{\min}}^{n_{\max}} \left[\frac{n^2 I_n^2}{Q^2 n_0^2 + n^2}\right] \times 10^3 \text{ kW} \tag{6.74}$$

Total cost

Applying the present-value factor to energy costs and collecting terms in S and in $1/S$ as for the single-tuned filter, it can be shown that once again the total cost is given by

$$\text{TCOST} = U_T + AS + \frac{B}{S} \tag{6.75}$$

where

$$A = \left[U_c + \frac{U_L}{n_0^2} + 8760 P_v U_u F_u \left(K_{CL} + \frac{10^3}{Q_L n_0} + \frac{10^3}{Q n_0^3}\right)\right](n_0^2/(n_0^2-1)) \tag{6.76}$$

and

$$B = [n_0^2/(n_0^2-1)]V_s^2 \sum_{n=n_{\min}}^{n_{\max}} I_n^2 \left[\frac{U_c}{n} + \frac{Q^2 U_L n}{Q^2 n_0^2 + n^2} + 8760 P_v U_u F_u \left(\frac{K_{CL}}{n} + \frac{Q^2 n_0 \times 10^3}{Q_L(Q^2 n_0^2 + n^2)} + \frac{Q n^2 \times 10^3}{n_0(Q^2 n_0^2 + n^2)}\right)\right] \tag{6.77}$$

As before, TCOST is a minimum when

$$S = S_{\text{MIN}} = \sqrt{\frac{B}{A}} \quad \text{MVAr} \tag{6.78}$$

6.12 D.C. Side Filters

Although the d.c. side voltage ripple of static converters generates harmonic currents, these are rarely filtered out because they do not have a direct effect on other processes or consumers.

High-voltage d.c. transmission is a special case, where overhead lines are used, because of communications interference. The amplitudes of the harmonic currents, discussed in Chapter 3, depend on the delay, extinction and commutation overlap angles as well as the various impedances of the d.c. circuit (i.e. smoothing reactors, damping circuits, surge capacitors and the line itself). The inclusion of the stray capacitances in a three-pulse model of the converter produces a standing wave pattern of the total

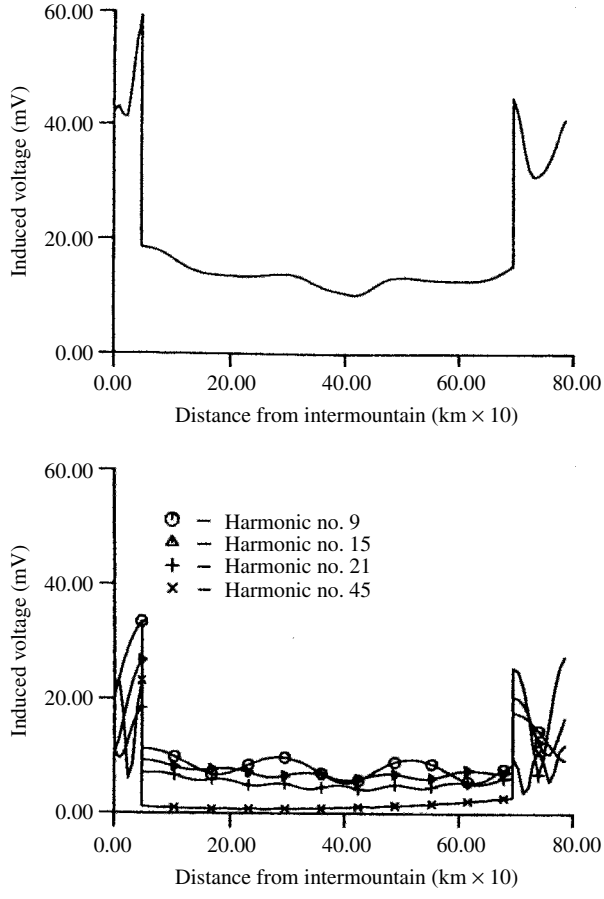


Figure 6.21 Example of induced voltage versus distance. Copyright © 2003 IEEE

earth mode equivalent disturbing current along the line distance, or alternatively the total induced voltage on an open circuit test line at a specified distance from the d.c. line (typically 1 km). An example of such calculation is shown in Figure 6.21, where the discontinuities are caused by parallel sections of electrode line at the ends of the d.c. line.

Other criteria used to define the performance of the d.c. filters in d.c. transmission schemes are the maximum voltage TIF on the high-voltage bus and the maximum permissible noise to ground in telephone lines close to the high voltage d.c. line.

Typical types and location of d.c. filters used in existing schemes are illustrated in Figure 6.22, and the subject is discussed thoroughly in [10].

Component ratings are considerably different to those for an a.c. filter, since the harmonic current is reduced to a relatively small value by the large d.c. smoothing reactor; consequently the capacitor cost is almost entirely dependent on its capacitance and the d.c. voltage level. The capacitor has the greatest cost and is chosen first; the inductor is then fixed for a given frequency. The selection of the quality factors is made as for an a.c. filter (e.g. by using equation (6.29)).

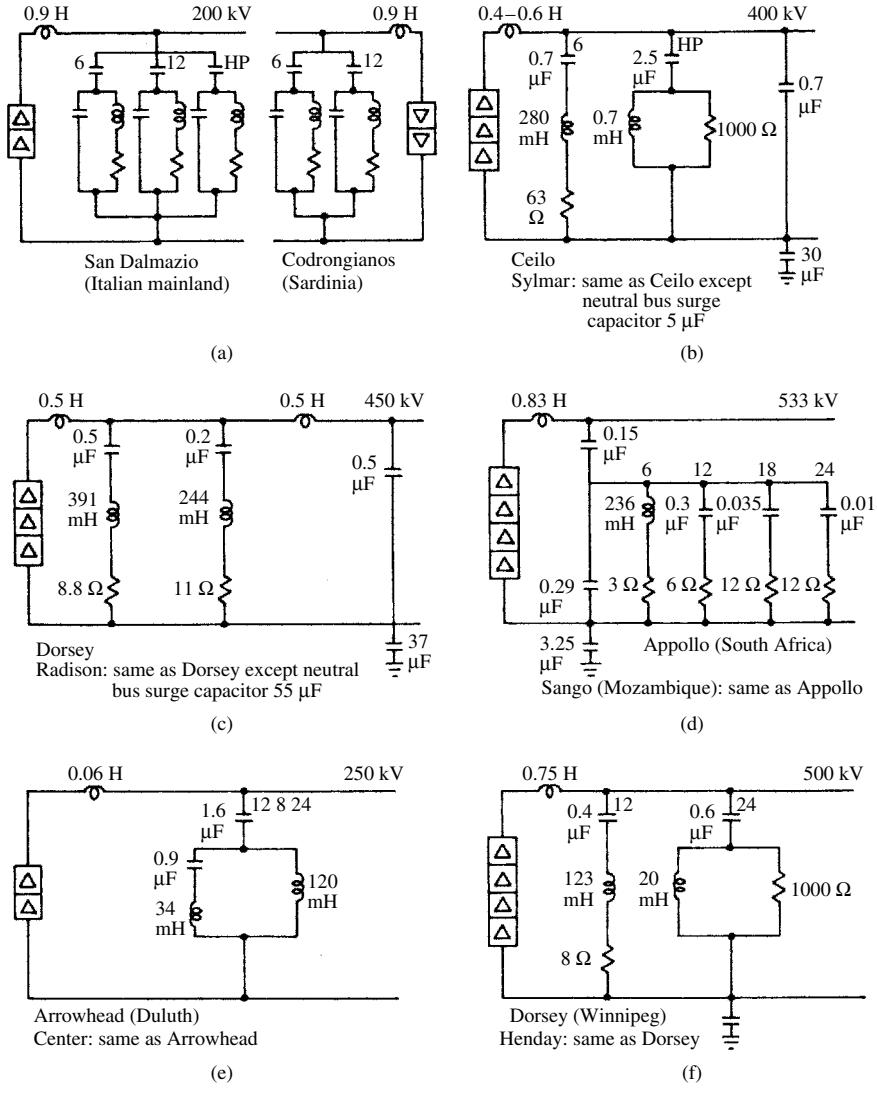


Figure 6.22 D.c. filter circuits of various HVd.c. schemes [10]

If the conventional stringent telephone interference criteria is imposed on HVd.c. lines the result is expensive filtering arrangements. However, the propagation of harmonics can be predicted with much greater accuracy in HVd.c. lines (as compared with a.c. lines) and it is possible to make more realistic cost comparisons with alternative changes in the telecommunications system.

6.13 Active Filters

The design complexity and high cost of losses of the conventional passive filters, as well as their restricted capability to eliminate inter-harmonics and non-characteristic

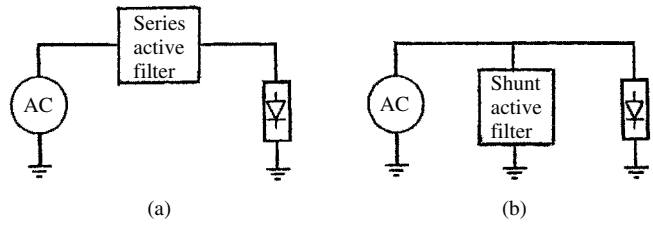


Figure 6.23 Active filters: (a) series; (b) shunt

harmonics, has encouraged the development of harmonic compensation by means of power electronic devices, commonly referred to as active filters.

According to their connection to the network, active filters can be of the series type, as shown in Figure 6.23(a), to prevent the transfer of harmonic current, or of the shunt type, shown in Figure 6.23(b), to reduce the harmonic content in the network.

The operating characteristics and limitations of the two types of active filter are discussed in the following sections.

6.13.1 Series Connection of Active Filters

As the generation of harmonic content is an inherent part of the operation of the nonlinear components, a path must be provided for them to flow. Therefore the use of series-connected filters in isolation is not normally viable and they have to be combined with some type of passive filtering. The latter absorb the current harmonics generated by the nonlinear plant, while the active filters blocks the transfer of harmonics in either direction. This combination isolates the passive filters from the a.c. system impedance, improving their response and reducing possible overloads.

Figure 6.24 shows a single phase diagram of the series active and shunt passive filtering combination. The harmonics are represented by a current source i_L and the network and passive filter by the impedances Z_S and Z_F, respectively. The active filter is represented by a voltage source V_C in series.

The controlled voltage source offers no impedance to the flow of the fundamental component but introduces a very large resistance between the network and the nonlinear

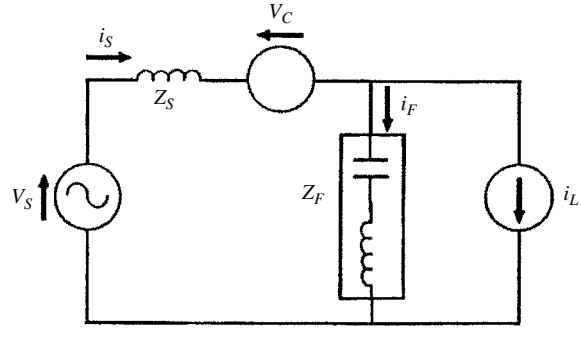


Figure 6.24 Single-phase circuit of a series active filter

plant for the harmonic frequencies. In practice, due to the limitation of the active filter bandwidth, there is a maximum level for that resistance.

In the ideal case, the nonlinear plant current harmonic content is forced to circulate via the passive filter, and the active filter voltage is the sum of the supply and passive filter voltages. The power rating of the series active filter is of the order of 2–5% of the nonlinear plant nominal power (in VA) [11].

The main limitation of the active/passive filter configuration is that it is restricted to a fixed fundamental frequency.

6.13.2 Shunt Connection of Active Filters

An early proposal for the shunt active filter connection was made in 1971 [12] for the elimination of the converter current harmonics via magnetic compensation, as shown in Figure 6.25.

In this configuration a current transformer captures information about the total converter current. The fundamental current is then eliminated by means of a series resonant circuit. The remaining content of the current is amplified to the appropriate level by means of a linear amplifier, the output of which is fed back via a tertiary winding in the converter transformer.

More recently there has been considerable research in this field, especially in the derivation and processing of the signal representing the current harmonic components in order to derive the appropriate compensation current [13–15].

Besides harmonic elimination, the active compensation systems can be designed to improve the power factor. Figure 6.26 shows a circuit based on the use of a signal processor unit (SPU) for the compensation of a load harmonic current and the displacement angle of the current fundamental frequency. In this unit the sampled harmonic current content is transmitted to the SPU. The SPU synthesises a sinusoidal wave in phase with the fundamental component of the load current (for the purpose of harmonic elimination) or with the terminal voltage (for the combined compensation of harmonics and displacement factor improvement). The synthesised sinusoidal current is then subtracted from the signal representing the load current to obtain the required compensating current; this signal is fed to an amplifier and then combined, via a reinjection transformer (or by direct connection using an inductor), with the load current in order to form an almost sinusoidal system current.

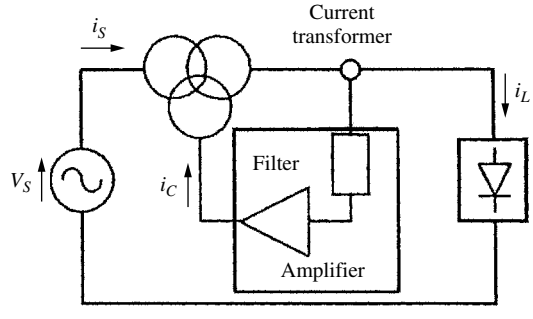


Figure 6.25 Magnetic compensation of converter harmonics

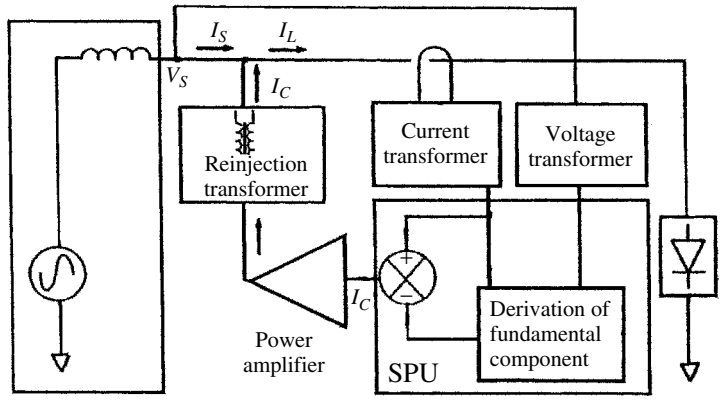


Figure 6.26 Active system for the compensation of the harmonic distortion

The main characteristic of this processing system is that the SPU operates in the time domain and thus avoids the need for complex processing to extract the harmonic components. Therefore the shunt-connected active filter is not tied to a specific fundamental frequency and thus the compensation achieved is effective at any source frequency within the limits imposed by the design.

Although the shunt active filter has definite advantages over passive filtering, its use in real industrial applications has so far been limited. This is because the cost of the inverter is still higher than the passive filter solution. A recent contribution [16] has proposed the connection of a shunt active filter in series with a passive filter. In this case the rating of the active filter is reduced and improves the performance of the passive filter.

The compensating effect of an active filter prototype [17] is illustrated in Figure 6.27. Figure 6.27(a) shows the current waveform absorbed by a single-phase bridge rectifier feeding a resistive load, and Figure 6.27(b) illustrates the compensating effect achieved by the active filter.

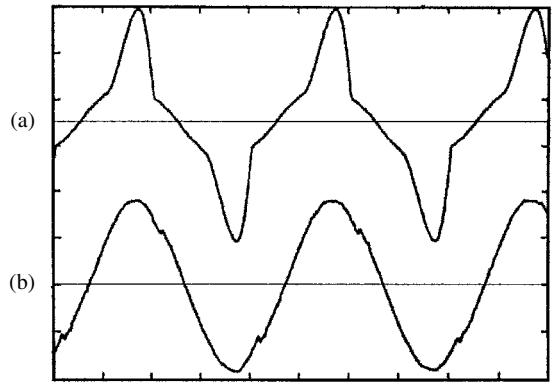


Figure 6.27 Typical magnitudes of an active filter: (a) load current; (b) compensated supply current

6.14 Discussion

The decision on the magnitude and type of harmonic reduction to be used is always made by economic considerations. Filters of whatever type are always expensive and thus, if at all possible, must be avoided. One of the problems in this respect is the difficulty in determining the extent of liability by the different parties involved. The installation of passive harmonic filters at a point in the system normally has a positive effect on the system as a whole. However, often the cost of providing such general welfare is rarely shared between the parties benefiting from it. On the negative side, the parallel combination of the filters and system impedances produces resonances (normally at non-characteristic harmonics) and, thus increases substantially the distortion at those frequencies.

Active filters, on the other hand, can be designed to compensate the harmonic content of the particular nonlinear load consideration, without providing an attractive path for the harmonics of neighbouring plant. Looking at it from the supplier viewpoint, though, too much active elimination can have a negative effect on the rest of the system, because active filters do not provide damping for existing harmonics. With the increasing use of highly controllable power electronic devices, especially in distributed generation with active waveform control, the lack of system damping is going to be a growing problem in the future.

6.15 References

1. CIGRE WG-14 03 (1989) AC harmonic filters and reactive compensation for HVdc with particular reference to non-characteristic harmonics, Supplement to *Electra* **63**.
2. Arrillaga, J., Juhlin, L., Lathinen, M., Ribeiro, P. and Saavedra, A.R. (1996) A.C. system modelling for a.c. system design, an overview of impedance modelling, *Electra*, **164**, 133–151.
3. Kimbark, E.W. (1971) *Direct Current Transmission*, John Wiley & Sons, New York, Ch. 8.
4. Ainsworth, J.D. (1965) Filters, damping circuits and reactive voltamperes in HVdc convertors, in *High Voltage Direct Current Convertors and Systems* (B.J. Cory, ed.), Macdonald, London, pp. 137–74.
5. Stanley, C.H., Price, J.J. and Brewer, G.L. (1977) Design and performance of a.c. filters for 12-pulse HVdc schemes, *IEE Conf. Publ.*, **154**, 158–61.
6. Ortmeyer, T.H. and Hiyama, T. (1996) Distribution system harmonic filter planning, *Trans. IEEE Power Delivery*, **11**(4), 2005–12.
7. Ortmeyer, T.H., Kakimoto, N. Hiyama, T. and Hammam, M.S.A.A. (1998) Harmonic performance of individual and group loads, *Proc. ICHPS*, 277–83.
8. Hiyama, T., Hammam, M.S.A.A. and Ortmeyer, T.H. (1989) Distribution system modelling with distributed harmonic sources, *Trans. IEEE Power Delivery*, **4**(2), 1297–1304.
9. Powell, R.O.M. (1966) The design of capacitor components of large high voltage a.c. filter networks, *IEE Conf. Publ.*, **22**, 275–6.
10. Harrison, R.E. and Krishnayya, P.C.S. (1978) System considerations in the application of d.c. filters for HVdc transmission, CIGRE paper 14-09, Paris.
11. Battacharya, D.D.M. and Barnejee, B. (1991) Synchronous frame harmonic isolator using active series filter, *European Power Electronics Conference, Firenze*, Vol. 3, pp. 30–5.
12. Sasaki, H. and Machida, T. (1971) A new method to eliminate a.c. harmonic currents by magnetic flux compensation—considerations on basic design, *Trans. IEEE Power Apparatus Systems*, **PAS-90**(5), 2009–19.

13. Akagi, H., Navea, A. and Atoh, S. (1986) Control strategy of active power filters using multiple voltage-source PWM converters, *Trans. IEEE Industry Applications*, **IA22**(3), 460–5.
14. Enslin, J.H.R. and Van Harmelen, G.L. (1990) Real-time dynamic control of dynamic power filters in supplies with high contamination, Proceedings of Power Electronic Specialists Conference, pp. 887–94.
15. Hayafune, K., Ueshiba, T., Masada, E and Ogiwara, Y. (1984) Microcomputer controlled active power filter, International Conference on Industrial Electronics, Control and Instrumentation, Tokyo, pp. 1221–26.
16. Detjen, O., Jacobs, J., De Doncker, R.W. and Mall, H.G. (2001) A new hybrid filter to dampen resonances and compensate harmonic currents in industrial power systems with power factor correction equipment, *Trans. IEEE Power Electronics*, **16**(6), 821–7.
17. Round, S. (1992) Active filtering and VAR compensation, PhD thesis, University of Canterbury, New Zealand.

7

Computation of Harmonic Flows

7.1 Introduction

Although the title specifically refers to *harmonic flows*, the analysis and algorithms described in this chapter are equally applicable to other frequencies in the region of interest such as inter-harmonics and subharmonics.

The simplest harmonic flow involves a single harmonic source and single-phase network analysis. This model is commonly used to derive the system harmonic impedances at the point of common coupling in filter design. In general, however, the network will be unbalanced and may contain several harmonic sources. Therefore, the derivation of the harmonic voltages and currents requires multi-source three-phase harmonic analysis. If the harmonics generated by the nonlinear components are reasonably independent of the voltage distortion level in the a.c. system, the derivation of the harmonic sources (the subject of Chapter 3) can be decoupled from the analysis of harmonic penetration and a direct (nodal) solution is possible. Since most nonlinearities manifest themselves as harmonic current sources, this is normally called the current injection method. In such cases, the expected voltage levels or the results of a fundamental frequency load flow are used to derive the current waveforms, and with them the harmonic content of the nonlinear components.

After a description of the direct harmonic analysis algorithm, the following sections discuss the modelling of network components and the formulation of the nodal admittance matrix as well as the computer implementation of the harmonic flow algorithm.

7.2 Direct Harmonic Analysis

The distribution of voltage and current harmonics throughout a linear power network containing one or more harmonic current sources is normally carried out using nodal analysis [1]. The asymmetry inherent in transmission systems cannot be studied with any simplification by using the symmetrical component frame of reference, therefore phase components are used.

Power System Harmonics, Second Edition J. Arrillaga, N.R. Watson
© 2003 John Wiley & Sons, Ltd ISBN: 0-470-85129-5

The nodal admittance matrix of the network at frequency f is of the form

$$[Y_{\mathrm{f}}] = \begin{bmatrix} Y_{11} & Y_{12} & \dots & Y_{1i} & \dots & Y_{1k} & \dots & Y_{1n} \\ Y_{21} & Y_{22} & \dots & Y_{2i} & \dots & Y_{2k} & \dots & Y_{2n} \\ \vdots & \vdots & \ddots & \vdots & \ddots & \vdots & \ddots & \\ Y_{i1} & Y_{i2} & \dots & Y_{ii} & \dots & Y_{ik} & \dots & Y_{in} \\ \vdots & \vdots & \ddots & \vdots & \ddots & \vdots & \ddots & \\ Y_{k1} & Y_{k2} & \dots & Y_{ki} & \dots & Y_{kk} & \dots & Y_{kn} \\ \vdots & \vdots & \ddots & \vdots & \ddots & \vdots & \ddots & \\ Y_{n1} & Y_{n2} & \dots & Y_{ni} & \dots & Y_{nk} & \dots & Y_{nn} \end{bmatrix} \tag{7.1}$$

where Y_{ki} is the mutual admittance between busbars k and i at frequency f, and Y_{ii} is the self-admittance of busbar i at frequency f.

A separate system admittance matrix is generated for each frequency of interest. The main difficulty is to determine which model best represents the various system components at the required frequency and obtain appropriate parameters for them. With this information, it is straightforward to build up the system fundamental and harmonic frequency admittance matrices.

The three-phase nature of the power system always results in some load or transmission line asymmetry, as well as circuit coupling. These effects give rise to unbalanced self- and mutual admittances of the network elements.

For the three-phase system, the elements of the admittance matrix are themselves 3×3 matrices consisting of self- and transfer admittances between phases, i.e.

$$Y_{ii} = \begin{bmatrix} Y_{aa} & Y_{ab} & Y_{ac} \\ Y_{ba} & Y_{bb} & Y_{bc} \\ Y_{ca} & Y_{cb} & Y_{cc} \end{bmatrix} \tag{7.2}$$

Figure 7.1 shows a case of two three-phase harmonic sources and an unbalanced a.c. system. The current injections, i.e. $I_{1h} - I_{3h}$ and $I_{4h} - I_{6h}$, can be unbalanced in magnitude and phase angle.

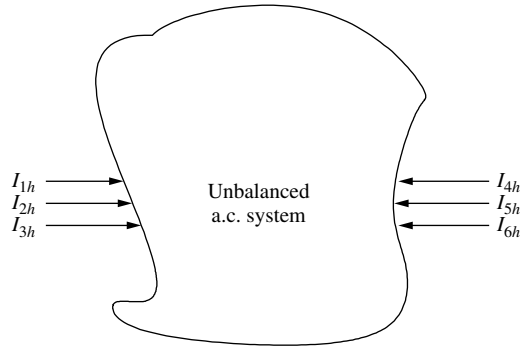


Figure 7.1 Unbalanced current injection into an unbalanced a.c. system

The system harmonic voltages are calculated by direct solution of the linear equation

$$[I_h] = [Y_h]\,[V_h] \qquad \text{for } h \neq 1 \tag{7.3}$$

where $[Y_h]$ is the system admittance matrix.

Therefore, the direct solution involves $h - 1$ independent sets of linear simultaneous equations, i.e.

$$\begin{array}{ccccc} [I_h] & = & [Y_h] & & [V_h] \\ \cdot & & \cdot & & \cdot \\ \cdot & & \cdot & & \cdot \\ \cdot[I_3] & = & [Y_3] & & \cdot[V_3] \\ [I_2] & = & [Y_2] & & [V_2] \end{array} \tag{7.4}$$

The injected currents at most a.c. busbars will be zero, since the sources of the harmonic considered are the nonlinear devices. To calculate an admittance matrix for the reduced portion of a system comprising just the injection busbars, the admittance matrix is formed with those buses at which harmonic injection occurs ordered last. Advantage is taken of the symmetry and sparsity of the admittance matrix [2], by using a row ordering technique to reduce the amount of off-diagonal element build-up. The matrix is triangulated using Gaussian elimination, down to but excluding the rows of the specified buses.

The resulting matrix equation for an n-node system with $n - j + 1$ injection points is

$$\begin{bmatrix} 0 \\ \vdots \\ 0 \\ \hline I_j \\ \vdots \\ I_n \end{bmatrix} = \left[\begin{array}{ccc} & 0 & \\ & & \\ 0 & \begin{matrix} Y_{jj} & \dots & Y_{jn} \\ \vdots & & \vdots \\ Y_{nj} & \dots & Y_{nn} \end{matrix} \end{array}\right] \cdot \begin{bmatrix} V_1 \\ \vdots \\ V_{j-1} \\ \hline V_j \\ \vdots \\ V_n \end{bmatrix} \tag{7.5}$$

As a consequence, $I_j \dots I_n$ remain unchanged since the currents above these in the current vector are zero. The reduced matrix equation is

$$\begin{bmatrix} I_j \\ \vdots \\ I_n \end{bmatrix} = \begin{bmatrix} Y_{jj} & \dots & Y_{jn} \\ \vdots & \dots & \vdots \\ Y_{nj} & \dots & Y_{nn} \end{bmatrix} \cdot \begin{bmatrix} V_j \\ \vdots \\ V_n \end{bmatrix} \tag{7.6}$$

and the order of the admittance matrix is three times the number of injection busbars for a three-phase system. The elements are the self- and transfer admittances of the reduced system as viewed from the injection busbars. Whenever required, the impedance matrix may be obtained for the reduced system by matrix inversion.

Reducing a system to provide an equivalent admittance matrix, as viewed from a specific bus, is an essential part of filter design. The reduction of the admittance matrix to a set of busbars where nonlinearities exist is an essential step to allow accurate

a.c. system representation in many other types of analysis, such as iterative harmonic analysis or as frequency-dependent equivalents in time-domain analysis.

7.2.1 Frequency Scan Analysis

The simplest application of the direct method described above is the frequency scan. It involves the derivation of the frequency response of a network looking from a specified busbar. A one per unit sinusoidal current is injected into the bus at a range of frequencies and the set of equations (7.3) is used to calculate the voltage response. This calculation is repeated at discrete frequency steps covering the specified frequency spectrum.

This process can be equally used with phase or sequence components. In the latter case, one per unit positive- or zero-sequence current is injected to derive the positive- or zero-sequence driving-point network impedances seen from the specified bus.

Frequency scan analysis is widely used in filter design. It is also a preliminary step in the derivation of frequency-dependent equivalents for use in electromagnetic transients simulation.

Instead of injecting one per unit current, the use of one per unit voltage can be used to investigate the effect of background harmonic voltages present at any specified point in the network. The set of equations (7.3) is then used to derive the harmonic voltage transfer to the rest of the network.

7.2.2 Incorporation of Harmonic Voltage Sources

Most power system nonlinearities manifest themselves as harmonic current sources, but sometimes harmonic voltage sources are used to represent the distortion background present in the network prior to the installation of the new nonlinear load. Moreover, some recent power electronic devices based on GTO and IGBT switching, act as voltage sources behind an impedance.

A system containing harmonic voltages at some busbars and harmonic current injections at other busbars is solved by partitioning the admittance matrix and performing a partial inversion. This then allows the unknown busbar voltages and unknown harmonic currents to be found. If V_2 represents the known voltage sources then I_2 are the unknown variables. The remaining busbars are represented as a harmonic current injection I_1 (which can be either zero or specified by harmonic current source) and the corresponding harmonic voltage vector V_1 represents the unknown variables.

Partitioning the matrix equation to separate the two types of nodes gives

$$\begin{bmatrix} Y_{11} & Y_{12} \\ Y_{21} & Y_{22} \end{bmatrix} \begin{bmatrix} V_1 \\ V_2 \end{bmatrix} = \begin{bmatrix} I_1 \\ I_2 \end{bmatrix} \tag{7.7}$$

The unknown voltage vector V_1 is found by solving

$$[Y_{11}]\,[V_1] = [I_1] - [Y_{12}]\,[V_2] \tag{7.8}$$

The harmonic currents injected by the harmonic voltage sources are then found by solving

$$[Y_{21}]\,[V_1] + [Y_{22}]\,[V_2] = [I_2] \tag{7.9}$$

With this formulation some extra processing is required to obtain the reduced admittance matrix, which is not generated as part of the solution.

7.2.3 Cascading Sections

Mutually coupled transmission lines with different tower geometries over the line length need special consideration. If only terminal voltage information is required, the line sections may be combined into one equivalent section using *ABCD* parameters, as shown in Figure 7.2.

All the individual sections must contain the same number of mutually coupled three-phase elements, to ensure that the parameter matrices are of the same order and that matrix multiplications are executable. In this respect, uncoupled sections will use the coupled format with zero coupling elements to maintain the correct dimensions.

For the case of a non-homogeneous line with n different sections

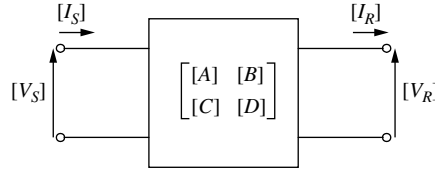
$$\begin{bmatrix} V_S \\ I_S \end{bmatrix} = \begin{bmatrix} [A_1]\ [B_1] \\ [C_1]\ [D_1] \end{bmatrix} \times \begin{bmatrix} [A_2]\ [B_2] \\ [C_2]\ [D_2] \end{bmatrix} \times \cdots \times \begin{bmatrix} [A_n]\ [B_n] \\ [C_n]\ [D_n] \end{bmatrix} \begin{bmatrix} V_R \\ -I_R \end{bmatrix}$$

$$\begin{bmatrix} V_S \\ I_S \end{bmatrix} = \begin{bmatrix} [A]\ [B] \\ [C]\ [D] \end{bmatrix} \begin{bmatrix} V_R \\ -I_R \end{bmatrix} \tag{7.10}$$

It must be noted that in general $[A] \neq [D]$ for a non-homogeneous line.

Once the resultant *ABCD* parameters have been found, the equivalent nodal admittance matrix for the subsystem can be calculated from

$$[Y] = \begin{bmatrix} [D]\,[B]^{-1} & [C] - [D]\,[B]^{-1}[A] \\ [B]^{-1} & -[B]^{-1}[A] \end{bmatrix}. \tag{7.11}$$



(a)

$$\begin{bmatrix} V_S \\ I_S \end{bmatrix} = \begin{bmatrix} [A] & [B] \\ [C] & [D] \end{bmatrix} \begin{bmatrix} V_R \\ -I_R \end{bmatrix}$$

(b)

Figure 7.2 Two-port network transmission parameters: (a) multi-two-port network; (b) matrix transmission parameters

If, however, extra information along the line is required, appropriate fictitious nodes are created at specified points and/or at regular intervals, and the following nodal matrix equation is formed, inverted (factorised) and solved. The resultant vector provides the harmonic voltage profile along the line. Alternatively, instead of creating fictitious nodes during the solution, and thus increasing the computation, a more detailed voltage profile can be derived by analysing the harmonic flow along the line once the overall solution has been obtained.

$$\begin{bmatrix} I_S \\ I_1 \\ I_2 \\ \vdots \\ I_n \\ I_R \end{bmatrix}_h = \begin{bmatrix} [Y_{SS}] & -[Y_{S1}] & & & & \\ -[Y_{1S}] & [Y_{SS}]+[Y_{11}] & -[Y_{12}] & & & \\ & -[Y_{21}] & [Y_{11}]+[Y_{22}] & \ddots & & \\ & & \ddots & \ddots & \ddots & \\ & & & \ddots & [Y_{nn}]+[Y_{RR}] & -[Y_{nR}] \\ & & & & -[Y_{Rn}] & [Y_{RR}] \end{bmatrix}_h \begin{bmatrix} V_S \\ V_1 \\ V_2 \\ \vdots \\ V_n \\ V_R \end{bmatrix} \tag{7.12}$$

7.3 Derivation of Network Harmonic Impedances from Field Tests

In the absence of more accurate information, existing harmonic standards and recommendations often refer to harmonic impedance sources derived from the balanced short-circuit impedance of the system at fundamental frequency. The inadequacy of such an approach has become apparent with the help of online tests and computer studies.

The availability of voltage and current transducers throughout the power system provides the basis for the indirect derivation of harmonic impedances. Their assessment is therefore dependent on the performance of such transducers, which may not have been designed to respond accurately to harmonic frequencies.

The present techniques for the derivation of harmonic impedances can be divided into three groups, depending on the origin of harmonics or inter-harmonics:

- Use of existing harmonics sources (non-invasive)
- Direct injection (invasive)
- Analysis of transient waveforms (non-invasive).

7.3.1 Use of Existing Sources (Online Non-Invasive Tests)

In the non-invasive test the information required is obtained purely from measurements of existing waveforms, i.e. using the harmonic content already present in the system. This is the simplest and most commonly used technique.

Electricit de France [3] has proposed two alternative ways of deriving information on harmonic impedances, in the form of sequence components, using the principle of digital filtering rather than Fourier analysis. One method uses numerical techniques to perform the digital filtering of the physical input values, and retains only the frequencies contained in a selected bandwidth. The information is then used to identify the network with a simple impedance model which is only valid over a relatively narrow frequency range. The identification is carried out separately for the zero-sequence and positive-(negative-) sequence values. The second method uses electronic filters to transform the six voltage and current values into four (two zero-sequence and two positive-sequence), after eliminating the 50 Hz component.

The harmonic content produced by an existing high-voltage d.c. converter station has been used [4] to obtain the harmonic impedances directly from the ratios of voltage and current readings. This assumes that all other important harmonic sources in the power system are disconnected; however, measurements taken without the existing high-voltage d.c. converter station operating, or operating at a different operating point, could have been used to account for the other harmonic sources in the system.

When the harmonic voltage levels are high and affected by the connection of a shunt capacitor bank the method illustrated in Figure 7.3 has been used to identify the main source of harmonics.

The harmonic current injection and harmonic impedances (for the Norton equivalents) are obtained by solving the linear set of equations

$$\begin{bmatrix} 1 & 0 & -V'_m & 0 \\ 0 & -1 & 0 & V'_m \\ 1 & 0 & -V''_m & 0 \\ 0 & -1 & 0 & V''_m \end{bmatrix} \begin{bmatrix} I_1 \\ I_2 \\ Y_1 \\ Y_2 \end{bmatrix} = \begin{bmatrix} I'_m \\ I'_m \\ I''_m \\ I''_m - Y_c V''_m \end{bmatrix} \tag{7.13}$$

where V'_m and I'_m are the measured harmonic voltage and current prior to connecting the capacitor and V''_m and I''_m after.

This method assumes that the components of the Norton equivalents are not affected by the switching operation. In general, however, this is not the case as the related variation in the system harmonic impedances, and particularly their phase angle variation [5], can have considerable effect on the Norton equivalent impedances of the nonlinear load.

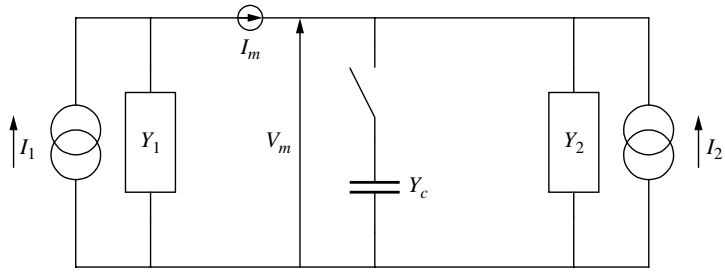


Figure 7.3 Identification of main harmonic source by capacitor switching

7.3.2 Direct Injection (Online Invasive Tests)

In principle, it is possible to design a source of harmonic power which absorbs fundamental frequency power and converts it into harmonic power of the appropriate frequencies, magnitudes and phases. However, the measurement of harmonic impedance requires a distorting source of considerable capacity.

In practice, measurements are usually taken at points where there is considerable distortion due to existing harmonic sources in the network. The effect of injecting a further source needed for harmonic measurement is superimposed on these. The result is a low signal to noise ratio, which makes the measurement unreliable.

To overcome this problem, the Electricity Council Centre (Capenhurst, UK) [6] designed a system which generates power at frequencies mid-way between the characteristic harmonic frequencies of interest, i.e. at the odd multiples of 25 Hz, on the assumption that interpolation between these frequencies is justifiable. The power ratings of the distorting source for measurements at 11 kV, 33 kV and 132 kV are 9 kW, 36 kW and 180 kW, respectively, and the units consist of a switching modulator in series with a resistive load in the form of a fan heater. The 11 kV and 33 kV systems are portable and the 132 kV system is located in a purpose-built van.

Figure 7.4 illustrates the results of typical measurements carried out with this equipment in combination with a harmonic impedance instrument [7], specially designed to provide simultaneous information about voltage and current with their phase relationship.

7.3.3 From Transient Waveforms (Online Non-Invasive Tests)

The methods discussed above involve measurement of the steady-state levels of particular frequencies. Alternatively, the network frequency characteristics can be derived

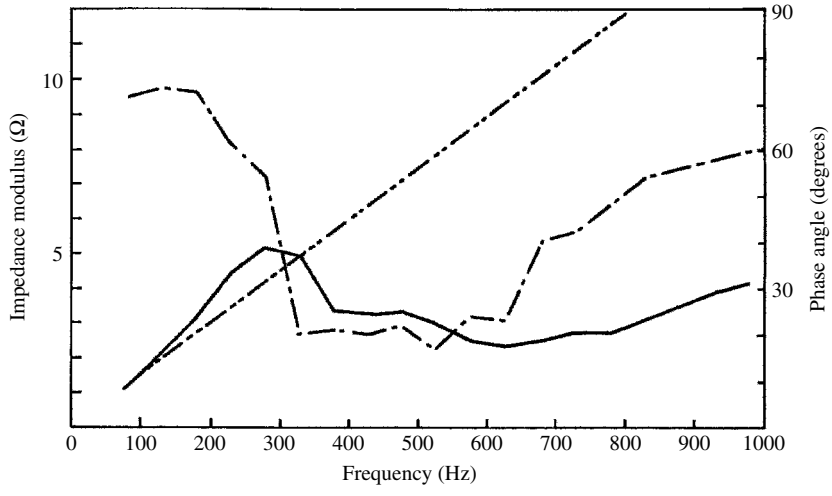


Figure 7.4 Source impedance seen from an 11 kV busbar supplying a commercial load: (· · –· · –), Obtained from the short-circuit impedance at 50 Hz; (———), measured impedance magnitude; (–· –·), measured impedance phase angle

from the transient voltage and current waveforms produced by normal switching operations. These include the switching of capacitor banks and transformers or even the system natural variations [8].

The advantage of using capacitor banks is their widespread use and their frequent switching, which produces a rich spectrum of inter-harmonics. However, the resulting harmonic currents are unsymmetrical, of short duration and depend on the point of wave of switching.

The transient inrush current produced by transformer switching produces high harmonic current levels compared to existing harmonics with a spectrum, ranging from 100 Hz to about 7000 Hz. Moreover, the signals are present for several seconds. Again the currents are highly unsymmetrical and depend on the switching moment and core remanence.

The use of natural system variations for spectral analysis can also provide time-dependent system impedances. Although this method is generally applicable, it can only achieve good precision in the presence of some predominant disturbing load.

The accuracy of applying the FFT to the voltage and current time-domain recordings in the presence of noise can be improved by correlation analysis in conjunction with spectral analysis. Spectral analysis of the auto- and cross-power spectra has been used to determine the frequency response of two 26.6 kV feeders [9] and also to determine the 3×3 impedance matrices [10]. With these methods, correlation indices are used to reject measurements where the signal to noise ratio causes the calculated values to be suspect. With least squares estimates, the matrix condition number also indicates the accuracy of the answer.

Identification techniques that do not require the use of FFT have also been applied to time-domain responses. Prony analysis and the direct ARMA method are two identification techniques suitable for determining frequency characteristics [11] from time-domain waveforms.

The main advantage of these non-invasive techniques is that they can be readily applied without the need for special injection equipment; however, they are equally applicable to invasive testing, where an impulse or other frequency-rich signal is injected.

7.4 Transmission Line Models

A transmission line consists of distributed inductance and capacitance, which affect the magnetic and electrostatic conditions of the line, and resistance and conductance, which affect the losses. These electrical parameters are calculated from the line geometry and conductor data. The effects of ground currents and earth wires are included in the calculation of these parameters. The calculated parameters are expressed as a series impedance and shunt admittance per unit length. A simple representation of the line includes the line total inductance, capacitance, resistance and conductance as lumped parameters, as shown in Figure 7.5 (nominal PI model). However, when the line length becomes an appreciable part of the wavelength of the frequency of interest, errors become apparent. Subdividing the line and using cascaded nominal PI sections to represent the line can alleviate this problem. The more nominal PI sections used, the closer the model represents the distributed nature of the line, and hence the more

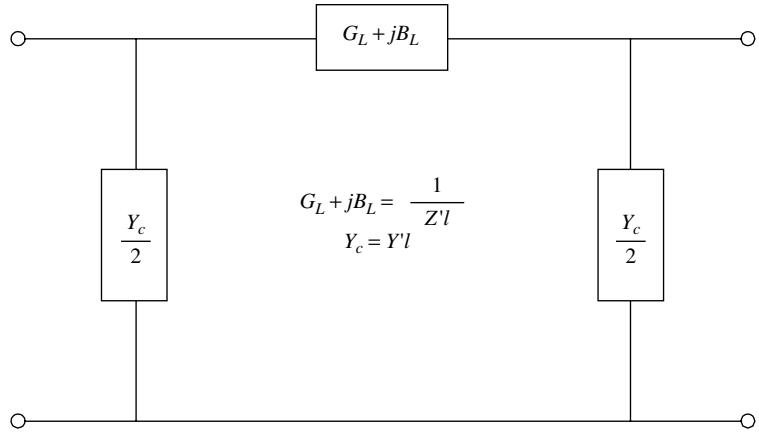


Figure 7.5 Nominal PI representation of transmission line

accurate the model. However, computational burden also greatly increases due to the increase in the number of busbars and lumped elements.

Before considering long line effects in detail, the lumped component representation of a three-phase transmission line with ground wire and earth return, suitable for inclusion in the system admittance matrix, will be considered next.

The impedance of a three-phase transmission line with an overhead earth wire is illustrated in Figure 7.6. Each conductor has resistance, inductance and capacitance, and is mutually coupled to the others.

With respect to Figure 7.6, the following equation can be written for the series impedance equivalent of phase a

$$V_{\mathrm{a}} - V'_{\mathrm{a}} = I_{\mathrm{a}}(R_{\mathrm{a}} + j\omega L_{\mathrm{a}}) + I_{\mathrm{b}}(j\omega L_{\mathrm{ab}}) + I_{\mathrm{c}}(j\omega L_{\mathrm{ac}}) + j\omega L_{\mathrm{ag}} I_{\mathrm{g}} - j\omega L_{\mathrm{an}} I_{\mathrm{n}} + V_{\mathrm{n}} \tag{7.14}$$

where

$$V_{\mathrm{n}} = I_{\mathrm{n}}(R_{\mathrm{n}} + j\omega L_{\mathrm{n}}) - I_{\mathrm{a}} j\omega L_{\mathrm{na}} - I_{\mathrm{b}} j\omega L_{\mathrm{nb}} - I_{\mathrm{c}} j\omega L_{\mathrm{nc}} - I_{\mathrm{g}} j\omega L_{\mathrm{ng}} \tag{7.15}$$

and substituting

$$I_{\mathrm{n}} = I_{\mathrm{a}} + I_{\mathrm{b}} + I_{\mathrm{c}} + I_{\mathrm{g}} \tag{7.16}$$

gives

$$V_{\mathrm{a}} - V'_{\mathrm{a}} = I_{\mathrm{a}}(R_{\mathrm{a}} + j\omega L_{\mathrm{a}}) + I_{\mathrm{b}} j\omega L_{\mathrm{ab}} + I_{\mathrm{c}} j\omega L_{\mathrm{ac}} + j\omega L_{\mathrm{ag}}\ I_{\mathrm{g}} - j\omega L_{\mathrm{an}}\ (I_{\mathrm{a}} + I_{\mathrm{b}} + I_{\mathrm{c}} + I_{\mathrm{g}}) + V_{\mathrm{n}} \tag{7.17}$$

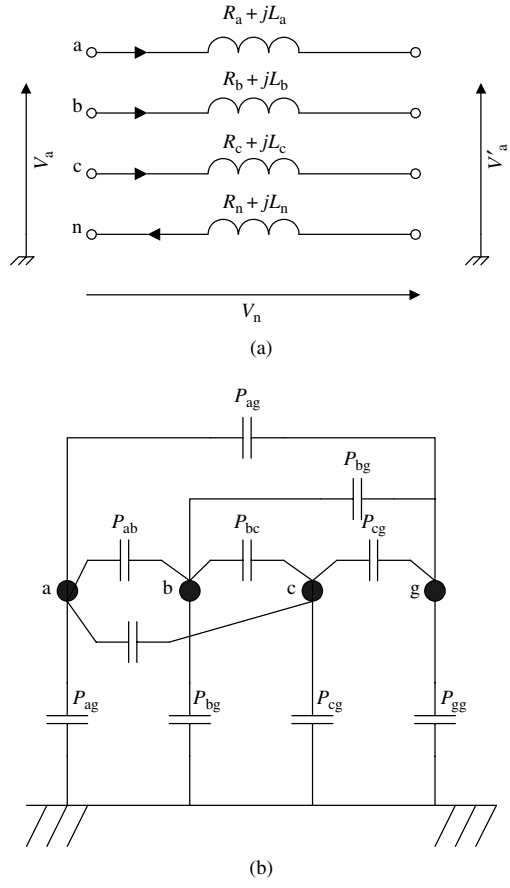


Figure 7.6 (a) Three-phase transmission series impedance equivalent; (b) three-phase transmission shunt impedance equivalent

Regrouping and substituting for V_n, i.e.

$$\begin{aligned}\Delta V_a &= V_a - V'_a \\ &= I_a(R_a + j\omega L_a - j\omega L_{an} + R_n + j\omega L_n - j\omega L_{na}) \\ &\quad + I_b(j\omega L_{ab} - j\omega L_{an} + R_n + j\omega L_n - j\omega L_{nb}) \\ &\quad + I_c(j\omega L_{ac} - j\omega L_{an} + R_n + j\omega L_n - j\omega L_{nc}) \\ &\quad + I_g(j\omega L_{ag} - j\omega L_{an} + R_n + j\omega L_n - j\omega L_{ng}) \qquad (7.18)\end{aligned}$$

$$\begin{aligned}\Delta V_a &= I_a(R_a + j\omega L_a - 2j\omega L_{an} + R_n + j\omega L_n) \\ &\quad + I_b(j\omega L_{ab} - j\omega L_{bn} - j\omega L_{an} + R_n + j\omega L_n) \\ &\quad + I_c(j\omega L_{ac} - j\omega L_{cn} - j\omega L_{an} + R_n + j\omega L_n) \\ &\quad + I_g(j\omega L_{ag} - j\omega L_{gn} - j\omega L_{an} + R_n + j\omega L_n) \qquad (7.19)\end{aligned}$$

or

$$\Delta V_a = Z_{aa-n} I_a + Z_{ab-n} I_b + Z_{ac-n} I_c + Z_{ag-n} I_g \tag{7.20}$$

and writing similar equations for the other phases and earth wire, the following matrix equation results:

$$\begin{bmatrix} \Delta V_a \\ \Delta V_b \\ \Delta V_c \\ \Delta V_g \end{bmatrix} = \begin{bmatrix} Z_{aa-n} & Z_{ab-n} & Z_{ac-n} & Z_{ag-n} \\ Z_{ba-n} & Z_{bb-n} & Z_{bc-n} & Z_{bg-n} \\ Z_{ca-n} & Z_{cb-n} & Z_{cc-n} & Z_{cg-n} \\ Z_{ga-n} & Z_{gb-n} & Z_{gc-n} & Z_{gg-n} \end{bmatrix} \begin{bmatrix} I_a \\ I_b \\ I_c \\ I_g \end{bmatrix} \tag{7.21}$$

Usually we are interested only in the performance of the phase conductors, and it is more convenient to use a three-conductor equivalent for the transmission line. This is achieved by writing matrix equation (7.21) in partitioned form as follows:

$$\begin{bmatrix} \Delta V_{abc} \\ \Delta V_g \end{bmatrix} \quad \begin{bmatrix} Z_A & Z_B \\ Z_C & Z_D \end{bmatrix} \quad \begin{bmatrix} I_{abc} \\ I_g \end{bmatrix} \tag{7.22}$$

From (7.22)

$$[\Delta V_{abc}] = [Z_A]\,[I_{abc}] + [Z_B]\,[I_g] \tag{7.23}$$

$$[\Delta V_g] = [Z_C]\,[I_{abc}] + [Z_D]\,[I_g] \tag{7.24}$$

From equations (7.23) and (7.24), and assuming that the earth wire is at zero potential,

$$[\Delta V_{abc}] = [Z_{abc}]\,[I_{abc}] \tag{7.25}$$

where

$$[Z_{abc}] = [Z_A] - [Z_B]\,[Z_D]^{-1}[Z_C] = \begin{bmatrix} Z'_{aa-n} & Z'_{ab-n} & Z'_{ac-n} \\ Z'_{ba-n} & Z'_{bb-n} & Z'_{bc-n} \\ Z'_{ca-n} & Z'_{cb-n} & Z'_{cc-n} \end{bmatrix} \tag{7.26}$$

With reference to Figure 7.6(b), the potentials of the line conductors are related to the conductor charges by the matrix equation [12]

$$\begin{bmatrix} V_a \\ V_b \\ V_c \\ V_g \end{bmatrix} = \begin{bmatrix} P_{aa} & P_{ab} & P_{ac} & P_{ag} \\ P_{ba} & P_{bb} & P_{bc} & P_{bg} \\ P_{ca} & P_{cb} & P_{cc} & P_{cg} \\ P_{ga} & P_{gb} & P_{gc} & P_{gg} \end{bmatrix} \begin{bmatrix} Q_a \\ Q_b \\ Q_c \\ Q_g \end{bmatrix} \tag{7.27}$$

considerations as for the series impedance matrix, lead to

$$[V_{abc}] = [P'_{abc}]\,[Q_{abc}] \tag{7.28}$$

where P'_{abc} is a 3×3 matrix which includes the effects of the earth wire. The capacitance matrix of the transmission line of Figure 7.6 is given by

$$[C'_{abc}] = [P'_{abc}]^{-1} = \begin{array}{|c|c|c|} \hline C_{aa} & -C_{ab} & -C_{ac} \\ \hline -C_{ba} & C_{bb} & -C_{bc} \\ \hline -C_{ca} & -C_{cb} & C_{cc} \\ \hline \end{array} \tag{7.29}$$

The series impedance and shunt admittance lumped PI model representation of the three-phase line is shown in Figure 7.7(a) and its matrix equivalent is illustrated in Figure 7.7(b). These two matrices can also be represented by compound admittances [13] (Figure 7.7(c)).

Using the compound component concept, the nodal injected currents of Figure 7.7(c) are related to the nodal voltages by the equation

$$\underset{6\times 1}{\begin{array}{|c|}\hline [I_i] \\ \hline [I_k] \\ \hline \end{array}} = \underset{6\times 6}{\begin{array}{|c|c|}\hline [Z]^{-1} + [Y]/2 & -[Z]^{-1} \\ \hline -[Z]^{-1} & [Z]^{-1} + [Y]/2 \\ \hline \end{array}} \underset{6\times 1}{\begin{array}{|c|}\hline [V_i] \\ \hline [V_k] \\ \hline \end{array}} \tag{7.30}$$

This forms the element admittance matrix representation for the short line between busbars i and k in terms of 3×3 matrix quantities.

7.4.1 Mutually Coupled Three-Phase Lines

When two or more transmission lines occupy the same right of way for a considerable length, the electrostatic and electromagnetic coupling between those lines must be taken into account.

Consider the simplest case of two mutually coupled single-circuit three-phase lines. The two coupled lines are considered to form one subsystem composed of four system busbars. The coupled lines are illustrated in Figure 7.8, where each element is a 3×3 compound admittance and all voltages and currents are 3×1 vectors.

The coupled series elements represent the electromagnetic coupling while the coupled shunt elements represent the capacitive or electrostatic coupling. These coupling parameters are lumped in a similar way to the standard line parameters.

With the admittances labelled as in Figure 7.8, and applying the rules of linear transformation for compound networks, the admittance matrix for the subsystem is

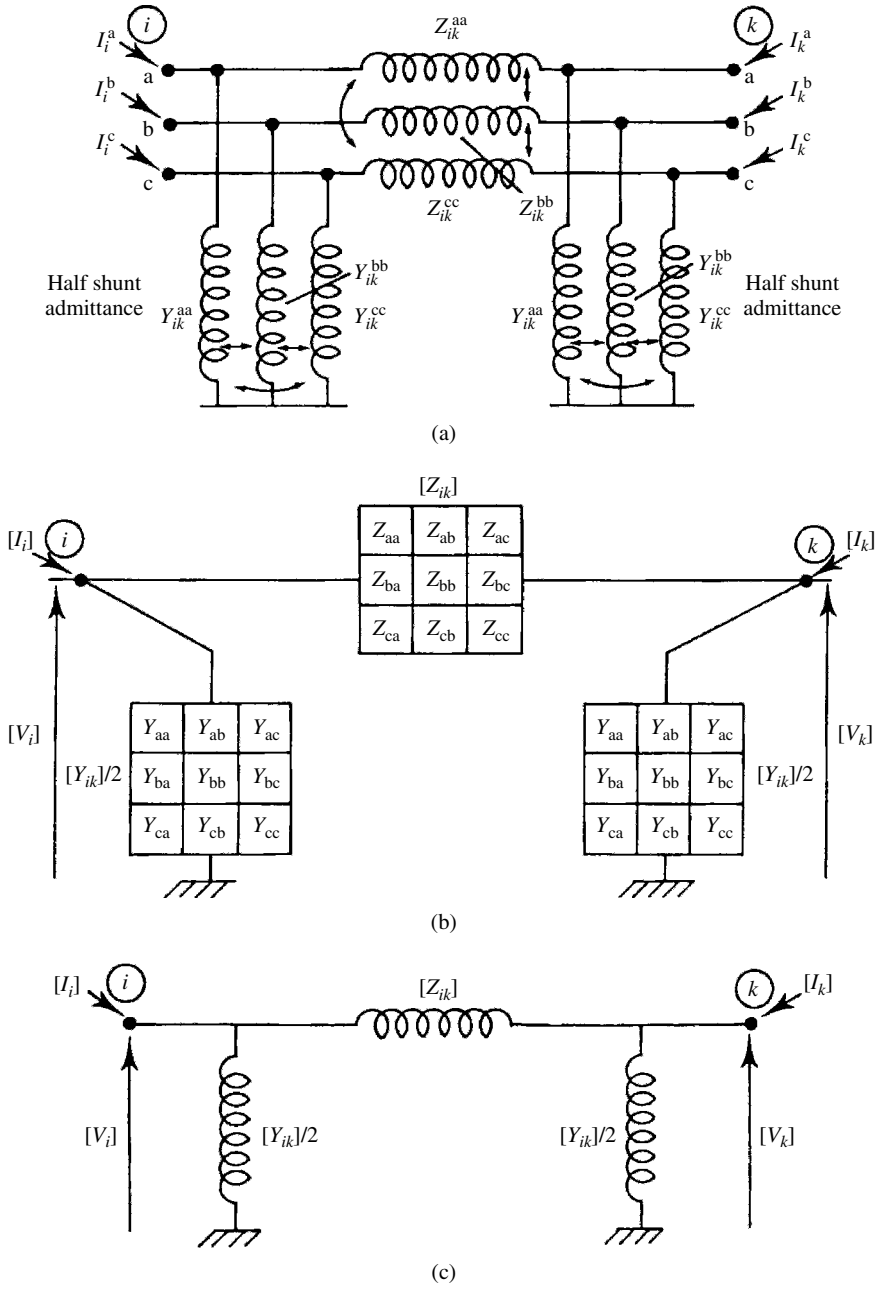


Figure 7.7 Lumped *PI* model of a short three-phase line series impedance: (a) full circuit representation; (b) matrix equivalent; (c) using three-phase compound admittances

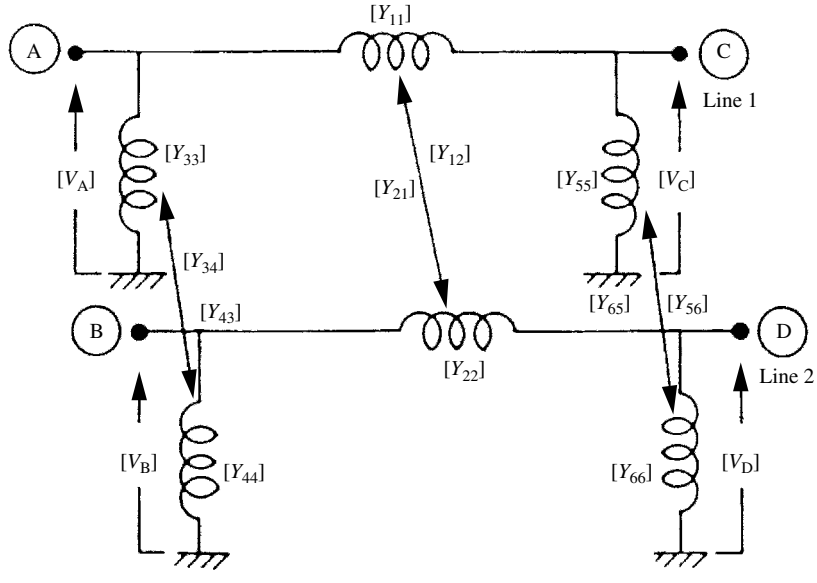


Figure 7.8 Two-coupled three-phase lines

defined as follows:

$$\underset{12\times 1}{\begin{bmatrix} I_A \\ I_B \\ I_C \\ I_D \end{bmatrix}} = \underset{12\times 12}{\begin{bmatrix} Y_{11}+Y_{33} & Y_{12}+Y_{34} & -Y_{11} & -Y_{12} \\ Y_{12}^T+Y_{34}^T & Y_{22}+Y_{44} & -Y_{12}^T & -Y_{22} \\ -Y_{11} & -Y_{12} & Y_{11}+Y_{55} & Y_{12}+Y_{56} \\ -Y_{12}^T & -Y_{22} & Y_{12}^T+Y_{56}^T & Y_{22}+Y_{66} \end{bmatrix}} \cdot \underset{12\times 1}{\begin{bmatrix} V_A \\ V_B \\ V_C \\ V_D \end{bmatrix}} \tag{7.31}$$

It is assumed here that the mutual coupling is bilateral. Therefore $Y_{21} = Y_{12}^T$, etc.

The subsystem may be redrawn as in Figure 7.9. The pairs of coupled 3×3 compound admittances are now represented as a 6×6 compound admittance. The matrix representation is also shown. Following this representation and the labelling of the admittance block in the figure, the admittance matrix may be written in terms of the 6×6 compound coils as

$$\underset{12\times 1}{\begin{bmatrix} \begin{bmatrix} I_A \\ I_B \end{bmatrix} \\ \begin{bmatrix} I_C \\ I_D \end{bmatrix} \end{bmatrix}} = \underset{12\times 12}{\begin{bmatrix} [Z_s]^{-1}+[Y_{s1}] & -[Z_s]^{-1} \\ -[Z_s]^{-1} & [Z_s]^{-1}+[Y_{s2}] \end{bmatrix}} \underset{12\times 1}{\begin{bmatrix} \begin{bmatrix} V_A \\ V_B \end{bmatrix} \\ \begin{bmatrix} V_C \\ V_D \end{bmatrix} \end{bmatrix}} \tag{7.32}$$

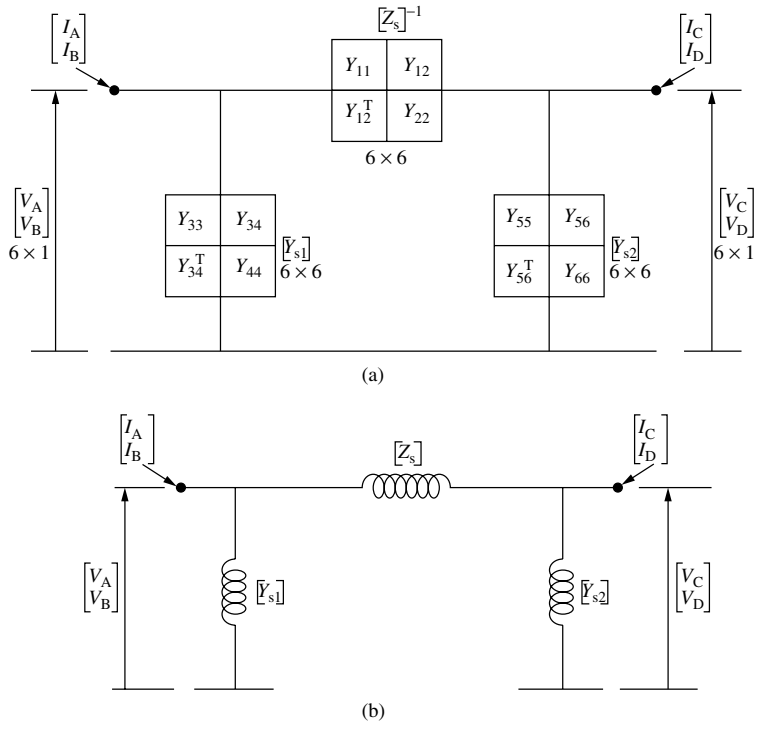


Figure 7.9 A 6×6 compound admittance representation of two coupled three-phase lines: (a) 6×6 matrix representation; (b) 6×6 compound admittance representation

This is clearly identical to equation (7.31) with the appropriate matrix partitioning.

The representation of Figure 7.9 is more concise and the formation of equation (7.32) from this representation is straightforward, being exactly similar to that which results from the use of 3×3 compound admittances for the normal single three-phase line.

The data which must be available, to enable coupled lines to be treated in a similar manner to single lines, is the series impedance and shunt admittance matrices. These matrices are of order 3×3 for a single line, 6×6 for two coupled lines, 9×9 for three and 12×12 for four coupled lines.

Once the matrices $[Z_s]$ and $[Y_s]$ are available, the admittance matrix for the subsystem is formed by application of equation (7.32).

When all the busbars of the coupled lines are distinct, the subsystem may be combined directly into the system admittance matrix. However, if the busbars are not distinct then the admittance matrix as derived from equation (7.32) must be modified. This is considered in the following section.

7.4.2 Consideration of Terminal Connections

The admittance matrix as derived above must be reduced if there are different elements in the subsystem connected to the same busbar. As an example, consider two parallel transmission lines as illustrated in Figure 7.10.

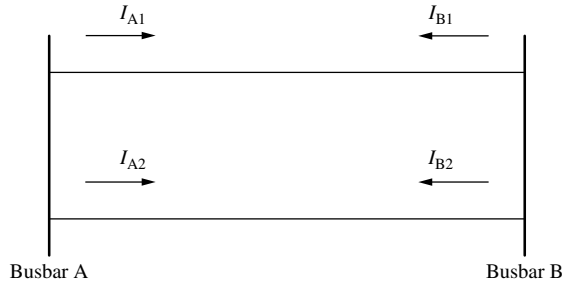


Figure 7.10 Mutually coupled parallel transmission lines

The admittance matrix derived previously related the currents and voltages at the four busbars A1, A2, B1 and B2. This relationship is given by

$$\begin{bmatrix} I_{A1} \\ I_{A2} \\ I_{B1} \\ I_{B2} \end{bmatrix} = \begin{bmatrix} [Y_{A1A2B1B2}] \end{bmatrix} \begin{bmatrix} V_{A1} \\ V_{A2} \\ V_{B1} \\ V_{B2} \end{bmatrix} \tag{7.33}$$

The nodal injected currents at busbars A and B are given by

$$I_A = I_{A1} + I_{A2} \tag{7.34a}$$

$$I_B = I_{B1} + I_{B2} \tag{7.34b}$$

Also, from inspection of Figure 7.10

$$V_A = V_{A1} = V_{A2} \tag{7.35a}$$

$$V_B = V_{B1} = V_{B2} \tag{7.35b}$$

The required matrix equation relates the nodal injected currents, I_A and I_B, to the voltages at these busbars. This is readily derived from equation (7.33) and the conditions specified above. It is simply a matter of adding appropriate rows and columns, and yields

$$\begin{bmatrix} I_A \\ I_B \end{bmatrix} = \begin{bmatrix} [Y_{AB}] \end{bmatrix} \begin{bmatrix} V_A \\ V_B \end{bmatrix} \tag{7.36}$$

where $[Y_{AB}]$ is the required nodal admittance matrix for the subsystem.

It should be noted that the matrix in equation (7.33) must be retained, as it is needed for the calculation of the individual line currents.

7.4.3 Equivalent PI Model

For long lines a number of nominal PI models are connected in series to improve the accuracy of voltages and currents, which are affected by standing wave effects.

For example, a three-section PI model provides an accuracy to 1.2% for a quarter wavelength line (a quarter wavelength corresponds to 1500 km and 1250 km at 50 Hz and 60 Hz, respectively).

As the frequency increases, the number of nominal PI sections to maintain a particular accuracy increases proportionally, e.g. a 300 km line requires 30 nominal PI sections to maintain the 1.2% accuracy for the 50th harmonic. However, near resonance the accuracy departs significantly from an acceptable value.

The computational effort can be greatly reduced and the accuracy improved with the use of an equivalent PI model derived from the solution of the second-order linear differential equations describing wave propagation along transmission lines [14]. These are:

$$\frac{\mathrm{d}^2 V(x)}{\mathrm{d}x^2} = Z'Y'V(x) \tag{7.37a}$$

$$\frac{\mathrm{d}^2 I(x)}{\mathrm{d}x^2} = Z'Y'I(x), \tag{7.37b}$$

where

$Z' = r + j2\pi fL$ is the series impedance per unit length and $Y' = g + j2\pi fC$ is the shunt admittance per unit length

The solution of the wave equations at a distance x from the sending end of the line is

$$V(x) = \exp(-\gamma.x)V_\mathrm{i} + \exp(\gamma.x)V_\mathrm{r} \tag{7.38}$$

$$I(x) = (Z')^{-1}\gamma[\exp(-\gamma.x)V_\mathrm{i} - \exp(\gamma.x)V_\mathrm{r}] \tag{7.39}$$

where $\gamma = \sqrt{Z'Y'} = \alpha + j\beta$ is the propagation constant, and V_i and V_r are the forward and reverse travelling voltages, respectively.

Depending on the problem in hand, e.g. if the evaluation of terminal quantities only is required, it is more convenient to formulate a solution using two-port matrix equations. This leads to the equivalent PI model, shown in Figure 7.11, where

$$Z = Z_0 \sinh(\gamma.l) \tag{7.40}$$

$$Y_1 = Y_2 = \frac{1}{Z_0}\frac{\cosh(\gamma.l) - 1}{\sinh(\gamma.l)} = \frac{1}{Z_0}\tanh\frac{(\gamma.l)}{2} \tag{7.41}$$

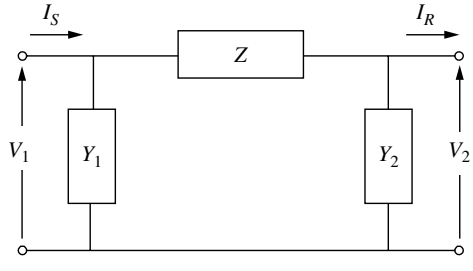


Figure 7.11 The equivalent PI model of a long transmission line

and

$$Z_0 = \sqrt{Z'/Y'} \tag{7.42}$$

is the characteristic impedance of the line.

To illustrate the characteristics of the impedances in Figure 7.11, these are plotted against frequency in Figure 7.12 for a 220 kV, 230 km line. The parameters of the line were calculated using geometric mean distances and three equal length transposition sections. The shunt resistance and shunt reactance are formed by inverting the shunt admittance.

The series and shunt reactances are the predominant components and both have a period of 1300 Hz for the test line. The line length of 230 km corresponds with one wavelength at this frequency. The series reactance increases from its inductive 50 Hz value up to a maximum at 325 Hz (the quarter wavelength frequency) and then decreases, passing through zero at 650 Hz (the half wavelength frequency). Between the half and full wavelength frequencies the series reactance is capacitive. By contrast, the shunt reactance is capacitive and large at fundamental frequency, reducing in magnitude to zero at the half wavelength frequency. Beyond this it becomes inductive.

The series resistance is small at audio frequencies. This is to be expected in a system designed to transmit power at fundamental frequency with minimum losses. Also, the peak magnitudes increase slowly as frequency increases. Since the series resistance does not get appreciably larger over the audio frequency range, the attenuation does not increase significantly. Thus, currents with frequencies in this range will propagate large distances on the power system. The negative resistances are a mathematical artifice and are not physically measurable. However they give the correct terminal conditions for a distributed parameter transmission line.

The shunt resistance, which is normally considered to be zero in a nominal PI model, has considerable effect at resonant frequencies and, as can be observed from Figure 7.12, becomes very large as the wavelength frequency is approached.

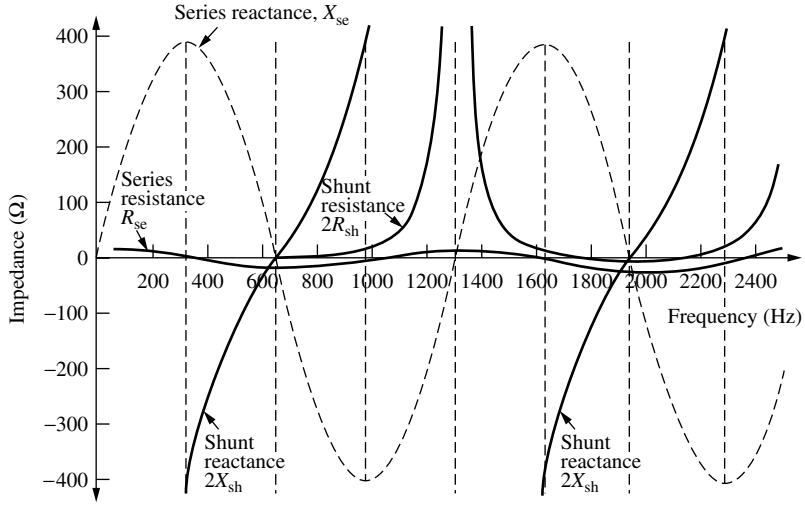


Figure 7.12 Impedance versus frequency for the equivalent PI model (skin effect included)

The impedance variation of a transmission line at resonance is similar to the case of a series and parallel resonating tuned circuit. In Figure 7.12 the series and shunt reactances are equal in magnitude but of opposite sign at 325 Hz, i.e. there is a series resonance (or node) with a low purely resistive impedance. This effect is better illustrated in Figure 7.13, where the impedance of the open circuited line is plotted. In this case the low impedance magnitude (series resonance) only contains the series and shunt resistances and occurs at the odd quarter wavelength frequencies.

At 650 Hz, although both the series and shunt reactances are small, the transmission line has a high impedance equivalent to a parallel resonating tuned circuit. This condition is called an antinode and can also be observed in Figure 7.13. The parallel resonances occur at the half wavelength frequencies.

Low impedance at the odd quarter wavelength frequencies and large impedance at the half wavelength frequencies indicate the low level of attenuation of the audio frequency signals. The addition of other system components such as loads and generators must provide the harmonic damping.

The asymptotes of Figure 7.13 are calculated from knowledge of the total series impedance, Z, and shunt admittance, Y, of the line [14]. The propagation constant γ is

$$\gamma = \sqrt{(ZY)} = \alpha + j\beta \tag{7.43}$$

where α is the attenuation constant and β is the phase constant. The characteristic impedance Z_0 is

$$Z_0 = \sqrt{(Z/Y)}$$

The upper asymptote or maximum impedance is

$$Z_0 \coth \alpha l$$

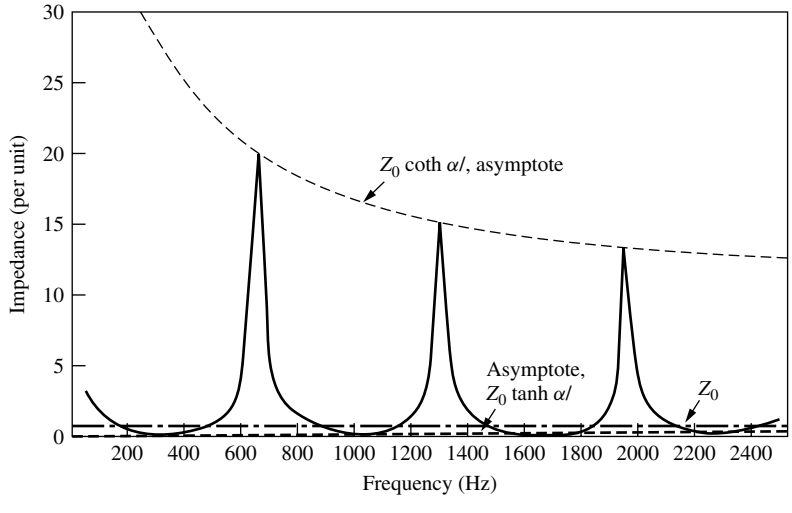


Figure 7.13 Impedance versus frequency for the open circuited Islington to Kikiwa transmission line (skin effect included)

and the lower asymptote or minimum impedance is

$$Z_0 \tanh \alpha l$$

The lower asymptote is small in value and slowly increases with frequency, while the upper asymptote decreases from an infinite value as frequency increases. For large frequencies these two asymptotes approach a value equal to the characteristic impedance.

In the case of multiconductor transmission lines, the nominal PI series impedance and shunt admittance matrices per unit distance, $[Z']$ and $[Y']$ respectively, are square and their size is fixed by the number of mutually coupled conductors.

The derivation of the equivalent PI model for harmonic penetration studies from the nominal PI matrices is similar to that of the single-phase lines, except that it involves the evaluation of hyperbolic functions of the propagation constant, which is now a matrix

$$[\gamma] = ([Z'] \, [Y'])^{1/2} \tag{7.44}$$

There is no direct way of calculating sinh or tanh of a matrix, thus a method using eigenvalues and eigenvectors, called *modal analysis*, is employed [15] that leads to the following expressions for the series and shunt components of the equivalent PI circuit [16]:

$$[Z]_{\text{EPM}} = l[Z'] \, [M] \left[\frac{\sinh \gamma l}{\gamma l} \right] [M]^{-1} \tag{7.45}$$

where l is the transmission line length, $[Z]_{\text{EPM}}$ is the equivalent PI series impedance matrix, $[M]$ is the matrix of normalised eigenvectors,

$$\left[\frac{\sinh \gamma l}{\gamma l} \right] = \begin{bmatrix} \dfrac{\sinh \gamma_1 l}{\gamma_1 l} & 0 & \cdots & 0 \\ 0 & \dfrac{\sinh \gamma_2 l}{\gamma_2 l} & \cdots & 0 \\ \vdots & \vdots & \vdots & \\ 0 & 0 & \dfrac{\sinh \gamma_j l}{\gamma_j l} & \end{bmatrix} \tag{7.46}$$

and γ_j is the jth eigenvalue for $j/3$ mutually coupled circuits. Similarly

$$\frac{1}{2}[Y]_{\text{EPM}} = \frac{1}{2} l[M] \left[\frac{\tanh(\gamma l/2)}{\gamma l/2} \right] [M]^{-1} [Y'] \tag{7.47}$$

where $[Y]_{\text{EPM}}$ is the equivalent PI shunt admittance matrix.

Computer derivation of the correction factors for conversion from the nominal PI to the equivalent PI model, and their incorporation into the series impedance and shunt admittance matrices, is carried out as indicated in the structure diagram of Figure 7.14. The LR2 algorithm of Wilkinson and Reinsch [17] is used with due regard for accurate calculations in the derivation of the eigenvalues and eigenvectors.

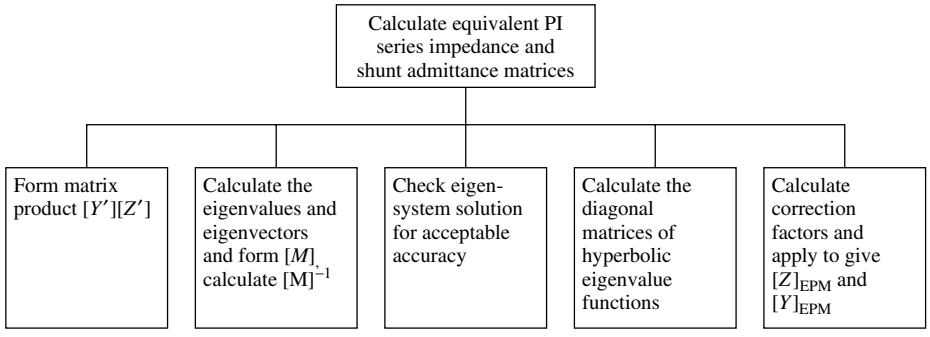

Calculate equivalent PI series impedance and shunt admittance matrices
Form matrix product [Y′][Z′]
Calculate the eigenvalues and eigenvectors and form [M], calculate [M]−1
Check eigen-system solution for acceptable accuracy
Calculate the diagonal matrices of hyperbolic eigenvalue functions
Calculate correction factors and apply to give [Z]EPM and [Y]EPM

Figure 7.14 Structure diagram for calculation of the equivalent PI model

7.4.4 Evaluation of Transmission Line Parameters

The lumped series impedance matrix $[Z]$ of a transmission line consists of three components, while the shunt admittance matrix $[Y]$ contains one.

$$[Z] = [Z_e] + [Z_g] + [Z_c] \tag{7.48}$$

$$[Y] = [Y_g] \tag{7.49}$$

where $[Z_c]$ is the internal impedance of the conductors $(\Omega \cdot \text{km}^{-1})$, $[Z_g]$ is the impedance due to the physical geometry of the conductor's arrangement $(\Omega \cdot \text{km}^{-1})$, $[Z_e]$ is the earth return path impedance $(\Omega \cdot \text{km}^{-1})$, and $[Y_g]$ is the admittance due to the physical geometry of the conductor $(\Omega^{-1} \cdot \text{km}^{-1})$.

In multiconductor transmission all *primitive matrices* (the admittance matrices of the unconnected branches of the original network components) are symmetric and, therefore, the functions that define the elements need only be evaluated for elements on or above the leading diagonal.

Earth Impedance Matrix $[Z_e]$ The impedance due to the earth path varies with frequency in a nonlinear fashion. The solution of this problem, under idealised conditions, has been given in the form of either an infinite integral or an infinite series [18].

As the need arises to calculate ground impedances for a wide spectrum of frequencies, the tendency is to select simple formulations aiming at a reduction in computing time, while maintaining a reasonable level of accuracy.

Consequently, what was originally a heuristic approach [19] is becoming the more favoured alternative, particularly at high frequencies.

Based on Carson's work, the ground impedance can be concisely expressed as

$$Z_e = 1000 J(r, \theta)(\Omega \cdot \text{km}^{-1}) \tag{7.50}$$

where

$$Z_e \in [Z_e]$$

$$J(r, \theta) = \frac{\omega \mu_a}{\pi}\{P(r, \theta) + jQ(r, \theta)\}$$

$$r_{ij} = \sqrt{\frac{\omega\mu_a}{\rho}} \quad D_{ij}$$

$$D_{ij} = \sqrt{(h_i + h_j)^2 + d^2{}_{ij}} \qquad \text{for } i \neq j$$

$$D_{ij} = 2h_i \qquad \text{for } i = j$$

$$\theta_{ij} = \arctan \frac{d_{ij}}{h_i + h_j} \qquad \text{for } i \neq j$$

$$\theta_{ij} = 0 \qquad \text{for } i = j$$

$\omega = 2\pi f\,(\text{rad} \cdot \text{s}^{-1})$

f is frequency (Hz)

h_i is the height of conductor i (m)

d_{ij} is the horizontal distance between conductors i and j (m)

μ_a is the permeability of free space $= 7\pi \times 10^{-7}(\text{H} \cdot \text{m}^{-1})$

ρ is the earth resistivity $(\Omega \cdot \text{m})$.

Carson's solution to equation (7.50) is defined by eight different infinite series which converge quickly for problems related to transmission line parameter calculation, but the number of required computations increases with frequency and separation of the conductors.

More recent literature has described closed form formulations for the numerical evaluation of line-ground loops, based on the concept of a mirroring surface beneath the earth at a certain depth. The most popular complex penetration model, which has had more appeal is that of C. Dubanton [20], due to its simplicity and high degree of accuracy for the whole frequency span for which Carson's equations are valid.

Dubanton's formulae for the evaluation of the self- and mutual impedances of conductors i and j are

$$Z_{ii} = \frac{j\omega\mu_o}{2\pi} \times \ln \frac{2(h_i + p)}{r_i} \tag{7.51}$$

$$Z_{ij} = \frac{j\omega\mu_o}{2\pi} \times \ln \frac{\sqrt{2(h_i + p)}}{\sqrt{(h_i - h_j)^2 + d^2{}_{ij}}} \tag{7.52}$$

where $p = 1/\sqrt{j\omega\mu_o\sigma}$ is the complex depth below the earth at which the mirroring surface is located.

An alternative and very simple formulation has been proposed [21], which for the purpose of harmonic penetration yields accurate solutions when compared to those obtained using Carson's equations.

Geometrical Impedance Matrix $[Z_g]$ and Admittance Matrix $[Y_g]$ If the conductors and the earth are assumed to be equipotential surfaces, the geometrical impedance can be formulated in terms of potential coefficients theory.

The self-potential coefficient ψ_{ii} for the ith conductor and the mutual potential coefficient ψ_{ij} between the ith and jth conductors are defined as follows:

$$\psi_{ii} = \ln(2h_i / r_i) \tag{7.53}$$

$$\psi_{ij} = \ln(\mathrm{D}_{ij} / d_{ij}) \tag{7.54}$$

where r_i is the radius of the ith conductor (m) while the other variables are as defined earlier.

Potential coefficients depend entirely on the physical arrangement of the conductors and need only be evaluated once.

For practical purposes the air is assumed to have zero conductance and

$$[Z_\mathrm{g}] = j\omega \mathrm{K}'[\psi]\ \Omega/\mathrm{km} \tag{7.55}$$

where $[\psi]$ is a matrix of potential coefficients and $\mathrm{K}' = 2 \times 10^{-4}$.

The lumped shunt admittance parameters [**Y**] are completely defined by the inverse relation of the potential coefficients matrix, i.e.

$$[Y_\mathrm{g}] = 1000 j\omega 2\pi \varepsilon_\mathrm{a} [\psi]^{-1} \tag{7.56}$$

where ε_a is permittivity of free space $= 8.857 \times 10^{-12}$ $(\mathrm{F} \cdot \mathrm{m}^{-1})$.

As $[Z_\mathrm{g}]$ and $[Y_\mathrm{g}]$ are linear functions of frequency, they need only be evaluated once and scaled for other frequencies.

Conductor Impedance Matrix [Z_c] This term accounts for the internal impedance of the conductors. Both resistance and inductance have a nonlinear frequency dependence. Current tends to flow on the surface of the conductor, the *skin effect,* which increases with frequency and needs to be computed at each frequency. An accurate result for a homogeneous nonferrous conductor of annular cross-section involves the evaluation of long equations based on the solution of Bessel functions, as shown in equation (7.57).

$$\mathrm{Z_c} = \frac{j\omega\mu_\mathrm{o}}{2\pi} \frac{1}{x_\mathrm{e}} \frac{\mathrm{J_o}(x_\mathrm{e})\mathrm{N'_o}(x_\mathrm{i}) - \mathrm{N_o}(x_\mathrm{e})\mathrm{J'_o}(x_\mathrm{i})}{\mathrm{J'_o}(x_\mathrm{e})\mathrm{N'_o}(x_\mathrm{i}) - \mathrm{N'_o}(x_\mathrm{e})\mathrm{J'_o}(x_\mathrm{i})} \tag{7.57}$$

where

$x_\mathrm{e} = j\sqrt{j\omega\mu_\mathrm{o}\sigma_\mathrm{c}} r_\mathrm{e}$
$x_\mathrm{i} = j\sqrt{j\omega\mu_\mathrm{o}\sigma_\mathrm{c}} r_\mathrm{i}$
r_e is the external radius of the conductor (m)
r_i is the internal radius of the conductor (m)
$\mathrm{J_o}$ is the Bessel function of the first kind and zero order
$\mathrm{J'_o}$ is the derivative of the Bessel function of the first kind and zero order
$\mathrm{N_o}$ is the Bessel function of the second kind and zero order
$\mathrm{N'_o}$ is the derivative of the Bessel function of the second kind and zero order
σ_c is the conductivity of the conductor material at the average conductor temperature.

The Bessel functions and their derivatives are solved, within a specified accuracy, by means of their associated infinite series. Convergence problems are frequently encountered at high frequencies and low ratios of conductor thickness to external radius i.e. $(r_e - r_i)/r_e$, necessitating the use of asymptotic expansions.

A new closed form solution has been proposed [19] based on the concept of complex penetration; unfortunately errors of up to 6.6% occur in the region of interest.

To overcome the difficulties of slow convergence of the Bessel function approach and the inaccuracy of the complex penetration method at relatively low frequencies, an alternative approach based upon curve fitting to the Bessel function formula has been proposed [21].

For long lines, skin effect resistance (R_{ac}/R_{dc}) ratios and their effect on the resonant voltage magnitudes are important. Because the series resistance of a transmission line is a small component of the series impedance when the transmission line is not at resonance, the harmonic voltages, shown in Figure 7.15, do not change to any significant extent when skin effect is included. At resonance the series resistance and shunt conductance become the dominant system components. Changes in the series resistance magnitude change the voltage peaks but do not affect the resonance frequency.

In Figure 7.15 the voltage calculated with skin effect is, at resonance, 50% higher than without skin effect; these results correspond with an R_{ac}/R_{dc} ratio of 2. In a single-phase model without ground return the ratio of voltages at resonance, with and without skin effect, is the same as the skin effect ratio. In a three-phase model the presence of shunt conductance and series resistance coupling between phases, and the different resonant frequencies of the phases, reduces the resonant peak voltages compared with single-phase modelling.

Skin effect is also taken into account in modelling the earth return as a conductor. The depth of penetration of the earth currents decreases with an increase in frequency or a decrease in earth resistivity. The series inductance decreases as a result of these changes.

As an alternative to the rigorous analysis described above, power companies often use approximations to the skin effect by means of correction factors. Typical corrections in current use by the NGC (UK) and EDF (France) are given in Table 7.1.

Lewis and Tuttle [22] presented a practical method for calculating the skin effect resistance ratio by approximating ACSR (aluminium conductor steel reinforced)

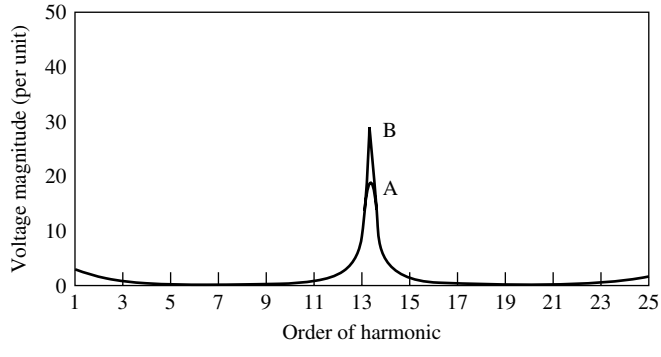


Figure 7.15 The result of modelling: curve A, skin effect included; curve B, no skin effect

Table 7.1 Corrections for skin effect in overhead lines

Company	Voltage (kV)	Harmonic order	Resistance
NGC	400, 275 (based on 0.4 sq.in. steel-core al. conductors)	$h \leq 4.21$	$R_1\left(1+\dfrac{3.45h^2}{192+2.77h^2}\right)$
	132	$4.21 < h \leq 7.76$	$R_1(0.806+0.105h)$
		$h > 7.76$	$R_1(0.267+0.485\sqrt{h})$
			$R_1\left(1+\dfrac{0.6465h^2}{192+0518h^2}\right)$
EDF	400, 225	$h \leq 4$	$R_1\left(1+\dfrac{3.45h^2}{192+2.77h^2}\right)$
		$4 < h < 8$	$R_1(0.864-0.024\sqrt{h}+0.105h)$
		$8 < h$	$R_1(0.267+0.485\sqrt{h})$
	150, 90		$R_1\left(1+\dfrac{0.646h^2}{192+0.518h^2}\right)$

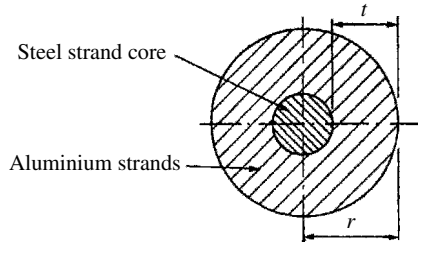


Figure 7.16 ACSR hollow tube conductor representation

conductors to uniform tubes having the same inside and outside diameters as the aluminium conductors (Figure 7.16). Figure 7.17 illustrates the skin effect ratio for different models and various tube ratios for ACSR conductors. Skin effect modelling is important for long lines. Although the series resistance of a transmission line is typically a small component of the series impedance, it dominates its value at resonances.

7.5 Underground and Submarine Cables [23]

A unified solution similar to that of overhead transmission is difficult for underground cables because of the great variety in their construction and layouts.

The cross-section of a cable, although extremely complex, can be simplified to that of Figure 7.18 and its series per unit length harmonic impedance is calculated by the

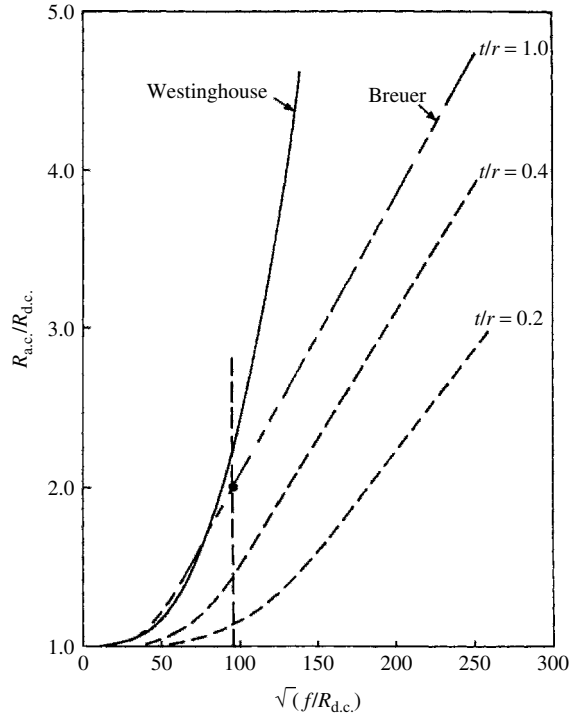


Figure 7.17 Skin effect resistance for different models

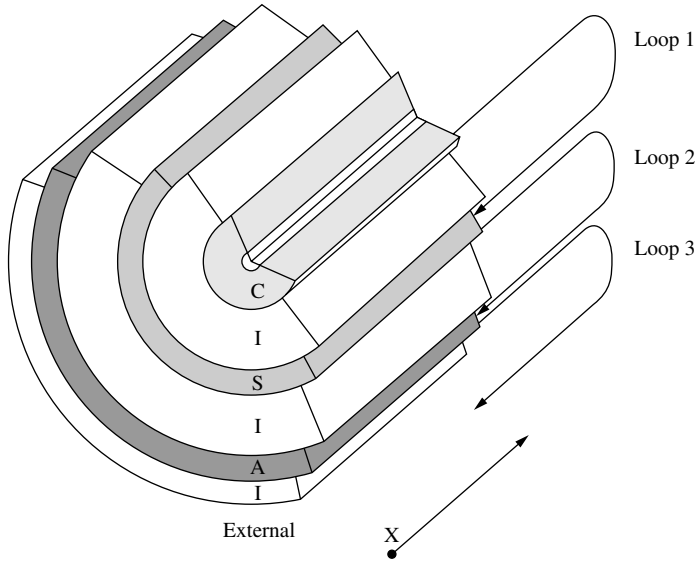


Figure 7.18 Cable cross-section

following set of loop equations.

$$-\begin{bmatrix} dV_1/dx \\ dV_2/dx \\ dV_3/dx \end{bmatrix} = \begin{bmatrix} Z'_{11} & Z'_{12} & 0 \\ Z'_{21} & Z'_{22} & Z'_{23} \\ 0 & Z'_{32} & Z'_{33} \end{bmatrix} \begin{bmatrix} I_1 \\ I_2 \\ I_3 \end{bmatrix} \tag{7.58}$$

where Z'_{11} is the sum of the following three component impedances:

$Z'_{\text{core-outside}}$: internal impedance of the core with the return path outside the core

$Z'_{\text{core-insulation}}$: impedance of the insulation surrounding the core

$Z'_{\text{sheath-inside}}$: internal impedance of the sheath with the return path inside the sheath.

Similarly

$$Z'_{22} = Z'_{\text{sheath-outside}} + Z'_{\text{sheath/armour-insulation}} + Z'_{\text{armour-inside}} \tag{7.59}$$

and

$$Z'_{33} = Z'_{\text{armour-outside}} + Z'_{\text{armour/earth-insulation}} + Z'_{\text{earth-inside}} \tag{7.60}$$

The coupling impedances $Z'_{12} = Z'_{21}$ and $Z'_{23} = Z'_{32}$ are negative because of opposing current directions (I_2 in negative direction in loop 1, and I_3 in negative direction in loop 2), i.e.

$$Z'_{12} = Z'_{21} = -Z'_{\text{sheath-mutual}} \tag{7.61}$$

$$Z'_{23} = Z'_{32} = -Z'_{\text{armour-mutual}} \tag{7.62}$$

where

$Z'_{\text{sheath-mutual}}$: mutual impedance (per unit length) of the tubular sheath between inside loop 1 and the outside loop 2

$Z'_{\text{armour-mutual}}$: mutual impedance (per unit length) of the tubular armour between the inside loop 2 and the outside loop 3

Finally, $Z'_{13} = Z'_{31} = 0$ because loop 1 and loop 3 have no common branch.

The impedances of the insulation are given by

$$Z'_{\text{insulation}} = j\omega \frac{\mu}{2\pi} \ln \frac{r_{\text{outside}}}{r_{\text{inside}}} \quad \text{in } \Omega/m \tag{7.63}$$

where μ is the permeability of insulation in H/m, r_{outside} is the outside radius of insulation and r_{inside} is the inside radius of insulation.

If there is no insulation between the armour and earth, then Z' insulation $= 0$.

The internal impedances and the mutual impedance of a tubular conductor are a function of frequency, and can be derived from Bessel and Kelvin functions.

$$Z'_{\text{tube-inside}} = \frac{\sqrt{j}.\omega.\mu}{2\pi.mq.D}[I_o(\sqrt{j}mq)K_1(\sqrt{j}mr) + K_o(\sqrt{j}mq)I_1(\sqrt{j}mr)] \tag{7.64}$$

$$Z'_{\text{tube-outside}} = \frac{\sqrt{j}.\omega.\mu}{2\pi.mr.D}[I_o(\sqrt{j}mr)K_1(\sqrt{j}mq) + K_o(\sqrt{j}mr)I_1(\sqrt{j}mq)] \tag{7.65}$$

$$Z'_{\text{tube-mutual}} = \frac{\omega.\mu}{2\pi.mq.mr.D} \tag{7.66}$$

with

$$D = I_1(\sqrt{j}mr)K_1(\sqrt{j}mq) - I_1(\sqrt{j}mq)K_1(\sqrt{j}mr) \tag{7.67}$$

where

$$mr = \sqrt{K\frac{1}{1-s^2}} \tag{7.68}$$

$$mq = \sqrt{K\frac{s^2}{1-s^2}} \tag{7.69}$$

with

$$K = \frac{8\pi.10^{-4}.f.\mu_r}{R'_{\text{dc}}} \tag{7.70}$$

$$s = \frac{q}{r} \tag{7.71}$$

where q is the inside radius, r is the outside radius and R'_{dc} is the d.c. resistance in Ω/Km.

The only remaining term is $Z'_{\text{earth-inside}}$ in equation (7.60), which is the earth return impedance for underground cables, or the sea return impedance for submarine cables. The earth return impedance can be calculated approximately with equation (7.64) by letting the outside radius go to infinity. This approach, also used by Bianchi and Luoni [24] to find the sea return impedance, is quite acceptable considering the fact that sea resistivity and other input parameters are not known accurately.

Equation (7.58) is not in a form compatible with the solution used for overhead conductors, where the voltages with respect to local ground and the actual currents in the conductors are used as variables. Equation (7.58) can easily be brought into such a form by introducing the appropriate terminal conditions, namely with

$$\begin{aligned} V_1 &= V_{\text{core}} - V_{\text{sheath}} & I_1 &= I_{\text{core}} \\ V_2 &= V_{\text{sheath}} - V_{\text{armour}} & I_2 &= I_{\text{core}} + I_{\text{sheath}} \\ V_3 &= V_{\text{armour}} & I_3 &= I_{\text{core}} + I_{\text{sheath}} + I_{\text{armour}} \end{aligned}$$

Equation (7.58) can be rewritten as

$$-\begin{bmatrix} dV_{\text{core}}/dx \\ dV_{\text{sheath}}/dx \\ dV_{\text{armour}}/dx \end{bmatrix} = \begin{bmatrix} Z'_{\text{cc}} & Z'_{\text{cs}} & Z'_{\text{ca}} \\ Z'_{\text{sc}} & Z'_{\text{ss}} & Z'_{\text{sa}} \\ Z'_{\text{ac}} & Z'_{\text{as}} & Z'_{\text{aa}} \end{bmatrix} \begin{bmatrix} I_{\text{core}} \\ I_{\text{sheath}} \\ I_{\text{armour}} \end{bmatrix} \tag{7.72}$$

where

$$
\begin{aligned}
Z'_{cc} &= Z'_{11} + 2Z'_{12} + Z'_{22} + 2Z'_{23} + Z'_{33} \\
Z'_{cs} &= Z'_{sc} = Z'_{12} + Z'_{22} + 2Z'_{23} + Z'_{33} \\
Z'_{ca} &= Z'_{ac} = Z'_{sa} = Z'_{as} = Z'_{23} + Z'_{33} \\
Z'_{ss} &= Z'_{22} + 2Z'_{23} + Z'_{33} \\
Z'_{aa} &= Z'_{33}
\end{aligned}
$$

Because a good approximation for many cables having bonding between the sheath and the armour, and the armour earthed to the sea, is $V_{\text{sheath}} = V_{\text{armour}} = 0$, the system can be reduced to

$$-\mathrm{d}V_{\text{core}}/\mathrm{d}x = ZI_{\text{core}} \tag{7.73}$$

where Z is a reduction of the impedance matrix of equation (7.72).

Similarly, for each cable the per unit length harmonic admittance is

$$-\begin{bmatrix} \mathrm{d}I_1/\mathrm{d}x \\ \mathrm{d}I_2/\mathrm{d}x \\ \mathrm{d}I_3/\mathrm{d}x \end{bmatrix} = \begin{bmatrix} j\omega C'_1 & 0 & 0 \\ 0 & j\omega C'_2 & 0 \\ 0 & 0 & j\omega C'_3 \end{bmatrix} \begin{bmatrix} V_1 \\ V_2 \\ V_3 \end{bmatrix} \tag{7.74}$$

where $C'_i = 2\pi\varepsilon_o\varepsilon_r / l_n(r/q)$. Therefore, when converted to core, sheath and armour quantities,

$$-\begin{bmatrix} \mathrm{d}I_{\text{core}}/\mathrm{d}x \\ \mathrm{d}I_{\text{sheath}}/\mathrm{d}x \\ \mathrm{d}I_{\text{armour}}/\mathrm{d}x \end{bmatrix} = \begin{bmatrix} Y'_1 & -Y'_1 & 0 \\ -Y'_1 & Y' + Y'_2 & -Y'_2 \\ 0 & -Y'_2 & Y'_2 + Y'_3 \end{bmatrix} \begin{bmatrix} V_{\text{core}} \\ V_{\text{sheath}} \\ V_{\text{armour}} \end{bmatrix} \tag{7.75}$$

where $Y'_i = j\omega l_i$. If, as before, $V_{\text{sheath}} = V_{\text{armour}} = 0$, equation (7.75) reduces to

$$-\mathrm{d}I_{\text{core}}\mathrm{d}x = Y'_1 V_{\text{core}} \tag{7.76}$$

Therefore, for frequencies of interest, the cable per unit length harmonic impedance, Z', and admittance, Y', are calculated with both the zero- and positive-sequence values being equal to the Z in equation (7.73), and the Y' in equation (7.76), respectively.

In the absence of rigorous computer models, such as described above, power companies often use approximations to the skin effect by means of correction factors. Typical corrections used by the NGC (UK) and EDF (France) are given in Table 7.2.

7.6 Three-Phase Transformer Models

The basic three-phase two-winding transformer is shown in Figure 7.19. Its primitive network, on the assumption that the flux paths are symmetrically distributed between

Table 7.2 Corrections for skin effect in cables

Company	Voltage (kV)	Harmonic order	Resistance
NGC	400, 275 (based on 2.5 sq.in. conductor at 5 in. spacing between centres)	$h \geq 1.5$	$0.74\ R_1\ (0.267 + 1.073\sqrt{h})$
	132	$h \geq 2.35$	$R_1\ (0.187 + 0.532\sqrt{h})$
EDF	400, 225	$h \geq 2$	$0.74\ R_1\ (0.267 + 1.073\sqrt{h})$
	150, 90	$h \geq 2$	$R_1\ (0.187 + 0.532\sqrt{h})$

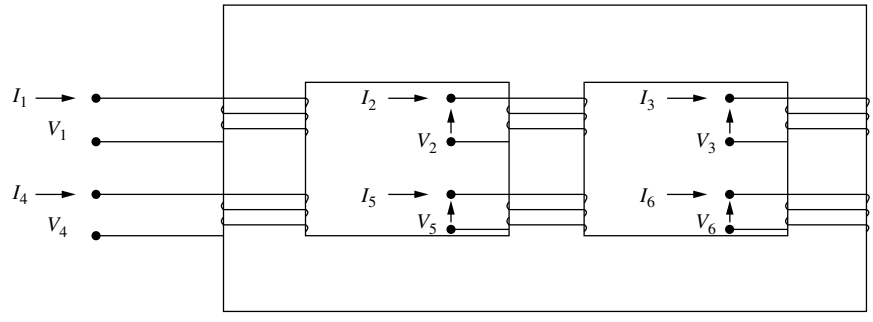


Figure 7.19 Diagrammatic representation of a two-winding transformer

all windings, is represented by the equation

$$\begin{bmatrix} I_1 \\ I_2 \\ I_3 \\ I_4 \\ I_5 \\ I_6 \end{bmatrix} = \begin{bmatrix} y_p & y'_m & y'_m & -y_m & y''_m & y''_m \\ y'_m & y_p & y'_m & y''_m & -y_m & y''_m \\ y'_m & y'_m & y_p & y''_m & y''_m & -y_m \\ -y_m & y''_m & y''_m & y_s & y'''_m & y'''_m \\ y''_m & -y_m & y''_m & y'''_m & y_s & y'''_m \\ y''_m & y''_m & -y_m & y'''_m & y'''_m & y_s \end{bmatrix} \begin{bmatrix} V_1 \\ V_2 \\ V_3 \\ V_4 \\ V_5 \\ V_6 \end{bmatrix} \tag{7.77}$$

where y'_m is the mutual admittance between primary coils, y''_m is the mutual admittance between primary and secondary coils on different cores, and y'''_m is the mutual admittance between secondary coils.

If a tertiary winding is also present, the primitive network consists of nine (instead of six) coupled coils and its mathematical model will be a 9×9 admittance matrix.

The interphase coupling can usually be ignored (e.g. the case of three single-phase separate units) and all the primed terms are effectively zero.

The connection matrix $[C]$ between the primitive network and the actual transformer buses is derived from the transformer connection.

By way of example, consider the Wye G-Delta connection of Figure 7.20. The following connection matrix applies:

$$\begin{bmatrix} V_1 \\ V_2 \\ V_3 \\ V_4 \\ V_5 \\ V_6 \end{bmatrix} = \begin{bmatrix} 1 & 0 & 0 & 0 & 0 & 0 \\ 0 & 1 & 0 & 0 & 0 & 0 \\ 0 & 0 & 1 & 0 & 0 & 0 \\ 0 & 0 & 0 & 1 & -1 & 0 \\ 0 & 0 & 0 & 0 & 1 & -1 \\ 0 & 0 & 0 & -1 & 0 & 1 \end{bmatrix} \begin{bmatrix} V_p^a \\ V_p^b \\ V_p^c \\ V_s^A \\ V_s^B \\ V_s^C \end{bmatrix} \tag{7.78}$$

or

$$[V]_{\text{Branch}} = [C]\,[V]_{\text{node}} \tag{7.79}$$

We can also write

$$[Y]_{\text{NODE}} = [C]^{\text{T}}[Y]_{\text{PRIM}}[C] \tag{7.80}$$

and using $[Y]_{\text{PRIM}}$ from equation (7.77)

$[Y]_{\text{NODE}} =$

y_p	y'_m	y'_m	$-(y_m + y''_m)$	$(y_m + y''_m)$	0	A
y'_m	y_p	y'_m	0	$-(y_m + y''_m)$	$(y_m + y''_m)$	B
y'_m	y'_m	y_p	$(y_m + y''_m)$	0	$-(y_m + y''_m)$	C
$-(y_m + y''_m)$	0	$(y_m + y''_m)$	$2(y_s - y'''_m)$	$-(y_s - y'''_m)$	$-(y_s - y'''_m)$	A
$(y_m + y''_m)$	$-(y_m + y''_m)$	0	$-(y_s - y'''_m)$	$2(y_s - y'''_m)$	$-(y_s - y'''_m)$	B
0	$(y_m + y''_m)$	$-(y_m + y''_m)$	$-(y_s - y'''_m)$	$-(y_s - y'''_m)$	$2(y_s - y'''_m)$	C

(7.81)

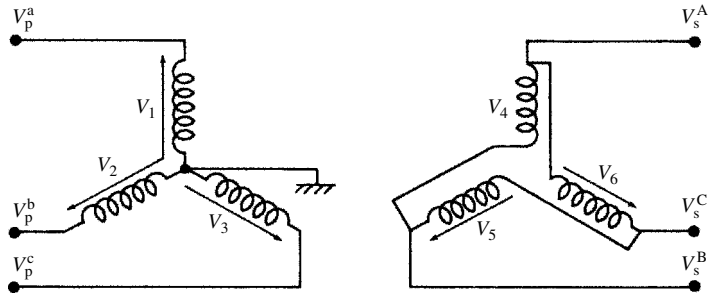


Figure 7.20 Network connection diagram for a Wye G-delta transformer

If the primitive admittances are expressed in per unit the upper-right and lower-left quadrants of matrix (7.81) must be divided by $\sqrt{3}$ and the lower-right quadrant by 3. Then, in the absence of interphase coupling, the nodal admittance matrix equation of the Wye G-delta connection becomes

$$\begin{bmatrix} I_p^a \\ I_p^b \\ I_p^c \\ I_s^A \\ I_s^B \\ I_s^C \end{bmatrix} = \begin{bmatrix} y & & & -y/\sqrt{3} & y/\sqrt{3} & \\ & y & & & -y/\sqrt{3} & y/\sqrt{3} \\ & & y & y/\sqrt{3} & & -y/\sqrt{3} \\ -y/\sqrt{3} & & y/\sqrt{3} & 2/3y & -1/3y & -1/3y \\ y/\sqrt{3} & -y/\sqrt{3} & & -1/3y & 2/3y & -1/3y \\ & y/\sqrt{3} & -y/\sqrt{3} & -1/3y & -1/3y & 2/3y \end{bmatrix} \begin{bmatrix} V_p^a \\ V_p^b \\ V_p^c \\ V_s^A \\ V_s^B \\ V_s^C \end{bmatrix} \tag{7.82}$$

where y is the transformer leakage admittance in per unit, which is approximated by

$$Y_{th} = \frac{1}{R\sqrt{h} + jX_1 h} \tag{7.83}$$

where R is the resistance at fundamental frequency and X_l is the transformer's leakage reactance.

An example of a typical variation of the inductive coefficient of a transformer with frequency is shown in Figure 7.21.

The magnetising admittance is usually ignored since under normal operating conditions its contribution is not significant. If, however, the transformer is under severe saturation, appropriate current harmonic sources must be added at the transformer terminals.

In general, any two-winding three-phase transformer may be represented by two coupled compound coils as shown in Figure 7.22 where $[Y_{sp}] = [Y_{ps}]^T$.

If the parameters of the three phases are assumed balanced, all the common three-phase connections can be modelled by three basic submatrices. The submatrices $[Y_{pp}]$, $[Y_{ps}]$, etc. are given in Table 7.3 for the common connections in terms of the following matrices:

$$Y_1 = \begin{bmatrix} y_t & & \\ & y_t & \\ & & y_t \end{bmatrix} \quad Y_{11} = \begin{bmatrix} 2y_t & -y_t & -y_t \\ -y_t & 2y_t & -y_t \\ -y_t & -y_t & 2y_t \end{bmatrix} \quad Y_{111} = \begin{bmatrix} -y_t & y_t & \\ & -y_t & y_t \\ y_t & & -y_t \end{bmatrix}$$

For transformers with neutrals connected through an impedance, an extra coil is added to the primitive network for each unearthed neutral and the primitive admittance increases in dimension. However, by noting that the injected current in the neutral is

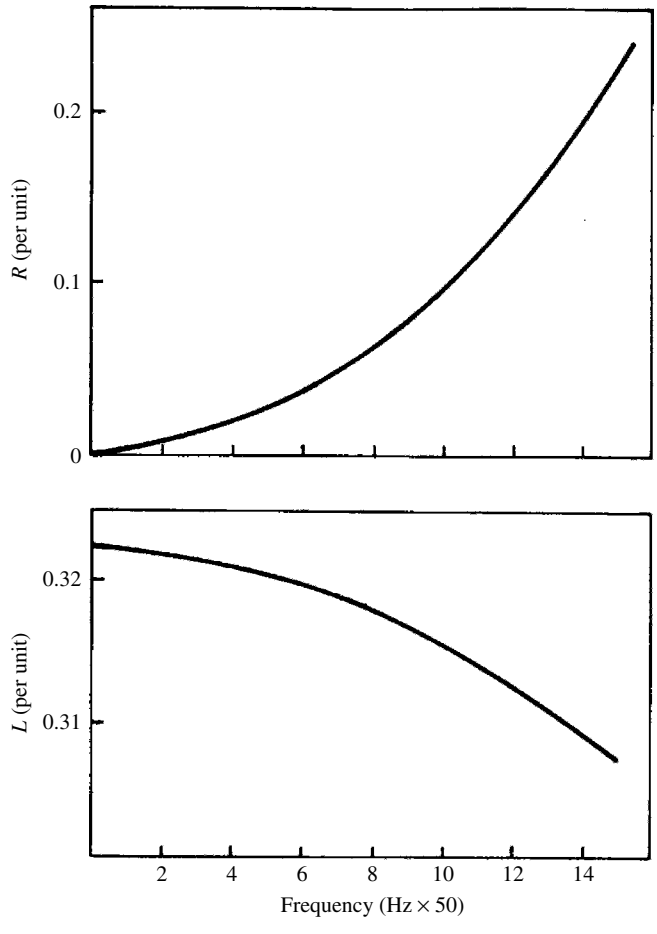


Figure 7.21 Transformer parameter frequency dependency

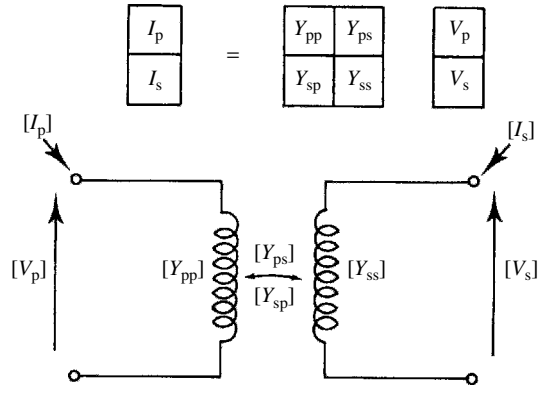


Figure 7.22 Two-winding three-phase transformer

Table 7.3 Characteristic submatrices used in forming the transformer admittance matrices

Transformer connection		Self-admittance		Mutual admittance
Bus P	Bus S	Y_{pp}	Y_{ss}	Y_{ps}, Y_{sp}
Wye G	Wye G	Y_1	Y_1	$-Y_1$
Wye G	Wye	Y_1	$Y_{11/3}$	$-Y_{11/3}$
Wye G	Delta	Y_1	Y_{11}	Y_{111}
Wye	Wye	$Y_{11/3}$	$Y_{11/3}$	$-Y_{11/3}$
Wye	Delta	$Y_{11/3}$	Y_{11}	Y_{111}
Delta	Delta	Y_{11}	Y_{11}	$-Y_{11}$

zero (no direct connection), these extra terms can be eliminated from the connected network admittance matrix. This results in the matrix:

$$Y = \begin{array}{|c|c|c|} \hline y_t - c & -c & -c \\ \hline -c & y_t - c & -c \\ \hline -c & -c & y_t - c \\ \hline \end{array} \quad \text{where } c = y_t.y_t/(3.y_t + y_n)$$

Once the admittance matrix has been formed for a particular connection it represents a simple subsystem composed of the two busbars interconnected by the transformer.

7.7 Generator Modelling

For the purpose of determining the network harmonic admittances, the generators can be modelled as a series combination of resistance and inductive reactance, i.e.

$$Y_{gh} = \frac{1}{R\sqrt{h} + jX''_d h} \tag{7.84}$$

where R is derived from the machine power losses and X''_d is the generator's sub-transient reactance.

A frequency-dependent multiplying factor can be added to the reactance terms to account for skin effect. It should be noted that equation (7.84) is not valid at fundamental frequency as the positive sequence component still sees the synchronous impedance due to the flux not rotating with respect to the rotor.

7.8 Shunt Elements

Shunt reactors and capacitors are used in a transmission system for reactive power control. The data for these elements is usually given in terms of their rated megavolt-amps and rated kilovolts, and the equivalent phase admittance in per unit is calculated from this data.

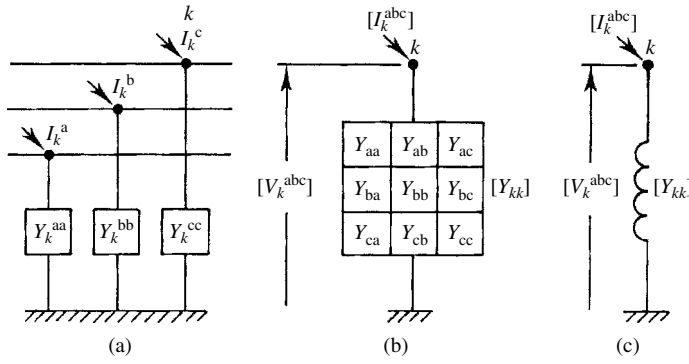


Figure 7.23 Representation of a shunt element: (a) coupled admittance; (b) admittance matrix; (c) compound admittance

The coupled admittances to ground at bus k are formed into a 3×3 admittance matrix as shown in Figure 7.23, and this reduces to the compound admittance representation indicated. The admittance matrix is incorporated directly into the system admittance matrix, contributing only to the self-admittance of the particular bus.

While provision for off-diagonal terms exists, the admittance matrix for shunt elements is usually diagonal, as there is normally no coupling between the components of each phase.

Consider, as an example, the three-phase capacitor bank shown in Figure 7.24. A 3×3 matrix representation similar to that for a line section is illustrated.

The megavolt-amp rating at fundamental frequency (Q) and the nominal voltage (V) are normally used to calculate the capacitive reactance at the n harmonic, i.e. $X_c = V^2/nQ$.

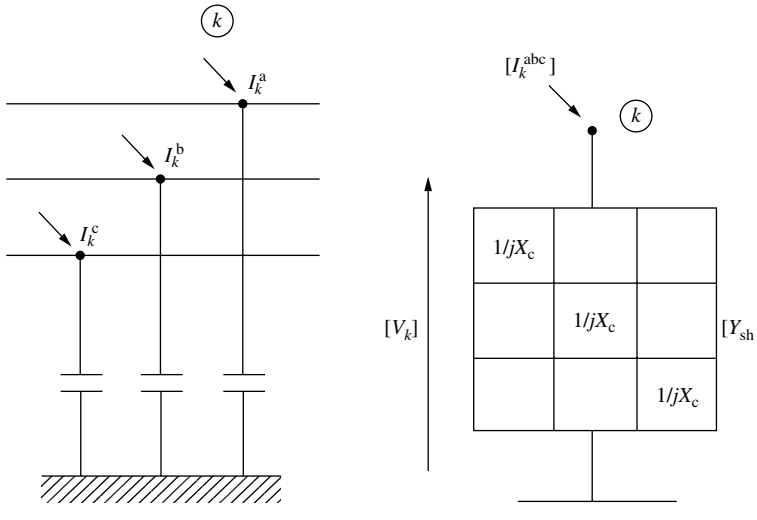


Figure 7.24 Representation of a shunt capacitor bank

In terms of *ABCD* parameters the matrix equation of a shunt element is:

$$\begin{bmatrix} V_s \\ I_s \end{bmatrix} = \begin{bmatrix} [U] & \\ [Y_{sh}] & [U] \end{bmatrix} \times \begin{bmatrix} V_r \\ -I_r \end{bmatrix} \tag{7.85}$$

where $[Y_{sh}]$ = Diag (shunt admittance of each phase) and $[U]$ = Identity matrix.

However, in harmonic analysis, any added inductance, often placed in series with shunt capacitors, must be explicitly represented. For floating star or delta-connected configurations, the procedure used in Section 7.6. for the transformer representation should be followed.

7.9 Series Elements

Series elements are connected directly between two buses and for modelling purposes they constitute a subsystem in the network subdivision.

A three-phase coupled series admittance between two busbars i and k is shown in Figure 7.25(a), as well as its reduced nodal admittance matrix (Figure 7.25(b)) and compound admittance (Figure 7.25(c)).

The series capacitor, used for transmission line reactance compensation, is an example of an uncoupled series element; in this case the admittance matrix is diagonal. For a lumped series element, the *ABCD* parameter matrix equation is:

$$\begin{bmatrix} V_s \\ I_s \end{bmatrix} = \begin{bmatrix} [U] & [Z_{se}] \\ & [U] \end{bmatrix} \times \begin{bmatrix} V_r \\ -I_r \end{bmatrix} \tag{7.86}$$

where $[Z_{se}]$ = Diag (series impedance of each phase) and [U] is the identity matrix.

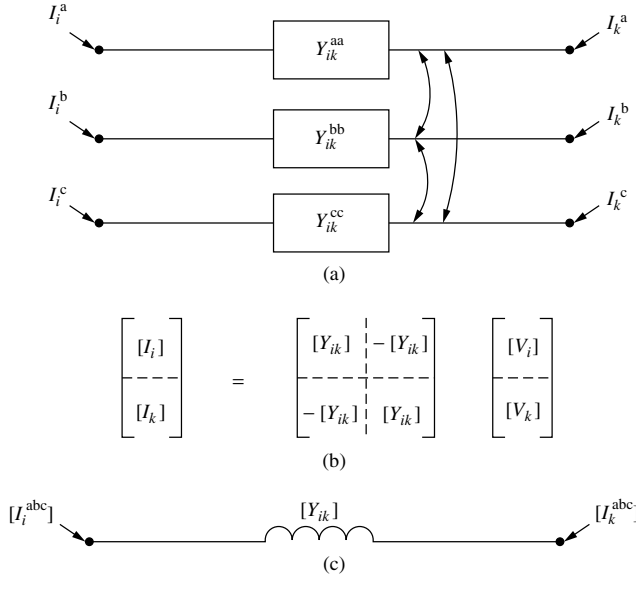


Figure 7.25 Representation of a series element: (a) coupled admittances; (b) admittance matrix; (c) compound admittance

7.10 Distribution System Modelling

The harmonic impedances seen from primary transmission system buses are greatly affected by the degree of representation of the distribution system and the consumer loads fed radially from each busbar. Moreover, the distribution system should also be modelled in the three-phase frame to take into account unbalanced loading, transformers of different connections and earth residual currents.

A typical simplified *dominant* configuration of a distribution feeder is shown in Figure 7.26. Generally, the bulk of the load fed from distribution feeders is located behind two transformers downstream. Thus, to calculate the harmonic impedances seen from the high-voltage primary transmission side it may be sufficient to use a discrete model of the composite effect of many loads and distribution system lines and transformers at the high voltage side of the main distribution transformers; typically the 110 kV in a system using 400 kV and 220 kV transmission.

The following guidelines are recommended for the derivation of distribution feeder equivalents:

- Distribution lines and cables (e.g. 69–33 kV) should be represented by an equivalent-π model. For short lines, the total capacitance at each voltage level should be estimated and connected at that busbar. Due to their relatively low X/R ratio, the resistance of lines and cables plays an important part in damping resonant conditions and should always be included in the equivalent circuit.
- Transformers between distribution voltage levels should be represented by an equivalent element.
- As the active power absorbed by rotating machines does not correspond to a damping value, the active and reactive power demand at the fundamental frequency may not be used in a straightforward manner. Alternative models for load representation should be used according to their composition and characteristics. Groups of small motors may actually provide some damping for the harmonic content depending on the X/R ratio of their blocked rotor circuit.
- Power factor correction (PFC) capacitance should be estimated as accurately as possible and allocated at the corresponding voltage level.
- Other elements, such as transmission line inductors, filters and generators, should be represented according to their actual configuration and composition.

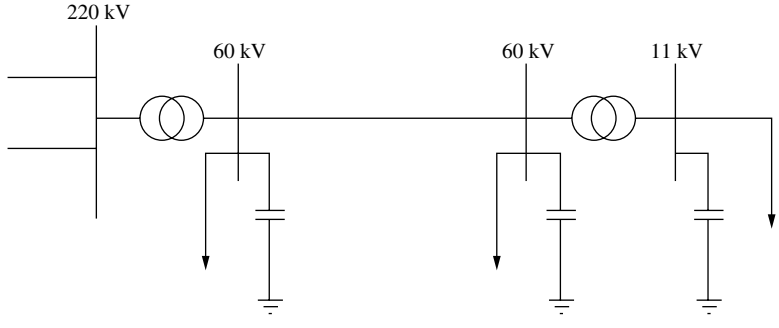


Figure 7.26 Typical distribution feeder

- The representation should be more detailed nearer the points of interest. Simpler equivalents for the transmission and distribution systems should be used only for remote points.
- All elements should be uncoupled three-phase branches, including unbalanced phase parameters.

7.11 Load Models

There are no *generally acceptable* load equivalents for harmonic analysis [25]. In each case the derivation of equivalent conductance and susceptance harmonic bandwidths from specified P (active) and Q (reactive) power flows will need extra information on the actual composition of the load. Power distribution companies will have a reasonable idea of the proportion of each type in their system depending on the time of day and should provide such information.

The aggregate nature of the load makes it difficult to establish models based purely on theoretical analysis. Attempts to deduce models from measurements have been made [26] but lack general applicability. Utilities should be encouraged to develop databases of their electrical *regions,* with as much information as possible to provide accurate equivalent harmonic impedances for future studies.

Consumers' loads constitute not only the main element of the damping component but may affect the resonance conditions, particularly at higher frequencies. Some early measurements [27] showed that maximum plant conditions can result in reduced impedances at lower frequencies and increased impedances at higher frequencies. Simulation studies [28] have also demonstrated that the addition of detailed load representation can result in either an increase or decrease in harmonic flow.

The energy utilisation systems are themselves growing contributors to the harmonic problem as a result of the increased content of nonlinear appliances as explained in Chapter 3.

There are basically three types of loads: passive, motive and power electronic.

(1) Predominantly passive loads (typically domestic) can be represented approximately by a series R, X impedance, i.e.

$$Z_{\mathrm{r}}(\omega) = R_{\mathrm{r}}\sqrt{h} + jX_{\mathrm{r}}h \tag{7.87}$$

where R_{r} is load resistance at the fundamental frequency, X_{r} is load reactance at the fundamental frequency and h is harmonic order (ω/ω_1).
The weighting coefficient $\sqrt{h}$, used above for frequency dependence of the resistive component, is different in different models; for instance, reference [25] uses a factor of 0.6 $\sqrt{h}$ instead. The equivalent inductance represents the relatively small motor content when known. In studies concerning mainly the transmission network the loads are usually equivalent parts of the distribution network, specified by the consumption of active and reactive power. Normally a parallel model is used, i.e.

$$Y_{\mathrm{L}}(\omega) = 1/R_{\mathrm{p}} + j1/(X_{\mathrm{p}}h) \tag{7.88}$$

where R_p is Load resistance at the fundamental frequency, X_p is load reactance at the fundamental frequency and h is harmonic order (ω/ω_1).

$$X_p = \frac{V^2}{Q} \qquad R = \frac{V^2}{P} \tag{7.89}$$

There are many variations of this parallel form of load representation. For example, the parallel load model suggested by reference [25] is a parallel connection of inductive reactance and resistance whose values are

$$X = j\frac{V^2}{(0.1h + 0.9)Q} \qquad R = \frac{V^2}{(0.1h + 0.9)P} \tag{7.90}$$

where P and Q are fundamental frequency active and reactive powers.

(2) Various models of predominantly motive loads have been suggested using resistive-inductive equivalents, their differences being often due to the boundary of system

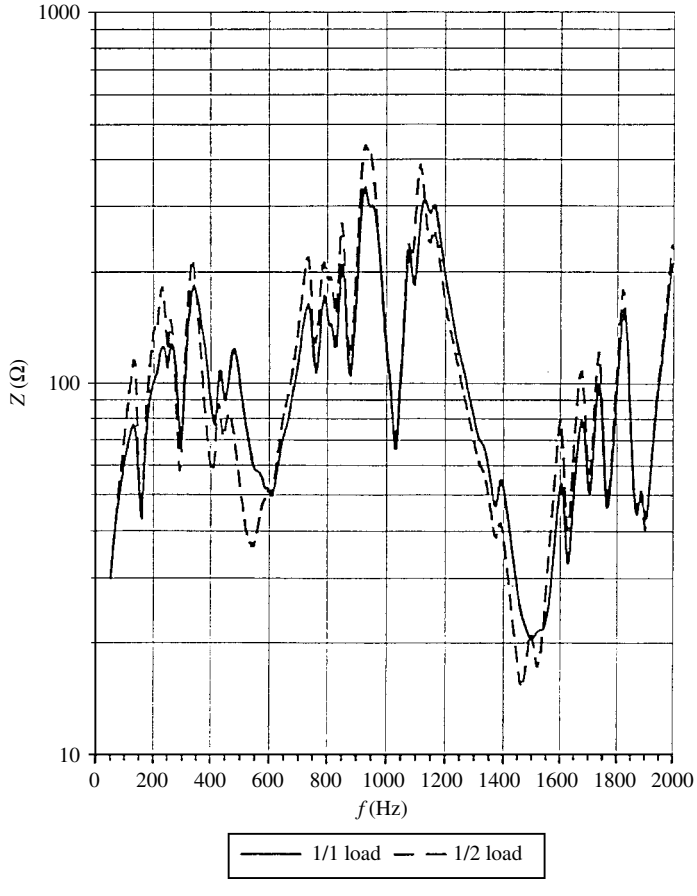


Figure 7.27 Load effect on the magnitude of the network harmonic impedances.(Reproduced from [29] by permission of CIGRE)

representation. A detailed analysis of the induction motor response to harmonic frequencies, leading to a relatively simple model, is described later in this section.

(3) Modelling the power electronic loads is a more difficult problem because, besides being harmonic sources, these loads do not present a constant R, L, C configuration and their nonlinear characteristics cannot fit within the linear harmonic equivalent model. In the absence of detailed information, the power electronic loads are often left open-circuited when calculating harmonic impedances. However, their effective harmonic impedances need to be considered when the power ratings are relatively high, such as arc furnaces, aluminium smelters, etc.

When studying the transmission network it is strongly recommended to model at least part of the next lower voltage level and place the load equivalent there. To illustrate the importance of the loading level on the harmonic impedances, Figures 7.27 and 7.28 show the effect of halving the load level on the magnitude and phase of the individual harmonics at a converter bus connected to a 400 kV system [29].

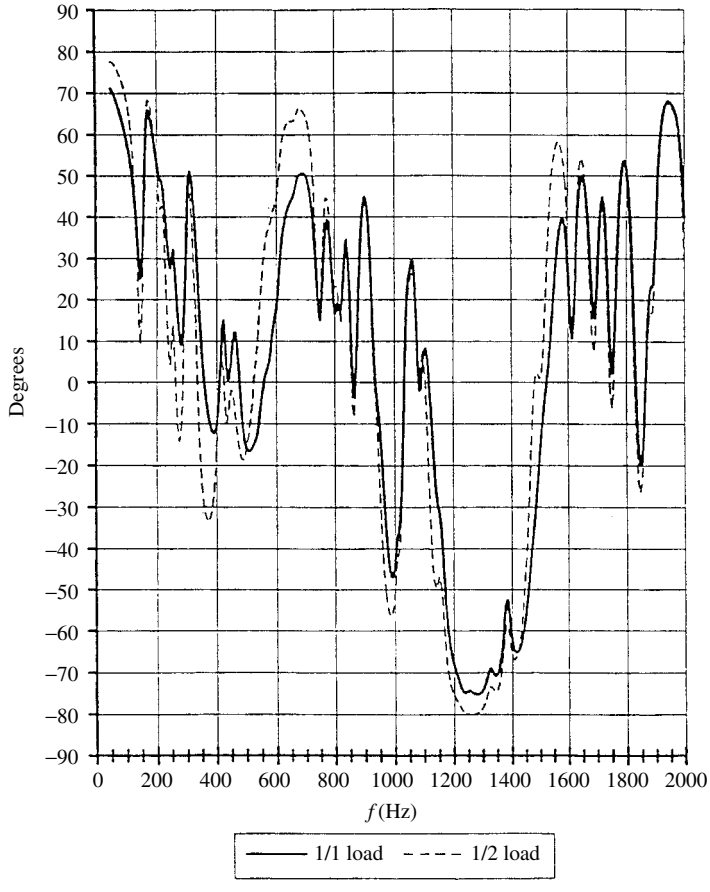


Figure 7.28 Load effect on the phase angle of the network harmonic impedances. (Reproduced from [29] by permission of CIGRE)

7.11.1 Induction Motor Model

The circuit shown in Figure 7.29 is an approximate single-phase representation of the induction motor, with the magnetising impedance ignored.

The motor impedance at any frequency can be expressed as:

$$Z_{\mathrm{m}}(\omega) = R_{\mathrm{mh}} + jX_{\mathrm{mh}} \tag{7.91}$$

At the fundamental frequency ($h = 1$)

$$X_{\mathrm{m1}} = X_1 + X_2 = X_{\mathrm{B}} \tag{7.92}$$

$$R_{\mathrm{m1}} = R_1 + \frac{R_2}{S} = R_{\mathrm{B}}\left(a + \frac{b}{S}\right) \tag{7.93}$$

where R_{B} is the total motor resistance with the rotor locked, R_1 is the stator resistance related to R_{B} by coefficient a (which is typically 0.45), R_2 is the rotor resistance related to R_{B} by coefficient b (which is typically 0.55), and X_{B} is the total motor reactance with the rotor locked.

$$S - \mathrm{Slip} = \frac{\omega_{\mathrm{s}} - \omega_{\mathrm{r}}}{\omega_{\mathrm{s}}}$$

At harmonic frequencies

$$X_{\mathrm{mh}} = h \cdot X_{\mathrm{B}} \tag{7.94}$$

$$R_{\mathrm{mh}} = R_{\mathrm{B}}\left(a.\mathrm{k}_a + \frac{b}{S_{\mathrm{h}}}.k_b\right) \tag{7.95}$$

where k_a, k_b are correction factors to take into account skin effect in the stator and rotor, respectively, and S_{h} is apparent slip at the superimposed frequency, i.e.

$$S_{\mathrm{h}} = \frac{\pm h\omega_{\mathrm{s}} - \omega_{\mathrm{r}}}{\pm h\omega_{\mathrm{s}}} \tag{7.96}$$

$$S_{\mathrm{h}} \approx 1 - \frac{\omega_{\mathrm{r}}}{h\omega_{\mathrm{s}}} \quad \text{for the positive-sequence harmonics}$$

$$S_{\mathrm{h}} \approx 1 + \frac{\omega_{\mathrm{r}}}{h\omega_{\mathrm{s}}} \quad \text{for the negative-sequence harmonics}$$

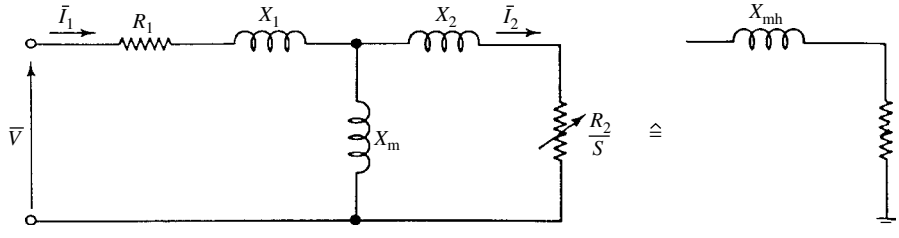


Figure 7.29 Approximate representation of the induction motor

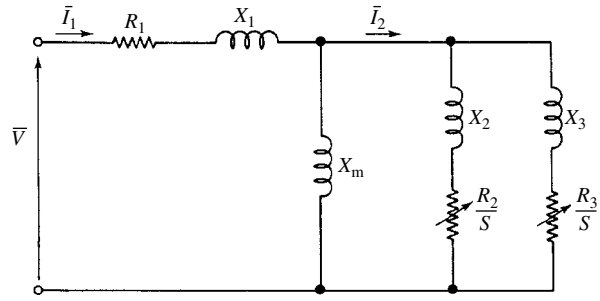


Figure 7.30 Accurate induction motor model

Assuming an exponential variation of the resistances with frequency, i.e.

$$k_a = h^{\alpha}$$
$$k_b = (\pm h - 1)^{\alpha}$$

the motor equivalent resistance for $\alpha = 0.5$ becomes

$$R_{mh} = R_B[a\sqrt{h} + (\pm h.b\sqrt{\pm h - 1})/(\pm h - 1)] \tag{7.97}$$

An accurate model of a double cage induction motor is shown in Figure 7.30.

7.11.2 Norton Equivalents of Residential Loads

In practice there is always a mix of the three types of load and no general guidelines can be given for their representation without detailed knowledge of their composition. However, the latter are reasonably predictable in the case of radial distribution systems feeding domestic customers. In these cases, and with judicious estimation of the load mix, it is possible to derive accurate equivalents for the composite residential load.

The Pspice program is used in reference [30] to derive equivalent components for specified combinations of linear and nonlinear appliances as well as the low-voltage distribution network of a residential feeder. The nonlinear appliances include personal computers, compact fluorescent lamps, television sets and fluorescent lighting. It is a bottom-up approach, whereby the instantaneous voltages and currents of the network are calculated and then the Fourier transform of the waveshapes obtained. The linear load is represented as a single branch with a lumped circuit derived at the point of common coupling (PCC) [31].

The different load combinations used in the test system were decided based on extensive household interviews in the area. The third, fifth and seventh harmonic currents on the LV side of the distribution transformer were also monitored over a period of several days for the purpose of model verifications. The simulation results substantially agreed with the recorded values.

While requiring considerable effort, this approach can be used to derive harmonic equivalent circuits at PCCs of residential feeders to be used in further system

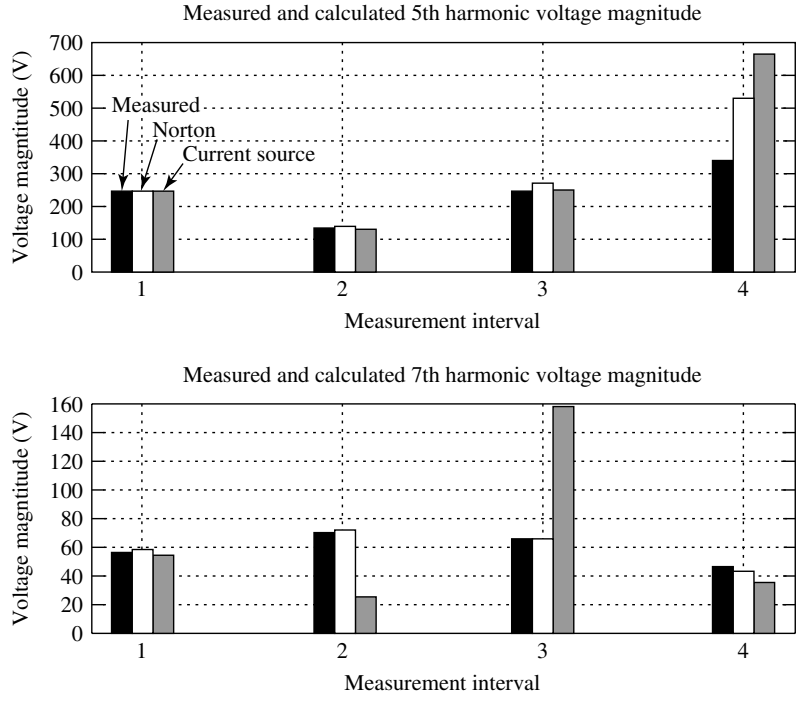


Figure 7.31 Measured and calculated harmonic voltage magnitude

development. It is envisaged, however, that the application of this method to industrial feeders is not straightforward considering the greater variety of their loads and operating cycles.

7.11.3 Empirical Models Based on Measurements

An alternative approach to explicit load representation is the use of empirical models derived from measurements.

In particular, information obtained from harmonic current and voltage measurements with different operating conditions, for example by switching a shunt capacitor (as described in Section 7.3.1), can be used to derive approximate Norton harmonic equivalents of the load or group of loads connected at a distribution bus. By way of example, Figure 7.31 shows measured and calculated harmonic voltages at four 10-minute time intervals for an 11 kV distribution bus fed from the 220 kV transmission system via a 40 MVA transformer [32]. Clearly the Norton approach gives a better estimation of the harmonic voltages than the constant current source.

7.12 Computer Implementation [33]

The evolution of computer technology has removed many of the limitations that affected implementation decisions in the past.

Earlier implementations were restricted by the use of mainframe computers, and limitations in graphical support, memory and storage space.

The main factor affecting recent implementations has been the acceptability of the personal computer (PC) as the main computing platform in terms of capability and price. The PC platform has been enhanced by the use of several graphical operating systems and particularly Microsoft Windows™. Other important developments have been the availability of ample computer bandwidths, reduced cost of memory modules, making memory limitation secondary, cheaper storage modules with much larger capacity, and great improvement in software support and development support tools.

To cope with the larger size and complexity of computer programs, new facilities have become available to make the software more modular and easier to maintain. Three important examples are multitasking operating systems, graphical user interfaces (GUIs), and object-oriented design methodology.

In line with the steps described in the previous sections of the chapter, the computer implementation involves the following stages:

- Computation of the admittance matrices of individual components at the specified harmonic frequencies.
- Formation of the system admittance matrices at individual frequencies according to the network topology.
- Calculation of the system harmonic voltages at all the system nodes given the harmonic current injections at the nodes containing nonlinear plant components.

7.12.1 Harmonic Penetration Overview

A modern harmonic penetration program includes a GUI, the simulation algorithm engine and a database handling data structure.

The GUI is used for data entry (component parameters and network topology), and for the presentation of the simulation results.

The simulation algorithm engine performs the calculations required and has traditionally been written in the FORTRAN language, although recently object-oriented languages have also been used. Mixed-language programming makes it possible to use FORTRAN's advantage of built-in complex number manipulation with other languages to benefit from the strengths of each.

Database handling routines are used to store and retrieve the power system data from disk. However, the traditional fixed format, still widely used today, is very rigid and inflexible. The use of a platform-independent text format, such as ASCII, provides far greater flexibility.

7.12.2 An Advanced Program Structure

Lack of memory space has in the past forced simulation packages to be fragmented into several programs. Moreover, lack of computer power has often made it necessary to store intermediate results rather than recalculate them as and when needed.

The structure of a typical software package for harmonic analysis is illustrated in Figure 7.32. The computational effort required to generate the harmonic admittance matrices of transmission lines and cables usually exceeds that of forming the system admittance matrix and solving for the harmonic voltages and currents. Therefore, these matrices are usually computed separately and stored in disk files, which are then read by the main simulation program when forming the system admittance matrices. The modelling of nonlinear loads is also separated from the main program; the calculated current injections are then stored in disk files and read by the main program when performing the harmonic penetration analysis. The results of the harmonic penetration study are also output to disk files to be imported into plotting tools for presentation. These can also be used by other tools such as Matlab™ for further analysis or spreadsheets for reporting purposes.

Although the above subdivisions have enabled complex analysis to be performed successfully despite the limitations presented by earlier computers, their main drawback is the use of many intermediary files, the maintenance of which becomes laborious when the simulated system is large, as all these files must be updated before the succeeding program is activated. Moreover, the conversion of complex or floating numbers into the text format typically used in these files introduces truncation or round-off errors. These errors may distort the final results, especially at high harmonic frequencies when the distortion levels are generally low, particularly when the analysis process involves many such conversions. The use of unformatted data has the advantages of reduced file size, and faster reading and writing to disk operations without introducing truncation errors; however, the data in the file cannot be readily inspected.

Typically, a graphical data entry or editor is added to the package to help the user to construct the simulation cases. These editors are usually separate applications that are able to generate the necessary data files required in the simulation. The simulation results are imported into plotting applications such as Matlab™ or Microsoft Excel™ for further analysis or reporting purposes.

Several advances in computer technology have made it possible to integrate all the above processes into a single framework without the need to combine them all into a single huge executable binary. The most important developments are abundance of cheap memory (which includes virtual memory and dynamic memory allocation

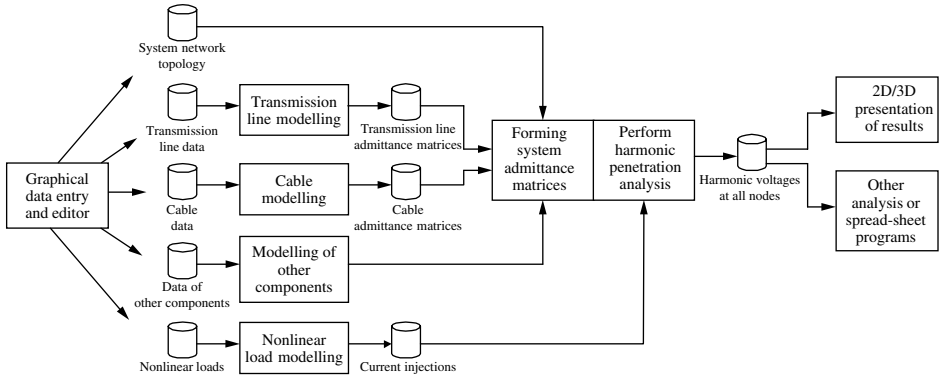


Figure 7.32 Structure of harmonic analysis software

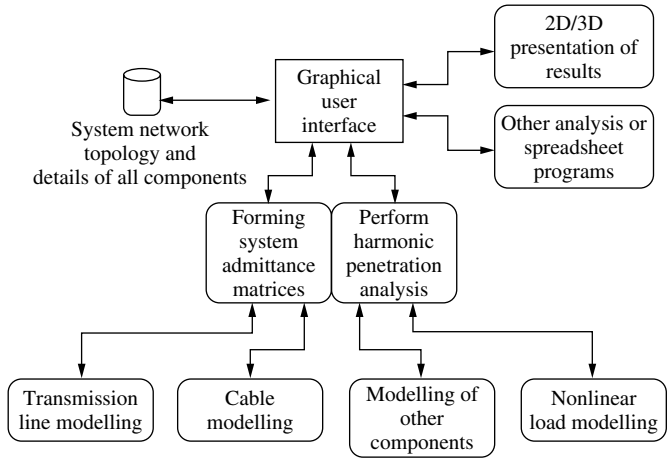

2D/3D presentation of results
Graphical user interface
System network topology and details of all components
Other analysis or spreadsheet programs
Forming system admittance matrices
Perform harmonic penetration analysis
Transmission line modelling
Cable modelling
Modelling of other components
Nonlinear load modelling

Figure 7.33 Functional overview

technologies), dynamic linked libraries, object-oriented development tools and mixed-language programming.

Making use of these new technologies, Figure 7.33 depicts how a harmonic penetration simulation program is put together. The mathematical modelling of the power system components, including nonlinear loads, and the harmonic penetration are programmed as relocatable dynamic linked libraries and these are made accessible to the GUI. Through this GUI, users can construct the power system simulation network by joining different power system components together and specifying the component parameter settings. The constructed simulation network consists of lists of power system components and their settings; these are passed to the harmonic penetration library to carry out the tasks required by the simulation study.

7.12.3 Data Structure

The essence of the object-oriented methodology is a family of classes that make up the application. Each of the classes has its own unique properties or settings and includes procedures to alter the settings. At execution, objects of the classes are created when they are needed to perform certain tasks and they are usually deleted upon completion of these tasks.

The data used in the harmonic penetration study includes the power system components and the topology by which they are connected to form a system. Therefore, based on the object-oriented methodology, a simulation case can be regarded as a drawing page or canvas object, which acts as a container for all the power system components objects making up the system. The various classes of objects making up an object-oriented version of harmonic analysis are summarised in Figure 7.34.

The two main classes are the Power System Canvas and the Power System Component class, both inherited from the Generic Graphical Component, which provides the interfaces to the low-level graphical functions of the GUI operating system (which is Microsoft Windows™ in this implementation).

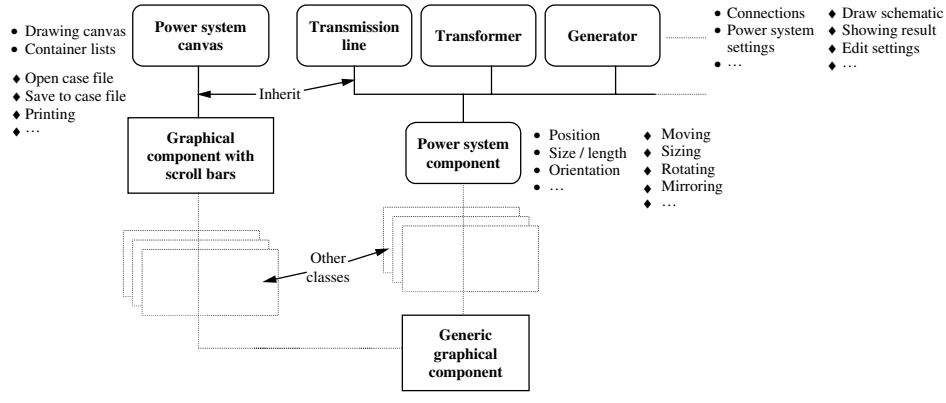


Figure 7.34 Power system component models

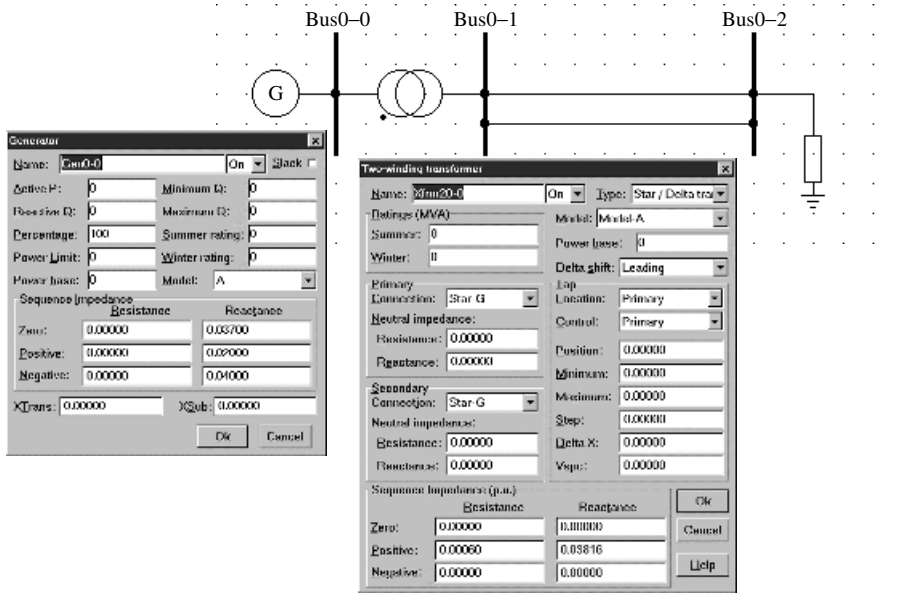


Figure 7.35 Typical interface

Figure 7.35 illustrates the use of the object-oriented method in building a network for simulation studies. It shows a three-busbar power system consisting of a generator and a load connected through a two-winding transformer, and a double-circuit transmission line. All of these components are inherited from the common Power System Component class. They differ from each other by the functions used to draw them, resulting in different images and requiring different editing forms, as shown for the generator and transformer in the figure. Consequently, the simulation test case is made up of three objects of busbar class and one object each of the generator, transformer, transmission lines and load classes. The busbar objects are differentiated from each other by their busbar name property.

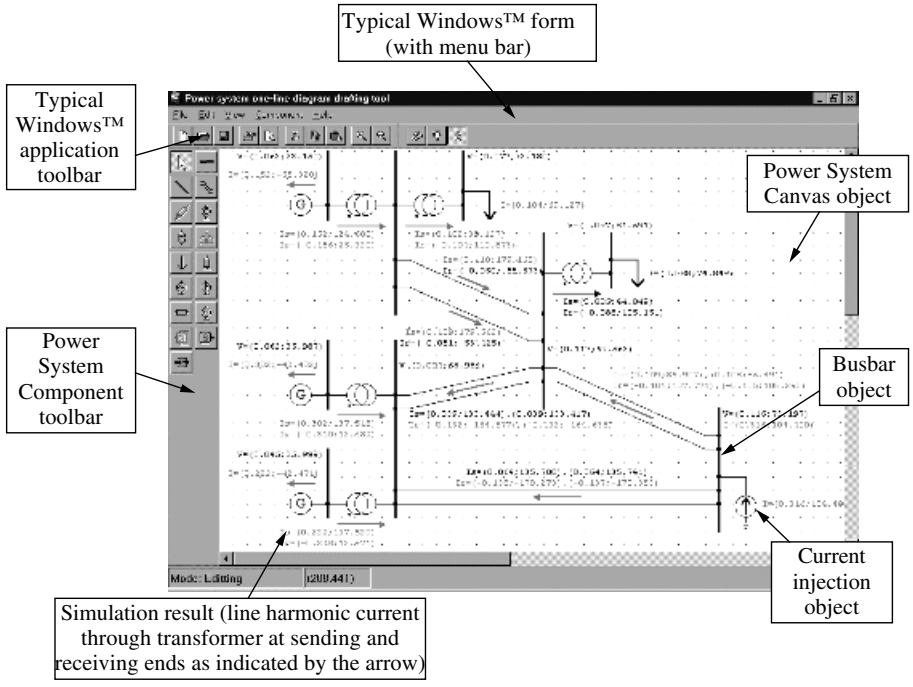

Typical Windows™ form (with menu bar)
Typical Windows™ application toolbar
Power System Canvas object
Power System Component toolbar
Busbar object
Current injection object
Simulation result (line harmonic current through transformer at sending and receiving ends as indicated by the arrow)

Figure 7.36 View of solution results

In this object-oriented manner, a power system network is described by lists of these Power System Component objects. There are altogether five container lists in the example above, corresponding to the five different classes. These lists can be created automatically as the network is built up using a graphical editor, or they are constructed according to the information stored in the data file. These lists are then passed to the simulation engine, which constructs the system admittance matrices at the respective harmonic frequencies, and carries out the harmonic penetration studies, as outlined in earlier sections. Each of the power system component objects also contains properties for recording simulation results. Hence, the GUI can then extract the result values from the lists of objects and display them on the canvas as shown in Figure 7.36. The presentation of results is customised, allowing them to be presented differently according to the component type. Harmonic voltages are only shown on the busbar objects while multi-terminal objects such as transformers and transmission lines will show the harmonic currents at the terminals, with the direction of the flow indicated using arrows. Finally, the colour of the arrows and the result texts can be used to indicate if the values exceed certain limits.

The database used in harmonic penetration analysis can be divided into graphical and power system data. The graphical database contains information required for displaying the power system network in a GUI. The power system database, on the other hand, contains network topology information that describes the make-up of the simulated power system network.

The power system database is designed to be a text file so that it is easier to transfer from one operating system to another. This has the disadvantage of increasing the

file size and the accessing time. Data reading is still a considerable proportion of the solution time; for a 110 bus, 50 harmonics solution, the data reading time is about 20% of the total.

Generally, power systems have a fixed and rigid structure and their design takes advantage of data formats such as the well-known IEEE common data format and the PTI (Power Technology Incorporated) data format. These types of database typically

```
09/25/93 UW ARCHIVE           100.0  1962 W IEEE 14 Bus Test Case
BUS DATA FOLLOWS                            14 ITEMS
   1 Bus 1     HV  1  1  3 1.060    0.0      0.0      0.0    232.4   -16.9      0.0  1.060     0.0     0.0
0.0    0.0        0
   2 Bus 2     HV  1  1  2 1.045   -4.98     21.7     12.7     40.0    42.4      0.0  1.045    50.0   -40.0
0.0    0.0        0
   3 Bus 3     HV  1  1  2 1.010  -12.72     94.2     19.0      0.0    23.4      0.0  1.010    40.0     0.0
0.0    0.0        0
   4 Bus 4     HV  1  1  0 1.019  -10.33     47.8     -3.9      0.0     0.0      0.0  0.0       0.0     0.0
0.0    0.0        0
   5 Bus 5     HV  1  1  0 1.020   -8.78      7.6      1.6      0.0     0.0      0.0  0.0       0.0     0.0
0.0    0.0        0
   6 Bus 6     LV  1  1  2 1.070  -14.22     11.2      7.5      0.0    12.2      0.0  1.070    24.0    -6.0
0.0    0.0        0
   7 Bus 7     ZV  1  1  0 1.062  -13.37      0.0      0.0      0.0     0.0      0.0  0.0       0.0     0.0
0.0    0.0        0
   8 Bus 8     TV  1  1  2 1.090  -13.36      0.0      0.0      0.0    17.4      0.0  1.090    24.0    -6.0
0.0    0.0        0
   9 Bus 9     LV  1  1  0 1.056  -14.94     29.5     16.6      0.0     0.0      0.0  0.0       0.0     0.0
0.0    0.19       0
  10 Bus 10    LV  1  1  0 1.051  -15.10      9.0      5.8      0.0     0.0      0.0  0.0       0.0     0.0
0.0    0.0        0
  11 Bus 11    LV  1  1  0 1.057  -14.79      3.5      1.8      0.0     0.0      0.0  0.0       0.0     0.0
0.0    0.0        0
  12 Bus 12    LV  1  1  0 1.055  -15.07      6.1      1.6      0.0     0.0      0.0  0.0       0.0     0.0
0.0    0.0        0
  13 Bus 13    LV  1  1  0 1.050  -15.16     13.5      5.8      0.0     0.0      0.0  0.0       0.0     0.0
0.0    0.0        0
  14 Bus 14    LV  1  1  0 1.036  -16.04     14.9      5.0      0.0     0.0      0.0  0.0       0.0     0.0
0.0    0.0        0
-999
BRANCH DATA FOLLOWS                          20 ITEMS
   1    2  1  1 1 0  0.01938   0.05917    0.0528     0     0     0    0 0  0.0       0.0 0.0    0.0
0.0    0.0   0.0
   1    5  1  1 1 0  0.05403   0.22304    0.0492     0     0     0    0 0  0.0       0.0 0.0    0.0
0.0    0.0   0.0
   2    3  1  1 1 0  0.04699   0.19797    0.0438     0     0     0    0 0  0.0       0.0 0.0    0.0
0.0    0.0   0.0
   2    4  1  1 1 0  0.05811   0.17632    0.0374     0     0     0    0 0  0.0       0.0 0.0    0.0
0.0    0.0   0.0
   2    5  1  1 1 0  0.05695   0.17388    0.0340     0     0     0    0 0  0.0       0.0 0.0    0.0
0.0    0.0   0.0
   3    4  1  1 1 0  0.06701   0.17103    0.0346     0     0     0    0 0  0.0       0.0 0.0    0.0
0.0    0.0   0.0
   4    5  1  1 1 0  0.01335   0.04211    0.0128     0     0     0    0 0  0.0       0.0 0.0    0.0
0.0    0.0   0.0
   4    7  1  1 1 1  0.0       0.20912    0.0        0     0     0    0 0  0.978     0.0 0.0    0.0
0.0    0.0   0.0
   4    9  1  1 1 1  0.0       0.55618    0.0        0     0     0    0 0  0.969     0.0 0.0    0.0
0.0    0.0   0.0
   5    6  1  1 1 1  0.0       0.25202    0.0        0     0     0    0 0  0.932     0.0 0.0    0.0
0.0    0.0   0.0
   6   11  1  1 1 0  0.09498   0.19890    0.0        0     0     0    0 0  0.0       0.0 0.0    0.0
0.0    0.0   0.0
   6   12  1  1 1 0  0.12291   0.25581    0.0        0     0     0    0 0  0.0       0.0 0.0    0.0
0.0    0.0   0.0
   6   13  1  1 1 0  0.06615   0.13027    0.0        0     0     0    0 0  0.0       0.0 0.0    0.0
0.0    0.0   0.0
   7    8  1  1 1 0  0.0       0.17615    0.0        0     0     0    0 0  0.0       0.0 0.0    0.0
0.0    0.0   0.0
   7    9  1  1 1 0  0.0       0.11001    0.0        0     0     0    0 0  0.0       0.0 0.0    0.0
0.0    0.0   0.0
   9   10  1  1 1 0  0.03181   0.08450    0.0        0     0     0    0 0  0.0       0.0 0.0    0.0
0.0    0.0   0.0
   9   14  1  1 1 0  0.12711   0.27038    0.0        0     0     0    0 0  0.0       0.0 0.0    0.0
0.0    0.0   0.0
  10   11  1  1 1 0  0.08205   0.19207    0.0        0     0     0    0 0  0.0       0.0 0.0    0.0
0.0    0.0   0.0
  12   13  1  1 1 0  0.22092   0.19988    0.0        0     0     0    0 0  0.0       0.0 0.0    0.0
0.0    0.0   0.0
  13   14  1  1 1 0  0.17093   0.34802    0.0        0     0     0    0 0  0.0       0.0 0.0    0.0
0.0    0.0   0.0
-999
LOSS ZONES FOLLOWS                    1 ITEMS
  1 IEEE 14 BUS
-99
INTERCHANGE DATA FOLLOWS                 1 ITEMS
 1    2 Bus 2     HV    0.0  999.99  IEEE14  IEEE 14 Bus Test Case
-9
TIE LINES FOLLOWS                     0 ITEMS
-999
END OF DATA
```

Figure 7.37 IEEE common data format example

start with several lines of comments or general descriptions of the power system network. These are followed by sections of lines delimited by some code word such as '999' or 'End'. Each section corresponds to a type of power system components. Each line (or several subsequent lines) within a section has a fixed format with multiple fixed-width columns for specifying the setting values of a particular component. An example of this is the IEEE common data format illustrated in Figure 7.37.

7.13 Examples of Application of the Models

7.13.1 Harmonic Flow in a Homogeneous Transmission Line [34]

A 230 km 220 kV line of flat configuration is used as the first test system; the parameters of this line are shown in Figure 7.38. A three-dimensional graphic representation is used to provide simultaneous information on the harmonic levels along the line. At each harmonic (up to the 25th harmonic), one per unit positive-sequence current is injected at the Islington end of the line. The voltages caused by this current injection are, therefore, the same as the calculated impedance, i.e. V_+ gives Z_{++}, V_- gives Z_{+-} and V_0 gives Z_{+0} (the subscripts $+$, $-$, 0 refer to the positive, negative and zero sequences, respectively).

Figures 7.39–7.41 illustrate the effect of two extreme cases of line termination (at Kikiwa), i.e. the line open-circuited and short-circuited, respectively. The differences in harmonic magnitudes along the line are due to standing wave effects and shifting of the resonant frequencies caused by line terminations.

Figure 7.39 indicates the existence of high voltage levels at both ends of the open-circuited line at the half wavelength frequencies. The 25th harmonic clearly illustrates the standing wave effect, with voltage maxima and minima alternating at quarter wavelength intervals.

At any particular frequency, a peak voltage at a point in the line will indicate the presence of a peak current of the same frequency at a point about a quarter wavelength away. This is clearly seen in Figure 7.40

When the line is short-circuited at the extreme end, the harmonic current penetration is completely different, as shown in Figure 7.41(a). The high current levels at the receiving end of the line are due to the short-circuit condition. Figure 7.13 shows that

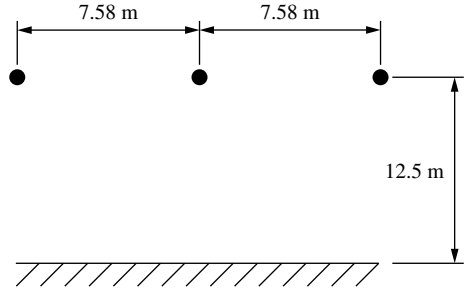


Figure 7.38 Conductor information for the Islington to Kikiwa line: conductor type, Zebra (54/3.18 + 7/3.18); length, 230 km; resistivity, 100 Ωm

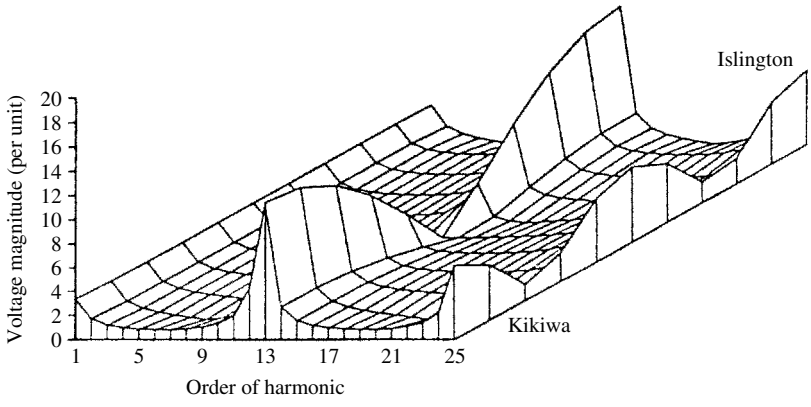


Figure 7.39 Positive sequence voltage versus frequency along the open-ended Islington to Kikiwa line

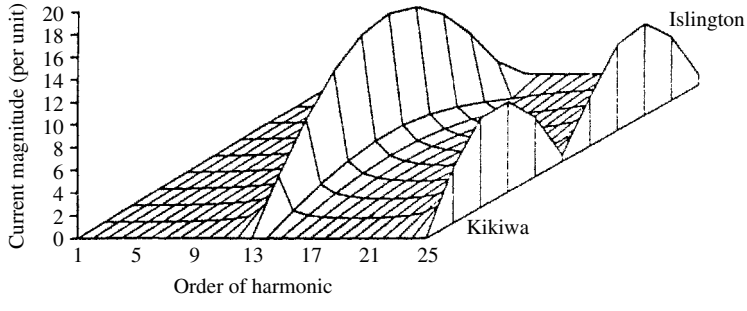


Figure 7.40 Positive sequence current along the open-ended line for a 1 per unit positive-sequence current injection at Islington

the resonant maxima decrease as frequency increases. However, this does not appear to be the case in Figure 7.41(a). The reason is that the points plotted correspond only to harmonic frequencies, and resonances do not fall exactly on these frequencies; i.e. the peak magnitudes at non-harmonic frequencies can be greater than the values plotted in the figure.

Coupling between Harmonic Sequences It is the zero-sequence penetration, rather than the positive sequence, that provides relevant information for the assessment of possible harmonic interference in neighbouring telephone systems. The presence of zero sequence in a transmission line connected to a converter bridge is entirely due to asymmetries in either the converter a.c. plant components or the transmission line itself.

In Figure 7.41 the locations of maximum zero-sequence current (Figure 7.41(c)) coincide with those of the positive sequence (Figure 7.41(a)), and the highest level produced in the test line, about 10% of the injected positive-sequence current, occurs at the 19th harmonic, at the Kikiwa end of the short-circuited line. However, the levels of zero sequence current are low (notice the scale change between positive- and zero-sequence plots).

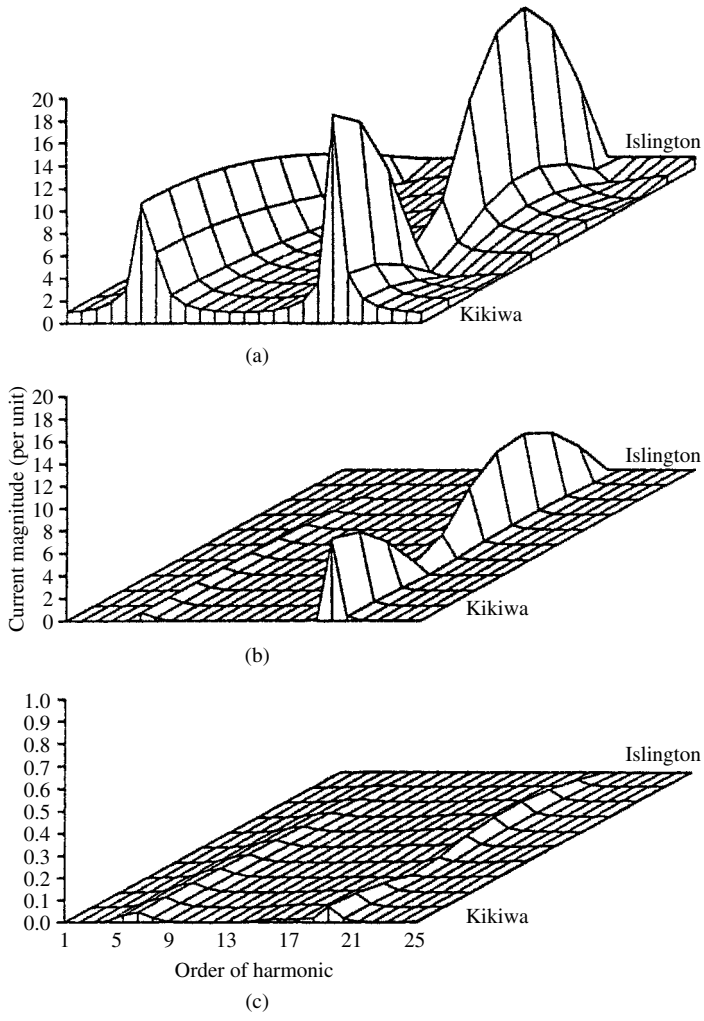


Figure 7.41 Sequence currents along the short-circuited line for a 1 per unit positive-sequence current injection at Islington: (a) positive-sequence current; (b) negative-sequence current; (c) zero-sequence current

Differences in Phase Voltages In conventional harmonic analysis using single-phase positive sequence models, a transmission line is assumed to have one resonant frequency. However, the use of the three-phase algorithm to model the Islington–Kikiwa unbalanced transmission line shows that the resonant frequencies are different for each phase. In this case, the spread of frequencies can be seen from Figure 7.42 to be approximately 6 Hz.

The different magnitudes of the resonant frequencies (up to 30%) of the three phases partly explains the problems encountered with correlating single-phase modelling and measurements on the physical network. The results clearly indicate that harmonics in the transmission system are unbalanced and three-phase in nature.

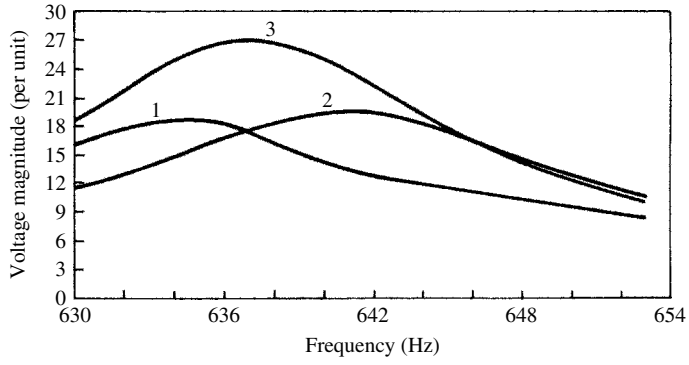


Figure 7.42 Three-phase resonant frequencies of the Islington to Kikiwa line with a 1 per unit positive sequence current injection (skin effect included)

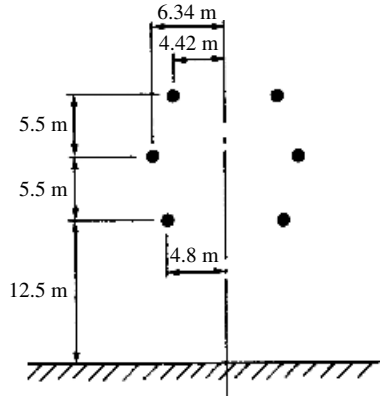


Figure 7.43 Line geometry of a double circuit line. Length, 167 km; earth resistivity, 100 Ωm; two conductors per bundle; bundle spacing, 0.45 m; conductor, 30/3.71 + 7/3.71

Effect of Mutual Coupling in Double Circuits The unbalanced behaviour of double circuit lines is well documented at fundamental frequency [35,36]. The three-phase harmonic penetration algorithm is used in this section to determine the importance of modelling mutual coupling at harmonic frequencies. The line used is shown in Figure 7.43.

Figure 7.44 displays the harmonic impedance (Z_{++}, Z_{00}) seen from the point of harmonic injection, both for a 1 per unit positive-sequence current and 1 per unit zero-sequence injections. The figure also displays the coupling between the positive sequence and the other sequence networks, i.e. Z_{+-} and Z_{+0}.

Results for the case of a coupled line are illustrated in Figure 7.44(a) and those of two single-circuit lines in Figure 7.44(b).

The magnitudes and resonant frequencies of the Z_{++} and Z_{+0} impedances are not affected by the modelling of mutual coupling. However, the level of Z_{+-} has changed substantially at resonance, showing appreciable imbalance. Moreover, the magnitude and resonant frequency of Z_{00} is very different in the two cases.

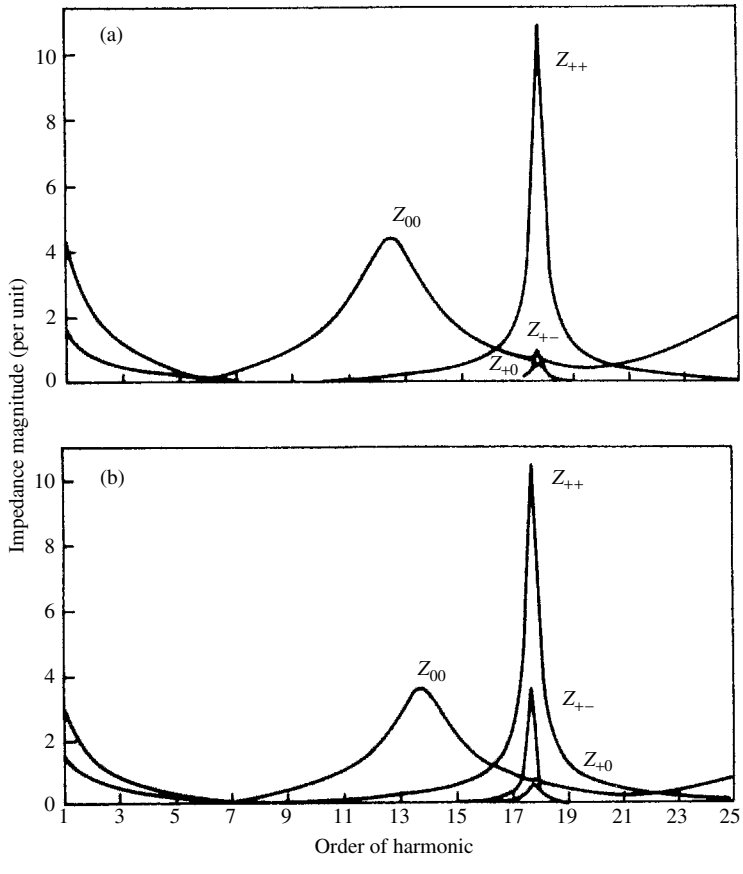


Figure 7.44 Sequence impedance magnitude versus frequency: (a) double-circuit coupled line; (b) two single-circuit lines

Robinson [37] reported that telephone interference caused by zero-sequence currents did not coincide with high levels of power system harmonics. This can partly be explained by the different resonant frequencies of the Z_{++} and Z_{00} observed.

Maximum Values of Currents and Voltages along Transmission Lines Due to the standing wave effect of voltages and currents on transmission lines, the maximum values of these are likely to occur at points other than at the receiving end or sending end busbars. These local maxima could result in insulation damage, overheating or electromagnetic interference. It is thus necessary to calculate the maximum values of currents and voltages along the line and determine the points at which they occur.

Knowing the receiving end current and voltage, for each harmonic frequency, the current and voltage at any point on the line can be calculated for each frequency by the following equations [38]:

$$I(x) = \frac{I_R}{2Z_0}\left[(Z_R + Z_0)e^{\gamma x} + (Z_0 - Z_R)e^{-\gamma x}\right] \tag{7.98}$$

$$V(x) = \frac{I_R}{2}\left[(Z_R + Z_0)e^{\gamma x} + (Z_R - Z_0)e^{-\gamma x}\right] \tag{7.99}$$

where x is the distance from the receiving end, I_R is the receiving end current, V_R is the receiving end voltage and $Z_R = V_R/I_R$. The points on the transmission line at which these are maximum are obtained by considering the currents and voltages as forward (incident) and backward (reflected) travelling waves with respect to the receiving end.

For example, consider the current equation (7.100). The incident current at the receiving end is

$$I_R^+ = \frac{(Z_R + Z_0)}{2Z_0} I_R \tag{7.100}$$

and the reflected current at the receiving end

$$I_R^- = \frac{(Z_0 - Z_R)}{2Z_0} I_R \tag{7.101}$$

The angles associated with these currents at any point along the line are given by

$$\theta^+ = \theta_R^+ + \beta x, \quad \theta^- = \theta_R^- - \beta x, \tag{7.102}$$

where θ_R^+, θ_R^- are the angles of the current at the receiving end.

The current will be a maximum for θ_R^+ equal to θ_R^- . Thus

$$\theta_R^+ + \beta x = \theta_R^- - \beta x, \tag{7.103}$$

or

$$x = \frac{\theta_R^- - \theta_R^+}{2\beta} \tag{7.104}$$

The current will also have local maxima at intervals of one half wavelength along the line.

While the total r.m.s. voltage and current (over the fundamental and all harmonics) are of greatest importance, the location of the maximum total r.m.s. voltage and current will most likely be dominated by that harmonic which is closest to a resonant frequency of the system.

The harmonic analysis described above uses phase components whereas for telephone interference the zero-sequence component is of primary importance. The sequence components (indicated by subscripts $+$, $-$, 0 for the positive, negative and zero sequences, respectively) are obtained from the phase quantities (1, 2, 3) using the relationship

$$[V_{+-0}] = [T_s]^{-1}[V_{123}] \tag{7.105}$$

$$\begin{aligned}[I_{+-0}] &= [T_s]^{-1}[I_{123}] \\ &= [T_s]^{-1}[Y_{123}][T_s][V_{+-0}]\end{aligned} \tag{7.106}$$

where $[T_s]$ is the transformation matrix.

$$[T_s]^{-1} = \frac{1}{3}\begin{bmatrix} a & a^2 & 1 \\ a^2 & a & 1 \\ 1 & 1 & 1 \end{bmatrix} [T_s] = \begin{bmatrix} a^2 & a & 1 \\ a & a^2 & 1 \\ 1 & 1 & 1 \end{bmatrix} \text{ and } a = -\frac{1}{2} + j\frac{\sqrt{3}}{2}$$

The sequence voltages and currents are thus related by the sequence admittance matrix

$$[Y_{+-0}] = [T_s]^{-1}[Y_{123}][T_s] \tag{7.107}$$

In practice, a transmission line will contain sections with different tower geometry. Each of these sections can then be explicitly represented by its equivalent PI circuit or these can be cascaded to obtain an overall equivalent of the complete line. The most efficient solution is to carry out the system harmonic flow analysis without explicit representation of the individual sections and then use a post-processing technique whereby the end terminals, voltages and currents are used to calculate the harmonic current profile along the transmission line section of interest. An example of the end result is shown in Figure 7.45 for a 110 kV double-circuit line.

When performing telephone interference studies often the harmonic sources are not well known yet need to be represented in the simulation. For example, the troublesome harmonics could be entering the 110 kV circuits from the local low-voltage distribution system or from the 220 kV system. Without resorting to a system-wide Harmonic State Estimation, it is difficult to overcome this problem for telephone interference studies. A number of simulations are performed for different injection scenarios. Usually a

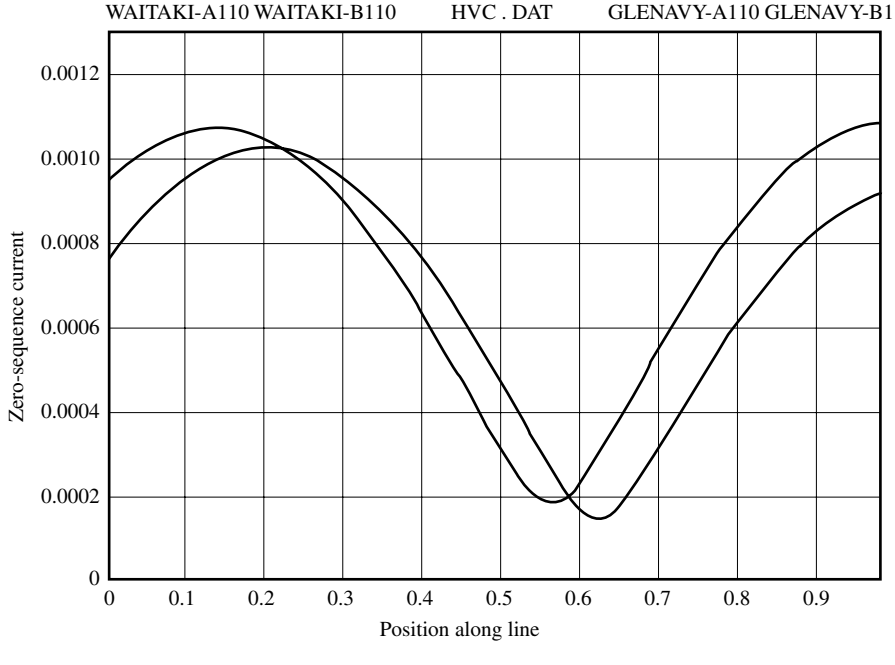


Figure 7.45 Zero-sequence harmonic current profile along a double-circuit transmission line

1 per unit injection is used and the post-processing program scales all the harmonic penetration results to match given measurements levels at one point in the system. Measurements are taken at a second point and these are compared to the scaled results of the other scenarios. Injection scenarios that do not result in the correct harmonic profile are then discarded. This can be taken a step further by opening some circuit breakers to produce a different harmonic flow pattern to distinguish between scenarios that are not easily distinguished from measurements at two locations.

7.13.2 Impedance Loci

This section considers the progressive formation of the harmonic impedances of an interconnected system from the individual component characteristics. The test system, shown in Figure 7.46, is a nine-bus network comprising the 220 kV transmission system below Roxburgh in the south island of New Zealand. The current harmonic source is an existing aluminium smelter at the Tiwai bus.

The double-circuit lines are symmetrical about the tower axis and the transformers have star or delta connections depending on their location in the system, as indicated in Figure 7.47.

Generator transformers have deltas on the generator, or low-voltage side, and grounded star connection on the high-voltage side. Transmission substation transformers have grounded star on the high-voltage side and low-voltage windings with delta-connected tertiaries. Distribution transformers supplying the electrical supply authorities are delta-connected on the high voltage and grounded star on the low-voltage side.

The connection is important in considering the flow of zero-sequence harmonic currents. A delta-connected winding will act as an open circuit and a star-connected winding, with neutral point grounded, as a short-circuit to the zero-sequence harmonic currents. The zero-sequence impedance of the system will thus be considerably different to that presented to positive- or negative-sequence currents.

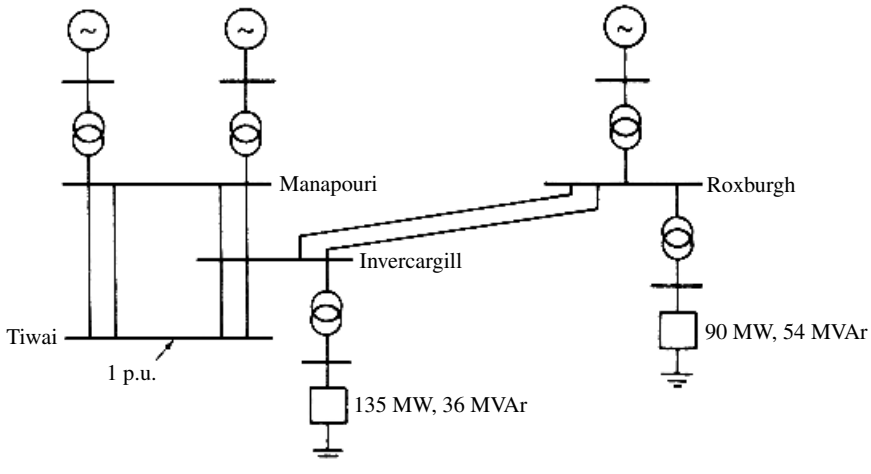


Figure 7.46 Test system including load and generation

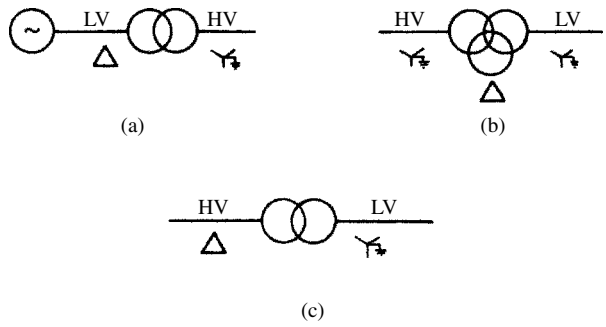


Figure 7.47 Transformer connections: (a) generating station; (b) transmission substation; (c) distribution substation

Generator, Transformer and Load Impedances at Roxburgh With reference to Figure 7.46, a step-by-step formation of the system impedances is initiated by examining the effect of the various components at Roxburgh.

The harmonic impedance locus of the generator, considered in isolation, is shown in Figure 7.48 (curve A). The addition of the generator transformer produces the impedance locus of curve B. Finally, curve C illustrates the damping effect of a 90 MW and 54 MVAR load connected through a transformer to the Roxburgh bus.

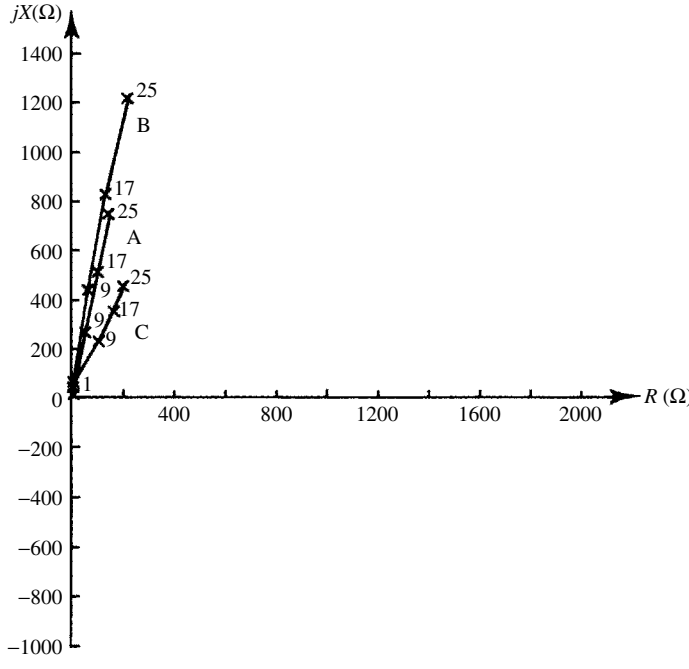


Figure 7.48 Polar plot of the generator, transformer and load impedances at Roxburgh: curve A, generator only; curve B, generator and generator transformer; curve C, generator, generator transformer, load (100%) and load transformer

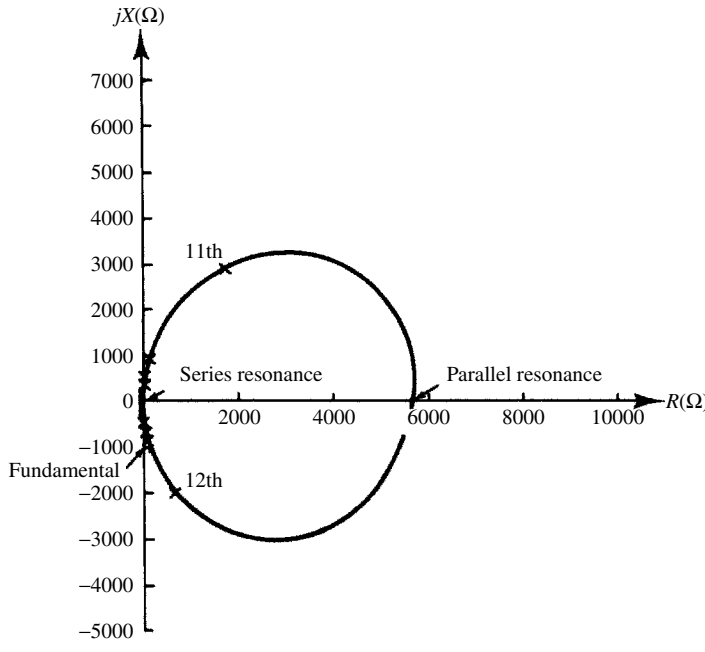


Figure 7.49 Polar plot of the impedance of the open-circuited Invercargill to Roxburgh lines with 50 Hz intervals marked

Interconnection Between Invercargill and Roxburgh The double 220 kV transmission line between Invercargill and Roxburgh in isolation (i.e. open-circuited at Roxburgh) has the impedance locus of Figure 7.49.

At fundamental frequency the line is capacitive, although this is difficult to observe. As the frequency increases the line approaches a series resonance, at which point the impedance is very small and purely resistive, the phase angle becoming inductive. From this point the impedance increases in magnitude in a clockwise direction with increasing frequency. Somewhere between the 11th and 12th harmonics a parallel resonance occurs, manifested by a large, purely resistive impedance. As frequency increases further the line again becomes capacitive.

The effect of line termination is shown in Figure 7.50 for a one per unit harmonic injection at Invercargill. When the line is isolated (i.e. corresponding to the locus of Figure 7.49) the per unit voltages of the various harmonics are illustrated in curves A of Figure 7.50. Figure 7.50(a) gives the voltage magnitudes and Figure 7.50(b) their phase angles.

The same graphs show corresponding voltage magnitudes and phases when the line is short-circuited (Figure 7.50, curves B), loaded by the generator-transformer group (Figure 7.50, curves C) and by the complete system at Roxburgh (Figure 7.50, curves D).

Left-Hand Side of the System Referring now to the left-hand side part of the system of Figure 7.46, with the lines between Invercargill and Roxburgh open, Figure 7.51 illustrates the effect of one per unit harmonic current injections at Tiwai. Curves A

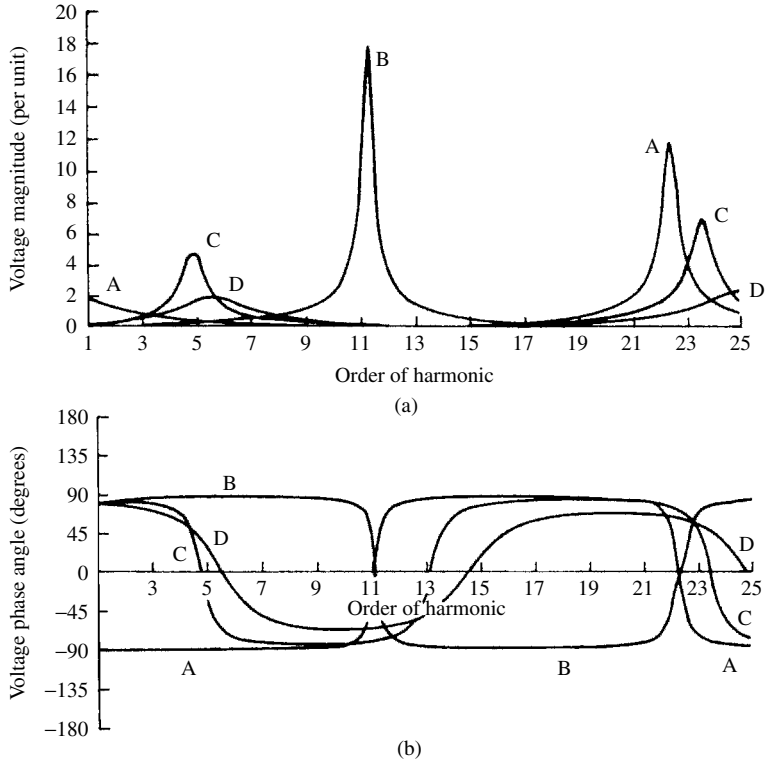


Figure 7.50 Positive-sequence voltages at Invercargill versus frequency for different terminations of the Roxburgh to Invercargill lines: (a) voltage magnitudes; (b) voltage phase angles. Curves A, open circuit; curves B, short-circuit; curves C, generator and generator transformer; curves D, generator, generator transformer, load and load transformer

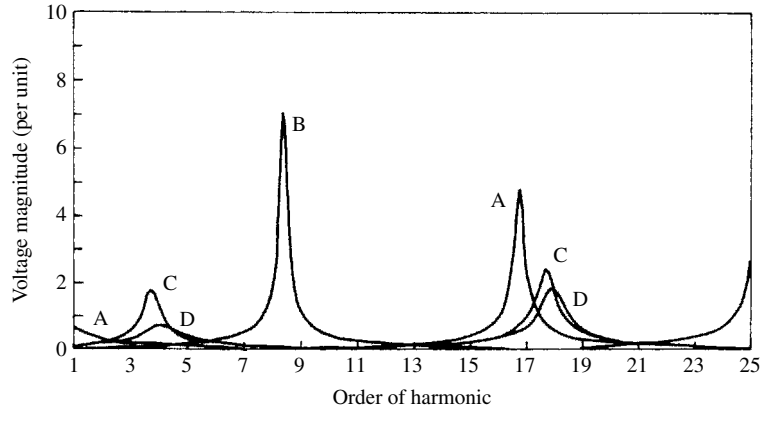


Figure 7.51 Positive-sequence voltage magnitude at Tiwai versus frequency for different termination: curve A, open circuit; curve B, short-circuit; curve C, generator and generator transformer; curve D, generator, generator transformer, load and load transformer

and B of Figure 7.51 show the voltage spectra at Tiwai with the rest of the system open and short-circuited, respectively.

When, first, generation (Figure 7.51, curve C) and then load (Figure 7.51, curve D) are added with the associated transformers, similar effects to the previous section are observed. The resonant points lie between those of the open and short-circuit cases, with reduced magnitudes as compared with the extreme cases of termination.

Complete Test System By combining the two individual systems considered in the two preceding subsections, the progressive formation of the test network (Figure 7.47) is completed.

Figure 7.52 compares the voltage magnitudes at the Tiwai bus for different loading conditions. Curve A shows the effect of the transmission system in isolation (i.e. with all the generators and loads disconnected); the resulting resonance frequencies of the interconnected system do not correspond to those of the two individual parts of the system described in the two preceding subsections. There are now two resonances around the 18th harmonic, one smaller in magnitude. The effect of this latter resonance is to create an extra loop in the impedance locus (as shown in Figure 7.53).

Figure 7.53 illustrates the progressive complexity of the impedance locus as the a.c. system increases.

An appreciation of the variation of the harmonic voltages throughout the complete system is obtained using the three-dimensional diagram of Figure 7.54. Lower voltages are observed on the transformer secondaries, namely at the generator and load busbars. Two major resonances occur at all the busbars. The first is between the 4th and 5th harmonics and the second between the 19th and 20th harmonics; these correspond with the resonances observed in Figure 7.52 at Tiwai.

Three-Phase Impedances of the Test System at Tiwai The unbalanced nature of the transmission network can be illustrated by plotting the three individual equivalent phase impedances. Figure 7.55 shows that the imbalance is low at fundamental frequency, but increases towards the first parallel resonance which occurs between the fourth and

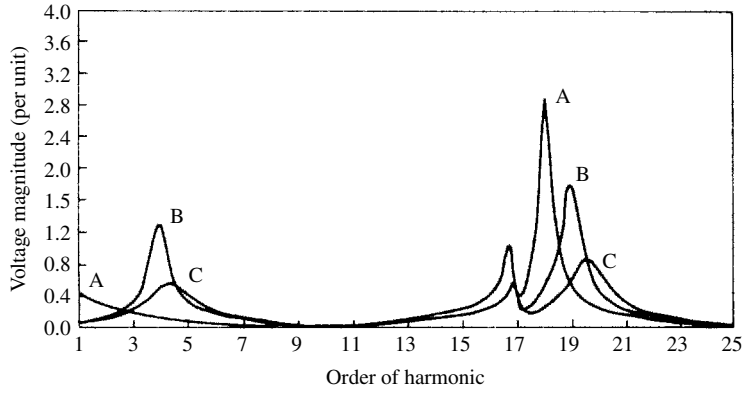


Figure 7.52 Positive-sequence voltages at Tiwai versus frequency for different terminations: curve A, open circuit; curve B, generators and generator transformers; curve C, generators, generator transformers, loads and load transformers

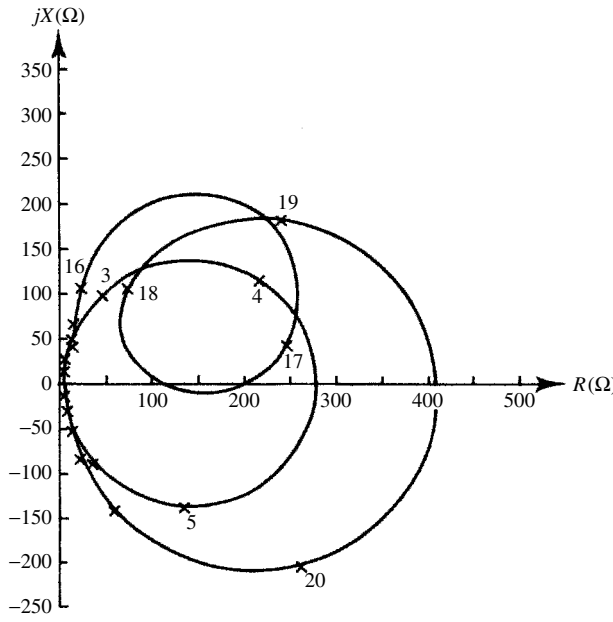


Figure 7.53 Positive-sequence impedances of the test system from Tiwai with harmonic intervals indicated

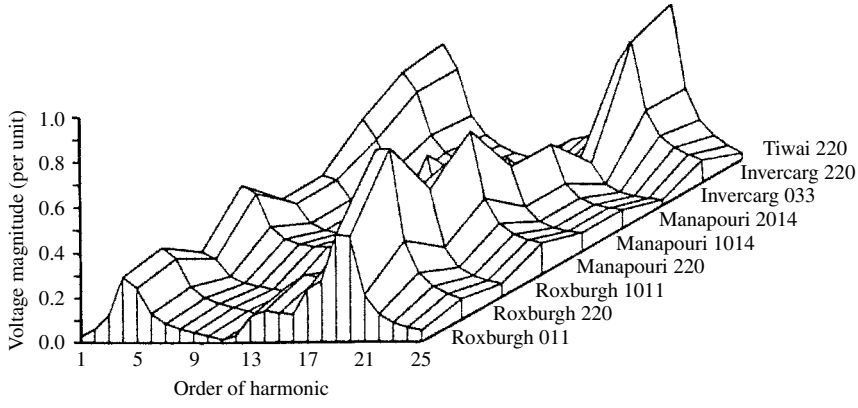


Figure 7.54 Positive-sequence voltage magnitude versus frequency at all test system busbars

fifth harmonics, where the magnitude differences are of the order of 30%. This effect is mainly caused by differences in the mutual impedances between phases, resulting from the asymmetry in transmission line conductor geometries.

The series resonance at the 11th harmonic exhibits low levels of imbalance, and the second parallel resonance between the 19th and 20th harmonics again shows considerable differences in the impedances between phases. High levels of imbalance at parallel resonant frequencies assist in explaining the difficulties experienced with correlating single-phase simulation results with measured tests [39].

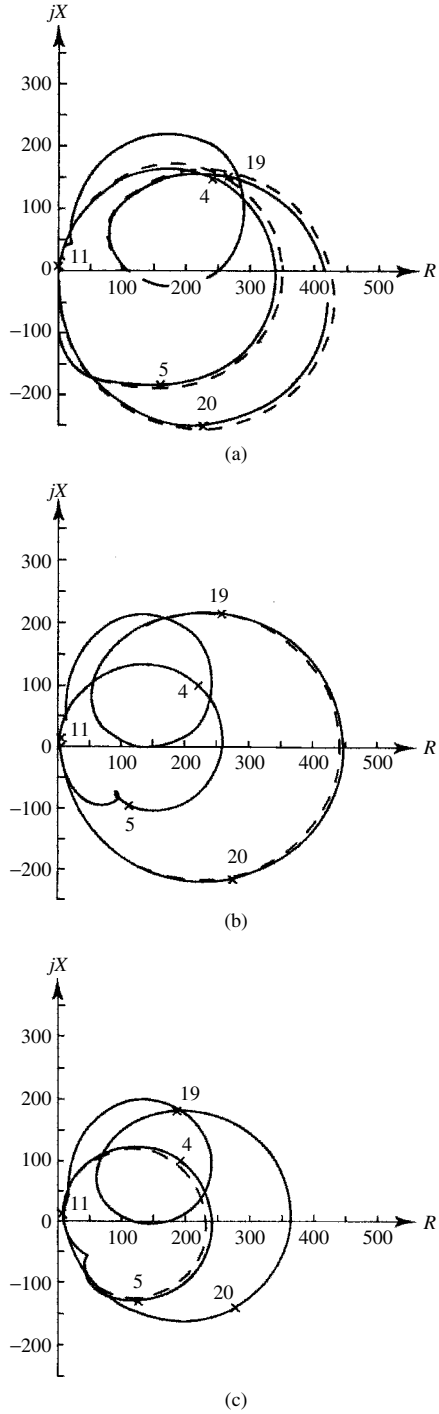


Figure 7.55 Equivalent phase impedances for the test system: (a) red phase; (b) yellow phase; (c) blue phase. (———), balanced load; (- - - -), unbalanced load

While most system loads are nearly balanced, this is not the case with single-phase traction supplies [40]. This effect has been simulated by reducing phase 1 load by 10% and increasing phase 3 load by 10%. The results, also plotted in Figure 7.55, indicate that the level of impedance imbalance at the parallel resonant points increases with load imbalance.

Voltage Sensitivity to Line Parameter Variation By selectively reducing the line lengths and observing the voltages at Tiwai, the lines which most affect resonant conditions are determined. The results are illustrated in Figure 7.56.

A 5% reduction in length in the Tiwai to Manapouri lines (Figure 7.56, curve B) causes the two resonant frequencies around the 18th harmonic to shift by approximately 20 Hz. A 5% decrease in the lengths of the lines from Roxburgh to Invercargill has practically no effect on the smaller resonant frequency, but changes the resonance between the 19th and the 20th harmonics by approximately 10 Hz.

The lines close to the point of the current injection appear to have the largest effect on the system resonance frequencies, and thus their parameters must be represented with a greater level of accuracy than the lines more distant in the network.

Harmonic Imbalance Factor Any harmonic imbalance in the a.c. system will affect the three-phase voltage waveforms, and hence the zero crossings used for the converter control. As a consequence, harmonic imbalance will affect the non-characteristic harmonics produced by converter plant.

At fundamental frequency an imbalance factor has been used to indicate the extent of unbalanced system conditions [41]. The use of such an index at harmonic frequencies gives a simple measure of imbalance. With reference to the reduced system of Figure 7.46, Table 7.4 lists the values of the imbalance factor at parallel resonances, defined as the ratio of negative-sequence voltage, for a balanced one per unit harmonic current injection. The values of the imbalance factor are largest at parallel resonant frequencies; Table 7.4 represents maximum levels.

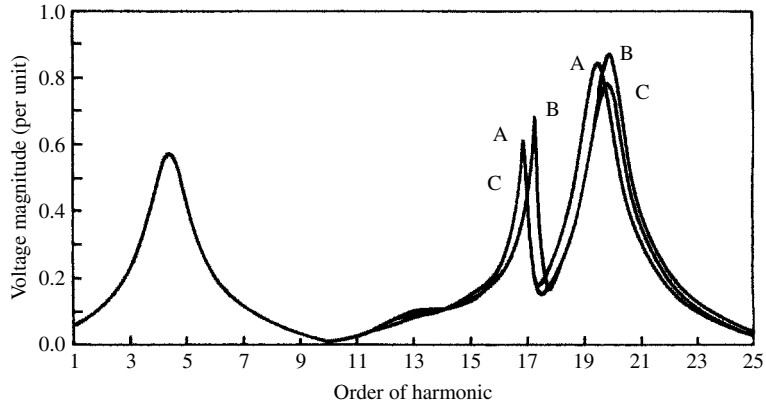


Figure 7.56 Positive-sequence voltage magnitude at Tiwai versus frequency for line length variations: curve A, test system including generation and loads; curve B, Tiwai to Manapouri lines 5% shorter; curve C, Invercargill to Roxburgh lines 5% shorter

Table 7.4 Values of the imbalance factor at parallel resonances for various terminations of the reduced system

	Harmonic	Imbalance factor (%)
Reduced system, no generation or load	17	24.8
Reduced system, generation only	19	10.1
Reduced system, generation and 100% load	20	6.2
With phasing the same on each circuit	20	17.2

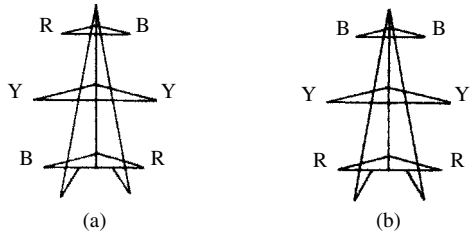


Figure 7.57 Examples of different tower conductor arrangements: (a) common arrangement; (b) phase positions the same in each circuit

The imbalance factor is greatest with a network comprising only the transmission lines. The connection of both generation and load, the models of which are balanced, reduces the imbalance factor. At periods of light load, therefore, the a.c. system tends to be more unbalanced than at times of high load, and the generation of converter uncharacteristic harmonics will increase accordingly. At light load, however, the level of harmonics will be higher and so imbalance is only one factor in the production of these uncharacteristic harmonics.

The last two entries in Table 7.4 are for the system with both load and generation, for line phasings as indicated in Figure 7.57(a) and (b) respectively.

The position of phases in double-circuit lines is normally varied in each circuit as in Figure 7.57(a) to minimise the fundamental frequency imbalance. When the phase positions are altered to be the same in each circuit, as illustrated in Figure 7.57(b), the imbalance factor rises substantially to 17%. Conductor geometries are thus important in unbalanced harmonic penetration analysis.

7.13.3 Harmonic Analysis of Transmission Line with Transpositions [42]

The conductor geometries of high-voltage transmission lines produce considerable impedance asymmetry, which in turn causes corresponding voltage imbalance at the far end of the line.

It is generally accepted that, for practical distances, the effect of line asymmetry can be eliminated by the use of phase transpositions dividing the line into three, or multiples of three, equal lengths. Accordingly, transpositions are often used in long-distance transmission as a means of balancing the fundamental frequency impedances of the line.

In fundamental frequency studies the effect of transpositions is generally accounted for by averaging the distributed parameters of the three transposed sections and using them in a single nominal or equivalent PI circuit. Such a method, however, assumes that the line geometry is perfectly symmetrical at all points, whereas the transpositions occur at two discrete distances, at different points on the standing wave.

The series impedance and shunt equivalent matrices are combined into one admittance matrix that represents the transposed section, i.e.

$$\mathbf{Y}' = \begin{array}{|c|c|}\hline \mathbf{Y}'_{SS} & -\mathbf{Y}'_{SR} \\ \hline -\mathbf{Y}'_{RS} & \mathbf{Y}'_{RR} \\ \hline \end{array} \tag{7.108}$$

where

$$[\mathbf{Y}_{SS}] = [\mathbf{Y}_{RR}] = [\mathbf{Z}]^{-1} + \tfrac{1}{2}[\mathbf{Y}]$$
$$[\mathbf{Y}_{SR}] = [\mathbf{Y}_{RS}] = [\mathbf{Z}]^{-1}$$

The admittance parameters for the individual sections are then transformed into $\mathbf{A}'$, $\mathbf{B}'$, $\mathbf{C}'$, $\mathbf{D}'$ parameters, such that they can be cascaded, i.e.

$$[\mathbf{A}] = [\mathbf{A}_1][\mathbf{A}_2][\mathbf{A}_3] \tag{7.109}$$

Finally, the resultant transmission parameters $\mathbf{A}$, $\mathbf{B}$, $\mathbf{C}$, $\mathbf{D}$ are converted back into an admittance matrix which properly represents the effects of transpositions.

The nodal admittance matrix equation of the three-phase transmission line may be written as

$$\begin{array}{|c|}\hline \mathbf{I}_S \\ \hline \mathbf{I}_R \\ \hline \end{array} = \begin{array}{|c|c|}\hline \mathbf{Y}_{SS} & -\mathbf{Y}_{SR} \\ \hline -\mathbf{Y}_{RS} & \mathbf{Y}_{RR} \\ \hline \end{array} \begin{array}{|c|}\hline \mathbf{V}_S \\ \hline \mathbf{V}_R \\ \hline \end{array} \tag{7.110}$$

where $\mathbf{I}_S$, $\mathbf{I}_R$, $\mathbf{V}_S$ and $\mathbf{V}_R$ are vectors of a size determined by the number of coupled conductors.

Applying a partial inversion algorithm to equation (7.110), the following matrix of inverse hybrid parameters is obtained.

$$\begin{array}{|c|}\hline I_S \\ \hline V_R \\ \hline \end{array} = \begin{array}{|c|c|}\hline Y_{SS} - Y_{SR}Y^{-1}{}_{RR}Y_{RS} & -Y_{SR}Y^{-1}{}_{RR} \\ \hline Y_{RR}^{-1}Y_{RS} & Y_{RR}^{-1} \\ \hline \end{array} \begin{array}{|c|}\hline V_S \\ \hline I_R \\ \hline \end{array} \tag{7.111}$$

or

$$V_R = Y^{-1}{}_{RR}Y_{RS}V_S + Y^{-1}{}_{RR}I_R \tag{7.112}$$

Two different cases are of interest and will be used in the following sections. The first relates to a harmonic voltage excited open-ended line, specified as $V_S = 1$ p.u. and $I_R = 0$. This case produces the highest voltage harmonic levels and must, therefore, be considered for design purposes. The second important case is the harmonic current

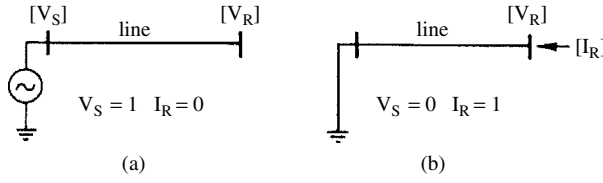


Figure 7.58 Diagram of terminal conditions: (a) voltage source and open-ended line; (b) current source and short-circuited line

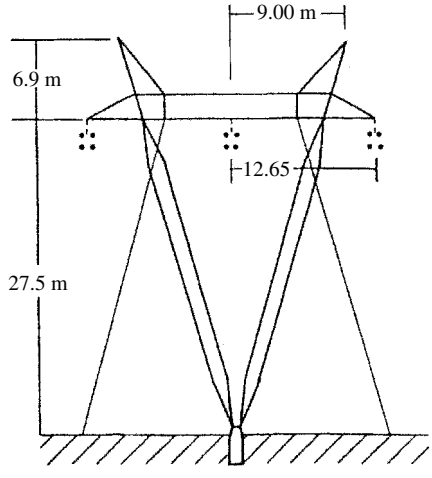


Figure 7.59 Test line

excited short-circuited ended line, specified as $V_S = 0$ and $I_R = 1$ p.u., which is more likely to be of practical interest. These two cases are illustrated by the simplified diagrams of Figure 7.58(a) and (b), respectively.

Details of the Test Line The test line, shown in Figure 7.59, is of flat configuration without earth wires, and the main parameters are:

Nominal voltage = 500 kV
Conductor type: Panther (30/3.00 + 7/3.00 ACSR)
Resistivity = 100 Ω/m
Equal distances between transpositions and the natural impedance matrix

Effect of Transpositions with Voltage Excitation Harmonic voltage sources are often ignored when assessing harmonic distortion. However, under non-ideal system conditions, synchronous generators can produce harmonic EMFS [43]. Moreover, some power electronic circuits operate as harmonic voltage sources [44,45]. It is thus appropriate to consider the effectiveness of transpositions in the presence of harmonic as well as power frequency voltage sources.

The test line is fed from 1 p.u. voltage sources at fundamental and harmonic frequencies. It is realised that the presence of 1 p.u. harmonic voltage sources is unrealistic, but such a figure provides a good reference for comparability between the effects at different frequencies. The expected harmonic voltage levels are likely to be about 1–3% of the fundamental and, therefore, the results plotted in later figures should be scaled down proportionally.

Open-Ended Line The fundamental frequency behaviour of the open-ended line is illustrated in Figure 7.60(a) and (b) for the line untransposed and transposed, respectively. In each case, the receiving end voltages are plotted for line distances varying from 50 to 1500 km.

These figures indicate that in the absence of voltage compensation, the effectiveness of transpositions is limited to line distances under one-eighth of the wavelength (i.e. 750 km at 50 Hz). For distances approaching the quarter wavelength, the transposed line produces considerably greater imbalance than the untransposed.

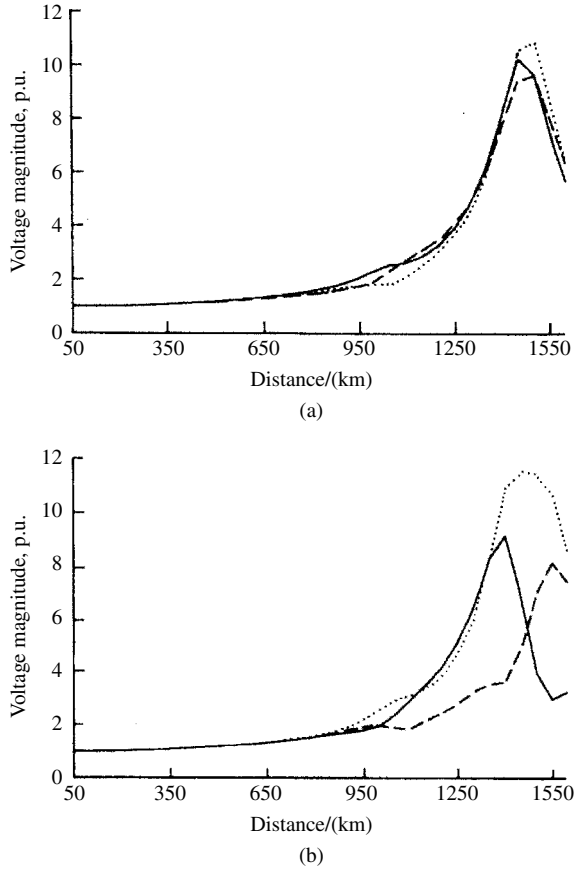


Figure 7.60 Fundamental frequency three-phase voltages at the end of the test line (open-circuited) versus line distance. (a) without transpositions: (———), R; (- - - -), Y; (· · · · · ·), B; (b) with transpositions: (———), Y; (- - - -), B; (· · · · · ·), R

Although such transmission distances are impractical without compensation, the results provide some indication of the behaviour to be expected with shorter lines at harmonic frequencies. Such behaviour is exemplified in Figure 7.61, which corresponds to the case of a line excited by 1 p.u. 3rd harmonic voltage. However, the results plotted in Figure 7.61, obtained at 50 km intervals, are not sufficiently discriminating around the points of resonance. Thus the region of resonant distances has been expanded in Figure 7.62 to illustrate more clearly the greatly increased imbalance caused by the transpositions. The resonant peaks of the three phases occur at very different distances, e.g. Figure 7.61(b) shows 50 km diversity between the peaks. Therefore, for a given line distance the resonant frequencies will vary, thus increasing the risk of a resonant condition.

It is also interesting to note the dramatic voltage amplification which occurs for electrical distances equal to the first quarter wavelength. Figure 7.62 shows a peak of 35 per unit for the 3rd harmonic when the line is 500 km long, and the 5th harmonic peak (not shown) reaches 45 per unit at about 300 km.

Figure 7.61(a) and (b) also show the effect of attenuation with distance, i.e. the considerable reduction of the peaks at resonant distances at the odd quarters of wavelength

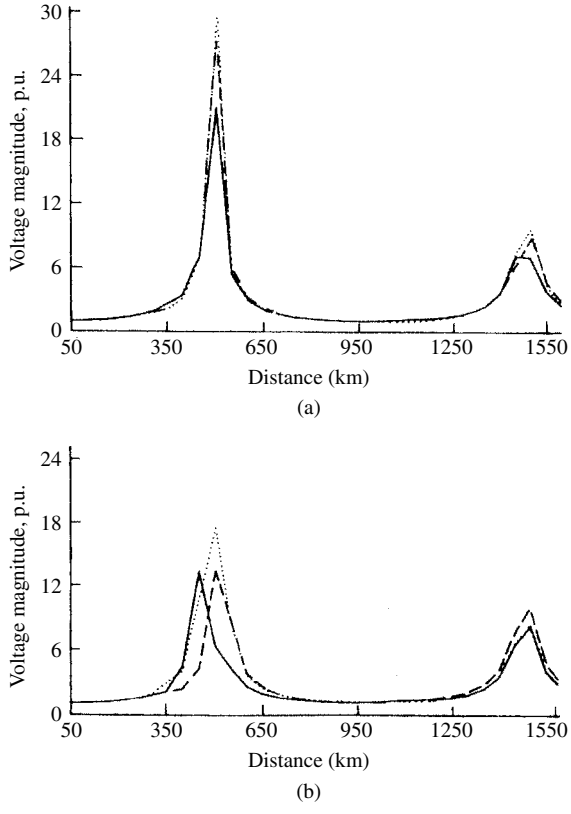


Figure 7.61 Three-phase third harmonic voltages at the end of the test line (open-circuited) versus line distance. For key see Figure 7.60

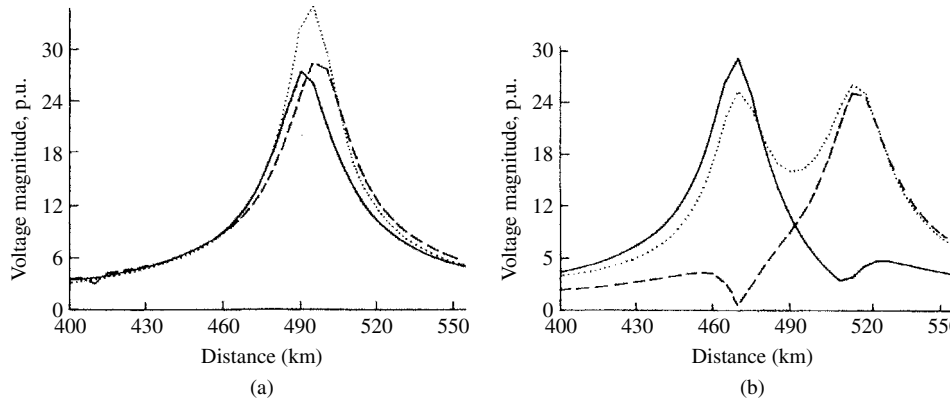


Figure 7.62 Results of Figure 7.61 expanded in the region of resonance. For key see Figure 7.60

other than the first. Such attenuation is caused by the series and shunt resistive components of the equivalent PI model.

The immediate effect of the transpositions is the compensation of geometrical line asymmetry. This can only result in electrical symmetry if the average currents in each of the transposed sections are similar. Thus the deterioration of voltage balances current standing wave along the line. The improved symmetry of the phase voltages at the three-quarter wave distance, seen in Figure 7.61, is due to the averaging effect produced by the third harmonic standing wave, as illustrated by the idealised waveforms of Figure 7.63.

From the above discussion the effectiveness of transpositions should improve as the voltage and current profile throughout the line becomes more uniform, i.e. closer to the natural loading condition, which is discussed in the next section.

Line Loaded If an ideal (uncoupled and unattenuated) line is loaded with its characteristic impedance, the sending end voltage will be sustained throughout the line, provided that the phase angle difference between the sending and receiving end voltages is kept below 45° (or 750 km at 50 Hz). To assess the effectiveness of transpositions with loading, the test line was loaded with its characteristic impedance calculated at 50 Hz. It must be noted that in a coupled multiconductor line such impedance is a matrix, of which only the diagonal elements are being used for the loading. Furthermore, the three diagonal elements are different and are also frequency dependent. We cannot therefore expect to see the uniform 1 p.u. voltage predicted by conventional theory.

For a line loaded with its characteristic impedance, the effectiveness of transpositions is limited to distances of about 350 km and 200 km for the 3rd and 5th harmonics, respectively. Beyond those distances the transposed lines produce higher levels of imbalance. Subsequent harmonic peaks are seen to reduce rapidly with loading. By way of example, the 5th harmonic voltages without and with transpositions are shown in Figure 7.64(a) and (b), respectively.

The harmonic behaviour of a loaded transmission line without and with transpositions is illustrated in Figure 7.65(a) and (b), respectively. This figure displays the

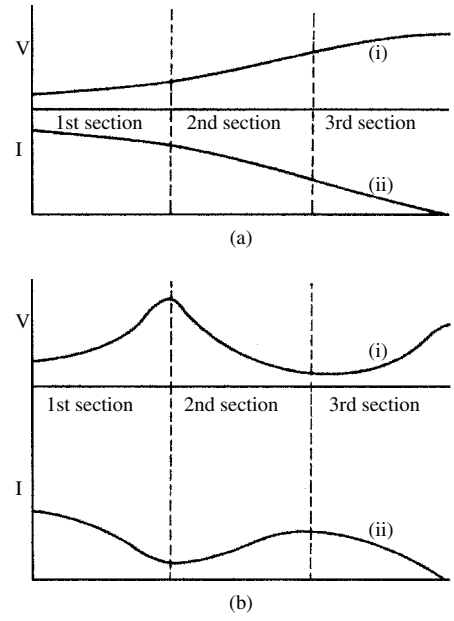


Figure 7.63 (a) Standing waves along a line of quarter wavelength: (i) voltage wave; (ii) current wave. (b) Third harmonic standing waves along a line of three quarter wavelength: (i) voltage wave; (ii) current wave

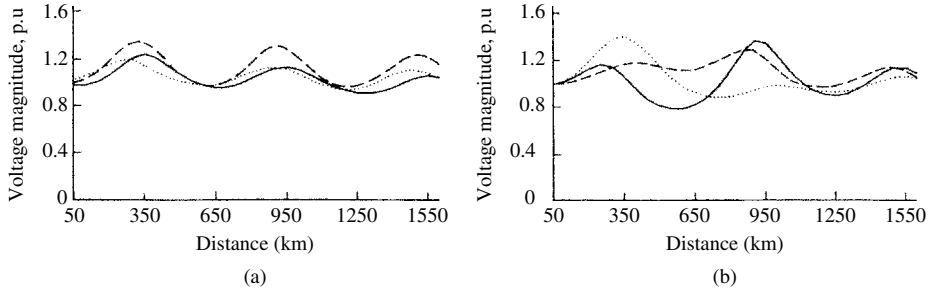


Figure 7.64 Three-phase fifth harmonic voltages at the end of the test line (loaded with the characteristic impedance). For key see Figure 7.60

variation of 5th harmonic voltage at the receiving end of a 250 km line with one per unit voltage injection at the sending end. The level of imbalance of the untransposed line (Figure 7.65(a)) shows a gradual increase up to about the natural load (1 p.u. admittance) and very little change thereafter. In contrast, Figure 7.65(b) illustrates a dramatic increase in the voltage imbalance as the load reduces from the natural level (1 p.u. admittance) to the open-circuit condition. A qualitative justification for this behaviour has been made in Figure 7.63. As the line load increases above the natural level, Figure 7.65(b) shows that effectiveness of the transposition increases.

Considering the relatively insignificant levels of harmonic voltage excitation expected from a well-designed system, the resulting voltage distortion in a transposed

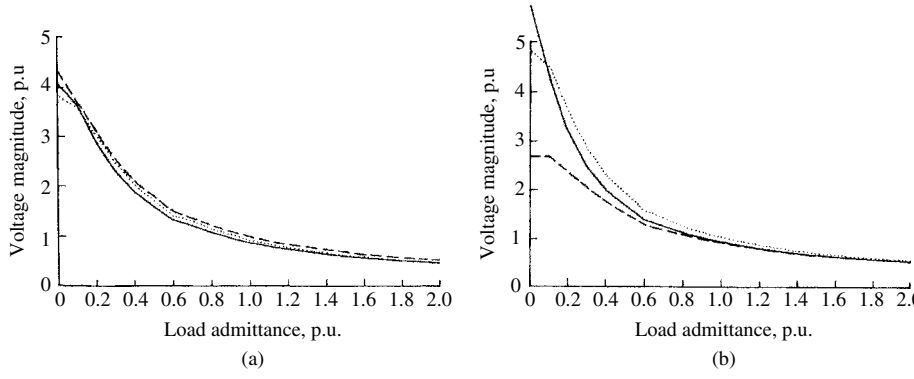


Figure 7.65 Three-phase fifth harmonic voltages at the end of a 250 km test line versus loading admittance (referred to the characteristic admittance). For key see Figure 7.60

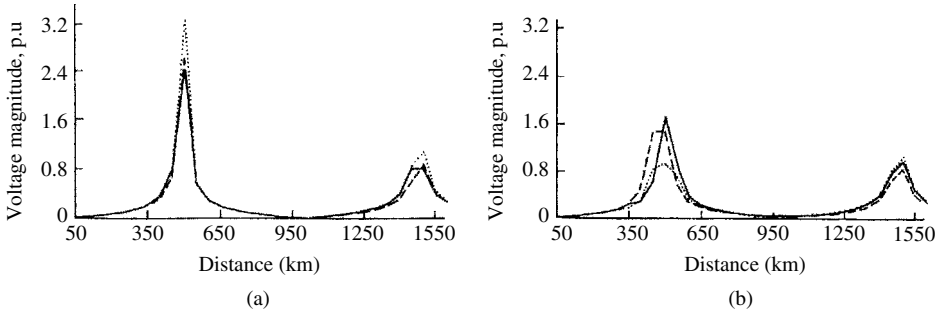


Figure 7.66 Three-phase third harmonic voltages caused by 1 p.u. third harmonic current at the point of harmonic current injection. For key see Figure 7.60

or untransposed load line is not expected to cause problems, except when the line is lightly loaded. With harmonic current excitation the situation may be quite different, and its effect is examined next.

Effect of Transpositions with Current Excitation The main cause of power system harmonic distortion is the large static power converter, such as used in HVd.c. transmission and in the metal reduction industry. Because of their large d.c. smoothing inductance compared to the a.c. system impedance, static converters can be considered as current sources on the a.c. side and voltage sources on the d.c. side [46].

Thus, the harmonic modelling of a long transmission line feeding a static converter is basically that of Figure 7.58(b), i.e. a harmonic current source at the receiving end of the line with the sending end shorted to ground through a relatively low impedance.

The harmonic voltages at the point of current harmonic injection follow the same pattern as those of the open circuit line with harmonic voltage excitation. This is clearly illustrated in Figure 7.66 for a case of 3rd harmonic current injection. Similarly to the voltage excited open line, substantial voltage distortion results when the line length is close to a quarter wavelength, although the imbalance caused by transpositions is less pronounced in the case of current injection.

7.13.4 Harmonic Analysis of Transmission Line with VAR Compensation [47]

Matrix Model of a Compensated Line Generally, long transmission lines are divided into two or three sections of equal length and VAR compensating equipment is connected between them in the form of series capacitors and shunt inductors or capacitors. An equivalent circuit of a typical long-distance transmission line with conventional compensation elements is illustrated in Figure 7.67.

Each line section is represented by its harmonic admittance matrix

$$Y = \begin{bmatrix} [Y_{SS}] & [-Y_{SR}] \\ [-Y_{RS}] & [Y_{RR}] \end{bmatrix}_h \tag{7.113}$$

where

$$[Y_{SS}] = [Y_{RR}] = [Z]^{-1}{}_{EPM} + \tfrac{1}{2}[Y]_{EPM}$$
$$[Y_{SR}] = [Y_{RS}] = [Z]^{-1}{}_{EPM}$$

the suffix EPM indicating equivalent PI model.

With the assumption that the compensating inductances and capacitances are uncoupled and linearly dependent with frequency, their corresponding harmonic matrix admittances are:

$$Y_c = \begin{bmatrix} jh_o\omega_o C_c & 0 & 0 \\ 0 & jh_o\omega_o C_c & 0 \\ 0 & 0 & jh_o\omega_o C_c \end{bmatrix} \quad Y_L = \begin{bmatrix} \dfrac{-j}{h\omega_o L_c} & 0 & 0 \\ 0 & \dfrac{-j}{h\omega_o L_c} & 0 \\ 0 & 0 & \dfrac{-j}{h\omega_o L_c} \end{bmatrix} \tag{7.114}$$

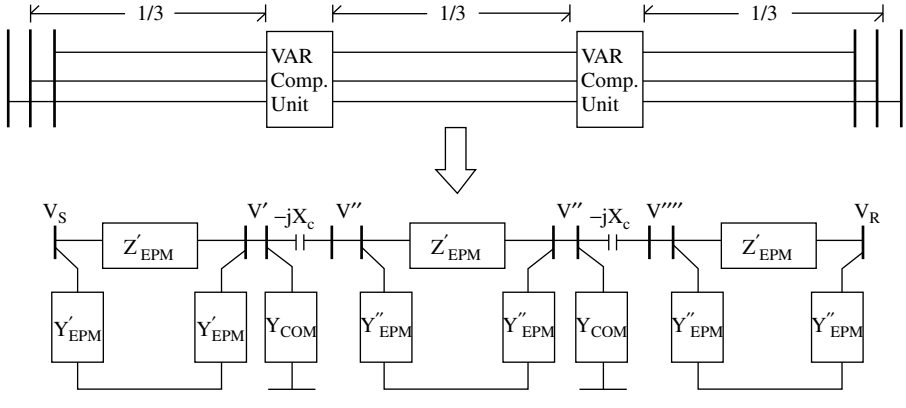


Figure 7.67 Equivalent circuit of VAR compensated transmission line point of harmonic current injection

where L and C are the fundamental frequency values of the compensating inductance and capacitance derived from load flow studies, and h is the harmonic order.

Finally, the admittance matrices of the individual subsystems, i.e. the line sections and VAR compensating units, must be combined into a single admittance matrix.

If the purpose is to observe harmonic voltages at the far end of the transmission system, the individual subsystems must be transformed to *ABCD* parameters and then cascaded to obtain an equivalent *ABCD* matrix equation. This in turn can be converted back to an equivalent admittance matrix, which relates the currents and voltages at the two ends of the line, as described by equations (7.112), (7.113) and (7.114) and Figure 7.58

Harmonic Voltage Excitation The test line is a 1000 km line of the same configuration as shown in Figure 7.59.

The addition of shunt inductive compensation effectively increases the characteristic impedance and thus reduces the load that causes the optimum voltage profile.

For the positive-sequence shunt admittance values of the test system, a standard load flow program was used to derive the optimal discrete shunt inductances required to provide a practically constant voltage along the line at the fundamental frequency.

However, the addition of shunt inductance isolates the line from ground (reducing its ability to act as a low-pass filter) and thus reduces its ability to dampen harmonics.

The results, plotted in Figure 7.68, correspond to an open-ended line and show that while the fundamental frequency voltage profile is good, the line performance at harmonic frequencies is worse than without compensation. In particular, the level of the receiving end voltage for second-harmonic injection has increased dramatically.

In the absence of compensation, the natural load of the line under consideration is approximately 950 MW, but the maximum nominal loading planned is 1450 MW, i.e. 1.5 times the natural load.

For this loading condition, Figure 7.69 shows the effect of a combined compensation scheme, consisting of shunt and series capacitors. It is noted that shunt capacitors tend to amplify harmonic distortion at the compensation points, while having the opposite effect elsewhere.

Harmonic Current Excitation In this case, a one per unit harmonic current was injected at the receiving end of the line.

The effect of shunt inductive compensation in the harmonic behaviour of the unloaded line is shown in Figure 7.70; again the second harmonic shows the greater amplification.

The results of combining series and shunt capacitive compensation for the case of a heavily loaded line, shown in Figure 7.71, indicate that the magnitudes of the harmonic voltages for the loaded line are smaller than those of an open-ended line.

7.13.5 Harmonic Analysis of an HVD.C. Transmission Line [48]

Due to the limited number of phases and switching devices, the d.c. output voltages at converter stations contain considerable ripple. Under perfectly symmetrical a.c. supply and switching conditions, the voltage ripple consists only of twelve pulse-related harmonics. In practice, however, a.c. system imbalance and asymmetrical firing may lead to other frequencies being present in the d.c. voltage waveforms.

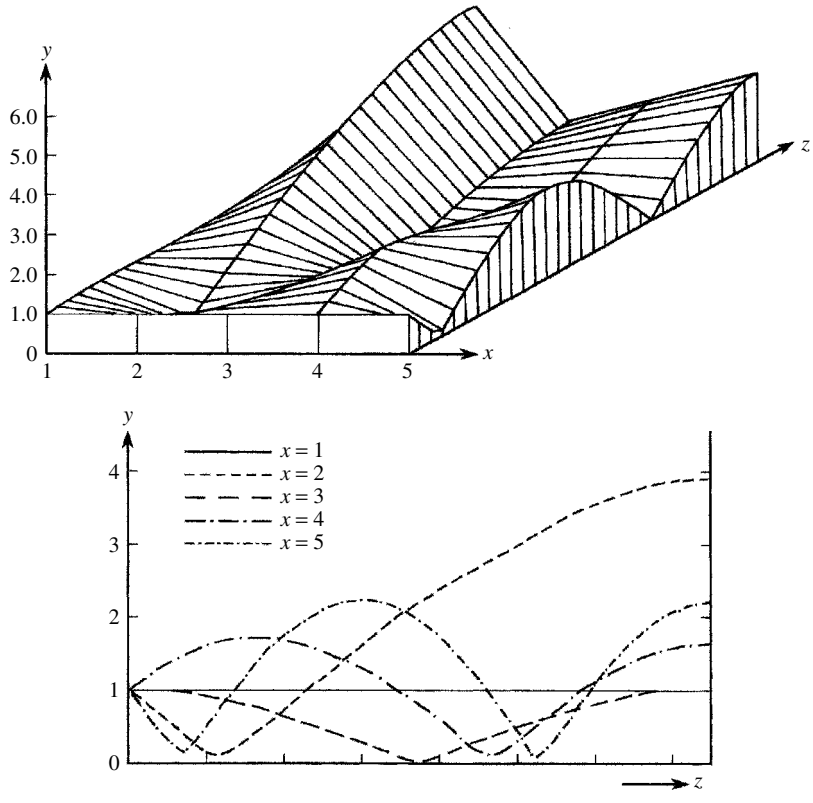


Figure 7.68 Fundamental and harmonic voltage levels along the unloaded line with shunt inductive compensation and 1 per unit voltage at the sending end. x, harmonic order; y, voltage magnitude; z, line position with reference to point of harmonic injection. For key see Figure 7.60

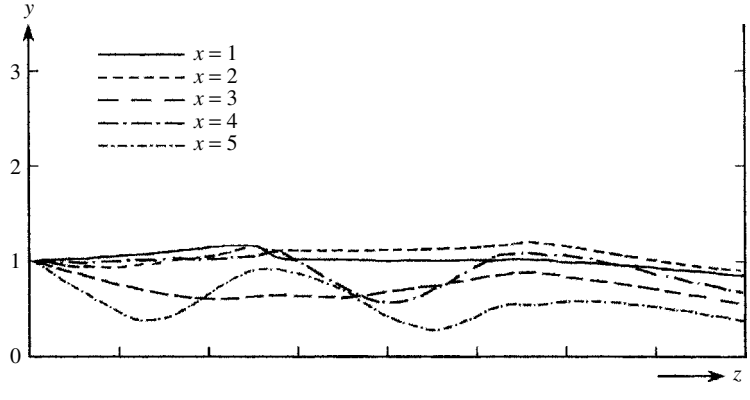


Figure 7.69 Standing waves along the heavy-loaded line with series as well as shunt capacitive compensation

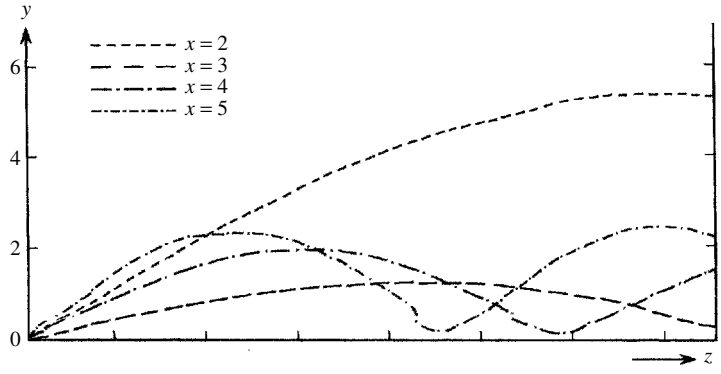


Figure 7.70 Harmonic voltage levels along the unloaded line with shunt inductive compensation

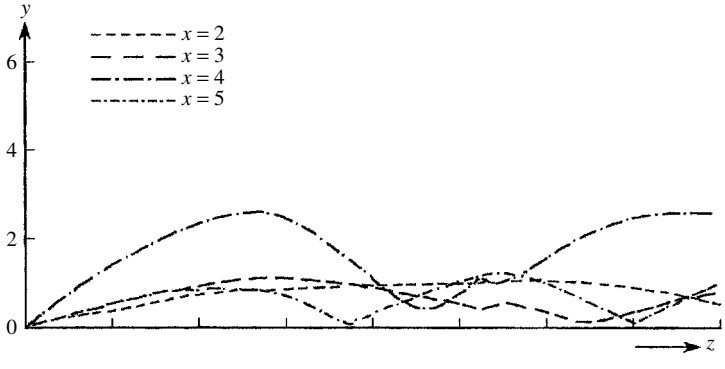
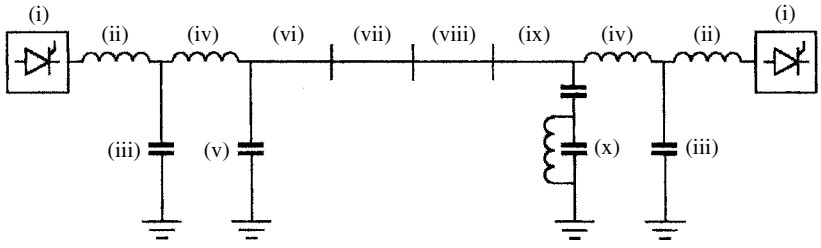


Figure 7.71 Harmonic voltage levels along the loaded line with series as well as shunt capacitive compensation

It is, therefore, necessary to derive the full spectrum of harmonic admittances of the d.c. link. For generality, the test system, based on the New Zealand system, contains overhead lines and submarine cables, and each of them must be represented by the frequency-dependent models derived in earlier sections. The New Zealand HVd.c. link, illustrated in Figure 7.72, consists of six major subsystems, (ii), (v), (vi), (vii), (viii) and (ix), and three auxiliary components (iii), (iv) and (x). The distances of the main transmission components are:

SI inland line	484 km
SI coastal line	49 km
Cook Strait cable	37 km
NI coastal line	34.5 km

Figure 7.73 shows a typical tower, with relevant data (for the inland line section) given in Table 7.5.



(i) Convertor terminal
(ii) Smoothing reactor
(iii) High frequency capacitor (0.1 μF)
(iv) Line trap (1.05 mH)
(v) Surge capacitor (0.9 μF)
(vi) SI inland line section
(vii) SI coastal line section
(viii) Cook Strait cable
(ix) NI coastal line section
(x) 600 Hz damping circuit

Figure 7.72 Layout of NZ d.c. link, including ancillary components

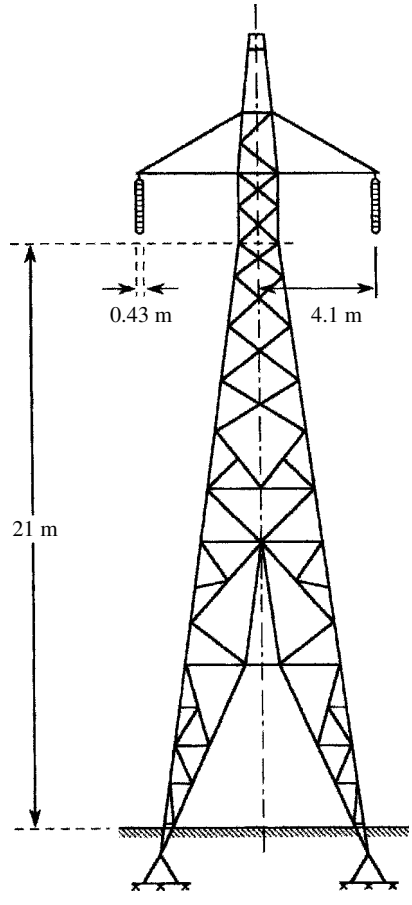


Figure 7.73 Typical d.c. tower

Table 7.5 Inland line section data

	Main conductors	Earth wire
Resistance	0.351	3.1 ohms/km
Diameter	38.4 mm	11.5 mm
Skin ratio T/D	0.3859	0.5
Bundle spacing	431.8 mm	–

Table 7.6 Data for the New Zealand cable system

Conductor	Inside diameter (mm)	Outside diameter (mm)	Resistance
Core	13.462	33.477	0.0331 Ohms/km
Sheath	63.242	71.044	0.2865 Ohms/km
Armour	88.189	98.958	0.1148 Ohms/km
Sea	110.896	–	0.21 Ohms-metres

Towers in the coastal sections are identical to those in Figure 7.73 except that the spacing between conductors is increased from 7.23 m to 12.8 m.

A cross-section of the submarine cable is shown in Figure 7.18, and relevant information for the cable is given in Table 7.6.

A relative permittivity of 3.5 and a relative permeability of 1.0 for the insulation are also assumed.

Derivation of Parameters [48] Considering the perfectly balanced self- and mutual impedance of the line, the HVd.c. scheme is best analysed using sequence networks (of positive and zero sequence). With reference to the circuit diagram of Figure 7.74, the positive-sequence current is defined as the average current flowing from node 1 to node 2, i.e.

$$I_+ = (I_1 - I_2)/2 \tag{7.115}$$

and the zero-sequence component is the average current flowing into the network, and returning by some other path, i.e.

$$I_0 = (I_1 + I_2)/2 \tag{7.116}$$

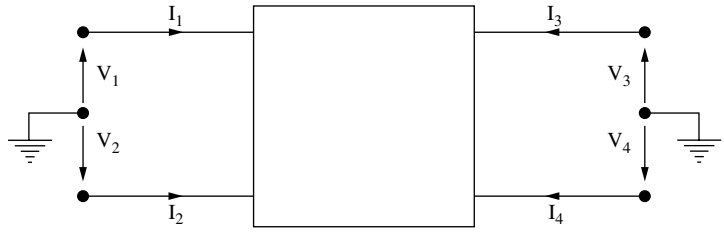


Figure 7.74 Components of a two-phase system

The relationships between the phase and sequence components of current and voltage are:

$$\begin{bmatrix} I_0 \\ I_+ \end{bmatrix} = [T] \begin{bmatrix} I_1 \\ I_2 \end{bmatrix} \tag{7.117}$$

$$\begin{bmatrix} V_0 \\ V_+ \end{bmatrix} = [T] \begin{bmatrix} V_1 \\ V_2 \end{bmatrix} \tag{7.118}$$

where

$$[T] = \frac{1}{2} \times \begin{bmatrix} 1 & 1 \\ 1 & -1 \end{bmatrix} \tag{7.119}$$

In terms of sequence components the impedances and admittances of the series and shunt elements of the equivalent PI circuits of the subsystems are:

$$[Z_{\text{sequence}}] = \begin{bmatrix} Z_o & 0 \\ 0 & Z_+ \end{bmatrix} \tag{7.120}$$

$$[Y_{\text{sequence}}] = \begin{bmatrix} Y_o & 0 \\ 0 & Y_+ \end{bmatrix} \tag{7.121}$$

The above equation may be written as

$$\begin{bmatrix} Z_s & Z_m \\ Z_m & Z_s \end{bmatrix} = 0.5 \begin{bmatrix} 1 & 1 \\ 1 & -1 \end{bmatrix} \begin{bmatrix} Z_o & 0 \\ 0 & Z_p \end{bmatrix} \begin{bmatrix} 1 & 1 \\ 1 & -1 \end{bmatrix} \tag{7.122}$$

Therefore

$$Z_s = 0.5\ [Z_o + Z_p] \text{ and } Z_m = 0.5\ [Z_o - Z_p] \tag{7.123}$$

Similarly

$$Y_s = 0.5\ [Y_o + Y_p] \text{ and } Y_m = 0.5\ [Y_o - Y_p] \tag{7.124}$$

The impedance and admittance matrices for each of the sections must be transformed in *ABCD* parameter matrices in order to cascade the section. For the circuit of Figure 7.75, the *ABCD* parameter transformation equations are as follows:

$$\begin{aligned} A &= 1 + Y_2 Z \\ B &= Z \\ C &= Y_1 + Y_2 + Z\ Y_1 Y_2 \\ D &= 1 + Y_1 Z \end{aligned} \tag{7.125}$$

For the situation under consideration, the scalar quantities Z, Y_1 and Y_2 must be replaced with the appropriate matrices, i.e.

$$\begin{aligned} Y_1 = Y_2 &= 0.5\ [Y_{\text{phase}}] \\ Z &= [Z_{\text{phase}}] \end{aligned} \tag{7.126}$$

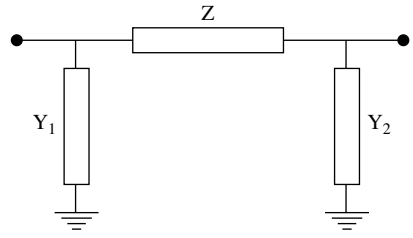


Figure 7.75 Circuit for calculating *ABCD* parameters

Therefore, the *ABCD* parameter matrix equations become

$$\begin{aligned}
[A] &= [\mathrm{U}] + 0.5[\mathrm{Y}_{\mathrm{phase}}][\mathrm{Z}_{\mathrm{phase}}] \\
[B] &= [\mathrm{Z}_{\mathrm{phase}}] \\
[C] &= [\mathrm{Y}_{\mathrm{phase}}] + 0.5[\mathrm{Z}_{\mathrm{phase}}][\mathrm{Y}_{\mathrm{phase}}]^2 \\
[D] &= [A]
\end{aligned} \tag{7.127}$$

The final form of the *ABCD* parameter matrix for a particular section is, therefore

$$[ABCD] = \begin{bmatrix} [A] & [B] \\ [C] & [D] \end{bmatrix} \tag{7.128}$$

The sections may then be cascaded by simply multiplying their respective *ABCD* matrices together, i.e.

$$\begin{bmatrix} [A] & [B] \\ [C] & [D] \end{bmatrix} = \begin{bmatrix} [A^1] & [B^1] \\ [C^1] & [D^1] \end{bmatrix} \mathrm{x—x} \begin{bmatrix} [A^n] & [B^n] \\ [C^n] & [D^n] \end{bmatrix} \tag{7.129}$$

The resulting 4×4 matrix must be converted back into a 4×4 admittance using the following inverse equations:

$$\begin{aligned}
[\mathrm{Y}_{11}] &= [D][B]^{-1} \\
[\mathrm{Y}_{12}] &= [C] - [D][B]^{-1}[A] \\
[\mathrm{Y}_{21}] &= -[B]^{-1} \\
[\mathrm{Y}_{22}] &= [B]^{-1}[A]
\end{aligned} \tag{7.130}$$

The final admittance matrix, in terms of phase components, is

$$[\mathrm{Y}] = \begin{bmatrix} \mathrm{Y}_{11} & \mathrm{Y}_{12} & \mathrm{Y}_{13} & \mathrm{Y}_{14} \\ \mathrm{Y}_{21} & \mathrm{Y}_{22} & \mathrm{Y}_{23} & \mathrm{Y}_{24} \\ \mathrm{Y}_{31} & \mathrm{Y}_{32} & \mathrm{Y}_{33} & \mathrm{Y}_{34} \\ \mathrm{Y}_{41} & \mathrm{Y}_{42} & \mathrm{Y}_{43} & \mathrm{Y}_{44} \end{bmatrix} = \begin{bmatrix} [\mathrm{Y}_{11}] & [\mathrm{Y}_{12}] \\ [\mathrm{Y}_{21}] & [\mathrm{Y}_{22}] \end{bmatrix} \tag{7.131}$$

Thus the transmission network of Figure 7.74 may be represented by the following equation:

$$[I] = [Y][V] \tag{7.132}$$

where $[I] = [I_1, I_2, I_3, I_4]$ and $[V] = [V_1, V_2, V_3, V_4]$.

In order to calculate the impedance seen from the sending end terminals, the 4×4 admittance matrix must first be reduced to a 2×2 matrix by eliminating the receiving end voltages and currents. Since the receiving end converter can be approximated by a voltage source, it appears as a short circuit to harmonic frequencies. It may, therefore, be assumed that

$$V_3 = V_4 \quad \text{and} \quad I_3 = -I_4$$

This leads to the 2×2 admittance matrix in terms of I_1, V_1 and I_2, V_2 only:

$$Y' = \begin{bmatrix} Y_{11} - Y_a & Y_{12} - Y_b \\ Y_{21} - Y_c & Y_{22} - Y_d \end{bmatrix} \tag{7.133}$$

where

$$Y_a = \frac{(Y_{13} + Y_{14})(Y_{31} + Y_{41})}{(Y_{33} + Y_{34} + Y_{43} + Y_{44})}$$

$$Y_b = \frac{(Y_{13} + Y_{14})(Y_{32} + Y_{42})}{(Y_{33} + Y_{34} + Y_{43} + Y_{44})}$$

$$Y_c = \frac{(Y_{23} + Y_{24})(Y_{31} + Y_{41})}{(Y_{33} + Y_{34} + Y_{43} + Y_{44})}$$

$$Y_d = \frac{(Y_{23} + Y_{24})(Y_{32} + Y_{42})}{(Y_{33} + Y_{34} + Y_{43} + Y_{44})}$$

Moreover, if the midpoint between the two poles at the far end is earthed, then $V_3 = V_4 = 0$, and the above matrix simplifies to:

$$Y' = \begin{bmatrix} Y_{11} & Y_{12} \\ Y_{21} & Y_{22} \end{bmatrix} \tag{7.134}$$

Finally, the positive-sequence admittance is

$$Y_{pos} = 0.5[Y_{11} - Y_{12}] \tag{7.135}$$

Impedance Plots Figure 7.76 compares the impedance plots, as seen from the Benmore terminal, obtained both with and without ancillary components. As can be readily seen, the effect of including the ancillary components is quite dramatic at high frequencies, shifting all the resonances to the left, and markedly altering the magnitude of the very first peak.

Figure 7.77 compares the same impedance plots as seen from the Haywards end. Although the resonances are again shifted to the left, the effect of the cable, as discussed in the previous section, tends to mask out the standing wave effects occurring in the SI inland line section. Of note here, however, is the 600 Hz damping circuit, with the

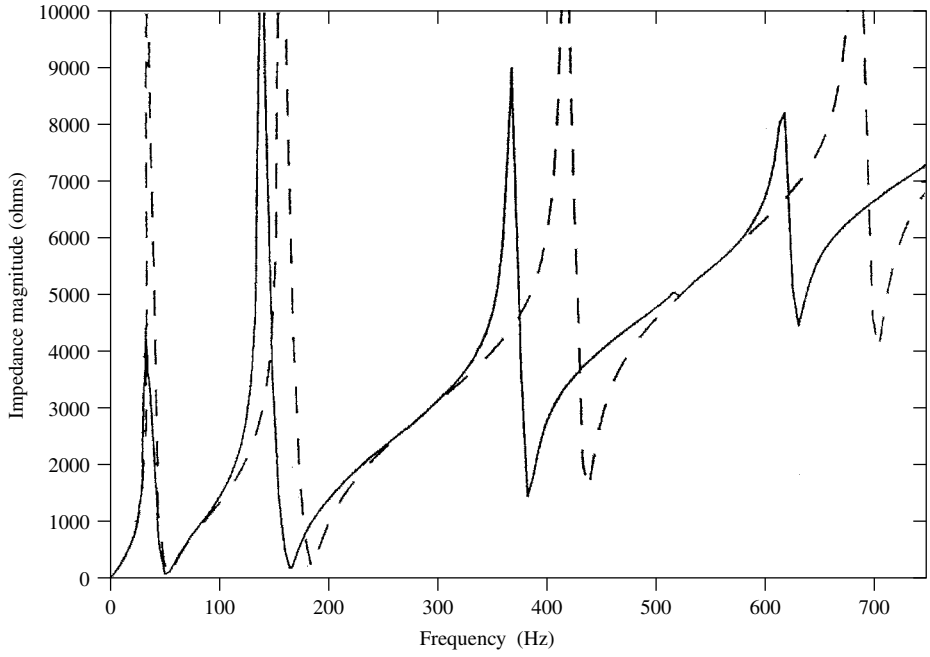


Figure 7.76 Harmonic impedances seen from Benmore: (———), with ancillary components; (- - - -), without ancillary components

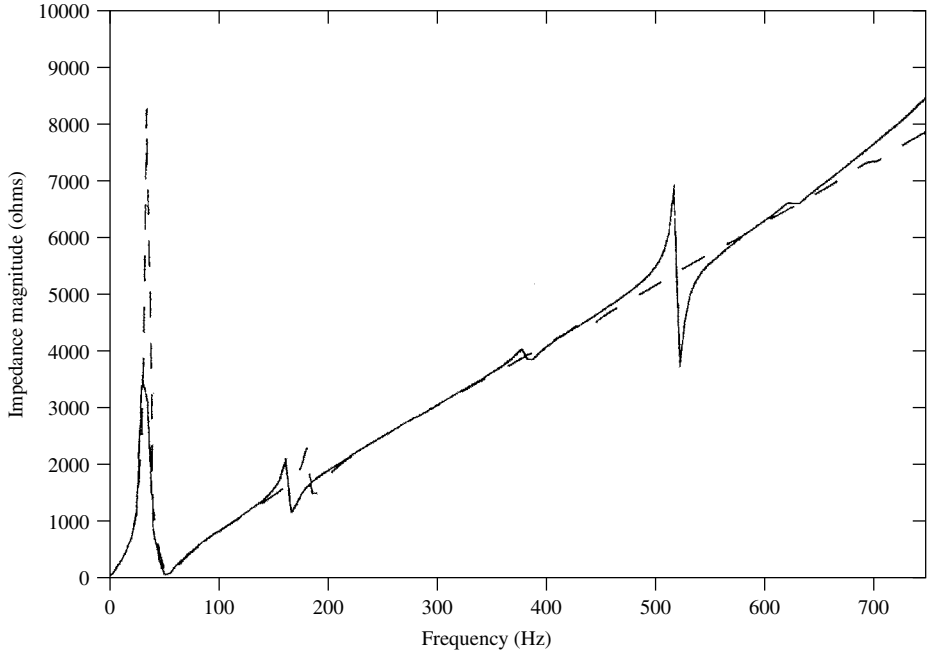


Figure 7.77 Harmonic impedances seen from Haywards: (———), with ancillary components; (- - - -), without ancillary components

resonant point modified by the surrounding components. This resonant point may also be observed from the Benmore end, in Figure 7.76, although its magnitude is reduced by the masking effect of the cable.

7.14 Simulation Backed by Field Tests

The harmonic sources are not normally well known and yet they need to be represented when performing harmonic penetration studies. Thus the analytical predictions must be backed by limited field measurements to provide confidence on the adequacy of the model representation.

The analytical model must provide information on the location of the harmonic sources, possibly without resorting to the complexity of global state estimation techniques. A variety of harmonic injection scenarios can be used to try to help to locate these sources, e.g. to decide whether a particular troublesome harmonic penetrates a 110 kV system from the higher-voltage transmission side or from the local low-voltage distribution network.

As an illustration, let us consider a set of field tests carried out in the New Zealand system to detect the source of telephone interference experienced on the Timaru–Temuka 110 kV line following the removal of the 110 kV line between Ashburton and Temuka. Preliminary measurement determined that the 47th and 49th harmonics were creating the problem. A number of simulations were carried out, and those that did not show increases in the 47th and 49th harmonic content on the Timaru end of the line were discarded (at that end of the line power and telecom lines share the same poles).

The harmonic sources were lumped at strategic locations. On the 220 kV network alternative harmonic injections were placed at Tiwai (the site of an aluminium smelter) and at Benmore (the site of an HVd.c. converter); another source was considered at low-voltage level in the Timaru area. The exciting source was a one per unit current injection and a post-processing program was used to scale the harmonic penetration results to match the measurement levels at one point in the system. The measurements were then made at a second point and the scaled results were compared to those of the previous scenario. This approach was repeated several times and the injection scenarios that did not produced the correct harmonic profile were discarded. The results of this tests indicated that the 47th and 49th harmonics were entering the 110 kV from the 220 kV system and that the 110 kV levels were insensitive to the location of these sources in the 220 kV system.

Figure 7.78 shows the predicted profile before and after removing the Ashburton–Temuka line. This profiles matches the 110 mA of 49th harmonic measured at Timaru and 10 mA measured at the Temuka end of this line. Various ways of reducing the harmonic levels were then investigated and studies carried out to determine the sensitivity of the harmonic content to loading levels, length of lines (since the actual length normally exceeds the map lengths due to the terrain of the countryside), sequence of the harmonic injections and harmonic source locations.

Figure 7.78(b) shows the zero sequence obtained from the sequence components transformation of the phase values in Figure 7.78(a). The zero-sequence currents along other transmission lines in the South Island, displayed in Figure 7.79, show that some of them are significantly larger.

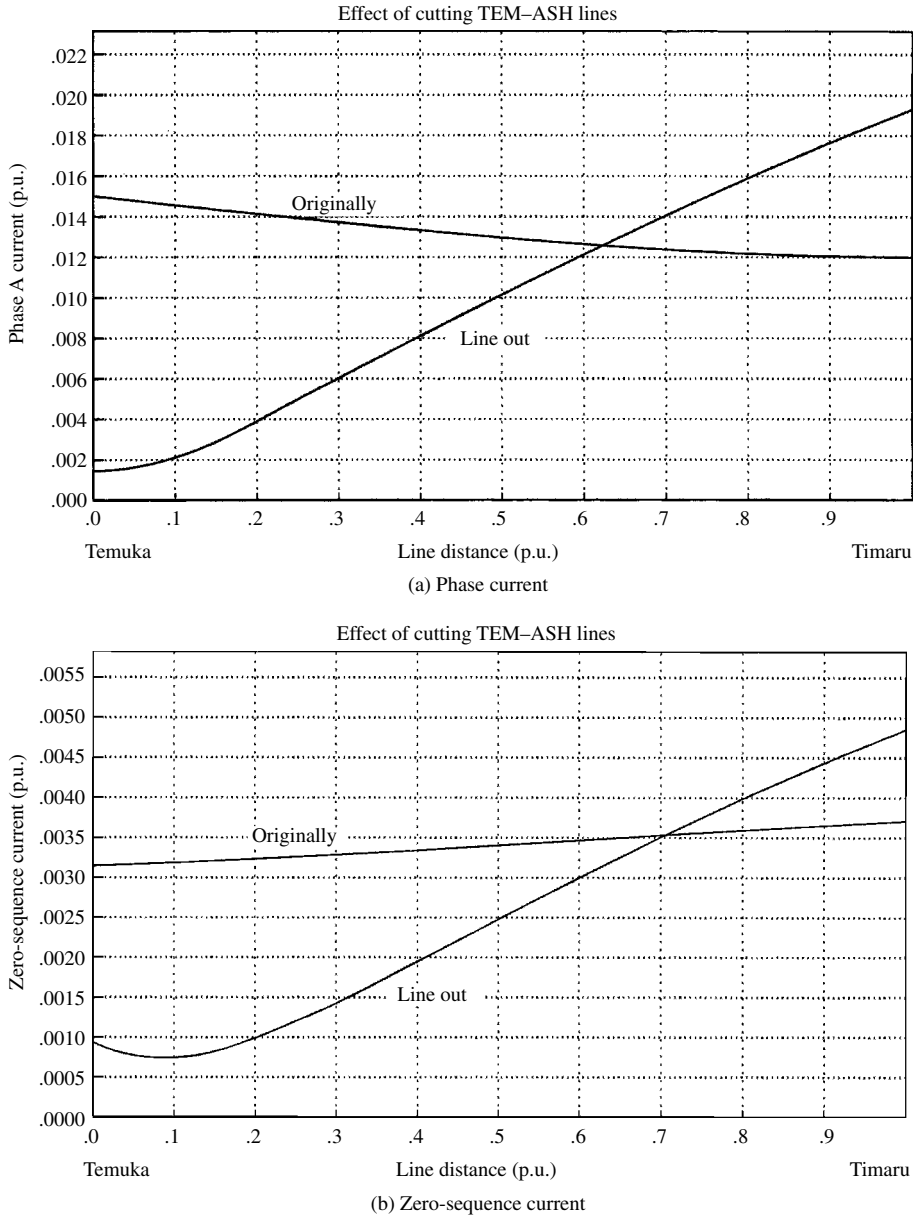


Figure 7.78 Effect of removal of the Ashburton–Temuka line on the 49th harmonic in the Timaru–Temuka lines

The computer model was also used to evaluate the effect of either extra series inductances or shunt capacitances. A promising solution was a possible system reconfiguration; this was tested by opening some circuit breakers to produce a different harmonic flow pattern, which was then compared to the computer predictions. The results indicated that the 47th and 49th harmonic levels dropped when the circuit

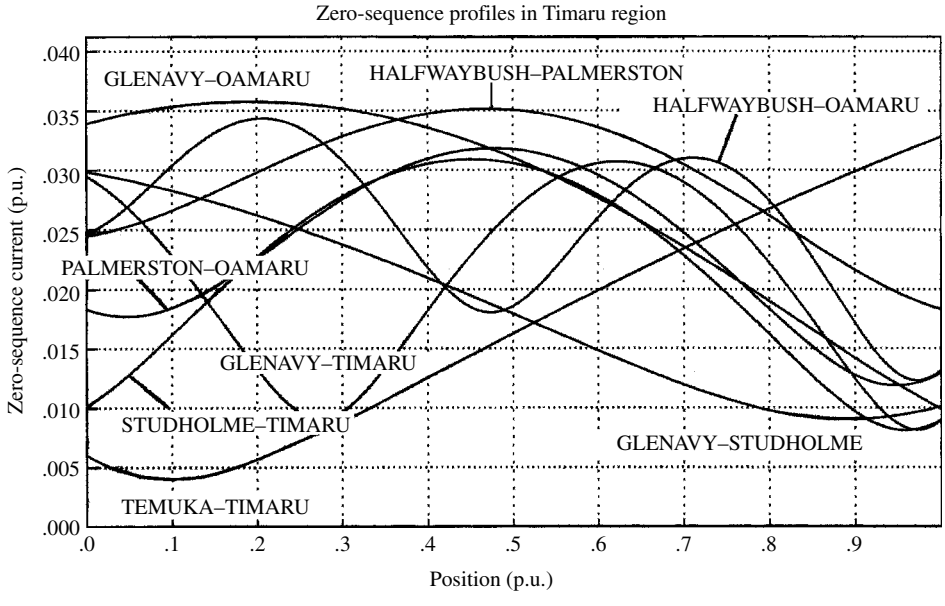


Figure 7.79 Zero sequence 49th harmonic current profile in New Zealand (SI)

breakers were opened to disconnect the 110 kV network south of Timaru. This is consistent with the fact that a significant amount of the harmonics are entering the 110 kV system from the 220 kV side.

A relatively simple field test to verify the theoretical models is the use of ripple control signal injection on the system and then comparing the results with the computer predicted values. For example, a test with a ripple signal of 175 Hz at the 66 kV busbar in Christchurch (New Zealand) gave a measured value of 9.76, while the predicted value was 8.92.

7.14.1 Post-Processing of Transmission Line Harmonics for Test Result Comparisons

Restricted measurements on the physical network limit the ability to compare a three-phase model with test results. Also, the data obtained from live three-phase systems only includes the phase voltages and currents of the coupled phases. To compare measured and simulated impedances at a current injection busbar it is thus necessary to derive equivalent phase impedances from the 3×3 admittance matrix. If the sequence of a given harmonic current injection is known, this can be used to give a phase impedance incorporating mutual coupling. For example assuming positive sequence and making $I_1 = \mathrm{I}\angle 0^\circ$ per unit, $I_2 = \mathrm{I}\angle -120^\circ$ per unit, $I_3 = \mathrm{I}\angle +120^\circ$ per unit, the matrix equation

$$\begin{bmatrix} I_1 \\ I_2 \\ I_3 \end{bmatrix} = \begin{bmatrix} Y_{11} & Y_{12} & Y_{13} \\ Y_{21} & Y_{22} & Y_{23} \\ Y_{31} & Y_{32} & Y_{33} \end{bmatrix} \cdot \begin{bmatrix} V_1 \\ V_2 \\ V_3 \end{bmatrix} \tag{7.136}$$

can be solved for V_1, V_2 and V_3, yielding the following equivalent phase impedances:

$$Z_1 = \frac{V_1}{I_1} \qquad Z_2 = \frac{V_2}{I_2} \qquad Z_3 = \frac{V_3}{I_3} \tag{7.137}$$

Often three-phase analysis results need to be compared against single-phase results (i.e. positive-sequence model), either from measurements or single-phase analysis. Consider the comparison of harmonic impedance.

In terms of sequence components, equation (7.136) becomes

$$\begin{pmatrix} I_+ \\ I_- \\ I_0 \end{pmatrix} = \begin{bmatrix} Y_{++} & Y_{+-} & Y_{+0} \\ Y_{-+} & Y_{--} & Y_{-0} \\ Y_{0+} & Y_{0-} & Y_{00} \end{bmatrix} \cdot \begin{pmatrix} V_+ \\ V_- \\ V_0 \end{pmatrix} \tag{7.138}$$

If a pure positive sequence current is injected, all sequences of voltage are produced due to the coupling between sequences. This coupling can be derived using a Kron reduction, i.e.

$$\begin{pmatrix} I_+ \\ I_- \\ I_0 \end{pmatrix} = \begin{bmatrix} [A] & [B] \\ [C] & [D] \end{bmatrix} \begin{pmatrix} V_+ \\ V_- \\ V_0 \end{pmatrix} \tag{7.139}$$

where

$$[A] = [Y_{++}][B] = [\, Y_{+-} \quad Y_{+0} \,]$$

$$[C] = [\, Y_{-+} \quad Y_{0+} \,]^t \text{ and } [D] = \begin{bmatrix} Y_{--} & Y_{-0} \\ Y_{0-} & Y_{00} \end{bmatrix}$$

Setting $I_- = 0$ and $I_0 = 0$ and rearranging gives:

$$I_+ = ([A] - [B]^{-1}[D][C])V_+ = Y_+^{\text{effective}} V_+ \tag{7.140}$$

which results in the following positive-sequence impedance:

$$[Z_+] = ([A] - [B]^{-1}[D][C])^{-1} \tag{7.141}$$

7.15 Discussion

The main content of this chapter has been a review of the harmonic models in current use for the network and load components of a linear power system. These models and a set of specified harmonic sources (as described in Chapter 3) have been used to develop a direct harmonic flow to calculate the distribution of voltage and current harmonics throughout the linear power system. The harmonic flow algorithm has been described as multi-phase and multi-source, although the single-phase, single-source model is still in common use in filter design.

However, the direct solution is based on the assumption of fixed harmonic sources, i.e. ignoring harmonic interactions between the nonlinear sources and the linear system. This is a reasonable approximation when the power rating of the nonlinear source

is small relative to the system fault level. The direct solution can lead to unsatisfactory designs when large converter plant is involved, and more advanced solutions are presented in the next chapter covering such cases.

7.16 References

1. Fortescue, C.L. (1918) Method of symmetrical co-ordinates applied to the solution of polyphase networks. *Trans. AIEE*, **37**(2), 1027–1140.
2. Zollenkopf, K. (1960) Bifactorisation-basic computational algorithm and programming techniques, Conference on Large Sets of Sparse Linear Equations, Oxford.
3. Lemoine, M. (1977) Methods of measuring harmonic impedances, CIRED Publication no. 151, London, pp. 5–6.
4. Brewer, G.D., Chow, J.H., Gentile, T.J. *et al.* (1982) HVDC-AC harmonic interaction. I. Development of a harmonic measurement system hardware and software, *IEEE Trans. Power Apparatus Systems*, **PAS-101**, 701–8.
5. Arrillaga, J., Smith, B.C., Watson, N.R. and Wood, A.R. (1997) *Power System Harmonic Analysis*, John Wiley & Sons, London, Ch. 10.
6. Baker, W.P. (1981) The measurement of the system impedance at harmonic frequencies, Paper presented at the Int. Conf. on Harmonics in Power Systems, UMIST, Manchester.
7. Barnes, H. (1976) An automatic harmonic analyser for the supply industry, IEE Conference on Sources and Effects of Power System Disturbances, London.
8. Robert, A. and Deflandre, T. (1997) Guide for assessing the network harmonic impedance, 14th International Conference and Exhibition on Electricity Distribution, Pt 1: Contributions. CIRED, IEE Conference Publication no. 438, **1**, pp. 3.1–1.3.10.
9. Morched, A.S. and Kundur, P. (1984) Identification and modeling of load characteristics at high frequencies, *IEEE Trans. Power Apparatus Systems*, **PAS-1-3**(3), 619–30.
10. Nagpal, M., Zu, W. and Sawada, J. (1998) Harmonic impedance measurement using three-phase transient, *IEEE Trans. Power Delivery*, **13**(1), 8–13.
11. Smith, J.R., Hauer, J.F. and Trudnowski, D.J. (1993) Transfer function identification in power system applications, *IEEE Trans. Power Systems*, **8**(3), 1282–8.
12. Chen, M.S. and Dillon, W.E. (1974) Power system modelling, *Proc. IEE*, **62**, 901.
13. Arrillaga, J., Arnold, C.P. and Harker, B.J. (1983) *Computer Modelling of Electrical Power Systems*, John Wiley & Sons, London.
14. Kimbark, E.W. (1950) *Electrical Transmission of Power and Signals*, John Wiley & Sons, New York.
15. Galloway, R.H., Shorrocks, W.N. and Wedepohl, L.M. (1964) Calculation of electrical parameters for short and long polyphase transmission lines, *Proc. IEE*, **111**, 2051–9.
16. Bowman, W.I. and McNamee, J.M. (1964) Development of equivalent PI and T matrix circuits for long untransposed transmission lines, *IEEE Trans.*, **PAS-84**, 625–32.
17. Wilkinson, J.H. and Reinsch, C. (1971) *Handbook for Automatic Computations*, vol. II, *Linear Algebra*, Springer-Verlag, Berlin.
18. Carson, J.R. (1926) Wave propagation in overhead wires with ground return. *Bell System Technical Journal*, **5**, 539–56.
19. Deri, A., Tevan, G., Semlyen, A. and Castanheira, A. (1981) The complex ground return plane, a simplified model for homogeneous and multi-layer earth return, *IEEE Trans. Power Apparatus Systems*, **PAS-100**, 3686–93.
20. Semlyen, A. and Deri, A. (1985) Time domain modelling of frequency dependent three-phase transmission line impedance, *IEEE Trans. Power Apparatus Systems*, **PAS-104**, 1549–55.

21. Acha, E. (1988) Modelling of power system transformers in the complex conjugate harmonic space, PhD Thesis, University of Canterbury, New Zealand.
22. Lewis, V.A. and Tuttle, P.D. (1958) The resistance and reactance of aluminium conductors steel-reinforced, *IEEE/Trans.*, **PAS-77**, 1189–215.
23. Dommel, H.W. (1978) Line constants of overhead lines and underground cables, Course E.E. 553 notes, University of British Columbia.
24. Bianchi, G. and Luoni, G. (1976) Induced currents and losses in single-core submarine cables, *IEEE Trans.*, **PAS-95**, 49–58.
25. Pesonen, J.A. (1981) Harmonics, characteristic parameters, method of study, estimates of existing values in the network, *Electra*, **77**, 35–56.
26. Ribeiro, P.F. (1985) Investigations of harmonic penetration in transmission systems, PhD Thesis, UMIST, Manchester.
27. Huddart, K.W. and Brewer, G.L. (1966) Factors influencing the harmonic impedance of a power system, *IEE Conference on High Voltage D.C. Transmission,* no. 22, pp. 450–2.
28. Mahmoud, A.A. and Shultz, R.D. (1982) A method for analyzing harmonic distribution in a.c. power systems, *IEEE Trans.*, **PAS-101**(6), 1815–26.
29. Arrillaga, J. (convener), (1996) AC system modelling for ac filter design—An overview of impedance modelling, *ELECTRA*, **164**, 133–151.
30. Capasso, A., Lamedica, R. and Prudenzi, A. (1998) Estimation of net harmonic currents due to dispersed non-linear loads within residential areas, *International Conference on Harmonics and Quality of Power (ICHQP'98)*, Athens, pp. 700–5.
31. Lamedica, R., Prudenzi, A., Tironi, F. and Zaninelli, D. (1997) A model of large loads for harmonic studies in distribution networks, *IEEE Trans. Power Delivery*, **12**(1).
32. Thunberg, E. and Söder, L. (1998) A harmonic Norton model of a real distribution network, *International Conference on Harmonics and Quality of Power (ICHQP'98)*, Athens, pp. 279–86.
33. Arrillaga, J., Watson, N.R. and Chen, S. (2000) *Power System Quality Assessment*, John Wiley & Sons, Chichester.
34. Arrillaga, J., Densem, T.J. and Harker, B.J. (1983) Zero sequence harmonic current generation in transmission lines connected to large converter plant, *IEEE Trans.*, **PAS-102**(7), 2357–63.
35. Hesse, M.H. (1966) Circulating currents in parallel untransposed multicircuit lines. I. Numerical evaluations, *IEEE Trans.*, **PAS-85**, 802–11.
36. Edison Electric Institute (1968) *EHV Transmission Line Reference Book*, New York.
37. Robinson, G.H. (1966) Harmonic phenomena associated with the Benmore-Haywards HVd.c. transmission scheme, *New Zealand Engineer*, **21**, 16–29.
38. Shultz, R.D., Smith, R.A. and Hickey, G.L. (1983) Calculation of maximum harmonic currents and voltages on transmission lines, *IEEE Trans.* **PAS-102**, 817–21.
39. McGranahan, M.F., Dugan, R.C. and Sponsler, W.L. (1981) Digital simulation of distribution system frequency response characteristics, *IEEE Trans.*, **PAS-100**, 1362–9.
40. Winthrop, D.A. (1983) Planning for a railway traction load on the New Zealand power system, *IPENZ Conference*, New Zealand.
41. Robert, R.D. and Leedham, P.J. (1974) A review of the cause and effects of distribution system three-phase unbalance, *IEE Conference Publication*, **110**, 83–92.
42. Arrillaga, J., Acha, E. and Bodger, P.S. (1986) Ineffectiveness of transmission line transpositions at harmonic frequencies, *Proc. IEE*, **123C**(2), 99–104.
43. Semlyen, A., Eggleston, J.F. and Arrillaga, J. (1987) Admittance matrix model of a synchronous machine for harmonic analysis, *IEEE Trans.*, **PWRS-2**(4), 833–40.
44. Arrillaga, J. and Duke, R.M. (1979) Thyristor-controlled quadrature boosting, *Proc. IEE*, **126**(6), 493–8.
45. Stemmler, H. and Guth, G. (1982) The thyristor-controlled static phase-shifter, *Brown Bovery Rev.*, **69**(3), 73–8.

46. Arrillaga, J. (1983) *High Voltage Direct Current Transmission*, Peter Peregrinus, London.
47. Arrillaga, J., Acha, E., Watson, N.R. and Veale, N. (1988) Ineffectiveness of transmission line VAR compensation at harmonic frequencies, International Conference on Harmonics in Power Systems, (ICHPS III), Nashville, **IN**, pp. 233–8.
48. Eggleston, J.F., Callaghan, C.D., Arrillaga, J. and Dommel, H.W. (1988) Derivation of harmonic impedances of the inter-island HVd.c link, *Trans. IPENS* (New Zealand), **EMCh-15**(1), 9–24.

8

Advanced Harmonic Assessment

8.1 Introduction

Given the lack of detailed information normally available on the characteristics of the harmonic sources, the latter are often represented as approximate harmonic current injections. In an existing system these can be derived from selective measurements, whereas for planning studies the current injections are obtained from relatively simple models as described in Chapter 2.

In the static converter case the current injection method normally assumes a steady firing delay angle, either no commutation period or one of unvarying duration, an undistorted a.c. system voltage and perfect d.c. current. In practice this is rarely the case. Some voltage distortion and/or unbalance will exist on the a.c. side and current ripple on the d.c. side. Through the current controller the firing angle will not be steady and the commutation period duration will also vary. Therefore not only will harmonic voltages and currents be transferred through the converter, but they may also be amplified through the variation of the valves' switching instants. These interactions have particular relevance for non-characteristic harmonics.

Although the current injection method is used extensively in the design of filters, as explained in Chapter 6, this approach can lead to unsatisfactory solutions in applications involving very large power ratings such as an HVd.c. converter [1]. By ignoring or oversimplifying the interaction that exists between the converter and the a.c. and d.c. systems, an important low-order harmonic (or inter-harmonic) parallel resonance can be missed, leading to operational problems and even harmonic instabilities [2].

This chapter describes several algorithms with more advanced representation of the critical harmonic sources, taking into account their interactions with the rest of the power system components. Other topics discussed are the prospects for global harmonic state estimation and harmonic source identification. The chapter ends with a thorough assessment of the potential application of the electromagnetic transients simulation programs for harmonic analysis.

8.2 Transfer Function Model

Based on modulation theory and small signal linearisation, the transfer function concept provides an accurate direct solution of the converter response when the input voltage waveform is modulated by a signal at any specified frequency [3].

Power System Harmonics, Second Edition J. Arrillaga, N.R. Watson
© 2003 John Wiley & Sons, Ltd ISBN: 0-470-85129-5

In the case of the six-pulse converter, two transfer functions $Y_{\psi dc}$ and $Y_{\psi ac}$ are needed to describe the interconnection between the d.c. and a.c. sides of the converter. The d.c. voltage is calculated by summing each phase voltage multiplied by its associated transfer function, i.e.

$$v_d = N \sum_{\psi} Y_{\psi \mathrm{dc}} v_{\psi} \tag{8.1}$$

where $\psi = 0^\circ$, 120° and 240° for phases a, b and c, N is the converter transformer ratio and v_ψ are the three phase voltages. $Y_{\psi \mathrm{dc}}$ has values between -1 and $+1$, where $+1$ signifies a connection of the d.c. side positive bus to the phase in question, -1 signifies a connection of the d.c. side negative bus to the phase in question, and 0 indicates no connection. By assigning the transfer function a value of 0.5 for the two commutating phases, the d.c. voltage is correctly represented during the commutation process.

The a.c. current in each phase can be defined by

$$i_\psi = N Y_{\psi \mathrm{ac}} i_{\mathrm{dc}} \tag{8.2}$$

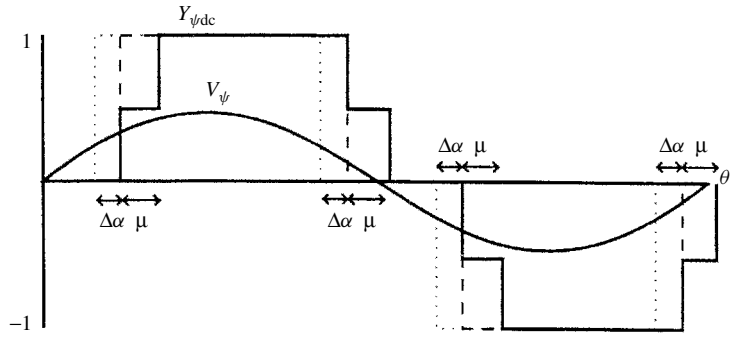
where i_{dc} is the d.c. side current, and $Y_{\psi \mathrm{ac}}$ is similar to $Y_{\psi \mathrm{dc}}$, except that during the commutation period the a.c. current rises or falls in a continuous manner and is approximated by a linear transfer of the d.c. current from one phase to the next.

Both transfer functions are built up by the summation of a basic function (no commutation period and steady firing angle), a firing angle variation function, and a commutation function. The process is illustrated in Figure 8.1, where the dotted line represents the basic transfer function, the dashed line the function revised to include a firing angle variation of $\Delta\alpha$, and the solid line the function further revised to include the effect of a commutation period. Breaking up the transfer function in this way allows the frequency spectra to be more easily written.

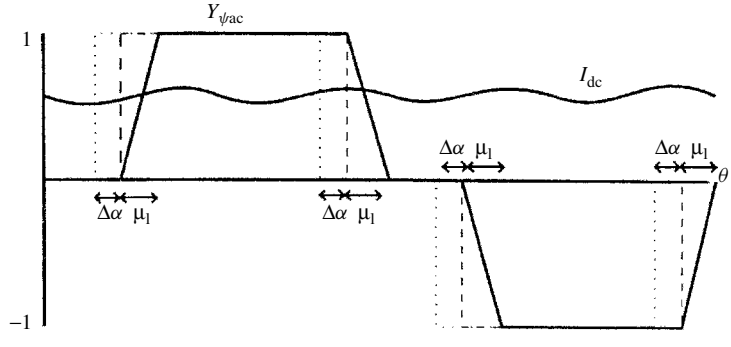
The firing angle variation function is characterised as a set of pulses, with fixed leading edges and variable trailing edges. For $Y_{\psi \mathrm{dc}}$, the commutation function comprises a set of rectangular pulses, of which the leading edges match the firing angle variation, and the trailing edges vary somewhat differently. For $Y_{\psi \mathrm{ac}}$, the commutation function comprises a set of saw-tooth pulses, of which the leading and trailing edges match the firing angle variation. When the spectrum of this waveform is written, the current-time area of the commutation function has the dominant effect. An effective commutation period duration μ_1 is defined, such that the area of the $Y_{\psi \mathrm{dc}}$ commutation function matches the area of the true commutation waveform. In addition a small variable triangular pulse is added to account for the variation in this area consequential to the a.c. voltage, d.c. current, or firing angle variations.

The frequency spectra of the transfer functions is derived in Chapter 5 of reference [3].

The transfer function is a very useful concept for the design of control systems because it provides information on cause–effect relationships. However, to reduce the complexity of the formulation, the linearisation process is truncated at the first term of Taylor's series. This simplification has little effect on the accuracy of the results for the low harmonic orders but the solution accuracy decreases with increasing distortion magnitude and frequency.



(a) Transfer function to d.c. voltage



(b) Transfer function to a.c. current

Figure 8.1 Transfer functions: (a) $Y_{\psi dc}$; (b) $Y_{\psi ac}$

The main limitation of the direct solution is its inability to model the interaction between the harmonic source and the system harmonic flow.

8.3 Iterative Harmonic Analysis (IHA)

8.3.1 Fixed-Point Iterative Method

The simplest iterative scheme uses the fixed-point iteration (or Gauss) concept. At each iteration the latest values of the distorted terminal voltages are used to calculate the harmonic current injections. The direct analysis described in Chapter 7 is invoked to update the a.c. voltage harmonics for the next iteration. With reference to the three-phase static converter, the updated terminal voltages are used as the commutating voltages for the converter solution. The calculated d.c. voltage waveform is then impressed upon the d.c. side impedance to derive the d.c. current waveform, which in turn, together with the switching instants and commutation process, provides the a.c. current harmonic injections. The latter are then used to derive the a.c. voltage harmonics in the frequency domain for the next iteration.

Early fixed-point iterative methods involved the solution of the switching instants [4,5]. An alternative approach is to derive time-domain waveforms for the

direct voltage and a.c. side phase currents by evaluating analytical expressions for those quantities on a point-by-point basis and then applying the FFT to yield the desired harmonic information [6].

The fixed-point solution is likely to diverge when the d.c. system harmonic impedance is large and the commutating reactance small.

8.3.2 The Method of Norton Equivalents

In the fixed-point iteration, the nonlinear component is represented at each iteration by a constant current source. Far better convergence can be expected with the use of a Norton equivalent for the nonlinear component, with the Norton admittance representing a linearisation, possibly approximate, of the component response to variation in terminal voltage harmonics.

Time-invariant characteristics of some plant components, such as the transformer magnetisation, can be described by the static voltage–current relationship,

$$i(t) = f(v(t)) \tag{8.3}$$

in the time domain. In this case, the current injection and the Norton admittance can be calculated by an elegant procedure involving an excursion into the time domain [7]. At each iteration, the applied voltage harmonics are inverse Fourier transformed to yield the voltage waveform. The voltage waveform is then applied point-by-point to the static voltage/current characteristic, to yield the current waveform. By calculating the voltage and current waveform at $2n$ equi-spaced points, a fast Fourier transform (FFT) is readily applied to the current waveform, to yield the total harmonic injection. This process is illustrated in Figure 8.2 for the case of the transformer magnetisation nonlinearity.

8.3.3 Hybrid Time/Frequency Domain Solution

However, the characteristics of time-variant nonlinear components, such as power electronic devices, do not fall in the category defined by equation (8.3). Instead, their voltage–current relationships result from many interdependent factors, such as phase and magnitude of each of the a.c. voltage and current harmonic components, control system functions, firing angle constraints, etc. Moreover, the solution accuracy achieved with IHA methods when applied to static conversion is very limited due to the over-simplified modelling of the converters (in particular the idealised representation of the valve switching instants). The more accurate and generally applicable time-domain solution (such as the state variable or the EMTP method) has been proposed to represent the behaviour of the nonlinear components in a hybrid frequency/time domain solution [8,9].

The hybrid solution proceeds in two stages. First the periodic steady state of the individual components is derived from a load flow program and then updated using voltage corrections from the second stage. The calculations are performed in the frequency domain where appropriate (e.g. in the case of transmission lines) and in the

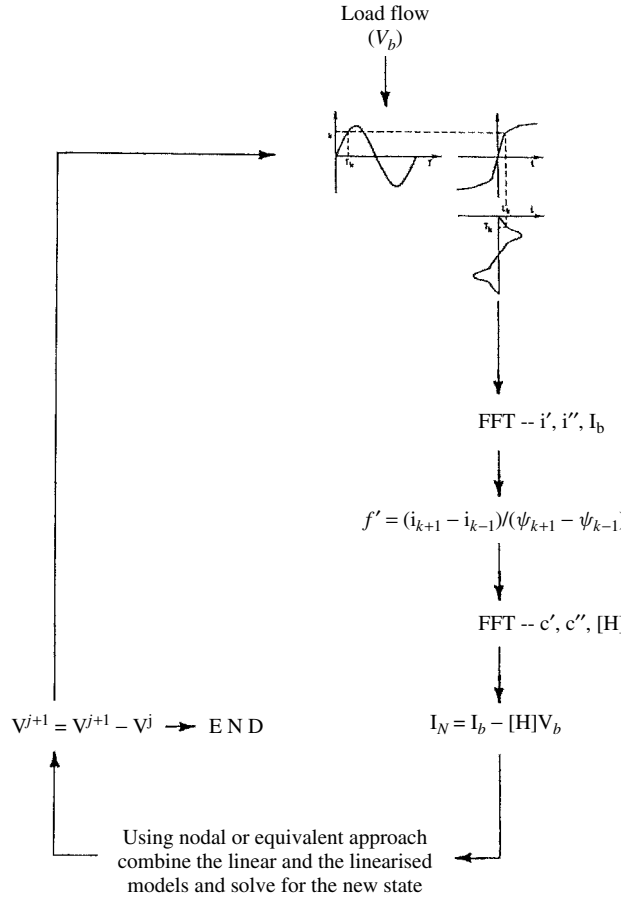

Load flow
(V_b)
FFT -- i′, i″, I_b
$f' = (i_{k+1} - i_{k-1})/(\psi_{k+1} - \psi_{k-1})$
FFT -- c′, c″, [H]
$V^{j+1} = V^{j+1} - V^j$ → E N D
$I_N = I_b - [H]V_b$
Using nodal or equivalent approach
combine the linear and the linearised
models and solve for the new state

Figure 8.2 Iterative solution for the modelling of transformer magnetisation nonlinearities

time domain otherwise. In stage two the currents obtained in the first stage are used to derive the current mismatches Δi, expressed in the frequency domain. These become injections into a system-wide incremental harmonic admittance matrix Y, calculated in advance from such matrices for all the individual components. The equation $\Delta i = Y \Delta v$ is then solved for Δv to be used in the first stage to update all bus voltages.

The first stage approach is modular, but in the second stage the voltage corrections are calculated globally, i.e. for the whole system. However, convergence is only achieved linearly, because of the approximations made on the accuracy of Δv. A separate iterative procedure is needed to model the controllers of active nonlinear devices, such as a.c.–d.c. converters, and this procedure relies entirely on information from the previous iteration.

Acceleration Technique Time-domain simulation, whether performed by the EMTP, state variable or any other method, may require large computation times to reach steady state, thus the use of accelerating techniques [10,11] is advocated to speed up the solution. These techniques take advantage of the two-point boundary value inherent in

the steady-state condition. Thus a correction term is added to the initial state vector, calculated as a function of the residuum of the initial and final state vectors and the mapping derivative over the period. A concise version of the Poincare method described in reference [11] is given here.

A nonlinear system of state equations is expressed as

$$\dot{x} = g(x, u) \qquad x(t_o) = x_o \tag{8.4}$$

where $u = u(t)$ is the input, and x_o the vector of state variables at $t = t_o$ close to the periodic steady state. This state is characterised by the condition

$$f(x_o) = x(t_o + T) - x(t_o) \tag{8.5}$$

where $x(t_o + T)$ is derived by numerical integration over the period t_o to $t_o + T$ of the state equations (8.4).

Equation (8.5) represents a system of n nonlinear algebraic equations with n unknowns x and can thus be solved by the Newton–Raphson method.

The linearised form of equation (8.5) around an approximation $x_o^{(k)}$ at step k of its solution is

$$f(x_o) \cong f(x_o^{(k)}) + J^{(k)}(x_o^{(k+1)} - x_o^{(k)}) = 0 \tag{8.6}$$

where $J^{(k)}$ is the Jacobian (the matrix of partial derivatives of $f(x_o)$ with respect to x_o, evaluated at $x_o^{(k)}$).

With

$$x_o^{(k)} \rightarrow f(x_o^{(k)}) \tag{8.7}$$

and

$$x_o^{(k)} + \varepsilon e_i \rightarrow f(x_o^{(k)} + \varepsilon e_i) \quad i = 1, \ldots, n \tag{8.8}$$

where e_i are the columns of the unity matrix and ε is a small scalar, the $J^{(k)}$ is assembled from the vectors

$$\frac{1}{\varepsilon}(f(x_o^{(k)} + \varepsilon e_i) - f(x_o^{(k)})) \quad i = 1, \ldots, n \tag{8.9}$$

obtained in equations (8.7) and (8.8).

Finally, using the above approximation $J^{(k)}$ of the Jacobian, the updated value $x_o^{(k+1)}$ for x_o is obtained from equation (8.6).

The process described above is quasi-Newton but its convergence is close to quadratic. Therefore, as in a conventional Newton power flow program, only three to five iterations are needed for convergence to a highly accurate solution, depending on the closeness of the initial state x_o to the converged solution.

8.3.4 The Harmonic Domain

An important step in solution accuracy and reliability is provided by the so-called harmonic domain [12], a full Newton solution that takes into account the modulating

effect of a.c. voltage and d.c. current distortion on the switching instants and converter control functions. This method performs a linearisation around the operating point, that provides sufficient accuracy. Modelling a distorting source in the harmonic domain requires the derivation of a set of nonlinear equations describing the harmonic transfer through the device in the steady state. A different model is thus required for each nonlinear device.

So far this method has been applied to three-phase static power conversion equipment. The converter model must be differentiable with respect to the solution variables and this is achieved by the convolution technique, which calculates the transfers analytically using easily differentiable real-valued functions. The advantage of describing the system in real-valued terms is that both electrical and non-electrical variables, such as control variables, can be solved simultaneously.

Each of the six-pulse bridges of a converter terminal can be viewed as a four-port circuit, i.e. consisting of two inputs and two outputs. The inputs in this case are the a.c. phase voltage spectra and the d.c. current spectra. The outputs are the a.c. current and d.c. voltage spectra. The convolution technique approximates the transferred waveshapes (d.c. voltage and a.c. phase currents) to piece-wise waveshapes consisting of twelve distinct periods of conduction. These periods are defined explicitly by the switching angles of the converter. In the case of the d.c. voltage transfer, twelve analytic frequency-domain expressions are derived from nodal analysis of the twelve commutation circuits which describe steady-state waveshapes valid for those circuits. The spectra calculated using these expressions are then convolved with those of band-limited rectangular windowing functions. The resultant sum of the convolved spectra is that of the total waveshape. Figure 8.3 illustrates one convolution for the d.c. voltage of an inverter as seen in the time domain.

A similar process is followed to obtain the harmonic spectra of the a.c. phase currents. These transfers are general for both inverter and rectifier, with only the direction of d.c. current flow and the resultant sign of the d.c. voltage across the bridge being different.

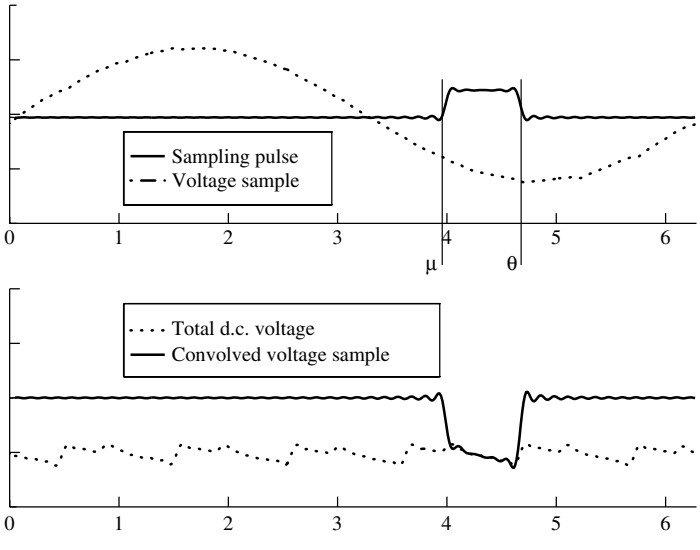


Figure 8.3 Convolution sampling waveforms for a six-pulse converter

The harmonic transfers across a converter are largely dependant upon the accuracy of determining the switching instants, particularly the end of commutation angle. For the convolution model these angles are obtained from twelve single-variable Newton–Raphson steps. The commutation angles are defined by the cross-over points of the commutation currents with the d.c. current (harmonics included). The firing angles are dependant upon the control strategy but are also solved using single-variable iterative steps. As the full solution Jacobian includes the effect of modulating these switching instants, the main solution is still of a full Newton nature.

To solve the standard twelve-pulse configuration, two convolution models are needed for the star/star and star/delta connected bridges. The harmonic transfers from each model are added together to yield the full transfer characteristic.

Each frequency is ordered by phase components and is partitioned into real and imaginary parts. This leads to six variables for each harmonic at an a.c. busbar, and two at a d.c. busbar. Consequently, for a study to the 50th harmonic, 300 variables need to be defined at the converter a.c. terminal and 100 at the d.c. terminal. The remaining required mismatches are those for the average d.c. current and the control variables. For a current-controlled rectifier these are the firing angles, which are modulated by the d.c. current through a PI (proportional integral) controller. The minimum gamma controlled inverter assumes equidistant firings but requires the commutating voltage zero crossings as variables in order to calculate the extinction angles.

The Jacobian, in Newton's solution, only needs to be approximate, and therefore only the significant terms need to be retained. Thus the full harmonic Jacobian can be about 96% sparse without affecting convergence. The Jacobian elements can be calculated either by numerical partial differentiation or by analytically derived expressions for the partial derivatives. Numerical calculation of the Jacobian has the advantage of ease of coding, but is very slow; it is achieved by sequentially perturbing each variable and calculating the change in all the mismatches. The analytical method of calculating the Jacobian matrix requires considerable effort to obtain all the partial derivatives in analytic form, but is exceptionally fast. Thus the latter method is preferred because the solution speed is increased by a factor of 50 with respect to using one obtained numerically.

Good variable initialisation is achieved in a two-stage process. The first stage uses a positive-sequence power flow estimation and classical converter equations. This information is used to start a three-phase power-flow solution including the control variables; the results of the latter are then used to initialise the full harmonic solution.

As the two converters of an HVd.c. link interact nonlinearly with each other, it is necessary to solve them simultaneously. At each converter busbar the variables represent the specified harmonics in ascending order. The structure of the Jacobian is illustrated in Figure 8.4, although for simplicity it only includes 13 harmonics.

The two a.c. systems of the d.c. link are not directly connected, and therefore there is no direct coupling between the two a.c. busbars represented by numbers 1 and 2. This can be seen in the matrix by the presence of zero blocks A2 and B1. The two d.c. busbars at 3 and 4 are directly coupled through the nodal analysis of the system; blocks C4 and D3 are the diagonal linear linking elements.

Some refinements have been made to the harmonic domain algorithm to make it suitable for the efficient computation of inter-harmonics [13]. Inter-harmonics can be accommodated efficiently by means of an adaptive technique complemented by

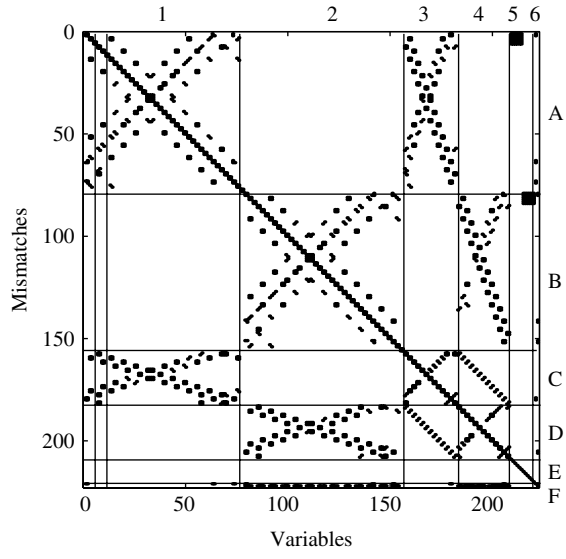


Figure 8.4 Jacobian of the CIGRE Hvd.c. test system for 13 harmonics

interpolation between integer frequencies [14]. These refinements take advantage of the inherent sparsity present in the harmonic arrays, which provide several orders of improvement in solution time with no significant degradation in solution accuracy. As a result, the increase in computation is now almost linear with the number of power frequency cycles, as opposed to cubic with the original full method.

Although in principle any type of nonlinear component can be accommodated in the harmonic domain solution, the formulation of each new component requires considerable skill and effort. Accordingly, a program for the calculation of the non-sinusoidal periodic steady state may be of very high dimension and complexity, as well as being difficult to use and develop further. However, this method is extremely useful to assess the harmonic interaction between a.c. system and large power converters and has already been adopted by several large manufacturers.

8.4 Harmonic Power Flow

The concept of harmonic power flow (HPF) was introduced in an early contribution by Xia and Heydt [15] for the case of a symmetrical power system. Although there have been further publications discussing this subject in the three-phase frame of reference [16–19], most of the power quality contributions still use the HPF concept with exclusive reference to symmetrical operation on the basis that at the fundamental frequency the power system is designed to operate under strict limits of unbalance. However, the symmetrical solution is of very limited value to the industry because the experience of many field tests indicates that asymmetry is the rule rather than the exception with power system harmonics (both at characteristic and non-characteristic harmonic frequencies) and such information can not be represented in a balanced HPF.

Further compelling reasons for replacing the symmetrical HPF concept by the three-phase alternative are:

(1) System unbalance produces non-characteristic harmonics in power electronic equipment, particularly non-zero-sequence triplens. These are not normally filtered and penetrate into the a.c. network regardless of the type of transformer connection.
(2) Often the filters of large power conversion plant resonate with the a.c. system impedance at low-order non-characteristic harmonics such as the third.
(3) Transmission system unbalance is greatly affected by line geometry, and the use of transpositions, calculated to reduce fundamental frequency imbalance, is ineffective at harmonic frequencies [20].
(4) Harmonic flows are affected by the transformer connections, which only a three-phase model can represent.
(5) The need to model harmonic interactions between geographically separated converter units.

The derivation of voltage inbalance requires a three-phase power flow solution. With this information a three-phase model of the converter plant derives the characteristic and non-characteristic harmonic currents injected by the converter, which constitute the exciting sources for the harmonic penetration model described in Chapter 7.

Generally a direct solution based on the inbalance calculated from a preliminary three-phase power flow will provide sufficiently accurate information. A few sequential iterations of the three-phase power flow and the harmonic penetration study may be required for greater accuracy [16].

However, under difficult resonant conditions the sequential solution is likely to diverge and a unified Newton solution provides a more reliable alternative.

8.4.1 Components of a Three-Phase Newton HPF Solution

The three constituent parts of an HPF for use in systems containing large power converters are:

(1) a three-phase a.c.–d.c. power flow [21] at the fundamental frequency;
(2) a multi-harmonic three-phase representation of the linear part of the power system (the subject of Chapter 7);
(3) a harmonic domain representation of the individual converters, as described in Section 8.3.4.

These three components need to be coupled with each other in a large, mostly block-diagonal, Jacobian matrix.

Power Flow Requirements Unification of the three-phase power flow and harmonic interaction at the converter terminals imposes a different set of requirements on the power flow implementation than those that led to the development of the decoupled algorithms. First, the converter harmonic model is necessarily in Cartesian

co-ordinates [22]. If the power flow equations are in polar co-ordinates, as required by the decoupling concept, nonlinear polar transforms must be carried out at each iteration to interface with the converter a.c. terminal (at fundamental frequency). This is likely to increase the number of iterations to convergence substantially, as well as complicate the power flow implementation. An additional factor to consider is that the converter equations take longer to calculate than the solution of the prefactorised Jacobian system. It is therefore desirable to reduce the number of converter mismatch equation evaluations by reducing the number of iterations to convergence. This can be achieved by using the full Jacobian matrix, with no decoupling. Taken together, these points indicate that a unified power flow and harmonic solution in Cartesian co-ordinates will be more efficient than one in polar co-ordinates.

Combined Jacobian The nine-busbar network of Figure 8.5 is used to illustrate the structure of the combined power flow and harmonic solution. The slack busbar is at ROXBURGH-011, and loads are placed at ROXBURGH-220, INVERCARG-011 and TIWAI-220. Also, the rectifier end of the CIGRE benchmark model [23] is connected at the TIWAI busbar.

The combined Jacobian is illustrated in Figure 8.6. In this figure, the busbars and specifications of the power flow solution can be observed at the top left-hand side. Of

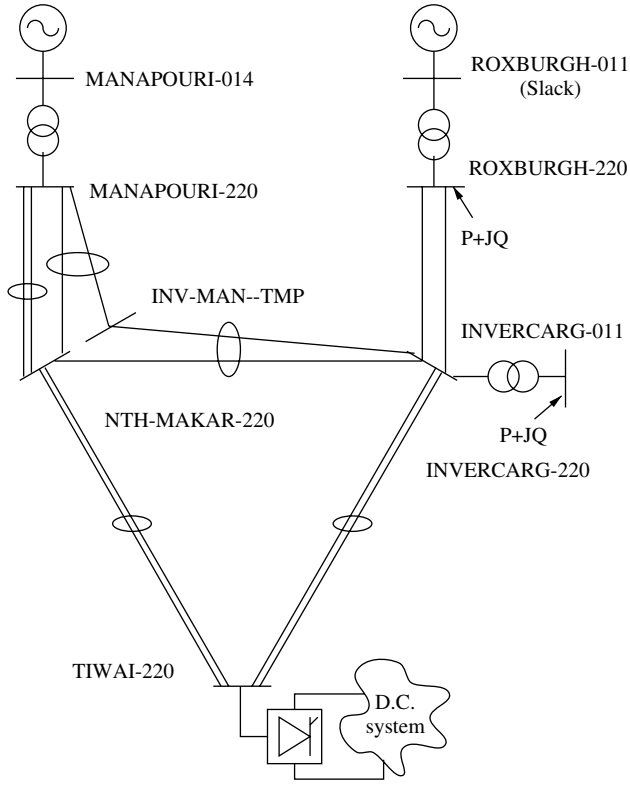


Figure 8.5 Test system for three-phase power flow

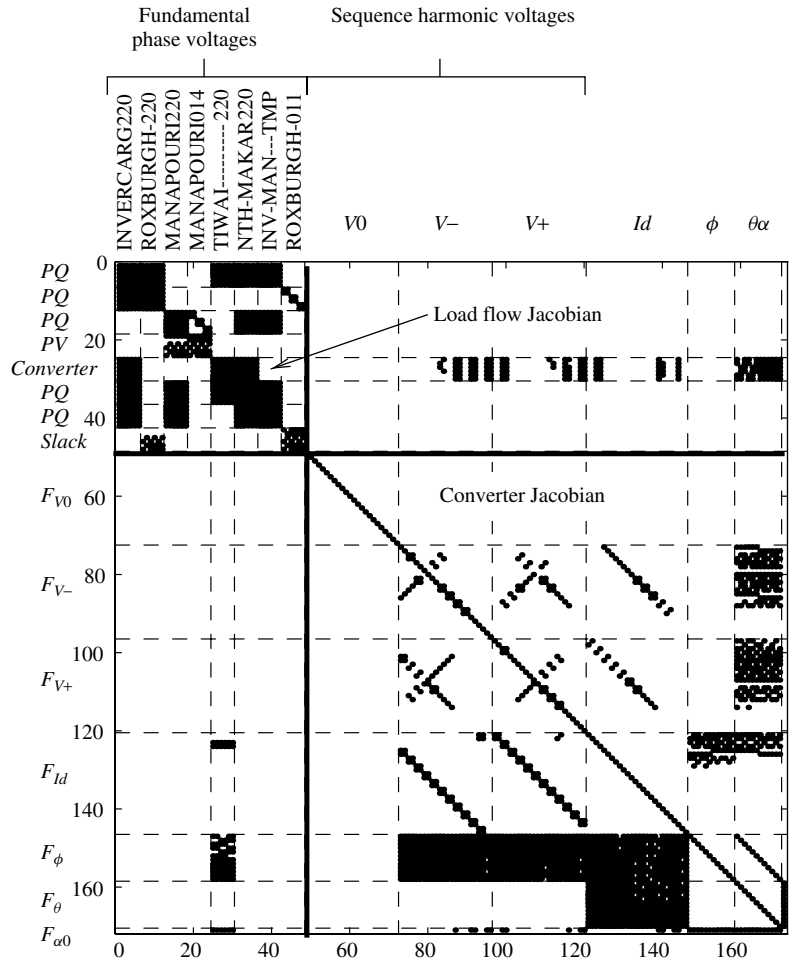


Figure 8.6 Jacobian matrix for an integrated power flow and harmonic solution

course, the structural sparsity would be much greater for a realistically sized system, and is clearly not symmetric. The lower right-hand side matrix block represents the converter harmonics solution, which is seen to be coupled only to the fundamental frequency voltages at the converter terminals.

The combined Jacobian contains no more terms than the separate Jacobians of the load flow and converter, and yet convergence has been found to be faster and more robust than a fixed-point iteration between separate load flow and converter model updates, which usually diverges.

The Thevenin equivalent of the a.c. system is retained at all harmonic frequencies except the fundamental, which is the point of coupling to the power flow equations. Similarly, three-phase power flow equations are retained at every bus except the converter bus. It is assumed that were it not for the converter, the converter bus would be *PQ* specified. Since the power flow is three-phase, six mismatch equations (real and imaginary parts) are required at the converter bus at fundamental frequency.

Because the processing required at every iteration is dominated by the converter equations, it is essential that convergence of the load flow part of the system be faster than that of the converter model, which typically converges in seven iterations. The decoupled load flow method is not suitable as it requires more iterations for convergence. As explained above, integration of the converter model with a load flow requires that the load flow be reformulated in Cartesian components, with no decoupling in the Jacobian matrix.

General HPF Framework for Systems with Multiple Converters The method and components of the Newton solution have already been discussed in previous sections with reference to a single 12-pulse converter connected to an a.c. power system. This section describes the structure of a general Jacobian capable of accommodating, as well as a three-phase power flow, multiple converters of different pulse numbers and d.c. configurations placed in separate locations.

While all the system busbars must be explicitly represented at the power frequency, due to the nonlinear nature of the power flow specifications, only the converter busbars are nonlinear at the harmonic frequencies. Thus, in the latter case, the linear network can be reduced to an equivalent system that links the nonlinear device busbars. The linear reduction used also produces equivalent current injections for remote constant voltage or current harmonic sources.

By way of illustration, Figure 8.7 shows the structure of the Jacobian representing the power and harmonic flows in the New Zealand South Island transmission system. This system consists of 100 busbars, of which 14 are generation busbars, 24 *PQ* loads and 4 large rectifier busbars. The total system loading is about 2500 MW, of which over half is rectified. Consequently there has been a question mark over the degree of interaction between the four rectifier busbars (shown in Figure 8.8).

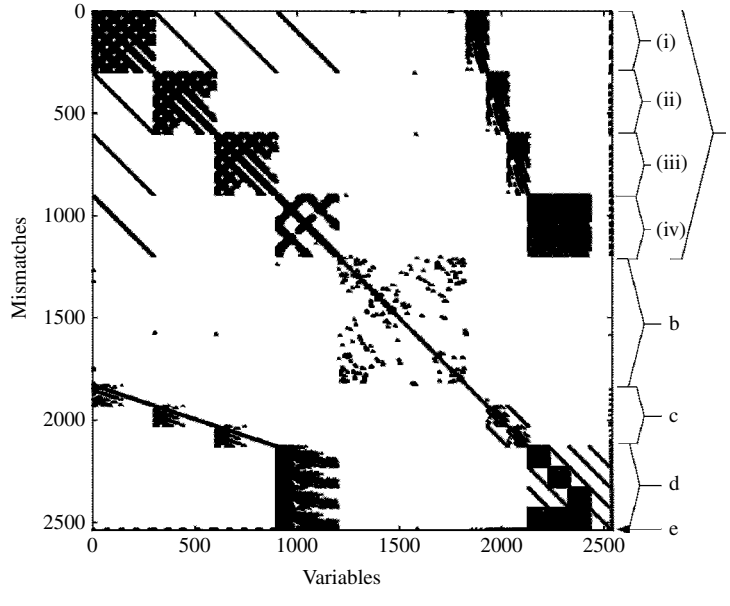


Figure 8.7 Jacobian structure of the New Zealand South Island system

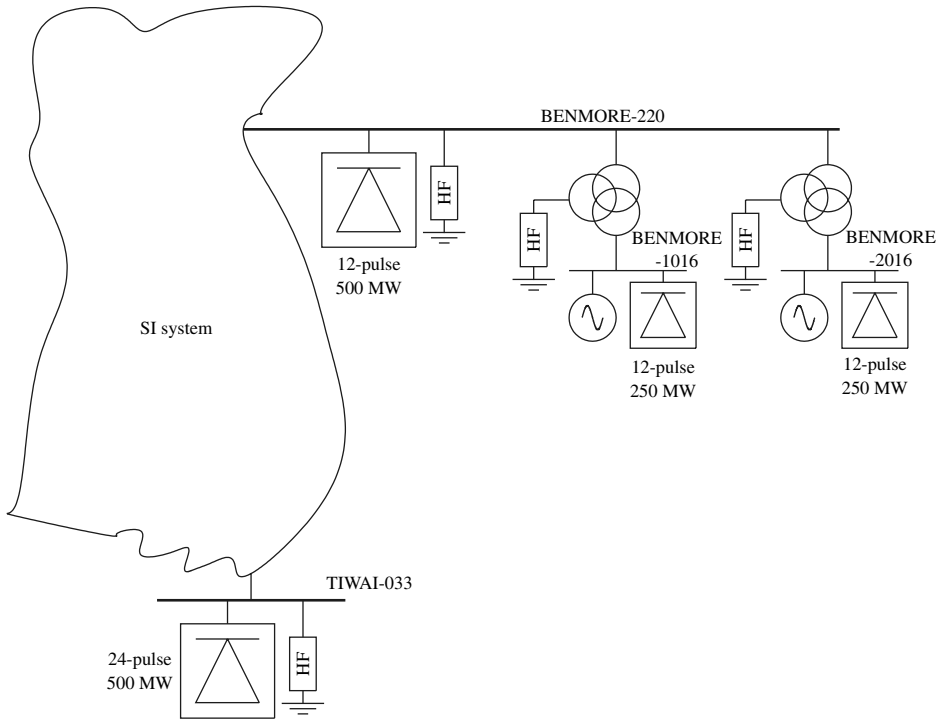


Figure 8.8 Multiconverter system (New Zealand South Island)

Three of the busbars are grouped together at Benmore in the middle of the South Island and form one end of the 1000 MW bipolar HVd.c. link. The fourth is located at Tiwai, at the southern end of the South Island, and is a 500 MW aluminium smelter.

As explained in Section 8.3.4, 426 variables and mismatches are needed at each converter bus, consisting of 300 a.c. voltages and 100 d.c. currents, the remaining 26 being switching and control terms. These three components are separated in the generalised Jacobian, as shown in Figure 8.7, where all the switching terms are placed last.

The 300×300 uppermost diagonal block contains the Benmore converter a.c. voltage variables and mismatches. Similarly, the next block diagonal matrix (also of order 300×300) contains the a.c. voltages of the Tiwai converters. The remaining elements in the upper left-hand side region represents the couplings (harmonic interactions) between the Benmore and Tiwai converters. Further down, and also on the right, are the (100×100) d.c. current harmonic terms and their coupling elements to the rest of the converter variables. The low right-hand side matrix contains the elements of the three-phase power flow (100 buses $\times$ 3 phases $\times$ 2 real and imaginary parts). Finally, the bottom and far right parts of the Jacobian contain the relatively few switching and control terms (26 per converter).

The test system is used to assess the ability of the unified algorithm to determine the degree of interaction between the multiple converters. At light load the Benmore-220 filters are normally out of service to minimise excessive VAR generation. Under these conditions, the results of the unified algorithm, shown by the black trace in Figure 8.9, are considerably different than those of the simplified model; this indicates

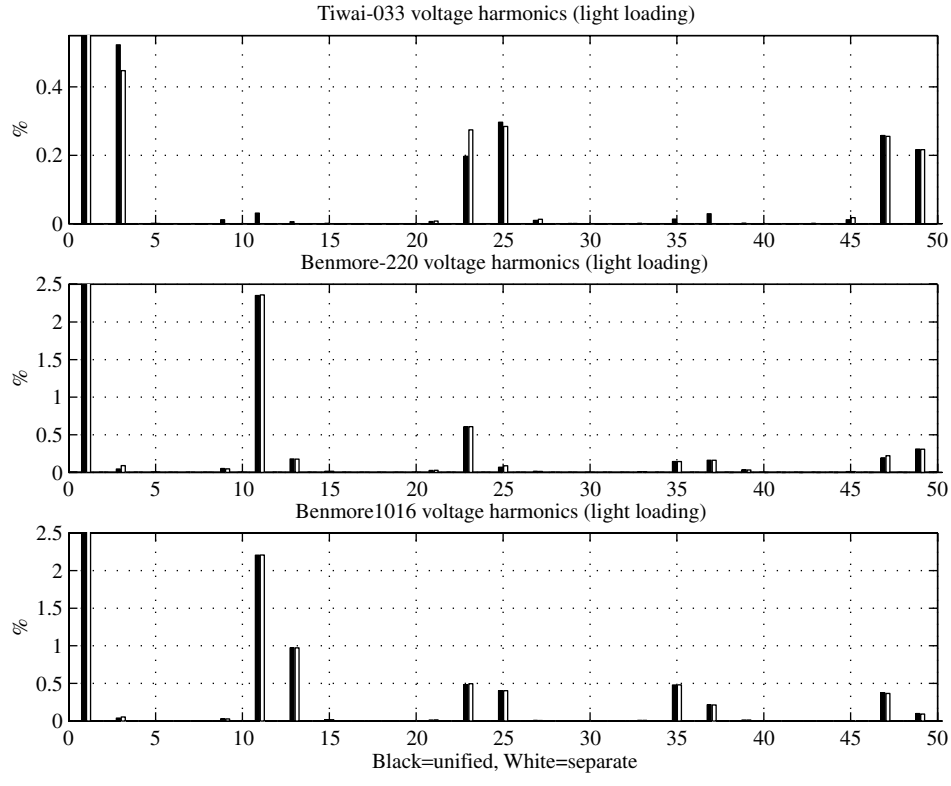


Figure 8.9 Comparison of harmonic voltages with the Benmore filters out of service

that in this case there is a noticeable harmonic interaction between the Tiwai-033 and Benmore converters.

8.5 Harmonic State Estimation

Recent contributions [24–33] have extended the concept of power system state estimation to harmonic frequencies. However, full measurement of the system states, by first recording the voltage and current waveforms at nodes and lines and then deriving their frequency spectra, is prohibitive for a large system. Only partial measurement (not necessarily made at the harmonic sources) is practical and, therefore, the measurements must be complemented by system simulation.

The framework of harmonic state estimation is illustrated in Figure 8.10. It uses a three-phase system model to describe asymmetrical conditions such as circuit mutual couplings, impedance and current injection unbalance. A partial measurement set is also needed consisting of some bus voltages, injection currents and line currents, or bus injection volt-amperes and line volt-amperes. Instead of system-wide harmonic state estimation, some contributions [34,35] discuss the issue with reference to the estimation of the harmonic components from the voltage or current waveform at a measurement point.

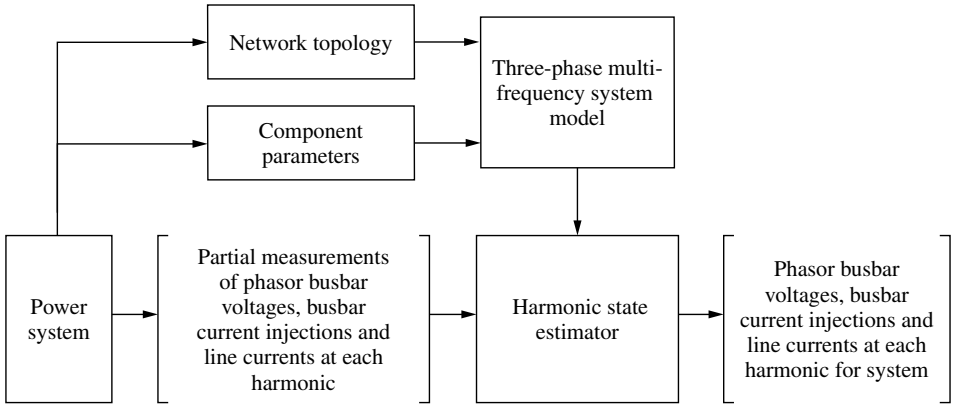

Network topology
Component parameters
Three-phase multi-frequency system model
Power system
Partial measurements of phasor busbar voltages, busbar current injections and line currents at each harmonic
Harmonic state estimator
Phasor busbar voltages, busbar current injections and line currents at each harmonic for system

Figure 8.10 Framework for harmonic state estimation

Based on the network topology, a harmonic state estimator (HSE) is formulated from the system admittance matrix at harmonic frequencies and the placement of measurement points. Measurements of voltage and current harmonics at selected busbars and lines are sent to a central workstation for the estimation of bus injection current, bus voltage and line current spectra at all or selected positions in the network.

The placement of measurement points is normally assumed symmetrical (e.g. either three or no phases of injection currents of a busbar are measured). However, this requirement restricts the search for optimal placement of measurement points in three-phase asymmetrical power systems.

The implementation of existing algorithms is in practice limited by poor synchronisation of conventional instrumentation schemes, lack of continuity of measurements or lack of processing speed. A system-wide or partially observable HSE requires synchronised measurement of phasor voltage and current harmonics made at the different measurement points, as illustrated in Figure 8.11.

HSE turns multi-point measurement to *system-wide measurement* in a very economic way. Two important optimisation problems in HSE are the maximum observable subsystem for a given measurement placement, and the minimum number of measurement channels needed for the observability of a given system. The HSE can be implemented continuously in real time if the measurement is continuous and the processing speed fast enough. Potentially, the harmonic monitoring instrument and estimator can be integrated into an existing supervisory control and data acquisition (SCADA) system.

State estimation is thus an alternative, or a supplement, to the direct measurement of electrical signals. Strictly speaking, a system state is a mathematically definable, although not necessarily measurable, electrical quantity such as a nodal voltage or a line current. In practice, however, the *state* concept is often extended to other variables, such as the voltage phase angle difference of a transmission line; it is also used for complex combinations of individual variables.

The task of the HSE is to generate the 'best' estimate of the harmonic levels from limited measured harmonic data, corrupted with measurement noise. The three issues involved are the choice of state variables, some performance criteria and the selection of measurement points and quantities to be measured.

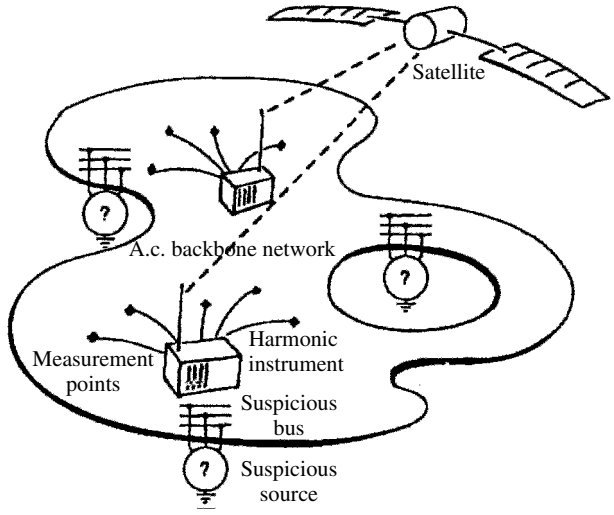


Figure 8.11 System-wide harmonic state estimation

State variables are those variables that, if known, completely specify the system. The voltage phasors at all the busbars are usually chosen, as they allow the branch currents, shunt currents and currents injected into the busbar to be determined.

Various performance criteria are possible, the most widely used being the weighted least-squares (WLS)

Observability analysis (OA) [29] is required in HSE to identify its solvability. A power system is said to be observable if the set of available measurements is sufficient to calculate all the state variables of the system uniquely. Observability is dependent on the number, locations and types of available measurements, and the network topology, as well as the system admittance matrix. For a different network topology, or the same network topology but different measurement placements, an OA is to be performed in each case.

It is important for OA not only to decide whether the system is observable and hence system-wide HSE can be performed, but also to provide information about the observable/unobservable islands as well as redundant measurement points if not completely observable. This allows the repositioning of measurement points to maximise their usefulness.

A system is observable if a unique solution can be obtained for the given measurements. A unique solution exists if and only if the rank of $[h]$ equals the number of unknown state variables. Therefore, for observability the number of measurements must not be less than the number of state variables to be estimated. However, this condition is not sufficient since linear dependency may exist among rows of the measurement matrix. The rank of $[h]$ does not depend on the quality of the measurements and therefore the noise vector can be assumed to be zero.

Existing OA can be divided into three groups of methods: numerical (floating-point calculations), topological and symbolic. A detailed coverage of this topic is made in [24,25].

8.5.1 Load and Harmonic Source Identification

The harmonic simulation and HSE algorithms differ regarding the way loads are treated. In general, a load bus may contain linear (passive) and nonlinear components. These can be modelled in detail in harmonic simulation, which represents separately the current injections and the passive components. HSE, on the other hand, may have no information about the composition of the load and is only capable of estimating the net current flow into or out of the load busbar.

Therefore, the current injection information supplied to the HSE algorithm is the sum of the harmonic current source and harmonic current flowing in the load. The harmonic voltages at the suspicious buses, and harmonic currents injected from the suspicious sources to the backbone, are provided by the estimator at the end of HSE and each suspicious source is classified as a harmonic injector or a harmonic absorber.

In general, a suspicious harmonic source can be considered as a Norton equivalent circuit at each harmonic frequency (Figure 8.12), and the following relationship applies for a harmonic of order n:

$$\hat{I}_i(n) - I_i(n) = V_i(n)\ Y_i(n) \tag{8.10}$$

In equation (8.10), $V_i(n)$ and $I_i(n)$ are the nodal voltage and current injection, respectively, as provided by the estimator, while $\hat{I}_i(n)$ and $Y_i(n)$ are the unknown Norton harmonic current injection and admittance within the suspicious source ($i = 1, 2, 3$). In theory, it should be possible to derive some information on the nature of the load from the estimated harmonic voltages and injected currents at the bus.

When no harmonic current injection exists at a node, it is possible to identify the load impedance using the nodal harmonic voltage and current information at two different harmonics. This calculated impedance can be verified using information at other frequencies. When a harmonic source is present, it is not possible to identify the components without additional information. This information may come from measurements obtained under different operating conditions (e.g. a component switched in or out)

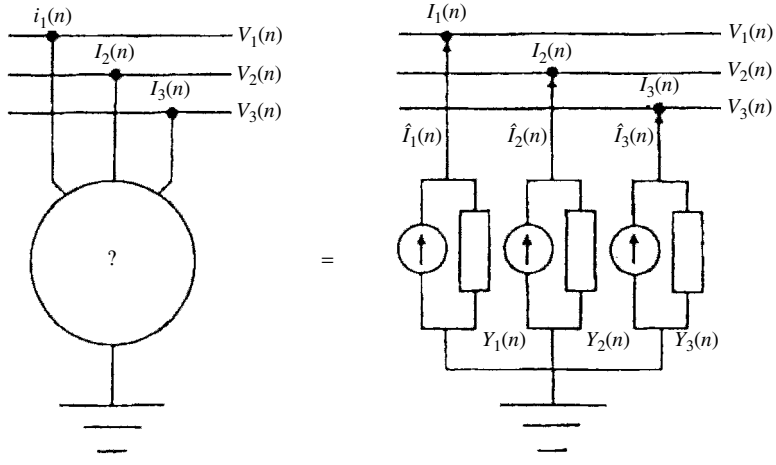


Figure 8.12 Norton equivalent for suspicious harmonic sources

or may take the form of an assumed ratio of the harmonic current injection to the fundamental based on the converter pulse number. In the latter case, if the following two assumptions are made for the suspicious source,

$$Y_i(n) = G_i - j\ B_i/n \tag{8.11}$$

$$|\hat{I}_i(n)| = \delta_i(n, n_0)|\hat{I}_i(n_0)| \tag{8.12}$$

where G_i and B_i are unknown parameters for node i, n_0 is a chosen reference harmonic (e.g. the 11th harmonic for the cases of 6-pulse and 12-pulse converters), and $\delta_i(n, n_o)$ is a chosen ratio of $|\hat{I}_i(n)|$ to $|\hat{I}_i(n_0)|$, then for any two harmonics n_1 and n_2 which are not n_0, the set of quadratic equations (equations (8.10)–(8.12)) is solvable to obtain the unknown Norton parameters $\hat{I}_i(n)$ and $Y_i(n)$ for each harmonic n of interest.

It can be shown, by sensitivity analysis, that the estimated Norton parameters using the above method are very dependent on the chosen ratio when the suspicious source contains non-zero Norton current injections, and very insensitive to the chosen ratio when the suspicious source does not contain Norton current injections. Therefore, the above method can at least be used to identify whether a suspicious source is a purely passive load and, in such case, estimate the equivalent harmonic admittances of the passive load.

8.6 The Electromagnetic Transients Solution

The EMTP method, although designed for the simulation of transients, can also be used for the derivation of the steady-state voltage and current waveforms taking into account the variety of system nonlinearities and the effect of the control functions. Its potential extension to the steady-state solution should therefore simplify the calculation of power system harmonics. Two different modelling philosophies have been proposed for this purpose. One is the hybrid solution outlined above, which is basically a frequency-domain solution with periodic excursions into the time domain to update the contribution of the nonlinear components. The alternative is a basically time-domain solution to the steady state followed by FFT processing of the resulting waveforms. The latter alternative offers greater user simplicity, given the general availability of EMTP packages, and is thus described further in the remaining part of the chapter.

Starting from standstill, the basic time domain uses a 'brute force' solution, i.e. the system equations are integrated until the steady state is reached within a specified tolerance. The voltage and current waveforms, represented by sets of discrete values at equally spaced intervals (*corresponding* with the integration steps), are subjected to FFT processing to derive the harmonic spectra. This is a very simple method but can be slow when the network has components with light damping.

The use of acceleration techniques, described in Section 8.3.3 for the hybrid solution, is not recommended here for the following reason. The number of periods to be processed in the time domain required by the acceleration technique is almost directly proportional to the number of state variables multiplied by the number of Newton iterations. Therefore the solution efficiency reduces very rapidly as the a.c. system size increases. This is not a problem in the case of the hybrid algorithm, because in that

case the time-domain solutions require no explicit representation of the a.c. network. On the other hand, when the solution is carried out entirely in the time domain, the a.c. system components are included in the formulation and thus the number of state variables is always large. Moreover, as the time-domain algorithm requires only a single transient simulation to steady state run, the advantage of the acceleration technique is questionable in this case, due to the additional complexity.

This method is very easy to use given the general availability of EMTP packages with flexible and detailed modelling of the nonlinear components. However, their accuracy is limited by the restricted frequency-dependence representation of the a.c. system components, although this problem can be greatly reduced with the use of frequency-dependent equivalents for the linear part of the system (a subject described later in this section).

8.6.1 Time Step Selection

The time step selection is critical to model accurately the resonant conditions when converters are involved. A resonant system modelled with 100 μS or 50 μS steps can miss a resonance, while the use of a 10 μS does not. Moreover, the higher the resonant frequency the smaller the step should be. A possible way of checking the effectiveness of a given time step is to reduce the step and then compare the results with those obtained in the previous run. If there is a significant change around the resonant frequency, then the time step is too large. The main reason for the small time step requirement is the need to pin-point the commutation instants very accurately, as these have great influence on the positive feedback that appears to occur between the a.c. harmonic voltages and the corresponding driven converter currents.

8.6.2 A.C. System Representation

The main requirement of a harmonic solution is the use of an accurate frequency-dependent model for the system components. This is best achieved in the frequency domain and has been the main reason for the development of the hybrid algorithms.

The next important question is the size of detailed system representation. To illustrate this point, Figure 8.13 shows the effect of the extent of system representation on the harmonic impedances. The solid line indicates a representation of the entire transmission system (11 kV and above) of the New Zealand South Island system. The dash-dotted line relates to a system reduced down to the local 220 kV network and only significant loads and generators represented. The dashed line represents the case of the 220 kV transmission network without generators, transformers or loads. The differences between these cases are very pronounced.

8.6.3 Frequency-Dependent Network Equivalents

The use of a frequency-dependent network equivalent (FDNE) avoids the need to model any significant part of the a.c. system in detail, yet can still provide an accurate picture of the system impedance across the selected range of harmonic frequencies.

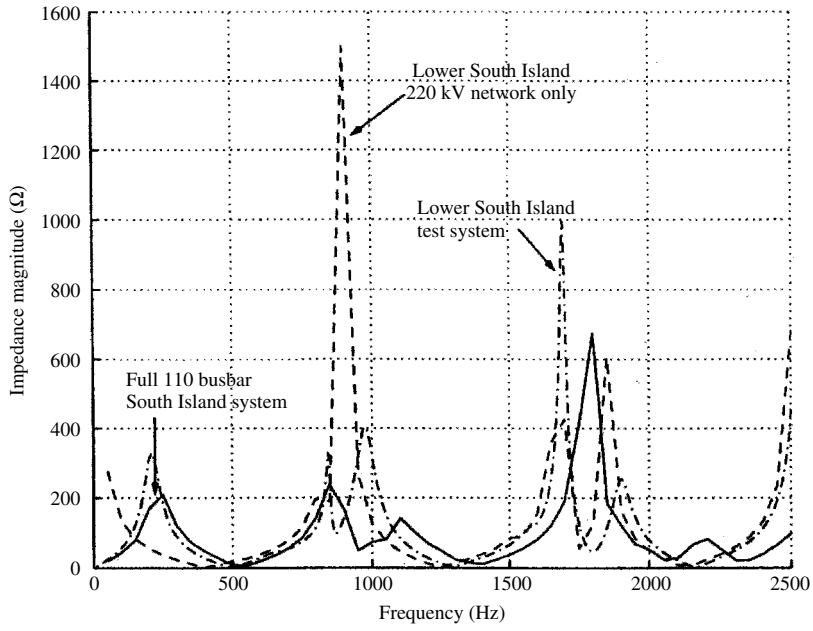


Figure 8.13 Comparison of depth of system representation

An early proposal [36] used the resonant points of the network frequency response to derive a set of tuned branches that can be easily incorporated into the EMTP program. Although the synthesis of those branches is direct, this method first ignores the losses to determine the L and C values for the required resonant frequencies and then determines the R values to match the response at minima points. In practice an iterative optimisation procedure is necessary after this process to improve the fit.

The equivalents of multiterminal circuits, such as a three-phase system with mutual couplings between phases, requires the fitting of admittance matrices instead of scalar admittances [37].

A criticism of the above technique for general transients use is that it can not model an arbitrary response. An alternative approach is to fit a rational function to a response and implement it directly in the transients program without the need for an equivalent circuit. In the latter, however, the parameters are functions of the time step and hence the fitting must be performed again when the time step is altered. Moreover the stability of the fit, without which the system can not be simulated, is still a problem with the rational function methods. Thus the parallel branches *RLC* equivalent provides greater simplicity and reliability at the expense of accuracy over the rational function methods. For (steady state) harmonic studies, where transient performance is not an issue, the parallel branches *RLC* equivalent can be fitted with high Q tuned branches for each harmonic, giving good accuracy at each harmonic but not at intermediate frequencies.

8.6.4 Case Study

The application of FDNE to harmonic analysis is illustrated here with reference to the CIGRE benchmark link [23] with the rectifier a.c. system replaced by the New Zealand

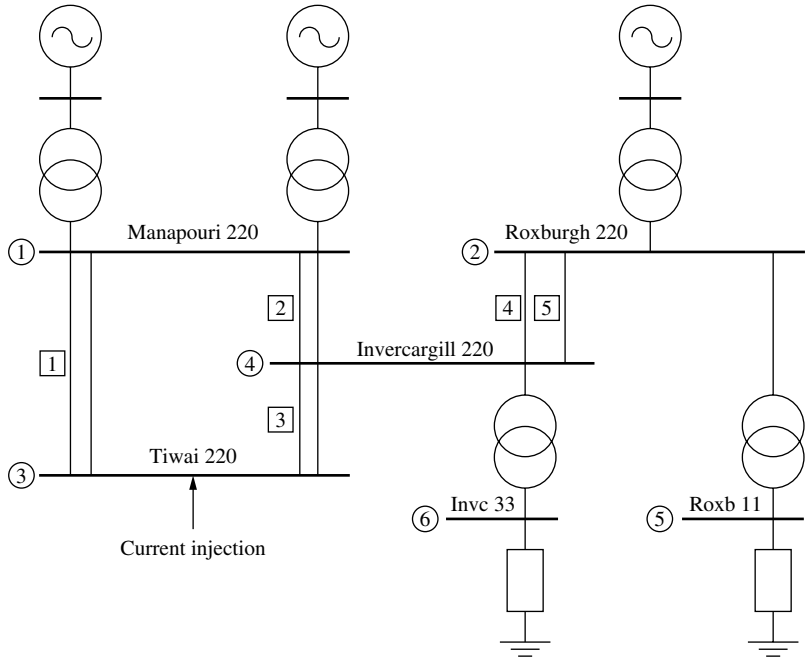


Figure 8.14 Lower South Island of New Zealand

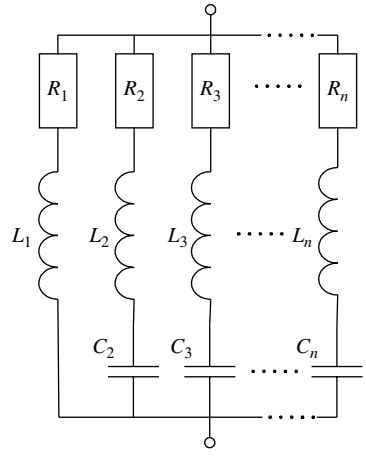


Figure 8.15 *RLC* network

Lower South Island test system [3] (Figure 8.14), which will be represented by a frequency-dependent network equivalent with the admittance terms emulated either by rational functions in the z domain or parallel *RLC* branches (as shown in Figure 8.15). Being a three-phase system, the equivalent will be of the form shown in Figure 8.16. The harmonic filters on the rectifier side of the d.c. link have been disconnected to accentuate the harmonic levels, as the presence of harmonic filters tends to mask any differences.

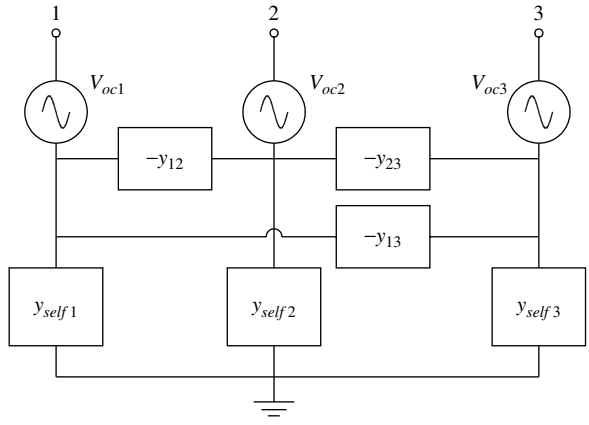


Figure 8.16. Three-phase FDNE

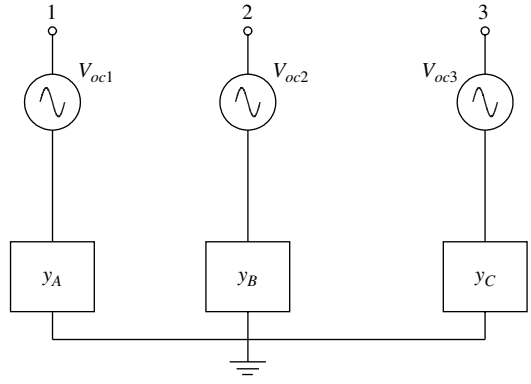


Figure 8.17 Simplified three-phase FDNE

A simplified FDNE, shown in Figure 8.17, is also considered using only the positive-sequence component. Its admittance elements are obtained by post-multiplying each 3×3 matrix by the matrix:

$$\begin{bmatrix} 1 & a^2 & a \\ a & 1 & a^2 \\ a^2 & a & 1 \end{bmatrix}$$

and then extracting the diagonal terms. This method is valid for systems with little phase current asymmetry. The effectiveness of the three FDNE equivalent alternatives is by comparison with the full representation of the system.

The first step in forming an FDNE is the calculation of the frequency response of the system to be represented. Although this is best achieved using frequency-domain programs, to enable comparison with simulations of the full system the frequency response of the test system is determined from time-domain simulations.

Figure 8.18 shows the phase voltages at the point of injection resulting from three current injection tests (at each phase of the Tiwai bus). These voltages are used to derive

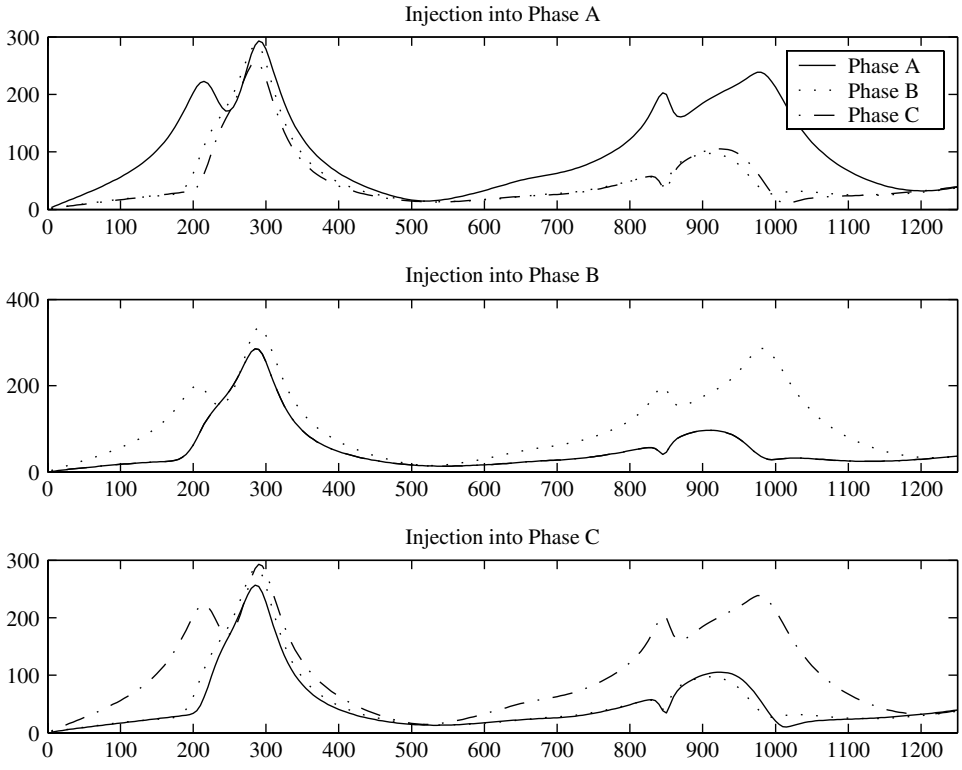


Figure 8.18 Voltages from injection tests

the self- and mutual impedances at each frequency. The 3×3 impedance matrices are then inverted to derive the nodal admittance matrices to be fitted (their respective magnitude and phase for the test system are shown in Figures 8.19 and 8.20).

In a nodal admittance matrix the off-diagonal elements are the negative of the interconnecting branch admittance and the diagonal terms the sum of all the branch admittances connected to a node; thus the latter are fitted by adding all admittances in the row or column (as the admittance matrices are symmetrical) of the particular node. Only six terms need to be fitted as Y_{12} and Y_{13} are the same as Y_{21} and Y_{31} respectively.

With the rational function approach each term is represented by a rational function of the form

$$H(z) = \frac{a_0 + a_1 z^{-1} + a_2 z^{-2} \cdots + a_n z^{-n}}{1 + b_1 z^{-1} + b_2 z^{-2} \cdots + b_n z^{-n}}$$

The values of the a and b coefficients are determined by setting up an over-determined system of linear equations of the form

$$\begin{bmatrix} [A_{11}] & [A_{12}] \\ [A_{21}] & [A_{22}] \end{bmatrix} \begin{pmatrix} \underline{a} \\ \underline{b} \end{pmatrix} = \begin{pmatrix} \underline{C} \\ \underline{D} \end{pmatrix}$$

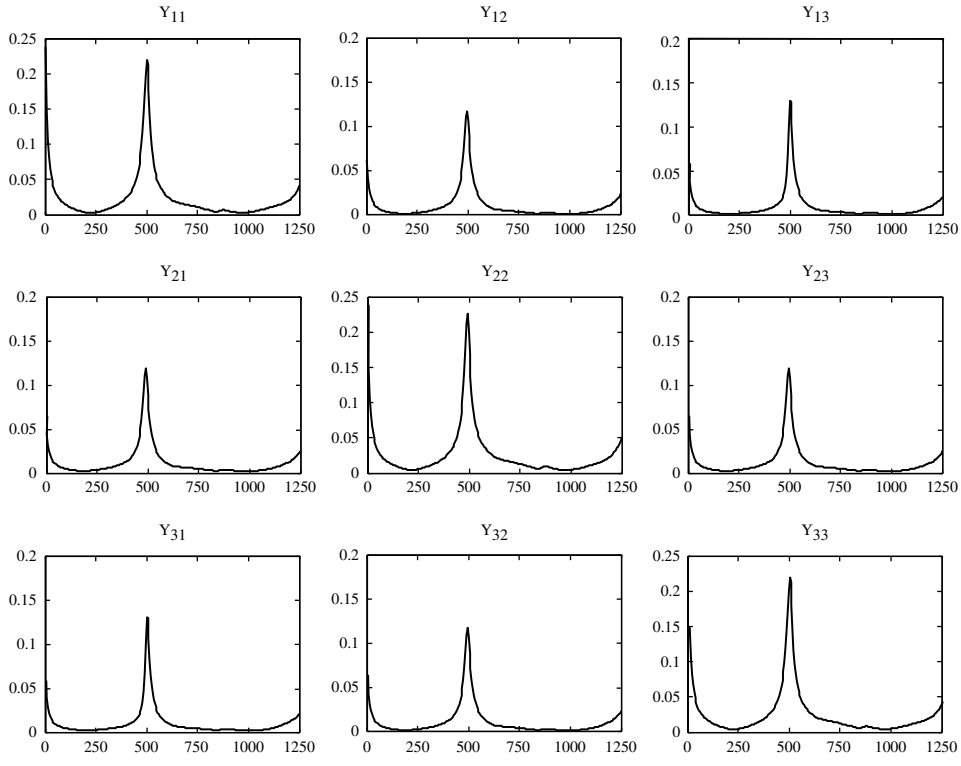


Figure 8.19 Admittance magnitude

where $\underline{a}$ and $\underline{b}$ are vectors of the a and b coefficients. $\underline{C}$ and $\underline{D}$ are vectors of the negative of the real and imaginary parts, respectively, of the sample data at each frequency. The system of linear equations is derived by evaluating the frequency response of $H(z)$ and equating to the required response at each sample point. This is solved via weighted least-squares. Two equations result from each sample point, one for the real component and the other for the imaginary component. A weighting factor of 100 is applied to equations representing the fundamental frequency so as to ensure minimal steady-state error. The rational function is implemented in PSCAD/EMTDC as a Norton equivalent (a current source with a parallel resistance). As $H(z) = I(z)/V(z)$, multiplying by the denominator and rearranging for $I(z)$ gives

$$I(z) = \underbrace{a_0 V(z)}_{\substack{\text{Instantaneous} \\ \text{term}}} + \underbrace{\left\{ \begin{array}{l} V(z)(a_1 z^{-1} + a_2 z^{-2} \cdots + a_n z^{-n}) \\ -I(z)(b_1 z^{-1} + b_2 z^{-2} \cdots + b_n z^{-n}) \end{array} \right\}}_{\text{History terms}}$$

The resistance represents the instantaneous term ($R = 1/a_0$) while the current source represents all the past history terms in current ($a_1, a_2 \ldots a_n$) and voltage ($b_1, b_2 \ldots b_n$). The complete formulation and implementation for this approach is given in [38]. The following tables contain the parameters for the model of the lower South Island of New Zealand. These have all been weighted for 50 Hz to minimize error at the fundamental.

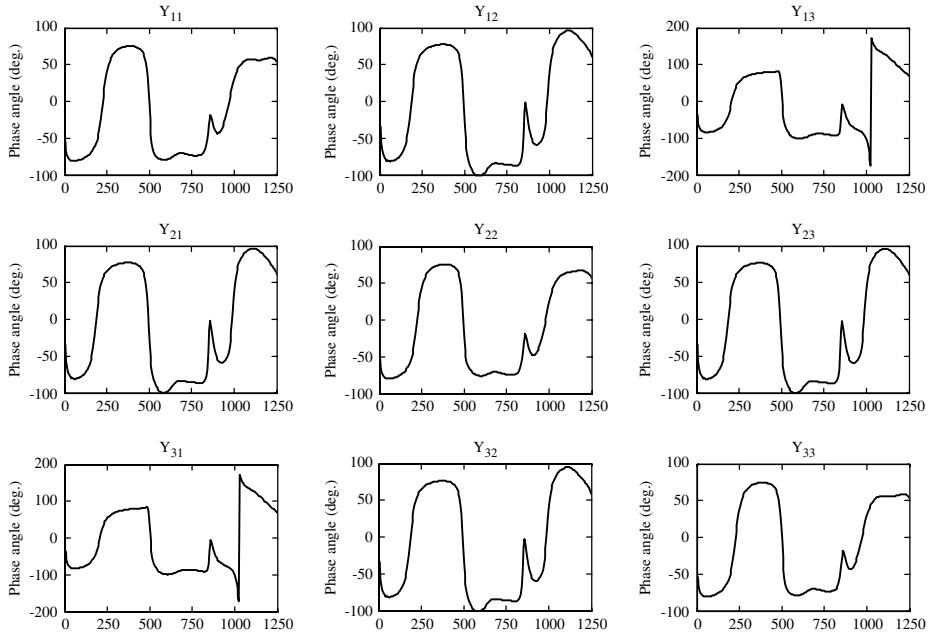


Figure 8.20 Admittance phase angle

Table 8.1 Coefficients of rational function representing Y_{self1} term

Order	Y_{self1}	
	a	*b*
0	2.4518139802491529e−003	1.0
1	−1.5523400352713717e−002	−6.6654302428731960e+000
2	4.2380331810221161e−002	1.9230399247655740e+001
3	−6.4641019199195751e−002	−3.1130273213778576e+001
4	5.9457300767762414e−002	3.0538485772657317e+001
5	−3.2959346847465210e−002	−1.8155446247494950e+001
6	1.0187297977530718e−002	6.0572751686602073e+000
7	−1.3529372195878338e−003	−8.7501014304358138e−001

The rational function forms a finally balanced system that represents the frequency response of the system. The positive and negative coefficients result in very similar numbers being subtracted and hence precision is important in the calculations. Thus a large number of decimal places is needed; this is illustrated in Tables 8.1 and 8.2 for the Y_{self1} and Y_{12} coefficients used in PSCAD/EMTDC simulation.

Rounding the coefficients to less significant digits can have a dramatic effect on the frequency response and often results in the system being unstable.

Figures 8.21 and 8.22 display the typical fitting accuracy for the Y_{12} and Y_{self1} terms respectively. The Y_{12} is fitted by an 11th order rational function while the Y_{self1} term by a 7th order. Although increasing the order of the Y_{self1} improves the fit, some poles are unstable.

Table 8.2 Coefficients of rational function representing Y_{12} term

Order	Y_{12}	
	a	*b*
0	1.9501107426634562e−003	1.0
1	−1.8984910246341156e−002	−1.0472045700750085e+001
2	8.4077491417341846e−002	5.0242749736612936e+001
3	−2.2327784954520663e−001	−1.4577147599444638e+002
4	3.9436282600293848e−001	2.8416307981056764e+002
5	−4.8528978431109171e−001	−3.9078405955678375e+002
6	4.2318006985401002e−001	3.8685683419253877e+002
7	−2.6026788334542772e−001	−2.7568394845148111e+002
8	1.0983931015277194e−001	1.3859815103973341e+002
9	−2.9928875612837458e−002	−4.6818484850277628e+001
10	4.6331885907560004e−003	9.5644565932267973e+000
11	−2.9369352575267255e−004	−8.9525681690543701e−001

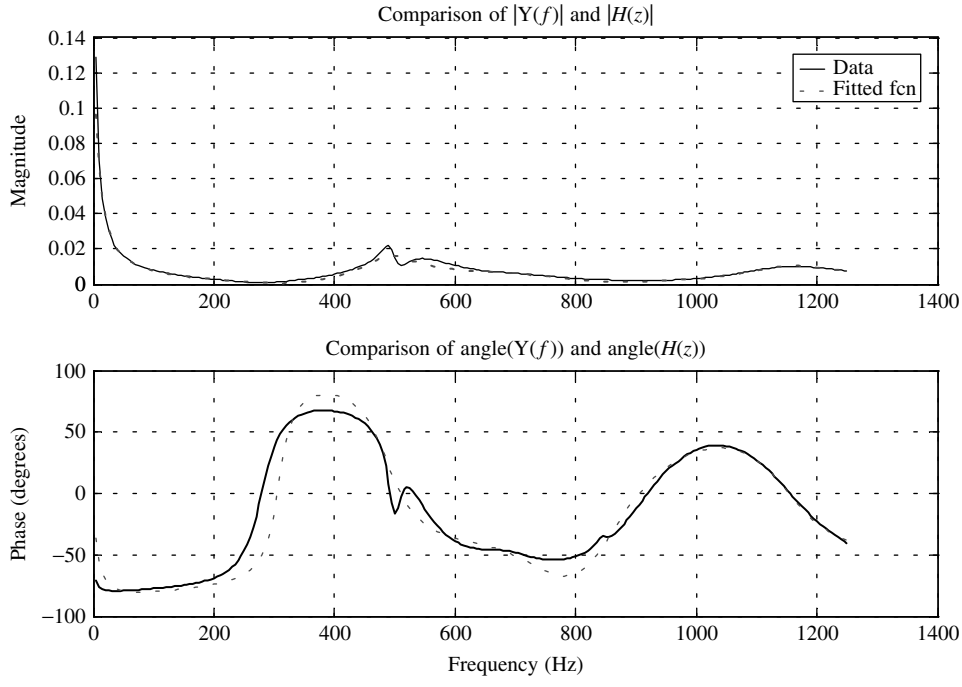


Figure 8.21 Comparison of Y_{self1} admittance term

To implement an *RLC* network, the features of the frequency response, that is the frequencies of peaks and troughs and trough magnitudes, are determined. For example, running the Y_{self1} term through a feature extraction program gives the results shown in Table 8.3.

Inspection of the frequency response allows some of the minor features to be removed, such as the 510 Hz and 545 Hz peak and trough, respectively, as these

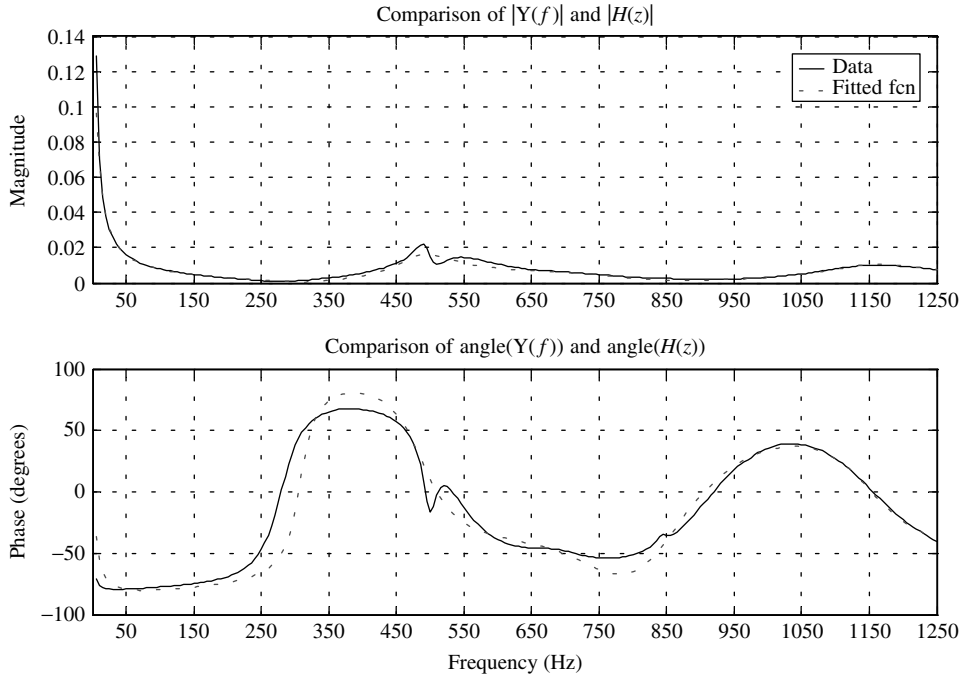


Figure 8.22 Comparison of Y_{12} admittance term

Table 8.3 Features of Y_{self1}

Frequency (Hz)	Type	Z magnitude (Ω)
280.0	Peak	1155.31
490.0	Trough	45.19
510.0	Peak	94.23
545.0	Trough	68.07
840.0	Peak	322.26
845.0	Trough	322.17
910.0	Peak	522.90
1160.0	Trough	98.09

only cause a small deviation from the overall trend. Extra peaks and troughs can be added outside the 5–1250 Hz frequency range to shape the response at the extremity of the frequency range.

The fitting procedure starts by ignoring the resistances when determining the L and C values so as to give the correct resonant frequencies. The resistances are set to be the impedance at the troughs and then all the L and C values are scaled, while maintaining the resonant frequencies, to give the correct circuit impedance at a specified match frequency. In this case the scaling frequency is 200 Hz and the match value 366.47 Ω.

The resistances of the branches are then adjusted to further improve the size of the resonant peaks. This can be achieved by modification of the impedance at the troughs

Table 8.4 Final selection of features used for Y_{self1} term

Frequency (Hz)	Type	Z magnitude Ω
0	Trough	10.0
280.0	Peak	–
490	Trough	90.18931
840.0	Peak	–
845.0	Trough	400.0
910.0	Peak	–
1160.0	Trough	98.091
1900	Peak	–

Table 8.5 Features for *RLC* FDNE (3 × 3)

		Trough frequency (Hz)	Trough magnitude (Ω)	Peak frequency (Hz)
Y_{self1}	1	0.0	10.0	280.0
	2	490	90.18931	840.0
	3	845.0	400.0	910.0
	4	1160.	98.091	1900.0
Y_{self2}	1	0.0	4.0	315.0
	2	440.0	300.0	465.0
	3	500.0	134.3544	945.0
	4	1155.0	292.0187	1900.0
Y_{self3}	1	0.0	0.1	1.0
	2	5.0	7.75	280.0
	3	490.0	90.1893	910.0
	4	1160.0	98.0910	1900.0
12	1	0.0	20.0000	185
	2	495	18.3576	845.0
	3	875	339.1000	990.0
	4	2250	5.0000	2500.0
13	1	0.0	20.000	205.0
	2	500.0	20.000	850.0
	3	880.00	300.000	1015.0
	4	1250.0	5.000	2500.0
23	1	0.0	20.000	185.0
	2	495.0	18.3576	845.0
	3	875.0	339.100	990.0
	4	2250.0	5.000	2500.0

or directly modifying the R values. Increasing the resistance effectively reduces the peak on either side. The final features used for the fitting are shown in Table 8.4. The complete set of features obtained is shown in Table 8.5. Often after this process extra branches are added to further improve the response in particular regions. The final *RLC* values obtained are given in Table 8.6, while Table 8.7 gives the matching frequency

Table 8.6 FDNE *RLC* 3 × 3

		R (Ω)	*L* (mH)	*C* (μF)
11	1	10.000	167.99566	–
	2	90.18931	94.8172641875	1.1126554076
	3	400.000	11671.3350	0.0030395291
	4	98.091	74.6789304842	0.2520729217
22	1	4.000	171.8693160074	–
	2	300.000	425.2498126926	0.3076739870
	3	134.3544	238.0594943090	0.4256128660
	4	292.018674	138.1816356405	0.1374124129
33	1	0.100	4205.3875120966	–
	2	7.750	175.2641568245	5781.0556064702
	3	90.18931	94.3575961209	1.1180757678
	4	98.091	76.6775418608	0.2455026041
12	1	20.000	311.0932318150	–
	2	18.3576	66.3414891513	1.5582769607
	3	339.100	1660.0376649282	0.0199299503
	4	5.000	9.2106855866	0.5432294040
	5	2000.00	4300.0	0.1720726
13	1	20.000	383.6827097296	–
	2	20.000	89.0417534485	1.1379064284
	3	300.000	1305.8401298774	0.0250486837
	4	5.000	94.3258081564	0.1718658944
	5	2000.000	3881.828	0.1552731
23	1	20.000	311.0932318150	–
	2	18.35760	66.3414891513	1.5582769607
	3	339.100	1660.0376649282	0.0199299503
	4	5.000	9.2106855866	0.5432294040
	5	2000.000	4300.00	0.1720726

Table 8.7 Match frequency and values

Term	Match frequency (Hz)	Match magnitude (Ω)
Y_{self1}	200.0	366.47
Y_{self2}	200.0	300.47
Y_{self3}	200.0	366.47
Y_{12}	140.0	600.0
Y_{13}	100.0	305.0
Y_{23}	140.0	600.0

and magnitude. Note that terms Y_{12}, Y_{13} and Y_{23} have an extra branch added (i.e. five *RLC* branches and yet there are only four peak/trough combinations) to improve the response at the first parallel resonance (approximately 185 Hz). Figures 8.23 and 8.24 display the comparison between the FDNE and required response.

Assuming balanced phase currents and diagonalising the impedance matrices results in three uncoupled frequency responses, each of which can be fitted with an *RLC* circuit. Applying the same procedure of feature extraction and synthesis of the *RLC*

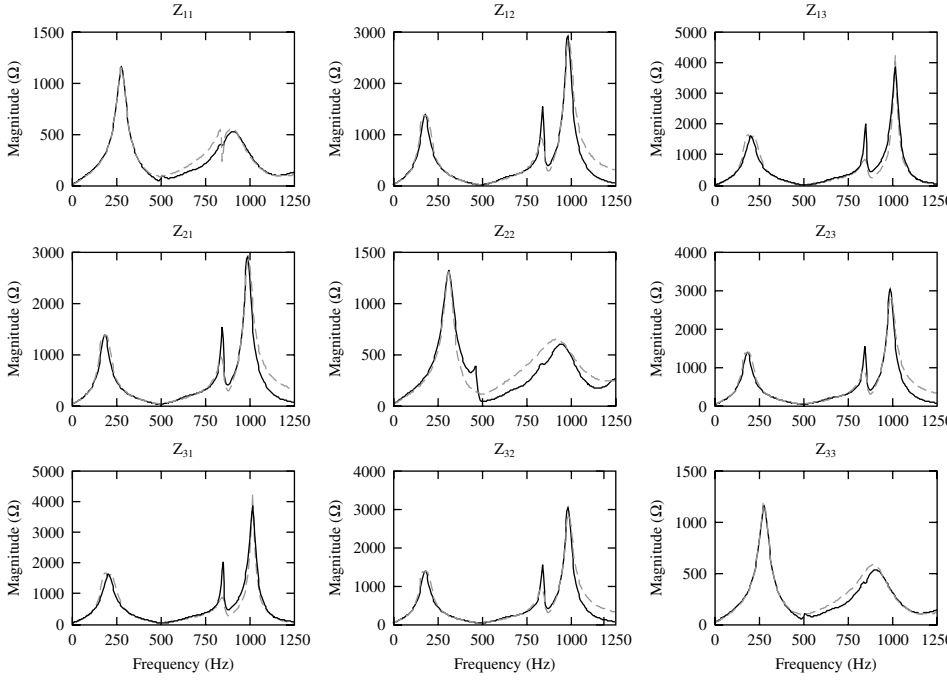


Figure 8.23 Comparison of magnitude response (*RLC* 3 × 3 FDNE)

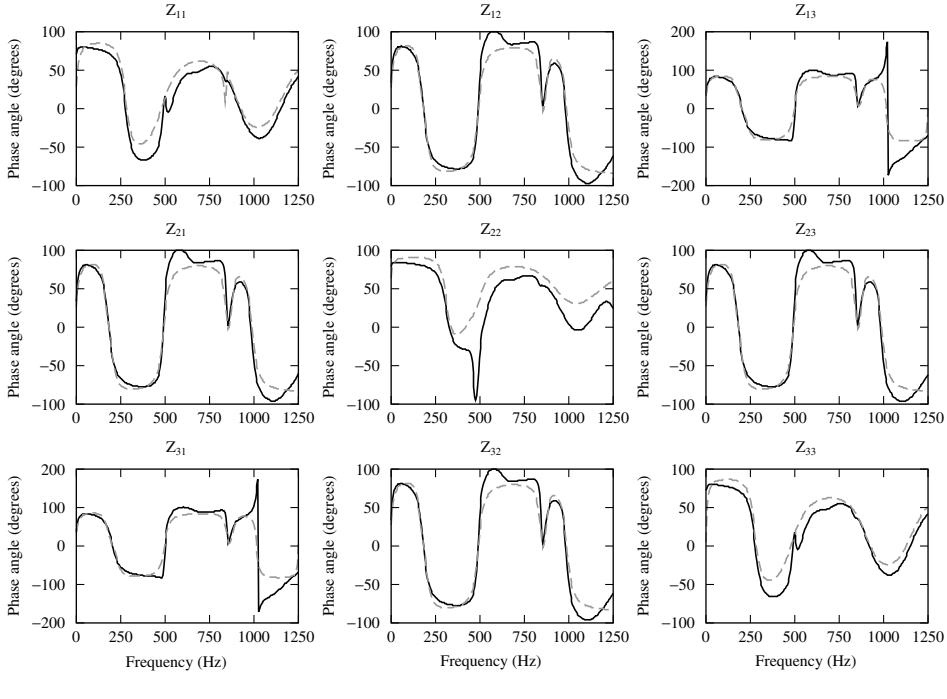


Figure 8.24 Comparison of phase angle response (*RLC* 3 × 3 FDNE)

circuit results in the values shown in Table 8.8. Each phase has a correction branch (branch 5 for phases A and C, and branch 6 for phase B) designed to give a better match at fundamental frequency (50 Hz). These branches are series resonant at 45 Hz, so at 50 Hz the impedance magnitude and phase angle are far closer to what is required. Figure 8.25 displays the match for the phase A term. A better match can be achieved by adding more branches to shape the response even further, particularly between 800 Hz and 1000 Hz.

Table 8.8 FDNE, *RLC* simplified

		R (Ω)	L (mH)	C (μF)
A	1	30.000	74.838	–
	2	1.400	21.554	4.8549
	3	91.30	1167.1335	0.068249
	4	10.00	15.296	0.9799
	5	5.0	530.5	23.58
B	1	30.000	74.072	–
	2	89.700	77.518	0.45837
	3	4.0	21.825	4.6423
	4	65.4	463.24	0.072409
	5	10.0	14.684	1.0207
	6	5.0	530.5	23.58
C	1	35.000	68.236	–
	2	7.000	19.959	5.1795
	3	40.000	36.513	0.090611
	4	10.000	13.795	1.0865
	5	1.0	530.5	23.58

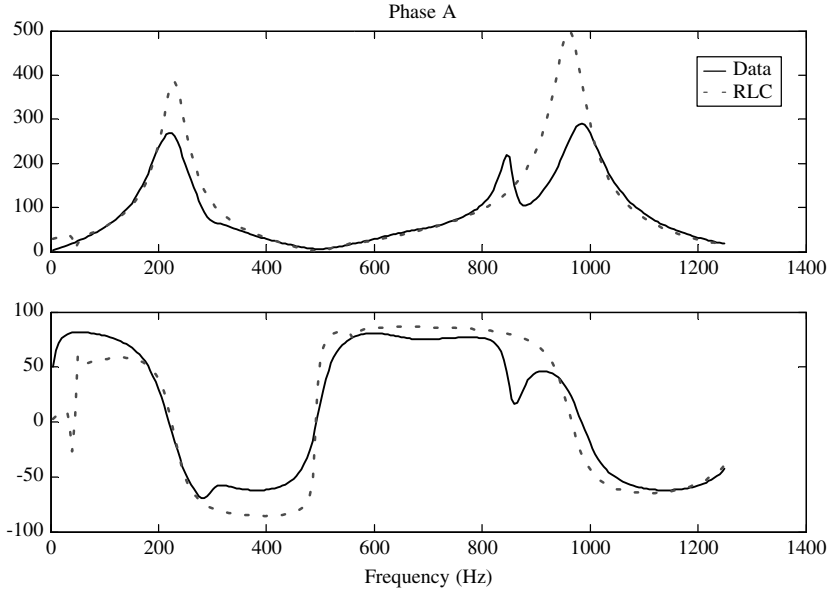


Figure 8.25 Phase A term after diagonalising

Table 8.9 FDNE voltage source parameters

	Voltage (phase to neutral)	
	Magnitude (kV)	Phase angle (degrees)
Phase A	121.599	61.16755
Phase B	121.599	−59.15545
Phase C	121.599	180.66100

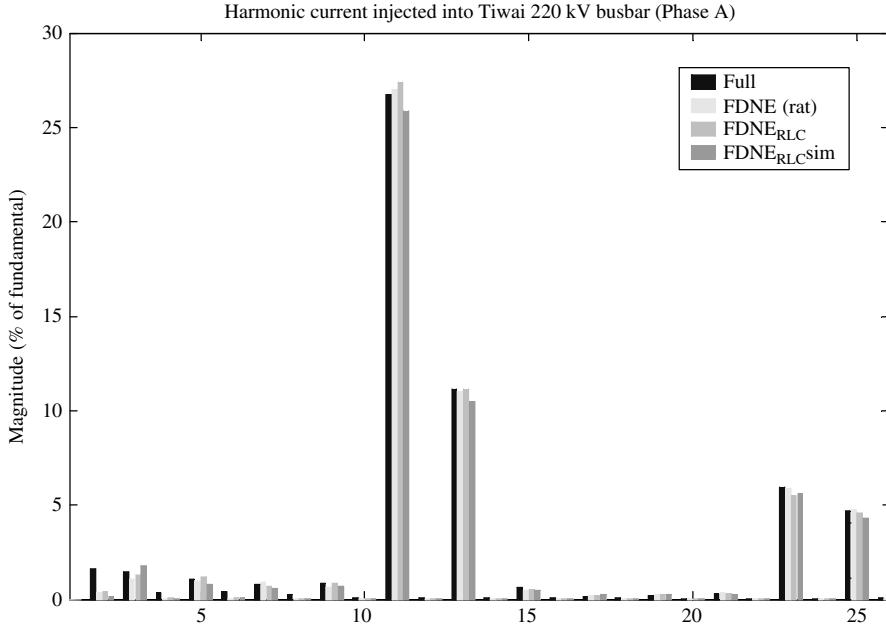


Figure 8.26 Harmonic current injection (phase A)

The voltage source magnitude and phase angle for all the FDNEs are set to be that of the full system under open circuit. These values are given in Table 8.9.

Setting the rectifier α order to 0.6 radians and inverter order to 2.42 and simulating the four cases (full, FDNE rational functions, FDNE *RLC* and FDNE *RLC* simplified) give the results displayed in Figures 8.26 and 8.27. This example shows that the assessed injected current from the d.c. link is very close for all cases. The harmonic levels predicted by the FDNE (rational function) match the full system best. The injected current into the rectifier a.c. system by the HVd.c. link is similar, with the rational function FDNE being the most accurate and the simplified *RLC* the worst. The RLC FDNE circuits show a large discrepancy in the 25th harmonic on the terminal voltage, which does not appear in the injected current. This is understandable when the fitting errors are considered (Figure 8.23 for the *RLC* FDNE and Figure 8.25 for the simplified *RLC* FDNE).

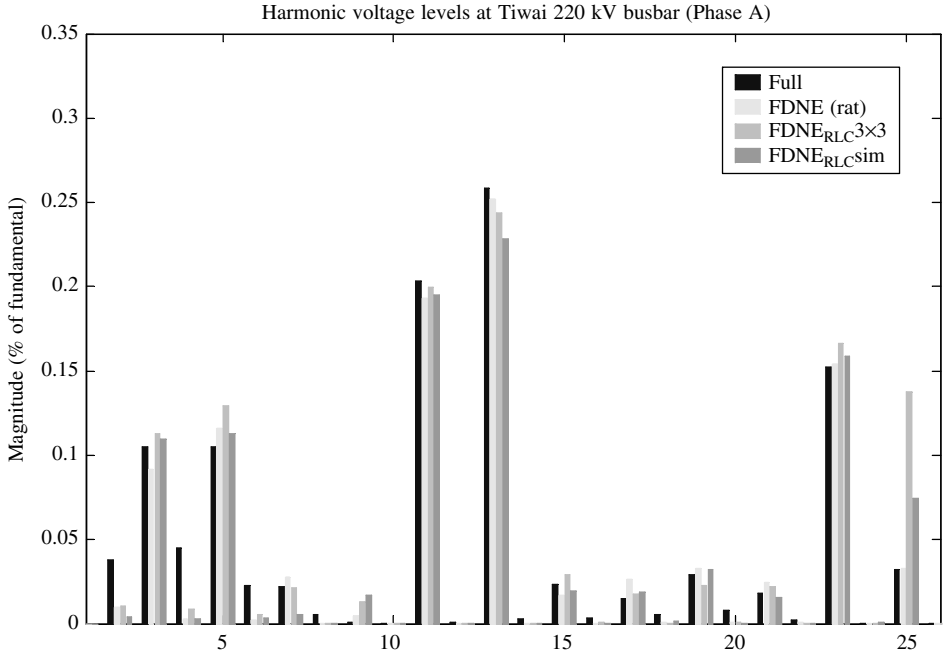


Figure 8.27 Harmonic voltage at terminal busbar (phase A)

The system impedances are unbalanced, as they are in most practical systems, resulting in uncharacteristic harmonics being generated by the converter. It is essential that the FDNE accurately represents the system at fundamental frequency as any discrepancy, particularly in the imbalance, has a dramatic impact on the operation of the converter, through the controller, and hence on the injected harmonic current, particularly the uncharacteristic harmonics. This in turn results in very large errors in assessed voltage distortion, even if the FDNE correctly represents the system impedance at these harmonic frequencies. Hence the need for correction branches at fundamental frequency for *RLC* FDNE or weighting factors for the rational function approach. Tables 8.10 and 8.11 show the fundamental frequency conditions for this comparison. Getting the fundamental frequency matching right is more important than getting the matching correct at harmonic frequencies.

If the interaction of a nonlinear device with the a.c. system is not modelled; that is, the device is represented by a fixed current injection, then the assessed harmonic

Table 8.10 Fundamental phase-neutral voltage at Tiwai 220 kV busbar

	Full		FDNE (rational fcn)		*RLC* 3 × 3		*RLC* (simplified)	
	Magnitude (kV)	Angle (degrees)	Magnitude (kV)	Angle (degrees)	Magnitude (kV)	Angle (degrees)	Magnitude (kV)	Angle (degrees)
Phase A	120.208	−27.48	120.183	−28.25	120.280	−28.22	120.411	−27.99
Phase B	120.551	−147.82	120.558	−148.45	120.678	−148.44	120.678	148.26
Phase C	119.804	92.14	120.133	91.44	120.247	91.45	120.343	91.64

Table 8.11 Fundamental current injected into Tiwai 220 kV busbar

	Full		FDNE (rational fcn)		*RLC* 3 × 3		*RLC* (simplified)	
	Magnitude (kA)	Angle (degrees)	Magnitude (kA)	Angle (degrees)	Magnitude (kA)	Angle (degrees)	Magnitude (kA)	Angle (degrees)
Phase A	0.060	−87.19	0.060	−85.90	0.060	−85.32	0.060	−85.90
Phase B	0.056	154.02	0.054	151.78	0.053	151.51	0.054	151.78
Phase C	0.057	26.89	0.059	26.09	0.060	25.71	0.059	26.09

levels given by the FDNE will be even closer to the full system run under the same conditions. The only difference will be the fitting errors. This provides one method for finding modelling errors, by performing injection tests on the FDNE model in the EMTP-type program, then taking the FFT to obtain the frequency response and comparing it to the matched response in the frequency domain.

Although the modelling of the frequency dependency of overhead lines and cables is well advanced in EMTP packages, this is not true for the other components. The standard models for generators, transformers and loads do not represent the increase in resistance (or slight reduction in inductance) associated with skin effect. This increase in resistance will be most noticeable when a resonance occurs. Hence, using a frequency-domain program to obtain the frequency response of the a.c. system to be represented by an FDNE will give a frequency response closer to reality. Having developed an FDNE from frequency data obtained using a frequency-domain program, it is very hard to verify the accuracy of the final FDNE without accurate measurements of the actual system. Hence, the above approach of using the less accurate time-domain derivation of frequency data has been used, as this allows the complete time-domain model to be used as the benchmark. Improved representation of components and their frequency dependency can be achieved by using *RL* networks, as illustrated in Figure 8.28 for a generator.

Figures 8.29–8.31 display the impedance magnitude, phase angle and impedance loci, respectively, for frequency-domain and time-domain generation of frequency responses. Frequency-dependent transmission line models with standard generator, transformer and load models were used in the time domain. As expected, there is reasonable agreement except at resonance, where the frequency domain generates a higher peak. The impedance loci look a lot worse, as the impedance changes very fast with frequency, near resonances. Hence the loops represent very narrow frequency bands and are the regions where discrepancies in resistances are most pronounced.

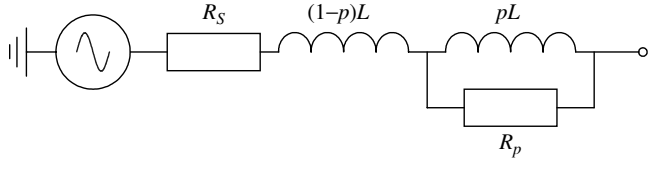


Figure 8.28 Generator model with improved frequency response

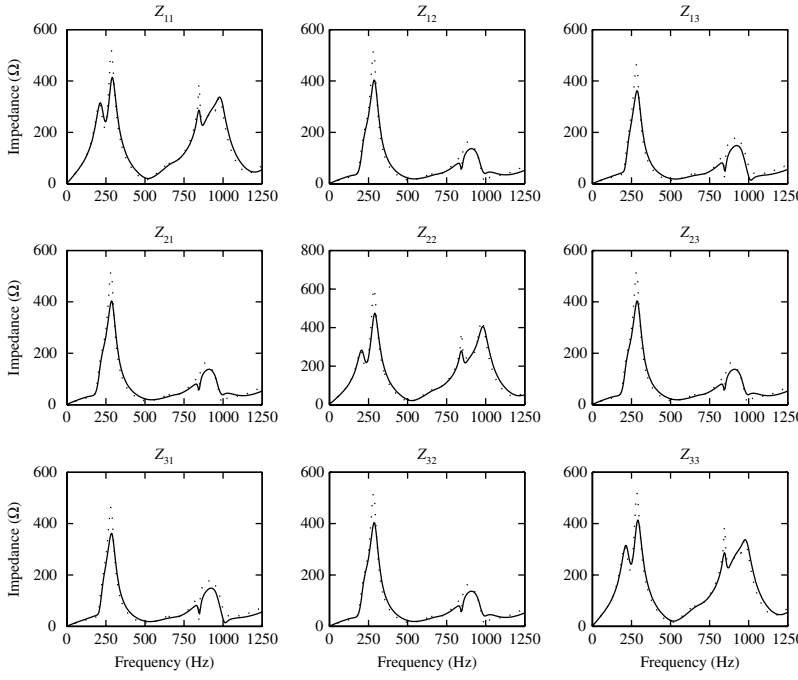


Figure 8.29 Comparison between (———) time- and (· · · · · ·) frequency-domain assessment of system impedance

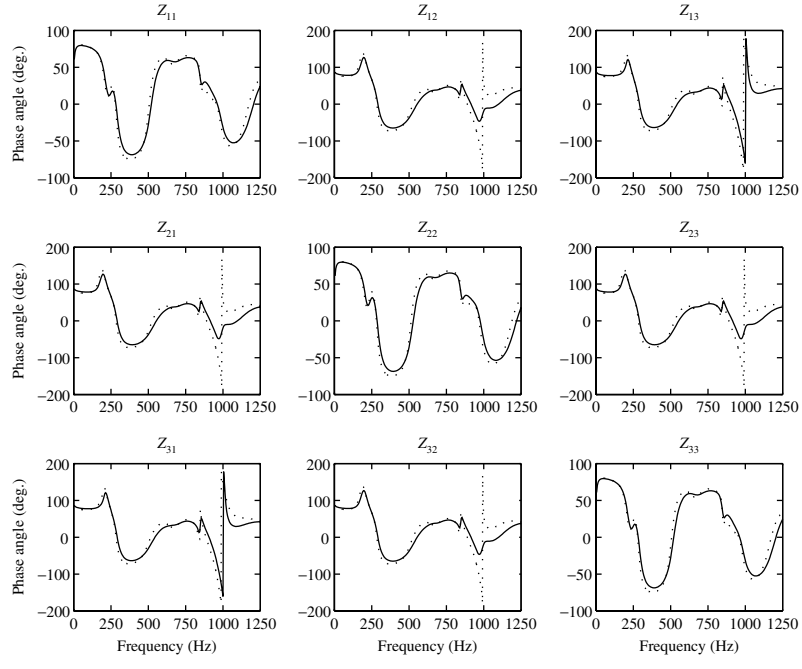


Figure 8.30 Comparison between (———) time- and (· · · · · ·) frequency-domain assessment of system impedance

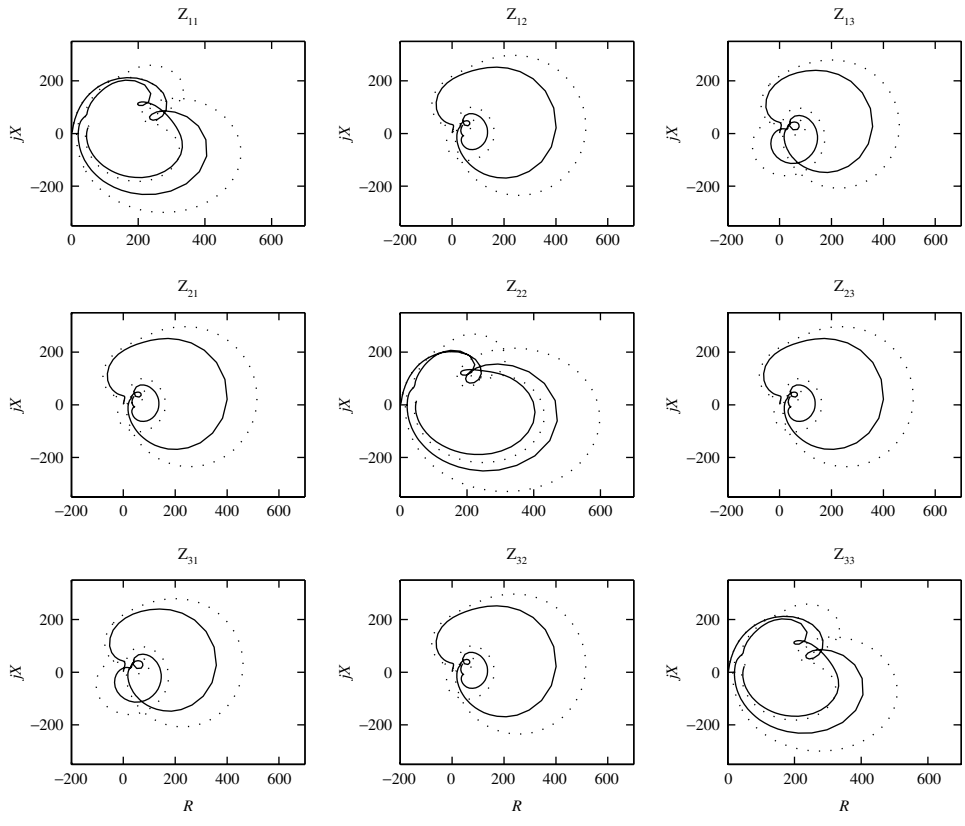


Figure 8.31 Comparison between (———) time- and (· · · · · ·) frequency-domain assessment of system impedance

8.7 Discussion on Advanced Harmonic Modelling

Three advanced methods have been described in this chapter for the simulation of the power system harmonic sources. These are the harmonic domain, the time domain and a hybrid combination of the conventional frequency and time domains.

The harmonic domain includes a linearised representation of the nonlinear components around the operating point in a full Newton solution. The fundamental frequency load flow is also incorporated in the Newton solution, which thus provides the ideal tool for general steady-state assessment. However, the complexity of the formulation to derive the system Jacobian may well prevent its final acceptability.

The hybrid proposal takes advantage of the characteristics of the frequency and time domains for the linear and nonlinear components, respectively. The hybrid algorithm is conceptually simpler and more flexible than the harmonic domain but it is not a full newton solution and therefore not as reliable under weak system conditions.

The direct time-domain solution, using EMTP-type programs, can be used for the derivation of the steady-state voltage and current waveforms and harmonics levels, and is particularly good at taking into account complex nonlinear devices and their controllers. Care is required to ensure a realistic resistance at harmonic frequencies.

FDNE can be used to represent the arbitrary frequency response of an a.c. system. When representing the interaction between the a.c. system and nonlinear devices, an accurate match at fundamental frequency must be achieved otherwise the incorrect operating conditions will result, with wrong harmonic injection estimates being obtained. This will follow through to wrong harmonic voltages.

With fixed harmonic current injections only the match at harmonic frequencies is important.

The rational function representation is more accurate and more methodical than the fitting of *RLC* networks, as the latter requires a certain amount of manual tuning of parameters. However, the rational function approach has the problem of stability, and hence trial and error is usually required to find the highest order that is stable.

8.8 References

1. Dickmander, D.L., Lee, S.Y., Desilets, G.L. and Granger, M. (1994) AC/DC harmonic interactions in the presence of GIC for the Quebec–New England phase II HVdc transmission, *IEEE Trans. Power Delivery*, **9**(1), 68–78.
2. Hammad, A.E. (1992) Analysis of the second harmonic instability for the Chateauguay HVdc/svc scheme, *IEEE Trans. Power Delivery*, **7**(1), 410–15.
3. Arrillaga, J., Smith, B.C., Watson, N.R. and Wood, A.R. (1997) *Power System Harmonic Analysis*, John Wiley & Sons, Chichester.
4. Yacamini, R. and De Oliveira, J.C. (1980) Harmonics in multiple converter systems: a generalised approach, *Proc. IEE*, **127**(2), 96–106.
5. Reeve, J. and Baron, J.A. (1971) Harmonic interaction between HVdc converters and a.c. power systems, *IEEE Trans. Power Apparatus and Systems*, **90**(6), 2785–93.
6. Callaghan, C. and Arrillaga, J. (1989) A double iterative algorithm for the analysis of power and harmonic flows at a.c.–d.c. terminals, *Proc. IEE*, **136**(6), 319–24.
7. Semlyen, A., Acha, E. and Arrillaga, J. (1992) Newton-type algorithms for the harmonic phasor analysis of non-linear power circuits in periodical steady state with special reference to magnetic non-linearities, *Trans. IEEE Power Delivery*, **PWRD-7**(3), 1090–8.
8. Semlyen, A. and Medina, A. (1995) Computation of the periodic steady state in system with non-linear components using a hybrid time and frequency domain methodology, *Trans. IEEE Power Systems*, **10**(3), 1498–1504.
9. Usaola, J. and Mayordomo, J.G. (1994) Multifrequency analysis with time domain simulation, *ETEP*, **6**(1), 53–9.
10. Usaola, J. and Mayordomo, J.G. (1990) Fast steady state technique for harmonic analysis, *ICHQP IV*, Budapest, pp. 336–42.
11. Semlyen, A. and Shlash, M. (2000) Principles of modular harmonic power flow methodology, *Proc. IEE Gener. Transm. Distrib.*, **147**(1), 1–6.
12. Smith, B.C., Watson, N.R., Wood, A.R. and Arrillaga, J. (1995) Steady state model of the ac-dc converter in the harmonic domain, *Proc. IEE Gener. Transm. Distrib.*, **142**(2), 109–18.
13. Bathurst, G.N., Watson, N.R. and Arrillaga, J. (2000) Adaptive frequency-selection method for a Newton solution of harmonics and inter-harmonics, *Proc. IEE Gener. Transm. Distrib.*, **142**(2), 126–30.
14. Arrillaga, J., Bathurst, G.N. and Watson, N.R. (2001) Adaptive derivation of inter-harmonics in variable speed drives, EPE 2001 Conference, Gratz, Austria.
15. Xia, D. and Heydt, G.T. (1982) Harmonic power flow studies, Part I—Formulation and solution, Part II—Implementation and practical application, *IEEE Trans. Power Apparatus Systems*, **PAS-101**, 1257–70.

16. Arrillaga, J. and Callaghan, C.D. (1991) Three-phase a.c.–d.c. load and harmonic flows, *IEEE Trans. Power Delivery*, **6**(1), 238–44.
17. Xu, W., Marti, J.R. and Dommel, H.W. (1991) A multiphase harmonic load flow solution technique, *IEEE Trans. Power Apparatus and Systems*, **PS-6**, 174–82.
18. Valcarcel, M. and Mayordomo, J.G. (1993) Harmonic power flow for unbalanced systems, *IEEE Trans. Power Delivery*, **8**(4), 2052–9.
19. Bathurst, G.N., Smith, B.C., Watson, N.R. and Arrillaga, J. (2000) A modular approach to the solution of the three-phase harmonic power flow, *IEEE Trans. Power Delivery*, **15**(3), 984–9.
20. Arrillaga, J., Acha, E., Densem, T. and Bodger, P.S. (1986) Ineffectiveness of transmission line transpositions at harmonic frequencies, *Proc. IEE*, **133C**(2), 99–104.
21. Harker, B.J. and Arrillaga, J. (1979) Three-phase a.c.–d.c. load flow, *Proc. IEE*, **126**(12), 1275–81.
22. Arrillaga, J. and Watson, N.R. (2001) *Computer Modelling of Electrical Power Systems*, John Wiley & Sons, Chichester.
23. Szetchman, M., Weiss, T. and Thio, C.V. (1991) First benchmark model for HVdc control studies, *Electra*, **135**, 55–75.
24. Heydt, G.T. (1989) Identification of harmonic sources by a state estimation technique, *IEEE Trans. Power Delivery*, **4**(1), 569–76.
25. Arrillaga, J., Watson, N.R. and Chen, S. (2000) *Power System Quality Assessment*, John Wiley & Sons, Chichester.
26. Beides, H.M. and Heydt, G.T. (1991) Dynamic state estimation of power system harmonics using Kalman filter methodology, *IEEE Trans. Power Delivery*, **6**(4), 1663–70.
27. Meliopoulos, A.P.S., Zang, F. and Zellingher, S. (1994) Power system harmonic state estimation, *IEEE Trans. Power Delivery*, **9**(3), 1701–9.
28. Du, Z.P., Arrillaga, J. and Watson, N.R. (1996) Continuous harmonic state estimation of power systems, *Proc. IEE*, **143 Pt.C**(4), 329–36.
29. Du, Z.P., Arrillaga, J. and Watson, N.R. (1996) A new symbolic method of observability analysis for harmonic state estimation of power systems, *Proc. IEE*, **1**, 431–5.
30. Farach, J.E., Grady, W.M. and Arapostathis, A. (1996) Optimal harmonic sensor placement in fundamental network topologies, *Proc. IEE Gener. Transm. Distrib.*, **143**(6), 608–12.
31. Ma, H. and Grigis, A.A. (1996) Identification and tracking of harmonic sources in a power system using a Kalman filter, *IEEE Trans. Power Delivery*, **11**(3), 1659–65.
32. Hartana, R.K. and Richards, G.G. (1990) Harmonic source monitoring and identification using neural network, *IEEE Trans. Power Systems*, **5**(4), 1098–104.
33. Soliman, S.A., Christensen, G.S., Kelly, D.H. and El-Naggar, K.M. (1990) A state estimation algorithm for identification and measurement of power system harmonics, *Electric Power Research*, no. 19, 195–206.
34. Osowski, S. (1994) SVD technique for estimation of harmonic components in a power system: a statistical approach, *Proc. IEE Gener., Transm. Distrib.*, **141**(5), 473–9.
35. Moo, C.S. and Chang, Y.N. (1995) Group-harmonic identification in power systems with non-stationary waveforms, *Proc. IEE Gener., Transm. Distrib.*, **142**(5), 517–22.
36. Hingorani, N.G. and Burbury, M. (1970) Simulation of ac system impedance in HVdc system studies, *IEEE Trans. Power Apparatus Systems*, **89**(5/6), 820–8.
37. Watson, N.R. and Arrillaga, J. (1988) Frequency-dependent ac system equivalents for harmonic studies and transient converter simulation, *Trans. IEEE*, **PD-3**(3), 1196–1203.
38. Watson, N.R. and Arrillaga, J. (2003) Power systems electromagnetic transients simulation, IEE Power and energy series 39, London.